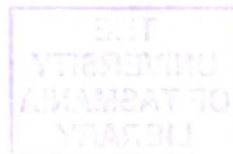


Computer Simulation and Investigation of Underwater Two-Part
and Multi Tow Systems

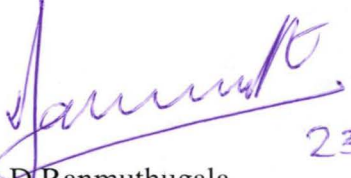
Susantha Devapriya
Susantha D Ranmuthugala

Civil and Mechanical Engineering
Submitted in fulfilment of the requirements for the degree of
Doctor of Philosophy in Engineering

University of Tasmania
December 2000



This thesis contains no material which has been accepted for a degree or diploma by the University or any other institution, except by way of background information and duly acknowledged.


S D Ranmuthugala 23/12/00

This thesis may be made available for loan and limited copying in accordance with the *Copyright Act 1968*.


S D Ranmuthugala

23/12/00

Note:

This thesis contains a number of colour photographs and graphs. Reproducing it without colour may affect the quality of the photographs and hinder the identification of the data in the graphs.

ABSTRACT

To maximise effectiveness, towed underwater sonar bodies generally require perturbations from the steady state motion to be minimised. The instantaneous position of the towed body is influenced by the unsteady, wave-induced motion of the surface vessel, transmitted via the tow cable. This can render the trajectory of the underwater body beyond acceptable limits for sonar operations.

In an effort to decouple this motion, a two-part tow configuration has been employed. This thesis describes a three-dimensional dynamic computer model developed to investigate two-part tows by modelling the individual cables separately and coupling them dynamically. This approach also enables the modelling of series and parallel multiple tow configurations. The cable system, modelled using a three degree-of-freedom finite difference approach, is then coupled to the six degree-of-freedom underwater towed bodies at the appropriate locations of the cable system. The modelling of the cable as a continuous medium and the derivation of the stress wave speeds are also presented, followed by the validity and effects of representing it as a discretised model.

The solution to the dynamic equations describing the motion of the discretised tow configuration is carried out using an implicit multi-step numerical technique, subject to specific boundary conditions. This allows the values to be *improved* through an iterative procedure, until sufficient convergence is achieved.

An introduction into the use of such numerical techniques in engineering and an analysis of the numerical procedure used in the solution are also presented. The requirements for accuracy and numerical stability of the integration technique are investigated and a guide to the time interval for the time stepping algorithm is deduced.

The computer model is successfully validated using experimental results from scaled model tests in a circulating water channel. These results together with those obtained from full scale sonar trials utilising small coastal craft are used to further investigate the behaviour of the two-part tow configuration to varying parameters. The experimental results and the computer model enables the user to identify the optimum tow configuration for the prevailing conditions.

The thesis also presents a detailed review of the various methods available to investigate underwater cables and vehicles, together with prediction methods for their hydrodynamic coefficients. The latter coefficients for the scaled models used in the project are obtained via experimental procedures.

Although a number of investigations have been carried out dealing with aspects of underwater towing operations, the strength of this investigation lies in that it combines these aspects, *i.e.* mathematical modelling, computer simulation, prediction of the hydrodynamic coefficients, scaled model experiments, full scale trials, and the analysis of the numerical technique, into one study.

ACKNOWLEDGEMENTS

I wish to thank the following for their assistance and valuable contribution during the project.

My supervisors Professor Michael Davis from the University of Tasmania and Dr Stan Gottschalk from AMC for their guidance, support, and encouragement. Dr Gottschalk's ability to make sense of my somewhat disorganised draft material at such short notice, and return them with in-depth comments and recommendations has been a major factor in the completion of this project.

Mr Brendon Anderson and Mr Garry Campanella from DSTO for their assistance in organising the experimental work and providing the ever important industry input. Special mention must be made of Mr Anderson for his patience, encouragement, and for reminding me on numerous occasions that timeframes are not infinitely expandable.

Robert Evans from AMC, Peter Graham, Greg Wright, Darryl Gaston, and Darius Juchnevicius from DSTO, Tim Mak from AMECRC and a number of staff members from AMC and DSTO for their assistance in the experimental stages of the project. Ross Warden from DSTO for assistance in video recording the scaled model tests and their subsequent analysis. Dr Ian MacGillivray from DSTO for assisting with analysing experimental data.

Special thanks to Dr Paul McShane, Dr Colin Buxton, and Mr Ian Cartwright, my line managers during the project, for their support and understanding that enabled me to complete the work. My colleagues at AMC for their encouragement, even if only to ask "when will you ever finish?".

AMC, DSTO, and AMECRC for their assistance, including financial and in-kind contributions, throughout the project.

Finally my wife Preeni for putting up with a short tempered husband who spent all his spare time staring at a computer screen, not to mention the mountain of paper that defied all her efforts at cleaning, my parents for all their support during the project, and my two children who made a supreme effort to stay out of Dad's path and expressed everyone's relief at the end of the project by stating "Dad can now stop *playing* with the computer and play with us".

TABLE OF CONTENTS

Abstract	i
Acknowledgements	iii
List of Illustrations	viii
List of Tables	xiii
Nomenclature	xiv
Abbreviations	xxii
Equation Numbering Scheme	xxii
 <u>Chapter 1</u>	
Introduction	1
1.1 Definition of Problem	1
1.2 Outline of Thesis	5
1.3 Tow Configuration	6
1.4 Static and Quasi-Static Cable Models	8
1.5 Dynamic Cable Models	13
1.6 Tow Cable / Fish Models	20
1.7 Solution Techniques	24
1.8 Underwater Vehicle Models	28
1.9 Experimental Investigation and Validation	30
 <u>Chapter 2</u>	
Modelling Techniques	32
2.1 Introduction	32
2.2 Dynamic Cable Models	33
2.2.1 The Method of Characteristics	33
2.2.2 Finite Difference Method	40
2.2.3 Hinged Rod Method	45
2.2.4 Finite Element Method	52
2.2.5 Lumped-Mass Method	60

2.3	Cable Drag and Inertia Forces	62
2.3.1	Flow Past a Smooth Long Rigid Cylinder	63
2.3.2	Effects on Drag Coefficient due to Surface Roughness and Turbulence	70
2.3.3	Drag on a Rigid Cylinder Inclined to the Flow	71
2.3.4	Morison's Equation	74
2.3.5	Hydrodynamic Cylinder Coefficients in Harmonic Flow	76
2.3.6	Vortex Induced Hydrodynamic Forces	83
2.3.7	Hydrodynamic Coefficients Selected	91
2.4	Towed Fish Models	91
2.5	Towed Fish Hydrodynamic and Acceleration Coefficients	93
2.5.1	Towed Fish Acceleration Coefficients	93
2.5.2	Towed Fish Static and Dynamic Hydrodynamic Coefficients	96

Chapter 3

Cable and Fish Model	104
3.1 Modelling of the System	104
3.2 Axes System	105
3.2.1 Cable System Transformation Matrix	105
3.2.2 Tow Fish Transformation Matrix	107
3.3 Cable Model	109
3.3.1 Drag Force	112
3.4 Equations of Motion for Cable Nodes	114
3.4.1 Junction	118
3.4.2 Boundary Nodes	120
3.5 Tow Fish Model	122
3.5.1 Force Equations for Tow Fish	125
3.5.2 Moment Equations for Tow Fish	131
3.5.3 Linearisation of Equations	134
3.5.4 Equations of Motion for Tow Fish	137

Chapter 4

Solution Algorithm and Program Outputs	143
4.1 Overview	143
4.2 Quasi-Static Model	145

4.3	Dynamic Model Solution Algorithm	150
4.3.1	Boundary Nodes	154
4.3.2	Junction	155
4.3.3	Matrix Solution	157
4.3.4	Angular Displacement of Tow Fish	161
4.3.5	Solution Procedure	162
4.4	Program Outputs	164
4.5	Multiple Tows in Series	167
4.6	Multiple Tows in Parallel	173

Chapter 5

Analysis of the Numerical Method	177
5.1 Introduction	177
5.1.1 Derivation of the Houbolt Scheme	181
5.2 Comparison between the Lumped Mass Model and the Continuous Cable Model	185
5.2.1 Continuous Cable Model	185
5.2.2 Wave Speeds	192
5.2.3 Relationship between Continuous and Discrete Systems	192
5.2.4 Effects due to Discretisation	197
5.3 Stability and Accuracy	200
5.4 von Neumann (Fourier) and Routh-Hurwitz Methods	202
5.4.1 von Neumann (Fourier) Method	203
5.4.2 Routh-Hurwitz Method	204
5.5 Matrix Stability Method	205
5.5.1 Modal Superposition	205
5.5.2 Stability Analysis	209
5.5.3 Stability of the Houbolt Integration Scheme	212
5.5.4 Non-linear Systems	215
5.6 Accuracy	217
5.6.1 Accuracy Analysis of the Houbolt Scheme	220
5.7 Natural Frequencies of the Model	226
5.8 Estimation of the Time Step	231

<u>Chapter 6</u>	
Experimental Methods and Validation	236
6.1 Introduction	236
6.2 Scaled Model Trials	236
6.2.1 Scaled Model Trial Configurations	238
6.3 Scaled Model Test Results	240
6.3.1 Response of the Two-Part Tow due to Vertical Excitation	241
6.3.2 Response of the Two-Part Tow due to Horizontal Excitation	253
6.3.3 Conclusion from the Scaled Model Trial Results	260
6.4 Full Scale Trials	261
6.4.1 Full Scale Trial Results	263
6.5 Scaled Model Hydrodynamic Coefficients	267
6.6 Validation of the Computer Program	269
 <u>Chapter 7</u>	
Conclusion	275
7.1 Summary	275
7.2 Conclusions and Recommendations	279
7.3 Future Work	281
 <u>Bibliography</u>	283
 <u>Appendix A</u>	
Experimental Results	299
 <u>Appendix B</u>	
Computer Program Flowcharts	331
List of Program Flowcharts	331

LIST OF ILLUSTRATIONS

Figure	Page No.
1.1 Tow Configurations (a) to (i)	2 and 3
1.2 Two-Part Tow	4
1.3 Conventional Tow	7
1.4 Typical Transfer Function for Shallow and Deep Water Mooring Cases	12
2.1 Cartesian Coordinates of Cable	34
2.2 Continuous Cable Element	34
2.3 t-s Solution Mesh	39
2.4 Hinged Rod Segment	46
2.5 Finite Element Model	53
2.6 Equivalent Nodal Forces on Finite Element	54
2.7 Tension Forces in Finite Element	55
2.8 Lumped Mass Model	61
2.9 Flow Past a Cylinder (a) to (e)	67
2.10 Drag Coefficient for Cylinders and Spheres	68
2.11 Typical Variation of Drag Coefficient with Reynolds Number for a Smooth Cylinder	68
2.12 The Drag of Sand Roughened Cylinders	71
2.13 Direction of Drag Forces on a Cable in a 3D Flow Field	72
2.14 Variation of Drag Coefficient for Inclined, Smooth Cylinders	73
2.15 Drag Coefficient versus Reynolds Number for $KC = 20$ and for Various Values of Relative Roughness	79
2.16 Drag Coefficient versus Reynolds Number for $KC = 40$ and for Various Values of Relative Roughness	79
2.17 Inertia Coefficient versus Reynolds Number for $KC = 20$ and for Various Values of Relative Roughness	80
2.18 Inertia Coefficient versus Reynolds Number for $KC = 40$ and for Various Values of Relative Roughness	80
2.19 Lift Coefficient versus Reynolds Number for Smooth Cylinders	81
2.20 Lift Coefficient versus KC for a Relative Roughness of $1/200$	81
2.21 Effective Lift Coefficient during Vortex Shedding against Effective Displacement Amplitude	86

2.22	Drag Coefficient Amplification during Vortex Shedding against Wake Response Parameter	87
2.23	Drag Coefficient during Vortex Shedding against Reduced Velocity	88
2.24	Orientation of an Underwater Vehicle	94
3.1	Coordinate Transformation for Cable	106
3.2	Right Hand Coordinate System for Towed Fish	106
3.3	Coordinate Transformation for Towed Fish	108
3.4	Lumped Mass Model of the Two-Part Tow	109
3.5	Cable Node “i”	110
3.6	Cable Junction Node “j”	119
3.7	Boundary Nodes	121
	(a) Towed Fish, (b) Depressor, (c) Surface Vessel	
3.8	Three-Dimensional Towed Fish	124
3.9	Geometry of the Towed Fish	124
3.10	Rotation of Unit Vectors of Towed Fish	127
	(a) Rotation about X Axis, (b) Rotation about Y Axis	
	(c) Rotation about Z Axis	
3.11	Forces and Moments at Tow Point (1) and Centre of Gravity (G) of Towed Fish	131
4.1	Two-Part Tow Modelled with a Single Cable	144
4.2	Two-Part Tow Modelled with Two Cables	144
4.3	Multiple Tow in Series Modelled with a Single Cable	145
4.4	Multiple Tow in Series Modelled with Separate Cable Systems	145
4.5	Quasi-Static Fish Model	147
4.6	Conventional Tow – Surge	165
4.7	Two-Part Tow 1 – Surge	165
4.8	Conventional Tow – Heave	165
4.9	Two-Part Tow 1 – Heave	165
4.10	Conventional Tow - Pitch Angle	165
4.11	Two-Part Tow 1 – Pitch Angle	165
4.12	Change in Pitch Angle with Location of Junction	166
4.13	Two-Part Tow 1 – Path of Vehicles	167
4.14	Two-Part Tow 1 – Depth	167
4.15	Two-Part Tow 1 - Pitch Angle	167
4.16	Multiple Tow Fish in Series	168
4.17	Tow Fish with Two Cables at Two Separate Nodes	168

4.18	Series Multi-Tow - Path – Fast	171
4.19	Series Multi-Tow - Path - Fast – Slow	171
4.20	Series Multi-Tow - Depth – Fast	171
4.21	Series Multi-Tow – Depth – Slow	171
4.22	Series Multi-Tow - Pitch Angle – Fast	171
4.23	Series Multi-Tow - Pitch Angle – Slow	171
4.24	Difference Curve – X Direction	172
4.25	Difference Curve – Y Direction	172
4.26	Difference Curve – Depth	172
4.27	Difference Curve – Pitch Angle	172
4.28	Multiple Tow Fish in Parallel	173
4.29	Parallel Multi-Tow – Path	176
4.30	Parallel Multi-Tow – Depth	176
4.31	Parallel Multi-Tow - Pitch Angle	176
5.1	Spectral Radius of Numerical Integration Schemes with Zero Damping	215
5.2	Amplitude Decay and Period Elongation	219
5.3	Amplitude Decay and Period Elongation of Numerical Integration Schemes	219
6.1	Circulating Water Channel	237
6.2	Top View of Channel	237
6.3	Experimental Procedure	237
6.4	Scaled Models	237
6.5	Recording of Vertical Motion	240
6.6	Recording of Horizontal Motion	240
6.7	Surface Excitation Mechanism	240
6.8	Depressor and Towed Fish Response for Configurations C11 to C13	243
6.9	Depressor and Towed Fish Response for Configurations C21 to C23	243
6.10	Depressor and Towed Fish Response for Configurations C31 to C33	243
6.11	Depressor and Towed Fish Response for Configurations B31 to B33	243
6.12	Depressor and Towed Fish Response for Configurations A31 to A33	243
6.13	Depressor and Towed Fish Response for Configurations I21 to I23	245
6.14	Depressor and Towed Fish Response for Configurations I31 to I33	245
6.15	Depressor and Towed Fish Response for Configurations H31 to H33	245
6.16	Depressor and Towed Fish Response for Configurations G31 to G33	245
6.17	Depressor and Towed Fish Response for Configurations B31 to B33	247

6.18	Depressor and Towed Fish Response for Configurations E31 to E33	247
6.19	Depressor and Towed Fish Response for Configurations H31 to H33	247
6.20	Depressor and Towed Fish Response for Configurations K31 to K33	247
6.21	Depressor and Towed Fish Response for Configurations C21 to C23	249
6.22	Depressor and Towed Fish Response for Configurations X21 to X23	249
6.23	Depressor and Towed Fish Response for Configurations F21 to F23	249
6.24	Depressor and Towed Fish Response for Configurations T21 to T23	249
6.25	Depressor and Towed Fish Response for Configurations I21 to I23	249
6.26	Depressor and Towed Fish Response for Configurations AH21 to AH23	249
6.27	Depressor and Towed Fish Response for Configurations C31 to C33	251
6.28	Depressor and Towed Fish Response for Configurations AA62 to AA64	251
6.29	Depressor and Towed Fish Response for Configurations AA42 to AA44	252
6.30	Depressor and Towed Fish Response for Configurations AB42 to AB44	252
6.31	Depressor and Towed Fish Response for Configurations J31 to J33	252
6.32	Depressor and Towed Fish Response for Configurations AC22 to AC24	252
6.33	Depressor and Towed Fish Response for Configurations AD22 to AD24	252
6.34	Towed Fish Response for Configurations YY21 to YY23	253
6.35	Towed Fish Response for Configurations YA11 to YA14	253
6.36	Towed Fish Response for Configurations YA21 to YA24	253
6.37	Towed Fish Response for Configurations WA21 to WA23	253
6.38	Towed Fish Response for Configurations YD21 to YD23	255
6.39	Towed Fish Response for Configurations YG21 to YG23	255
6.40	Towed Fish Response for Configurations YC21 to YC23	255
6.41	Towed Fish Response for Configurations WC21 to WC24	255
6.42	Towed Fish Response for Configurations WA21 to WA23	255
6.43	Towed Fish Response for Configurations WB21 to WB24	255
6.44	Towed Fish Response for Configurations YA21 to YA24	257
6.45	Towed Fish Response for Configurations YB21 to YB23	257
6.46	Towed Fish Response for Configurations WA21 to WA23	257
6.47	Towed Fish Response for Configurations WD21 to WD24	257
6.48	Towed Fish Response for Configurations YD21 to YD23	258
6.49	Towed Fish Response for Configurations WC21 to WC24	258

6.50	Towed Fish Response for Configurations YG21 to YG23	259
6.51	Towed Fish Response for Configurations YE21 to YE23	259
6.52	Towed Fish Response for Configurations YF21 to YF23	259
6.53	Towed Fish Response for Configurations WA21 to WA23	259
6.54	Towed Fish Response for Configurations WE21 to WE24	259
6.55	Towed Fish Response for Configurations WF21 to WF24	259
6.56	Full Scale Trial Single Part Tow	261
6.57	Full Scale Trial Two-Part Tow	261
6.58	Aft Deck of Deploying Vessel	261
6.59	Deploying of Two-Part Tow	261
6.60	Use of HPMM to obtain the Hydrodynamic Coefficients	267
6.61	Coefficients for Tow Fish	268
6.62	Vertical Coefficients for Depressor	268
6.63	Horizontal Coefficients for Depressor	268
6.64	Pitch Angle of Tow Fish for I31 – Computer – Degrees	270
6.65	Pitch Angle of Tow Fish for I31 – Experiment – Degrees	270
6.66	Heave of Tow Fish for I31 – Computer – Centimetres	271
6.67	Heave of Tow Fish for I31 – Experiment – Centimetres	271
6.68	Surge of Tow Fish for I31 – Computer – Centimetres	271
6.69	Surge of Tow Fish for I31 – Experiment – Centimetres	271
6.70	Tension at Surface for I31 – Computer – Kilograms	271
6.71	Tension at Surface for I31 – Experimental – Kilograms	271
6.72	Pitch Angle of Tow Fish and Depressor for C31 – Computer – Degrees	272
6.73	Pitch Angle of Tow Fish and Depressor for C31 – Experiment – Degrees	272
6.74	Heave of Tow Fish and Depressor for C31 – Computer – Centimetres	272
6.75	Heave of Tow Fish and Depressor for C31 – Experiment – Centimetres	272
6.76	Surge of Tow Fish for C31 – Computer – Centimetres	272
6.77	Surge of Tow Fish for C31 – Computer – Centimetres	272
6.78	Tension at Surface for C31 – Computer – Kilograms	273
6.79	Tension at Surface for C31 – Experimental – Kilograms	273
6.80	Yaw Angle of Tow Fish for YA22 – Computer – Degrees	273
6.81	Yaw Angle of Tow Fish for YA22 – Experiment – Degrees	273
6.82	Sway of Tow Fish for YA22 – Computer – Centimetres	273
6.83	Sway of Tow Fish for YA22 – Experiment – Centimetres	273

LIST OF TABLES

Table	Page No.
4.1 Conventional and Two-Part Tow Configuration Information	164
4.2 Series Multi-Tow Configuration Information	170
4.3 Parallel Multi-Tow Configuration Information	175
6.1 Full Scale Trail – Limiting Parameters	262
6.2 Trial 1 – Summary of Results	264
6.3 Trial 2 – Summary of Results	264
6.4 Tow Configuration Information for Validation Runs	270
6.5 Statistical Analysis of the Computer and Experimental Results	274
A1 Scaled Model Tests AMC – Information	299
A2 Scaled Model Tests AMC – Results	304
A3 Trial 1 - Tow Information	309
A4 Trial 2 - Tow Information	311
A5 Trial 1 - Tow Results	313
A6 Trial 2 - Tow Results	317
A7 Trial 2 - Results - Direction to Swell	320
A8 Trial 2 - Results - Cable Length	322
A9 Trial 2 - Results - Tow Velocity	324
A10 Trial 2 - Results - Depressor Wing	327
A11 Trial 2 - Results - Types of Tows	329
A list of Flowcharts in Appendix B is given at the beginning of the Appendix	331

NOMENCLATURE

The following defines the major symbols used in this thesis. Since the work in this thesis encompasses the fluid mechanics and solid mechanics disciplines, some symbols traditionally have more than one meaning. In order to maintain consistency throughout the thesis, the symbols selected reflect those used by other authors in this field. Some variables and constants are defined at the relevant locations in the text.

General Convention

SI units are implicit.

For a dummy variable “A”:

\vec{A}	vector A
$\underline{\underline{A}}$	matrix A
[A]	matrix A
\dot{A}	derivative of A with respect to time
\ddot{A}	second derivative of A with respect to time
\hat{A}	unit vector A

Variables and Constants

A	cross sectional area
$\vec{A}, \dot{\vec{A}}, \ddot{\vec{A}}$	vectors representing the body rotational angles and their derivatives
A_i	cross sectional area of cable segment “i”
Am_n	normal added mass coefficient of cable segment “i”
Am_t	tangential added mass coefficient of cable segment “i”
$Am_{fx',y',z'}$	added mass of the towed fish in the X', Y', and Z' directions
$\underline{\underline{Am}}$	hydrodynamic inertia (added mass) matrix of cable element
$AI_{x',y',z'}$	added inertia of the towed fish about the X', Y', and Z' axes
A_{ab}	where $a = 1, 2, 3$ and $b = 1, 2, 3$ mass matrix terms of the <i>manipulated</i> equation of motion of the fish as defined in equations (3.97)
Af_{ab}	where $a = 1$ to 6 and $b = 1$ to 6 mass matrix terms of the equation of motion of the fish as defined in equations (3.89) to (3.94), [refer also to equations (3.85) and (2.93)]
A_{fl}, B_{fl}	variables defined in equations (3.95)

A_{fx}	cross sectional area of the fish perpendicular to the X axis
A_g	geometrical area of the body, (usually the cross-sectional area to the flow <i>or</i> the surface area)
A_x	projected area of cylinder in the plane perpendicular to the direction of flow
$\underline{\underline{A_p}}$	amplification matrix
$\underline{\underline{A_u}}, \underline{\underline{B_u}}$	matrices defined in equations (2.9), (2.17), and (5.46)
$[A]^T$	transpose of matrix $[A]$
$[A]^{-1}$	inverse of matrix $[A]$
B_{21}, B_{23}	variables defined in equations (3.96)
C_a	added mass coefficient
C_d	drag coefficient
C_{dE}	equivalent drag coefficient
C_e	linearised equivalent damping coefficient in equation (2.77)
C_H	hydrodynamic coefficient
C_L	lift coefficient
C_m	inertia coefficient
C_n	cable drag coefficient in the normal direction
C_t	cable drag coefficient in the tangential direction
C_w	wave speed
$CT_{x,y,zi}$	trigonometric terms defined in equations (3.29)
C_b and D_b	<i>where $b = 1, 2, 3, 4, \dots$</i> <i>extra</i> terms of the constraint equation for the junction in comparison to the standard constraint equation (4.18), defined in equations (4.31) and (4.47)
C^t	<i>where $t = 0, 1, 2, 3, 4, \dots$</i> constants defined in equations (5.11) and (5.20)
$\underline{\underline{c}}$	damping matrix
D	diameter
D_i	diameter of cable segment “i”
DEN	variable defined in equation (3.23)
E	modulus of elasticity
$E_i, -F_i, G_i$	partial differential terms as defined in equations (4.19) to (4.21)
ER_i^{t+1}	error in the cable segment length “i”, between the span of the nodal positions and the stretched length of the segment due to the tension
$[E_i F_i G_i CD]$	matrix connecting the tension correction terms with the error terms, as defined in equations (4.32) and (4.33)

$[E_i F_i G_i]$	$[E_i F_i G_i CD]$ converted to a true tri-diagonal matrix, as defined in equation (4.35)
\bar{F}, \bar{f}	force vectors
$F_{ix,y,z}$	forces on node “i” in the X, Y, and Z directions
$F_{dix,y,z}$	drag forces (global) on segment “i” in the X, Y, and Z directions
$F_{dix',y',z'}$	drag forces (local) on segment “i” in the X', Y', and Z' directions
F_{do}	mean drag force in equation (2.77)
$F_{eix,y,z}$	any additional forces on node “i” in the X, Y, and Z directions
$F_{iox,y,z}$	represents all forces <i>except</i> tension forces, acting on node “i”
\bar{F}_f	force vector acting on the fish
$F_{f,x',y',z'}$	components of \bar{F}_f along the X', Y', and Z' (local) axes
$F'_{fx',y',z'}$	<i>summed</i> forces in the equation of motion of the fish, defined in equations (3.84) and (3.85)
$F_{fix',y',z'}$	<i>summed</i> forces in the <i>manipulated</i> equations of motion of the fish, defined in equations (3.98)
\bar{F}_H	hydrodynamic force, <i>i.e.</i> drag, lift, or side force
F_m	measured force
$\bar{F}_{T,i}$	tension vector along element “i” as defined in equation (2.49) and (2.52)
f	frequency
f_n	natural frequency
G	centre of gravity of towed fish
G_u, H_u	variables defined in equations (2.21)
$\bar{G}(\bar{U})$	vectors defined in equations (2.23)
g	acceleration due to gravity (9.81 m/s^2)
I, J, K_1, K_2	variables defined in equations (3.18)
$I_{Gx',y',z'}$	moments of inertia of the towed fish at the centre of gravity about the X', Y', and Z' axes, respectively
$I_{x',y',z'}$	moments of inertia of the towed fish at the tow point about the X', Y', and Z' axes, respectively
$\hat{i}, \hat{j}, \hat{k}$	unit vectors along u, v, and w (local) axes system
$\underline{\underline{J}}$	Jordan form of $\underline{\underline{A_p}}$, with eigenvalues (λ_{p_i}) of $\underline{\underline{A_p}}$ along its leading diagonal.
$\underline{\underline{k}}$	stiffness matrix
$\underline{\underline{k}}_E$	cable element elastic stiffness matrix
$\underline{\underline{k}}_G$	cable element geometric stiffness matrix
k_n	normal stiffness of a single lumped mass
k_r	height of roughness of cylinder

k_t	tangential stiffness of a single lumped mass
k_w	wave number
KC	Keulegan-Carpenter number
L, M, N_1, N_2	variables defined in equations (3.25)
$L_{\Delta t}(\bar{R}^N \Delta t)$	local truncation error of the integration scheme
<u>L_p</u>	load operator
l_i	length of cable segment “i”
l_f	length of fish
l_m	length of the smallest element in the lumped mass model
l_w	wavelength
m	mass terms
<u>m</u>	mass matrix
m_i	mass of node “i”, <i>ie.</i> the addition of half the mass of each adjacent segments
m_{ab}	<i>where a = 1, 2, 3 and b = 1, 2, 3</i> mass matrix terms
$m_{eix,y,z}$	mass and added mass of any additional weight attached to node “i”
m_f	mass of towed fish
$m_c(s)$	cable mass per unit length
\bar{M}	moment vector
\bar{M}_{fG}	moment vector acting on the fish, about its centre of gravity
$\bar{M}_{fGx',y',z'}$	components of \bar{M}_{fG} about the X', Y', and Z' (local) axes
\bar{M}_{f1}	moment vector acting on the fish, about its tow point
$\bar{M}_{fx',y',z'}$	components of \bar{M}_{f1} about the X', Y', and Z' (local) axes
$\bar{M}'_{fx',y',z'}$	<i>summed</i> moments in the equation of motion of the fish, defined in equations (3.84) and (3.85)
P_{ai}, R_{ai}, S_{ai}	<i>where a = x, y, z</i> variables defined in equations (3.29a)
$P_{Dx,y,z}$	variables defined in equations (3.32)
p, q, r	angular velocity components (roll, pitch, and yaw) of the fish about the X', Y', and Z' axes
$\dot{p}, \dot{q}, \dot{r}$	angular acceleration components of the fish about the X', Y', and Z' axes
<u>P</u>	matrix of eigenvectors of <u>A_p</u>
<u>P_i</u>	tensor defined in equations (2.39) and (2.40)
P_{ab}	<i>where a = 1, 2, 3...,n and b = 1, 2, 3...,n</i> eigenvector terms of <u>A_p</u>

$p(\underline{Ap})$	spectral radius of the amplification matrix (\underline{Ap})
\bar{R}_G	distance from the tow point (1) to the centre of gravity (G)
$\bar{R}, \dot{\bar{R}}, \ddot{\bar{R}}$	displacement, velocity, and acceleration vectors
Re	Reynolds number
$\bar{R}_m, \dot{\bar{R}}_m, \ddot{\bar{R}}_m$	modal displacement, velocity, and acceleration vectors
r_i	cable element mass ratio defined in equations (2.39) and (2.40)
s	arc length of any point along the cable
Str	Strouhal number
T	tension of cable
T_i	tension of cable segment “i”
\tilde{T}_i	tentative tension of cable segment “i”
T_f	tension of cable segment attached to towed fish
$T_{fx,y,z}$	component of the cable tension in the X, Y, and Z (global) directions
$T_{fx',y',z'}$	component of the cable tension in the X', Y', and Z' (local) directions
\hat{t}	unit vector in cable element direction from bottom to top
t	time
$t_{n,min}$	minimum natural period of the cable mesh
$t_{n,a}$	natural period of “a” mode
t_p	period of the cycle
\bar{U}	vector defined in equations (2.9), (2.17), and (5.46)
\bar{U}_G	velocity vector of the towed fish at its centre of gravity (G)
$\dot{\bar{U}}_G$	acceleration vector of the towed fish at its centre of gravity (G)
\bar{U}_1	velocity vector of the towed fish at its tow point
$\dot{\bar{U}}_1$	acceleration vector of the towed fish at its tow point
u, v, w	local velocity components along the local (X', Y', and Z') axes system
$\dot{u}, \dot{v}, \dot{w}$	local acceleration components along the local axes system
V	velocity
\bar{V}	velocity vector
$V_{cx,y,z}$	water current velocities along the X,Y, and Z directions
V_m	maximum velocity
V_R	reduced velocity
V_r	relative velocity between the body and the surrounding fluid
\bar{V}_r	relative velocity vector
$V_i(t)$	time dependent relative velocity
$V_{ix,y,z}$	velocities (global) of node “i” relative to the water in the X, Y, and Z directions

$VS_{rix,y,z}$	velocities (global) of cable segment “i” relative to the water in the X, Y, and Z directions
$VS_{rix',y',z'}$	velocities (local) of cable segment “i” relative to the water in the X', Y', and Z' directions
W_i	net weight of node “i” in water, <i>i.e.</i> the addition of half the net weight of each adjacent segments
w_R	wake response parameter
X, Y, Z	global axis system as defined in sub-section 3.2
x, y, z	displacement along the X, Y and Z directions
$\dot{x}, \dot{y}, \dot{z}$	velocities in the X, Y, and Z directions
$\ddot{x}, \ddot{y}, \ddot{z}$	acceleration in the X, Y, and Z directions
X', Y', Z'	local axes system as defined in sub-section 3.2
x', y', z'	displacement of node along the X', Y' and Z' directions
X_G, Y_G, Z_G	components of the distance (\overline{R}_G) from the tow point (1) to the centre of gravity (G), measured from the tow point and positive in the directions of the local axes system
Y_m	cross flow displacement amplitude
Y_{RMS}	root mean square anti-nodal displacement

Greek Symbols

α, β, γ	right hand rotation of the fish about the Y (pitch), X' (roll), and Z (yaw) axes
$\alpha^i, \beta^i, \gamma^i$	<i>where $i = 0, 1, 2, 3, \dots$</i> parameters of multi-step integration algorithm, (see equation (5.4))
β_f	frequency parameter defined by equation (2.86)
ϕ	horizontal angle of the cable with the X axis
ψ	vertical angle of the cable with the X-Y plane
ρ	density of the water in which the towing occurs
ρ_c	density of cable
σ	stress in cable or cable element when stretched
ϵ	local strain in cable or cable element when stretched
λ	eigenvalues
$\underline{\underline{\lambda}}$	matrix that stores the eigenvalues along its main diagonal
λ_{wi}	<i>where $i = 1, 2, 3, 4, 5, 6$</i> wave propagation speed along a continuous cable system
λ_{wL}	longitudinal wave speed along a continuous cable system
λ_{wT}	transverse wave speed along a continuous cable system

λ_{pi}	where $i = 1, 2, 3, \dots, n$ eigenvalues of <u>A_p</u>
κ	visco-elastic damping coefficient
υ	coefficient to allow for hysteresis
$\overline{\omega}$	angular velocity vector of cable element
ω_n	natural frequency
$\overline{\Omega}$	angular velocity vector of the towed fish having components α , β , and γ
μ_c	mass per unit length of the cable
μ_w	mass of the displaced water per unit length of the element
μ_i, η_i	variable to solve the tri-diagonal matrix $[E_i F_i G_i]$ recursively, as defined in equations (4.38) and (4.39)
φ_a	where $a = 1, 2$ characteristic lines associated with λ_a , defined in equations (2.13),
$\overline{\varphi}(s)$	shape function of cable element
ξ	variable length along the element divided by the element length, (s/l_i)
ζ	damping ratio
ν	$\text{Cos}^{-1} \zeta$
Γ	$\omega_n (-\text{Cos } \nu \pm i \text{Sin } \nu)$
$\tilde{\Gamma}$	$\Gamma + \delta$
$[\Lambda]$	cable system transformation matrix
$[\Lambda_f]$	tow fish transformation matrix
<u>Λ_m</u>	modal transformation matrix defined in equation (5.88)
Δt	time step (increment)
δ	represents the change in a parameter or
δ	error
δ_a	amplitude error, which increases the damping by a small quantity δ_a
δ_p	phase error, which increases the frequency of oscillation by a small quantity $\delta_a/2\pi$.
δ_{ij}	Kronecker delta,
δT_i^{t+1}	tension correction term of cable segment “i”
ϑ	variables defined in equation (2.80)
$\overline{\theta}$	eigenvectors
<u>Θ</u>	matrix that stores the eigenvectors along its columns
$O(\Delta t^a)$	asymptotic notation of the error having an order of “a”.

Subscripts

D	depressor
e	additional forces or weights
f	towed fish
G	centre of gravity of tow fish
i	i^{th} cable node, (or i^{th} cable segment located between nodes “i” and “i+1”)
i+1/2	cable element just after node “i”
i-1/2	cable element just prior to node “i”
j	cable node representing the junction
n	cable node representing the surface towing vessel
u, v, w	direction along axes of local coordinate system
x, y, z	direction along X, Y and Z axes
t	time
0	centroid of tow fish
1	tow point on tow fish

Superscripts

k	iteration index
m	convergence correction superscript in equation (4.7)
t	time
o	equilibrium position (configuration)
(1)	top of cable rod element
(2)	bottom of cable rod element

ABBREVIATIONS

2D	two dimensional
3D	three dimensional
AMC	Australian Maritime College
AMECRC	Australian Maritime Engineering Cooperative Research Centre
DOF	degree of freedom
DSTO	Defence, Science and Technology Organisation
FDM	finite difference method
FEM	finite element method
HPMM	horizontal planar-motion-mechanism
LMM	lumped mass method
RAN	Royal Australian Navy
ROV	Remotely Operated Vehicle

EQUATION NUMBERING SCHEME

All equations are numbered aligned to the relevant chapter and in ascending order through that chapter. For example equations in Chapter 3 will commence from (3.1) and continue as (3.2), (3.3) and onwards.

When an equation number represents a set of equations, the number is usually subdivided, *e.g.* equations (3.8a), (3.8b), and (3.8c). When referring to such a set of equations, if all of the equations in that set are being addressed, then they will be referred to as ***equations (3.8)***. However, if only some of the equations from the set are addressed, then those being addressed will be specified, *i.e.* ***equation (3.8b)***.

CHAPTER 1

INTRODUCTION

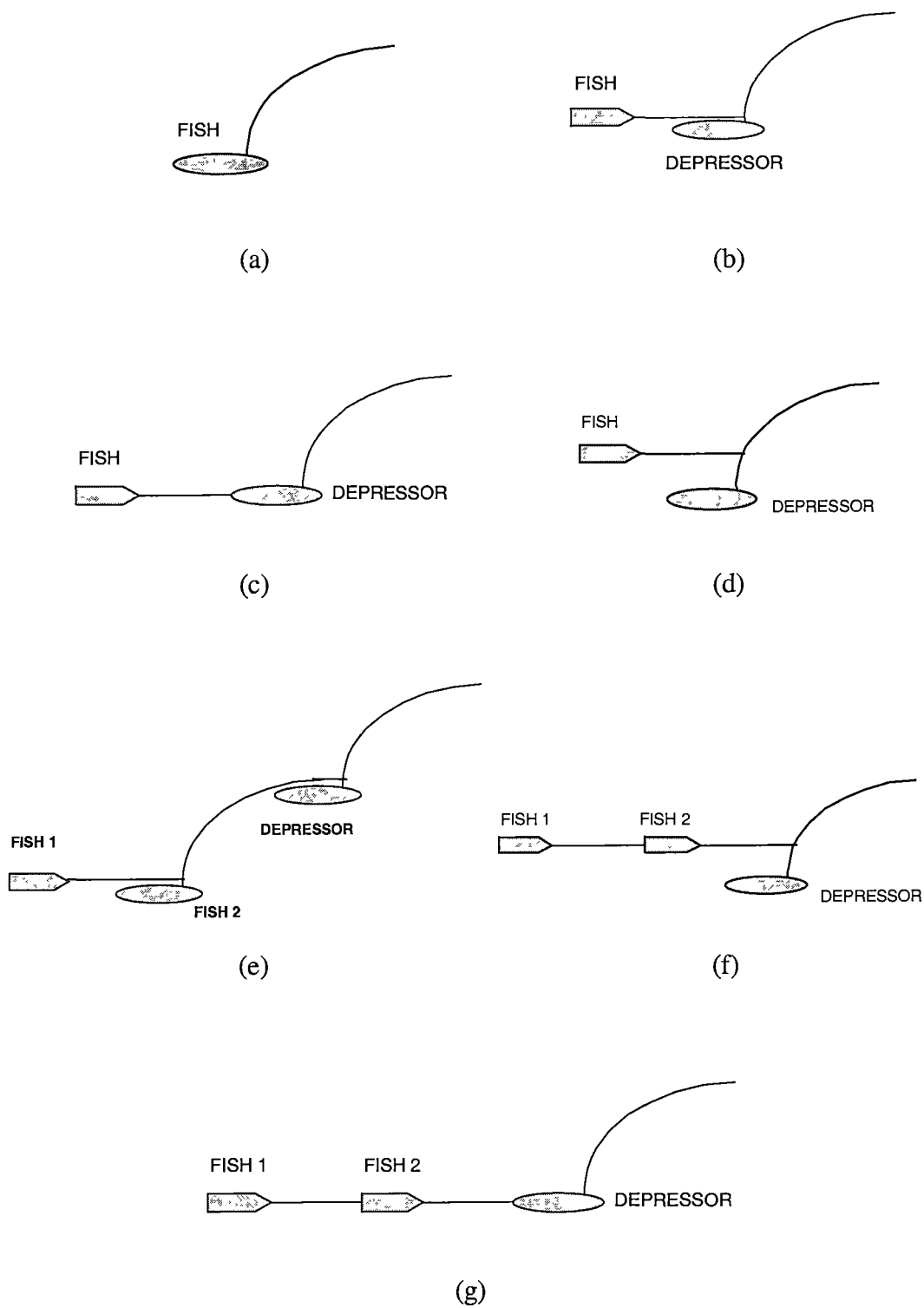
1.1 Definition of Problem

A sonar platform is an example of a submerged body that is towed behind a surface vessel. Such platforms are used extensively in offshore, military, hydrography, and oceanography activities, (see Figure 1.1). They generally require that perturbations from the steady state motion are minimised in order to ensure clear sonar imaging.

The instantaneous position of the submerged towed object (referred to as the “fish” in this text), is influenced by the relative motion between the cable and the water, the hydrodynamic characteristics of the fish, and the unsteady wave induced motion of the surface vessel. Depending on the sea state and the towing vessel's response to it, the wave induced motion can be sufficiently large to render the trajectory of the tow fish beyond acceptable limits for sonar operations. This motion is transmitted to the fish along the tow cable.

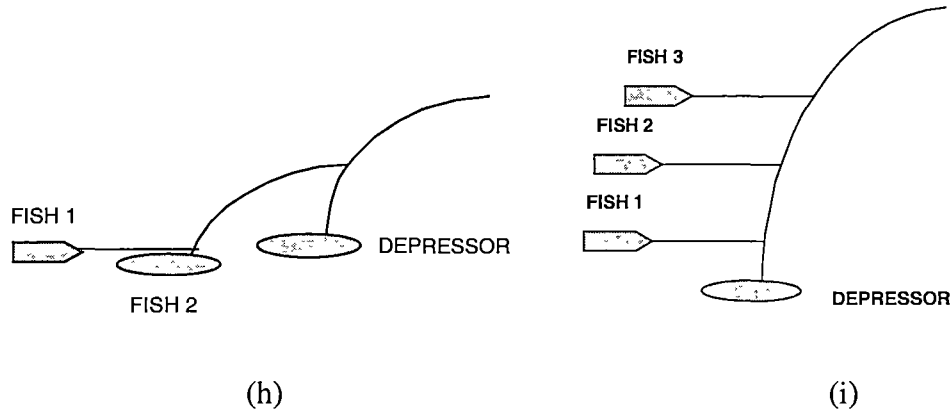
The Royal Australian Navy (RAN) uses towed sonar vehicles for a variety of operations. One task is the deployment of side scan sonar from small vessels to detect mines in coastal waters. As the operation is in coastal (shallow) waters, the length of the tow cable can be relatively short, *e.g.* 25 metres. In addition, the relatively small size of the surface vessel can lead to large wave induced motions. These conditions can adversely affect the motion of the sonar vehicle, resulting in imperfect sonar operations.

The wave induced motion of a towed body attached to a conventional tow system used by the RAN, exceeds the acceptable motion rates in the six-degrees of freedom by more than 60%, (see Tables 6.2 and 6.3 in Chapter 6). In order to reduce this motion, and thus improve the efficiency of sonar operations, the Defence, Science and Technology Organisation (DSTO) of Australia was tasked with optimising the tow configuration. The investigation was carried out by the Australian Maritime College (AMC), DSTO, and the University of Tasmania with assistance from the Australian Maritime Engineering Cooperative Research Centre (AMECRC).



Tow Configurations (PTO)

Figure 1.1



Tow Configurations (Continued)

Figure 1.1

Since the surface vessel's motion is usually beyond the control of the operator, the transmission of the wave induced motion of the surface vessel to the towed fish can be reduced by:

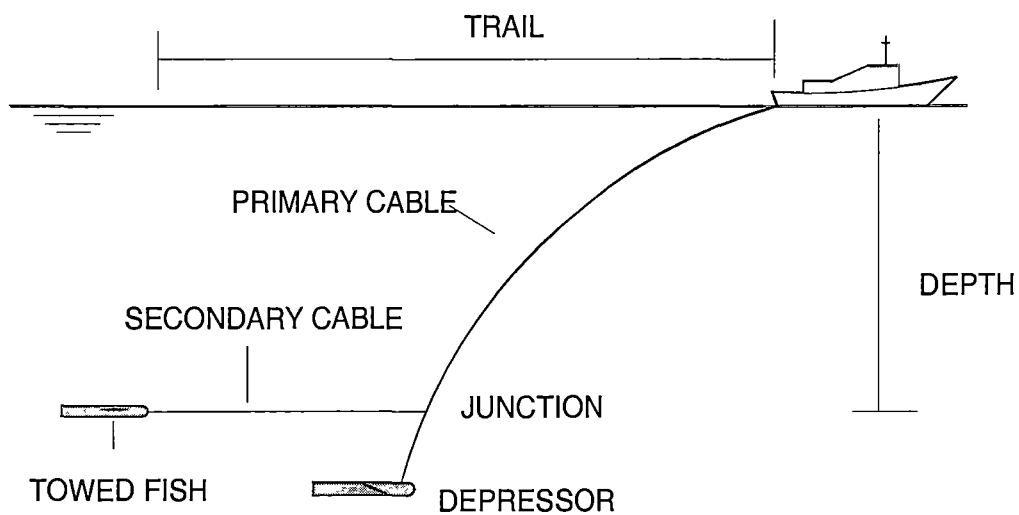
- designing the fish to be more hydrodynamically stable;
- incorporating adaptive control surfaces on the fish; and/or
- decoupling the surface vessel motion from the fish.

This investigation centres around the third option, since it is an effective, cost efficient method of achieving the required objective.

Various methods have been employed in tow configurations to increase decoupling of the motions. One such method is the two-part tow shown in Figure 1.2. It consists of a primary cable attached at its top end to the surface vessel (*i.e.* the vessel towing the sonar), while the bottom end is attached to a depressor. The latter ensures that the tow configuration maintains the required depth. The fish is attached to the lower end of the primary cable by a secondary cable. The point of attachment (referred to as the “junction”) can be varied along the cable length, thus influencing the behaviour of the towed fish. The two-part tow configuration and its behaviour are explained in Asplin and Christensson (1988), Preston (1989) and Hopkin *et al.* (1990).

In order to investigate and optimise the tow configuration, the project was carried out in three stages:

1. the development of a three-dimensional (3D) dynamic computer model incorporating the decoupling effect, to predict the motion of the fish due to the excitation at the surface;
2. scaled model tests of the tow configuration; and
3. full scale trials.



Two-Part Tow
Figure 1.2

The computer model of the two-part tow incorporates tow line and fish dynamics as well as the decoupling effect of the two separate lines. The response envelop of the configuration can be determined by varying the parameters of the model. This allows the configuration to be optimised to give an acceptable trajectory for the tow fish.

Since the attachment point between the two cables can be varied along the length of the primary cable, it is inadequate to model the tow configuration as a single cable system, with an “extra” lumped mass representing the depressor. One must model the two cables separately and then dynamically couple them at the junction. Following a comprehensive review of the literature, the author was unable to find any contributions dealing with the required tow configuration.

This concept allows the investigation of not only varying points of attachment, but also **multiple towed bodies**, *i.e.* more than one secondary cable attached at various points along the primary cable, (see Figure 1.1(i))

The results from the computer model were validated and supplemented using:

- experimental data from scaled model tests of the two-part tow configuration conducted in the circulating water channel at the Australian Maritime College in Launceston; and
- full scale trials at Jervis Bay and Port Phillip Bay.

1.2 Outline of Thesis

The remainder of this chapter outlines the tow configurations investigated and reviews the literature relevant to the modelling of such systems. This review includes static, quasi-static and dynamic cable modelling techniques, current underwater tow models, numerical procedures employed to solve cable / tow models, and the modelling of underwater vehicle. Finally the experimental investigation is introduced. The rest of the chapters are structured as follows.

Chapter 2 looks at the methods available to investigate cable and underwater bodies. It first looks at the more popular mathematical representations of dynamic cable modelling and the time domain solution techniques utilised. The selected method for this study is justified based on the ability and suitability of the various methods. The prediction of drag and inertia coefficients of cables is yet a highly researched area. Chapter 2 details some of the investigations, analyses the behaviour of the fluid flow around the cable, and presents current methods used to predict the relevant coefficients. Finally the modelling techniques available for underwater vehicles and the prediction of the relevant coefficients are discussed.

In Chapter 3, the mathematical modelling of the quasi-static and dynamic two-part and multi tow configurations is detailed. This includes the modelling approach used for the cable junction, series and parallel multiple tows, and the integration of the tow / depressor fish into the cable model. This is followed by the numerical solution procedure in Chapter 4, where the numerical integration scheme and the required iteration procedure are introduced. The incorporation of the discontinuity due to the cable junction into the solution technique is also detailed, as are the variations

required to deal with the two types of multiple tow configurations. Typical results for the various configurations are also presented.

Chapter 5 analyses the numerical procedure used in the solution, and includes an introduction into such numerical techniques in engineering. The modelling of the cable as a continuous medium and the derivation of the stress wave speeds are presented, followed by the validity and effects of representing it as a discretised model. The stability and accuracy of the numerical procedure utilised is analysed and the prediction of a suitable time step to meet these criteria is discussed.

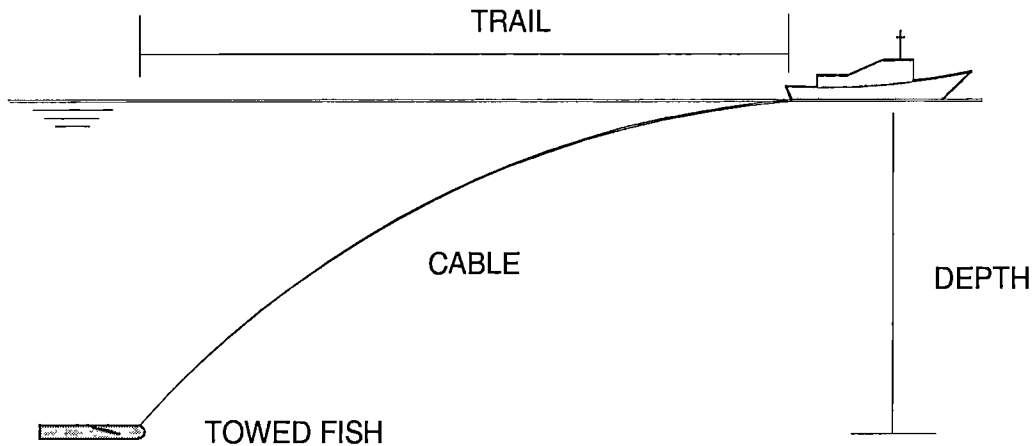
Chapter 6 details the scaled model experiments and the full scale trials, and analyses the results in order to investigate the behaviour of the two-part tow. The scaled model test results are also used to validate the computer model, which includes the experimental calculation of the hydrodynamic coefficients of the scaled models. Finally Chapter 7 presents the conclusions and recommendations.

Appendix A gives the results from the scaled model tests and the full scale trials, while Appendix B presents detailed flowcharts of the computer model.

1.3 Tow Configuration

Conventional towing arrangements consist of a tow cable attached at its upper end to the surface towing vessel and its lower end to the fish, (Figure 1.3). This configuration leads to large coupling effects, thus giving unacceptable fish motion due to the transmission of the excitation at the cable's upper end down to the fish. The two-part tow, shown in Figure 1.2, consists of a primary cable towed from the surface vessel in a similar manner to the conventional tow, except that the fish is replaced by a depressor to maintain the required depth of the cable's configuration. The fish is then attached to the *depressor* (Figure 1.1(c)) or to the *lower end of the primary cable* (Figure 1.1(d)) by a secondary cable.

Usually the primary cable is negatively buoyant, while the towed fish and the secondary cable are neutrally buoyant. However, these conditions could differ depending on the operator's requirements. The fish can be modified to be neutrally buoyant by simply adding ballast or buoyancy at the appropriate locations within the fish.



Conventional Tow

Figure 1.3

The computer model was developed to simulate both conventional and two-part tow configurations. In the latter case, it can consist of a two-part tow without a junction (Figure 1.1(b)) or a two-part tow with a junction (Figure 1.1(d)). This enables the use of one computer model to simulate and compare various tow configurations.

In order to expand the scope of the investigation, it was decided to incorporate multi-tow configurations in the computer model. These included:

- **Series Multiple Tow** (Figures 1.1(e) to 1.1(h)), where a number of towed fish are attached in series. Each towed fish is attached via its tow (secondary) cable to the fish preceding it.
- **Parallel Multiple Tow** (Figure 1.1(i)), where a number of towed fish are attached in parallel. Each towed fish is attached via its tow (secondary) cable to the primary cable, thus creating a number of junctions along the length of the primary cable.

Following an extensive literature survey into various underwater tow investigations, it was noted that most tow models dealt with conventional tow configurations, while some were able to deal with multiple tow configurations similar to that shown in Figure 1.1(g), (these will be discussed later in this chapter). However, none were found that could deal with the discontinuity created by having a “junction” at a point along the primary cable, (*i.e.* as in Figure 1.1(d)).

The tow configuration consists of two major components, *i.e.* the cable(s) and the tow / depressor fish. Therefore the investigation looked into the modelling of underwater cables, underwater bodies, and the coupling of the two. In Chapter 2 the various methods available for the modelling of underwater cables, including the governing equations and the recommended solution techniques, are described. This is followed by a description of the modelling techniques (again including the equations) commonly utilised for underwater vehicles.

In this Chapter, an overview of the various methods used in modelling underwater towed systems will be discussed, which includes a review of the cable models and solution techniques as well as the modelling of underwater vehicles.

1.4 Static and Quasi-Static Cable Models

Early work with cable systems dates back to the Greek civilisation, when eminent figures such as Pythagoras and Aristotle investigated cable tensions and frequencies. In the more recent past well known mathematicians and researchers such as Leonardo da Vinci, Mersenne, and Galileo continued the investigation. Early analytical work in the eighteenth century is attributed to Taylor who published the first dynamic solution of transverse cable dynamics, and Bernoulli, who published theories of oscillation for hanging chains and the superposition principle of several harmonics for taut string. The latter was illustrated by Fourier in the nineteenth century.

D'Alembert was the first to derive the partial differential equations for small transverse dynamics of taut wire, which were then solved by Lagrange. Euler derived the equation for a hanging chain and then obtained a series solution for the first three natural frequencies. Poisson derived and solved equations of a cable element subjected to a general force.

The above description can easily be taken to represent a *who is who* in the mechanical / structural engineering arena. This highlights the importance placed upon cable structures from the beginning of known civilisation.

Up till the early part of the 20th century, the analytical work was based on the prediction of the shape of a hanging uniform static cable using the so called *classical theory*. Here the longitudinal extension is neglected as are the dynamic effects. The

cable is assumed to achieve its stiffness through a change in its shape as the tension forces change at the ends. The equations describing the configuration are readily available from most structural mechanics text books dealing with compliant structures, *e.g.* Berteaux (1976), Wilson (1984) and Patel (1989).

The solution to these equations are obtained by approximate solutions or an iterative process. These models can be classified as “static” and have in the past been used to investigate underwater cable structures. Around World War I, analytical models were developed to predict the height of *barrage balloons* in varying wind conditions and to analyse aircraft towed cable configurations / systems. Between the wars, investigations primarily dealt with steady state towing of gliders, targets, and minesweeping equipment as well as steady state mooring of buoys and ships.

When considering the ocean environment, the effects of the surrounding water and the nature of the excitations encountered requires a more thorough investigation, especially if the flexible structure is long. Thus, the inclusion of the non-linear drag forces into the mathematical model results in a quasi-static model.

Quasi-static models ignore the affects of inertia and added mass in the calculations, taking into consideration only the forces such as mass, buoyancy, cable tensions, lift, and drag due to the cable / fluid interface. Equations for static equilibrium are then developed for the system and solved subject to given boundary conditions. (The inclusion of drag forces is important when considering an underwater catenary due to the magnitude of such forces that are experienced). The quasi-static models are able to incorporate non-linearities that are present in the cable model, which include:

- changes in geometry due to the change in the cable shape; and
- fluid loading, which is usually proportional to the square of the relative velocity between the cable and the surrounding fluid.

Modelling techniques for quasi-static cables can be broadly divided into the continuous, lumped mass, finite element, and hinged rod methods. The above classification is dependent on the method utilised to represent the cable system.

A number of researchers have developed quasi-static models and only a selected number are given in this review. The reference list at the end of the thesis gives a number of papers / text describing quasi-static models, and the paper by Casarella and

Parsons (1970) is an excellent review of the work carried out in this area. Berteaux (1976) gives a concise hierarchical chart outlining the various quasi-static and static model approaches.

Possibly the first quasi-static model was developed by McLoed in 1918 (Casarella and Parsons (1970)), based on the experimental work by Relf and Powell. This was then extended by Glauert in 1934. Landweber and Protter in 1944 included a constant tangential hydrodynamic force, and the former modelled an anchor chain in 1947. O'Hara in 1945 was the first to include the effect of cable stretching on cable density, cable length, and drag forces. Eames in 1956 and Whicker in 1957 developed two-dimensional (2D) steady state models including the use of faired section cables.

Pode (1951) investigated quasi-static inelastic continuous cables under constant tangential drag, and published a set of tables to be used in conjunction with a set of pre-determined equations to give the tension, length, scope, and/or depth of the configuration. The tables produced covered, among others, mooring, underwater towing, and surface towing configurations. To overcome the constant tangential drag limitation in Pode's data, Wilson (1960) produced a set of tables and graphs that included variable tangential cable drag forces.

Patton (1972) and Berteaux (1976) give detailed descriptions on the modelling and solution techniques of the quasi-static inelastic continuous cable configuration used for mooring of buoy systems. Similar models are also presented by a number of other researchers including Eames (1967), Ferriss (1980), and Huang and Vassalos (1993), with the former dealing with faired sectioned cables.

The quasi static lumped mass and hinged rod models have also been used by a number of researchers, especially as a starting configuration for the respective dynamic models. Dryer and Murray (1984) describe the two quasi static models in both two and three-dimensional configurations, and identify their merits and demerits through a series of numerical examples. Finite element models can also be used to model quasi static configurations by neglecting the inertia terms.

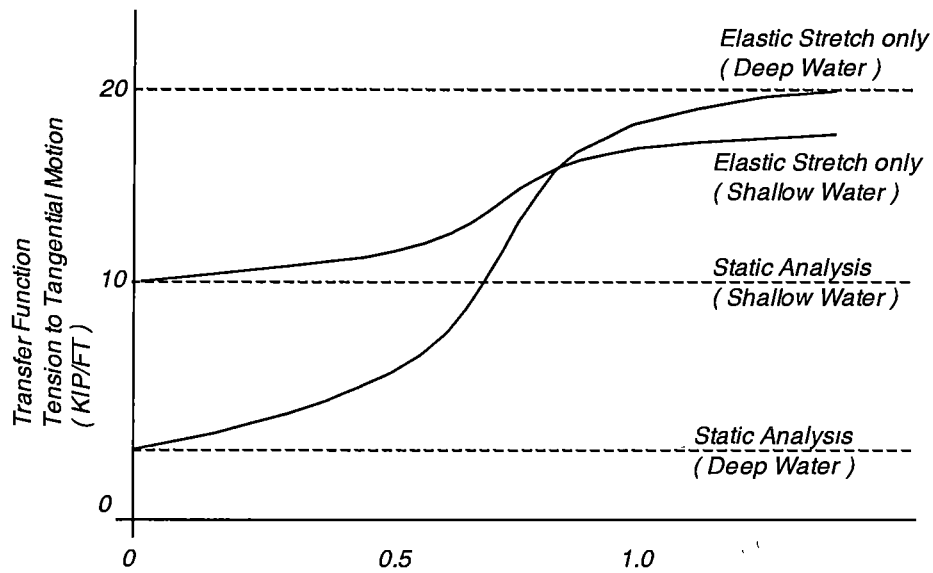
The above three discrete models offer simple straightforward modelling, although the iteration process to achieve the required equilibrium configuration may be tedious, with possible convergence problems, (Thomas and Hearn (1994)). One method of determining the equilibrium configuration of redundant cable arrays was introduced by Skop and O'Hara (1972) and was termed the method of imaginary reactions.

Peyrot and Goulois (1979) use the procedure suggested by O'Brien (1967) to develop a three-dimensional quasi-static cable model from basic catenary equations to analyse the equilibrium configuration of cable structures. The use of the catenary equation is claimed by Connaire and McNamara (1997) to give very little difficulty in convergence, as opposed to the problems encountered by finite element and finite difference quasi static models. This is attributed to the model being based on the catenary equations, thus providing an exact solution for the quasi static configuration of a curved cable. By contrast, the straight cable segments used in finite element and finite difference methods, introduce errors due to the approximated configuration.

Some researchers use the quasi-static model to carry out time stepping algorithms in an attempt to represent the “dynamic” motion of systems. This is usually carried out by the use of *cable derivatives* obtained by differentiating the steady state solution. An example is the method proposed by Ivers and Mudie (1973), in which the inertial forces are ignored and the cable configuration for a towed system is obtained using a force balance that is influenced by the surface vessel motion. Another, proposed by Peyrot and Goulois (1979), uses a three-dimensional quasi-static cable model to analyse the equilibrium configuration of structures with a number of cables, such as multi-leg mooring systems. Polderdijk (1985) uses modified quasi-static models to predict the anchor line response in preliminary studies.

Although quasi-static models are still used for certain applications, it is clear from a number of experimental validations (*e.g.* Bergdahl and Rask (1987)), that the dynamic effects, such as inertia and added mass, cannot be neglected as they have a significant influence on the cable tension and motion. From Kuwan and Bruen (1991) it is seen that quasi-static models tend to under-predict the cable tension. The ratio between the dynamic tension and the quasi-static tension, approaches 20, although when considering the total tension the under-prediction reduces to around 40%. Thus, the under-prediction in quasi-static models is significant, especially at the higher frequencies of excitation, *e.g.* wave induced surface vessel motion.

The discrepancy between the dynamic and quasi-static tensions can be explained by considering Figure 1.4, which shows the transfer function between the cable tension and the tangential motion of the upper end of a mooring line. At very low frequencies of motion, the dynamic tension transfer function is approximately equal to that for the quasi-static model.



(Kuwana and Bruen (1991))

Typical Transfer Function for Shallow and Deep Water Mooring Cases
Figure 1.4

However, as the frequency of the motion increases, the dynamic tension increases until it reaches the upper bound value defined by pure elastic stretching of the cable. This increase in tension is due to the higher hydro-dynamic damping on the cable from the surrounding fluid, thus restraining the change in shape of the cable. This results in the cable stretching to accommodate the motion. Although this effect reduces in shallow water (due to the lower static stiffness), it has a significant effect on the amplitude at higher frequencies of motion.

This under-prediction will lead to errors in the prediction of the cable behaviour, and thus the behaviour of the towed body. This is especially significant at the higher frequencies of excitation, *e.g.* excitation due to wave induced surface vessel motion. In addition, if cable specifications are based on computer model predictions, then the strength of the cable selected may be insufficient, leading to possible failure during operation. Further, by neglecting the dynamic influence, the effect (and possible damage) on the cable due to fatigue may be seriously under-predicted.

For these reasons, the simulation of underwater of towed bodies is now almost exclusively carried out using dynamic models. However, as shown in Chapter 3, the quasi-static model is used as a starting point in a number of dynamic models. It also has a limited use in preliminary investigations and in simulation models where the

cable influence is marginal, for example as tether models of Remotely Operated Vehicles (ROV). Some examples of the use of quasi static models are given by de Wit (1982), Cordelle (1983), Ishii *et al.* (1986), Hopkin *et al.* (1990), and Brook (1992).

1.5 Dynamic Cable Models

The dynamic models are based on Newton's equation of motion. Therefore, the effect of mass and added mass is incorporated into the equations, which are "driven" by an exciting displacement or force, and solved to defined boundary conditions.

Although the solution is usually carried out in time domain, some investigations (*e.g.* Koterayama (1977), Triantafyllou and Bilek (1983), Leonard and Tuah (1986), Suhara *et al.* (1987), and Larsen *et al.* (1992)), use a frequency domain approach. In the time domain solution, the non-linearities can be modelled, and solved at each time step. However, as the terms such as mass, added mass, damping, stiffness, etc. have to be calculated at each time step, the computation can become complex and time consuming.

On the other hand, the frequency domain method is always linear, as linear principles of superposition are used. Therefore, all non-linearities are eliminated either by direct linearisation or by iterative linearisation procedures. Triantafyllou *et al.* (1986), Chen and Lin (1989), Chakrabarti (1990), Teng and Li (1991), Kwan and Bruen (1991), and Clauss *et al.* (1992) give such procedures relevant to cable models and drag terms. An example of the linearising procedure is given in sub-section 2.3.4 in Chapter 2, dealing with the cable / fluid drag force.

In carrying out linearisation, the motion of the system is assumed to be a set of small deviations from an equilibrium position. The modelling for a frequency domain solution is usually carried out by a linear spring-mass-damper system. This model can have a number of degrees of freedom, depending on the modelling technique used, thus yielding a set of equations of motion. Early linear modelling of cable systems was carried out by a number of researchers including Kerney, Reid, Schram, Phillips, Whicker, Nath, etc., (see Choo and Casarella (1973)).

Triantafyllou and Bilek (1983) give an example of the use of the linear frequency domain method to solve non-linear taut cable systems. In order to solve the set of

coupled linear equations of motion derived for the cable system, most researchers use modal analysis, from which the modal frequency response is obtained. Examples of this method are given in Jeffery and Patel (1982) and Leonard and Tuah (1986). Nakamura (1990) utilises the frequency domain solution in a time domain simulation of a moored semi-submersible. However, Yilmaz and Incecik (1996) claim that the time domain solution must be used to deal with the strong non-linearities.

Leira and Olufsen (1987) use the frequency domain approach to estimate the fatigue damage to an underwater riser, and conclude that it is ideally suited for this task. However, they also identify that there are discrepancies between the results obtained for this solution technique and that from an equivalent time domain solution.

Jeffery and Patel (1982) compare the modal solution of a linearised model against a non-linear finite element model for a taut mooring system, concluding that the former offers a relatively poor performance for the computational effort required.

It is therefore concluded that although the frequency domain approach has its uses for specific situations, the time domain solution is preferred for most cable systems with strong non-linearities.

Possibly the first time domain dynamic model was by Phillip in 1949 (Casarella and Parsons (1970)), for airborne towing configurations. In 1957 Whicker indicated a solution for a two-dimensional dynamic towing model, and in 1958 solved the one dimensional (axial) motion of a deep mooring cable for the dynamic tension, (without including the effects of drag and weight).

Modelling the dynamic cable as a **continuous elastic medium** and solving it using either the method of characteristics (*e.g.* Reid (1968) and Patton (1972)) or finite difference approximation (*e.g.* Brooks (1990)) is a method utilised by a number of researchers to investigate various configurations of cable systems. This method develops a set of coupled partial differential equations to represent the continuous cable system.

The solution by the method of characteristics put forward by Reid (1968) is a direct integration solution of the equations of motion. It uses the stress wave fronts to replace the partial differential equations by ordinary differential equations, and then integrates them along the characteristic lines in the space-time domain. This method

gives an exact solution to the cable system, although some approximation is usually required within the numerical solution.

Syck (1981) highlights the difficulties with this method, including the slow execution due to use very small time steps required by the high longitudinal stress wave speeds along the cable. In order to speed up the calculation, Patton (1972) developed a lumped mass method (LMM) to solve the cable system using a low order integration scheme. Patton shows that the simulation using the lumped mass model is faster, although the high frequency response is truncated.

Brooks (1990) solves the partial differential equations by representing them using a finite difference scheme. However, the solution technique uses a large amount of computer space and time.

Many consider the paper by Walton and Polachek (1959) to be the foundation for the **lumped mass** solution to underwater cable models. The paper presents a two-dimensional dynamic model to represent a mooring cable. The cable system is represented by inelastic segments, (although they did include elasticity in a subsequent paper in 1963), with all external forces on the segments distributed to the adjacent nodes. The added mass and drag forces in the tangential directions are considered small in comparison with those acting in the normal direction, and thus neglected.

The equations of motion obtained for the nodes are solved using an explicit finite difference integration technique, *i.e.* the central difference technique. Since the equations of motion are non-linear, an explicit solution is impractical and an iterative process based on the Newton-Raphson method of successive approximations is employed. The tentative tension values for a time step are corrected through the iteration process to conform to the segment length constraint equation.

Walton and Polachek also carry out a stability analysis of the equations and solution technique by employing the von Neumann (Fourier) stability method, thus providing a limiting time step to be used in the solution process.

Nakajima *et al.* (1982) refined the mooring cable model developed by Walton and Polachek. Their model (in two-dimensions), includes tangential added mass, drag forces, and cable elasticity. The explicit central difference integration technique is replaced by an implicit algorithm, which should give unconditional numerical stability. However, as shown in Chapter 5, the modified Newton-Raphson iteration

process required for the non-linear system, introduces errors that result in numerical instability if large time steps are used. The time stepping process of the dynamic model commences from a quasi-static configuration.

Nakajima *et al.* validate the model successfully against scaled model experiments of a number of mooring cable / chain configurations. Results show that the dynamic tension can be much larger than the quasi-static tension and is dependent on the frequency of motion. It also increases as the drag forces on the cable increases.

Tsinipizoglou, (1984) expands the model developed by Nakajima *et al.* (1982) into three-dimensions and incorporates wave / current interaction with the cable. However, Tsinipizoglou reverts back to the central difference integration technique and ignores elasticity and tangential drag forces.

Van den Boom (1985) developed a two-dimensional model using the technique presented by Nakajima *et al.* The paper also briefly gives a comparison between the lumped mass model and an equivalent finite element model, concluding that the latter is less computer time efficient. Van den Boom also briefly dwells on the discretisation effect, developing approximate equations for the parasitical motion of the lumped masses. The method suggested to reduce this affect is to increase the number of segments used in the discrete representation. However, the effect of this on the stability of the numerical technique is not investigated.

Validation is carried out by comparing against results from scale model experiments, including those obtained from excitations in irregular waves. In the resulting discussion, the effect of “flying” and associated slackness is identified, even at low frequencies.

In van den Boom *et al.* (1987), the above model was expanded into three-dimensions. The inclusion of bending moments and shear forces enabled the modelling of risers and pipelines, in addition to mooring systems. Further model experiments were carried out to validate the three-dimensional cable, riser, and pipe models.

Peuker *et al.* (1987) also carry out the modelling of underwater flexible structures along the line described by van den Boom *et al.* (1987), however, the implicit time integration method used is different, thus demonstrating the versatility of the lumped mass method. The use of implicit, unconditionally stable algorithms in preference to the conditionally stable explicit algorithms is also briefly discussed, highlighting the

requirement for a time step smaller than the period of the highest natural frequency of the system for the latter case. It is claimed that by using the implicit algorithm it is possible to use a much larger time step to accurately predict the lower modes. Although this is true, in Chapter 5 it will be shown that the time step is limited by the propagation of the error introduced by the iteration process. The paper however, makes no mention of this, implying that the time step is purely limited by the accuracy of the results.

Two co-authors from Peuker *et al.* further discuss the model in Kokkinowrachos and Giese (1987), and include an explanation of the calculation of the system natural frequencies as an eigenvalue problem. These are then used to produce a simplified model that is used to carry out preliminary design work of underwater flexible structures, as the non-linear time domain model is claimed to be far too complex for such work. However, the advent of faster computers with larger memory capacities, especially in the last decade, has substantially reduced this problem.

Huang (1994) dynamically modelled underwater cable systems for mooring and towing using the lumped mass method in three-dimensions, and includes an investigation on the suitability and limits of the method. The modelling is similar to that given by van den Boom *et al.* (1987), however, the solution technique employs an implicit difference scheme introduced by O'Brian *et al.* (1950-51). This scheme is investigated utilising von Neumann (Fourier) stability method, showing it to be unconditionally stable. The paper also investigates the discretisation effect, especially on the dissipation or otherwise of high frequency waves along the lumped mass model, with its possible influence on numerical stability. Huang also briefly outlines the merits of the lumped mass method over other compatible methods available for cable modelling.

In Huang and Vassalos (1995) a slightly modified version of the above model is integrated using an explicit method, *i.e.* a modified Euler method, in order to reduce computational effort by eliminating the iteration process. Therefore, the time step has to be smaller than a critical value for stability.

Winget and Huston (1976) present a finite segment cable model that consist of ball and socket connected rigid links (segments). Cable stiffness is modelled as spring-dampers between the segments. Along the same lines, Chapman (1987) developed a three-dimensional dynamic **hinged rod** underwater tow model by dividing the cable into a number of rigid, non-extensible rods, with their mass uniformly distributed

along them. Equations of motion are then developed for each rod, yielding relationships between the forces and accelerations at the bottom of the rod to those at the top.

With the rapid development in computers and their increasing use in the solution of engineering structures, it was inevitable that the **finite element method** (FEM) would be used to model and solve cable structures. In fact most researchers today model cable systems either using the lumped mass method or the finite element method, each school being keen to emphasise the respective merits of its approach.

There are a number of ways of carrying out the modelling using finite elements. However, the basic concept is the representation of a cable by a series of segments (elements) joined together at nodes. The model calculates the motion from a known equilibrium system due to forces acting on the cable elements. The equations for the elements are developed by a Lagrangian approach or by Hamilton's principle. Forces distributed along the element are transformed to equivalent nodal forces through the principle of virtual work.

The shape and configuration of the element will depend on the modelling method used. Johansson (1976) and Webster (1975) introduced the modelling of cable systems using straight line elements, solving the non-linear matrix based equation using an iterative process. The former decoupled the force terms over a short period of time and used a trial and error process to obtain the final state at each time interval, while the latter used an implicit integration scheme to iterate towards the solution. In order to obtain accurate results, the finite element method requires the cable model to consist of a large number of elements. This effectively reduces the time step, thereby increasing the required computer space and run time.

Leonard and Recker (1972) use a solution technique based on the theory of incremental deformation, where the non-linear equations are reduced to a system of quasi-linear equations dependent of the prior history of the system. In Leonard (1973), the model was extended to have internal curvature and slope continuity at the nodes. This reduced the number of elements required to represent the cable accurately, thus reducing the computer requirements. Haritos and He (1989) modelled the cable configuration using three and four node parabolic isoparametric elements, allowing a further reduction in the number of elements. However, the time step used in Haritos and He (1992) is similar to that required by a lumped mass model, the only

advantage coming from the reduced computational effort due to the reduced number of cable elements.

Peyrot (1980) used the basic catenary equations to develop the finite element model to deal with dynamic cable structures, enabling the element to be longer than the traditional straight or curved cable element. Lindahl and Sjoberg (1983) transformed the equations of motion to ordinary differential equations by using the principle of virtual work, and an explicit numerical method is utilised to solve the equations without iteration.

McNamara and O'Brien (1986) developed a hybrid finite element model to deal with a variety of underwater flexible structures such as mooring cables, pipes, and risers. The hybrid element treats the axial forces and the bending shear forces as independent unknowns. It is claimed that the hybrid element gives greater stability and accuracy in the solution over a range of bending stiffness, *i.e.* from zero for a mooring cable to rigid pipelines.

Marichal and Jacquot (1988) developed a simplified Lagrangian model with a reduced number of variables (hence equations) and an explicit integration scheme, thus eliminating the need to carry out an iteration procedure within the finite difference solution. The model assumes an inelastic cable and is not validated in the paper.

Tuah and Leonard (1990) modified the finite element model with straight elements to deal with synthetic cables, *i.e.* modelled with viscoelastic cable elements.

Other researchers involved in modelling underwater cable systems include: Bernitsas (1982), Jeffery and Patel (1982), Kokkinowrachos *et al.* (1987), Pedersen and Junqi (1987), and Triantafyllou (1994). More information can be obtained from the reference list in this thesis.

From the discussion in this sub-section, it is seen that the dynamic modelling of cable systems can be divided into two broad groups:

- defining the cable elements primarily in physical terms, *e.g.* lumped mass and hinged rod models; or
- defining the cable elements primarily in mathematical terms, *e.g.* continuous cable and finite element models.

1.6 Tow Cable / Fish Models

Having reviewed the various cable models available, it is now appropriate to look at underwater tow models. Between the wars, a number of researchers investigated the towing of gliders and targets by aircraft, using static and quasi-static models. In 1936 Thews and Landweber (Casarella and Parsons (1970)), investigated cable tensions in towing surface targets using Glauert's cable model, with the inclusion of a constant tangential hydrodynamic force for the first time. During World War II, Richtmyer in 1941 and Reber in 1942 investigated the towing of minesweeping equipment using this analysis. In 1945 O'Hara included the effect of cable stretching on other cable parameters for an aircraft towed glider configuration. Whicker in 1957 and Eames in 1967 developed two-dimensional steady state towing models, including the use of faired-section cables, with the latter paper presenting valuable experimental data and formulae for drag coefficients of such cables.

The first dynamic cable model was by Phillip in 1949 for an airborne towing configuration. In 1957 Whicker indicated a solution for a two-dimensional dynamic towing model with a faired section cable. Strandhagen and Thomas in 1963 presented a three-dimensional underwater dynamic towing model based on the cable model of Walton and Polachek (1959), but failed to present a solution. The Boeing Company in 1966 modified this model and solved it using an analogue computer. In the same year Lagasse presented a two-dimensional model of a faired-section cable in a tethered towing system, with translation and rotational motion.

Schram and Reyle (1968) modelled a three-dimensional dynamic model of a towed body, with inextensible cables having faired-sections. Although the model is dynamic, it neglects the added mass. The partial differential equations are developed and solved in a similar manner to that introduced by Reid (1968) and Patton (1972) *i.e.* by the method of characteristics. The modelling of the tow body is basic, with its centre of gravity assumed to coincide with the tow point, thus eliminating the effect of the three rotational degrees of freedom of the body on the motion of the cable.

Ablow and Schechter (1983) modelled a three-dimensional dynamic towed cable in a slightly different manner to Schram and Reyle, by using an implicit finite difference numerical scheme with a Newton iteration method to solve the set of equations in matrix form. The cable is approximated by a sub-divided cable length. The model is claimed to be acceptable for a number of unsteady-state towed cable problems, with a fast and stable solution algorithm. As the model deals with free end cables (*e.g.*

arrays), it is unable in its current form to deal with towed bodies. Milinazzo *et al.* (1987) improved the model, especially the finite difference solution technique, (making it stable, faster, and more computationally efficient).

Paul and Soler (1972) modelled a two-dimensional towed underwater cable / vehicle configuration using a technique that lies “in between” a quasi-static and a dynamic model. The surface vessel is assumed to move along a straight line, while the submerged vehicle is assumed to travel in a vertical plane through this line. The discretisation of the cable is achieved by dividing the cable into a number of equal length straight line inelastic segments, with their masses “lumped” at the junctions, *i.e.* a lumped mass model. The drag force on the cable is assumed to act only in a direction normal to the cable. Inertia forces are neglected as it is assumed that these forces are small in comparison to weight and drag forces when considering slow motions.

The underwater vehicle is approximated as either a spherical or cylindrical clump, each giving drag forces in the two directions. Although the vehicle model is extremely rudimentary, it is able to incorporate a propulsion force to deal with vehicles having propulsive units.

Equations are developed by considering the force balance at each node and considering the geometric and kinematic relationship. The solution technique consists of first obtaining a quasi-static solution using the lumped mass model, which also yields the angular velocities of the cable segments. The “dynamic” solution is carried out starting with the quasi-static model and then employing a Runge-Kutta method over the time steps.

Sanders (1982) extended the modelling technique introduced by Paul and Soler (1972) to a three-dimensional towed cable system. This model also assumes that elasticity, added mass, and inertia effects are small and can be ignored, thus retaining only the weight and drag as external forces. The latter is considered in three-dimensions. The towed body considered is a long, slender neutrally buoyant body, *i.e.* a towed array, which is modelled in a similar manner to a cable segment. This restricts the model to towed arrays or similarly shaped bodies, thus reducing the versatility of the model.

It is interesting to note that Sanders did encounter stability problems with a predictor-corrector method, and a Runge-Kutta algorithm was successfully utilised with a sufficiently small time step. The requirement for the small time step is identified, but

the impression is that it was deduced by trial and error. Although an error analysis was carried out, details are not given in the paper.

Ivers and Mudie (1973) developed a three-dimensional model for extremely long tow cable systems, which was claimed to be dynamic, but as in the previous model ignores inertia (and the tangential drag force). The drag coefficient was obtained by minimising the root mean square error between the observed and calculated position of the towed fish. The towed fish model consisted of only the drag forces and its weight in water. The authors acknowledge that the model is a crude representation, but useful in simulating long tow lines using early ship-based computers.

Miller (1963) modelled a towed underwater system using a finite element model that used linear and rotational displacements of the elements. The model consisted of a six degree of freedom dynamic fish model with a varying attachment point and hydrodynamic fin forces. Webster (1975) used a straight segment finite element technique to model a three-dimensional dynamic towed cable / fish system. The solution is via an implicit integration scheme to iterate towards the solution. The towed body described in the paper is a sphere towed from its centre of gravity.

Delmer *et al.* (1983) used a “simplified finite element model” to dynamically simulate a towed cable suited for fishing purposes. The cable is modelled by coupled ordinary differential equations that describe the motion of discrete reference points along the cable. The computer model has four distinct types of reference points, that can be assembled to represent the cable. The elements that join the nodes are assumed to have constant properties along their length, *i.e.* the “simplified finite element model”. The equations are assembled into a matrix in a similar manner to the finite element method, and solved using an explicit integration scheme having flexible error control.

Kato (1987) carried out a vibration analysis of an underwater towed system by modelling the cable as an inextensible continuous system, and the towed fish in six degrees of freedom connected to the cable via gimbals. The equations are solved by first linearising and then taking an eigenvalue problem approach. The computational results are analysed in conjunction with compatible experimental results. A lumped mass quasi-static model is also used to compute the equilibrium state of the model.

Three-dimensional static and dynamic lumped mass tow models were developed by Koterayama *et al.* (1988) to investigate the motion of a depth controllable towed vehicle having six degrees of freedom, although the latter is simplified during the

modelling process. The required hydrodynamic coefficients for the simplified tow fish are obtained by scaled model experiments. The dynamic stability of the towed body is obtained by solving the equations of motions in frequency domain.

Kamman *et al.* (1989) also modelled a towed underwater system using a lumped mass method, solving the equations under both static and dynamic conditions. The three-dimensional towed body has six degrees of freedom with non-coinciding tow point and centre of gravity. The tension equations are linearised and used to obtain the acceleration terms, which are then used in numerical integration schemes to calculate the positions and velocities. No information is given on the integration technique and it is implied that no iteration is used in the solution. The paper also briefly discusses the use of the hinged rod cable model developed by Winget and Huston (1976) for towed systems, with a comparison of the results from the two models presented. The main draw back of the latter model is stated as the long execution time.

Among the configurations modelled by Huang (1992) is a three-dimensional dynamic lumped mass towed model solved using an implicit integration scheme. However, the sub-sea unit, (*i.e.* the towed fish or equivalent), is modelled with only its three linear degrees of freedom.

A three-dimensional dynamic hinged rod underwater tow model was developed by Chapman (1987) by dividing the cable into a number of rigid, non-extensible rods, with their mass uniformly distributed along the rod. Each rod is connected to the adjacent rods by frictionless ball joints that allows it to rotate in any direction, except spin along its axis. Equations of motion are then developed for each rod, which yield relationships between the forces and accelerations at the bottom of the rod to those at the top. Since the model does not support longitudinal wave propagation, it cannot represent the dynamic effects due to rapid cable top motion.

The use of an iterative “shooting” method, working from the top to meet the dynamic constraints of the fish at the bottom, proved to be numerically unstable for a system represented by 5 rods or more due to the propagation of errors down the cable. In order to overcome this, a direct functional relationship using tensors was developed between the forces and accelerations at the top of each rod as well as for the tow fish. The tow fish is modelled in 6 degrees of freedom with a variable tow point. Henderson and Wright (1991) extended Chapman’s model to deal with two-part tows similar to that given in Figure 1.1(c).

Interestingly, quasi-static models are still used in the analysis of towed systems, depending on their application. For example, Hopkin *et al.* (1990) models a two-dimensional two-part tow (similar to Figure 1.1(c)), using a quasi-static cable model coupled to a dynamic tow fish model, in order to study the controlled behaviour of the tow fish. However, by and large such models are reserved for preliminary work and as a starting configuration for dynamic models.

It was decided early in the programme to use a time domain three-dimensional dynamic simulation for the following reasons:

- the errors encountered in quasi-static models were unacceptably high; and
- frequency domain models did not allow easy and accurate representation of non-linearities envisaged in tow cable / fish modelling.

The popular cable modelling methods and the respective solution procedures are described in Chapter 2. The selection of the lumped mass method to use in the current problem is also justified in that chapter.

1.7 Solution Techniques

In engineering, the use of numerical techniques is widespread. The integration of ordinary differential equations can be classified as *implicit* or *explicit*. If during the integration, the values are obtained only from known values, the integration is said to be explicit. Thus, the value at a given step depends only upon the values *up to* that step. The most popular explicit integration scheme used in engineering is the Central Difference (CD) method, with Walton and Polachek (1959) probably being the first to use this explicit finite difference integration technique in the solution of cable systems.

However, if the values are obtained from those including the ones being calculated, then the integration is said to be implicit. In this case, the values at a given step depends upon the values *up to and inclusive* of that step. Therefore, these generally require an iteration process in the solution technique. A number of implicit schemes are used in engineering, including the Newmark, Houbolt, and Wilson- θ methods, (see Bathe (1982)).

The integration schemes for ordinary differential equations can be further divided into a number of groups depending on the number of steps and stages used in the scheme. In cable models the common algorithms used are multiple evaluation, single-step, and multi-step schemes. The first group reduces the error by calculating the values at a number of intermediate positions within the given step. An example is the *Runge-Kutta* method, used by Winget and Huston (1976), Sanders (1982), and Ractliffe (1984), with the second author dealing with underwater towed systems.

The single-step method uses simple low-order formulae based on a truncated Taylor series, (e.g. an Euler type integrator). Only one function is evaluated at each step, resulting in low accuracy. However, the accuracy can be improved, if the derivatives can be explicitly calculated. The hinged rod cable model of Chapman (1987) and the lumped mass model of Huang and Vassalos (1995) use such explicit methods in order to reduce computational effort by eliminating the iteration process.

The multi-step method uses a number of values obtained in previous iteration steps to recalculate their values. This allows their values to be *improved* through an iterative procedure, until sufficient convergence is achieved. Increasing the number of previous values in the iteration process enables schemes involving higher order terms to be incorporated, thus increasing accuracy. Common methods consist of *predictor-corrector* schemes, where an explicit formulae gives a *prediction* of the required solution of an implicit *corrector*. This type of scheme is extremely popular with cable model solution techniques, and is used in this project.

In quasi-static models, an iteration process is usually required to calculate the equilibrium configuration, as the equations are usually implicit. One method used is a Newton iteration process as described in Wilson (1975). However, as shown by Thomas and Hearn (1994), the procedure can be tedious and difficult to converge. Wilson (1975), Berteaux (1976), and Leonard and Tuah (1986) describe some techniques that can be employed to force a convergence in such situations.

The dynamic equations describing the motion of the cable and the fish are second order coupled non-linear partial differential equations, which are converted to ordinary differential equations. These are solved using a numerical integration scheme that gives the change in configuration of the cable / fish system with time. Since the equations are non-linear, an iteration process is required at each time step. Thus, the solution obtained from the numerical integration scheme is checked for accuracy with the aid of a constraint relationship. This relationship will enable the results to be

improved through the iteration process, until an acceptable level of accuracy is achieved. In addition to being accurate, the numerical technique must be stable.

The selection of the numerical solution procedure depends on the balance between accuracy / stability of the schemes versus the computational effort required. In dynamic cable / body models, modes of motion occur within the system and oscillate in scales of milliseconds. The ratio of the fastest to the slowest normal mode of motion is referred to as the “stiffness ratio”. A system having a large ratio (usually above a ratio of 10000), is deemed to be stiff.

Although these high frequency modes do not greatly influence the motion of the system, they affect the stability of the numerical scheme used in the solution process. Therefore, the step size used in explicit integration solution schemes should be sufficiently small to follow these rapid variations. Implicit integration schemes are usually stable for all time steps. However, the time step is limited due to two conditions, *i.e.* the loss of accuracy due to the size of the time step and the instability due to the propagation of errors introduced by the iteration scheme required for non-linear systems.

As stated previously, Walton and Polachek (1959) are probably the first to use the explicit finite difference integration technique, *i.e.* the central difference technique, in the solution of cable systems. Since the equations of motion are non-linear, an explicit solution is impractical and an iterative process based on the Newton-Raphson method is utilised. Since the central difference algorithm requires special starting procedures, (Bathe (1982)), a Taylor series expansion is used to obtain the initial tentative tension values to start the iteration. These values are then corrected through a modified Newton-Raphson iteration to conform to the segment length constraint equation. However, as shown later in Chapter 5, the special starting procedure can be omitted from the solution procedure, and a quasi-static or an approximate configuration used as an initial configuration to start the process, (Thomas (1993)).

Walton and Polachek also carry out a stability analysis of the equations and solution technique by employing the von Neumann (Fourier) stability method, described in Chapter 5. This provides a limiting time step to be used in the solution process in line with the explicit integration scheme. Although the limiting criteria are based on the equations being linear, they provides a good “guide” in choosing an appropriate time step. This will be discussed later in Chapter 5.

This *predictor-corrector* scheme is arguably the most popular method with solution techniques of discrete element cable models. For lumped mass models, finite difference schemes are used to approximate the cable equations, that are then solved by an appropriate procedure. Typical examples are given by Nakajima *et al.* (1982), van den Boom *et al.* (1987), Peuker *et al.* (1987), and Huang (1994).

In the finite element method, a number of the integration techniques are utilised to solve the matrix-based assembled equations of motion. For example, Johansson (1976) decoupled the force terms over a short period of time and used a trail and error process to obtain the final state at each time interval. Webster (1975) used an implicit integration scheme to iterate towards the solution, where the time step length was variable. Lindahl and Sjoberg (1983) used an explicit numerical integration scheme to solve the equations without iteration. Haritos and He (1989) used an implicit integration scheme to reduce the differential equations to a set of non-linear algebraic equations, that was solved using a modified Newton-Raphson iteration method.

McNamara and O'Brien (1986) used an implicit multi-step integration scheme, due to high intrinsic numerical damping and allowed large time increments. However, they later replaced this with an one-step scheme that allowed varying time steps. The latter was determined using a parameter referred to as the "current period" (Chaudhuri *et al.* (1987)). The two papers by Park and Underwood in 1980 present detailed information on the variable step central difference method, while Bergan and Mollestad (1985) present the method used by McNamara and O'Brien.

Although Walton and Polachek (1959) carried out a numerical stability analysis for their mathematical model, very little work has been carried out in analysing the stability and accuracy requirements for the numerical techniques utilised for underwater cable models. Some researchers (*e.g.* Peyrot (1980), Ractliffe (1984), Peuker *et al.* (1987)) have suggested limits for the time step, however, do not present analytical explanations for these limits. Huang (1992) carried out a stability analysis on the implicit scheme used in his model, while Thomas (1993) possibly offers the best investigation into the numerical solution of underwater cable systems by looking at one explicit and three implicit integration schemes. However, this area requires more investigation in order to fully understand the limitations imposed on the numerical schemes used in context of underwater catenary systems.

Considering numerical techniques in general, Bathe (1982) provides "engineers" with a brief but concise account of the stability and accuracy requirements of the popular

numerical schemes. Wood (1990) offers a more mathematical treatise, which is aimed more at mathematicians, rather than engineers. Other texts such as Ames (1969) and Gear (1971), also provide good analyses of such numerical methods. In addition, a number of publications offer information about, and analysis of these techniques.

One of the earliest analyses of numerical solution techniques is given O'Brien *et al.* (1950-51), which explains the von-Neumann (Fourier) stability method applied to the numerical solution of differential equations. Lax and Richtmyer (1956) expand on this work and looks at the requirement for stability for a number of finite difference equations.

Belytschko *et al.* (1975) investigated the spurious oscillation and stability of explicit integration schemes. It is claimed that in general, wave propagation problems are best solved by explicit techniques, while implicit techniques are best suited for inertial problems. The paper also develops limiting time steps to ensure stability with explicit integration schemes.

Hilber *et al.* (1977) developed an one-step unconditionally stable algorithm, which is compared with other popular integration methods. The development and investigation is detailed in Hilber (1976). Zienkiewicz (1977) provides the derivation of popular numerical schemes by applying a finite element weighted residual approach to the general linear equations of motion, using shape function descriptions of the displacements.

In Belytschko and Schoeberle (1975) and Hughes (1977), non-linear methods in structures are investigated for stability using an energy stability technique, *i.e.* the boundedness of the energy in the discrete system relative to its initial energy is postulated to imply stability.

1.8 Underwater Vehicle Models

It is not intended in this study to investigate the modelling of underwater vehicles in detail, as that is left respectfully to the naval architect. However, the underwater towed body (fish) model should be sufficiently detailed to predict accurately its dynamic motion along the three linear and three rotational degrees of freedom, *i.e.* six degrees of freedom. In addition, the fish model has to be dynamically interfaced with

the cable model at the appropriate location and lend itself to the solution procedure adapted for it.

In sub-section 1.5, a number of towed cable / fish models were reviewed, which included brief descriptions of the towed underwater vehicles. Some were rudimentary fish models, consisting of two or three-dimensional lumped mass models, with a coinciding tow point and centre of gravity, (*e.g.* Schram and Reyle (1968), Paul and Soler (1972), Ivers and Mudie (1973), Webster (1975), and Huang (1992)). A number of models consisted of only a towed cable model without a sub-sea unit, while others dealt only with towed arrays, (*e.g.* Sanders (1982), Ablow and Schechter (1983), Delmer *et al.* (1983), and Milinazzo *et al.* (1987)).

Hopkin *et al.* (1990) presents a two-dimensional dynamic model with fins, while models such as Miller (1963), Kato (1987), Chapman (1987), Kotera-yama *et al.* (1988), and Kamman *et al.* (1989) offer three-dimensional dynamic models of the tow fish, with 6 degrees of freedom, a variable tow point, and hydrodynamic fins. In addition, a number of authors have presented mathematical models for underwater vehicles, *e.g.* Abkowitz (1969), Humphreys (1976), Bhattacharyya (1978), and Papoulias (1992).

The modelling of underwater vehicles encompasses three areas, *i.e.* kinematics, dynamics, and hydrodynamics. The kinematics deals with the representation of the orientation and rotational rates of the fish. The dynamics develop the relationships between the forces / moments on the body to its motion. The hydrodynamic concepts produce the fluid induced forces and moments acting on the body at the given fish orientation and rotational rates.

The equation of motion will consist of coefficients that can be broadly divided into inertia (*i.e.* mass, moment of inertia, added mass and added moment of inertia), hydrodynamic (drag, lift and side force), gravity / buoyancy, and external forces (*e.g.* tow cable tension). The added mass terms will introduce coupling terms in the equations describing the motion of the body. This effect is compounded if the tow point(s) on the fish are located at points other than its centre of gravity. The prediction of the added mass / inertia coefficients is carried out by analytical (Clauss *et al.* (1992), Humphreys and Watkinson, (1978) and Imlay (1961)) or experimental procedures.

The forces and moments on the underwater body can be expressed as a function of its motion and orientation parameters, (*i.e.* displacements and velocities). Expressions for the forces and moments of an underwater body in six degrees of freedom are given in Gertler and Hagen (1967). The main hydrodynamic coefficients are the drag, lift, and side force coefficients in the linear and rotary directions.

Very little information is available to predict these coefficients using analytical methods. Some examples of such analytical predictions are given in Fidler (1978) and selected publications from the US Naval Sea Systems Command Hydromechanics Committee (SEAHAC). The preferred method is to obtain these coefficients using experimental data as explained in Abkowitz (1969) and Wingham and Henderson (1988).

1.9 Experimental Investigation and Validation

The experimental stage of this work was used for two purposes:

- to validate the computer model; and
- to further investigate the two-part tow.

The tests were carried out in two stages:

- scaled model trials in the circulating water channel at the Australian Maritime College; and
- full scale trials using RAN and DSTO side scan sonar vehicles.

The scaled model experimental stage of the two-part tow consisted of a number of tow configurations, obtained by varying the parameters of the configuration.. The tow was excited by an elliptical exciter located at the water surface, ensuring that the cable model remained submerged throughout the run. The tension values at the surface tow point was recorded via a load cell. The motion of the towed fish was obtained on video and digitised using reference points on the towed body. By locating the video camera at different positions, it was possible to record the surge, sway, heave, pitch, and yaw motions.

The drag and lift coefficients for the scaled models were obtained experimentally using a horizontal planar-motion-mechanism (HPMM), fitted with a six degree of freedom load cell and located at the circulating water channel. The coefficients and the testing procedure are described in Chapters 2 and 6 respectively.

The full scale trials consisted of towing the actual side scan sonar through a number of runs under varying conditions. The sonar gear in the sonar vehicle was replaced with accelerometers to record its motion, which was then fed back to the surface via the tow cable. The surface tow point cable tension was also recorded via a load cell. A number of experiments were carried out in Jervis Bay and Port Phillip Bay.

Chapter 6 and Appendix A describe the experiments in detail and evaluates the results obtained.

CHAPTER 2

MODELLING TECHNIQUES

2.1 Introduction

In this chapter, the various modelling techniques available to model underwater towed systems are investigated. The modelling requirements for such systems can be divided into two distinct areas:

- cable model; and
- towed body (fish) model.

The various three-dimensional dynamic models available to predict the behaviour of underwater cable systems are investigated in sub-section 2.2, thus enabling the selection of the most suitable cable model to simulate the behaviour of two-part and multi-tow configurations. The selected cable model should be sufficiently flexible to deal with cable junctions and to integrate the towed fish model.

Sub-section 2.4 deals with various methods available for the modelling of six degrees of freedom dynamic underwater bodies, (*i.e.* the towed fish). The fish model should be compatible with the selected cable model, enabling it to be incorporated into the cable model solution technique. Thus, the two models should allow for coupling of motions and forces between them.

The behaviour of underwater cables and bodies are influenced by the hydrodynamic loading on them from the surrounding fluid. This loading can be divided into two broad groups:

- hydrodynamic (drag, lift, side) forces; and
- inertia forces (mass, moment of inertia, added mass, and added moment of inertia).

In sub-section 2.3, the various methods available to predict the hydrodynamic loading on underwater cables are discussed. The effects of rough surfaces and vortex shedding are discussed and their influence on the relevant coefficients are identified. Sub-section 2.5 deals with the hydrodynamic coefficients of underwater bodies.

2.2 Dynamic Cable Models

There are a number of methods used to model underwater cables dynamically. A brief description of some of the more popular methods is given below.

2.2.1 The Method of Characteristics

The method of characteristics is commonly used for the solution of hyperbolic partial differential equations. It employs a set of characteristic curves along which the total differential equations are valid. A brief explanation of the method is given below, with a detailed description obtainable from Patton (1972) and Schram and Reyle (1968), which explain the modelling and solution technique for mooring and towed cable systems, respectively.

Figures 2.1 and 2.2 shows the Cartesian coordinate system and the tensile force for a cable segment (element) of length δs . By resolving the tension into the Cartesian coordinate directions, X, Y, and Z, the equations of motion are given by:

$$\mu_c \frac{\partial^2 x}{\partial t^2} = \frac{\partial}{\partial s} (T \cos \phi \cos \psi) + F_x \quad (2.1a)$$

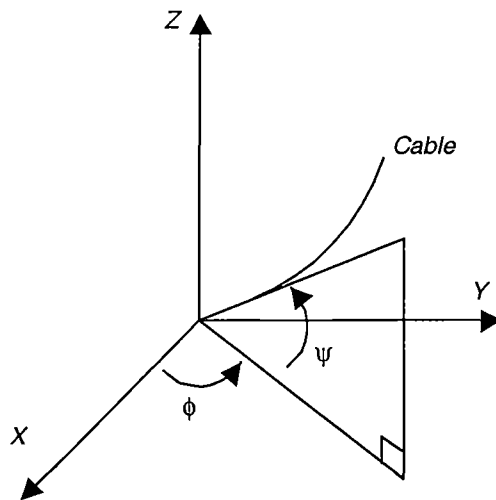
$$\mu_c \frac{\partial^2 y}{\partial t^2} = \frac{\partial}{\partial s} (T \sin \phi \cos \psi) + F_y \quad (2.1b)$$

$$\mu_c \frac{\partial^2 z}{\partial t^2} = \frac{\partial}{\partial s} (T \sin \psi) + F_z \quad (2.1c)$$

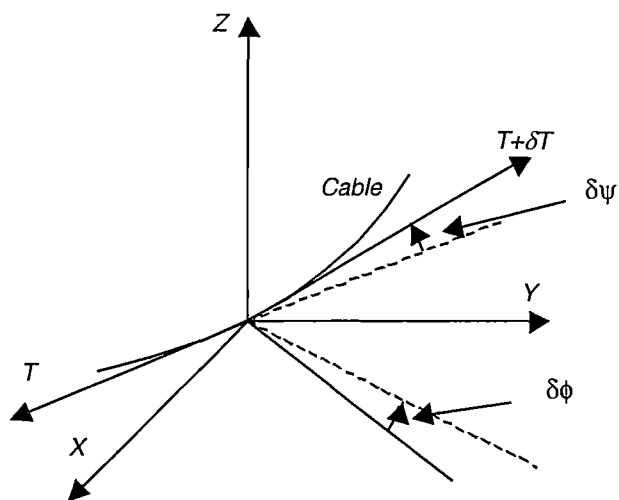
where

- $F_{x,y,z}$: hydrodynamic, mass, and buoyancy forces per unit stretched length of cable in the X, Y, and Z directions
- s : the arc length of any unstretched point along the cable
- T : cable tension

- μ_c : cable mass per unit length
 ϕ : horizontal angle of the cable with the X axis
 ψ : vertical angle of the cable with the X-Y plane
 x, y, z : displacement along the X, Y, and Z directions



Cartesian Coordinates of Cable
Figure 2.1



Continuous Cable Element
Figure 2.2

Also considering the geometric relationships, we have,

$$\frac{\partial x}{\partial s} = (1 + \epsilon) \cos \phi \cos \psi \quad (2.2a)$$

$$\frac{\partial y}{\partial s} = (1 + \epsilon) \sin \phi \cos \psi \quad (2.2b)$$

$$\frac{\partial z}{\partial s} = (1 + \epsilon) \sin \psi \quad (2.2c)$$

where ϵ is the local strain in a cable element when stretched.

From Figures 2.1 and 2.2, the transformation matrix $[\Lambda]$ between the Cartesian or global coordinate system (X, Y, Z) and the local coordinate system (X', Y', Z') along the cable is given by,

$$[\Lambda] = \begin{bmatrix} \cos \phi \cos \psi & \sin \phi \cos \psi & \sin \psi \\ -\sin \phi & \cos \phi & 0 \\ -\cos \phi \sin \psi & -\sin \phi \sin \psi & \cos \psi \end{bmatrix} \quad (2.3)$$

It can be easily shown that the inverse of the above transformation matrix is equal to the transpose of the matrix, *i.e.*,

$$[\Lambda]^{-1} = [\Lambda]^T \quad (2.4)$$

Thus, the hydrodynamic forces (F_x, F_y, F_z) and the cable velocities (V_x, V_y, V_z) in the Cartesian coordinates, can be transformed to the respective forces ($F_{x'}, F_{y'}, F_{z'}$) and velocities ($V_{x'}, V_{y'}, V_{z'}$) in the directions tangential and normal to the cable as,

$$[F_{x'}, F_{y'}, F_{z'}]^T = [\Lambda] \cdot [F_x, F_y, F_z]^T \quad (2.5)$$

$$[V_{x'}, V_{y'}, V_{z'}]^T = [\Lambda] \cdot [V_x, V_y, V_z]^T \quad (2.6)$$

In addition to the above equations, the relationship between the tension and strain in the cable is given by ,

$$\frac{\partial T}{\partial t} = \frac{\partial T}{\partial \epsilon} \cdot \frac{\partial \epsilon}{\partial t} \quad (2.7)$$

Assuming a linear variation of tension, equation (2.7) reduces to,

$$T = \frac{\partial T}{\partial \epsilon} \cdot \epsilon \quad (2.8)$$

As shown in Patton (1972), by using equations (2.5), (2.6), and (2.8) in equations (2.1) and (2.2), the following set of equations describing the motion of the cable in the directions tangential and normal to the cable are obtained,

$$\frac{\partial \bar{U}}{\partial t} + \underline{\underline{Au}} \frac{\partial \bar{U}}{\partial s} + \underline{\underline{Bu}} = 0 \quad (2.9)$$

where

$$\begin{aligned} \bar{U} &: \text{vector consisting of } [V_x', V_y', V_z', \epsilon, \phi, \psi]^T \\ \underline{\underline{Au}} &: 6 \times 6 \text{ matrix, (see Chapter 5 for the coefficients)} \\ \underline{\underline{Bu}} &: 6 \times 1 \text{ matrix, (see Chapter 5 for the coefficients)} \end{aligned}$$

For the six equations in (2.9), the determinant is,

$$|\underline{\underline{Au}} - \lambda_w \underline{\underline{I}}| = 0 \quad (2.10)$$

where $\underline{\underline{I}}$ is a unity matrix and λ_w represents the eigenvalues. The six characteristics are then derived as,

$$\lambda_{w1,2} = \pm \sqrt{\frac{1}{\mu_c} \cdot \frac{dT}{d\epsilon}} \quad (2.11a)$$

$$\lambda_{w3,4} = \pm \sqrt{\frac{1}{\mu_c} \cdot \frac{\epsilon}{(1+\epsilon)} \cdot \frac{dT}{d\epsilon}} \quad (2.11b)$$

$$\lambda_{w5,6} = \pm \sqrt{\frac{1}{\mu_c} \cdot \frac{\epsilon}{(1+\epsilon)} \cdot \frac{dT}{d\epsilon}} \quad (2.11c)$$

The characteristic roots are real, which indicates that equations (2.9) are hyperbolic partial differential equations. The characteristic values obtained in (2.11a) represent the speeds at which the *tensile disturbance* (wave) travels along the line, with the positive travelling down the line and the negative up the line. The characteristic values obtained in (2.11b) and (2.11c) represent the speeds at which the *transverse disturbance* (wave) travels along the line, again with the positive travelling down the line and the negative up the line. These are dealt at depth in Chapter 5.

Now by manipulating the six equations given in (2.9), the equivalent ordinary differential equations are developed for the motion of the disturbance along the cable. Thus, as shown in Patton (1972) we get,

$$\begin{aligned}
 dV_{x'} - Gu_{x'\epsilon} \cdot d\epsilon - Gu_{x'\psi} \cdot d\psi - Gu_{x'\phi} \cdot d\phi - Hu_{x'} \cdot dt &= 0 \\
 dV_{y'} - Gu_{y'\psi} \cdot d\psi - Gu_{y'\phi} \cdot d\phi - Hu_{y'} \cdot dt &= 0 \\
 dV_{z'} - Gu_{z'\phi} \cdot d\phi - Hu_{z'} \cdot dt &= 0
 \end{aligned}
 \tag{2.12}$$

where

$$Gu_{x'\epsilon} = \sqrt{\frac{1}{\mu_c} \frac{dT}{d\epsilon}}$$

$$Gu_{x'\psi} = V_{y'}$$

$$Gu_{x'\phi} = V_{z'} \cdot \cos \psi$$

$$Hu_{x'} = \frac{1}{\mu_c} \cdot F_{x'}$$

$$Gu_{y'\psi} = (1 + \epsilon) \sqrt{\frac{1}{\mu_c} \frac{1}{(1 + \epsilon)} \frac{dT}{d\epsilon}} - V_{x'}$$

$$Gu_{y'\phi} = V_{z'} \cdot \sin \psi$$

$$Hu_{y'} = \frac{1}{\mu_c} \cdot F_{y'}$$

$$Gu_{z'\phi} = (1 + \epsilon) \cos \psi \sqrt{\frac{1}{\mu_c} \frac{1}{(1 + \epsilon)} \frac{dT}{d\epsilon}} - (V_{x'} \cos \psi - V_{y'} \sin \psi)$$

$$Hu_{z'} = \frac{1}{\mu_c} F_{z'}$$

The characteristic equations representing the motions along the cable are given by,

$$\frac{dV_{x'}}{d\phi} \pm Gu_{x'\epsilon} \frac{d\epsilon}{d\phi} - Gu_{x'\psi} \frac{d\psi}{d\phi} - Gu_{x'\phi} \frac{d\phi}{d\phi} - Hu_{x'} \frac{dt}{d\phi} = 0 \quad (2.13a)$$

where $\phi = \phi_1, \phi_2$ are the characteristic lines associated with $\lambda_{w1}, \lambda_{w2}$, (*i.e.* the tensile disturbance down and up the cable), and the second term is – or + respectively.

$$\frac{dV_{y'}}{d\phi} \pm Gu_{y'\psi} \frac{d\psi}{d\phi} - Gu_{y'\phi} \frac{d\phi}{d\phi} - Hu_{y'} \frac{dt}{d\phi} = 0 \quad (2.13b)$$

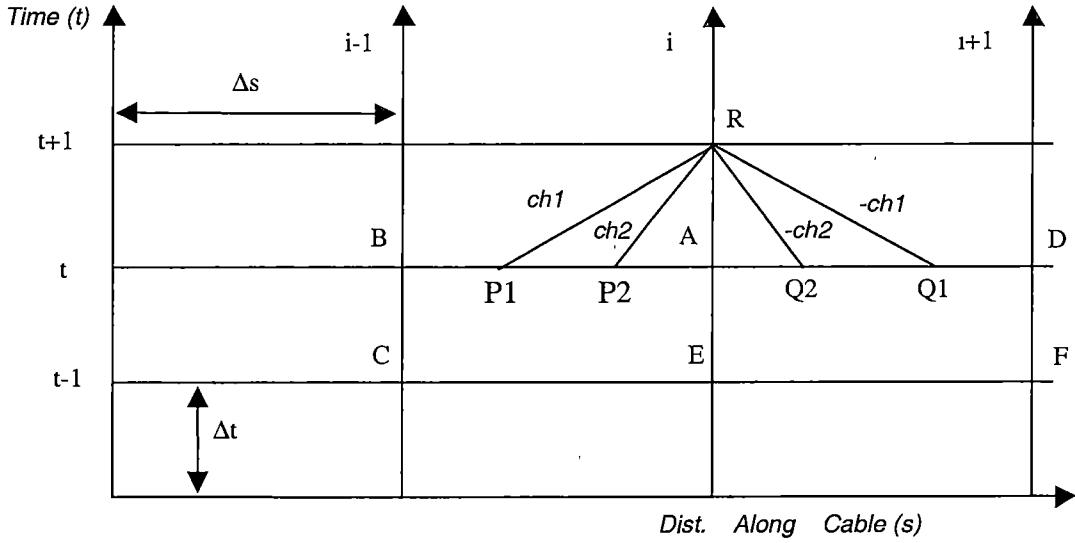
where $\phi = \phi_1, \phi_2$ are the characteristic lines associated with $\lambda_{w3}, \lambda_{w4}$, (*i.e.* the transverse disturbance in the X'-Y' plane, down and up the cable), and the second term is – or + respectively.

$$\frac{dV_{z'}}{d\phi} \pm Gu_{z'\phi} \frac{d\phi}{d\phi} - Hu_{z'} \frac{dt}{d\phi} = 0 \quad (2.13c)$$

where $\phi = \phi_1, \phi_2$ are the characteristic lines associated with $\lambda_{w5}, \lambda_{w6}$, (*i.e.* the transverse disturbance in the X'-Z' plane, down and up the cable), and the second term is – or + respectively.

By using the above characteristic equations, the *six partial differential equations* have been transformed into *six ordinary differential equations*. These can be solved using a numerical procedure as described below.

The cable is divided into a number of nodal points along its length. The resulting computational mesh or rectangular grid in the time-space (t-s) plane is shown in Figure 2.3. The initial values for the system is obtained from a quasi-static model. Assuming the values of the six independent parameters are known at the nodal points on the “t” time line, the solution is advance to the “t+1” time line.



t-s Solution Mesh

Figure 2.3

Note: A computation mesh is a grid with the variables of the partial differential equations represented along its axes. In the case of Figure 2.3, the variables are the spatial coordinates “s” along the cable on the X axis, and the time “t” on the Y axis. The grid spacing is the intervals used in the numerical scheme for each variable, *i.e.* Δs and Δt respectively. The mesh points represents the various time versus length points of the scheme.

Using the six parameters at B, A, and D, (see Figure 2.3), it is possible to linearly interpolate to find the values at points P₁, P₂, Q₁, and Q₂. Now using the characteristic curves from equations (2.13), the solution can be advanced to point R. Writing the characteristic equations in difference notation gives,

$$V_{x'(R)} - V_{x'(P1)} - Gu_{x'\epsilon(A)} \cdot (\epsilon_R - \epsilon_{P1}) - Gu_{x'\psi(A)} \cdot (\psi_R - \psi_{P1}) - Gu_{x'\phi(A)} \cdot (\phi_R - \phi_{P1}) - Hu_{x'(A)} \cdot dt = 0$$

$$V_{x'(R)} - V_{x'(Q1)} + Gu_{x'\epsilon(A)} \cdot (\epsilon_R - \epsilon_{Q1}) - Gu_{x'\psi(A)} \cdot (\psi_R - \psi_{Q1}) - Gu_{x'\phi(A)} \cdot (\phi_R - \phi_{Q1}) - Hu_{x'(A)} \cdot dt = 0$$

$$V_{y'(R)} - V_{y'(P2)} - Gu_{y'\psi(A)} \cdot (\psi_R - \psi_{P2}) - Gu_{y'\phi(A)} \cdot (\phi_R - \phi_{P2}) - Hu_{y'(A)} \cdot dt = 0$$

$$V_{y'(R)} - V_{y'(Q2)} + Gu_{y'\psi(A)} \cdot (\psi_R - \psi_{Q2}) - Gu_{y'\phi(A)} \cdot (\phi_R - \phi_{Q2}) - Hu_{y'(A)} \cdot dt = 0$$

$$\begin{aligned}
V_{z'(R)} - V_{z'(P2)} - Gu_{z'\phi(A)} \cdot (\phi_R - \phi_{P2}) - Hu_{z'(A)} \cdot dt &= 0 \\
V_{z'(R)} - V_{z'(Q2)} + Gu_{z'\phi(A)} \cdot (\phi_R - \phi_{Q2}) - Hu_{z'(A)} \cdot dt &= 0
\end{aligned}
\tag{2.14}$$

From the above difference equations, it is possible to calculate the parameters at R, *i.e.*,

$$\bar{U}_{(R)} = [V_{x'(R)}, V_{y'(R)}, V_{z'(R)}, \epsilon_{(R)}, \phi_{(R)}, \psi_{(R)}]^T \tag{2.15}$$

and equation (2.8) is used to calculate the tension T of the cable.

Thus, the numerical procedure can be summarised as:

Step 1: Compute all the coefficients for the six simultaneous equations (2.14) of all nodes using the values obtained for the previous two time steps.

Step 2: Solve the simultaneous equations to obtain the parameters for point R.

Step 3: Go back to steps 1 and 2 until sufficient convergence is achieved.

Step 4: Go to the next node and repeat steps 1 to 3 until end of cable.

Step 5: Go to the next time step and repeat steps 1 to 4 until end of simulation.

In this technique, the discontinuity due to the junction is difficult to model and would require complex calculation processes to solve. The modelling of multiple towed bodies would require substantial modification resulting in a complex and cumbersome solution procedure. In addition, the model fails under slack cable conditions, since the equations are ultra-hyperbolic and has an infinite number of equally valid solutions. Therefore, this technique was not pursued further for the use of the defined two-part and multi-tow systems.

2.2.2 Finite Difference Method

The partial differential equations obtained in (2.9) have been solved by various authors using a number of finite difference techniques. These methods are explained in detail in Ablow and Schechter (1983), Milinazzo *et al.* (1987), and Brook (1990),

with the first two dealing with underwater towed systems. A brief explanation of the method outlined in Brook (1990) is given below.

In this method the cable is divided into a number of segments (say n), and equations describing the motion of each of these segments are developed as explained in sub-section 2.2.1. Then a finite difference technique is used to force a solution to the known boundary conditions.

In sub-section 2.2.1, the set of partial differential equations explaining the motion of the cable was given by equation (2.9). Therefore, for each node along the cable there will be a set of six equations.

In order to control the numerical stability of the solution, visco-elastic damping (κ) is included in equation (2.8) as shown in Brook (1990) to give,

$$v \cdot \frac{\partial T}{\partial t} + T = AE \left(\epsilon + \kappa \cdot \frac{\partial \epsilon}{\partial t} \right) \quad (2.16)$$

where

- A : cross sectional area of cable
- E : modulus of elasticity
- κ : visco-elastic damping coefficient
- v : coefficient to allow for hysteresis

Using equations (2.9) and equation (2.16), a system of coupled non-linear first order partial differential equations are obtained, which are presented in matrix form as,

$$\frac{\partial \bar{U}}{\partial t} + \underline{\underline{Au}} \frac{\partial \bar{U}}{\partial s} + \underline{\underline{Bu}} = 0 \quad (2.17)$$

where

- \bar{U} : vector consisting of $[V_x, V_y, V_z, T, \epsilon, \phi, \psi]^T$
- $\underline{\underline{Au}}$: 7x7 matrix
- $\underline{\underline{Bu}}$: 7x1 matrix

A finite difference technique is now developed to solve the above set of equations subject to the known boundary conditions. The method shown here is based on a Taylor series expansion and solved iteratively using Newton's method.

Since the matrices in equation (2.17) are dependent on time (t) and space (s), they can be defined as,

$$\bar{U}_i^t = \bar{U}(s_i, t_i) \quad (2.18a)$$

$$\underline{\underline{Au}}_i^t = \underline{\underline{Au}}[\bar{U}(s_i, t_i)] \quad (2.18b)$$

$$\underline{\underline{Bu}}_i^t = \underline{\underline{Bu}}[\bar{U}(s_i, t_i)] \quad (2.18c)$$

where s_i and t_i denote a position and time give by $i\Delta s$ and $t\Delta t$ respectively. Δs and Δt are the space and time increments.

Therefore, the matrix equation (2.17) can be expressed as a finite difference approximation by,

$$\frac{\partial \bar{U}_i^{t+1}}{\partial t} + \frac{\partial \bar{U}_i^t}{\partial t} + \underline{\underline{Au}}_i^{t+1} \frac{\partial \bar{U}_i^{t+1}}{\partial s} + \underline{\underline{Au}}_i^t \frac{\partial \bar{U}_i^t}{\partial s} + \underline{\underline{Bu}}_i^{t+1} + \underline{\underline{Bu}}_i^t = 0 \quad (2.19)$$

Now using Taylor's theorem to expand \bar{U}_i^t with respect to time "t",

$$\begin{aligned} \bar{U}_i^{t+1} &= \bar{U}_i^t + \Delta t \frac{\partial \bar{U}_i^t}{\partial t} + \frac{\Delta t^2}{2} \frac{\partial^2 \bar{U}_i^t}{\partial t^2} + 0(\Delta t^3) \\ \bar{U}_i^{t-1} &= \bar{U}_i^t - \Delta t \frac{\partial \bar{U}_i^t}{\partial t} + \frac{\Delta t^2}{2} \frac{\partial^2 \bar{U}_i^t}{\partial t^2} + 0(\Delta t^3) \end{aligned} \quad (2.20)$$

Rearranging the above equations to express the partial derivatives with respect to time, substituting them into equation (2.19), and neglecting the higher order terms gives,

$$\bar{U}_i^{t+1} - \bar{U}_i^t + \frac{\Delta t}{2} \left(\underline{\underline{Au}}_i^{t+1} \frac{\partial \bar{U}_i^{t+1}}{\partial s} + \underline{\underline{Au}}_i^t \frac{\partial \bar{U}_i^t}{\partial s} + \underline{\underline{Bu}}_i^{t+1} + \underline{\underline{Bu}}_i^t \right) = 0 \quad (2.21)$$

Now by using Taylor's theorem to expand \bar{U}_i^t with respect to "s",

$$\begin{aligned}\bar{U}_i^{t+1} &= \bar{U}_i^t + \Delta s \frac{\partial \bar{U}_i^t}{\partial s} + \frac{\Delta s^2}{2} \frac{\partial^2 \bar{U}_i^t}{\partial s^2} + O(\Delta s^3) \\ \bar{U}_i^{t-1} &= \bar{U}_i^t - \Delta s \frac{\partial \bar{U}_i^t}{\partial s} + \frac{\Delta s^2}{2} \frac{\partial^2 \bar{U}_i^t}{\partial s^2} + O(\Delta s^3)\end{aligned}\tag{2.22}$$

The partial derivatives can be approximated by rearranging the above equations. Substituting these into equation (2.21) gives the finite difference scheme as,

$$\begin{aligned}\bar{G}(\bar{U}) &= \bar{U}_i^{t+1} + \frac{\Delta t}{4\Delta s} \underline{\underline{Au}}^{t+1} (\bar{U}_{i+1}^{t+1} + \bar{U}_i^{t+1}) + \frac{\Delta t}{2} \underline{\underline{Bu}}^{t+1} - \bar{U}_i^t \\ &+ \frac{\Delta t}{4\Delta s} \underline{\underline{Au}}^t (\bar{U}_{i+1}^t + \bar{U}_i^t) + \frac{\Delta t}{2} \underline{\underline{Bu}}^t = 0\end{aligned}\tag{2.23}$$

The terms in equation (2.23) include the boundary conditions, (*e.g.* the values at the cable ends). In addition, the parameters at time “*t*”, *i.e.* \bar{U}_i^t , are known from the previous time step. For the first iteration this is taken from the quasi-static configuration.

The equations are solved iteratively using Newton’s method, *i.e.*,

$$\bar{U}^{k+1} = \bar{U}^k + \Delta \bar{U}\tag{2.24}$$

where

\bar{U} : vector consisting of $[V_x, V_y, V_z, T, \epsilon, \phi, \psi]^T$
 $\Delta \bar{U}$: correction value of vector \bar{U}
k : iteration index

The correction value $\Delta \bar{U}$ can be obtained by solving the finite difference linear system. Thus,

$$\bar{G}(\bar{U}) + \frac{\partial \bar{G}(\bar{U})}{\partial \bar{U}} \cdot \Delta \bar{U} = 0\tag{2.25}$$

This produces a system of linear equations in the form of a *block tri-diagonal* system. The solution can be achieved by alternate column and row pivoting strategy or any other compatible technique.

Note: the term $\frac{\partial \overline{G}(\overline{U})}{\partial \overline{U}}$ is the Jacobian of the system of equations in (2.25), and can be expressed as,

$$\frac{\partial \bar{G}(\bar{U})}{\partial \bar{U}} = \begin{bmatrix} \underline{\underline{A}}_{0,1} & \underline{\underline{A}}_{0,2} & & & \\ \underline{\underline{A}}_{1,0} & \underline{\underline{A}}_{1,1} & \underline{\underline{A}}_{1,2} & & \\ & & & \underline{\underline{A}}_{m,m-1} & \underline{\underline{A}}_{m,m} & \underline{\underline{A}}_{m,m+1} \\ & & & & & \\ & & & & & \underline{\underline{A}}_{n-1,n-2} & \underline{\underline{A}}_{n-1,n-1} & \underline{\underline{A}}_{n-1,n} \\ & & & & & & \underline{\underline{A}}_{n,n-1} & \underline{\underline{A}}_{n,n} \end{bmatrix} \quad (2.26)$$

where each term in the matrix is a *block* consisting of the partial differential of $G(u)$ with respect to each of the relevant parameters.

For example, $\underline{A}_{1,2}$ is a 7x7 block and will be in the form,

$$\mathbf{A}_{1,2} = \begin{bmatrix} \frac{\partial \bar{G}(\bar{U}_{u1})}{\partial \bar{U}_{u2}} & \frac{\partial \bar{G}(\bar{U}_{u1})}{\partial \bar{U}_{v2}} & \frac{\partial \bar{G}(\bar{U}_{u1})}{\partial \bar{U}_{w2}} & \frac{\partial \bar{G}(\bar{U}_{u1})}{\partial \bar{U}_{T2}} & \text{etc} & \text{etc} & \frac{\partial \bar{G}(\bar{U}_{u1})}{\partial \bar{U}_{\psi2}} \\ \frac{\partial \bar{G}(\bar{U}_{v1})}{\partial \bar{U}_{u2}} & \frac{\partial \bar{G}(\bar{U}_{v1})}{\partial \bar{U}_{v2}} & \frac{\partial \bar{G}(\bar{U}_{v1})}{\partial \bar{U}_{w2}} & & & & \\ \frac{\partial \bar{G}(\bar{U}_{w1})}{\partial \bar{U}_{u2}} & & \text{etc} & & & & \\ \frac{\partial \bar{G}(\bar{U}_{T1})}{\partial \bar{U}_{u2}} & & & \text{etc} & & & \\ \text{etc} & & & & \text{etc} & & \\ \text{etc} & & & & & \text{etc} & \\ \frac{\partial \bar{G}(\bar{U}_{\psi1})}{\partial \bar{U}_{u2}} & & & & & & \frac{\partial \bar{G}(\bar{U}_{\psi1})}{\partial \bar{U}_{\psi2}} \end{bmatrix} \quad (2.27)$$

However, a large number of the terms will be zero. Thus, although the number of equations are $(7n-1)$, the calculation and computer memory / time required will be lower. Once the angles of the cable segments are known, their positions can be calculated from equations (2.2).

The numerical procedure can be summarised as:

Step 1: Compute $\overline{G}(\overline{U})$ from equation (2.23) and the coefficients for the system of block matrices (2.26), for all nodes using the values obtained for the previous time step.

Step 2: Solve the system of equations (2.25) to give the correction values for the required parameters.

Step 3: Update the parameters, (using equation (2.24)).

Step 4: Go back to steps 1 to 3 until sufficient convergence is achieved.

Step 5: Go to the next time step and repeat steps 1 to 4 until end of simulation.

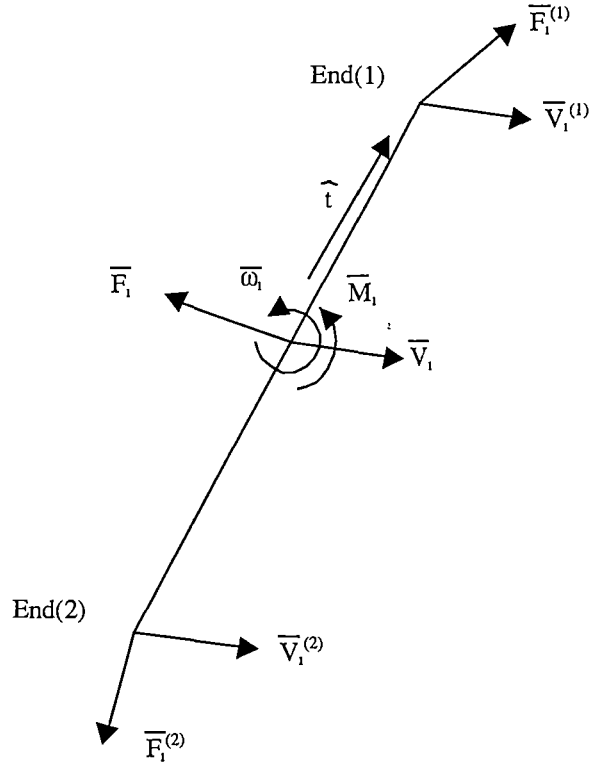
As the mathematical modelling follows the explanation in sub-section 2.2.1, the mathematical representation of the discontinuity due to the cable junction and the inclusion of parallel multi-tows will significantly increase the complexity. As seen from equations (2.26) and (2.27), the number of equations required to be solved is large, especially if a large number of cable segments are used. Thus, the inclusion of cable junctions or multiple tow configurations will substantially increase the number of equations and the complexity involved in the solution. Therefore, this technique was not pursued further for the use of the defined two-part and multi-tow systems.

2.2.3 Hinged Rod Method

Chapmen (1987) employed a hinged rod method to solve underwater towed body systems. A similar method was previously proposed by Winget and Huston (1976), with differences, especially in the solution technique, where the multiple evaluation *Runge-Kutta* scheme is utilised. In this sub-section a brief description of the former model, including its development and solution technique is given. For a detailed explanation the reader is referred to Chapmen (1987).

The hinged rod cable model is developed by dividing the cable into a number of rigid, non-extensible rods, with their mass uniformly distributed along the rod. Each rod is connected to the adjacent rods by frictionless ball joints that allows it to rotate in any direction, except spin along its axis. Figure 2.4 shows an element of a hinged rod cable, for which equations of motion are then developed.

Vectors and tensor are used in the equations to simplify their manipulation, *i.e.* they will be devoid of coordinates. The resulting final equations can then be solved using the components of the vectors.



Hinged Rod Segment

Figure 2.4

Applying Newton's equation of motion to the centre of gravity of rod element "i" in the linear and angular directions (see Figure.2.4), gives,

$$\mu_c l \dot{\vec{V}} = \vec{F}^{(1)} + \vec{F}^{(2)} + \vec{F} \quad (2.28)$$

$$\frac{1}{12} \mu_c l^3 \dot{\vec{\omega}} = \vec{M} + \frac{1}{2} l \hat{t} \times (\vec{F}^{(1)} - \vec{F}^{(2)}) \quad (2.29)$$

where

\vec{F} : force acting on the rod element

\vec{M} : moment acting on rod element

μ_c : mass per unit length of the cable

l : length of the rod element

$\bar{\mathbf{V}}$: linear velocity vector of rod element
 $\bar{\boldsymbol{\omega}}$: angular velocity vector of rod element
 $\hat{\mathbf{t}}$: unit vector in rod direction from bottom to top

and the superscripts are

(1) : top of rod
 (2) : bottom of rod

Note: the subscript “i” has been dropped for the sake of clarity. From Newton’s third law and kinematic considerations, it is seen that,

$$\bar{\mathbf{F}}_i^{(1)} = -\bar{\mathbf{F}}_{i-1}^{(2)} \quad (2.30)$$

$$\bar{\mathbf{V}}_i^{(1)} = \bar{\mathbf{V}}_{i-1}^{(2)} \quad (2.31)$$

$$\dot{\bar{\mathbf{V}}} = \frac{1}{2}(\dot{\bar{\mathbf{V}}}^{(1)} + \dot{\bar{\mathbf{V}}}^{(2)}) \quad (2.32)$$

$$l\dot{\bar{\boldsymbol{\omega}}} \times \hat{\mathbf{t}} = \dot{\bar{\mathbf{V}}}^{(1)} - \dot{\bar{\mathbf{V}}}^{(2)} + l\dot{\bar{\boldsymbol{\omega}}}^2 \hat{\mathbf{t}} \quad (2.33)$$

Note: $|\bar{\mathbf{F}}_i^{(1)}|$ is the tension of the i^{th} rod.

Now using equations (2.30) to (2.33), to manipulate equations (2.28) and (2.29), it is possible to eliminate $\dot{\bar{\mathbf{V}}}$ and $\dot{\bar{\boldsymbol{\omega}}}$, and to express $\bar{\mathbf{F}}^{(2)}$ and $\dot{\bar{\mathbf{V}}}^{(2)}$ as functions of $\bar{\mathbf{F}}^{(1)}$ and $\dot{\bar{\mathbf{V}}}^{(1)}$. Thus,

$$\dot{\bar{\mathbf{V}}}^{(2)} = \{-2(\underline{\mathbf{1}} - \hat{\mathbf{t}}\hat{\mathbf{t}}) + \hat{\mathbf{t}}\hat{\mathbf{t}}\} \cdot \dot{\bar{\mathbf{V}}}^{(1)} + \frac{6}{m}(\underline{\mathbf{1}} - \hat{\mathbf{t}}\hat{\mathbf{t}}) \cdot \left(\frac{1}{2}\bar{\mathbf{F}} + \bar{\mathbf{F}}^{(1)} + \frac{1}{l}\bar{\mathbf{M}} \times \hat{\mathbf{t}}\right) + l\omega\hat{\mathbf{t}} \quad (2.34)$$

$$\bar{\mathbf{F}}^{(2)} = \{2(\underline{\mathbf{1}} - \hat{\mathbf{t}}\hat{\mathbf{t}}) - \hat{\mathbf{t}}\hat{\mathbf{t}}\} \cdot \bar{\mathbf{F}}^{(1)} + \frac{1}{2}\{(\underline{\mathbf{1}} - \hat{\mathbf{t}}\hat{\mathbf{t}}) - 2\hat{\mathbf{t}}\hat{\mathbf{t}}\} \cdot (\bar{\mathbf{F}} - m\dot{\bar{\mathbf{V}}}^{(1)} + \frac{6}{l}\bar{\mathbf{M}} \times \hat{\mathbf{t}} - \frac{1}{2}ml\omega^2\hat{\mathbf{t}}) \quad (2.35)$$

where $m = \mu_c l$.

The forces and accelerations at the bottom of the rod are related to those at the top *via* equations (2.34) and (2.35). Therefore, by using equations (2.30) and (2.31), it is possible to obtain the forces and accelerations at the top of the next rod, (*i.e.* rod $i+1$).

At the bottom of the cable, the towed fish is modelled as a lumped mass to give,

$$\bar{\mathbf{F}}_{n+1} - \bar{\mathbf{F}}_n^{(2)} = m_f \dot{\bar{\mathbf{V}}}_n^{(2)} \quad (2.36)$$

where “n” is the number of rod elements used in the modelling and m_f is the mass of the fish.

However, as shown in Chapmen (1987), the use of an iterative “shooting” method, working from the top to meet the dynamic constraints of the fish at the bottom, proved to be numerically unstable for a system represented by 5 rods or more. In this method, a value for the force at the top ($\bar{\mathbf{F}}_1^{(1)}$) is *chosen* and the forces and accelerations of all the rods are calculated using equations (2.34) and (2.35). The acceleration of the last link, thus obtained should satisfy equation (2.36). If not, the value for $\bar{\mathbf{F}}_1^{(1)}$ is modified and the procedure repeated until equation (2.36) is satisfied.

The resulting instability is explained as being due to the solution method not being correctly relating to the physics of the rod system. There is only *one* force at the top that will induce a given acceleration at the fish, and the use of arbitrary values create large errors that propagate down the cable.

In order to overcome this, a direct functional relationship between the forces and accelerations at the top of each rod and the tow fish was developed. This was achieved by a “tensor” to connect the forces and accelerations. This concept can be understood by considering the application of an additional force to a joint of the rod element. The resulting acceleration of the rod will not necessarily be in a direction parallel to that force.

This relationship can be represented for element “i” as,

$$\bar{\mathbf{F}}_i^{(1)} = \underline{\underline{\mathbf{m}}}_i \cdot \dot{\bar{\mathbf{V}}}_i^{(1)} + \bar{\mathbf{f}}_i \quad (2.37)$$

where

$\bar{\mathbf{f}}_i$: “residual force” vector representing the force required to prevent the acceleration of the top of the rod

$\underline{\underline{\mathbf{m}}}_i$: second rank mass tensor describing the anisotropic mass properties of each rod

and from equation (2.36) for the fish, the element at the bottom of the cable gives,

$$\underline{\underline{m}}_{n+1} = m_f \underline{\underline{1}} \quad (2.38a)$$

$$\bar{f}_{n+1} = \bar{F}_{n+1} \quad (2.38b)$$

which are known.

Using equations (2.30), (2.31), (2.34), (2.35), and (2.37), it is possible to develop a recursive relationship to express $\underline{\underline{m}}_i$ and \bar{f}_i in terms of $\underline{\underline{m}}_{i+1}$ and \bar{f}_{i+1} . Thus,

$$\underline{\underline{P}}_i = A^{-1} \cdot \{(1 + r_i) \underline{\underline{1}} - r_i \underline{\underline{P}}_{i+1}\} \quad (2.39)$$

$$\bar{f}_i = A^{-1} \cdot \left\{ \frac{1}{2} \bar{F} - \frac{\bar{M} \times \hat{t}}{1} - \bar{f}_{i+1} - \frac{1}{2} m l \bar{\omega}^2 [(1 + r_i) \underline{\underline{1}} - r_i \underline{\underline{P}}_{i+1}] \cdot \hat{t} \right\} - \frac{1}{2} \bar{F} - \frac{\bar{M} \times \hat{t}}{1} \quad (2.40)$$

where

$$A^{-1} = 3\{(1 + r_i) \underline{\underline{1}} - r_i \underline{\underline{P}}_{i+1}\} \cdot (\underline{\underline{1}} - \hat{t} \hat{t}) - \underline{\underline{1}}$$

$$\underline{\underline{P}}_i = \underline{\underline{1}} - \frac{2 \underline{\underline{m}}_i}{m_i}$$

$$r_i = \frac{m_{i+1}}{m_i}$$

From equations (2.38) the values for $\underline{\underline{m}}_i$ and \bar{f}_i are known for $i = n$, (*i.e.* the tow fish). Therefore, it is possible to start from the bottom, calculate $\underline{\underline{m}}_i$ and \bar{f}_i for all rods, and store them. Since the acceleration at the top ($\dot{\bar{V}}_1^{(1)}$) is known as a boundary condition, using equation (2.37) and (2.31) alternately down the cable will yield the force $\bar{F}_i^{(1)}$ for each rod. At the same time it is possible to calculate the angular acceleration ($\dot{\bar{\omega}}_i$) of each rod and the linear acceleration ($\dot{\bar{V}}_i^{(2)}$) at the bottom of each rod. These two values are obtained by manipulating equations (2.33) and (2.34) to give,

$$l \dot{\bar{\omega}} \times \hat{t} = 3(1 - \hat{t} \hat{t}) \cdot \{ \underline{\underline{P}}_i \cdot \dot{\bar{V}}^{(1)} - \frac{2}{m} (\bar{f}_i + \frac{1}{2} \bar{F} + \frac{\bar{M} \times \hat{t}}{1}) \} \quad (2.41)$$

$$\dot{\bar{V}}^{(2)} = \dot{\bar{V}}^{(1)} - l \dot{\bar{\omega}}^2 \hat{t} - l \dot{\bar{\omega}} \times \hat{t} \quad (2.42)$$

If the angular accelerations ($\dot{\omega}$) calculated above are integrated with respect to time, the angular velocities (ω) and the new orientation of the rods (\hat{t}) are obtained. An *Euler* type integrator, modified for second order equations is the integration method used in Chapmen (1987). This is briefly described below.

A Taylor series expansion about time “t” yields,

$$\hat{t}(t + \Delta t) = \hat{t}(t) + \Delta t \cdot \dot{\hat{t}}(t) + \frac{1}{2} \Delta t^2 \cdot \ddot{\hat{t}}(t) + \frac{1}{6} \Delta t^3 \cdot \dddot{\hat{t}}(t + \alpha \Delta t) + \dots \quad (2.43a)$$

$$\dot{\hat{t}}(t + \Delta t) = \dot{\hat{t}}(t) + \Delta t \cdot \ddot{\hat{t}}(t) + \frac{1}{2} \Delta t^2 \cdot \dddot{\hat{t}}(t + \beta \Delta t) + \dots \quad (2.43b)$$

where t is the time, Δt is the time increment, and \hat{t} is the unit vector in the direction of the rod. Using,

$$\dot{\hat{t}} = \omega \times \hat{t} \quad (2.44)$$

and normalising at each step gives the increments at $t + \Delta t$ as,

$$\hat{t}(t + \Delta t) = \frac{\hat{t}'}{|\hat{t}'|} \quad (2.45)$$

$$(\bar{\omega} \times \hat{t})(t + \Delta t) = \left(\underline{1} - |\hat{t}'|^{-2} \hat{t}' \hat{t}' \right) \cdot (\bar{\omega} \times \hat{t} + \Delta t \bar{\dot{\omega}} \times \hat{t}) \quad (2.46)$$

where

$$\hat{t}' = \hat{t} + \Delta t (\bar{\omega} \times \hat{t}) + \frac{1}{2} \Delta t^2 \bar{\dot{\omega}} \times \hat{t}$$

The truncation error is given by,

$$\text{Error} = \frac{\Delta t^2 \{ (\bar{\dot{\omega}} \times \hat{t})(t + \Delta t) - (\bar{\dot{\omega}} \times \hat{t})(\hat{t}) \}}{6} \quad (2.47)$$

The numerical procedure can be summarised as:

- Step 1:** Obtain all initial values (say from quasi-static model) and the boundary conditions (at the surface vessel).
- Step 2:** Calculate the acceleration of the fish, (which is also equal to $\dot{\bar{V}}_n^{(2)}$), using (2.38) and (2.37).
- Step 3:** Calculate and store \underline{P}_i and \bar{f}_i , starting from the bottom and recursively using (2.39) and (2.40).
- Step 4:** Calculate $\dot{\bar{V}}_i^{(1)}$, $\bar{F}_i^{(1)}$, and the rod tension ($|\dot{\bar{F}}_i^{(1)}|$), starting from the top ($i = 1$) and using (2.31) and (2.37).
- Step 5:** Use (2.41) and (2.42) to calculate the linear and angular accelerations $\dot{\bar{V}}_i^{(2)}$ and $(\dot{\bar{\omega}}_i \times \hat{t}_i)$
- Step 6:** Go to the next rod ($i+1$) and repeat steps 4 and 5, until the bottom is reached.
- Step 7:** Use (2.45) and (2.46) to integrate acceleration by Δt to give the new orientation of cable.
- Step 8:** Calculate truncation error from (2.47).
- Step 9:** If the error is greater than a predetermined value, restore to original configuration, reduce size of Δt and repeat steps 7 and 8 until the error is acceptable.
- Step 10:** Go to the next time step and repeat steps 1 to 9 until end of simulation.

In Henderson and Wright (1991), the hinged rod cable model was modified to represent a two-part tow. However, it is limited to deal with the situation shown in Figures 1.1(b, c, e, and g), *i.e.* where the secondary cables are connected to or adjacent to the preceding depressor / tow fish. It is not possible to successfully model configurations that have a “junction” located midway along the primary cable, *i.e.* as shown in Figures 1.1(d, f, h, and i).

The incorporation of the junction in the hinged rod model would be tedious. It would also complicate the representation of the parallel multi-tow configuration shown in Figure 1.1(i). In addition, as the model does not support longitudinal wave propagation, it cannot represent the dynamic effect due to rapid cable top motion. Thus, it is more suited to investigate the behaviour due to slowly changing conditions such as ship manoeuvring. Due to these shortcomings, this technique was not developed to model the defined two-part and multi-tow systems.

2.2.4 Finite Element Method

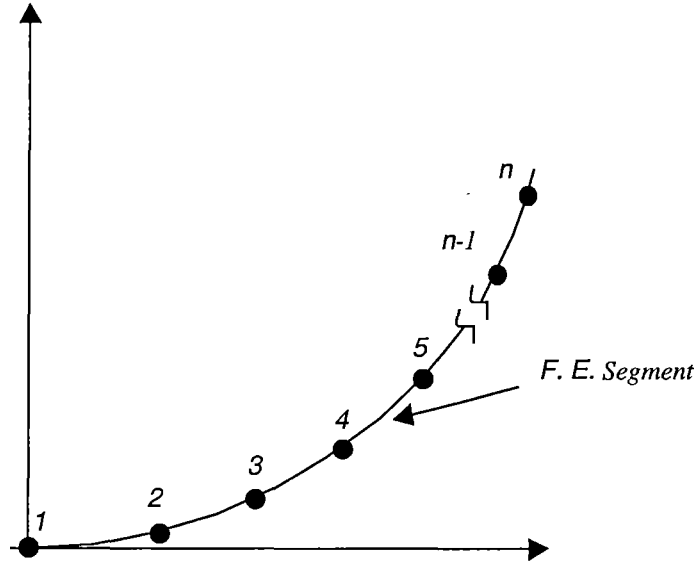
This method is used extensively in the modelling of mooring cables and flexible risers and is considered by many to be sufficiently flexible to meet a variety of conditions and configurations. Examples of finite element cable models include Leonard (1973), Johansson (1977), Peyrot (1980), Leonard and Nath (1981), Lindahl and Sjoberg (1983), McNamara *et al.* (1986), Kokkinowrachos *et al.* (1987), and Haritos and He (1989). It is also used in the modelling of towed cables as shown in Webster (1975) and Delmer *et al.* (1983).

There are a number of approaches to modelling cable systems using finite elements and it is not intended to explain all of these methods in detail here. However, a brief description of the general approach is given below for the sake of completeness. For more information, the readers are referred to the above references.

The basic concept of the finite element method is the representation of a cable by a series of elements (segments) joined together at nodes. The shape and configuration of the element used will depend on the modelling method employed. These include straight segments as in Johansson (1977) and curved segments as explained in Haritos and He (1989). In addition, Peyrot (1980) uses the basic catenary equation to develop the finite element configuration. In this section we will look at a finite element model based on straight elements. A curved element will only require slight modification to the equations, (*e.g.* the shape functions), and is described in detail by Leonard (1973) and Haritos and He (1989).

The finite element method is based upon a known equilibrium system. The model then calculates the motion *from* this equilibrium position due the forces acting on the cable elements.

The cable is considered to be a long slender structure with negligible moments and shear forces. It is divided into a number of straight elements connected at nodes as shown in Figure 2.5. As the modelling is carried out in three-dimensions, each node will have three degrees of freedom. The motion of the cable is described by the motion of the nodes.



Finite Element Model

Figure 2.5

The equations for the elements are developed through a Lagrangian approach. Forces distributed along the element are transformed to equivalent nodal forces through the principle of virtual work. Considering Figure 2.6, a distributed force on the element is represented by the shape function $\bar{\varphi}(s)$. The equivalent nodal forces can then be obtained as,

$$\bar{F}_1 = \int_0^1 (1 - \xi) \bar{\varphi}(\xi) d\xi \quad (2.48a)$$

$$\bar{F}_{i+1} = \int_0^1 \xi \bar{\varphi}(\xi) d\xi \quad (2.48b)$$

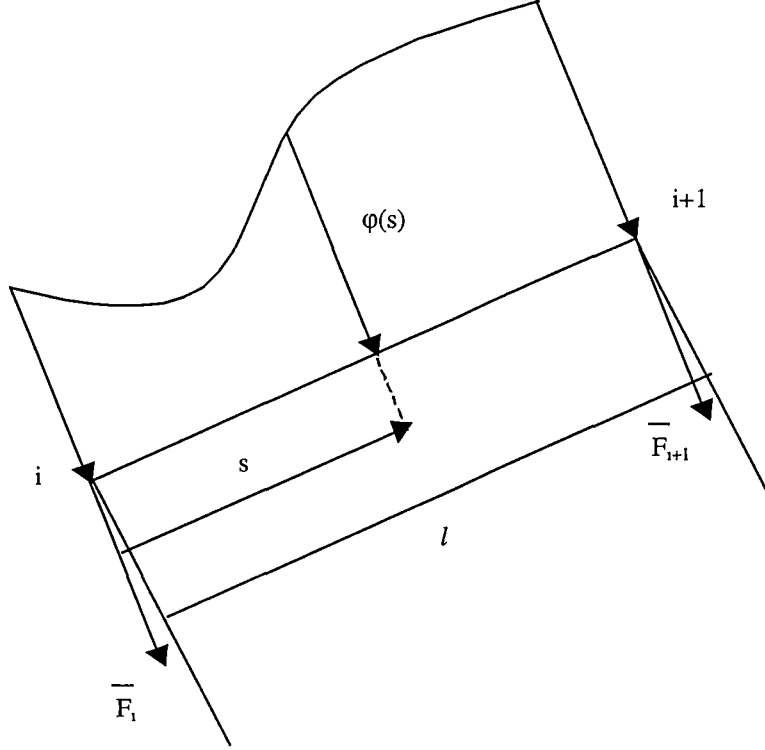
where

\bar{F}_i : equivalent nodal force on node “i”

$\bar{\varphi}(s)$: shape function of the distributed force

l_i : length of element

$\xi = \frac{s}{l_i}$, where “s” is the variable length along the element



Equivalent Nodal Forces on Finite Element

Figure 2.6

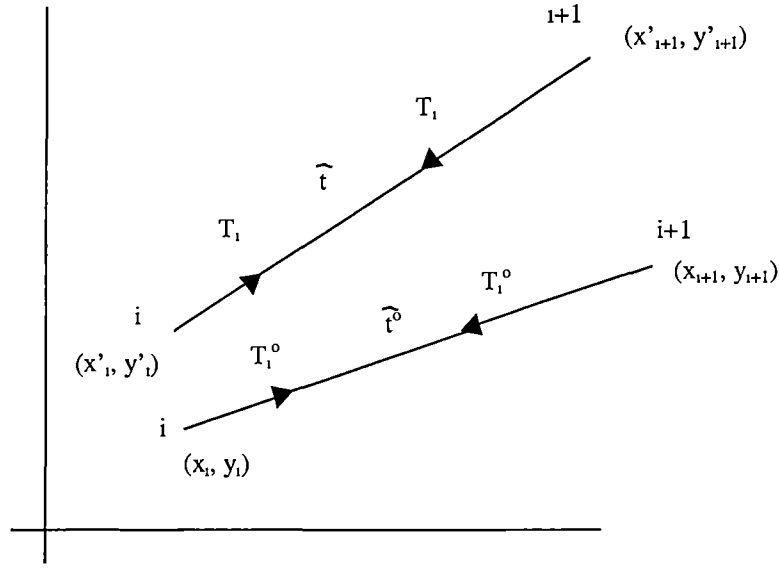
The forces acting on the cable element will consist of the following:

Tension Forces: Consider Figure 2.7. The element shown by the unit vector “ \hat{t}^o ” is in equilibrium state and has a length of l_i^o . The tension along the element at this configuration is given as T_i^o , and will act at the two nodes as,

$$\bar{F}_{T,i}^o = T_i^o \cdot \hat{t}^o \quad (2.49a)$$

$$\bar{F}_{T,i+1}^o = -T_i^o \cdot \hat{t}^o \quad (2.49b)$$

where $\bar{F}_{T,i}^o$ is the tension vector acting on node “i”.



Tension Forces in Finite Element

Figure 2.7

During motion, the element is displaced and undergoes changes in length and orientation to a position described by the unit vector “ \hat{t} ”. The new length and tension of the element are respectively,

$$l_i = l_i^0 + \Delta l_i \quad (2.50)$$

$$T_i = T_i^0 + k_E \cdot \Delta l_i \quad (2.51)$$

where “ k_E ” is the elastic stiffness of the element. Thus, the nodal forces can be written as,

$$\bar{F}_{T,i} = T_i \cdot \hat{t} \quad (2.52a)$$

$$\bar{F}_{T,i+1} = -T_i \cdot \hat{t} \quad (2.52b)$$

Therefore, the deviation of the nodal forces are,

$$\Delta \bar{F}_{T,i} = T_i \cdot \hat{t} - T_i^0 \cdot \hat{t}^0 \quad (2.53a)$$

$$\Delta \bar{F}_{T,i+1} = -T_i \cdot \hat{t} + T_i^0 \cdot \hat{t}^0 \quad (2.53b)$$

For a small deviation from the equilibrium position, the nodal forces (dropping the subscript “i” for clarity) are,

$$\bar{\mathbf{F}}_T = \bar{\mathbf{F}}_T^o - (\underline{\mathbf{k}}_E + \underline{\mathbf{k}}_G) \bar{\mathbf{R}} \quad (2.54)$$

where

$\underline{\mathbf{k}}_E$: elastic stiffness matrix

$\underline{\mathbf{k}}_G$: geometric stiffness matrix

$\bar{\mathbf{R}}$: displacement vector away from the equilibrium.

Thus, the tension forces for an arbitrary displacement “ $\bar{\mathbf{R}}$ ” from the equilibrium are,

$$\bar{\mathbf{F}}_T = \bar{\mathbf{F}}_T^o - (\underline{\mathbf{k}}_E + \underline{\mathbf{k}}_G) \bar{\mathbf{R}} + \Delta \bar{\mathbf{F}}_T \quad (2.55)$$

The elastic and geometric stiffness matrices for an axial element with three linear degrees of freedom at each end are obtained from,

$$\underline{\mathbf{k}}_E = [\Lambda]^T \cdot \underline{\mathbf{k}}_{EL} \cdot [\Lambda] \quad (2.56)$$

$$\underline{\mathbf{k}}_G = [\Lambda]^T \cdot \underline{\mathbf{k}}_{GL} \cdot [\Lambda] \quad (2.57)$$

where

$[\Lambda]$: transformation matrix, given in equation (2.3)

$[\Lambda]^T$: transpose of $[\Lambda]$

A_i : cross-sectional area of the cable

E : modulus of elasticity of the cable material.

and

$$\underline{\mathbf{k}}_{EL} = \text{local elastic stiffness matrix} = \frac{A_1 E}{l_1} \begin{bmatrix} 1 & 0 & 0 & -1 & 0 & 0 \\ 0 & 0 & 0 & 0 & 0 & 0 \\ 0 & 0 & 0 & 0 & 0 & 0 \\ -1 & 0 & 0 & 1 & 0 & 0 \\ 0 & 0 & 0 & 0 & 0 & 0 \\ 0 & 0 & 0 & 0 & 0 & 0 \end{bmatrix}$$

$$\underline{\underline{k}}_{GL} = \text{local geometric stiffness matrix} = \frac{T_1^0}{l_1^0} \begin{bmatrix} 0 & 0 & 0 & 0 & 0 & 0 \\ 0 & 1 & 0 & 0 & -1 & 0 \\ 0 & 0 & 1 & 0 & 0 & -1 \\ 0 & 0 & 0 & 0 & 0 & 0 \\ 0 & -1 & 0 & 0 & 1 & 0 \\ 0 & 0 & -1 & 0 & 0 & 1 \end{bmatrix}$$

Other Forces: The other forces included are the weight, buoyancy force, transverse and tangential drag forces, axial viscous force, and point loads. The equivalent nodal forces for any force that is distributed along the cable, *e.g.* transverse drag force, are obtained as explained in equations (2.48).

The inertia $\underline{\underline{m}}_L$ and hydrodynamic inertia (added mass, $\underline{\underline{Am}}$) matrices are described as,

$$\underline{\underline{m}}_L = \text{local mass matrix} = \frac{\mu_c l_1}{6} \begin{bmatrix} 2 & 0 & 0 & 1 & 0 & 0 \\ 0 & 2 & 0 & 0 & 1 & 0 \\ 0 & 0 & 2 & 0 & 0 & 1 \\ 1 & 0 & 0 & 2 & 0 & 0 \\ 0 & 1 & 0 & 0 & 2 & 0 \\ 0 & 0 & 1 & 0 & 0 & 2 \end{bmatrix} \quad (2.58)$$

$$\underline{\underline{Am}} = [\Lambda]^T \cdot \underline{\underline{Am}}_L \cdot [\Lambda] \quad (2.59)$$

where

μ_c : mass per unit length of the element

μ_w : mass of the displaced water per unit length of the element

C_m : hydrodynamic inertia coefficient.

and

$$\underline{\underline{Am}}_L = \text{local added mass matrix} = \frac{C_m \mu_w l_1}{6} \begin{bmatrix} 0 & 0 & 0 & 0 & 0 & 0 \\ 0 & 2 & 0 & 0 & 1 & 0 \\ 0 & 0 & 2 & 0 & 0 & 1 \\ 0 & 0 & 0 & 0 & 0 & 0 \\ 0 & 1 & 0 & 0 & 2 & 0 \\ 0 & 0 & 1 & 0 & 0 & 2 \end{bmatrix}$$

The element mass and added mass matrices are merged to give the element total mass matrix ($\underline{\underline{m}}$). Similarly the element elastic and geometric stiffness matrices are merged to give the element total stiffness matrix ($\underline{\underline{k}}$). Thus, the equation of motion for the element can be written as,

$$\underline{\underline{m}}.\ddot{\bar{\mathbf{R}}} + \underline{\underline{c}}.\dot{\bar{\mathbf{R}}} + \underline{\underline{k}}.\bar{\mathbf{R}} = \Delta\bar{\mathbf{F}}_T + \Delta\bar{\mathbf{F}}_D + \Delta\bar{\mathbf{F}}_I = \bar{\mathbf{F}} \quad (2.60)$$

where

- $\underline{\underline{m}}$: element mass matrix including added mass
- $\underline{\underline{c}}$: element damping matrix
- $\underline{\underline{k}}$: element stiffness matrix, including elastic and geometrical stiffness
- $\bar{\mathbf{F}}$: external forces on the element, including: $\Delta\bar{\mathbf{F}}_T$ = tension force deviation, $\Delta\bar{\mathbf{F}}_D$ = drag force deviation, and $\Delta\bar{\mathbf{F}}_I$ = inertia force deviation
- $\bar{\mathbf{R}}$: nodal incremental displacement vector, (*i.e.* displacement from the equilibrium state).

The above set of equations obtained for each element can be assembled to give a set of global equations for the complete system.

This set of non-linear differential equations can be solved either as a general eigenvalue problem or by using a predictor-corrector process such as a modified Newton-Raphson method. Either technique employs numerical integration techniques. The Newmark- β integration scheme (Newmark (1959)), that offers relationships between the nodal displacements, velocities, and accelerations is one of the most common numerical integration techniques used in cable solutions. It is described as,

$$\dot{\bar{\mathbf{R}}}^{t+1} = \dot{\bar{\mathbf{R}}}^t - (1-\gamma)\ddot{\bar{\mathbf{R}}}^t \Delta t + \gamma\ddot{\bar{\mathbf{R}}}^{t+1} \Delta t \quad (2.61)$$

$$\bar{\mathbf{R}}^{t+1} = \bar{\mathbf{R}}^t + \dot{\bar{\mathbf{R}}}^t \Delta t + (1-2\beta)\ddot{\bar{\mathbf{R}}}^t \frac{\Delta t^2}{2} + 2\beta\ddot{\bar{\mathbf{R}}}^{t+1} \frac{\Delta t^2}{2} \quad (2.62)$$

where $0 \leq \gamma \leq 1$ and $0 \leq \beta \leq 1$.

Using the above to obtain the nodal incremental velocity and acceleration vectors ($\dot{\bar{\mathbf{R}}}^{t+1}$ and $\ddot{\bar{\mathbf{R}}}^{t+1}$), and substituting into equation (2.60), the set of non-linear differential equations reduces to a set of non-linear algebraic equations in the form,

$$\underline{\underline{K}}_1 \bar{\mathbf{R}} = \bar{\mathbf{F}}' + \underline{\underline{K}}_2 \dot{\bar{\mathbf{R}}} + \underline{\underline{K}}_3 \ddot{\bar{\mathbf{R}}} \quad (2.63)$$

where

$\underline{\underline{K}}_1, \underline{\underline{K}}_2, \underline{\underline{K}}_3$: global matrices formed through a combination of the matrices in equation (2.60)

$\bar{\mathbf{F}}'$: global equivalent node force vector.

Hence, the matrices for each element given in (2.60) have been superimposed to give the global incremental equation of motion.

The solution procedure uses a modified Newton-Raphson approach. During an iteration process, the *residual* or “out-of-balance” force for equation (2.63) can be expressed as,

$$ER(\bar{\mathbf{R}}) = -\underline{\underline{K}}_1 \bar{\mathbf{R}} + (\bar{\mathbf{F}}' + \underline{\underline{K}}_2 \dot{\bar{\mathbf{R}}} + \underline{\underline{K}}_3 \ddot{\bar{\mathbf{R}}}) \quad (2.64)$$

Thus, the correction to the nodal incremental displacement vector “ $\bar{\mathbf{R}}$ ” is obtained by,

$$\delta(\bar{\mathbf{R}}) = -\underline{\underline{K}}_1^{-1} . ER(\bar{\mathbf{R}}) \quad (2.65)$$

The iteration process is summarised as follows:

- Step 1:** Obtain the initial equilibrium configuration, usually by solving the equation of motion (minus the inertia terms) and the boundary conditions.
- Step 2:** Calculate the nodal external force vectors, and the mass, damping and stiffness matrices.
- Step 3:** Obtain the tentative nodal incremental displacement vector “ $\bar{\mathbf{R}}$ ”, using equation (2.63).
- Step 4:** Recalculate the forces and system matrices for the “new” nodal incremental displacement vector.

- Step 5:** Calculate the “residual” force acting on the cable structure, using equation (2.64).
- Step 6:** Correct the nodal incremental displacement vector “ $\bar{\mathbf{R}}$ ” by the correction factor obtained from equation (2.65).
- Step 7:** Stop the iteration when the solution has converged, *i.e.* when the residual forces for all elements have reached an acceptably low level.
- Step 8:** Proceed to the next time step, “ $t+\Delta t$ ”, and repeat steps 2 to 7 using the “ $\bar{\mathbf{R}}$ ” vector obtained at “ t ”, until end of simulation.

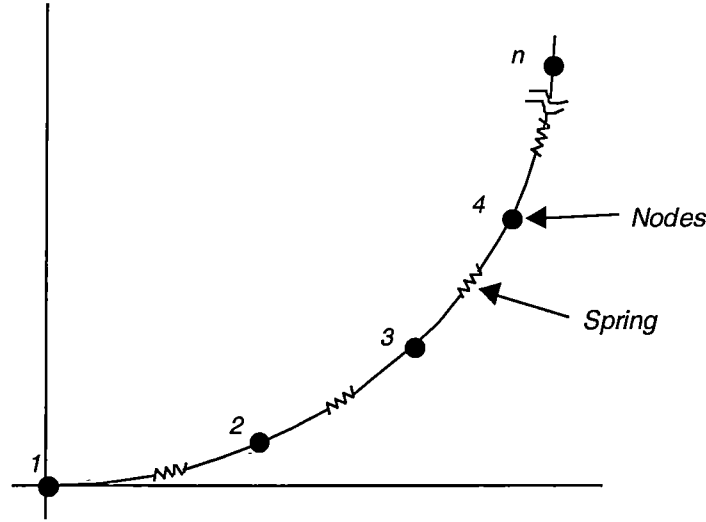
The finite element method would need to be modified to represent two-part tow configurations (with the junction located on the primary cable) and parallel multi-tow configurations. Although the nature of the model allows for such modifications, it offers no advantages over the lumped-mass method explained in sub-section 2.2.5. However, the set of equations for the finite element model were deemed to be more complex than that of the lumped mass system, and the solution process slower due to the use of matrix algebra. For these reasons and the advantages stipulated in sub-section 2.2.5, it was decided not to use the finite element technique to model the required tow configurations. However, it would be beneficial at a later date to compare the lumped-mass model against an equivalent finite element model dealing with two-part and multi-tow configurations.

2.2.5 Lumped-Mass Method

Together with the finite element method, this method is the most frequently used modelling technique for mooring cables and flexible risers. Examples of such lumped mass models are given by Walton and Polachek (1959), Nakajima *et al.* (1982), van den Boom (1985), and Kokkinowrachos *et al.* (1987)). It is also used in the modelling of conventional towed systems as shown in Koterayama *et al.* (1988) and Kamman *et al.* (1989). However, various researchers have resorted to different solution techniques for their models.

In a similar manner to the finite element method, the lumped-mass method divides the cable into a number of segments as shown in Figure 2.8. However, the distributions of the mass and forces are different. The lumped mass model represents the distributed mass of the cable by a series of discrete masses separated by weightless

elastic straight-line segments. The cable segments are assumed incapable of carrying compressive loads or bending moments. However, as shown in Kokkinowrachos *et al.* (1987), it is possible to include the effect of bending moments and shear forces to the overall model, thus enabling the modelling of flexible risers and underwater pipelines. As this method is explained in detail in Chapters 3 and 4, only a short description is given here.



Lumped Mass Model

Figure 2.8

All forces that act on the cable segment are redistributed to the adjacent nodes. Thus, by applying Newton's law of motion for each node, a set of equations of motion for each node is developed. This can be represented as,

$$\underline{\underline{m}} \cdot \ddot{\underline{\underline{R}}} = \underline{\underline{F}} \quad (2.66)$$

where

$\underline{\underline{m}}$: mass matrix including added mass

$\underline{\underline{F}}$: external forces on the node, including gravitational force, damping forces, cable tension, distributed loads, and concentrated loads

$\underline{\underline{R}}$: nodal displacement vector.

This approach replaces the non-linear partial differential equations describing the continuous cable system by a *set of non-linear ordinary differential equations* obtained by superimposing the contributions from all nodes in the cable structure.

The solution of this set of equations is achieved by numerical integration techniques, such as the Newmark- β scheme (equations (2.61) and (2.62)), central difference technique, or the Houbolt scheme (see Bathe (1982)). These schemes offer relationships between the nodal displacements, velocities, and accelerations.

Using tentative tension values, the accelerations of the nodes are obtained from the set of equations given by (2.66). These in turn are used in an appropriate numerical integration technique to predict the displacements and velocities of the nodes. The tentative tension values can then be corrected using a Newton-Raphson iteration process, to meet the constraint placed by the length of each segment. The iteration is continued until acceptable convergence is achieved.

Comparing the solution techniques employed for the lumped mass model and the finite element model, the former requires the solution of a set of simultaneous differential equations while the latter uses matrix algebra.

Due to the redistribution of forces from the segments to the adjacent nodes, the representation of the junction in the towed cable system is simplified. This provides an elegant method of modelling series and parallel multi-tow systems. In addition, the lumping of the forces at the nodes facilitates the integration of the towed fish model(s) with that of the cable(s).

For these reasons, it was decided to select the lumped mass model to represent the towed cable system. As shown in Leonard and Nath (1981) and Kokkinowrachos *et al.* (1987), there is little evidence of any advantage of the finite element method over the lumped-mass method. In fact Hearn and Thomas (1991) and Huang (1992) state that the lumped mass system is the most widely used method for cable modelling, and van den Boom (1985) concludes that the finite element method is less efficient with regard to computer time when compared against an equivalent lumped mass model.

2.3 Cable Drag and Inertia Forces

The relative motion between the cable and the surrounding fluid will result in hydrodynamic drag forces on the cable. In addition, if the cable motion is not steady, then the acceleration of the surrounding fluid will exert inertia or *added mass* forces on the cable.

To investigate the hydrodynamic drag forces on a cable, it is first required to understand how such forces are created on a body within a fluid stream. The hydrodynamic forces are primarily due to shear and pressure effects on the body. Forces are also generated when the body is at an angle of incidence to the flow, *i.e.* when the body undergoes angular displacement from its steady state configuration. Although some analytical methods are available to predict these forces (publications from the US Naval Sea Systems Command Hydromechanics Committee (SEAHAC)), the preferred option is to obtain them using experimental data.

The hydrodynamic forces acting on a body due to the surrounding fluid, will be a function of the density of the surrounding liquid, the relative velocity between the body and the surrounding liquid, the shape and size of the body, and the fluid viscosity. The usual method of expressing these forces is as a function of the “dynamic force”, (*i.e.* $\frac{1}{2}\rho \bar{V}^2$ x geometrical area). Thus, the hydrodynamic forces on the body are expressed as,

$$\bar{F}_H = \frac{1}{2} C_H \rho A_g \bar{V}_r^2 \quad (2.67)$$

where

\bar{F}_H : hydrodynamic force vector

ρ : density of the surrounding fluid

A_g : characteristic area of the body, (usually the cross-sectional area to the flow *or* the surface area)

C_H : hydrodynamic coefficient

\bar{V}_r : relative velocity vector between the body and the surrounding fluid

The hydrodynamic coefficients are non-dimensional and represent the combined effects due to the pressure, viscosity, surface condition, shape, etc. In many cases they are functions of the geometric shape, Reynolds number, Froude number, Weber number, and relative surface roughness. A general explanation of the calculation procedure of these coefficients is given in Abkowitz (1969), while the coefficients for standard shapes are given in Gerhart and Gross (1985).

2.3.1 Flow Past a Smooth Long Rigid Cylinder

A cable is a long, flexible cylinder. Therefore, before we consider the drag on the cable, let us revise the drag on a rigid cylinder. The flow past a cylinder, and

consequently the drag force, is a highly researched area in fluid dynamics. Thus, only a brief description of the work in this area is given.

Flow past a solid body can be considered in two regimes. The first is immediately adjacent to the surface of the body, where viscosity is predominant, hence generating frictional forces. The other is outside the boundary layer, where viscosity can be neglected. However, velocities and pressures are affected by the physical presence of the body, together with the associated boundary layer.

When a body is immersed in a flowing fluid (*i.e.* there is relative motion between the body and the fluid), a force will act on the body. The component of this force in the direction of relative motion is called the **drag** force. The component perpendicular to the drag force is called the **lift** force.

The drag force (also called the **profile drag**) is made up of two components, one which is due to the friction on the surface of the body, *i.e.* skin friction or **friction drag**, and the other which is due to the pressure distribution, *i.e.* the **pressure drag** or **form drag**. The latter depends on the pressure differences across the body, which in turn depend on its shape. Since both pressure and friction drag are dependent on the shape of the body, the total (profile) drag is a function of the shape of the body and its orientation to the flow.

Lift forces are **not** always present. They usually occur only if there is asymmetry, (which may be due to asymmetry of the body or misalignment between the body and the approaching flow). The angle of misalignment is called the “angle of attack”. In cables, a cyclic lift force may occur due to the effects of **vortex shedding**, which is explained later in this sub-section and in sub-section 2.3.6.

If the flow is completely asymmetrical, either due to the three-dimensional body having no symmetrical planes or the flow not being parallel to the symmetrical planes, then the resultant force will have three components. These three components will be perpendicular to each other, and are usually referred to as the **drag**, **lift**, and **side** forces. The latter force will be dealt with in sub-section 2.3.3.

The theoretical approach of calculating the drag and lift forces is difficult as it requires a knowledge of the pressure distribution and the shear stresses around the body. In practice, it is common to obtain drag and lift force components experimentally, *i.e.* in wind tunnels, circulating water channels, or flow tanks. It is usual to express these

forces as related to the fluid density, relative fluid stream velocity, and a characteristic of the body (*e.g.* the projected area of the body in the plane perpendicular to the direction of flow *or* the surface area).

Therefore, from equation (2.67), the drag and lift forces are given as,

$$F_d = 1/2 \cdot C_d \cdot \rho \cdot A \cdot V_r^2 \quad (2.68)$$

$$F_L = 1/2 \cdot C_L \cdot \rho \cdot A \cdot V_r^2 \quad (2.69)$$

where

F_d, F_L : drag and lift forces, respectively

C_d, C_L : drag and lift coefficients, respectively

ρ : density of the surrounding fluid

A : characteristic (usually area) of the body

V_r : relative velocity between the body and the fluid stream.

Since the drag and lift coefficients are non-dimensional, once they have been obtained, they can be used to calculate the drag and lift for geometrically similar bodies, over an equivalent speed range. These coefficients are not constant and will depend on the Reynolds Number (Re), Froude Number (Fr), and the Mach Number (Ma). Usually:

- Re will dominate when viscous forces are dominant;
- Fr will dominate when significant gravity waves are present (wave making drag); and
- Ma will dominate at high compressibility rates associated with flow near the speed of sound.

Other factors (such as surface condition and vibration frequency) may also influence the coefficients.

Consider an infinitely long circular cylinder placed transversely in a fluid stream. Due to the length of the cylinder, end flow can be neglected, giving rise to a two-dimensional flow regime. For a homogeneous fluid flowing past a given cylinder (*i.e.* a constant diameter), Re will be directly proportional to the velocity. Therefore, a change of Re can be imagined as a change in velocity.

In ideal flow, complete pressure recovery will occur across the cylinder placed in the flow. However, in real flow, complete pressure recovery will not occur.

From equation (2.68), the drag on the cylinder can be given as,

$$F_d = 1/2.C_d.\rho.D.l.V_o.|V_o| \quad (2.70)$$

where

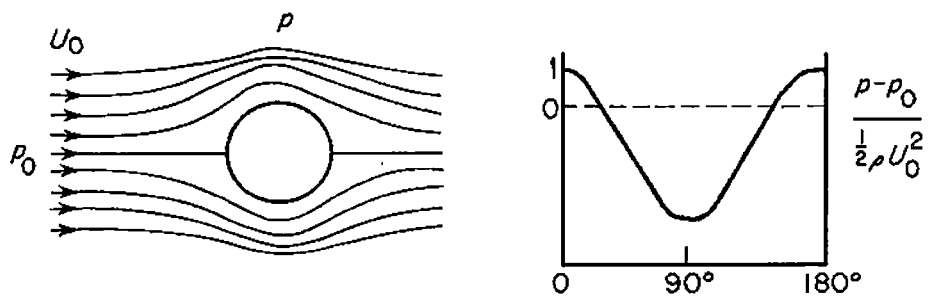
- F_d : drag force
- C_d : drag coefficient
- ρ : density of the surrounding fluid
- D : diameter of cylinder
- l : length of cylinder
- V_o : fluid free stream velocity

The drag coefficient (C_d) will depend on Re , the surface condition, and the shape of the body. Although various researchers have developed analytical and empirical formulae to predict C_d , (*e.g.* Soylemez (1996)), the usual method of prediction employed in practice is based on experimental data.

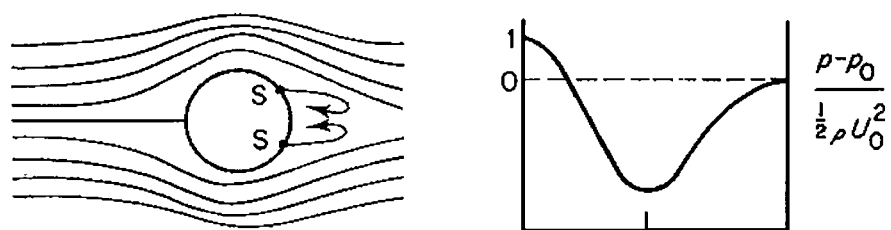
Figure 2.9 (Douglas *et al.* (1985)), gives the change of flow pattern and the pressure variation with the change in Re . Figures 2.10 (Gerhart and Gross (1985)) and 2.11 (Miller (1976)) show the change in the drag coefficient with Re . The former is across the full range of Re , while the latter looks at it across the practical range encountered in marine structures. Note: in Figure 2.11, the separated regimes are described in terms of the boundary layer behaviour near separation.

At low flow velocity ($Re < 0.5$), the inertia effect is negligible, thus allowing for near complete pressure recovery. This gives a near ideal flow-pressure distribution. Hence, the pressure (form) drag is negligible, and the profile drag is nearly all due to friction, (Figure 2.9(a)).

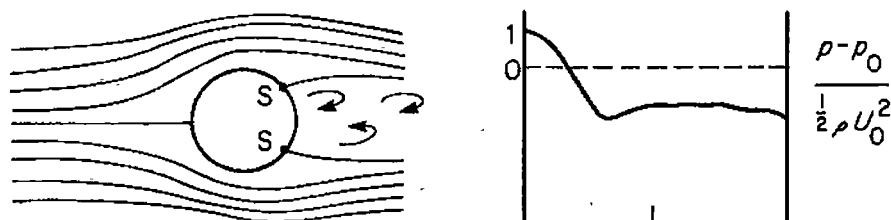
As Re increases to between 2 and 30, separation of the boundary layer will occur, (Figure 2.9(b)). At the points of separation, two symmetrical eddies will be formed rotating in an opposite direction to each other. These remain fixed and the flow will close beyond it.



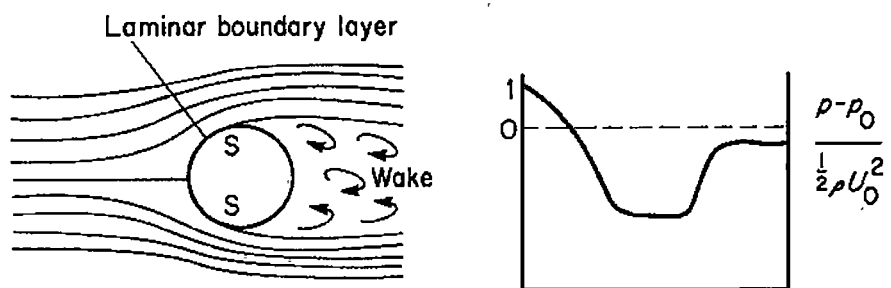
(a) $Re < 0.5$



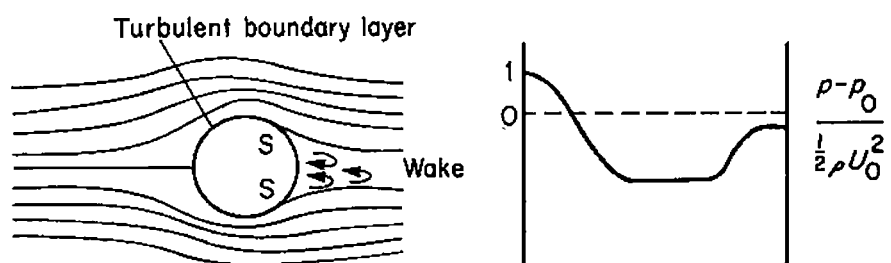
(b) $2 < Re < 30$



(c) $90 < Re < 10^3$



(d) $10^3 \leq Re \leq 2 \times 10^5$

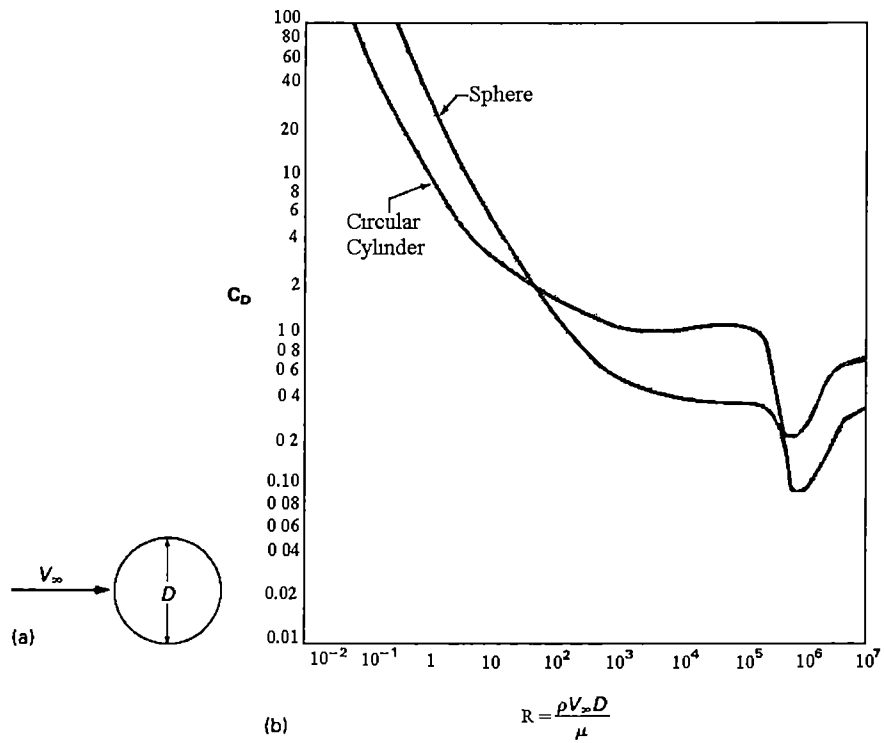


(e) $Re > 2 \times 10^5$

(Douglas *et al.* (1985))

Flow Past a Cylinder

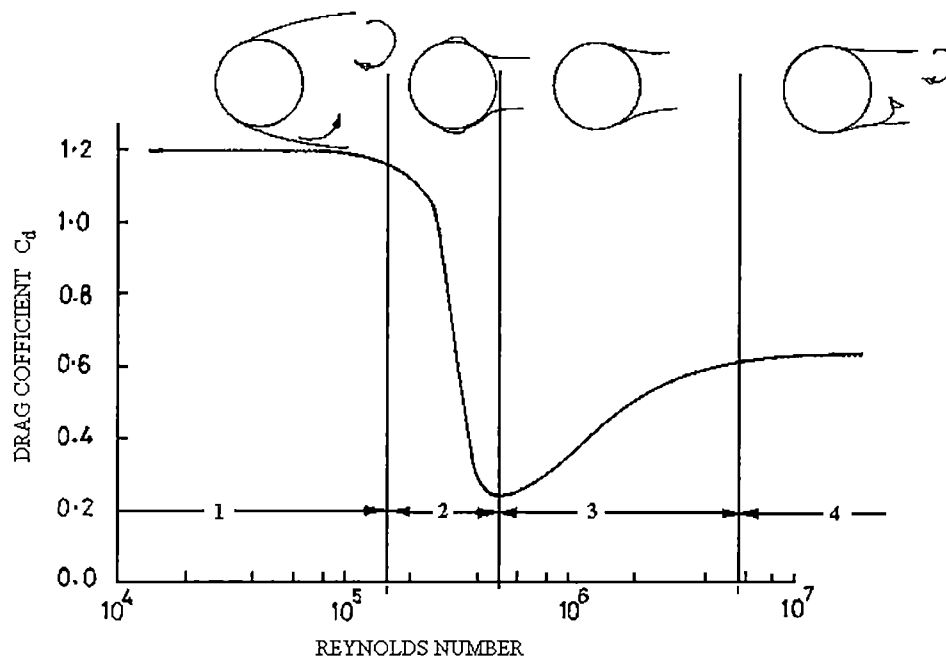
Figure 2.9



(Gerhart and Gross (1985))

Drag Coefficient for Cylinders and Spheres

Figure 2.10



Ranges of Reynolds Number:

1 - Subcritical; 2 - Critical; 3 - Supercritical; 4 - Postcritical

(Miller (1976))

Variation of Drag Coefficient with Reynolds Number for a Smooth Cylinder

Figure 2.11

A further increase in Re will elongate the fixed eddies, which will begin to oscillate, and at $Re > 90$, the oscillating eddies will break away from the cylinder (Figure 2.9(c)). These “*break away’s*” occur alternately from side to side and are transported downstream by the flow. As Re increases, the process is intensified, giving two discrete rows of alternating eddies in the wake. This is known as a “**vortex street**” or a “**von Karman vortex street**”. At this stage the pressure drag is about 75% of the total drag. The shedding of each vortex produces a circulation and hence a **lateral force** on the cylinder.

From Figure 2.11, it is seen that this region is called the **subcritical range**, and the drag coefficient is given as approximately 1.2. This is a result of the relatively low pressure region behind the cylinder due to the wide wake created by the early separation of the laminar boundary layer from the cylinder surface, *i.e.* approximately 80 degrees from the front stagnation point. The separated boundary layer becomes turbulent some distance downstream. The value of 1.2 is generally used as the drag coefficient of cables in a number of investigations, as the Re of this region covers the common velocities encountered. However, under dynamic conditions, the drag coefficient of marine cables (and similar structures) will substantially increase due to the vortex shedding effect. Therefore, investigators should take into consideration the possible changes in the drag coefficient and their consequences, (see sub-section 2.3.6).

As Re approaches 10^5 , a highly turbulent wake replaces the laminar boundary layer some distance downstream of the separation point, (Figure 2.9(d)). Pressure drag will now be responsible for nearly all the drag. As the Re increases further, the turbulent flow will cause the separation to move further back and the vortices will disappear. At $Re > 2 \times 10^5$, (Figure 2.9(e)), the transition from laminar to turbulent flow, occurs nearer to the separation point. It is seen from the **critical region** in Figure 2.11, ($2 \times 10^5 < Re < 4 \times 10^5$), that the turbulent shear layer then reattaches as a turbulent boundary layer, and commences to move the previously stagnant fluid at the wall. The relatively short region of separated flow between the laminar and turbulent boundary layers is called a separation bubble. Since the wake is now much smaller, the drag coefficient falls close to 0.2. Up to these Re levels, the flow though oscillatory, remains two-dimensional.

Miller (1976) states that in the **supercritical region** ($4 \times 10^5 < Re < 4 \times 10^6$), the details of the flow are uncertain, and the behaviour depends on the surface condition of the cylinder. It is believed that in this region the flow is three-dimensional, originating

either by flow caused by end constraints or by turbulent wedges streaming from local spanwise flow ahead of the average separation line.

In the **postcritical region**, the laminar boundary layer gets progressively more turbulent and less stable. Roshko (1961), found that at $Re > 4 \times 10^6$, the drag coefficient will appear to be independent of Re and remains around 0.6 to 0.7. In addition, it was also noted that the flow returns to a two-dimensional flow regime and wake vortex shedding becomes regular again.

2.3.2 Effects on Drag Coefficient due to Surface Roughness and Turbulence

The description given in the previous sub-section applies to smooth cylinders. However, most offshore structures will become roughened by corrosion and fouling. The surface condition of the cylinder and the free stream turbulence will effect the response of the boundary layer and its stability. Therefore, they will also effect the separation point, wake size, and the pressure distribution across the cylinder. These, as shown in the previous sub-section, influence the drag force on the cylinder.

A number of researchers, (Fage and Warsap (1930), Achenbach (1971), Miller (1976), and Sarpkaya (1977, 91)), have carried out experiments to determine the drag effects on roughened cylinders. Fage and Warsap found from their experiments that the increased level of free stream turbulence moved the drag curve towards lower Re , without altering the value of the drag coefficient. Similar experiments by other researchers found that the rate of fall of C_d with Re in the critical region reduced with increase turbulence.

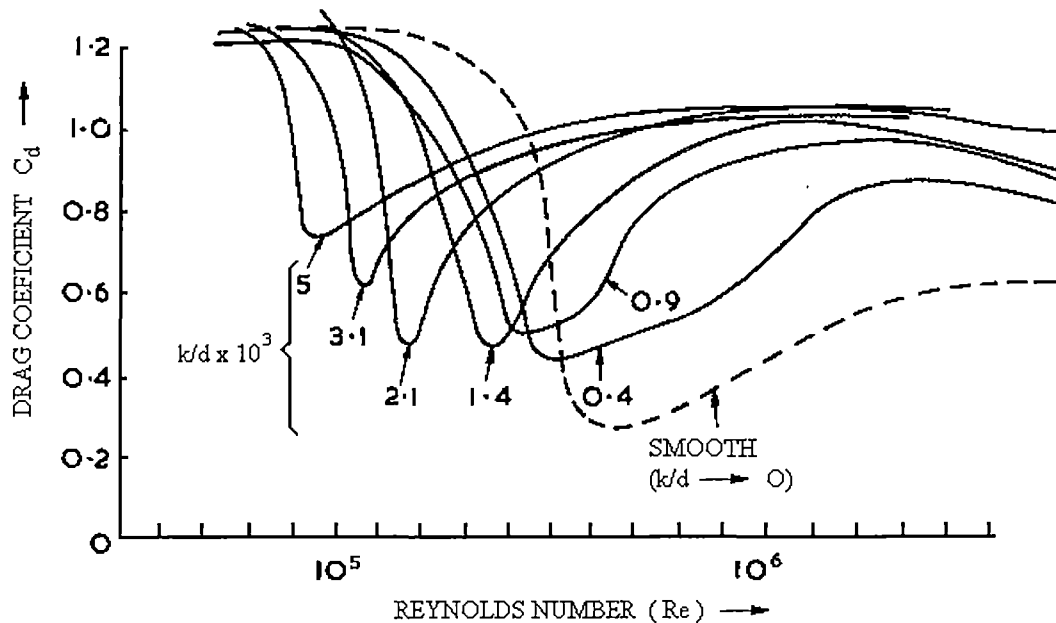
Fage and Warsap also examined the influence of the surface roughness by attaching various grades of abrasive paper to cylinders tested in a wind tunnel. The roughness of the cylinders was given as the *relative roughness*, defined by,

$$\text{relative roughness} = \frac{k_r}{D} \quad (2.71)$$

where k_r is the height of the physical roughness on the cylinder and D is its diameter.

Fage and Warsap (1930) found that an increase in the relative roughness shifted the critical region towards a lower Re . In addition, the minimum drag coefficient

increased in this region. Figure 2.12 reproduced from Miller (1976), shows the effect of surface roughness of a cylinder on its drag coefficient.



(Miller (1976))

The Drag of Sand Roughened Cylinders

Figure 2.12

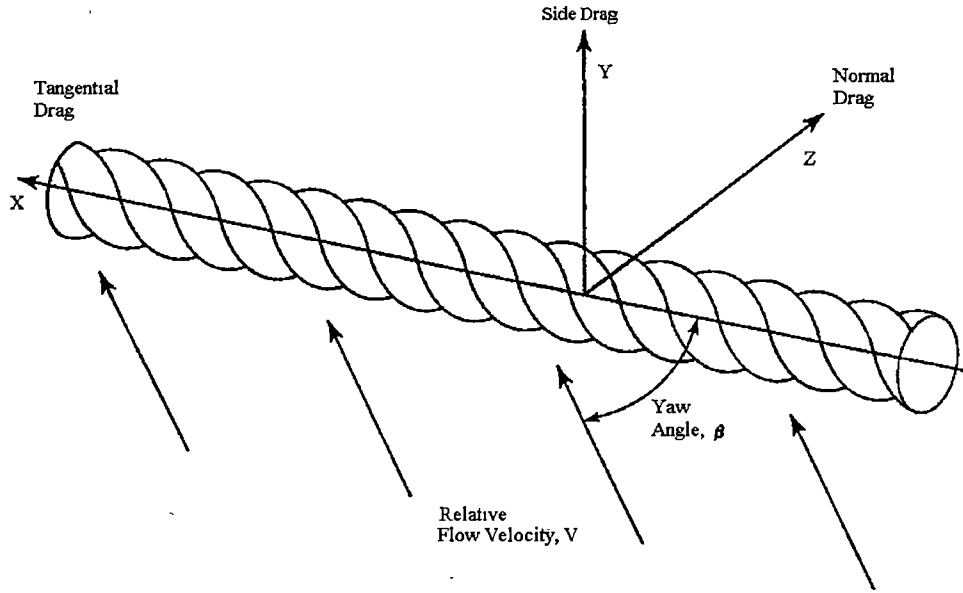
From similar experiments, Achenbach (1971) showed that beyond the critical region, the transition from laminar to turbulent flow occurred closer to the forward stagnation point, resulting in a constant drag coefficient, base pressure, and separation points. This constant drag coefficient at high Re , will increase as the relative roughness of the cylinder surface increases. However, after a certain relative roughness, the drag coefficient became virtually independent of the relative roughness.

Sarpkaya (1977) summarises the effects of roughness as follows. In the supercritical and postcritical regions, the drag coefficient is considerably larger than for a smooth cylinder. This is primarily due to the larger wake brought about by the earlier separation, which in turn is due to the retardation of the boundary layer. It was also noted by Sarpkaya that a higher turbulence level caused the critical range to be wider.

2.3.3 Drag on a Rigid Cylinder Inclined to the Flow

If the cylinder is at an angle to the uniform flow, then drag forces will be present in the tangential and normal directions to the cylinder. In a three-dimensional flow field

(Figure 2.13), there will be three drag forces perpendicular to each other, and are referred to as tangential, normal, and side drag forces. (note: in non-cable bodies, these forces may be referred to as the drag, lift, and side forces).



Direction of Drag Forces on a Cable in a 3D Flow Field

Figure 2.13

In addition to the factors specified in equation (2.70), these drag forces will depend on the angle of incidence to the flow. The usual practice of calculating these forces is to first resolve the relative velocity in the three directions. If the relative velocities along the tangential, normal, and side directions are found as V_{rt} , V_{rn} and V_{rs} , then the respective drag forces can be obtained by using equation (2.70) in each direction as,

$$F_{dt} = 1/2 \cdot C_t \cdot \rho \cdot D \cdot l \cdot V_{rt} \cdot |V_{rt}| \quad (2.72a)$$

$$F_{dn} = 1/2 \cdot C_n \cdot \rho \cdot D \cdot l \cdot V_{rn} \cdot |V_{rn}| \quad (2.72b)$$

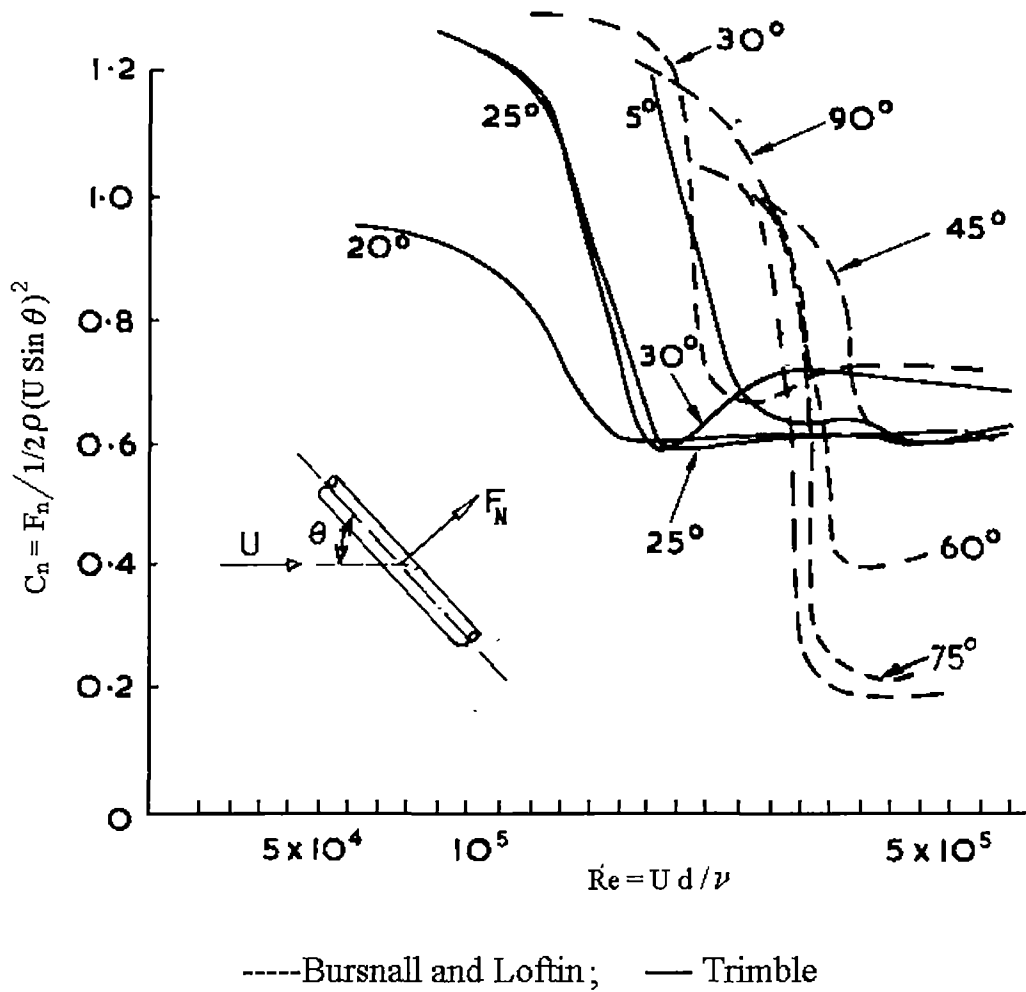
$$F_{ds} = 1/2 \cdot C_s \cdot \rho \cdot D \cdot l \cdot V_{rs} \cdot |V_{rs}| \quad (2.72c)$$

where

$V_{rt,n,s}$: velocities of the cable relative to the fluid in the tangential, normal, and side directions respectively

$F_{dt,n,s}$: drag forces in the tangential, normal, and side directions respectively

$C_{t,n}$: drag coefficient in the tangential and normal directions respectively



(Miller (1976))

Variation of Drag Coefficient for Inclined, Smooth Cylinders

Figure 2.14

Note:

1. In the above equations, it is assumed that the cable is of a non-faired section, thus C_n is used in both equations (2.72b) and (2.72c). However, if it is of a faired section, then the normal and side drag coefficients will be different. In such situations, the usual practice is to use the lift coefficient (C_L) for the side force, *i.e.* in equation (2.72c).
2. The dimension of the body used in all three equations is the projected area, ($D \times l$). However, it is also possible to use other dimensions, a common one being the surface area, ($\pi \times D \times l$). The drag coefficient is selected to suit the appropriate dimension used.

3. The square of the velocity is expressed in the given form to include the direction of the force.

Figure 2.14 reproduced from Miller (1976), shows the variation of the normal drag coefficient (C_n) for a smooth cylinder with the change of Re and cylinder inclination. Choo and Casarella (1971) give semi-empirical formulae for the calculation of the tangential and normal drag forces of cables in towed systems.

2.3.4 Morison's Equation

As stated previously, in addition to the hydrodynamic drag forces due to the relative motion between the cylinder (or cable) and the surrounding fluid, unsteady cable motion and hence the acceleration of the surrounding fluid will exert inertia (added mass) forces on the cable. Morison *et al.* (1950) suggested that the two flow regimes that generate drag and inertia forces be superimposed to give an equation to predict the horizontal force on a vertical pile. This equation has since been modified to deal with cylinders in various configurations and flow regimes. Chakrabati and Cotter (1983) and Shafiee-far *et al.* (1996), present some of the modifications to deal with stationary and moving structures in waves and currents.

The modified Morison's equation for cylinders and cables is given by,

$$F = \frac{1}{2} C_d \rho D |V_r| V_r + \frac{1}{4} C_m \rho \pi D^2 \dot{V}_r \quad (2.73)$$

where

V_r : relative velocity
 C_d : drag coefficient
 C_m : inertia coefficient.

The inertia coefficient can also be given as,

$$C_m = C_a + 1 \quad (2.74)$$

where C_a is added mass coefficient.

Since the drag component of Morison's equation (2.73) is non-linear, a number of methods have been proposed to linearise the terms, enabling its use in frequency

domain investigations, which employ the principle of superposition that requires linear functions. The numerical modelling carried out in this thesis uses the Morison's equation in its non-linear form. For those requiring an insight into the linearisation of the drag terms Triantafyllou *et al.* (1986), Chen and Lin (1989), Chakrabarti (1990), Teng and Li (1991), Kwan and Bruen (1991), and Clauss *et al.* (1992) are recommended. However for completeness, the linearisation technique for Morison's equation presented by Triantafyllou *et al.* is briefly described here. Note the linearisation presented is only for the drag force, *i.e.* the first term in Morison's equation (2.73).

Consider a cable in a steady current, with the cable velocity given by a random function of time. Thus, the relative fluid velocity (V_r) is assumed to be a Gaussian stationary random process of variance " σ " and mean relative velocity " V_{r0} ". Then the relative velocity " V_r " is given by,

$$V_r = V_{r0} + V_r(t) \quad (2.75)$$

where V_{r0} is the mean relative velocity and $V_r(t)$ is the time dependent relative velocity.

The drag force per unit length of the cable from Morison's equation is,

$$F_d = C_{d0} V_r |V_r| \quad (2.76)$$

where $C_{d0} = \frac{1}{2} C_d \rho D$.

Now an equivalent force can be expressed as,

$$F_d = F_{d0} + C_e \cdot V_r(t) \quad (2.77)$$

where the second term is proportionate to the time dependent relative velocity, and

F_{d0} : mean drag force

C_e : linearised equivalent damping coefficient.

The latter term is obtained by first expressing the residual, which is the difference between equation (2.76) and (2.77), and then minimising the mean square of the error. This is carried out by differentiating the square of the residual with respect to the

linearised equivalent damping coefficient (C_e) and then equating it to zero. This results in the coefficient being expressed as,

$$C_e = \sqrt{\frac{2}{\pi}} \rho C_{d0} D \sigma \left[\exp\left(-\frac{\mu^2}{2}\right) + \mu \sqrt{\frac{2}{\pi}} \operatorname{erf}\left(\frac{\mu}{\sqrt{2}}\right) \right] \quad (2.78)$$

where

$$\mu = \frac{V_{ro}}{\sigma}$$

$$\operatorname{erf}(R) = \frac{2}{\sqrt{\pi}} \int_0^{\infty} \exp(-R^2) dR, \quad \text{with "R" being a "dummy variable"}$$

σ = variance of the Gaussian stationary random process.

Note: the variables μ and σ defined here are not relevant to any other equations using the same symbols in this thesis.

2.3.5 Hydrodynamic Cylinder Coefficients in Harmonic Flow

Sarpkaya (1977), investigated the hydrodynamics of a roughened cylinder in fluctuating flow, producing graphs to predict the drag, lift, and inertia coefficients under these conditions.

For harmonic flow, Fourier averaged drag and inertia coefficients can be obtained from experimental results. These will vary with the Re , surface roughness, and the Keulegan-Carpenter number (KC). The latter is defined as,

$$KC = \frac{V_m t_p}{D} \quad (2.79)$$

where

V_m : maximum fluid velocity

t_p : period of the cycle

D : diameter

At $KC < 6$, the flow is dominated by inertia effects as there is little or no separated flow. When $KC > 25$, the flow is dominated by drag effects as the fluid velocity

varies little over a few cycles of vortex shedding. The region given by $6 \leq KC \leq 25$ consists of inertia and drag effects, with vortex shedding taking place on either side of the cylinder.

The governing parameters for the investigation carried out by Sarpkaya (1977) were obtained as follows. Consider an oscillating flow acting on a rough cylinder. The velocity of the flow is represented by,

$$v = -V_m \cos \vartheta \quad (2.80)$$

where

v : instantaneous velocity

V_m : maximum fluid velocity

$$\vartheta = \frac{2\pi t}{t_p}$$

t_p : period of the cycle

t : time

As shown by Keulegan and Carpenter (1958), the values for C_d and C_m for equation (2.73) are obtained by using Fourier averages of a measured force F_m , *i.e.*,

$$C_d = -0.75 \int_0^{2\pi} \frac{F_m \cos \vartheta}{\rho V_m^2 l D} d\vartheta \quad (2.81a)$$

$$C_m = \left(\frac{2V_m t_p}{\pi^3 D} \right) \int_0^{2\pi} \frac{F_m \sin \vartheta}{\rho V_m^2 l D} d\vartheta \quad (2.81b)$$

where l and D are the length and diameter of the cylinder, respectively.

For the transverse force, the maximum lift coefficient (C_L) is obtained as,

$$C_L = \frac{\text{maximum lift force in a cycle}}{0.5 \rho D l V_m^2} \quad (2.82)$$

Due to the cyclic nature of the forces, the coefficients given above are not constant throughout the cycle. They are either *time-invariant averages* or *peak values at a particular moment of the cycle*.

Dimensional analysis shows that the *time-dependent* coefficients can be expressed as,

$$[C_d, C_m, C_L] = f(V_m \cdot t_p / D, V_m \cdot D / \nu, k_r / D, t / t_p) \quad (2.83)$$

where ν is the fluid kinematic viscosity.

By considering *time-invariant* coefficients, and representing the first two terms by the relevant numbers, equation (2.83) reduces to,

$$[C_d, C_m, C_L] = f(KC, Re, k_r / D) \quad (2.84)$$

At low Re (*i.e.* $Re < 20,000$), it is not suitable to use Re in the above equation due to the low viscosity effect. Since the maximum velocity (V_m) is present in both KC and Re , equation (2.84) is rewritten as,

$$[C_d, C_m, C_L] = f(KC, \beta_f, k_r / D) \quad (2.85)$$

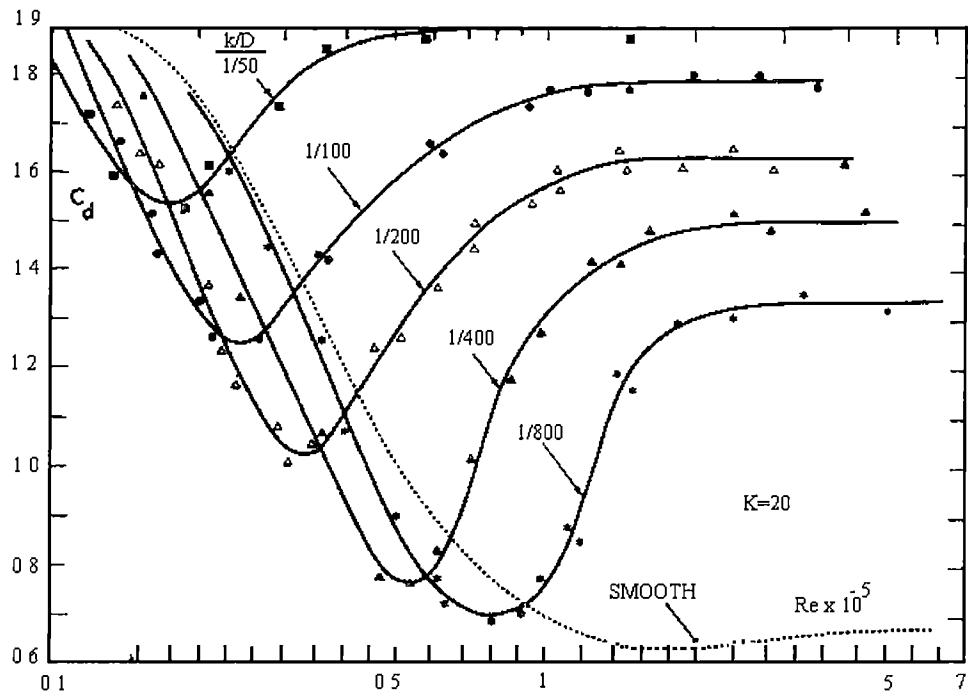
where

$$\beta_f = \text{frequency parameter} = \frac{Re}{KC} = \frac{D^2}{\nu t_p} \quad (2.86)$$

Thus, it is possible to use β_f or Re as an independent variable for dimensional analysis of the coefficients. Therefore, at a constant β_f , it is possible to create a series of curves for the coefficients for varying values of KC .

Note: the ratio β_f represents the ratio between the rate of diffusion of vorticity through the boundary layer thickness and the rate of diffusion to a distance equal to the diameter. It is therefore, equal to the square of the ratio: diameter / boundary layer thickness.

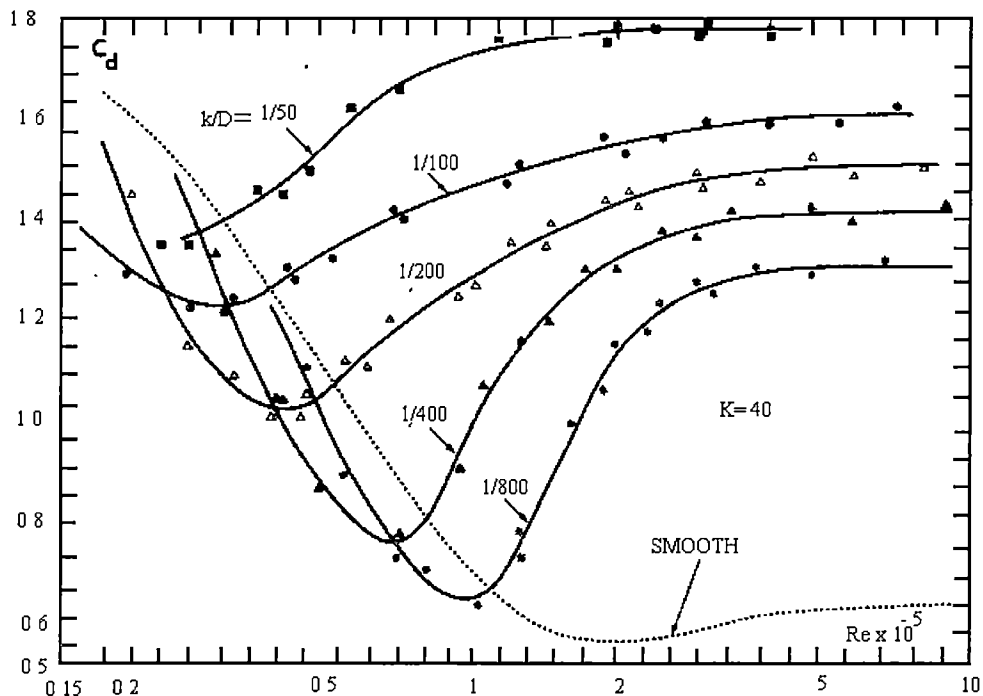
From the experiments carried out by Sarpkaya (1977), curves were produced for the three coefficients, (C_d , C_m , and C_L) for a number of cylinders of varying relative roughness k_r / D at constant β_f and different KC . It was then possible to present the curves for each relative roughness as function of the Re , k_r / D , and KC , with the former obtained by multiplying β_f by the relevant KC . Samples of these curves are reproduced in Figures 2.15 to 2.20, and show the variations of the coefficients within the critical and supercritical regions.



(Sarpkaya (1977))

Drag Coefficient versus Reynolds Number for $KC = 20$ and for Various Values of Relative Roughness

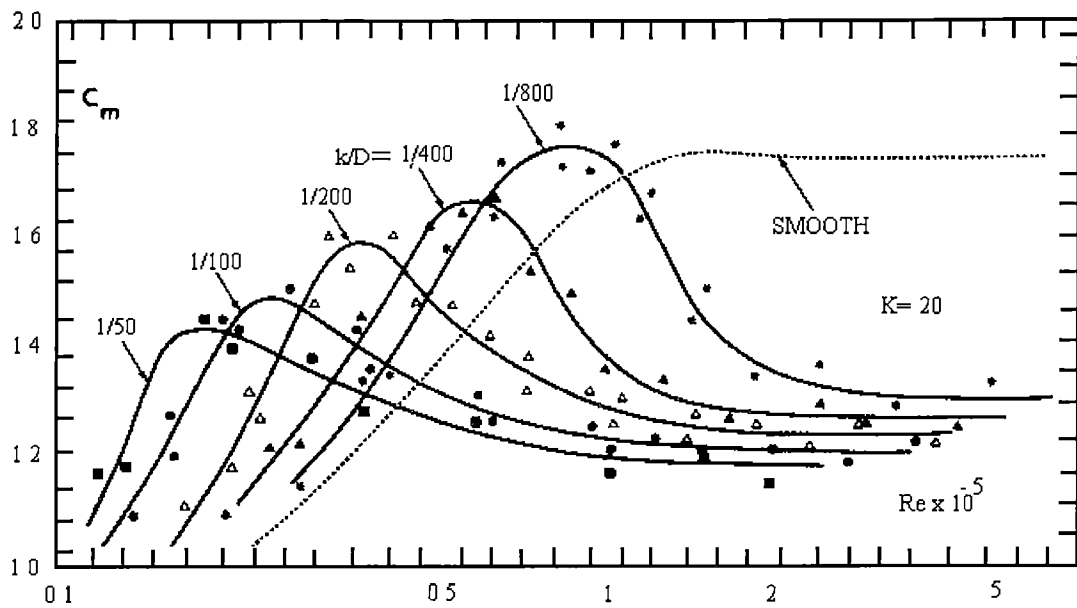
Figure 2.15



(Sarpkaya (1977))

Drag Coefficient versus Reynolds Number for $KC = 40$ and for Various Values of Relative Roughness

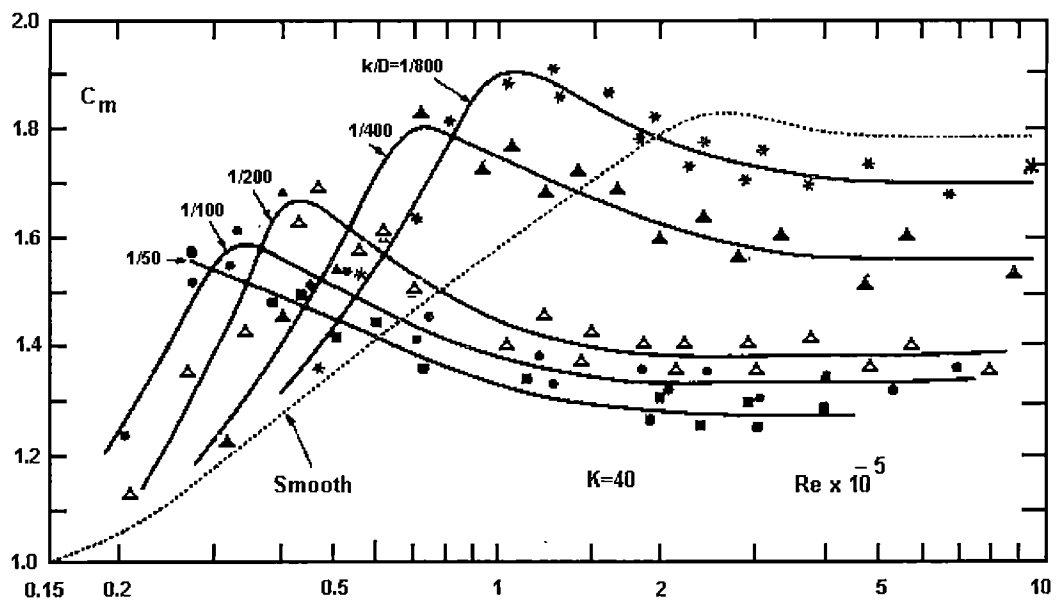
Figure 2.16



(Sarpkaya (1977))

Inertia Coefficient versus Reynolds Number for $KC = 20$ and for Various Values of Relative Roughness

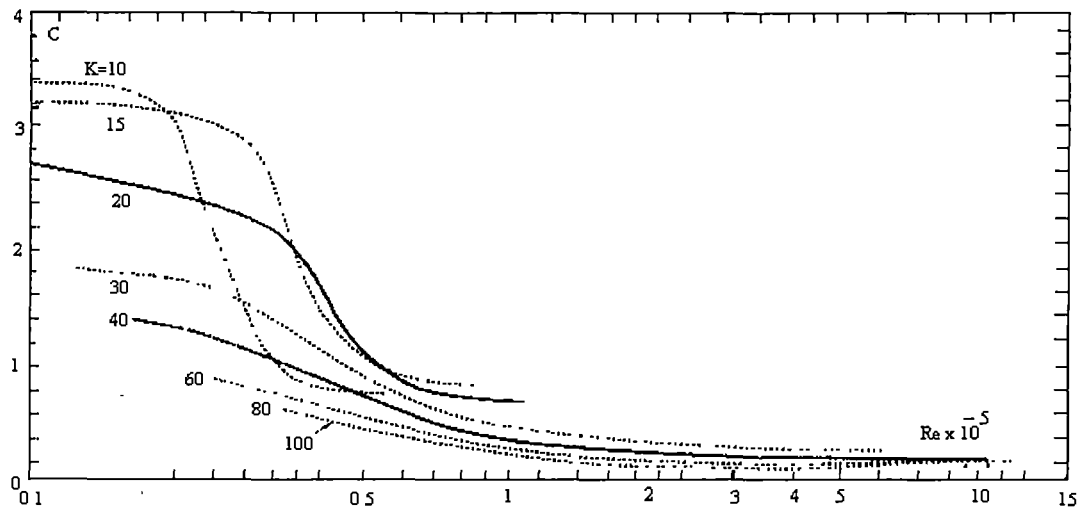
Figure 2.17



(Sarpkaya (1977))

Inertia Coefficient versus Reynolds Number for $KC = 40$ and for Various Values of Relative Roughness

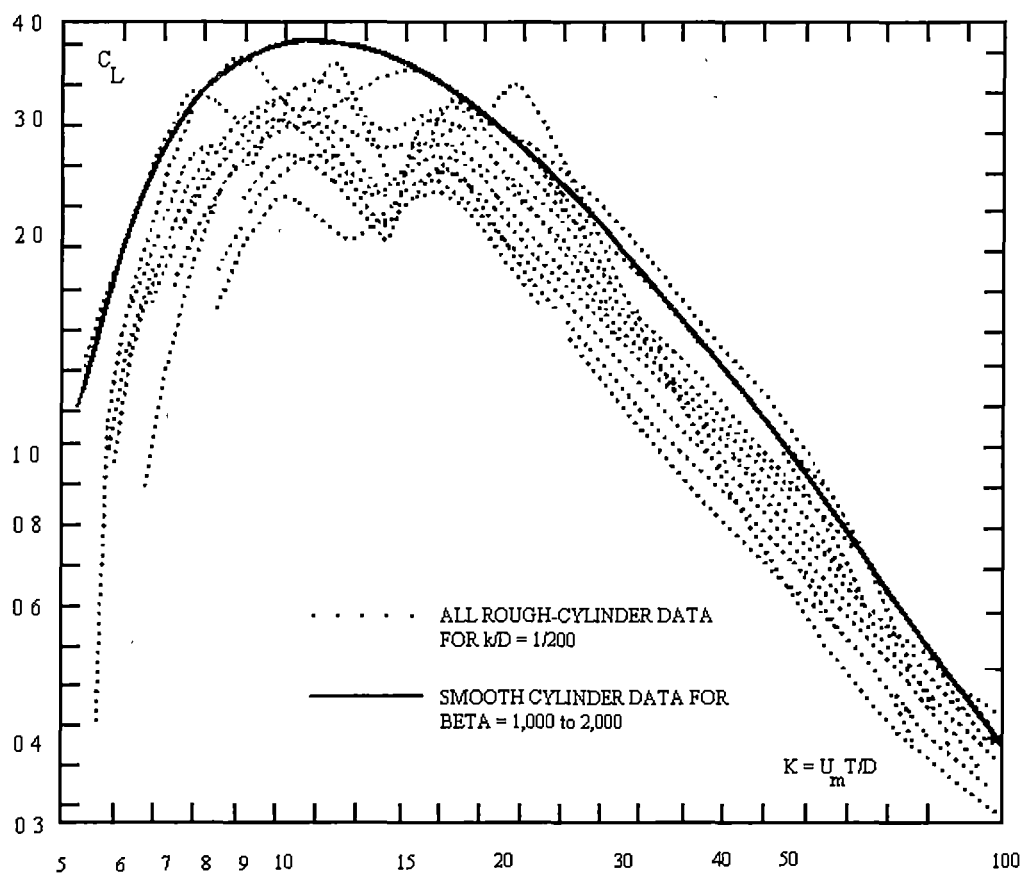
Figure 2.18



(Sarpkaya (1977))

Lift Coefficient versus Reynolds Number for Smooth Cylinders

Figure 2.19



(Sarpkaya (1977))

Lift Coefficient versus KC for a Relative Roughness of 1/200

Figure 2.20

Figures 2.15 and 2.16 show the change of the drag coefficient (C_d) with Re and k_r/D at $KC = 20$ and 40 . At lower Re values, C_d does not alter significantly as k_r/D changes. As Re increases to the critical region, the increase in k_r/D will cause the rapid drop in C_d to occur earlier. However, the actual drop will reduce as k_r/D increases, *i.e.* the minimum C_d will be higher. Further increase in Re to the supercritical region will result in the C_d increasing to a near-constant value closer to the postcritical region. This near constant C_d will be significantly higher for cylinders with higher k_r/D .

It was also noted that C_d for rough cylinders in oscillating flow is considerably higher than those for a similar cylinder in a steady flow. This emphasises the need to increase the drag coefficient when dealing with oscillatory motion.

Figures 2.17 and 2.18 show the change of the inertia coefficient (C_m) with Re and k_r/D at $KC = 20$ and 40 . At lower Re values, C_m is higher for cylinders with higher k_r/D . In the critical region where the drag coefficient (C_d) falls rapidly, C_m undergoes a steep increase. The Re for the maximum C_m , corresponds to that which yields the minimum C_d value. This maximum C_m value decreases as k_r/D increases. As Re passes the critical region, C_m falls marginally to reach a near constant value closer to the postcritical region. This near constant C_m value decreases as k_r/D increases.

It should be emphasised that the effect on the drag and lift coefficients is influenced by the relative roughness (k_r/D) and not only by the physical roughness (k_r).

Figure 2.19 shows the variation in lift coefficient (C_L) for a smooth cylinder with the change of Re and KC . As the Re approaches the critical region, C_L decreases rapidly to a value of around 0.25 . Figure 2.20 shows the change of C_L for a rough cylinder ($k_r/D = 1/200$) as a function of KC at various β_r . It is seen that C_L does not significantly vary with the change in β_r or Re . It was also noted by Sarpkaya (1977) that the change in k_r/D did not significantly affect C_L . It was further noted that due to the random nature of the shedding of vortices, a variation up to 25% was encountered in the C_L values obtained experimentally.

From Figure 2.20 it is seen that C_L reduces for rougher cylinders than those for smooth cylinders at lower Re , (*i.e.* lower β_r). In Kuhtz *et al.* (1997), values for the drag and inertia coefficients at very low β_r were obtained experimentally.

Due to the experiments being conducted with two-dimensional harmonic flow, the coefficients obtained represent the **maximum** values that may result in a three-dimensional wave induced flow that may actually be encountered.

Attempts have also been made by various researchers to develop formulae to predict the drag and lift coefficient of vibrating cylinders. For example, Kato *et al.* (1983) isolated the drag force at the oscillating frequency using a Fourier series, which was then used to calculate the drag and lift forces. However, for our needs the curves produced by Sarpkaya (1977) will be sufficient to predict the required coefficients.

2.3.6 Vortex Induced Hydrodynamic Forces

When a flow occurs across a cylinder at Re around 90 to 10^5 , oscillating eddies will occur and break away from the cylinder, *i.e.* von-Karman vortices shown in Figure 2.9(c). The shedding of these vortices produces a circulation and hence a lateral force on the cylinder. Due to the periodic alternating nature of the vortex shedding and its associated lateral force, the cylinder will be subjected to a lateral vibration, called **strumming**. If the vibration frequency coincides with a natural frequency, then resonance will occur leading to large vibration amplitudes and stresses, which in turn can lead to failure, *e.g.* collapsing of suspension bridges and damage to underwater petroleum riser. The vortex shedding effectively increases the drag force on the structure. Therefore, in practice to take into consideration the von-Karman vortices, the C_D values of cable / pipe structures are increased, and in some cases this can be to around three to four times the normal C_D value (Triantafyllou (1994)). The effect on the drag coefficient is considered later in this sub-section.

In addition, since the vibration accelerates the surrounding fluid, it will influence the inertia (or added mass) effect on the cable. This effect on C_m is usually obtained from experimental data such as those presented by Sarpkaya (1977) and Chakrabarti and Cotter (1983), (see sub-section 2.3.5).

The study of vortex induced vibration and its effects on the relevant hydrodynamic coefficients is complex and is beyond the scope of this thesis. Therefore, only a brief description of the work in this area is presented here.

Due to the flow past a cylinder, the frequency (f) of the forced vibration, also called “self-induced vibration”, is obtained as shown in Douglas *et al.* (1985) by,

$$\text{Str} = 0.198 \left(1 - \frac{19.7}{\text{Re}}\right) \quad (2.87)$$

where “Str” is the **Strouhal number**, given by,

$$\text{Str} = \frac{f D}{V} \quad (2.88)$$

where

f : frequency of vibration
D : diameter of cylinder
V : flow velocity

Note: other researchers have proposed similar equations to (2.87) to predict the frequency of vibration.

Equation (2.87) is valid for the range $250 < \text{Re} < 2 \times 10^5$. For circular cylinders, the Strouhal number has been empirically determined for a range of Re. Within the above Re range, the Strouhal number is approximately 0.2.

During cable strumming, the wake shedding frequency is influenced by the natural frequencies of the cable. For free cables, if the wake shedding frequency is within 25% of a natural frequency of the cable, it will **lock-on** to that natural frequency, (this phenomenon is also referred to as *wake capture*). Thus, the cable will vibrate at or near the locked-on natural frequency.

The maximum amplitude of the strumming cable is typically two to three cable diameters. It also increases the cable drag coefficient from around 1.2 to a value between 3 to 4. The effect on the drag coefficient of a cable is clearly demonstrated in the experiments carried out by Bourget and Marichal (1986 and 1990). When a cable was towed at a constant speed by one end, the shape of the cable was seen to be parabolic, as opposed to the straight line predicted by classical theories forwarded by Pode (1951). It was believed that the curvature was due to the change in the drag coefficient along the length of the cable, which in turn was attributed to the lateral vibration of the cable.

As shown in Horton *et al.* (1987), when a stranded cable (wire rope) is towed, mean steady drag and lift forces are created. Superimposed on these steady drag and lift

forces are fluctuating forces that cause the cable to vibrate, or “strum”. The normal drag on a cable is dominated by profile drag, while the tangential drag is dominated by friction drag.

Griffin (1985) collated the work of various researchers and plotted (Figure 2.21) the effective lift coefficient (C_{LE}) during vortex shedding (obtained by measuring the excitation force), against the effective displacement amplitude “ Y_{EFF} ”. (Note: Y_{EFF} is defined as the ratio between the displacement amplitude and the diameter). It is seen from Figure 2.21 that the maximum C_{LE} occurs around an amplitude of 0.6 to 1.0 cylinder diameters, and reaches a value of around 0.5 to 0.6. It then tends to fall off towards zero as Y_{EFF} increases.

Figure 2.22 (also collated by Griffin), shows a similar plot for the drag coefficient. This gives the amplification of the drag coefficient due to vortex shedding against the wake response parameter, which is defined as,

$$w_R = (1 + \frac{2 Y_m}{D}).(Str. V_R)^{-1} \quad (2.89)$$

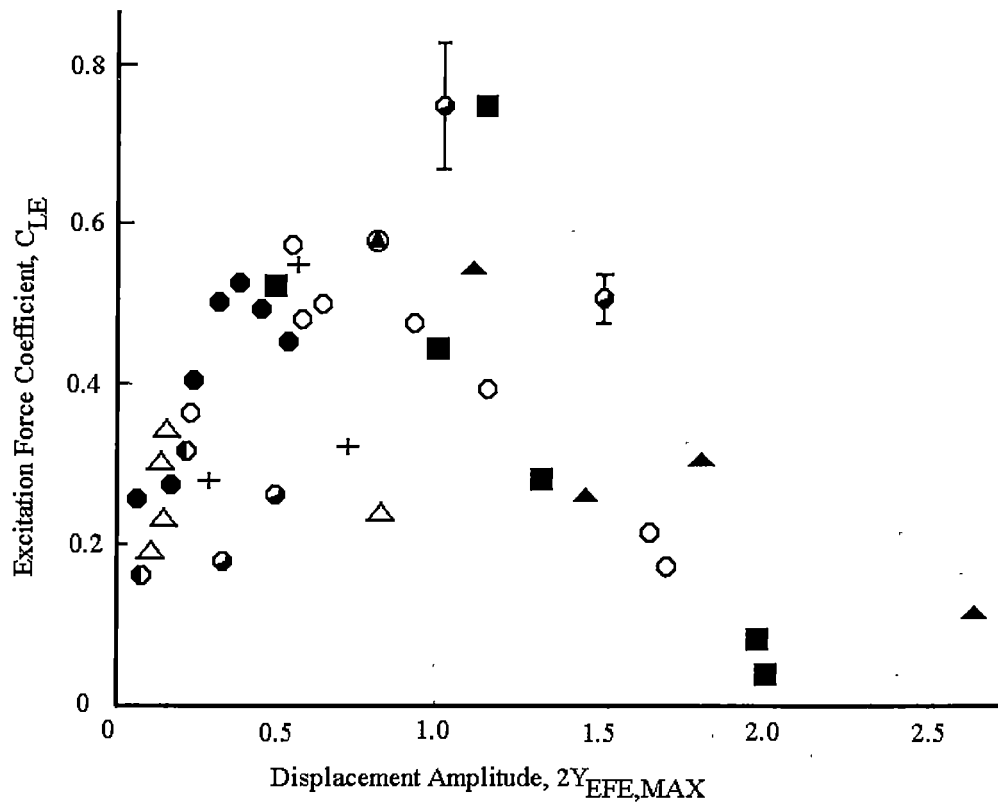
where

- w_R : wake response parameter
- Y_m : cross flow displacement amplitude
- V_R : reduced velocity
- f_n : natural frequency of the cylinder (or cable)

with the reduced velocity “ V_R ” defined as,

$$V_R = \frac{V}{f_n D} \quad (2.90)$$

The variation of the drag coefficient with the velocity is shown in Figure 2.23, (reproduced from Griffin (1985)). It shows that the drag undergoes a resonance-like behaviour, which is similar to that exhibited by the cross flow displacement amplitude. This magnification can result in major damage to offshore structures designed using standard drag coefficient data.

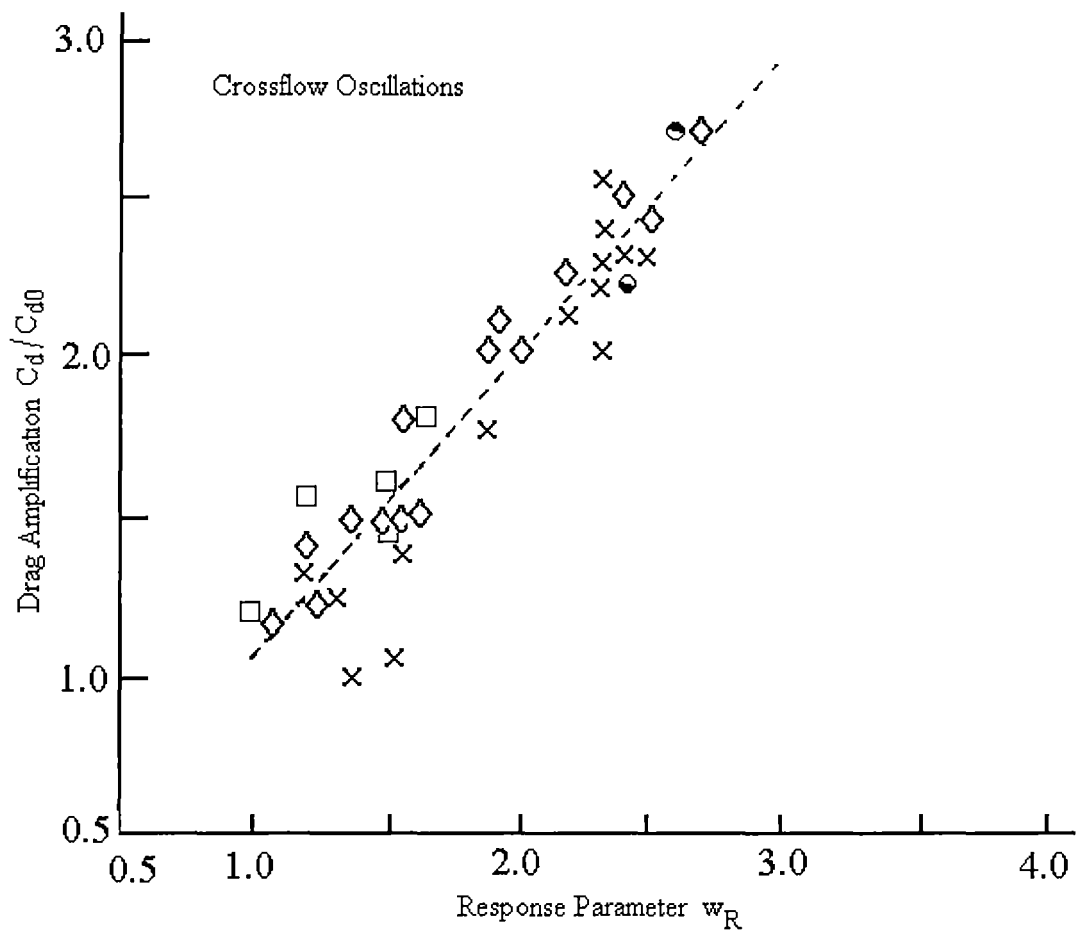


The component, C_{LE} , of the lift force plotted against the displacement amplitude $2Y_{EFE,MAX}$. The legend for the data points are given in the Table below

Symbol	Type of Cylinder	Medium	Cylinder Material	Investigator(s)
▲	Flexible Cantilever	Water	PVC	King (1977)
■			PVC Aluminium Stainless Steel	
○	Pivoted Rigid Cylinder	Water and Air	Brass	Vickery and Watkins (1964)
+	Spring Mounted Rigid Cylinder	Air		
⊙	Rigid Cylinder Forced Oscillations	Water	Aluminium Tubing	Sarpkaya (1978)
△	Flexible Cantilever	Air	Aluminium	Hartlen, Baines and Currie (1968)
●	Flexible Cylinder	Air	-	Farquharson and McHugh (1956)
⊙	Rigid Cylinder	Air	Brass	Simmons and Cleary (1979)

(Griffin (1985))

Effective Lift Coefficient during Vortex Shedding against Effective Displacement Amplitude
Figure 2.21



The drag coefficient amplification, C_d/C_{d0} , plotted as a function of the wake response parameter, $w_R = (1 + 2\bar{Y}/D)(Str.V_R)^{-1}$, for the cross flow vibrations of a circular cylinder. The legend for the data points is given in the table below.

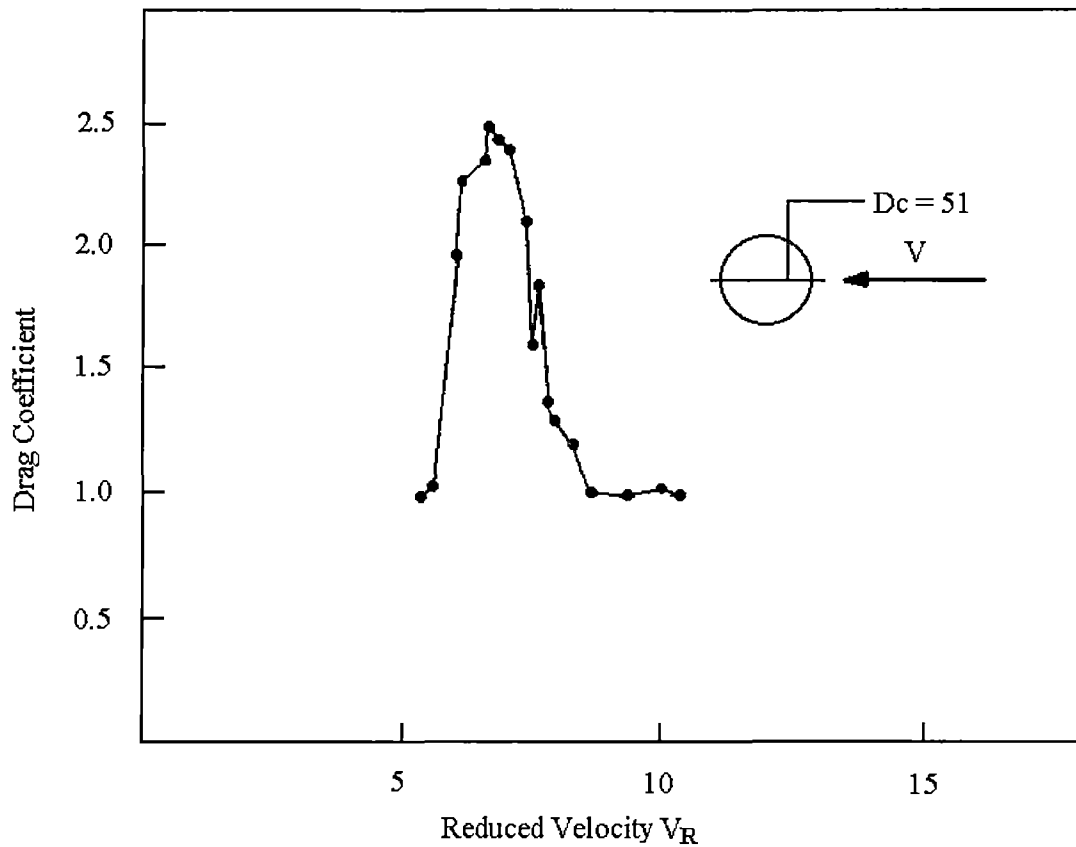
Table Drag Force Amplification on Vibrating Circular Cylinders; Description of the Data in Figure 2.22			
Symbol	Medium	Type of Vibration	Investigator/s
◊	Water	Cross flow, Forced	Sarpkaya (1977)
□	Water	Cross flow, Forced	Schargel (1980)
×	Water	Cross flow, Free	Overik (1982)
● ●	Water	Cross flow, Free	Moe (1982)

(Griffin (1985))

Drag Coefficient Amplification during Vortex Shedding against Wake

Response Parameter

Figure 2.22



The drag coefficient, C_d , plotted against the reduced velocity, V_R , for a spring mounted circular cylinder; from Overvik (1982). Peak cross flow displacement amplitude, $\bar{Y} = \pm 1$ to $1.1D$.

(Griffin (1985))

Drag Coefficient during Vortex Shedding against Reduced Velocity

Figure 2.23

From Figure 2.22 it is seen that the amplification of the drag coefficient due to vortex shedding reaches a factor of three. Using a least-squares fit to the data in the figure, an equation is derived for the drag coefficient amplification as,

$$C_d \text{ amplification} = 0.124 + 0.933 \cdot w_R \quad (2.91)$$

For a cylinder in a uniform flow, vortex shedding and the resulting vibration and forces are coherent over the length of the cylinder. However, when a long flexible cylinder, (e.g. marine cable), is in sheared flow, only some parts of the cable may exhibit vortex shedding. This will cause fluctuating transverse (lift) and in-line (drag) forces, resulting in transverse or in-line vibration of that portion of the cable. It is also possible that the vibration may lock-in to within 25% of the closest natural frequency of the cable, thus causing the whole cable to vibrate. However, since the rest of the

cable is not excited by vortex shedding, this vibration will result in a damping effect throughout the rest of the cable length. Thus, it can be summarised as: *the part of the cable shedding vortices will excite the cable, while the rest of the cable will act as a damper.*

At resonance, the frequency of the external excitation is equal to one of the natural frequencies of the system. If the corresponding modal damping ratio is small, then the response of this mode will dominate the response of all other non-resonance modes.

Very long cylinders with closely spaced natural frequencies, rarely exhibit lock-in and frequently behave as infinite strings. However, shorter cylinders with well separated natural frequencies, tend to lock-in with one mode. If two or more modes of vibration occurs, the response may be a multi-mode non-locking response, *i.e.* **beating** between modes may occur. Since it is difficult to predict which mode, if any, will dominate the response, it is difficult to predict the coefficients for the vibrating cable. It is interesting to note from Grosenbaugh *et al.* (1989) that the drag coefficient in a cable exhibiting beating was lower than that predicted for those in a locked-in condition.

The distinction between “long” and “short” cables is presented by Vandiver and Chung (1987) as follows. Given that “ n ” is the mode number of the highest resonantly excited mode in the system and that “ ζ ” is the damping coefficient of the system, then if,

- $n\zeta < 0.2$ the cable is “short” in the dynamic sense and single-mode resonant response will dominate the total response.
- $0.2 < n\zeta < 3$ significant attenuation occurs over the length of the cable, but an infinite cable response is not adequate. However normal superposition may be used.
- $3 < n\zeta$ the cable may be expected to behave dynamically as if it was infinitely long, and superposition models are not very useful, due to the large number of modes required. (Note: when excited near an end, a semi-infinite model may be used).

Many researchers have developed analytical or empirical formulae to predict the equivalent drag and lift coefficients in long flexible cylinders (cables) undergoing vortex-induced vibrations. One such empirical formula is that developed by Griffin

and Vandiver (1983) from full scale experiments to predict the equivalent drag coefficient during lock-in of a cylinder in shear flow as,

$$C_{dE} = C_d \left[1.16 + 1.67 \left(\frac{Y_{RMS}}{D} \right) \right] \quad (2.92)$$

where

C_{dE} : equivalent drag coefficient

C_d : drag coefficient of rigid cylinder, (usually 1.2)

Y_{RMS} : root mean square anti-nodal displacement

D : diameter of cylinder

Sarpkaya (1979), Vandiver (1983), and Boom & Walree (1990) among others present similar equations. In addition, various equations have been developed to predict the vibration amplitudes of cables / cylinders due to vortex shedding, and a selection of such equations are given in Sarpkaya (1979).

In addition to these formulae, a number of researchers have used various models and methods to calculate the equivalent drag and lift coefficient due to vortex shedding. Kim *et al.* (1985) used the non-linear static equations of the cable to calculate the average drag coefficients. Horton *et al.* (1987) predicted the increased drag and lift coefficients using the maximum drag and lift forces obtained from experiments and a loading function expressed in a Fourier series. Bourget and Marichal (1990) used the dissipated power from a towed cable to calculate the same. Slaouti and Bao (1997) also developed an amplification factor for the drag coefficient based on the transverse motion of the cylinder.

In order to investigate underwater cables, risers, and pipes influenced by vortex shedding in sheared flow, many researchers have developed numerical models, *e.g.* Whitney and Nikkel (1983) and Vandiver (1985). In most models, the energy input at the part of the cable being excited due to the fluctuating vortex induced force is balanced against the energy dissipation via the hydrodynamic damping due to the vibration of the rest of the cable.

A number of devices are fitted to underwater cables, pipes, and risers in order to reduce the shedding of vortices and thus, reduce the related adverse effects. Although this study does not venture into this area, a number of publications are available on

this topic. For example, Rogers (1983) and Jacobsen *et al.* (1996) present comprehensive assessments on such devices.

2.3.7 Hydrodynamic Coefficients Selected

The above sub-sections gave a brief insight into the calculation and prediction of the drag, lift, and inertia forces of underwater cables under varying conditions, such as fluctuating and sheared flow. For the work carried out in this thesis, the coefficients were selected from the data given by Sarpkaya (1977), with due regard to the findings by Shafiee-far *et al.* (1996) on the use of coefficients for Morison's equation. However, the selection of the coefficients can be changed to suit the conditions experienced by the towed system, as the computer model allows the input of the relevant coefficients to deal with these variations.

2.4 Towed Fish Model

A number of authors have presented models for underwater vehicles, *e.g.* Miller (1963), Abkowitz (1969), Humphreys (1976), Bhattacharyya (1978), Chapman (1984), and Papoulias (1992). This investigation uses a modified version of the existing models to simulate the behaviour of towed and depressor fish.

Since the purpose of this investigation is to minimise all perturbations of the towed fish from its steady state trajectory, the underwater bodies need to be dynamically modelled in six degrees of freedom, *i.e.* surge, sway, heave, roll, pitch, and yaw. However, each node of the cable in the lumped-mass method is modelled in three degrees of freedom. Therefore, it is required to dynamically integrate the six degrees of freedom fish model with the three degrees of freedom cable model. This task is further complicated in multi-tow configurations, where the number of towed fish increases.

The towed and depressor fish models require the following features:

- three-dimensional model;
- six degrees of freedom;
- inertia and added masses;
- drag and lift forces;
- lifting surfaces (wings and tail sections);

- tow cable forces;
- a second tow cable to attach other tow fish in series; and
- centre of gravity, centroid, and tow point at different locations within the fish.

The modelling consists of three areas: kinematics, dynamics, and hydrodynamics. The kinematics deals with the representation of the orientation and rotational rates of the fish. The dynamics develop the relationships between the forces / moments on the body to its motion. The hydrodynamic concepts produce the fluid-induced forces and moments acting on the body at the given fish orientation and rotational rates.

The hydrodynamic forces and moments are obtained from established fluid dynamic theories and practices. The required coefficients are obtained from experimental testing in wind tunnels or circulating water channels, supplemented by theoretical approximations.

The added mass terms of the towed / depressor fish will introduce coupling terms in the equations describing the motion of the body. This effect is compounded if the tow point(s) on the fish is located at points other than its centre of gravity. Therefore, the solution technique has to be sufficiently flexible to solve these coupled equations of motion together with the cable equations, *i.e.* the solution procedure has to incorporate the influence of the cable on the fish and *vice versa*.

As will be shown in sub-section 2.5.2, the equations of motion for an underwater body can be extremely long and cumbersome. Therefore, it is usual to linearise the equations about the initial equilibrium condition of motion. This reduces the higher order terms, yielding much simpler equations, thus simplifying the solution technique required.

For a dynamically stable vehicle, linear theory is acceptable for moderate manoeuvres, with the higher-order-terms required only for tight manoeuvres, (Abkowitz (1969)). Due to the nature of the operational conditions of the towed systems investigated, it is unlikely that the configuration will experience tight manoeuvres. The investigation is aimed at ascertaining the response of the vehicle after some infinitesimal disturbance from the equilibrium condition, and its ability to return to the original equilibrium position. Therefore, linearised equations for the underwater towed bodies are acceptable.

If all six degrees of freedom are included in all equations, even the linearised equations will be complex. Therefore, for most marine vehicles it is possible to separate the motion into the vertical and horizontal planes, (unless strong coupling exists between these motions). This approach is used in the modelling of all the towed and depressor fish in this study.

The vertical motion consists of surge, heave, and pitch. Roll motion is neglected as the underwater vehicles considered in the investigation have port-starboard symmetry, and the centre of gravity of the vehicle is located on the vertical plane through its longitudinal centreline. The horizontal motion covers surge, sway, yaw, and roll, since all vehicles do not have top and bottom symmetry, and the centre of gravity is usually below the centreline.

2.5 Towed Fish Hydrodynamic and Acceleration Coefficients

The equations describing the motion of an underwater body in six degrees of freedom are given by a number of researchers, including Miller (1963), Abkowitz (1969), Humphreys (1976), Bhattacharyya (1978), Chapman (1984), and Papoulias (1992). The derivation of the six degrees of freedom equations of motion used in this investigation and their incorporation into the cable model are considered in Chapter 3. Therefore, in this sub-section only a general representation of the equations will be used to explain the various terms.

The equation of motion will consist of coefficients that can be broadly divided into inertia (*i.e.* mass, moment of inertia, added mass, and added moment of inertia), hydrodynamic (drag, lift and side force), gravity / buoyancy, and external forces (*e.g.* tow cable tension). At low relative speeds the forces and moments due to the accelerated flow, (*i.e.* added mass and added moment of inertia), dominate. However, at higher relative speeds the steady hydrodynamic terms are dominant.

2.5.1 Towed Fish Acceleration Coefficients

The six-degree-of-freedom equations of motion of an underwater body in its local coordinate system (see Figure 2.24), are expressed as,

$$\begin{bmatrix} Af_{11} & Af_{12} & Af_{13} & Af_{14} & Af_{15} & Af_{16} \\ Af_{21} & Af_{22} & Af_{23} & Af_{24} & Af_{25} & Af_{26} \\ Af_{31} & Af_{32} & Af_{33} & Af_{34} & Af_{35} & Af_{36} \\ Af_{41} & Af_{42} & Af_{43} & Af_{44} & Af_{45} & Af_{46} \\ Af_{51} & Af_{52} & Af_{53} & Af_{54} & Af_{55} & Af_{56} \\ Af_{61} & Af_{62} & Af_{63} & Af_{64} & Af_{65} & Af_{66} \end{bmatrix} \begin{bmatrix} \dot{u} \\ \dot{v} \\ \dot{w} \\ \dot{p} \\ \dot{q} \\ \dot{r} \end{bmatrix} = \begin{bmatrix} F_{fx'} \\ F_{fy'} \\ F_{fz'} \\ M_{fx'} \\ M_{fy'} \\ M_{fz'} \end{bmatrix} \quad (2.93)$$

where

Af_{ab} : where $a = 1, 2, 3$ and $b = 1, 2, 3$

mass matrix terms of the equation of motion of the underwater body, incorporating the mass, added mass, inertia, and added inertia terms

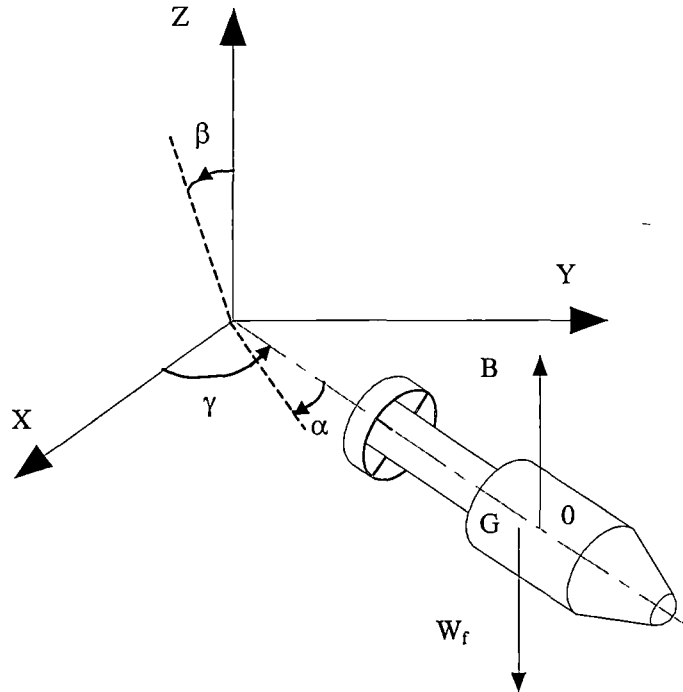
$\dot{u}, \dot{v}, \dot{w}$: local acceleration components of the body along the local axes system

$\dot{p}, \dot{q}, \dot{r}$: angular acceleration components of the body about the three axes, *i.e.* in the roll, pitch, and yaw directions

$F_{f,x',y',z'}$: forces acting on body along the local axes system

$M_{f,x',y',z'}$: moments acting on body about the local axes system

X', Y', Z' : local axes system



Orientation of an Underwater Vehicle

Figure 2.24

Depending on the shape and motion of the body, some of the mass matrix terms given by A_{fab} in equation (2.93) will be zero, while in most cases the matrix will be symmetrical about its leading diagonal.

The mass and moment of inertia terms can be obtained by employing usual techniques of solid mechanics. The moment of inertia of a towed vehicle can be obtained by suspending the body vertically and measuring the period of oscillation. If it is not possible to suspend the body from its tow point, then the parallel axis theorem can be utilised to transfer the moment of inertia from about the point of suspension to that about the tow point.

The prediction of the added mass / inertia coefficients is much more complex. Although the hydrodynamic forces on a body due to steady motion (*i.e.* drag and lift forces) are easily understood, the fluid forces created due to the acceleration of the body are less well understood. The fact that these forces are referred to by a range of names, *added mass*, *virtual mass*, *apparent mass*, *hydrodynamic mass*, etc. does little to clarify the issue. These added mass / inertia terms are briefly described below.

Any motion of the body through a fluid, causes the fluid surrounding it to move aside and then close in behind the body. This results in the fluid acquiring kinetic energy that would not be present if the body were stationary. Thus, the body has to impart that kinetic energy to the fluid by doing work on it.

When the motion of the body is steady, the corresponding fluid motion is steady, and the kinetic energy in the fluid is constant. Thus, no added mass / inertia terms are present in steady motion. However, when a body is accelerating through the fluid, it will result in a change in the kinetic energy within the fluid. Thus, the added mass is summarised as:

“The added mass effect is due to the work done on the fluid by a body as it accelerates”.

Note: steady speed of a body does not always result in steady motion. A common example of this is a body undergoing a steady turn. To achieve this motion, the body has to be accelerated “towards” the centre, thus changing the kinetic energy in the fluid. Therefore, under these conditions the added mass / inertia terms have to be included in the equations of motion.

These coefficients can be predicted by analytical or experimental procedures. The analytical method yields general expressions for the added mass / inertia coefficients for a number of bodies. Therefore, any changes to the shape of the body or its motion can be reflected by manipulating the terms in the expressions. This allows the investigation of the body without carrying out expensive experiments to determine the relevant coefficients for each of the conditions.

For simple shapes, the added mass / inertia coefficients can be obtained from fluid mechanics text, such as Clauss *et al.* (1992). For more complex shapes, the expressions for the coefficients are obtained by utilising the potential flow patterns and the kinetic energy in the fluid. Examples of such methods are presented in Humphreys and Watkinson (1978) and Imlay (1961).

Due to the complexities involved in analytically calculating these coefficients, the usual practice is to obtain them from experiments. However, each of the experimental outcomes represents a given configuration, *e.g.* in motion and shape. Thus, a range of experiments is needed to obtain the coefficients to deal with all the configurations that are to be investigated, since the data obtained for one configuration, in most cases will not “fit” other configurations. Therefore, the prediction of these terms using experimental data is time consuming and expensive. However, for most towed bodies (and underwater bodies), the coefficients are obtained using experimental data.

The experimental methods of obtaining the inertia coefficients usually employ a planar-motion-mechanism. Abkowitz (1969) gives an explanation on the planar-motion-mechanism and its use to calculate the relevant coefficients.

2.5.2 Towed Fish Static and Dynamic Hydrodynamic Coefficients

In the absence of external excitation forces (including tow cable forces) and assuming that no control surfaces can be deflected, the forces and moments on the underwater body can be expressed as,

$$\bar{\mathbf{F}} \text{ and } \bar{\mathbf{M}} = f(x, y, z, \alpha, \beta, \gamma, u, v, w, p, q, r, \dot{u}, \dot{v}, \dot{w}, \dot{p}, \dot{q}, \dot{r}) \quad (2.94)$$

where

$\bar{\mathbf{F}}$: force vector acting on the body
 $\bar{\mathbf{M}}$: moment vector acting on the body

x, y, z : displacement of the body along the X, Y, Z axes
 u, v, w : velocities of the body along the X, Y, Z axes
 β, α, γ : angular displacement of the body about the X, Y, Z axes, (*i.e.* roll, pitch, and yaw)
 p, q, r : angular velocities of the body about the X, Y, Z axes

The above function depends on the motion and orientation parameters. This function can be represented in a mathematical form with the use of a Taylor expansion. To explain this expansion, consider the function of one variable, say “x”. Thus,

$$\bar{F} = f(x) \quad (2.95)$$

If the function is required at a certain value of “x”, it can be described in terms of the value of the function and its derivatives at some other nearby value of x, say x_0 . Thus,

$$f(x) = f(x_0) + (x - x_0) \frac{df(x_0)}{dx} + \frac{(x - x_0)^2}{2!} \frac{d^2f(x_0)}{dx^2} + \frac{(x - x_0)^3}{3!} \frac{d^3f(x_0)}{dx^3} + \dots \quad (2.96)$$

where $f(x_0)$ is the value of the function at x_0 . Substituting,

$$D_x^n = \frac{d^n}{dx^n} \text{ and } \Delta x = (x - x_0)$$

we get,

$$f(x) = \left[1 + \Delta x D_x + \frac{(\Delta x D_x)^2}{2!} + \frac{(\Delta x D_x)^3}{3!} + \dots \right] f(x_0) \quad (2.97)$$

Using an exponential series expansion, *i.e.*,

$$e^a = 1 + a + \frac{a^2}{2!} + \frac{a^3}{3!} + \dots \quad (2.98)$$

the Taylor expansion in (2.97) can be expressed as,

$$f(x) = e^{\Delta x D_x} . f(x_0) \quad (2.99)$$

If two variables were considered, say x and y, then equation (2.99) can be written as,

$$f(x, y) = e^{\Delta x D_x + \Delta y D_y} \cdot f(x_o, y_o) \quad (2.100)$$

which can be expanded to give,

$$f(x, y) = \left[1 + (\Delta x D_x + \Delta y D_y) + \frac{(\Delta x D_x + \Delta y D_y)^2}{2!} + \dots \right] f(x_o, y_o) \quad (2.101)$$

$$\begin{aligned} f(x, y) = & f(x_o, y_o) + \Delta x \frac{\partial f(x_o, y_o)}{\partial x} + \Delta y \frac{\partial f(x_o, y_o)}{\partial y} \\ & + \frac{1}{2!} \left[(\Delta x)^2 \frac{\partial^2 f(x_o, y_o)}{\partial x^2} + (\Delta y)^2 \frac{\partial^2 f(x_o, y_o)}{\partial y^2} + 2 \Delta x \Delta y \frac{\partial^2 f(x_o, y_o)}{\partial x \partial y} \right] + \dots \end{aligned} \quad (2.102)$$

Similarly, the Taylor expansion for expression (2.94) is given by,

$$\bar{F} \text{ and } \bar{M} = \left[e^{\Delta x D_x + \Delta y D_y + \Delta z D_z + \dots + \Delta r D_r} \right] \cdot f(x_o, y_o, z_o, \dots, r_o) \quad (2.103)$$

Inspecting equations (2.102) and (2.103), it is noted that the partial differential terms will span from first order upwards, inclusive of cross products. This would yield a extremely long and cumbersome expression. However, a number of these terms will be zero, and the higher order terms are usually neglected. In the latter case, most simplification procedures neglect the terms above the third order.

Expressions for the forces and moments on an underwater body in six degrees of freedom are given in Gertler and Hagen (1967). These expressions, modified to deal with an underwater towed body, can be expressed as,

Note: the notations used for these equations are not strictly in line with those used in the rest of the thesis. For a more detailed explanation on the coefficients, refer to Gertler and Hagen (1967) and Abkowitz (1969).

$$\begin{aligned} F_x = & \frac{\rho}{2} l^4 [X_{qq} q^2 + X_{rr} r^2 + X_{rp} rp] + \frac{\rho}{2} l^3 [X_u \dot{u} + X_{vr} vr + X_{wq} wq] + \\ & + \frac{\rho}{2} l^2 [X_{uu} u^2 + X_{vv} v^2 + X_{ww} w^2] + (W - B) \sin \alpha + T_x \end{aligned} \quad (2.104a)$$

$$\begin{aligned}
F_y = & \frac{\rho}{2} l^4 \left[Y_r \dot{r} + Y_p \dot{p} + Y_{p|p|} p|p| + Y_{pq} pq + Y_{pr} qr \right] + \\
& \frac{\rho}{2} l^3 \left[Y_v \dot{v} + Y_{vq} vq + Y_{wp} wp + Y_{wr} wr \right] + \\
& \frac{\rho}{2} l^3 \left[Y_r ur + Y_p up + Y_{v|r|} \frac{v}{|v|} (v^2 + w^2)^{1/2} |r|p \right] + \\
& \frac{\rho}{2} l^2 \left[Y_{uu} u^2 + Y_v uv + Y_{v|v|} v (v^2 + w^2)^{1/2} + Y_{vw} vw \right] - \\
& (W - B) \cos \alpha \sin \beta + T_y
\end{aligned} \tag{2.104b}$$

$$\begin{aligned}
F_z = & \frac{\rho}{2} l^4 \left[Z_q \dot{q} + Z_{pp} p^2 + Z_{rr} r^2 + Z_{rp} rp \right] + \\
& \frac{\rho}{2} l^3 \left[Z_w \dot{w} + Z_{vr} vr + Z_{vp} vp + Z_q uq + Z_{w|q|} \frac{w}{|w|} (v^2 + w^2)^{1/2} |q| \right] + \\
& \frac{\rho}{2} l^2 \left[Z_{uu} u^2 + Z_w uw + Z_{w|w|} w (v^2 + w^2)^{1/2} \right] + \\
& \frac{\rho}{2} l^2 \left[Z_{|w|} u|w| + Z_{ww} |w| (v^2 + w^2)^{1/2} + Z_{vv} v^2 \right] - \\
& (W - B) \cos \alpha \cos \beta + T_z
\end{aligned} \tag{2.104c}$$

$$\begin{aligned}
M_x = & \frac{\rho}{2} l^5 \left[K_p \dot{p} + K_r \dot{r} + K_{qr} qr + K_{pq} pq + K_{p|p|} p|p| \right] + \\
& \frac{\rho}{2} l^4 \left[K_p up + K_r ur + K_v \dot{v} + K_{vq} vq + K_{wp} wp + K_{wr} wr \right] + \\
& \frac{\rho}{2} l^3 \left[K_{uu} u^2 + K_v uv + K_{v|v|} v (v^2 + w^2)^{1/2} + K_{vw} vw \right] - \\
& (Y_G W - Y_B B) \cos \alpha \cos \beta + (Z_G W - Z_B B) \cos \alpha \sin \beta + M_{Tx}
\end{aligned} \tag{2.104d}$$

$$\begin{aligned}
M_y = & \frac{\rho}{2} l^5 \left[M_q \dot{q} + M_{pp} p^2 + M_{rr} r^2 + M_{rp} rp + M_{q|q|} q|q| \right] + \\
& \frac{\rho}{2} l^4 \left[M_w \dot{w} + M_{vr} vr + M_{vp} vp + M_q uq + M_{w|q|} (v^2 + w^2)^{1/2} |q| \right] + \\
& \frac{\rho}{2} l^3 \left[M_{uu} u^2 + M_w uw + M_{w|w|} w (v^2 + w^2)^{1/2} \right] + \\
& \frac{\rho}{2} l^3 \left[M_{|w|} u|w| + M_{ww} |w| (v^2 + w^2)^{1/2} + M_{vv} v^2 \right] + \\
& (X_G W - X_B B) \cos \alpha \cos \beta + (Z_G W - Z_B B) \sin \alpha + M_{Ty}
\end{aligned} \tag{2.104e}$$

$$\begin{aligned}
M_z = & \frac{\rho}{2} l^5 \left[N_r \dot{r} + N_p \dot{p} + N_{pq} pq + N_{qr} qr + N_{r|r} r|r \right] + \\
& \frac{\rho}{2} l^4 \left[N_v \dot{v} + N_{wr} wr + N_{wp} wp + N_{vq} vq \right] + \\
& \frac{\rho}{2} l^4 \left[N_p up + N_r ur + N_{|v|r} |(v^2 + w^2)^{1/2}|r \right] + \\
& \frac{\rho}{2} l^3 \left[N_{uu} u^2 + N_v uv + N_{v|v|} v|(v^2 + w^2)^{1/2}| + N_{vw} vw \right] - \\
& (X_G W - X_B B) \cos \alpha \sin \beta - (Y_G W - Y_B B) \sin \alpha + M_{Tz}
\end{aligned} \tag{2.104f}$$

where, (refer also to equation (2.94)),

- $F_{x,y,z}$: forces on the underwater body along the X, Y, Z axes
 $M_{x,y,z}$: moments on the underwater body about the X, Y, Z axes
 ρ : density of the surrounding fluid
 l : length of the underwater body
 W : weight of the underwater body
 B : buoyancy force on the underwater body
 $T_{x,y,z}$: forces on the underwater body due to the tow cable tension along the X, Y, Z axes
 $M_{Tx,y,z}$: moments due to tow cable tension on the underwater body about the X, Y, Z axes
 X_G, Y_G, Z_G : distance from the tow point to the centre of gravity of the body.

and where the coefficients are as follows,

- X : force coefficient in direction along the X axis
 Y : force coefficient in direction along the Y axis
 Z : force coefficient in direction along the Z axis
 K : moment coefficient about X axis
 M : moment coefficient about Y axis
 N : moment coefficient about Z axis

For example,

- X_{qq} : second order hydrodynamic coefficient representing the side force as a function of q

It should also be noted that some first order terms will be zero, *e.g.* “ X_q ” - the first order hydrodynamic coefficient representing the side force as a function of q .

These hydrodynamic coefficients are primarily due to shear and pressure effects on the body. The main components are the drag, lift, and side force coefficients in the linear and rotary directions. In addition, moments will be produced about the tow point. These moments are usually due to an angle of incidence to the flow, *i.e.* when the towed body undergoes angular displacement from the steady state configuration.

Very little information is available for predicting these coefficients using analytical methods. Some examples of such analytical predictions based on semi-empirical slender body methods are given in Fidler (1978), Summey and Smith (1981), and selected publications from the US Naval Sea Systems Command Hydromechanics Committee (SEAHAC).

The Reynolds number encountered for most underwater vehicles is in the region of 10^6 to 10^7 , which is similar to those encountered by sub-sonic aircraft. This is the reason that hydrodynamic coefficients and their prediction methods developed for wing and tail surfaces of subsonic aircraft are applicable to most underwater vehicles. However, even in the aircraft industry, very little data exist for the analytical prediction of the coefficients of the body, possibly because these vehicles are wing dominated as opposed to underwater vehicles.

Therefore, the preferred method to obtain the coefficients for underwater vehicles remains the use of experimental data. These experiments are conducted using either a planar-motion-mechanism, rotating arm facility, wind tunnel, or water channel. The forces obtained from the above experiments are then used to calculate the relevant coefficients. The procedure can be summarised as follows.

The forces and moments acting on the body due to the fluid will be a function of the density of the surrounding liquid (ρ), velocity of the body relative to the surrounding liquid (\bar{V}), shape / size of the body, and the fluid viscosity. Consider the forces first. Using dimensional analysis the forces can be expressed as a function of the “dynamic force”, (*i.e.* $\frac{1}{2}\rho \bar{V}^2$ x geometrical area). Thus, the drag, lift, and side forces on the body are expressed as,

$$\bar{F}_d = \frac{1}{2} C_d \rho A_g \bar{V}_r^2 \quad (2.105a)$$

$$\bar{F}_L = \frac{1}{2} C_L \rho A_g \bar{V}_r^2 \quad (2.105b)$$

$$\bar{F}_S = \frac{1}{2} C_S \rho A_g \bar{V}_r^2 \quad (2.105c)$$

where

$\bar{F}_{d,L,S}$: drag, lift, and side forces respectively

ρ : density of surrounding fluid

A_g : characteristic area of the body, (usually the cross-sectional area to the flow *or* the surface area)

$C_{d,L,S}$: drag, lift, and side force coefficients respectively

\bar{V}_r : relative velocity between the body and the surrounding fluid

The drag, lift, and side force coefficients are non-dimensional coefficients that represent the combined effects due to the pressure, viscosity, surface condition, and shape. In many cases they are functions of the geometric shape, Reynolds number, Froude number, Weber number, relative surface roughness, etc.

Similarly the moments acting on the body can be expressed as,

$$\bar{M} = \frac{1}{2} C_{r,p,y} \rho A_g l \bar{V}_r^2 \quad (2.106)$$

where

\bar{M} : moments acting on the body

ρ : density of surrounding fluid

A_g : characteristic area of the body

l : length of the body, (in some cases the effective diameter “D” is used)

$C_{r,p,y}$: roll, pitch, and yaw moment coefficients respectively

\bar{V}_r : relative velocity between the body and the surrounding fluid

A general explanation of the calculation method of these coefficients is given in Abkowitz (1969), while a detailed explanation on the prediction of the coefficients for a towed sonar vehicle, including wind tunnel experiments, is given in Wingham and Henderson (1988). Similar tests were carried out by the author on the scaled models in the Circulating Water Channel using a horizontal planar-motion-mechanism

(HPMM). The various coefficients were obtained over a range of angles of incidence and plotted as shown in Figures 6.61, 6.62, and 6.63.

As stated earlier the Reynolds numbers encountered for most underwater towed vehicles in practice is in the region of 10^6 to 10^7 . Over this region the hydrodynamic coefficients tend to remain reasonably constant. Therefore, the curves obtained for the coefficients can be used for all practical speeds of the simulation. The digitisation of the curves is carried out by producing third order polynomials to represent the curves, with the tangent of the angle of incidence being the independent variable and the required coefficient the dependent variable. This allows the computer model to calculate the required coefficients for each time step, and thus calculate the relevant forces and moments.

If the towed fish or the towing envelop is such that the coefficients tend to change substantially with speed (or Re), it is a simple matter to incorporate this into the existing computer model. This however, would require the calculation of the coefficients at the required speeds and angles of incidence. The coefficients can then be digitised using curve fitting techniques or look-up tables to enable the calculation of the required coefficients.

The product coefficients (*e.g.* X_{vr}) and the rotary velocity coefficients (*e.g.* X_{qq}) are usually obtained from planar-motion-mechanism or rotary arm facility experiments. For simple models, these values can be obtained by approximation and fluid dynamic theory, as shown in Gerhart and Gross (1985) and Clauss *et al.* (1992).

CHAPTER 3

CABLE AND FISH MODEL

3.1 Modelling of the System

In Chapters 1 and 2, the techniques employed to model conventional towing arrangements were discussed, (*e.g.* Schram and Reyle (1968), Webster (1975), Ablow and Schechter (1983), Milinazzo *et al.* (1987), Chapmen (1987), Koterayama *et al.* (1988), Kamman *et al.* (1989), and Huang (1992)). From the various methods available to model cable systems, the lumped mass method was selected as it enables easy representation of the cable junction and readily integrates the towed fish model, (see sub-section 2.2 for detailed justification of the selection).

In the lumped mass method, the cable is modelled by dividing it into a number of discrete segments, which then yield a set of second order differential equations to describe the motion of each segment. The number of equations will depend on the degrees of freedom considered. Due to the large changes in the cable geometry and the cable / fluid interaction, these equations are non-linear. In Chapter 5, it will be shown that the lumped mass model equations are representative of the continuous cable system.

If the secondary cable is attached directly to the depressor (Figure 1.1(b)), then it is possible to model the system as a single cable with the depressor represented by an extra mass. This approach has been successfully modelled previously (Henderson and Wright (1991)). If however, the attachment point between the cables is relatively high above the depressor (Figure 1.1(d)), the above method is inadequate. To represent such configurations, the author models the two cables separately and dynamically couples them at the junction.

The coupling of the cables at the junction is essential when modelling multiple tows in parallel as shown in Figure 1.1(i). In systems consisting of multiple tows in series, (see Figures 1.1(f) and 1.1(g), the cables are separated by the tow fish, thus requiring each cable to be modelled separately and interfaced at the respective tow fish. Thus, the solution procedure has to be flexible to enable the investigation of multiple tow systems.

In order to represent fully the position and attitude of the tow fish, the system is modelled in three-dimensions. Although the fish is modelled to yield six degrees of freedom, *i.e.* surge, sway, heave, roll, pitch, and yaw, the cable model disregards the three angular displacements, as the linear displacements of the discrete cable segments are able to explain completely the position of the cable. Hence, the cable system is modelled and solved in the global coordinate system, although certain forces may need to be calculated in the local coordinate system.

However, when modelling the towed fish, one must develop and solve the differential equations describing the six degrees of freedom of the fish in the local coordinate system. This has to be integrated with the cable solution algorithm to ensure coupling between the fish and the cable systems. The model should also be versatile to deal with multiple fish, which again require integration with the cable system at the appropriate locations.

3.2 Axes System

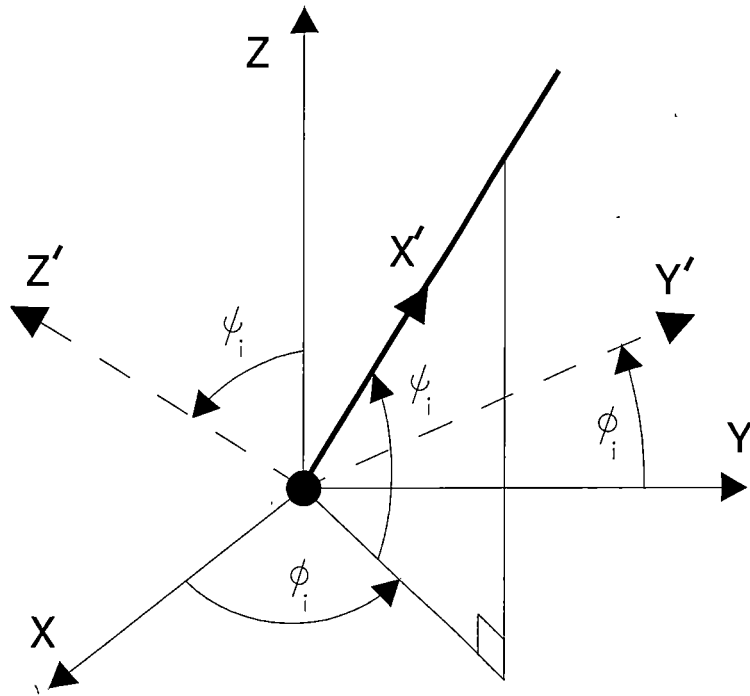
As the cable system is modelled as a discrete number of elements, and the tow fish is modelled as a separate entity to be integrated with the cable system, it is required to utilise the global and local coordinate systems to develop, solve, and describe the motions of the various components of the system.

3.2.1 Cable System Transformation Matrix

The cable model is developed and solved in the global coordinate system. However, terms such as cable drag forces and hydrodynamic added mass, need to be developed in the local coordinate system and transformed to the global coordinate system.

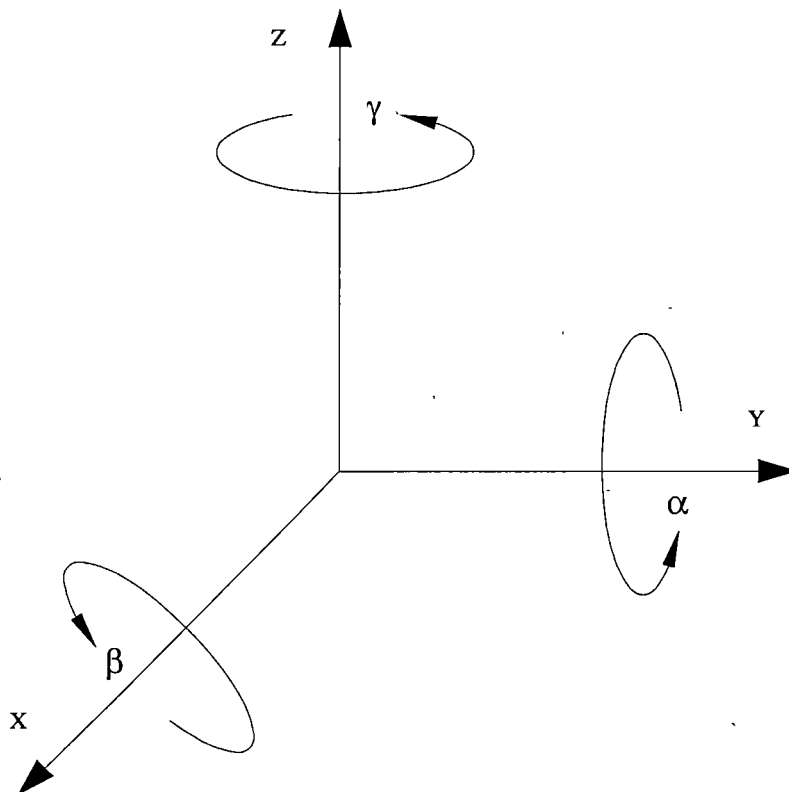
Figure 3.1 shows the global and local coordinate system as applied to the cable. The global coordinate system defined by X, Y, and Z represents the original axes of the surface tow point, *i.e.* the surface tow vessel. The positive directions of the global axes system are:

- X axis - the original direction of motion of the surface tow vessel;
- Y axis - to the left of the X axis; and
- Z axis - vertically upwards.



Coordinate Transformation for Cable

Figure 3.1



Right Hand Coordinate System for Towed Fish

Figure 3.2

The local coordinate system is obtained by rotating the cable segment horizontally in the right hand direction about the Z axis, and vertically in the left hand direction about the Y axis respectively. The end result is shown in Figure 3.1. The cable element is assumed to remain untwisted, *i.e.* allowing no rotation about the X axis. This is common among cable modelling techniques, with no significant difference to the results due to its omission (Chapman (1987) and Sun and Leonard (1998)). If the local coordinates are defined as X', Y' and Z', and if the horizontal (ϕ) and vertical (ψ) rotational angles are defined as:

- horizontal angle (ϕ) - angle of the cable with the X axis; and
- vertical angle (ψ) - angle of the cable with the X-Y plane

then the cable transformation matrix $[\Lambda]$ from the global coordinate system to the local coordinate system is given by,

$$[\Lambda] = \begin{bmatrix} \cos\phi \cos\psi & \sin\phi \cos\psi & \sin\psi \\ -\sin\phi & \cos\phi & 0 \\ -\cos\phi \sin\psi & -\sin\phi \sin\psi & \cos\psi \end{bmatrix} \quad (3.1)$$

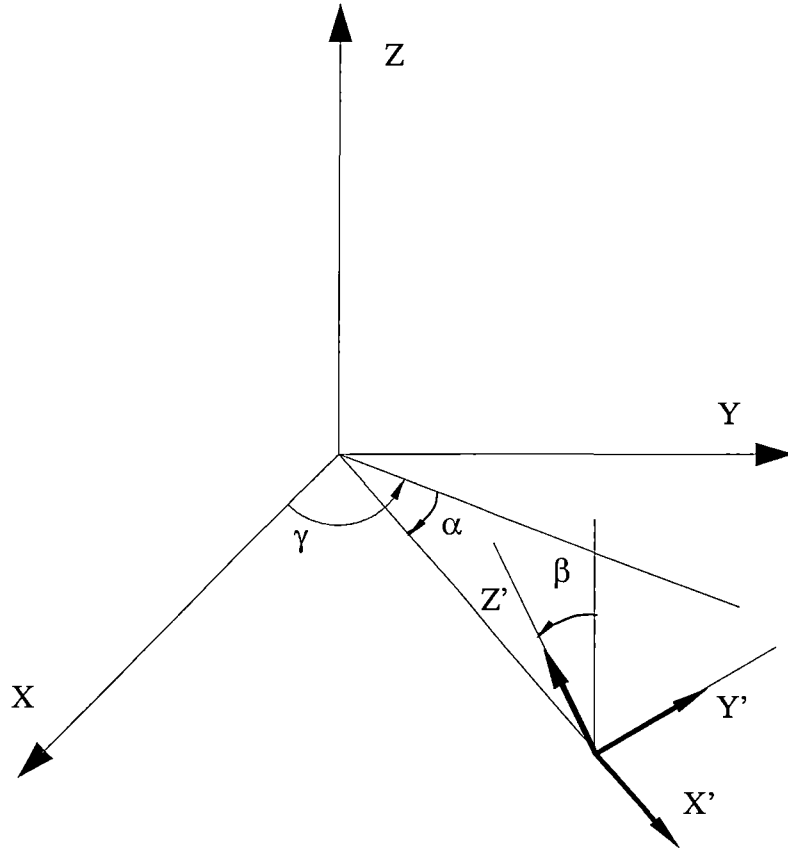
It can be shown that the inverse of the above transformation matrix is equal to the transpose of the matrix, *i.e.*,

$$[\Lambda]^{-1} = [\Lambda]^T \quad (3.2)$$

3.2.2 Tow Fish Transformation Matrix

The local coordinate system used to define the linear and angular position of the fish shown in Figure 3.2, is based on the *right-hand coordinate system*. Figure 3.3 shows the global and local coordinate system, with X, Y, and Z representing the former axes system and X', Y' and Z' representing the latter. The global axes system is identical to the global coordinate system described for the cable system. The local coordinate system is obtained by rotating the global system using the right hand rotation about each axis in turn. Thus,

- yaw motion (γ) - right hand rotation about the Z axis;
- pitch motion (α) - right hand rotation about the Y axis; and
- roll motion (β) - right hand rotation about the X axis.



Coordinate Transformation for Towed Fish

Figure 3.3

It is seen from Figure 3.3 that the towed fish transformation matrix $[\Lambda_f]$ from the global coordinate system to the local coordinate system is given by,

$$[\Lambda_f] = \begin{bmatrix} \cos\gamma \cos\alpha & \sin\gamma \cos\alpha & -\sin\alpha \\ -\sin\gamma \cos\beta + \cos\gamma \cos\alpha \sin\beta & \cos\gamma \cos\beta + \sin\gamma \sin\alpha \sin\beta & \cos\alpha \sin\beta \\ \cos\gamma \sin\alpha \cos\beta + \sin\gamma \sin\beta & \sin\gamma \sin\alpha \cos\beta - \cos\gamma \sin\beta & \cos\alpha \cos\beta \end{bmatrix} \quad (3.3)$$

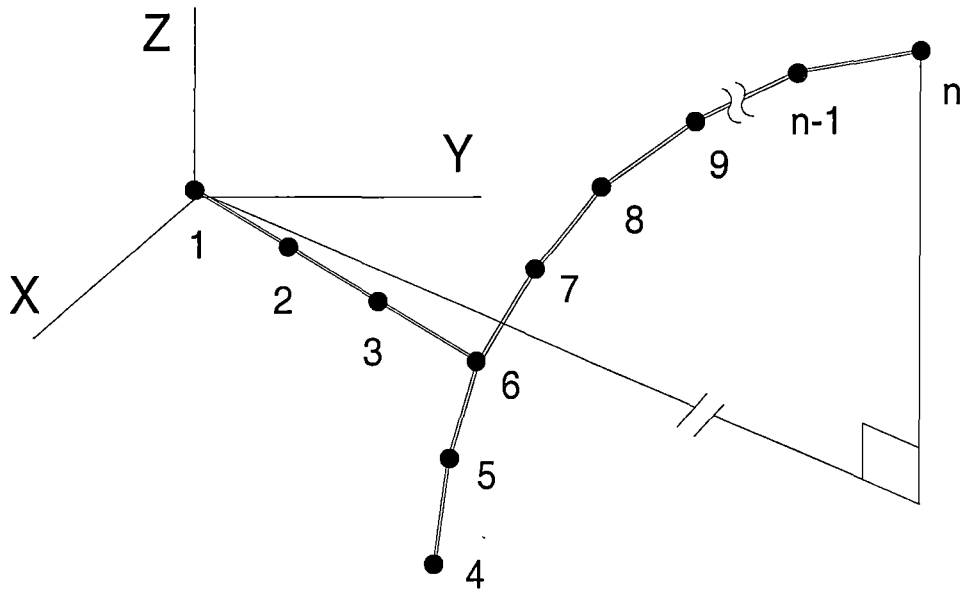
Just as for the cable transformation matrix, the inverse of the fish transformation matrix is equal to its transpose, *i.e.*,

$$[\Lambda_f]^{-1} = [\Lambda_f]^T \quad (3.4)$$

3.3 Cable Model

The modelling of the cable assumes the distributed mass of the tow cable to be represented by a series of discrete masses separated by weightless elastic straight-line segments, (*i.e.* the so called lumped mass approach). The cable segments are assumed incapable of carrying compressive loads or bending moments as is the practice with lumped mass models. The selection of this method over the others used in similar models, was due to the ease in representing the junction by defining the relevant boundary conditions for that node.

The lumped mass model is shown in Figure 3.4, with the nodes being numbered from the point of attachment of the cable to the tow fish, culminating at the upper end of the cable at the surface. The cable is assumed to be totally submerged throughout the simulation.



Lumped Mass Model of the Two-Part Tow

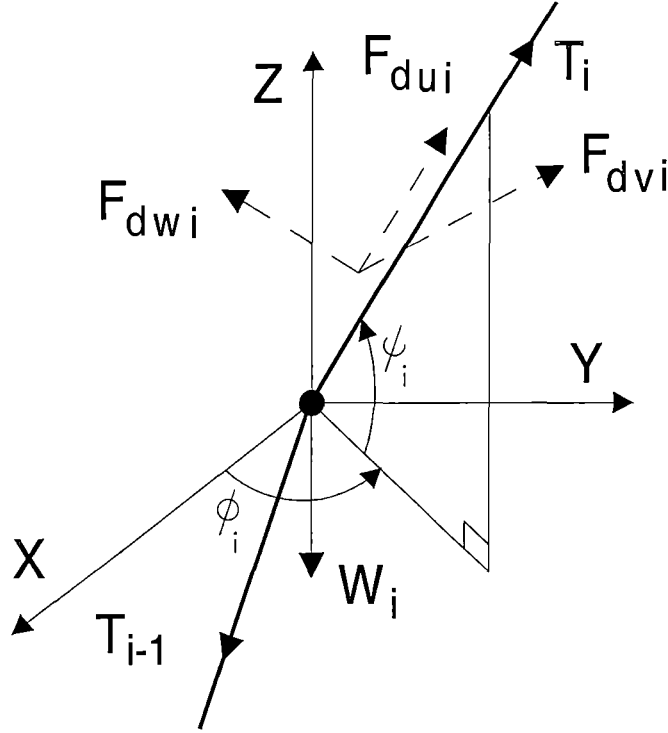
Figure 3.4

The motion of the cable can be described by applying Newton's law of motion to each node in turn. Figure 3.5 represents the “*i*”th node of the cable (excluding the junction and boundary nodes), from which the following equations of motion are obtained,

$$\underline{\underline{m}} \cdot \ddot{\underline{\underline{R}}} = \underline{\underline{F}} \quad (3.5)$$

where

$\underline{\underline{m}}$: element mass matrix
 $\ddot{\underline{R}}$: nodal acceleration vector
 $\underline{\underline{F}}$: nodal force vector.



Cable Node "i"

Figure 3.5

The node mass matrix ($\underline{\underline{m}}$) will include, half the mass of each segment adjacent to that node, any extra masses fitted to the node, and the added mass due to the acceleration of the surrounding fluid particles.

In obtaining the added mass, the cable acceleration is resolved in the tangential and normal directions to the cable axis and the resulting added mass effect is then resolved in the horizontal and vertical directions to ensure compatibility with the global axes system. These components plus the physical mass of the cable segments can be distributed to each node to yield a 3 x 3 mass matrix. Thus, the equations of motion for node "i" in matrix form are,

$$\begin{bmatrix} m_{111} & m_{112} & m_{113} \\ m_{121} & m_{122} & m_{123} \\ m_{131} & m_{132} & m_{133} \end{bmatrix} \cdot \begin{bmatrix} \ddot{x}_i \\ \ddot{y}_i \\ \ddot{z}_i \end{bmatrix} = \begin{bmatrix} F_{ix} \\ F_{iy} \\ F_{iz} \end{bmatrix} \quad (3.6)$$

where

- m_{iab} : where $a = 1, 2, 3$ and $b = 1, 2, 3$
the mass matrix terms of node “i”
 $\ddot{x}_i, \ddot{y}_i, \ddot{z}_i$: acceleration of node “i” in the X, Y, and Z directions respectively
 $F_{ix,y,z}$: forces on node “i” in the X, Y, and Z directions respectively

The mass matrix terms consisting of the mass, added mass and coupling terms are given by:

$$m_{i11} = m_i + m_{eix} + 0.5 \{ Am_{ti-1} \cos^2 \phi_{i-1} \cos^2 \psi_{i-1} + Am_{ti} \cos^2 \phi_i \cos^2 \psi_i + Am_{ni-1} [1 - \cos^2 \phi_{i-1} \cos^2 \psi_{i-1}] + Am_{ni} [1 - \cos^2 \phi_i \cos^2 \psi_i] \}$$

$$m_{i12} = 0.5 \{ [Am_{ti-1} - Am_{ni-1}] \sin \phi_{i-1} \cos \phi_{i-1} \cos^2 \psi_{i-1} + [Am_{ti} - Am_{ni}] \sin \phi_i \cos \phi_i \cos^2 \psi_i \}$$

$$m_{i13} = 0.5 \{ [Am_{ti-1} - Am_{ni-1}] \cos \phi_{i-1} \sin \psi_{i-1} \cos \psi_{i-1} + [Am_{ti} - Am_{ni}] \cos \phi_i \sin \psi_i \cos \psi_i \}$$

$$m_{i21} = m_{i12}$$

$$m_{i22} = m_i + m_{eiy} + 0.5 \{ Am_{ti-1} \sin^2 \phi_{i-1} \cos^2 \psi_{i-1} + Am_{ti} \sin^2 \phi_i \cos^2 \psi_i + Am_{ni-1} [1 - \sin^2 \phi_{i-1} \cos^2 \psi_{i-1}] + Am_{ni} [1 - \sin^2 \phi_i \cos^2 \psi_i] \}$$

$$m_{i23} = 0.5 \{ [Am_{ti-1} - Am_{ni-1}] \sin \phi_{i-1} \sin \psi_{i-1} \cos \psi_{i-1} + [Am_{ti} - Am_{ni}] \sin \phi_i \sin \psi_i \cos \psi_i \}$$

$$m_{i31} = m_{i13}$$

$$m_{i32} = m_{i23}$$

$$m_{i33} = m_i + m_{eiz} + 0.5 \{ Am_{ti-1} \sin^2 \psi_{i-1} + Am_{ti} \sin^2 \psi_i + Am_{ni-1} [1 - \cos^2 \psi_{i-1}] + Am_{ni} [1 - \cos^2 \psi_i] \}$$

(3.7)

where

- m_i : mass of node “i”, *i.e.* the addition of half the mass of each adjacent segments
 $m_{eix,y,z}$: mass and added mass of any additional weight attached to node “i”
 Am_{ti} : tangential added mass coefficient of cable segment “i”
 Am_{ni} : normal added mass coefficient of cable segment “i”.

The forces F_{ix} , F_{iy} , and F_{iz} will include the tensions in the adjacent segments, net weights of the cable segments in water, and the drag forces on the cables due to the cable - water interface. Hence, from Figure 3.5 these forces are given as,

$$F_{ix} = T_i \cos \phi_i \cos \psi_i - T_{i-1} \cos \phi_{i-1} \cos \psi_{i-1} + \frac{1}{2} F_{dix} + \frac{1}{2} F_{di-1x} - F_{eix} \quad (3.8a)$$

$$F_{iy} = T_i \sin \phi_i \cos \psi_i - T_{i-1} \sin \phi_{i-1} \cos \psi_{i-1} + \frac{1}{2} F_{diy} + \frac{1}{2} F_{di-1y} - F_{eiy} \quad (3.8b)$$

$$F_{iz} = T_i \sin \psi_i - T_{i-1} \sin \psi_{i-1} + \frac{1}{2} F_{diz} + \frac{1}{2} F_{di-1z} - F_{eiz} - W_i \quad (3.8c)$$

where

- T_i : tension of segment “i”
 $F_{dix,y,z}$: drag forces on segment “i” in the X, Y, and Z directions
 $F_{eix,y,z}$: any additional forces on node “i” in the X, Y, and Z directions
 W_i : net weight of node “i” in water, *i.e.* the addition of half the net weight of each adjacent segment

3.3.1 Drag Forces

The relative motion between the cable and the fluid will lead to a drag force resulting in a damping effect on the cable. In Chapter 2, the calculation of the drag forces on an underwater cable was dealt in detail. The method recommended to calculate these forces is the use of the modified Morison’s equation, *i.e.* equation (2.73), with the appropriate drag coefficients. Since the added mass of the cable is included in the cable’s mass matrix defined in equation (3.6), the inertia term in Morison’s equation (2.73) is ignored.

These drag forces will have components in the tangential and normal directions to the cable axis as shown in Figure 3.5, and will be proportional to the square of the relative cable velocity. These drag forces are first calculated in the local coordinate system

(see equations (2.72)) and transformed to the global coordinate system to be incorporated in equations (3.8).

In order to obtain the drag forces, it is first required to calculate the local relative velocities of the cable. The global relative nodal velocities (V_{nx} , V_{ny} , and V_{nz}) can be obtained by deducting the water current velocities (V_{cx} , V_{cy} , and V_{cz}) from the nodal global absolute velocities (\dot{x}_i , \dot{y}_i , and \dot{z}_i) as,

$$V_{nx} = \dot{x}_i - V_{cx} \quad (3.9a)$$

$$V_{ny} = \dot{y}_i - V_{cy} \quad (3.9b)$$

$$V_{nz} = \dot{z}_i - V_{cz} \quad (3.9c)$$

Segment “i” is located between nodes “i” and “i+1”. Therefore, the global relative velocities of cable segment “i” ($VS_{rix,y,z}$) can be obtained as the mean of the relative velocities of the two adjacent nodes, *i.e.*, nodes “i” and “i+1”. Thus,

$$VS_{rix} = (V_{rix} + V_{n+1x}) / 2 \quad (3.10a)$$

$$VS_{ny} = (V_{ny} + V_{n+1y}) / 2 \quad (3.10b)$$

$$VS_{nz} = (V_{nz} + V_{n+1z}) / 2 \quad (3.10c)$$

The local relative velocities ($VS_{rix',y',z'}$) of cable segment “i” are then obtained by multiplying the global relative velocities ($VS_{rix,y,z}$) by the transformation matrix $[A]$ for the cable element. Thus,

$$[VS_{rix',y',z'}] = [A] \cdot [VS_{rix,y,z}] \quad (3.11)$$

The local drag forces of cable segment “i” are then obtained from the reduced Morison's equation, (*i.e.* minus the inertia term) as,

$$F_{dix'} = 0.5 \cdot C_t \cdot \rho \cdot D_1 \cdot l_i \cdot VS_{rix'} \cdot |VS_{rix'}| \quad (3.12a)$$

$$F_{diy'} = 0.5 \cdot C_n \cdot \rho \cdot D_1 \cdot l_i \cdot VS_{ny'} \cdot |VS_{ny'}| \quad (3.12b)$$

$$F_{diz'} = 0.5 \cdot C_n \cdot \rho \cdot D_1 \cdot l_i \cdot VS_{nz'} \cdot |VS_{nz'}| \quad (3.12c)$$

The drag forces thus obtained are then transformed back to the global coordinate system using the inverse of the transformation matrix. Since $[\Lambda]^{-1} = [\Lambda]^T$,

$$[F_{dx,y,z}] = [\Lambda]^T \cdot [F_{dx',y',z'}] \quad (3.13)$$

Since the drag forces calculated above will influence the behaviour of the adjacent nodes, the former is distributed evenly between these nodes. Thus, the drag forces $F_{dx,y,z}$ for cable segment “i” is distributed evenly between nodes “i” and “i+1” respectively. Similarly the drag force on segment “i-1” is distributed evenly between nodes “i-1” and “i”, and so on. The distribution of the segment drag forces to the adjacent nodes is shown in equations (3.8).

3.4 Equations of Motion for Cable Nodes

Equation (3.6) describes the equations of motion for node “i”, (*i.e.* any node along the cable except the junction and boundary nodes), in matrix form. In this sub-section, this set of equations will be further developed. Expanding equation (3.6) gives,

$$m_{i11} \cdot \ddot{x}_i + m_{i12} \cdot \ddot{y}_i + m_{i13} \cdot \ddot{z}_i = F_{ix} \quad (3.14a)$$

$$m_{i21} \cdot \ddot{x}_i + m_{i22} \cdot \ddot{y}_i + m_{i23} \cdot \ddot{z}_i = F_{iy} \quad (3.14b)$$

$$m_{i31} \cdot \ddot{x}_i + m_{i32} \cdot \ddot{y}_i + m_{i33} \cdot \ddot{z}_i = F_{iz} \quad (3.14c)$$

From equation (3.14b), the acceleration in the Y-direction is obtained as,

$$\ddot{y}_i = \frac{F_{iy} - m_{i21} \cdot \ddot{x}_i - m_{i23} \cdot \ddot{z}_i}{m_{i22}} \quad (3.15)$$

Substituting equation (3.15) into equation (3.14a) gives,

$$\ddot{x}_i \cdot [m_{i11} \cdot m_{i22} - m_{i12} \cdot m_{i21}] + \ddot{z}_i \cdot [m_{i13} \cdot m_{i22} - m_{i12} \cdot m_{i23}] = m_{i22} \cdot F_{ix} - m_{i12} \cdot F_{iy} \quad (3.16)$$

Further, substituting (3.15) into equation (3.14c) gives,

$$\ddot{x}_i \cdot [m_{i31} \cdot m_{i22} - m_{i32} \cdot m_{i21}] + \ddot{z}_i \cdot [m_{i33} \cdot m_{i22} - m_{i32} \cdot m_{i23}] = m_{i22} \cdot F_{iz} - m_{i32} \cdot F_{iy} \quad (3.17)$$

Now defining:

$$I = (m_{i11} \cdot m_{i22}) - (m_{i12} \cdot m_{i21}) \quad (3.18a)$$

$$J = (m_{i33} \cdot m_{i22}) - (m_{i32} \cdot m_{i23}) \quad (3.18b)$$

$$K_1 = (m_{i13} \cdot m_{i22}) - (m_{i12} \cdot m_{i23}) \quad (3.18c)$$

$$K_2 = (m_{i31} \cdot m_{i22}) - (m_{i32} \cdot m_{i21}) \quad (3.18d)$$

and substituting equation (3.18) into equations (3.16) and (3.17) gives,

$$(I) \cdot \ddot{x}_i + (K_1) \cdot \ddot{z}_i = (m_{i22}) \cdot F_{ix} - (m_{i12}) \cdot F_{iy} \quad (3.19)$$

$$(K_2) \cdot \ddot{x}_i + (J) \cdot \ddot{z}_i = (m_{i22}) \cdot F_{iz} - (m_{i23}) \cdot F_{iy} \quad (3.20)$$

Solving equations (3.19) and (3.20) to give the accelerations \ddot{x}_i and \ddot{z}_i yields,

$$\ddot{x}_i = \{ J \cdot m_{i22} \cdot F_{ix} - K_1 \cdot m_{i22} \cdot F_{iz} + F_{iy} \cdot [K_1 \cdot m_{i32} - J \cdot m_{i12}] \} / \text{DEN} \quad (3.21)$$

$$\ddot{z}_i = \{ I \cdot m_{i22} \cdot F_{iz} - K_2 \cdot m_{i22} \cdot F_{ix} + F_{iy} \cdot [K_2 \cdot m_{i12} - I \cdot m_{i32}] \} / \text{DEN} \quad (3.22)$$

where

$$\text{DEN} = (I \cdot J) - (K_1 \cdot K_2) \quad (3.23)$$

Substituting (3.21) and (3.22) in (3.15) yields \ddot{y}_i as,

$$\begin{aligned} \ddot{y}_i = & \{ F_{ix} \cdot [K_2 \cdot m_{i23} - J \cdot m_{i21}] + F_{iz} \cdot [K_1 \cdot m_{i21} - I \cdot m_{i23}] + \\ & (F_{iy} / m_{i22}) \cdot [\text{DEN} - K_1 \cdot m_{i21} \cdot m_{i32} - K_2 \cdot m_{i23} \cdot m_{i12} - J \cdot m_{i21} \cdot m_{i12} - \\ & I \cdot m_{i32} \cdot m_{i23}] \} / \text{DEN} \end{aligned} \quad (3.24)$$

Now defining:

$$L = (\Delta t)^2 \cdot I / \text{DEN} \quad (3.25a)$$

$$M = (\Delta t)^2 \cdot J / \text{DEN} \quad (3.25b)$$

$$N_1 = (\Delta t)^2 \cdot K_1 / \text{DEN} \quad (3.25c)$$

$$N_2 = (\Delta t)^2 \cdot K_2 / \text{DEN} \quad (3.25d)$$

where “ Δt ” is the time step (increment). Substituting equations (3.25) into equations (3.21), (3.22), and (3.24) yields the accelerations as,

$$\ddot{x}_1 = \{ m_{i22} \cdot M \cdot F_{ix} - m_{i22} \cdot N_1 \cdot F_{iz} + F_{iy} \cdot [m_{i32} \cdot N_1 - m_{i12} \cdot M] \} / (\Delta t)^2 \quad (3.26a)$$

$$\begin{aligned} \ddot{y}_1 = & \{ F_{ix} \cdot [m_{i23} \cdot N_2 - m_{i21} \cdot M] + F_{iz} \cdot [m_{i21} \cdot N_1 - m_{i23} \cdot L] + \\ & (F_{iy} / m_{i22}) \cdot [(\Delta t)^2 - m_{i21} \cdot m_{i32} \cdot N_1 - m_{i23} \cdot m_{i12} \cdot N_2 - m_{i21} \cdot m_{i12} \cdot M - \\ & m_{i32} \cdot m_{i23} \cdot L] \} / (\Delta t)^2 \end{aligned} \quad (3.26b)$$

$$\ddot{z}_1 = \{ m_{i22} \cdot L \cdot F_{iz} - m_{i22} \cdot N_2 \cdot F_{ix} + F_{iy} \cdot [m_{i12} \cdot N_2 - m_{i32} \cdot L] \} / (\Delta t)^2 \quad (3.26c)$$

Now considering the forces on node “i” given by equations (3.8). It is possible to separate the tension terms and express them as,

$$F_{ix} = T_i \cos \phi_i \cos \psi_i - T_{i-1} \cos \phi_{i-1} \cos \psi_{i-1} + F_{iox} \quad (3.27a)$$

$$F_{iy} = T_i \sin \phi_i \cos \psi_i - T_{i-1} \sin \phi_{i-1} \cos \psi_{i-1} + F_{ioy} \quad (3.27b)$$

$$F_{iz} = T_i \sin \psi_i - T_{i-1} \sin \psi_{i-1} + F_{ioz} \quad (3.27c)$$

where $F_{iox,y,z}$ represents all forces acting on the node, except for the tension forces, *i.e.* drag forces, weight, buoyancy etc. Now substituting equations (3.27) into equations (3.26) gives the global accelerations \ddot{x}_1 , \ddot{y}_1 , and \ddot{z}_1 of the node as,

$$\ddot{x}_1 = (-P_{xi} T_{i-1} + R_{xi} T_i + S_{xi}) / (\Delta t)^2 \quad (3.28a)$$

$$\ddot{y}_1 = (-P_{yi} T_{i-1} + R_{yi} T_i + S_{yi}) / (\Delta t)^2 \quad (3.28b)$$

$$\ddot{z}_1 = (-P_{zi} T_{i-1} + R_{zi} T_i + S_{zi}) / (\Delta t)^2 \quad (3.28c)$$

where

$$\begin{aligned}
P_{xi} &= m_{i22} \cdot M \cdot CT_{xi-1} - m_{i22} \cdot N_1 \cdot CT_{zi-1} + (m_{i32} \cdot N_1 - m_{i12} \cdot M) \cdot CT_{yi-1} \\
P_{yi} &= (m_{i23} \cdot N_2 - m_{i21} \cdot M) \cdot CT_{xi-1} + (m_{i21} \cdot N_1 - m_{i23} \cdot L) \cdot CT_{zi-1} + P_{yie} \\
P_{zi} &= m_{i22} \cdot L \cdot CT_{zi-1} - m_{i22} \cdot N_2 \cdot CT_{xi-1} + (m_{i12} \cdot N_2 - m_{i32} \cdot L) \cdot CT_{yi-1} \\
R_{xi} &= m_{i22} \cdot M \cdot CT_{xi} - m_{i22} \cdot N_1 \cdot CT_{zi} + (m_{i32} \cdot N_1 - m_{i12} \cdot M) \cdot CT_{yi} \\
R_{yi} &= (m_{i23} \cdot N_2 - m_{i21} \cdot M) \cdot CT_{xi} + (m_{i21} \cdot N_1 - m_{i23} \cdot L) \cdot CT_{zi} + R_{yie} \\
R_{zi} &= m_{i22} \cdot L \cdot CT_{zi} - m_{i22} \cdot N_2 \cdot CT_{xi} + (m_{i12} \cdot N_2 - m_{i32} \cdot L) \cdot CT_{yi} \\
S_{xi} &= m_{i22} \cdot M \cdot F_{iox} - m_{i22} \cdot N_1 \cdot F_{ioz} + (m_{i32} \cdot N_1 - m_{i12} \cdot M) \cdot F_{ioy} \\
S_{yi} &= (m_{i23} \cdot N_2 - m_{i21} \cdot M) \cdot F_{iox} + (m_{i21} \cdot N_1 - m_{i23} \cdot L) \cdot F_{ioz} + S_{yie} \\
S_{zi} &= m_{i22} \cdot L \cdot F_{ioz} - m_{i22} \cdot N_2 \cdot F_{iox} + (m_{i12} \cdot N_2 - m_{i32} \cdot L) \cdot F_{ioy}
\end{aligned} \tag{3.29a}$$

and where

$$\begin{aligned}
P_{yie} &= \{ (\Delta t)^2 - (m_{i21} \cdot m_{i32} \cdot N_1 + m_{i12} \cdot m_{i23} \cdot N_2 - m_{i12} \cdot m_{i21} \cdot M - m_{i23} \cdot m_{i32} \cdot L) / m_{i22} \} \cdot CT_{yi-1} \\
R_{yie} &= \{ (\Delta t)^2 - (m_{i21} \cdot m_{i32} \cdot N_1 + m_{i12} \cdot m_{i23} \cdot N_2 - m_{i12} \cdot m_{i21} \cdot M - m_{i23} \cdot m_{i32} \cdot L) / m_{i22} \} \cdot CT_{yi} \\
S_{yie} &= \{ (\Delta t)^2 - (m_{i21} \cdot m_{i32} \cdot N_1 + m_{i12} \cdot m_{i23} \cdot N_2 - m_{i12} \cdot m_{i21} \cdot M - m_{i23} \cdot m_{i32} \cdot L) / m_{i22} \} \cdot F_{ioy} \\
CT_{xi-1} &= \cos \phi_{i-1} \cdot \cos \psi_{i-1} \\
CT_{yi-1} &= \sin \phi_{i-1} \cdot \cos \psi_{i-1} \\
CT_{zi-1} &= \sin \psi_{i-1} \\
CT_{xi} &= \cos \phi_i \cdot \cos \psi_i
\end{aligned}$$

$$CT_{y1} = \sin \phi_1 \cdot \cos \psi_1$$

$$CT_{z1} = \sin \psi_1$$

(3.29b)

3.4.1 Junction

Equations (3.6), (3.8) and hence (3.28) obtained from Figure 3.5 are not valid for the node representing the junction (j), shown in Figure 3.6. This node includes in addition to the segments adjacent to the node, the final segment of the secondary cable represented by segment number “D-1”, where “D” is the node representing the depressor (see Figure 3.4 for the numbering of the nodes). The addition of this extra cable segment will result in the mass matrix ($\underline{\underline{m}}$) in equation (3.5) being modified to include the physical mass and the added mass of this extra cable segment. In addition, the extra forces at the node due to the additional cable segment will change equation (3.8). If subscript “j” represents the junction, then the equation of motion for node “j” is,

$$\begin{bmatrix} m_{j11} & m_{j12} & m_{j13} \\ m_{j21} & m_{j22} & m_{j23} \\ m_{j31} & m_{j32} & m_{j33} \end{bmatrix} \cdot \begin{bmatrix} \ddot{x}_j \\ \ddot{y}_j \\ \ddot{z}_j \end{bmatrix} = \begin{bmatrix} F_{jx} \\ F_{jy} \\ F_{jz} \end{bmatrix} \quad (3.30)$$

where

$$m_{j11} = m_{i11} + 0.5 \{ Am_{iD} \cos^2 \phi_{D-1} \cos^2 \psi_{D-1} + Am_{nD} [1 - \cos^2 \phi_{D-1} \cos^2 \psi_{D-1}] \}$$

$$m_{j12} = m_{i12} + 0.5 \{ [Am_{iD} - Am_{nD}] \sin \phi_{D-1} \cos \phi_{D-1} \cos^2 \psi_{D-1} \}$$

$$m_{j13} = m_{i13} + 0.5 \{ [Am_{iD} - Am_{nD}] \cos \phi_{D-1} \sin \psi_{D-1} \cos \psi_{D-1} \}$$

$$m_{j21} = m_{j12}$$

$$m_{j22} = m_{i22} + 0.5 \{ Am_{iD} \sin^2 \phi_{D-1} \cos^2 \psi_{D-1} + Am_{nD} [1 - \sin^2 \phi_{D-1} \cos^2 \psi_{D-1}] \}$$

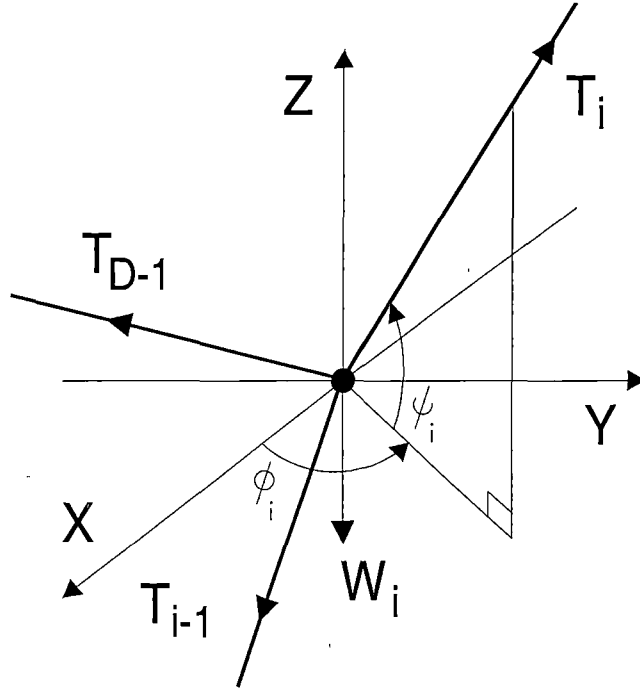
$$m_{j23} = m_{i23} + 0.5 \{ [Am_{iD} - Am_{nD}] \sin \phi_{D-1} \sin \psi_{D-1} \cos \psi_{D-1} \}$$

$$m_{j31} = m_{j13}$$

$$m_{j32} = m_{j23}$$

$$m_{j33} = m_{i33} + 0.5 \{ Am_{tD} \sin^2 \psi_{D-1} + Am_{nD} [1 - \cos^2 \psi_{D-1}] \}$$

where m_{i11} to m_{i33} are as defined in equations (3.7), however applied to the node representing the junction (*i.e.* node “j”). Am_{tD} and Am_{nD} are the tangential and normal added mass coefficients of the final cables segment of the secondary cable, *i.e.* segment number “D-1”.



Cable Junction Node “j”

Figure 3.6

The forces acting at the junction will include the terms in equation (3.8) applied to node “j”, plus the tension and drag forces of the secondary cable segment (D-1). Thus, the forces at node “j” are,

$$F_{ix} = T_j \cos \phi_j \cos \psi_j - T_{j-1} \cos \phi_{j-1} \cos \psi_{j-1} - T_{D-1} \cos \phi_{D-1} \cos \psi_{D-1} + \frac{1}{2} F_{dix} + \frac{1}{2} F_{dix} - \frac{1}{2} F_{dD-1x} - F_{ejx} \quad (3.31a)$$

$$F_{iy} = T_j \sin \phi_j \cos \psi_j - T_{j-1} \sin \phi_{j-1} \cos \psi_{j-1} - T_{D-1} \sin \phi_{D-1} \cos \psi_{D-1} + \frac{1}{2} F_{diy} + \frac{1}{2} F_{diy} + \frac{1}{2} F_{dD-1y} - F_{eiy} \quad (3.31b)$$

$$F_{Jz} = T_J \sin \psi_J - T_{J-1} \sin \psi_{J-1} - T_{D-1} \sin \psi_{D-1} + \frac{1}{2} F_{djz} + \frac{1}{2} F_{dj-1z} + \frac{1}{2} F_{dD-1z} - F_{ejz} - W_J \quad (3.31c)$$

The net weight W_J , will include the contribution by segment “D-1” in mass and buoyancy. Following the sequence described from equation (3.15) to (3.29), the equations of motion for the junction (*i.e.* equations (3.30)), will reduce to,

$$\ddot{x}_J = (-P_{xj} T_{J-1} + R_{xj} T_J + S_{xj} - P_{Dx} T_{D-1}) / (\Delta t)^2 \quad (3.32a)$$

$$\ddot{y}_J = (-P_{yj} T_{J-1} + R_{yj} T_J + S_{yj} - P_{Dy} T_{D-1}) / (\Delta t)^2 \quad (3.32b)$$

$$\ddot{z}_J = (-P_{zj} T_{J-1} + R_{zj} T_J + S_{zj} - P_{Dz} T_{D-1}) / (\Delta t)^2 \quad (3.32c)$$

where

$$P_{Dx} = m_{j22} \cdot M \cdot \cos \phi_{D-1} \cdot \cos \psi_{D-1} - m_{j22} \cdot N_1 \cdot \sin \psi_{D-1} + (m_{j32} \cdot N_1 - m_{j12} \cdot M) \cdot \sin \phi_{D-1} \cdot \cos \psi_{D-1}$$

$$P_{Dy} = (m_{j23} \cdot N_2 - m_{j21} \cdot M) \cdot \cos \phi_{D-1} \cdot \cos \psi_{D-1} + (m_{j21} \cdot N_1 - m_{j23} \cdot L) \cdot \sin \psi_{D-1} + P_{Dye}$$

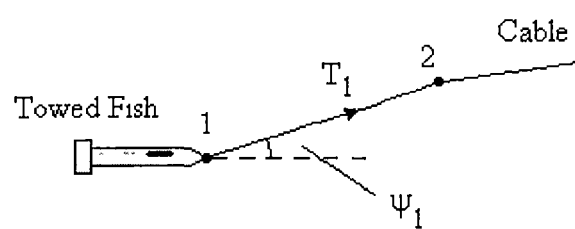
$$P_{Dz} = m_{j22} \cdot L \cdot \sin \psi_{D-1} - m_{j22} \cdot N_2 \cdot \cos \phi_{D-1} \cdot \cos \psi_{D-1} + (m_{j12} \cdot N_2 - m_{j32} \cdot L) \cdot \sin \phi_{D-1} \cdot \cos \psi_{D-1}$$

$$P_{Dye} = \{ (\Delta t)^2 - (m_{j23} \cdot m_{j32} \cdot N_1 + m_{j12} \cdot m_{j23} \cdot N_2 - m_{j12} \cdot m_{j21} \cdot M - m_{j23} \cdot m_{j32} \cdot L) \cdot \sin \phi_{D-1} \cdot \cos \psi_{D-1} \} / m_{j22}$$

Comparing equations (3.28) and (3.32), it is seen that the latter set of equations has an additional term due to the tension of the secondary cable acting on the node representing the junction (j).

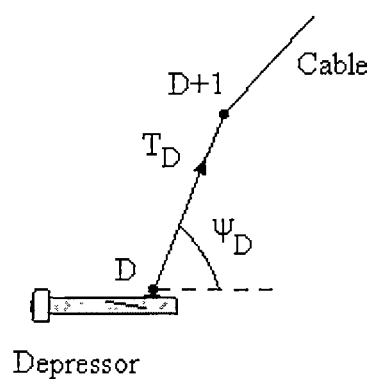
3.4.2 Boundary Nodes

When considering boundary nodes, (*e.g.* the surface, towed fish, and depressor node), only one cable segment is attached to the node, (see Figure 3.7). Therefore, equations (3.28) for node “i”, will need to be modified to reflect these changes.



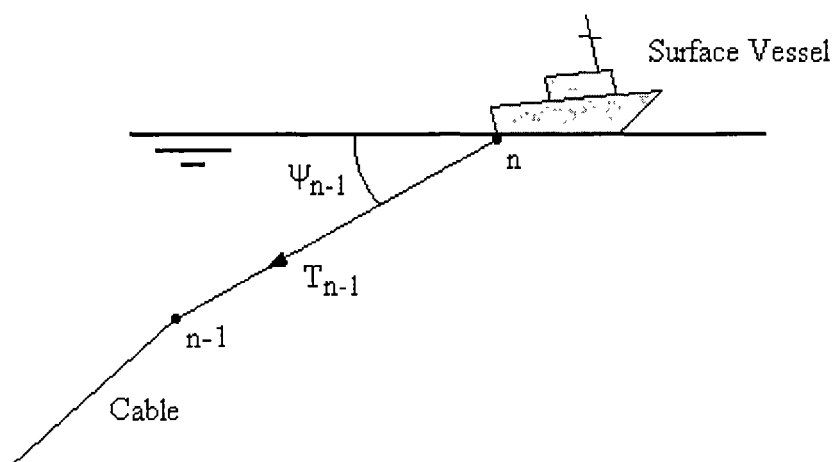
Towed Fish

(a)



Depressor

(b)



Surface Vessel

(c)

Boundary Nodes

Figure 3.7

Consider the nodes representing a towed or a depressor fish, with only one attached cable as shown in Figures 3.7(a) and 3.7(b), respectively. Therefore, the tension T_{i-1} in the set of equations in (3.28) will disappear, reducing them to,

$$\ddot{x}_i = (R_{xi} T_i + S_{xi}) / (\Delta t)^2 \quad (3.33a)$$

$$\ddot{y}_i = (R_{yi} T_i + S_{yi}) / (\Delta t)^2 \quad (3.33b)$$

$$\ddot{z}_i = (R_{zi} T_i + S_{zi}) / (\Delta t)^2 \quad (3.33c)$$

Similarly for the surface node (Figure 3.7(c)), the tension T_i will disappear and the set of equations in (3.28) reduces to,

$$\ddot{x}_i = (-P_{xi} T_{i-1} + S_{xi}) / (\Delta t)^2 \quad (3.34a)$$

$$\ddot{y}_i = (-P_{yi} T_{i-1} + S_{yi}) / (\Delta t)^2 \quad (3.34b)$$

$$\ddot{z}_i = (-P_{zi} T_{i-1} + S_{zi}) / (\Delta t)^2 \quad (3.34c)$$

3.5 Tow Fish Model

Since the model should be able to incorporate more than one fish, (see Figure 1.1), and the depressor used in the two-part tow configuration is in most cases a tow fish with negative lift, it is essential that the cable system be able to integrate the fish model into the solution algorithm. The modelling technique applied should be able to represent each tow fish at the appropriate node, thus enabling their integration into the cable solution, without affecting accuracy.

Unlike the cable system, which is modelled and solved in the global coordinate system, the fish needs to be modelled in a local coordinate system, thus enabling a true and easy representation of the six degrees of freedom necessary to describe the position and attitude of the body. However, in order to integrate the fish model into the solution algorithm of the cable system, the results from the local fish model has to be transformed to the global coordinate system. The appropriate transformation was explained in sub-section 3.2, resulting in the transformation matrix $[\Lambda_f]$ given by equation (3.3).

The modelling of the fish is based on the method described in Abkowitz (1969), modified by the author to suit the requirements of the tow configuration. Figure 3.8 shows the tow fish to be modelled in accordance with Newton's laws of motion. In order to apply the equations of motion, an origin for the tow fish has to be identified. The usual practice when applying equations of motion to submerged bodies, is to take the origin as its centre of gravity (G) or its geometric centre (O). However, since the fish model has to be solved as part of the cable system, the appropriate point to be selected as the origin would be the tow point, as it will be an integral part of the cable configuration.

In order to separate the force and moment equations, they will be considered as acting at the centre of gravity, however, they will be expressed in terms of components measured relative to the tow point. The latter point will be designated as "1", as the tow fish is usually fitted to the lower end of the cable system, and is therefore the first node in the system.

This notation will not be valid if the system consists of more than one tow fish or incorporate a depressor fish, as these additional fish will be attached to node numbers other than node 1, (see Figure 1.1). However, the notation described will be used to explain the modelling technique for tow fish, and may be modified as required for any additional fish in the system.

From hereon the subscripts used in this chapter are as follows:

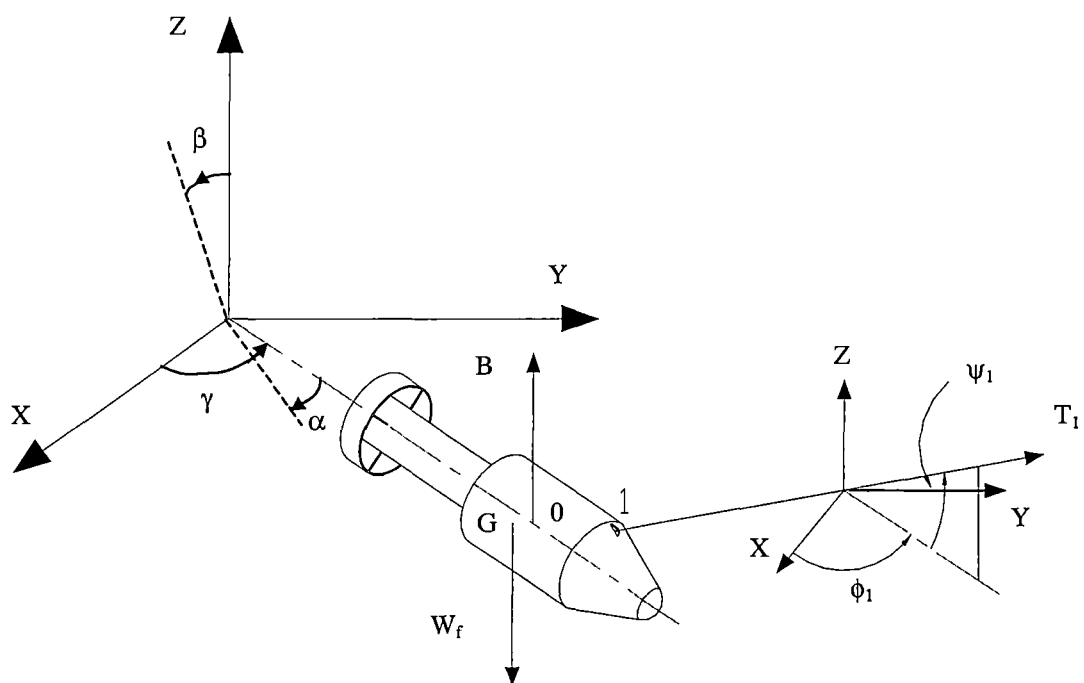
- F : tow (or depressor) fish
- G : centre of gravity
- O : geometric centre (centroid)
- 1 : tow point

From Figures 3.8 and 3.9, by applying linear and angular equations of motion to the centre of gravity (G), within the local coordinate system, we have,

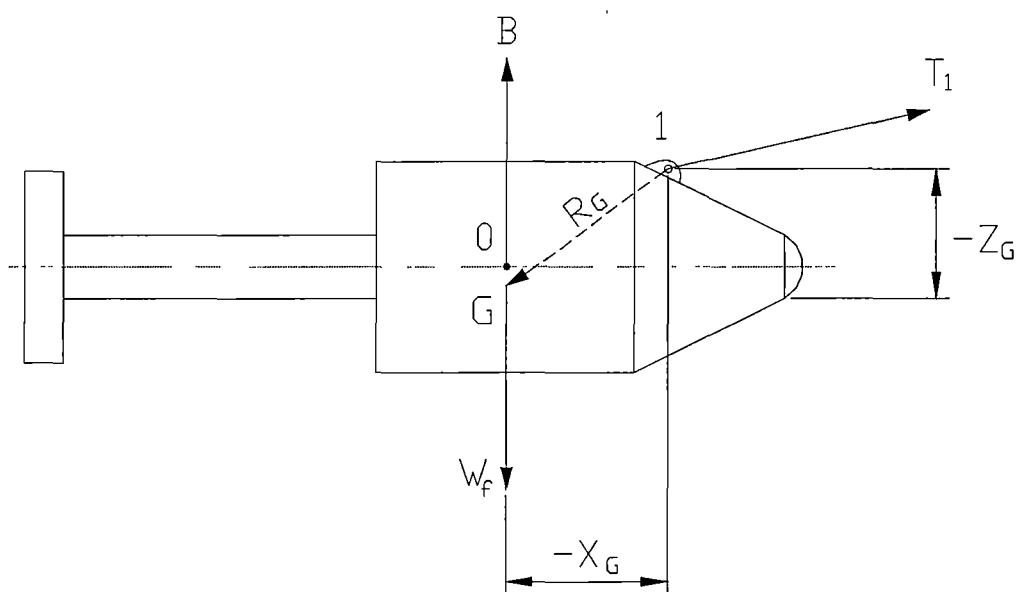
$$\overline{F}_f = \hat{i}.F_{fx'} + \hat{j}.F_{fy'} + \hat{k}.F_{fz'} = \frac{d(m_f \cdot \overline{U}_G)}{dt} \quad (3.35)$$

$$\overline{M}_{fG} = \hat{i}.M_{fGx'} + \hat{j}.M_{fGy'} + \hat{k}.M_{fGz'} = \frac{d(\text{Angular Momentum})_G}{dt} \quad (3.36)$$

where



Three-Dimensional Towed Fish
Figure 3.8



Geometry of the Towed Fish
Figure 3.9

- $\overline{\mathbf{F}}_f$: force vector acting on the fish
 $\overline{\mathbf{M}}_{fG}$: moment vector acting on the fish about its centre of gravity
 m_f : mass of fish
 $\overline{\mathbf{U}}_G$: velocity vector at the centre of gravity (G)
 $\hat{i}, \hat{j}, \hat{k}$: unit vectors along X', Y', and Z' (local) axes system.

It is now necessary to develop the equations expressed with the forces, moments, and velocities of the tow point (1). From Figure 3.9, the distance from the tow point (1) to the centre of gravity (G) is given by $\overline{\mathbf{R}}_G$, which has components X_G , Y_G , and Z_G , measured from the tow point and is positive in the directions of the local axes system.

3.5.1 Force Equations for Tow Fish

Let us first consider the force equation of motion given in (3.35).

$$\overline{\mathbf{F}}_f = \frac{d(m_f \cdot \overline{\mathbf{U}}_G)}{dt} = m_f \cdot \frac{d\overline{\mathbf{U}}_G}{dt} = m_f \cdot \dot{\overline{\mathbf{U}}}_G \quad (3.35)$$

The velocity vector $\overline{\mathbf{U}}_G$ at the centre of gravity G, will be equal to the velocity vector $\overline{\mathbf{U}}_1$ at the tow point (1), plus the velocity of “G” relative to “1”, *i.e.*,

$$\overline{\mathbf{U}}_G = \overline{\mathbf{U}}_1 + \frac{d(\overline{\mathbf{R}}_G)}{dt} = \overline{\mathbf{U}}_1 + \dot{\overline{\mathbf{R}}}_G \quad (3.37)$$

Since $\overline{\mathbf{R}}_G$ is a vector fixed within the fish, there will be no change in the length of $\overline{\mathbf{R}}_G$, as the fish is considered rigid. So the only change in $\overline{\mathbf{R}}_G$ will be in direction. Thus,

$$\dot{\overline{\mathbf{R}}}_G = \overline{\boldsymbol{\Omega}} \times \overline{\mathbf{R}}_G \quad (3.38)$$

where $\overline{\boldsymbol{\Omega}}$ is the angular velocity vector of the body, and will be the same at any point within the body. This angular velocity vector $\overline{\boldsymbol{\Omega}}$ is defined as,

$$\overline{\boldsymbol{\Omega}} = \hat{i} \cdot \frac{d\beta}{dt} + \hat{j} \cdot \frac{d\alpha}{dt} + \hat{k} \cdot \frac{d\gamma}{dt} \quad (3.39)$$

where α , β , and γ are the rotational motion of the fish defined in sub-section 3.2. Substituting equation (3.38) into equation (3.37) gives,

$$\bar{\mathbf{U}}_G = \bar{\mathbf{U}}_1 + \bar{\boldsymbol{\Omega}} \times \bar{\mathbf{R}}_G \quad (3.40)$$

Now substituting into equation (3.35) yields,

$$\bar{\mathbf{F}}_f = m_f \cdot \frac{d(\bar{\mathbf{U}}_1 + \bar{\boldsymbol{\Omega}} \times \bar{\mathbf{R}}_G)}{dt} \quad (3.41)$$

which expands to give,

$$\bar{\mathbf{F}}_f = m_f \cdot [\dot{\bar{\mathbf{U}}}_1 + (\dot{\bar{\boldsymbol{\Omega}}} \times \bar{\mathbf{R}}_G) + (\bar{\boldsymbol{\Omega}} \times \dot{\bar{\mathbf{R}}}_G)] \quad (3.42)$$

In order to solve equation (3.42), it is necessary to obtain expressions for the terms on the right hand side. Considering first the term $\bar{\mathbf{U}}_1$. The velocity vector $\bar{\mathbf{U}}_1$ will have three components u , v , and w along the local axes system, having unit vectors \hat{i} , \hat{j} , and \hat{k} respectively. Thus,

$$\bar{\mathbf{U}}_1 = \hat{i} \cdot u + \hat{j} \cdot v + \hat{k} \cdot w \quad (3.43)$$

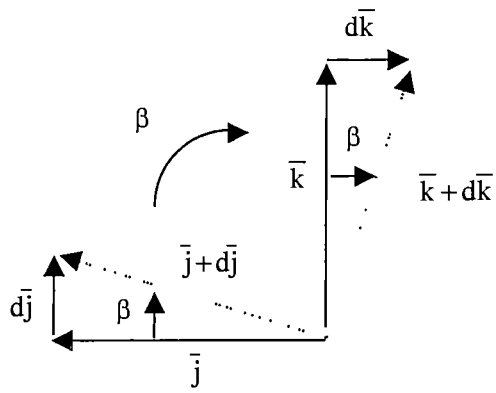
Differentiating with respect to time “ t ” gives,

$$\dot{\bar{\mathbf{U}}}_1 = \frac{d\bar{\mathbf{U}}_1}{dt} = \frac{d(\hat{i} \cdot u + \hat{j} \cdot v + \hat{k} \cdot w)}{dt} \quad (3.44)$$

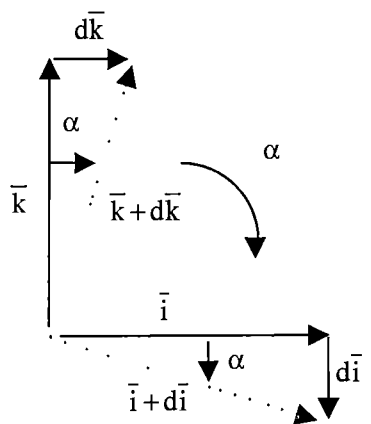
which expands to give,

$$\dot{\bar{\mathbf{U}}}_1 = \hat{i} \cdot \dot{u} + u \cdot \frac{d\hat{i}}{dt} + \hat{j} \cdot \dot{v} + v \cdot \frac{d\hat{j}}{dt} + \hat{k} \cdot \dot{w} + w \cdot \frac{d\hat{k}}{dt} \quad (3.45)$$

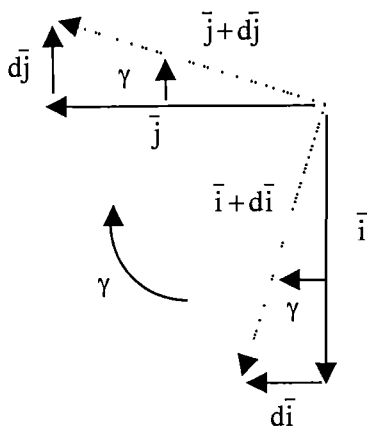
In order to simplify the above equation, it is necessary to obtain expressions for the terms $\frac{d\hat{i}}{dt}$, $\frac{d\hat{j}}{dt}$, and $\frac{d\hat{k}}{dt}$, which give the change in the unit vectors within the local axis system. These unit vectors \hat{i} , \hat{j} , and \hat{k} will not change in length over time. However, the same is not true for their directions, as they will change as the attitude of the body changes with body rotation. In order to develop expressions for this change, consider Figures 3.10(a, b, and c), which shows the rotation of the axes system about each axis separately, *i.e.* roll, pitch, and yaw. The changes to the vectors are given by $d\hat{i}$, $d\hat{j}$, and $d\hat{k}$, which is the product of the unit vector and the respective differential angle of rotation measured as a small angle in radians.



(a) Rotation about X Axis



(b) Rotation about Y Axis



(c) Rotation about Z Axis

Rotation of Unit Vectors of Towed Fish

Figure 3.10

From Figures 3.10(a, b, and c) respectively, the following can be deduced:

Rotation about the X axis - Roll - β

$$d\hat{i} = 0 \quad (3.46a)$$

$$d\hat{j} = \hat{k}.d\beta \quad (3.46b)$$

$$d\hat{k} = -\hat{j}.d\beta \quad (3.46c)$$

Rotation about the Y axis - Pitch - α

$$d\hat{i} = -\hat{k}.d\alpha \quad (3.47a)$$

$$d\hat{j} = 0 \quad (3.47b)$$

$$d\hat{k} = \hat{i}.d\alpha \quad (3.47c)$$

Rotation about the Z axis - Yaw - γ

$$d\hat{i} = \hat{j}.d\gamma \quad (3.48a)$$

$$d\hat{j} = -\hat{i}.d\gamma \quad (3.48b)$$

$$d\hat{k} = 0 \quad (3.48c)$$

As the rotational angles are small, the contributions of the three rotations can be added to yield,

$$d\hat{i} = \hat{i}.0 + \hat{j}.d\gamma - \hat{k}.d\alpha \quad (3.49a)$$

$$d\hat{j} = -\hat{i}.d\gamma + \hat{j}.0 + \hat{k}.d\beta \quad (3.49b)$$

$$d\hat{k} = \hat{i}.d\alpha - \hat{j}.d\beta + \hat{k}.0 \quad (3.49c)$$

Differentiating the above with respect to time “t” gives,

$$\frac{d\hat{i}}{dt} = \hat{i}.0 + \hat{j}.\frac{d\gamma}{dt} - \hat{k}.\frac{d\alpha}{dt} \quad (3.50a)$$

$$\frac{d\hat{j}}{dt} = -\hat{i}.\frac{d\gamma}{dt} + \hat{j}.0 + \hat{k}.\frac{d\beta}{dt} \quad (3.50b)$$

$$\frac{d\hat{k}}{dt} = \hat{i} \cdot \frac{d\alpha}{dt} - \hat{j} \cdot \frac{d\beta}{dt} + \hat{k} \cdot 0 \quad (3.50c)$$

Using the angular velocity vector $\overline{\Omega}$ defined in equation (3.39) gives,

$$\overline{\Omega} = \hat{i} \cdot p + \hat{j} \cdot q + \hat{k} \cdot r \quad (3.51)$$

where

$$p = \frac{d\beta}{dt}$$

$$q = \frac{d\alpha}{dt}$$

$$r = \frac{d\gamma}{dt}$$

Substituting into equations (3.50) yields,

$$\frac{d\hat{i}}{dt} = \hat{i} \cdot 0 + \hat{j} \cdot r - \hat{k} \cdot q \quad (3.52a)$$

$$\frac{d\hat{j}}{dt} = -\hat{i} \cdot r + \hat{j} \cdot 0 + \hat{k} \cdot p \quad (3.52b)$$

$$\frac{d\hat{k}}{dt} = \hat{i} \cdot q - \hat{j} \cdot p + \hat{k} \cdot 0 \quad (3.52c)$$

Substituting into equation (3.45) gives $\dot{\overline{U}}_1$ as,

$$\dot{\overline{U}}_1 = \hat{i} \cdot (\dot{u} + q \cdot w - r \cdot v) + \hat{j} \cdot (\dot{v} + r \cdot u - p \cdot w) + \hat{k} \cdot (\dot{w} + p \cdot v - q \cdot u) \quad (3.53)$$

Having obtained $\dot{\overline{U}}_1$, it is now needed to define $\overline{\Omega}$ and $\dot{\overline{\Omega}}$ in equation (3.42). Using the definition in equation (3.51), *i.e.*,

$$\overline{\Omega} = \hat{i} \cdot p + \hat{j} \cdot q + \hat{k} \cdot r \quad (3.51)$$

$\dot{\overline{\Omega}}$ is obtained by differentiating equation (3.51) with respect to time “t” as,

$$\dot{\bar{\Omega}} = \frac{d(\hat{i}.p + \hat{j}.q + \hat{k}.r)}{dt} = \hat{i}.\dot{p} + p.\frac{d\hat{i}}{dt} + \hat{j}.\dot{q} + q.\frac{d\hat{j}}{dt} + \hat{k}.\dot{r} + r.\frac{d\hat{k}}{dt} \quad (3.54)$$

Substituting from equations (3.52) into the above and simplifying gives,

$$\dot{\bar{\Omega}} = \hat{i}.\dot{p} + \hat{j}.\dot{q} + \hat{k}.\dot{r} \quad (3.55)$$

Now to obtain the term $\dot{\bar{R}}_G$ (see equation (3.42)), since,

$$\bar{R}_G = \hat{i}.X_G + \hat{j}.Y_G + \hat{k}.Z_G \quad (3.56)$$

By differentiating equation (3.56) with respect to time “t” gives $\dot{\bar{R}}_G$ as,

$$\dot{\bar{R}}_G = \frac{d\bar{R}_G}{dt} = \hat{i}.\dot{X}_G + X_G.\frac{d\hat{i}}{dt} + \hat{j}.\dot{Y}_G + Y_G.\frac{d\hat{j}}{dt} + \hat{k}.\dot{Z}_G + Z_G.\frac{d\hat{k}}{dt} \quad (3.57)$$

Now $\dot{X}_G = \dot{Y}_G = \dot{Z}_G = 0$, as \bar{R}_G is fixed within the body, (see equation (3.38)).

Substituting from equations (3.52) and simplifying gives,

$$\dot{\bar{R}}_G = \bar{\Omega} \times \bar{R}_G = \hat{i}.(q.Z_G - r.Y_G) + \hat{j}.(r.X_G - p.Z_G) + \hat{k}.(p.Y_G - q.X_G) \quad (3.58)$$

The right hand terms of equation (3.42) have now been obtained. Substituting equations (3.51), (3.53), (3.55), (3.56), and (3.58) into equation (3.42) and separating the respective local coordinate directions (*i.e.* X', Y', and Z') gives,

$$F_{fx'} = m_f . [\dot{u} + q.w - r.v - X_G (q^2 + r^2) + Y_G (p.q - \dot{r}) + Z_G (p.r + \dot{q})] \quad (3.59)$$

$$F_{fy'} = m_f . [\dot{v} + r.u - p.w - Y_G (r^2 + p^2) + Z_G (q.r - \dot{p}) + X_G (q.p + \dot{r})] \quad (3.60)$$

$$F_{fz'} = m_f . [\dot{w} + p.v - q.u - Z_G (p^2 + q^2) + X_G (r.p - \dot{q}) + Y_G (r.q + \dot{p})] \quad (3.61)$$

where

- u, v, w : linear velocities of the body along X', Y', and Z' (local) directions
- $\dot{u}, \dot{v}, \dot{w}$: linear accelerations of the body along X', Y', and Z' (local) directions
- p, q, r : angular velocities (roll, pitch, and yaw) defined in equation (3.51)
- $\dot{p}, \dot{q}, \dot{r}$: angular accelerations of the body about X', Y', and Z' axes

3.5.2 Moment Equations for Tow Fish

Now let us consider the moment equation given by equation (3.36), *i.e.*,

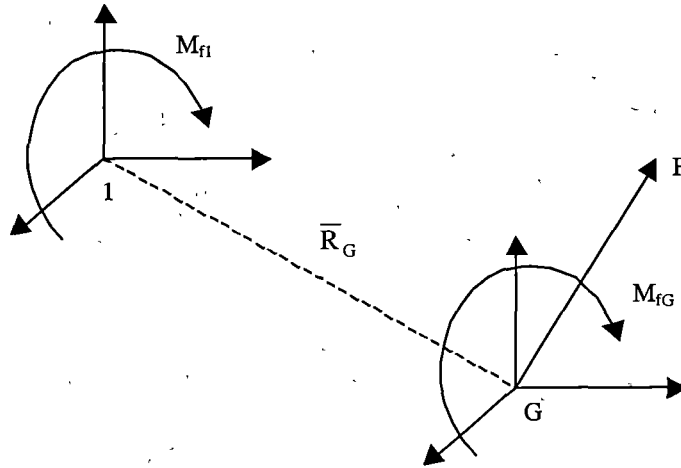
$$\overline{M}_{fG} = \hat{i}.M_{fGx} + \hat{j}.M_{fGy} + \hat{k}.M_{fGz} = \frac{d(\text{Angular Momentum})_G}{dt} \quad (3.36)$$

Using Figure 3.11, the moment about the tow point (1), *i.e.* \overline{M}_{f1} , can be expressed as:

The moment about the tow point (1), $(\overline{M}_{f1}) =$

the moment at the centre of gravity (G), $(\overline{M}_{fG}) +$

the moment caused by the force \overline{F}_f acting at the centre of gravity (G) at a distance \overline{R}_G from the tow point (1).



Forces and Moments at Tow Point (1) and Centre of Gravity (G) of Towed Fish

Figure 3.11

Thus,

$$\overline{M}_{f1} = \overline{M}_{fG} + (\overline{F}_f \times \overline{R}_G) \quad \text{or} \quad (3.62)$$

$$\overline{M}_{fG} = \overline{M}_{f1} - (\overline{F}_f \times \overline{R}_G) \quad (3.63)$$

Since the axes system considered at the centre of gravity (G), coincides with the principal axes of inertia, then the products of inertia are zero. Thus,

$$\overline{M}_{fG} = \frac{d\{(\hat{i}.I_{Gx}.\dot{\beta}) + (\hat{j}.I_{Gy}.\dot{\alpha}) + (\hat{k}.I_{Gz}.\dot{\gamma})\}}{dt} \quad (3.64)$$

where $I_{Gx',y',z'}$ are the moments of inertia of the towed fish at the centre of gravity around the X' , Y' , and Z' axes respectively.

The axes system at the origin, *i.e.* tow point (1), is parallel to the axes system at the centre of gravity (G) and have identical unit vectors, *i.e.* \hat{i} , \hat{j} , and \hat{k} . Thus, using the parallel axes theorem to express the moments of inertia ($I_{Gx',y',z'}$) at the centre of gravity (G), in terms of the moments of inertia ($I_{x',y',z'}$) at the tow point (1), we get,

$$I_{Gx'} = I_{x'} - m_f (Y_G^2 + Z_G^2) \quad (3.65a)$$

$$I_{Gy'} = I_{y'} - m_f (Z_G^2 + X_G^2) \quad (3.65b)$$

$$I_{Gz'} = I_{z'} - m_f (X_G^2 + Y_G^2) \quad (3.65c)$$

Substituting into equation (3.64) and using equation (3.58) gives,

$$\begin{aligned} \overline{M}_{fG} = & \frac{d}{dt} (\hat{i} \cdot I_{x'} \cdot p + \hat{j} \cdot I_{y'} \cdot q + \hat{k} \cdot I_{z'} \cdot r - \\ & - m_f [\hat{i} (Y_G^2 + Z_G^2) p + \hat{j} (Z_G^2 + X_G^2) q + \hat{k} (X_G^2 + Y_G^2) r]) \end{aligned} \quad (3.66)$$

$$\begin{aligned} \overline{M}_{fG} = & \frac{d}{dt} \{ \hat{i} \cdot I_{x'} \cdot p + \hat{j} \cdot I_{y'} \cdot q + \hat{k} \cdot I_{z'} \cdot r - m_f \cdot \overline{R}_G \times (\overline{\Omega} \times \overline{R}_G) \\ & - m_f [\hat{i} (X_G \cdot Y_G \cdot q + X_G \cdot Z_G \cdot r) + \hat{j} (X_G \cdot Y_G \cdot p + Y_G \cdot Z_G \cdot r) \\ & + \hat{k} (X_G \cdot Z_G \cdot p + Y_G \cdot Z_G \cdot q)] \} \end{aligned} \quad (3.67)$$

where p , q , and r are as defined in equation (3.51). Substituting equation (3.42) into (3.63), followed by its substitution into the left hand side of the above equation and expanding yields,

$$\begin{aligned} \overline{M}_{f1} = & \frac{d[\hat{i} \cdot I_{x'} \cdot p + \hat{j} \cdot I_{y'} \cdot q + \hat{k} \cdot I_{z'} \cdot r]}{dt} \\ & - m_f \cdot \frac{d[\overline{R}_G \times (\overline{\Omega} \times \overline{R}_G)]}{dt} + m_f \cdot \overline{R}_G \cdot \frac{d[\overline{U}_1 + (\overline{\Omega} \times \overline{R}_G)]}{dt} \\ & - m_f \cdot \frac{d}{dt} [\hat{i} (X_G \cdot Y_G \cdot q + X_G \cdot Z_G \cdot r) + \hat{j} (X_G \cdot Y_G \cdot p + Y_G \cdot Z_G \cdot r) \\ & + \hat{k} (X_G \cdot Z_G \cdot p + Y_G \cdot Z_G \cdot q)] \end{aligned} \quad (3.68)$$

Using equation (3.38) in the above and simplifying gives,

$$\begin{aligned}\overline{M}_{f1} = & \frac{d[\hat{i}.I_{x'} .p + \hat{j}.I_{y'} .q + \hat{k}.I_{z'} .r]}{dt} - m_f .(\overline{\Omega} \times \overline{R}_G) \times (\overline{\Omega} \times \overline{R}_G) \\ & + m_f .\overline{R}_G \times \frac{d\overline{U}_1}{dt} - m_f .\frac{d}{dt}[\hat{i}(X_G .Y_G .q + X_G .Z_G .r) \\ & + \hat{j}(X_G .Y_G .p + Y_G .Z_G .r) + \hat{k}(X_G .Z_G .p + Y_G .Z_G .q)]\end{aligned}\quad (3.69)$$

Consider the term $d[\hat{i}.I_{x'} .p + \hat{j}.I_{y'} .q + \hat{k}.I_{z'} .r] / dt$, in the above equation, it can be expanded to yield,

$$\begin{aligned}& \frac{d[\hat{i}.I_{x'} .p + \hat{j}.I_{y'} .q + \hat{k}.I_{z'} .r]}{dt} \\ & = \hat{i} .\frac{d(I_{x'} .p)}{dt} + I_{x'} .p .\frac{d\hat{i}}{dt} + \hat{j} .\frac{d(I_{y'} .q)}{dt} + I_{y'} .q .\frac{d\hat{j}}{dt} + \hat{k} .\frac{d(I_{z'} .r)}{dt} + I_{z'} .r .\frac{d\hat{k}}{dt}\end{aligned}\quad (3.70)$$

Since the inertia terms will remain constant over time, substituting equations (3.52) gives,

$$\begin{aligned}& \frac{d[\hat{i}.I_{x'} .p + \hat{j}.I_{y'} .q + \hat{k}.I_{z'} .r]}{dt} = \hat{i}.I_{x'} .\dot{p} + I_{x'} .p .(\hat{j}.r - \hat{k}.q) \\ & + \hat{j}.I_{y'} .\dot{q} + I_{y'} .q .(\hat{k}.p - \hat{i}.r) + \hat{k}.I_{z'} .\dot{r} + I_{z'} .r .(\hat{i}.q - \hat{j}.p)\end{aligned}\quad (3.71)$$

Separating the terms along the respective local axes gives,

$$\begin{aligned}& \frac{d[\hat{i}.I_{x'} .p + \hat{j}.I_{y'} .q + \hat{k}.I_{z'} .r]}{dt} = \hat{i}[I_{x'} .\dot{p} + (I_{z'} - I_{y'}) .q .r] + \hat{j}[I_{y'} .\dot{q} + (I_{x'} - I_{z'}) .r .p] \\ & + \hat{k}[I_{z'} .\dot{r} + (I_{y'} - I_{x'}) .p .q]\end{aligned}\quad (3.72)$$

Substituting equations (3.53), (3.56), and (3.72) into equation (3.69) and separating into the local (X', Y', and Z') axes system yields,

$$\begin{aligned}M_{fx'} = & I_{x'} .\dot{p} + (I_{z'} - I_{y'}) .q .r + m_f [Y_G (\dot{w} + p.v - q.u) - Z_G (\dot{v} + r.u - p.w) \\ & + X_G .Y_G (p.r - \dot{q}) - X_G .Z_G (p.q + \dot{r}) + Y_G .Z_G (r^2 - q^2)]\end{aligned}\quad (3.73)$$

$$\begin{aligned} M_{\dot{y}'} = I_{y'} \dot{q} + (I_{x'} - I_{z'}) r p + m_f [Z_G (\dot{u} + q w - r v) - X_G (\dot{w} + p v - q u) \\ + Y_G Z_G (q p - \dot{r}) - Y_G X_G (q r + \dot{p}) + X_G Z_G (p^2 - r^2)] \end{aligned} \quad (3.74)$$

$$\begin{aligned} M_{\dot{z}'} = I_{z'} \dot{r} + (I_{y'} - I_{x'}) p q + m_f [X_G (\dot{v} + r \dot{u} - p w) - Y_G (\dot{u} + q w - r v) \\ + Z_G X_G (r q - \dot{p}) - Z_G Y_G (r p + \dot{q}) + Y_G X_G (q^2 - p^2)] \end{aligned} \quad (3.75)$$

3.5.3 Linearisation of Equations

Equations (3.59), (3.60), (3.61), (3.73), (3.74), and (3.75) describe the motion of the tow fish, with the tow point (1) considered as the origin. In order to simplify the above set of equations, it is possible to separate the vertical and horizontal motions and then linearise the equations.

In separating the vertical and horizontal motions, we decouple the following degrees of freedom:

- Vertical Motion - surge, heave, and pitch (x' , z' , and α)
- Horizontal Motion - surge, sway, roll, and yaw (x' , y' , β , and γ).

In order to linearise the equations, let us consider the vertical motion first. In this case, any term having sway, roll, yaw, or their derivatives are neglected. In addition, equations (3.60), (3.73), and (3.75) can be neglected as they describe horizontal motions.

For the towed bodies considered, the term Y_G , *i.e.* the distance from the tow point (1) to the centre of gravity (G), along the Y axis is considered zero. This term can be incorporated into the model with little modification, however, it is rarely non-zero due to symmetry. Thus, equations (3.59), (3.61), and (3.74) will reduce to,

$$F_{\dot{x}'} = m_f [\dot{u} + \dot{\alpha} w - X_G \dot{\alpha}^2 + Z_G \ddot{\alpha}] \quad (3.76a)$$

$$F_{\dot{z}'} = m_f [\dot{w} - \dot{\alpha} u - Z_G \dot{\alpha}^2 - X_G \ddot{\alpha}] \quad (3.76b)$$

$$M_{\dot{y}'} = I_{y'} \ddot{\alpha} + m_f [Z_G (\dot{u} + \dot{\alpha} w) - X_G (\dot{w} - \dot{\alpha} u)] \quad (3.76c)$$

When linearising the above equations, all variables will be measured from an initial value. For example, heave velocity (w) is expanded as,

$$w = w_0 + \Delta w \quad (3.77)$$

where w_0 is the initial (or equilibrium) value and Δw is the change from the initial value. Now for all variables except surge velocity (u_0), the initial value will be zero. Thus, equation (3.77) reduces to,

$$w = \Delta w \quad (3.78)$$

However, since the body may have initial forward speed, the surge velocity value will be,

$$u = u_0 + \Delta u \quad (3.79)$$

Thus, all terms in equations (3.76) can be replaced by linearised terms to give,

$$F_{fx'} = m_f [\Delta \dot{u} + \Delta \dot{\alpha} \Delta w - X_G \Delta \dot{\alpha}^2 + Z_G \Delta \ddot{\alpha}] \quad (3.80a)$$

$$F_{fz'} = m_f [\Delta \dot{w} - u_0 \Delta \dot{\alpha} - \Delta \dot{\alpha} \Delta u - Z_G \Delta \dot{\alpha}^2 - X_G \Delta \ddot{\alpha}] \quad (3.80b)$$

$$M_{fy'} = I_y \Delta \ddot{\alpha} + m_f [Z_G (\Delta \dot{u} + \Delta \dot{\alpha} \Delta w) - X_G (\Delta \dot{w} - u_0 \Delta \dot{\alpha} - \Delta \dot{\alpha} \Delta u)] \quad (3.80c)$$

Neglecting the higher order terms and dropping the Δ prefix, equations (3.80) reduce to,

$$F_{fx'} = m_f [\dot{u} + Z_G \ddot{\alpha}] \quad (3.81a)$$

$$F_{fz'} = m_f [\dot{w} - X_G \ddot{\alpha} - u_0 \dot{\alpha}] \quad (3.81b)$$

$$M_{fy'} = I_y \ddot{\alpha} + m_f [Z_G \dot{u} - X_G \dot{w} - X_G u_0 \dot{\alpha}] \quad (3.81c)$$

Now considering the horizontal motion, any terms having heave, pitch, or their derivatives are neglected, together with equations (3.61) and (3.74) as they describe vertical motions. Again the term Y_G is considered to be zero. Thus, equations (3.59), (3.60), (3.73), and (3.75) will reduce to,

$$F_{fx'} = m_f [\dot{u} - \dot{\gamma} v - X_G (\dot{\gamma}^2) + Z_G (\dot{\beta} \dot{\gamma})] \quad (3.82a)$$

$$F_{fy'} = m_f [\dot{v} + \dot{\gamma} \cdot u + Z_G (\ddot{\beta}) + X_G (\ddot{\gamma})] \quad (3.82b)$$

$$M_{fx'} = I_{x'} \ddot{\beta} + m_f [-Z_G (\dot{v} + \dot{\gamma} \cdot u) - X_G \cdot Z_G (\ddot{\gamma})] \quad (3.82c)$$

$$M_{fz'} = I_{z'} \ddot{\gamma} + m_f [X_G (\dot{v} + \dot{\gamma} \cdot u) + Z_G \cdot X_G (-\ddot{\beta})] \quad (3.82d)$$

Following a similar linearisation exercise as described for the vertical motions, we obtain,

$$F_{fx'} = m_f \cdot \dot{u} \quad (3.83a)$$

$$F_{fy'} = m_f [\dot{v} + u_0 \cdot \dot{\gamma} - Z_G \ddot{\beta} + X_G \ddot{\gamma}] \quad (3.83b)$$

$$M_{fx'} = I_{x'} \ddot{\beta} - m_f [Z_G \cdot \dot{v} + Z_G \cdot u_0 \cdot \dot{\gamma} + X_G \cdot Z_G \ddot{\gamma}] \quad (3.83c)$$

$$M_{fz'} = I_{z'} \ddot{\gamma} + m_f [X_G \cdot \dot{v} + X_G \cdot u_0 \cdot \dot{\gamma} - Z_G \cdot X_G \ddot{\beta}] \quad (3.83d)$$

Now using equations (3.81) and (3.83), collecting the acceleration terms on one side and placing the equations in matrix form, gives the following set of equations in the local coordinate system,

$$\begin{bmatrix} F_{fx'} \\ F_{fy'} - m_f \cdot u_0 \cdot \dot{\gamma} \\ F_{fz'} + m_f \cdot u_0 \cdot \dot{\alpha} \\ M_{fx'} + m_f \cdot Z_G \cdot u_0 \cdot \dot{\gamma} \\ M_{fy'} + m_f \cdot X_G \cdot u_0 \cdot \dot{\alpha} \\ M_{fz'} + m_f \cdot X_G \cdot u_0 \cdot \dot{\gamma} \end{bmatrix} = \begin{bmatrix} m_f & 0 & 0 & 0 & m_f \cdot Z_G & 0 \\ 0 & m_f & 0 & -m_f \cdot Z_G & 0 & m_f \cdot X_G \\ 0 & 0 & m_f & 0 & -m_f \cdot X_G & 0 \\ 0 & -m_f \cdot Z_G & 0 & I_{x'} & 0 & -m_f \cdot X_G \cdot Z_G \\ m_f \cdot Z_G & 0 & -m_f \cdot X_G & 0 & I_{y'} & 0 \\ 0 & m_f \cdot X_G & 0 & -m_f \cdot X_G \cdot Z_G & 0 & I_{z'} \end{bmatrix} \cdot \begin{bmatrix} \dot{u} \\ \dot{v} \\ \dot{w} \\ \ddot{\beta} \\ \ddot{\alpha} \\ \ddot{\gamma} \end{bmatrix} \quad (3.84)$$

In the force and moment terms of the matrix, there will be terms representing the added mass and added inertia of the tow fish, which can be transposed into the mass matrix. Further, by representing all the left hand side terms within a row in equation (3.84) by the single terms $F'_{fx',y',z'}$ and $M'_{fx',y',z'}$ gives,

$$\begin{bmatrix} F'_{fx'} \\ F'_{fy'} \\ F'_{fz'} \\ M'_{fx'} \\ M'_{fy'} \\ M'_{fz'} \end{bmatrix} = [\text{Fish Mass Matrix}] \bullet \begin{bmatrix} \dot{u} \\ \dot{v} \\ \dot{w} \\ \ddot{\beta} \\ \ddot{\alpha} \\ \ddot{\gamma} \end{bmatrix} \quad (3.85)$$

where [Fish Mass Matrix] =

$$\begin{bmatrix} m_f + Am_{fx'} & 0 & 0 & 0 & m_f \cdot Z_G & 0 \\ 0 & m_f + Am_{fy'} & 0 & -m_f \cdot Z_G & 0 & m_f \cdot X_G \\ 0 & 0 & m_f + Am_{fz'} & 0 & -m_f \cdot X_G & 0 \\ 0 & -m_f \cdot Z_G & 0 & I_{x'} + AI_{x'} & 0 & -m_f \cdot X_G \cdot Z_G \\ m_f \cdot Z_G & 0 & -m_f \cdot X_G & 0 & I_{y'} + AI_{y'} & 0 \\ 0 & m_f \cdot X_G & 0 & -m_f \cdot X_G \cdot Z_G & 0 & I_{z'} + AI_{z'} \end{bmatrix}$$

3.5.4 Equations of Motion for Tow Fish

In order to solve the above set of equations, it is needed to find the forces and moments acting on the fish. Although it is possible to calculate these values using theoretical methods, in practice it is much simpler to obtain these values using experimental data. Either way, the values obtained are converted to a non-dimensional coefficient and plotted against the various vertical and horizontal angles of attack. The conversion to non-dimensional form is obtained using the relationships presented in sub-section 2.5 of Chapter 2, *i.e.* equations (2.105) and (2.106),

$$\text{Force coefficient} = \text{Force} / (0.5 \cdot \rho \cdot A_{fx} \cdot V_{fr}^2) \quad (3.86)$$

$$\text{Moment coefficient} = \text{Moment} / (0.5 \cdot \rho \cdot A_{fx} \cdot l_f \cdot V_{fr}^2) \quad (3.87)$$

where

ρ : density of liquid
 A_{fx} : cross sectional area of the fish perpendicular to the x axis
 l_f : length of fish
 V_{fr} : relative velocity between the fish and the surrounding liquid

The force or moment coefficient at any given angle of attack can then be obtained by a curve fitting method utilised to develop an appropriate equation. The coefficient is then multiplied by the appropriate equation defined in (3.86) and (3.87) to give the force or moment under the prevailing conditions. The experimental procedure to obtain the force and moment coefficients and the curve fitting technique are described in Chapter 6.

Since the origin of the fish is taken as the tow point (1) to enable its integration into the cable solution algorithm, the cable tension will not have any effect on the moments. However, the force equation will include the tension terms. If the fish has more than one cable segment attached to it (see Figure 1.1), then the second cable needs to be considered with due respect to the location of its attachment point, (see Chapter 4 for further discussion on this topic). Weight and buoyancy forces and their respective moments are simply calculated along the local coordinate system and added to the respective equations. The complete force and moment equations will be obtained along the local coordinate system and will include the following terms,

$$F_{fx',y',z'} = \text{cable tension(s) + cable drag forces + fish lift \& drag forces + weight + buoyancy.} \quad (3.88a)$$

$$M_{fx',y',z'} = \text{moments due to weight and buoyancy + moments due to fish attitude + moments due to hydrodynamic damping + moments due to second cable tension (if present).} \quad (3.88b)$$

Returning to the equations defined in (3.85), one needs to solve these in the local coordinate system before transforming the results to the global coordinate system. However, to include the equations in the cable solution algorithm, the six degree of freedom system has to be represented by a three degree of freedom system. Although this will yield a slight error in the solution, it will disappear during the iteration

process explained in Chapter 4. Writing the equations given in (3.85), with the mass matrix terms represented by Af_{11} to Af_{66} ,

$$F'_{fx} = Af_{11} \cdot \dot{u} + Af_{12} \cdot \dot{v} + Af_{13} \cdot \dot{w} + 0 + Af_{15} \cdot \ddot{\alpha} + 0 \quad (3.89)$$

$$F'_{fy} = Af_{21} \cdot \dot{u} + Af_{22} \cdot \dot{v} + Af_{23} \cdot \dot{w} + Af_{24} \cdot \ddot{\beta} + 0 + Af_{26} \cdot \ddot{\gamma} \quad (3.90)$$

$$F'_{fz} = Af_{31} \cdot \dot{u} + Af_{32} \cdot \dot{v} + Af_{33} \cdot \dot{w} + 0 + Af_{35} \cdot \ddot{\alpha} + 0 \quad (3.91)$$

$$M'_{fx} = 0 + Af_{42} \cdot \dot{v} + 0 + Af_{44} \cdot \ddot{\beta} + 0 + Af_{46} \cdot \ddot{\gamma} \quad (3.92)$$

$$M'_{fy} = Af_{51} \cdot \dot{u} + 0 + Af_{53} \cdot \dot{w} + 0 + Af_{55} \cdot \ddot{\alpha} + 0 \quad (3.93)$$

$$M'_{fz} = 0 + Af_{62} \cdot \dot{v} + 0 + Af_{64} \cdot \ddot{\beta} + 0 + Af_{66} \cdot \ddot{\gamma} \quad (3.94)$$

Now using equations (3.92), (3.93), and (3.94) to eliminate $\ddot{\alpha}$, $\ddot{\beta}$, and $\ddot{\gamma}$ as,

$$\ddot{\alpha} = \frac{M'_{fy} - Af_{51} \cdot \dot{u} - Af_{53} \cdot \dot{w}}{Af_{55}} \quad (3.95a)$$

$$\ddot{\beta} = \frac{1}{Af_{44}} \{ M'_{fx} \left[1 + \frac{Af_{46} \cdot A_{\Pi} \cdot Af_{64}}{Af_{44}} \right] - [Af_{46} \cdot A_{\Pi} \cdot M'_{fz}] - [Af_{42} - Af_{46} \cdot A_{\Pi} \cdot B_{\Pi}] \dot{v} \} \quad (3.95b)$$

$$\ddot{\gamma} = A_{\Pi} \left[M'_{fz} - \frac{Af_{64}}{Af_{44}} \cdot M'_{fx} - B_{\Pi} \cdot \dot{v} \right] \quad (3.95c)$$

where

$$A_{\Pi} = \frac{Af_{44}}{Af_{66} \cdot Af_{44} - Af_{64} \cdot Af_{46}}$$

$$B_{\Pi} = Af_{62} - \frac{Af_{64} \cdot Af_{42}}{Af_{44}}$$

and substituting into equations (3.89), (3.90), and (3.91) yields,

$$F'_{fx} - \frac{Af_{15}}{Af_{55}}.M'_{fy} = A_{11}.\dot{u} + A_{12}.\dot{v} + A_{13}.\dot{w} \quad (3.96a)$$

$$F'_{fy} - B_{21}.M'_{fx} - B_{23}.M'_{fz} = A_{21}.\dot{u} + A_{22}.\dot{v} + A_{23}.\dot{w} \quad (3.96b)$$

$$F'_{fz} - \frac{Af_{35}}{Af_{55}}.M'_{fy} = A_{31}.\dot{u} + A_{32}.\dot{v} + A_{33}.\dot{w} \quad (3.96c)$$

where

$$A_{11} = Af_{11} - \frac{Af_{15}.Af_{51}}{Af_{55}}$$

$$A_{12} = Af_{12}$$

$$A_{13} = Af_{13} - \frac{Af_{15}.Af_{53}}{Af_{55}}$$

$$A_{21} = Af_{21}$$

$$A_{22} = Af_{22} - \frac{Af_{24}}{Af_{44}}[Af_{42} - Af_{46}.A_{\Pi}.B_{\Pi}] - [Af_{26}.A_{\Pi}.B_{\Pi}]$$

$$A_{23} = Af_{23}$$

$$A_{31} = Af_{31} - \frac{Af_{35}.Af_{51}}{Af_{55}}$$

$$A_{32} = Af_{32}$$

$$A_{33} = Af_{33} - \frac{Af_{35}.Af_{53}}{Af_{55}}$$

$$B_{21} = \frac{Af_{24}}{Af_{44}}[1 + \frac{Af_{46}.A_{\Pi}.Af_{64}}{Af_{44}}] - [\frac{Af_{26}.A_{\Pi}.Af_{64}}{Af_{44}}]$$

$$B_{23} = Af_{26}.A_{\Pi} - [\frac{Af_{24}.A_{\Pi}.Af_{46}}{Af_{44}}]$$

(3.97)

The values for the moments $M_{fx',y',z'}$ are obtained from the previous iteration during the solution process outlined in Chapter 4. Any errors that enter due to this is dissipated during the iteration process. If all the left-hand-side forces and moments in equations (3.96) are represented by single variables $F_{fx',y',z'}$, then the equations reduce to,

$$F_{fx'} = A_{11} \cdot \ddot{u} + A_{12} \cdot \ddot{v} + A_{13} \cdot \ddot{w} \quad (3.98a)$$

$$F_{fy'} = A_{21} \cdot \ddot{u} + A_{22} \cdot \ddot{v} + A_{23} \cdot \ddot{w} \quad (3.98b)$$

$$F_{fz'} = A_{31} \cdot \ddot{u} + A_{32} \cdot \ddot{v} + A_{33} \cdot \ddot{w} \quad (3.98c)$$

These equations are similar to the equations derived for the cable segment “i”, given by equations (3.14). The terms $F_{fx',y',z'}$ include the tension terms of the cable segments attached to the fish. However, these terms are now included in the local coordinate system. The local tensions are obtained from the cable tension by transforming via the cable and fish transformation matrices $[\Lambda]$ and $[\Lambda_f]$ as follows:

$$[T_{fx,y,z}] = [\Lambda]^T \cdot [T_f] \quad (3.99a)$$

$$[T_{fx',y',z'}] = [\Lambda_f] \cdot [T_{fx,y,z}] \quad (3.99b)$$

where subscript “f” in the tension terms indicates the cable segment attached to the fish. Following the steps described by equations (3.15) to (3.29), equations (3.98) can be solved in the local coordinate system to yield the local accelerations as,

$$\ddot{u} = (-P_{x'i} T_{f-1} + R_{x'i} T_f + S_{x'i}) / (\Delta t)^2 \quad (3.100a)$$

$$\ddot{v} = (-P_{y'i} T_{f-1} + R_{y'i} T_f + S_{y'i}) / (\Delta t)^2 \quad (3.100b)$$

$$\ddot{w} = (-P_{z'i} T_{f-1} + R_{z'i} T_f + S_{z'i}) / (\Delta t)^2 \quad (3.100c)$$

By multiplying equations (3.100) by the inverse transformation matrix $[\Lambda_f]^{-1}$ for the fish, the local accelerations (\ddot{u} , \ddot{v} , and \ddot{w}) are converted to global accelerations (\ddot{x} , \ddot{y} , and \ddot{z}). However, since $[\Lambda_f]^{-1} = [\Lambda_f]^T$, pre-multiplying equations (3.100) by $[\Lambda_f]^T$ gives,

$$\ddot{x} = (-P_{xi} T_{f-1} + R_{xi} T_f + S_{xi}) / (\Delta t)^2 \quad (3.101a)$$

$$\ddot{y} = (-P_{yi} T_{f-1} + R_{yi} T_f + S_{yi}) / (\Delta t)^2 \quad (3.101b)$$

$$\ddot{z} = (-P_{zi} T_{f-1} + R_{zi} T_f + S_{zi}) / (\Delta t)^2 \quad (3.101c)$$

where $P_{x,y,xi}$, $R_{x,y,xi}$, and $S_{x,y,xi}$ are obtained by the multiplication of $P_{x',y',x'1}$, $R_{x',y',x'1}$, and $S_{x',y',x'1}$ by the relevant terms in the transpose of the towed fish transformation matrix, *i.e.* $[\Lambda_f]^T$.

Comparing equations (3.101) with the equations obtained for the cable system, *i.e.* equations (3.28), it is seen that the format is similar. Hence, the fish equations are now in a suitable format to be integrated into the solution algorithm of the cable system. The actual solution procedure is explained in Chapter 4.

If the fish has only one cable segment attached to it, *i.e.* a boundary node, then the terms $P_{xi,yi,zi}$ will disappear, since T_{f-1} will be zero. Thus, equations (3.101) will reduce to,

$$\ddot{x} = (R_{xi} T_f + S_{xi}) / (\Delta t)^2 \quad (3.102a)$$

$$\ddot{y} = (R_{yi} T_f + S_{yi}) / (\Delta t)^2 \quad (3.102b)$$

$$\ddot{z} = (R_{zi} T_f + S_{zi}) / (\Delta t)^2 \quad (3.102c)$$

For situations where a second cable is connected to a point other than the main tow point, the solution algorithm is slightly modified. This is explained in Chapter 4.

CHAPTER 4

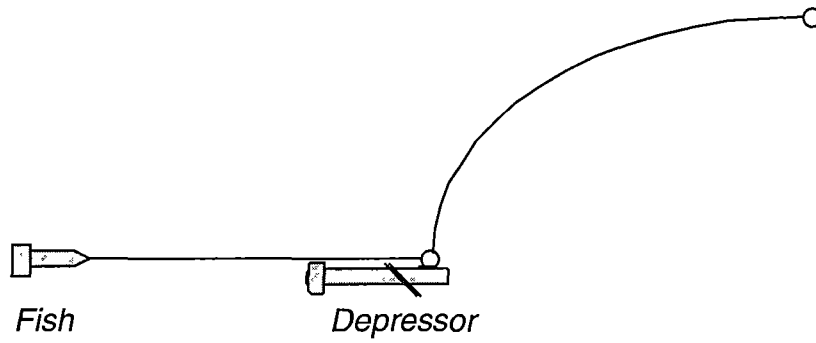
SOLUTION ALGORITHM AND PROGRAM OUTPUTS

4.1 Overview

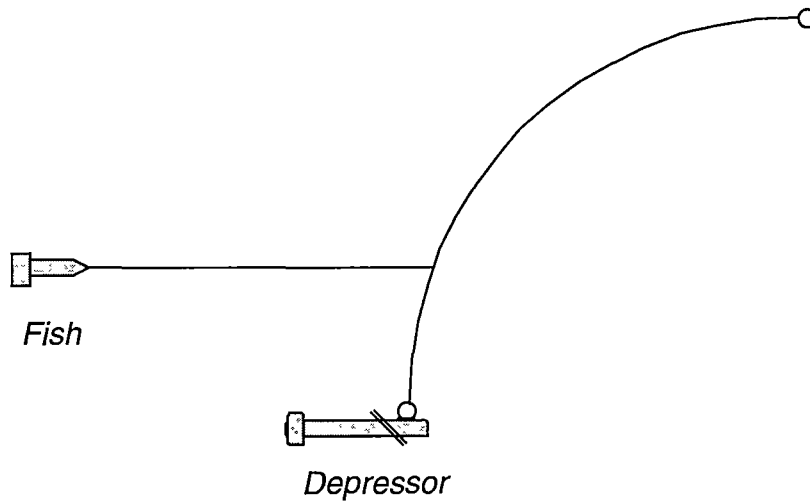
In Chapter 3, the dynamic equations describing the motions of the nodes and fish of the lumped mass model were derived. The technique employed to solve these equations consists of a time stepping method, where at each time step the model is iterated against a constraint equation until values within the tow configuration converge. In order to commence this solution technique, an initial configuration is required, with initial values for forces within the system. The ideal initial configuration for this problem was deemed to be the quasi-static configuration. Although the quasi-static model does have short comings as evidenced in sub-section 1.3 in Chapter 1, and in the next sub-section, the errors introduced by this model, will dissipate when the dynamic model is run for a sufficient length of time.

Since the dynamic solution is time consuming and requires a range of input data, it was decided to separate the quasi-static and dynamic model within the program structure, thus enabling the user to solve either the quasi-static model or to carry out a full dynamic solution. The results from the former, although insufficient for detailed investigation of the tow configuration, are sufficient for preliminary investigations, while offers the advantage of relatively low data input and shorter run time. This enables the user to rapidly obtain approximate tow configurations for a range of conditions. Once the number of configurations to be investigated has been finalised, the full dynamic solution can commence.

Although the computer model was originally developed to investigate the two-part tow, it was decided to expand it to investigate a range of other tow configurations as shown in Figure 1.1. In order to solve the respective models representing these configurations, it was required to include a range of modifications to the solution algorithm. For example, the solution techniques for the two configurations of the two-part tow as shown in Figures 4.1 and 4.2, (*i.e.* with the cable junction either at the bottom or midway along the primary cable respectively), will be different.



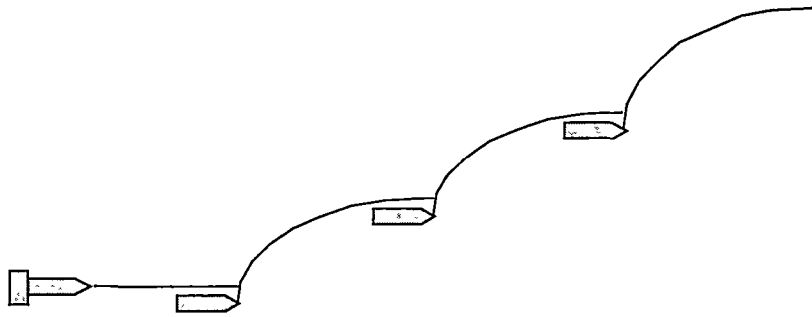
Two-Part Tow Modelled with a Single Cable
Figure 4.1



Two-Part Tow Modelled with Two Cables
Figure 4.2

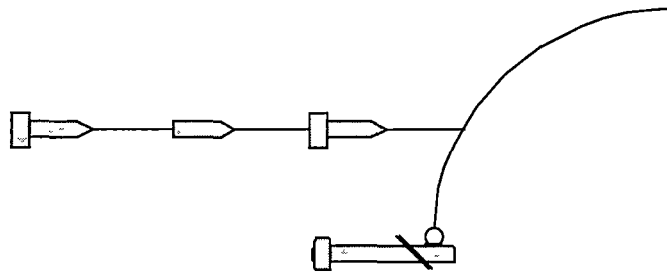
Further, multiple tows represented by Figures 4.3 and 4.4 will again require different solution algorithms, as the former can be described by one cable system, while the latter has the secondary cable separated by the tow fish resulting in separate cable sub systems.

In addition to the various two-part and multi tow configurations, the computer model is also required to simulate conventional tow systems, thus enabling comparisons between the various configurations.



Multiple Tow in Series Modelled with a Single Cable

Figure 4.3



Multiple Tow in Series Modelled with Separate Cable Systems

Figure 4.4

4.2 Quasi-Static Model

The quasi-static model assumes the system to be in static equilibrium, neglecting the effects due to inertia (including added mass) of the system. Although this simplified approach allows for a faster solution to the problem, the exclusion of the dynamics, affects its accuracy, limiting its value. If the quasi-static model is solved repeatedly for a surface excitation, the solution obtained will merely be a “snap shot” of the equilibrium configuration at the given instant. The instantaneous configuration predicted by the quasi-static model differs from the equilibrium configuration due to dynamic effects, and is unable to realistically predict the response of the system due to dynamic excitations. In addition, the resulting dynamic tension values can be more than three times the static value, which can lead to disastrous results when deploying tow fish in practice, if only a quasi-static model is used to predict the tensions for cable selection, (see sub-section 1.4 and Figure 1.4 in Chapter 1). Thus it is obvious that the solution technique has to include the dynamic effect, in order to yield realistic predictions.

However, since the quasi-static solution represents the steady state or equilibrium configuration of the system, it is an ideal starting point for the dynamic analysis. A quasi-static model, which requires to be solved in order to supply the dynamic model with an initial configuration and corresponding values was therefore incorporated within the overall model.

If the dynamic model is run for a sufficiently long time, the model will “re-configure” to represent the true configuration of the tow system. Therefore, the quasi-static model does not require to represent the static equilibrium position to a high degree of accuracy, as its primary task is to offer the dynamic model an initial configuration, thus enabling the latter to commence simulation without instability. This is essential, since large variations in the surface excitation can cause the dynamic model to diverge during its iterative solution procedure.

Due to the non-linear behaviour of the tow cable, the quasi-static model uses the same lumped mass approach, however with the equations derived for the statical equilibrium of each node. In order to simplify the solution technique (albeit at the expense of accuracy), the modelling is done in two-dimensions and then converted to a three-dimensional domain, thus preparing it for input into the dynamic model. The resulting loss of accuracy will dissipate as explained earlier, if the dynamic model is run for a sufficient length of time.

To develop the generic quasi-static equations, consider node “i” shown in Figure 3.5. Setting the sum of all tension, drag, weight, and buoyancy forces at the node to zero and neglecting all forces in the Y-direction, *i.e.* two-dimensions, it is possible to rewrite equations (3.8) as,

$$F_{ix} = T_i \cos \psi_i - T_{i-1} \cos \psi_{i-1} + \frac{1}{2} F_{dix} + \frac{1}{2} F_{di-1x} - F_{eix} = 0 \quad (4.1a)$$

$$F_{iz} = T_i \sin \psi_i - T_{i-1} \sin \psi_{i-1} + \frac{1}{2} F_{diz} + \frac{1}{2} F_{di-1z} - F_{eiz} - W_i = 0 \quad (4.1b)$$

where the drag forces ($F_{dix,z}$) are obtained by the relevant equations from equations (3.12).

The junction (*i.e.* node “j” in Figure 3.6), as explained in sub-section 3.4.1 in Chapter 3 will have the additional segment “D-1” of the secondary cable attached to it. Thus, from equation (4.1), the statical equilibrium equations become,

$$F_{jx} = T_j \cos \psi_j - T_{j-1} \cos \psi_{j-1} - T_{D-1} \cos \psi_{D-1} + \frac{1}{2} F_{djx} + \frac{1}{2} F_{dj-1x} + \frac{1}{2} F_{dD-1x} - F_{ejx} = 0 \quad (4.2a)$$

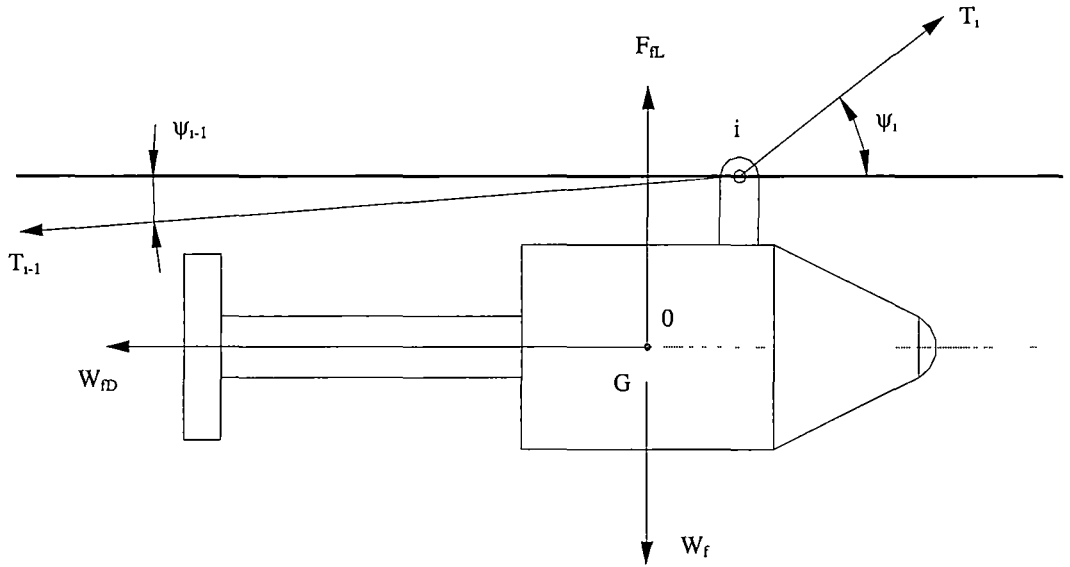
$$F_{jz} = T_j \sin \psi_j - T_{j-1} \sin \psi_{j-1} - T_{D-1} \sin \psi_{D-1} + \frac{1}{2} F_{djz} + \frac{1}{2} F_{dj-1z} + \frac{1}{2} F_{dD-1z} - F_{ejz} - W_j = 0 \quad (4.2b)$$

In order to simplify the quasi-static model, the fish model incorporated is much simpler than its equivalent in the dynamic model. The fish model is obtained by simply considering the tension, weight, buoyancy, lift, and drag forces on the body under statical equilibrium. The lift and drag forces are calculated in two-dimensions in the vertical plane using the appropriate equations from equations (2.105) as,

$$\text{Lift Force} = \bar{F}_{fL} = 0.5 \cdot C_{fL} \cdot \rho \cdot A_{fx} \cdot \bar{V}_{fr}^2 \quad (4.3a)$$

$$\text{Drag Force} = \bar{F}_{fD} = 0.5 \cdot C_{fD} \cdot \rho \cdot A_{fx} \cdot \bar{V}_{fr}^2 \quad (4.3b)$$

where C_{fL} and C_{fD} are the lift and drag coefficients of the fish, and all other variables are as defined in equations (3.86) and (3.87).



Quasi-Static Fish Model
Figure 4.5

Thus, referring to Figure 4.5, the statical equilibrium forces for the fish can be given as,

$$F_{ix} = T_i \cos \psi_i - T_{i-1} \cos \psi_{i-1} + \frac{1}{2} F_{dix} + \frac{1}{2} F_{di-1x} + F_{FD} = 0 \quad (4.4a)$$

$$F_{iz} = T_i \sin \psi_i - T_{i-1} \sin \psi_{i-1} + \frac{1}{2} F_{diz} + \frac{1}{2} F_{di-1z} + F_{FL} - W_i - W_{i-1} - W_f = 0 \quad (4.4b)$$

where node “i” represents the tow point. Note: the terms with subscript “i-1” will disappear, if a second cable is not fitted to the fish, (see Figure 4.5).

Once the statical equilibrium equations are obtained for all nodes of the system, they are solved subject to the required static boundary conditions. These will be the position of the upper end of the primary cable at the surface and the forces exerted at the lower end of the cables by the tow fish and the depressor, (if present).

Inspection of equations (4.1), (4.2), (4.3), and (4.4) show that the nodal point forces are non-linearly dependent on the nodal displacements. Therefore, it is necessary to utilise an iteration process to obtain the solution.

Prior to commencing the solution, approximate values are assigned to all cable segment angles and tensions. These can be specified by simply making each cable segment angle as 45 degrees and calculating the tensions as a function of the fish weight. The solution technique described below will then solve “along” the cable length, using an iterative procedure to meet the defined boundary conditions.

Referring to Figure 3.4, the static model for the secondary cable is solved beginning at the fish, *i.e.* node “1”, up to the node immediately prior to the junction, *i.e.* node “D-1” of the secondary cable. This yields the tension and angle of cable segment “D-1”. A similar approach is then adapted to the primary cable, starting at depressor “D” and working up the cable to the node immediately prior to the junction, *i.e.* node “j-1”, yielding the tension and the angle of cable segment “j-1”. Using the tensions and segment angles obtained in the above two cases, *i.e.* for segments “D-1” and “j-1”, the equilibrium equations for the junction node “j” are solved, and the solution then proceeds to the upper end of the primary cable, *i.e.* up to node “n”.

In the above solution process, the cable angle and tension can be obtained at each cable segment, by utilising the statical equilibrium equations and iterating until convergence is achieved. Thus, by rearranging equations (4.1) for node “i” yields the cable angle (ψ_i) and tension (T_i) of segment “i” as,

$$\tan\psi_i = \frac{T_{i-1} \cdot \sin\psi_{i-1} - \frac{1}{2}F_{diz} - \frac{1}{2}F_{di-1z} + F_{eiz} + W_i}{T_{i-1} \cdot \cos\psi_{i-1} - \frac{1}{2}F_{dix} - \frac{1}{2}F_{di-1x} + F_{eix}} \quad (4.5)$$

$$T_i = \frac{T_{i-1} \cdot \cos\psi_{i-1} - \frac{1}{2}F_{dix} - \frac{1}{2}F_{di-1x} + F_{eix}}{\cos\psi_i} \quad (4.6)$$

The angle and forces for the previous segment defined by subscript “i-1”, would have been calculated during the solution procedure for the previous node, *i.e.* utilising the equations for the previous node (i-1). Since the drag forces for cable segment “i” are non-linear functions of that segment angle, the values obtained in the previous iteration are used in the calculations. The iteration process then checks for convergence of the cable segment angle ψ_i , and adjusts the angle utilising the error between the iterations as,

$$\psi_i^{k+1} = \psi_i^k + \left[\frac{0.5}{2^m} \times (\psi_i^k - \psi_i^{k-1}) \right] \quad (4.7)$$

where superscript “k” defines the iteration and superscript “m” is equal to 1 in the first instance.

As the error reduces, it is possible that the error correction term can “swamp” the angle, which could result in a loss of convergence. In order to avoid this, the convergence is checked and the superscript “m” incremented to reduce the magnitude of the correction term, thus forcing the angle to convergence. Once the angle and tension of cable segment “i” have been obtained, the process is repeated for the next cable segment and so on, until the surface node “n” is reached. The nodes representing the junction and fish are solved in a similar manner, using the equations given by (4.2) and (4.4) respectively.

The two-dimensional configuration of the quasi-static cable system is then obtained by commencing from the surface node “n”, and calculating the nodal positions using the stretched length and orientation of each cable segment as,

$$x_i = x_{i+1} + \left[l_i \cdot \left(1 + \frac{T_i}{A_i E} \right) \cdot \cos\psi_i \right] \quad (4.8a)$$

$$z_i = z_{i+1} + \left[l_i \cdot \left(1 + \frac{T_i}{A_i E} \right) \cdot \sin\psi_i \right] \quad (4.8b)$$

If the tow was taking place in a three-dimensional velocity field, *i.e.* with a cross current, then the solution is first carried out in two-dimensions by converting the three-dimensional velocity field into two-dimensions. This is done by vectorially combining the horizontal velocities v_{xw} and v_{yw} , to give a resultant horizontal velocity.

Once the two-dimensional tow configuration has been obtained, it is returned to the three-dimensional field by adjusting the horizontal coordinates in equation (4.8a), *i.e.* by resolving x_i into X and Y directions. The horizontal angle ϕ_h , is obtained as the vector angle of the resultant horizontal velocity with the X axis in the three-dimensional field.

4.3 Dynamic Model Solution Algorithm

Using the values obtained from the quasi-static model as initial values at time “t”, the dynamic model can now be solved subject to the dynamic boundary conditions during each time interval “ Δt ”. The dynamic boundary conditions for the given tow configuration will be the path of motion of the primary cable’s upper end at the surface and the equations of motion of the tow fish and depressor at the lower ends. The following solution process is based on that described in van den Boom (1985), and modified to suit the discontinuity of the cable junction and multiple tow systems.

A numerical integration scheme is used to solve in the time domain the non-linear differential equations describing the motion of the system. Assuming that the nodal forces are functions of the node positions, velocities, and accelerations, a finite difference technique is employed to describe approximately the motions of the nodes at each time step. Although a number of numerical schemes were used during the computer modelling phase, only the one used extensively is discussed in this chapter.

The integration algorithm selected was the implicit multi-step integration scheme known as the Houbolt scheme (Bathe (1982)), where the tentative positions and velocities at the next time step are obtained as,

$$\dot{\bar{R}}^{t+1} = \frac{11.\bar{R}^{t+1} - 18.\bar{R}^t + 9.\bar{R}^{t-1} - 2.\bar{R}^{t-2}}{6.\Delta t} \quad (4.9)$$

$$\bar{R}^{t+1} = 2.5.\bar{R}^t - 2.\bar{R}^{t-1} + 0.5.\bar{R}^{t-2} + 0.5.(\Delta t)^2 \ddot{\bar{R}}^{t+1} \quad (4.10)$$

where $\bar{\mathbf{R}}$, $\dot{\bar{\mathbf{R}}}$, and $\ddot{\bar{\mathbf{R}}}$ are the nodal displacement, velocity, and acceleration vectors respectively. (Note: the above numerical scheme and other equivalent schemes are analysed in Chapter 5).

The tentative acceleration ($\ddot{\bar{\mathbf{R}}}^{t+1}$) for equation (4.10), can be obtained from the nodal equations of motion presented in (3.28), (3.32), (3.33), (3.34), (3.101), and (3.102) for the respective nodes, by utilising the quasi-static cable configuration and its tension values as initial tentative values. The tentative segment tensions so used, can then be corrected by using a Newton-Raphson iteration process, based on the constraint equation for the constitutive stress-strain relationship. Since the distance between two adjacent nodes “i” and “i+1”, should represent the stretched length of the cable segment “i”, and assuming that the cable follows Hook’s law of elasticity, it is possible to express the relationship, (*i.e.* the constraint equation of each segment length) as,

$$ER_i^{t+1} = (x_{i+1}^{t+1} - x_i^{t+1})^2 + (y_{i+1}^{t+1} - y_i^{t+1})^2 + (z_{i+1}^{t+1} - z_i^{t+1})^2 - [l_i^2 \cdot (1 + \frac{T_i^{t+1}}{A_i \cdot E})^2] \quad (4.11)$$

where

- A_i : cross sectional area of cable segment “i”
- E : modulus of elasticity of the cable material
- l_i : length of cable segment “i”
- T_i^{t+1} : tension in cable segment “i” at time “t+1”, (*i.e.* “t+Δt”)
- ER_i^{t+1} : error in the cable segment length “i”, between the span of the nodal positions and the stretched length of the segment due to the tentative tension.

It is now necessary to correct the tentative tension values T_i^{t+1} in order to reduce the error term ER_i^{t+1} to zero. Let us consider node “i” shown in Figure 3.5. The coordinates of node “i” can be obtained by substituting equations (3.28) into (4.10). Thus, it can be deduced that the coordinates of node “i” will be a function of the tensions of the adjacent cable segments “i” and “i-1”, and can be expressed as,

$$\bar{\mathbf{R}}_i^{t+1} = f(T_{i-1}^{t+1}, T_i^{t+1}) \quad (4.12)$$

Referring to equation (4.11) for cable segment “i”, it can be seen that the segment error term ER_i^{t+1} will be a function of nodes “i” and “i+1”. Therefore, from equations

(4.11) and (4.12) it is evident that ER_i^{t+1} will be a function of the tensions of cable segments “i-1”, “i”, and “i+1”. Thus,

$$ER_i^{t+1} = f(T_{i-1}^{t+1}, T_i^{t+1}, T_{i+1}^{t+1}) = 0 \quad (4.13)$$

since ER_i^{t+1} will be equal to zero when the length constraint is met. Now if the tension term T_i^{t+1} of cable segment “i” consists of two components, *i.e.*,

$$T_i^{t+1} = \tilde{T}_i^{t+1} + \delta T_i^{t+1} \quad (4.14)$$

where the tildes (\sim) represents the tentative values, *i.e.* \tilde{T}_i^{t+1} is the tentative value of the tension and δT_i^{t+1} is the tension correction term of cable segment “i”. Then, by expanding ER_i^{t+1} (equation (4.13)) in a Taylor series about point $\{\tilde{T}_{i-1}^{t+1}, \tilde{T}_i^{t+1}, \tilde{T}_{i+1}^{t+1}\}$, we obtain,

$$ER_i^{t+1} = \tilde{ER}_i^{t+1} + \frac{\partial \tilde{ER}_i^{t+1}}{\partial T_{i-1}^{t+1}} \cdot \delta T_{i-1}^{t+1} + \frac{\partial \tilde{ER}_i^{t+1}}{\partial T_i^{t+1}} \cdot \delta T_i^{t+1} + \frac{\partial \tilde{ER}_i^{t+1}}{\partial T_{i+1}^{t+1}} \cdot \delta T_{i+1}^{t+1} + \text{higher order terms} = 0 \quad (4.15)$$

Since the tentative tension values are sufficiently close to the correct values, (*i.e.* due to the initial configuration obtained under statical equilibrium being sufficiently close to the dynamic solution and the time interval “ Δt ” being small), the higher order terms in equation (4.15) can be neglected. Thus,

$$\frac{\partial \tilde{ER}_i^{t+1}}{\partial T_{i-1}^{t+1}} \cdot \delta T_{i-1}^{t+1} + \frac{\partial \tilde{ER}_i^{t+1}}{\partial T_i^{t+1}} \cdot \delta T_i^{t+1} + \frac{\partial \tilde{ER}_i^{t+1}}{\partial T_{i+1}^{t+1}} \cdot \delta T_{i+1}^{t+1} = -\tilde{ER}_i^{t+1} \quad (4.16)$$

It is now necessary to obtain the partial differential terms given above. Substituting the accelerations \ddot{x}_i^{t+1} , \ddot{y}_i^{t+1} , and \ddot{z}_i^{t+1} for node “i”, obtained from equations (3.28), into equation (4.10) gives,

$$x_i^{t+1} = 2.5 \cdot x_i^t - 2 \cdot x_i^{t-1} + 0.5 \cdot x_i^{t-2} + 0.5 \cdot [R_{xi} \cdot T_i^{t+1} - P_{xi} \cdot T_{i-1}^{t+1} + S_{xi}] \quad (4.17a)$$

$$y_i^{t+1} = 2.5 \cdot y_i^t - 2 \cdot y_i^{t-1} + 0.5 \cdot y_i^{t-2} + 0.5 \cdot [R_{yi} \cdot T_i^{t+1} - P_{yi} \cdot T_{i-1}^{t+1} + S_{yi}] \quad (4.17b)$$

$$z_i^{t+1} = 2.5 \cdot z_i^t - 2 \cdot z_i^{t-1} + 0.5 \cdot z_i^{t-2} + 0.5 \cdot [R_{zi} \cdot T_i^{t+1} - P_{zi} \cdot T_{i-1}^{t+1} + S_{zi}] \quad (4.17c)$$

Note: in the above equations, the nodal positions at “t”, “t-1”, and “t-2” (or “t”, “t-Δt”, and “t-2Δt”), will **not** depend on the tentative tensions, as they would have been calculated in previous time steps.

Similar equations can be written for the positions x_{i+1}^{t+1} , y_{i+1}^{t+1} , and z_{i+1}^{t+1} . Thus, by substituting these six equations into the length constraint equation (4.11), carrying out the partial differentiation with respect to T_{i-1}^{t+1} , T_i^{t+1} and T_{i+1}^{t+1} , and dropping the tildes (\sim) for clarity, yields,

$$E_i \cdot \delta T_{i-1}^{t+1} - F_i \cdot \delta T_i^{t+1} + G_i \cdot \delta T_{i+1}^{t+1} = -ER_i^{t+1} \quad (4.18)$$

where E_i , $-F_i$, and G_i are the partial differential terms in equation (4.16), with $-F_i$ the coefficient of the tension error term (δT_i^{t+1}) of the segment considered (*i.e.* segment “i”), while E_i and G_i are the coefficients of the tension error terms (δT_{i-1}^{t+1} and δT_{i+1}^{t+1}) of the adjacent segments, *i.e.* “i-1” and “i+1” respectively. These three coefficients are,

$$E_i = P_{x_i}(x_{i+1}^{t+1} - x_i^{t+1}) + P_{y_i}(y_{i+1}^{t+1} - y_i^{t+1}) + P_{z_i}(z_{i+1}^{t+1} - z_i^{t+1}) \quad (4.19)$$

$$F_i = (R_{x_i} + P_{x_{i+1}})(x_{i+1}^{t+1} - x_i^{t+1}) + (R_{y_i} + P_{y_{i+1}})(y_{i+1}^{t+1} - y_i^{t+1}) \\ + (R_{z_i} + P_{z_{i+1}})(z_{i+1}^{t+1} - z_i^{t+1}) + \frac{2 \cdot l_i^2}{A_i \cdot E} \left(1 + \frac{T_i^{t+1}}{A_i \cdot E}\right) \quad (4.20)$$

$$G_i = R_{x_{i+1}}(x_{i+1}^{t+1} - x_i^{t+1}) + R_{y_{i+1}}(y_{i+1}^{t+1} - y_i^{t+1}) + R_{z_{i+1}}(z_{i+1}^{t+1} - z_i^{t+1}) \quad (4.21)$$

Since ER_i^{t+1} is a function of the nodes “i” and “i+1”, and the nodes in turn are functions of the adjacent tensions (see equations (4.13) and (4.12)), E_i , F_i , and G_i can be obtained for all the relevant nodes.

For the segments adjacent to the nodes representing the boundaries and the junction, equation (4.18) will be slightly different, as the number of cables attached to these nodes are different. These nodes are shown in Figures 3.6 and 3.7, which include the junction, tow fish, depressor, and the surface node. The equivalent equations for these segments will now be developed.

4.3.1 Boundary Nodes

Consider Figure 3.7(a), which shows the first segment (*i.e.* segment “1”), attached to the towed fish, thus qualifying as a lower boundary node. It is noted that length (l_1) of the first segment, and hence its length error term (ER_1^{t+1}), is a function of the positions of nodes “1” and “2”.

Although the position of node “2” is a function of tensions T_1^{t+1} and T_2^{t+1} , the position of node “1” being a lower boundary node, will be a function of only tension T_1^{t+1} . Therefore, the error term ER_1^{t+1} will be a function of only two tensions, namely T_1^{t+1} and T_2^{t+1} . Thus,

$$ER_1^{t+1} = f(T_1^{t+1}, T_2^{t+1}) \quad (4.22)$$

Following a similar sequence of steps to those described from equations (4.15) to (4.18), yields,

$$-F_1 \cdot \delta T_1^{t+1} + G_1 \cdot \delta T_2^{t+1} = -ER_1^{t+1} \quad (4.23)$$

Comparing equation (4.23) for the towed fish (*i.e.* a lower boundary node), with equation (4.18) derived for any node “i”, it is seen that the term E_i in equation (4.23) is zero. This is because the position of node “1” is affected by only one tension (*i.e.* that of segment “1”), as opposed to the two adjacent segment tensions in normal nodes, (*i.e.* node “i”). In other words, there is no segment “0”.

A similar situation occurs for the depressor shown in Figure 3.7(b). Again, as this is a lower boundary node, with only one segment attached to the depressor, (*i.e.* segment “D”), we obtain,

$$-F_D \cdot \delta T_D^{t+1} + G_D \cdot \delta T_{D+1}^{t+1} = -ER_D^{t+1} \quad (4.24)$$

again with the term E_D equal to zero.

Considering cable segment “n-1” attached to the surface node “n” (see Figure 3.7(c)), a similar process will yield,

$$E_{n-1} \cdot \delta T_{n-2}^{t+1} - F_{n-1} \cdot \delta T_{n-1}^{t+1} = -ER_{n-1}^{t+1} \quad (4.25)$$

However, when compared with equation (4.18), it is noted that the term G_{n-1} is zero. This is because segment “n-1” is the last segment in the cable system, and the position of node “n” is only influenced by the tension of this segment.

4.3.2 Junction

From Figure 3.6, it is seen that the coordinates of the node representing the junction (j) will be a function of three tensions instead of the usual two. This is due to the additional cable segment “D-1” of the secondary cable also being attached to the junction node. Thus,

$$\bar{R}_j^{t+1} = f(T_{D-1}^{t+1}, T_{j-1}^{t+1}, T_j^{t+1}) \quad (4.26)$$

Therefore, the length error term ER_j^{t+1} of the cable segments adjacent to the junction, *i.e.* segments “D-1”, “j-1”, and “j”, will have an extra term, as they are functions of four tensions. Thus,

$$ER_{D-1}^{t+1} = f(T_{D-2}^{t+1}, T_{D-1}^{t+1}, T_{j-1}^{t+1}, T_j^{t+1}) \quad (4.27a)$$

$$ER_{j-1}^{t+1} = f(T_{D-1}^{t+1}, T_{j-2}^{t+1}, T_{j-1}^{t+1}, T_j^{t+1}) \quad (4.27b)$$

$$ER_j^{t+1} = f(T_{D-1}^{t+1}, T_{j-1}^{t+1}, T_j^{t+1}, T_{j+1}^{t+1}) \quad (4.27c)$$

Following a similar sequence of steps to those described from equations (4.15) to (4.18), the above equations can be reduced to a form similar to that given by equation (4.18), *i.e.*,

$$E_{D-1} \cdot \delta T_{D-2}^{t+1} - F_{D-1} \cdot \delta T_{D-1}^{t+1} + C_1 \cdot \delta T_{j-1}^{t+1} + C_2 \cdot \delta T_j^{t+1} = -ER_{D-1}^{t+1} \quad (4.28)$$

$$D_1 \cdot \delta T_{D-1}^{t+1} + E_{j-1} \cdot \delta T_{j-2}^{t+1} - F_{j-1} \cdot \delta T_{j-1}^{t+1} + G_{j-1} \cdot \delta T_j^{t+1} = -ER_{j-1}^{t+1} \quad (4.29)$$

$$D_2 \cdot \delta T_{D-1}^{t+1} + E_j \cdot \delta T_{j-1}^{t+1} - F_j \cdot \delta T_j^{t+1} + G_j \cdot \delta T_{j+1}^{t+1} = -ER_j^{t+1} \quad (4.30)$$

where the terms C_1 , C_2 , D_1 , and D_2 are the “extra” terms in comparison to the standard constraint equation obtained for segment “i” in equation (4.18). These extra terms are due to the additional secondary cable element “D-1”, and are expressed as,

$$C_1 = -P_{xj}(x_j^{t+1} - x_{D-1}^{t+1}) - P_{yj}(y_j^{t+1} - y_{D-1}^{t+1}) - P_{zj}(z_j^{t+1} - z_{D-1}^{t+1}) \quad (4.31a)$$

$$C_2 = R_{xj}(x_j^{t+1} - x_{D-1}^{t+1}) + R_{yj}(y_j^{t+1} - y_{D-1}^{t+1}) + R_{zj}(z_j^{t+1} - z_{D-1}^{t+1}) \quad (4.31b)$$

$$D_1 = -P_{Dx}(x_j^{t+1} - x_{j-1}^{t+1}) - P_{Dy}(y_j^{t+1} - y_{j-1}^{t+1}) - P_{Dz}(z_j^{t+1} - z_{j-1}^{t+1}) \quad (4.31c)$$

$$D_2 = P_{Dx}(x_{j+1}^{t+1} - x_j^{t+1}) + P_{Dy}(y_{j+1}^{t+1} - y_j^{t+1}) + P_{Dz}(z_{j+1}^{t+1} - z_j^{t+1}) \quad (4.31d)$$

where the terms $P_{Dx,y,z}$ were defined in equations (3.32).

It can also be seen from equation (4.28) representing the last segment on the secondary cable, *i.e.* segment “D-1”, that the term G_{D-1} is missing since no cable segment will be present beyond segment “D-1” on the secondary cable. This is similar to the equation developed for cable segment “n-1”, *i.e.* equation (4.25), which is adjacent to the surface node “n”, thus missing the term G_{n-1} , as there is no cable segment beyond node “n”.

The system of equations thus obtained in (4.18), (4.23), (4.24), (4.25), (4.28), (4.29), and (4.30) can now be expressed in matrix form to give,

$$[E_1 F_1 G_1 CD] [\delta T_1^{t+1}] = [ER_1^{t+1}] \quad (4.32)$$

where $[E_1 F_1 G_1 CD] =$

$$\begin{bmatrix} \begin{matrix} -F_1 & G_1 \\ E_2 & -F_2 \\ \dots & \dots \end{matrix} & \begin{matrix} G_2 \\ E_{D-1} \\ \dots \end{matrix} & \begin{matrix} \text{(col D-1)} \\ -F_{D-1} & 0 \\ 0 & -F_D \\ E_{D+1} & -F_{D+1} \\ \dots & \dots \end{matrix} & \begin{matrix} \text{(col j-1)} \\ C_1 \\ \dots \end{matrix} & \begin{matrix} \text{(col j)} \\ C_2 \\ \dots \end{matrix} & \begin{matrix} \text{(row D-1)} \\ \dots \end{matrix} \\ \begin{matrix} \text{(row j-1)} \\ \text{(row j)} \end{matrix} & \begin{matrix} D_1 \\ D_2 \end{matrix} & \begin{matrix} E_{j-1} \\ E_j \end{matrix} & \begin{matrix} -F_{j-1} \\ -F_j \end{matrix} & \begin{matrix} G_{j-1} \\ -F_j \\ E_{j+1} \end{matrix} & \begin{matrix} G_j \\ -F_{j+1} \\ G_{j+1} \end{matrix} & \begin{matrix} E_{n-2} \\ -F_{n-2} \\ E_{n-1} \end{matrix} & \begin{matrix} G_{n-2} \\ -F_{n-1} \end{matrix} \end{bmatrix} \quad (4.33)$$

and

$$\begin{aligned}
[\delta T_i] = \begin{bmatrix} \delta T_1 \\ \delta T_2 \\ - \\ \delta T_{D-1} \\ \delta T_D \\ \delta T_{D+1} \\ - \\ \delta T_{j-1} \\ \delta T_j \\ \delta T_{j+1} \\ - \\ \delta T_{n-2} \\ \delta T_{n-1} \end{bmatrix} \quad \text{and} \quad [ER_i] = \begin{bmatrix} -ER_1 \\ -ER_2 \\ - \\ -ER_{D-1} \\ -ER_D \\ -ER_{D+1} \\ - \\ -ER_{j-1} \\ -ER_j \\ -ER_{j+1} \\ - \\ -ER_{n-2} \\ -ER_{n-1} \end{bmatrix}
\end{aligned}
\tag{4.34}$$

4.3.3 Matrix Solution

Solving the set of equations given by (4.32) will yield the tension error terms δT_i , which can then be used to correct the tentative tensions. If the cable system consisted of a single cable, then matrix $[E_i F_i G_i C D]$ would be a **true tri-diagonal matrix** of the order $(n-1 \times n-1)$, where “n” is the number of nodes. Such matrices can be solved efficiently by a standard matrix inversion routine, *i.e.* the so called Thomas algorithm.

However, due to the discontinuity of the junction and the separate modelling of the two cables, the non-zero terms C_1 , C_2 , D_1 , and D_2 given in equations (4.31) lie outside the tri-diagonal band. The solution of such a matrix can be carried out either by conventional matrix theory, or by first transforming it into a true tri-diagonal form and then utilising the Thomas algorithm. In order to save computational time and memory space, it was decided to follow the latter approach, especially as the matrix can be large if the modelling utilises a large number of nodes. (Note: during the conversion, the zero terms on the outer diagonal of the tri-diagonal band have to be converted into non-zero terms, or they will cause divisions by zero during the Thomas algorithm).

The above transformation is carried out in a few elimination steps, since the positions of C_1 , C_2 , D_1 , and D_2 are known as a function of the depressor and junction node numbers “D” and “j” respectively, (see the row and column markings in matrix

$[E_i F_i G_i CD]$ in equation (4.33)). The elimination is carried out in two phases, summarised below.

Phase One

This phase consist of the elimination of terms D_1 and D_2 . The positions of these terms can be given as,

Position of D_1 : row “j-1” and column “D-1”

Position of D_2 : row “j” and column “D-1”

These terms are now eliminated by starting at row “2” and successively eliminating terms E_i until row “D-1” is reached. The elimination process is carried out for each row by utilising the row immediately above it. For example, E_2 is eliminated by multiplying row 1 by $\frac{E_2}{-F_1}$, and subtracting it from row “2”. Once row “D-1” is

reached, this row can be used to eliminate terms D_1 and D_2 . This is achieved by multiplying row “D-1” in turn by $\frac{D_1}{-F_{D-1}}$ and $\frac{D_2}{-F_{D-1}}$, and subtracting it from rows “j-

1” and “j” respectively. During these elimination steps, since terms C_1 and C_2 are on row “D-1”, the terms $-F_{j-1}$, G_{j-1} , ER_{j-1} , E_j , $-F_j$, and ER_j will be modified.

Phase Two

The second phase of the elimination process deals with terms C_1 and C_2 . Their positions within the matrix are given by,

Position of C_1 : row “D-1” and column “j-1”

Position of C_2 : row “D-1” and column “j”

Their elimination commences with term C_2 , which can be eliminated by multiplying row “j-1” by $\frac{C_2}{G_{j-1}}$ and subtracting it from row “D-1”. This elimination step will

result in an additional term at row “D-1” and column “j-2”. C_1 can then be eliminated by multiplying row “j-2” with $\frac{C_1}{G_{j-2}}$ and subtracting it from row “D-1”. Again this

will create a new term at row “D-1” and column “j-3”. To eliminate the additional terms created on row “D-1”, the process is continued in a similar manner until column “D+1” is reached. In other words, the successive elimination is carried out from column “j” using row “j-1”, to column “D+1” using row “D”. The last elimination step will also convert the zero term at row “D-1” and column “D”, *i.e.* G_{D-1} , to a non-

Once all equations in matrix $[E_i F_i G_i]$ are expressed in the above form, it is possible to carry out an elimination process commencing from row “1” and working down the rows within the matrix. This results in each tension correction term, δT_i^{t+1} , being expressed as a linear function of the first tension correction term δT_1^{t+1} , *i.e.*,

$$\delta T_i^{t+1} = \mu_i \delta T_1^{t+1} + \eta_i \quad (4.38)$$

where μ_i and η_i can be obtained recursively from (4.37) as,

$$\mu_{i+1} = \frac{F_i \mu_i - E_i \mu_{i-1}}{G_i} \quad (4.39a)$$

$$\eta_{i+1} = \frac{F_i \eta_i - E_i \eta_{i-1} - E R_i}{G_i} \quad (4.39b)$$

The first tension correction term, δT_1^{t+1} , can then be obtained from the last equation of the system of equations as,

$$\delta T_1^{t+1} = \frac{F_{n-1} \eta_{n-1} - E_{n-1} \eta_{n-2} - E R_{n-1}}{E_{n-1} \mu_{n-2} - F_{n-1} \mu_{n-1}} \quad (4.40)$$

The tension correction values δT_i^{t+1} , obtained for all segments of the cable system from equation (4.38), can now be used to update the tentative tension values T_i^{t+1} for each iteration process. Thus,

$$(T_i^{t+1})^{k+1} = (T_i^{t+1})^k + \delta T_i^{t+1} \quad (4.41)$$

where “k” is the iteration index. The corrected tensions can then be used to obtain the corrected accelerations from the respective equations of motion, *i.e.* equations (3.28); (3.32), (3.33), (3.34), (3.101), and (3.102), and hence the corrected coordinates and velocities from equations (4.9) and (4.10). The process is then repeated until acceptable convergence of the cable segment tension terms T_i^{t+1} , is achieved. The convergence is measured by comparing the largest tension correction term (δT_i^{t+1}) for that iteration against a pre-set tension error limit. The user can set this error limit, which can be established as a percentage (e.g. less than 10%) of the maximum static tension of the cable, (usually at the surface node). In the authors experience a tension error limit of 1 Newton produces satisfactory results.

4.3.4 Angular Displacement of Tow Fish

During the solution process, the linear displacements and velocities of the nodes are obtained at each iteration by equations (4.9) and (4.10). In order to obtain the attitude of the fish and the angular damping created by its motion, it is also required to calculate the angular displacements and velocities of the fish. This also influences the forces and moments acting on the fish, and hence those acting on the cable node it is attached to.

If the angular accelerations of the fish are known, the angular displacements and velocities of the fish can be obtained by utilising the Houbolt numerical integration scheme described in equation (4.9) and (4.10). The angular accelerations can be obtained by equations (3.95) in Chapter 3, reproduced below.

$$\ddot{\alpha} = \frac{M'_{fy} - Af_{51} \cdot \ddot{u} - Af_{53} \cdot \dot{w}}{Af_{55}} \quad (4.42a)$$

$$\ddot{\beta} = \frac{1}{Af_{44}} \{ M'_{fx} \cdot [1 + \frac{Af_{46} \cdot A_{\Pi} \cdot Af_{64}}{Af_{44}}] - [Af_{46} \cdot A_{\Pi} \cdot M'_{fz}] - [Af_{42} - Af_{46} \cdot A_{\Pi} \cdot B_{\Pi}] \dot{v} \} \quad (4.42b)$$

$$\ddot{\gamma} = A_{\Pi} [M'_{fz} - \frac{Af_{64}}{Af_{44}} \cdot M'_{fx} - B_{\Pi} \cdot \dot{v}] \quad (4.42c)$$

Inspecting the above equations reveal that the local linear accelerations of the node attached to the fish, (*i.e.* \ddot{u} , \dot{v} , and \dot{w}), are required. These accelerations are obtained by pre-multiplying the global acceleration terms, (*i.e.* \ddot{x} , \ddot{y} , and \ddot{z}), by the fish transformation matrix $[\Lambda_f]$, given in equation (3.3). Thus,

$$\begin{bmatrix} \ddot{u} \\ \dot{v} \\ \dot{w} \end{bmatrix} = [\Lambda_f] \cdot \begin{bmatrix} \ddot{x} \\ \ddot{y} \\ \ddot{z} \end{bmatrix} \quad (4.43)$$

The global acceleration terms are obtained from equations (3.101). The forces and moments for the angular acceleration equations (4.42) are obtained from the previous iteration step. Substituting these equations into equations (4.9) and (4.10) will yield the angular displacements and angular velocities as,

$$\dot{\bar{\mathbf{A}}}_{t+1} = \frac{11.\bar{\mathbf{A}}^{t+1} - 18.\bar{\mathbf{A}}^t + 9.\bar{\mathbf{A}}^{t-1} - 2.\bar{\mathbf{A}}^{t-2}}{6.\Delta t} \quad (4.44)$$

$$\bar{\mathbf{A}}^{t+1} = 2.5.\bar{\mathbf{A}}^t - 2.\bar{\mathbf{A}}^{t-1} + 0.5.\bar{\mathbf{A}}^{t-2} + 0.5.(\Delta t)^2.\ddot{\bar{\mathbf{A}}}^{t+1} \quad (4.45)$$

where $\bar{\mathbf{A}}$, $\dot{\bar{\mathbf{A}}}$, and $\ddot{\bar{\mathbf{A}}}$ represent the fish rotational angular displacement vector and its derivatives, *i.e.*,

$$\bar{\mathbf{A}} = \alpha, \beta, \text{ and } \gamma \quad (4.46a)$$

$$\dot{\bar{\mathbf{A}}} = \dot{\alpha}, \dot{\beta}, \text{ and } \dot{\gamma} \quad (4.46b)$$

$$\ddot{\bar{\mathbf{A}}} = \ddot{\alpha}, \ddot{\beta}, \text{ and } \ddot{\gamma} \quad (4.46c)$$

Thus, the angular displacements and angular velocities can be calculated at each iteration, which in turn will enable the calculation of the fish forces and moments for the next iteration to be carried out.

4.3.5 Solution Procedure

The dynamic model is initialised from the quasi-static configuration using the results from the latter model as initial tentative values. It is then driven by feeding in at appropriate time intervals the coordinates of the surface node representing the motion of the surface vessel. This is achieved by either a combination of sinusoidal X, Y, and Z excitations at the surface node, or through a data file representing its path of motion.

If the surface node motion is relatively large, it is advisable to reduce the transient response by gradually introducing this motion via an exponential decay term. If not, the sudden introduction of large excitations can result in numerical instability. It is also advisable to use small time steps to ensure accuracy and convergence. The accuracy / stability criteria for the numerical integration scheme and the selection of an appropriate time step are discussed at length in Chapter 5. The calculation procedure can be summarised as follows:

1. Obtain the quasi-static configuration of the towed system.
2. Introduce the surface motion for the given time step.

3. Calculate the cable segment transformation matrix and terms such as the drag forces and added mass for each node, using the current nodal displacements, velocities, and accelerations as tentative values for the next time step,
4. Obtain the transformation matrix for the towed and depressor fish. Then calculate the forces and moments on the fish in the local coordinate system and represent them within the appropriate cable node equations.
5. Obtain the accelerations of the cable nodes for the next time step, using the appropriate equations from (3.28), (3.32), (3.33), (3.34), (3.101), and (3.102), with the current tensions as the tentative tensions for the next time step.
6. Calculate the angular accelerations of the fish using equations (4.42), and the linear accelerations obtained for the nodes attached to the fish.
7. Obtain the nodal positions (including the segment angles), and the velocities for the next time step using equations (4.9) and (4.10) respectively.
8. Calculate the angular displacements and velocities of the fish from equations (4.44) and (4.45) using the angular accelerations obtained for the fish in step 6.
9. Obtain the segment length error terms ER_i^{t+1} using the cable length constraint equation (4.11).
10. Obtain the coefficients E_i , F_i , G_i , C_1 , C_2 , D_1 , and D_2 from equations (4.18), (4.23), (4.24), (4.25), (4.28), (4.29), and (4.30), thus giving equation (4.32). The terms C_1 , C_2 , D_1 , and D_2 will not be present for a single cable tow.
11. Convert the matrix (4.33) into a true tri-diagonal matrix, if it has non-zero terms for C_1 , C_2 , D_1 , and D_2 , *i.e.* due to a cable junction.
12. Solve equation (4.38) for the tension correction values δT_i^{t+1} . The tentative tensions are then updated using equation (4.41).
13. Repeat the iteration from step 3 to 12, until acceptable convergence is obtained for the tension terms T_i^{t+1} . This is achieved by comparing the largest tension correction term (δT_i^{t+1}) for that iteration against a pre-set tension error limit.

14. Increment the time step and using the calculated values for time “t+1”, as tentative values for the next time step, *i.e.* time “t+2”, repeat the procedure from step 2 to 13, until the required simulation time is reached.

A flowchart outlining the solution procedure described above is given as the “*Overall Computer Program Flowchart for the Two-Part Tow*” in Appendix B. The program enables various parameters to be saved to disc at selected time intervals. This information can then be viewed via a word processor or a spread sheet, and be plotted as required.

4.4 Program Outputs

Although the computer model was developed to simulate two-part tow configurations, it is also capable of simulating conventional tow systems. The input data identifies if the cable configuration is a conventional tow (Figure 1.1(a)), a two-part tow without a junction (Figure 1.1(b)), or a two-part tow with a junction (Figure 1.1(d)), and carries out the solution accordingly. The matrix conversion is required only in the latter case.

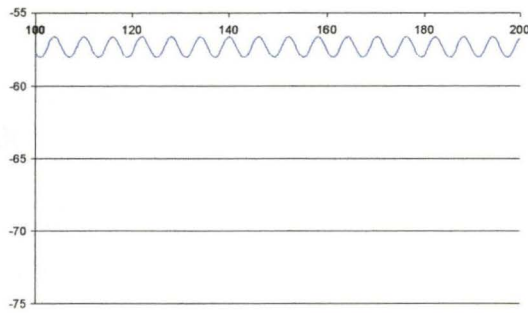
Figures 4.6 to 4.11 compare the response of equivalent conventional (Figure 1.1(a)) and two-part tow (Figure 1.1(d)) configurations in response to sinusoidal excitation at the surface node. The information on the tow configurations are given in Table 4.1, with the two-part tow represented as “*Two-Part Tow 1*”.

	Conventional Tow	Two-Part Tow 1	Two-Part Tow 2
Primary Cable	85 m	85 m	65 m
Secondary Cable	N/a	20 m	20 m
Depressor	N/a	300 kg	300 kg
Fish	300 kg	41.2 kg	41.2 kg
Number of Segments	6	8 (6 + 2)	6 (4 + 2)
Distance from Depressor to Junction	N/a	20 m	20 m

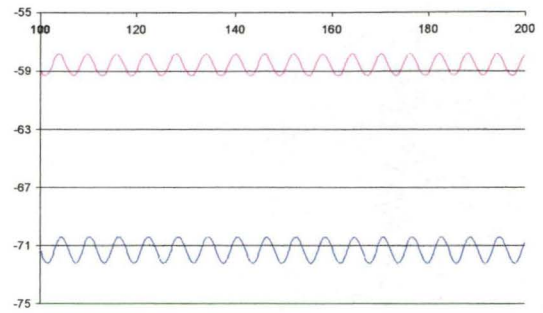
Conventional and Two-Part Tow Configuration Information

Table 4.1

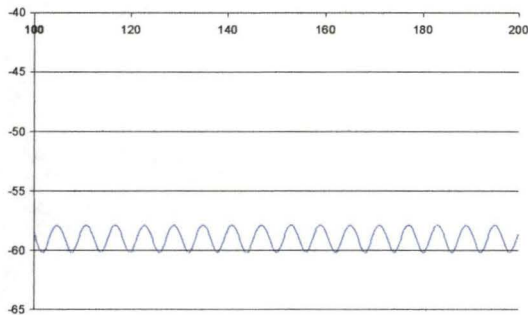
The surface excitation is sinusoidal in the X and Z directions, having an excitation period of 6 seconds and amplitudes of 1 meter and 2 metres in the X and Z directions respectively. The relative velocity of the tow to the surrounding water is 3 metres per second.



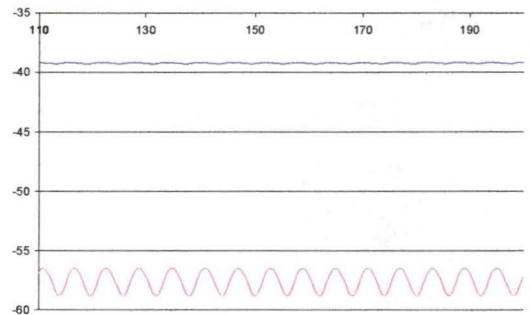
**Conventional Tow – Surge
Figure 4.6**



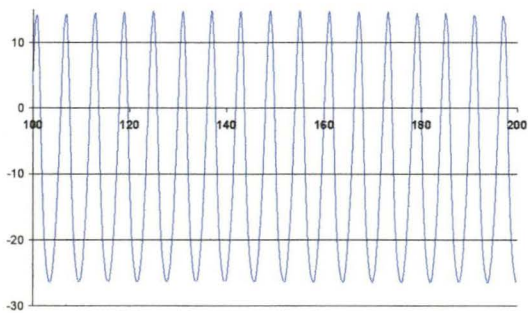
**Two-Part Tow 1 – Surge
Figure 4.7**



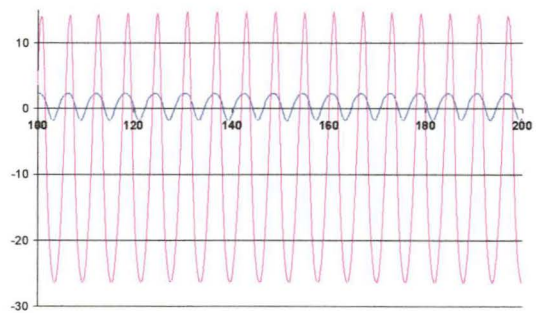
**Conventional Tow – Heave
Figure 4.8**



**Two-Part Tow 1 – Heave
Figure 4.9**



**Conventional Tow - Pitch Angle
Figure 4.10**



**Two-Part Tow 1 – Pitch Angle
Figure 4.11**

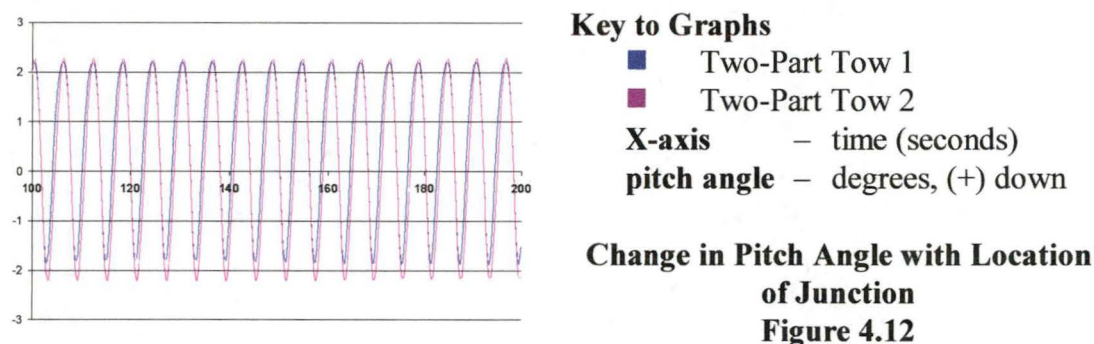
Key to Graphs

- fish
- depressor

- X-axis** – time (seconds)
- surge and heave** – metres
- pitch angle** – degrees, (+) down

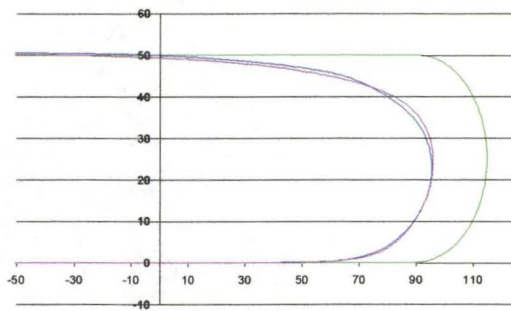
Interestingly, the heave and pitch angles reduce significantly with the use of the two-part tow, however the surge tends to marginally increase. This effect is confirmed in the experimental testing described later in Chapter 6.

Figure 4.12 compares the pitch angle response of two different two-part tow configurations under the same surface excitation. The configurations are described in Table 4.1 as “*Two-Part Tow 1 and 2*” respectively. The difference in the configurations is the attachment point (junction) of the secondary cable. The former has the junction located on the primary cable (Figure 1.1(d)), while the latter has the secondary cable attached adjacent to the depressor (Figure 1.1(b)). From Figure 4.12 it is seen that *Two-Part Tow 1* has a lower response amplitude. Again this effect is confirmed and discussed further in the experimental stage in Chapter 6.

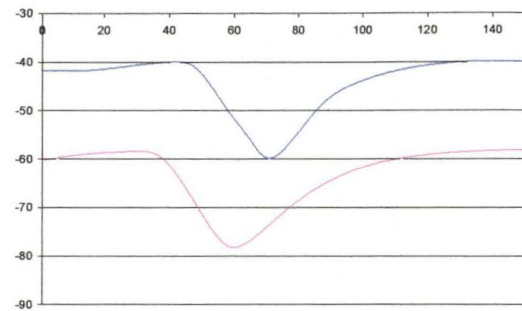


Figures 4.13 to 4.15 show the response of *Two-Part Tow 1* during a 180 degree manoeuvre (turn) of the surface vessel. The vessel is travelling at 3 metres per second and carries out the manoeuvre at a radius of 25 metres. From Figure 4.13 it is seen that both the depressor and fish turn inside the turning circle of the surface vessel. In addition, from Figure 4.14 the depth of the depressor and fish is seen to increase during the turn, due to the reduction in their speeds as they travel along the shorter paths. Both outcomes must be considered when carrying out such manoeuvres, as the towed fish and depressor may strike the sea bed or underwater objects. This highlights one of the advantages of simulation before carrying out the actual operation. Note: when considering the pitch angle in Figure 4.15, **positive is downwards**, (*i.e.* Right Hand Coordinate System - see Figure 3.2).

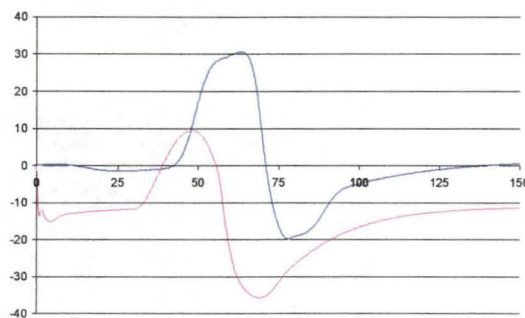
The solution procedure outlined above is for conventional or two-part tow configurations. However, the computer model is also able to solve multiple tow configurations, by modifying the solution procedure to deal with the additional tows. The multiple tow configurations investigated are divided into two distinct types, shown in Figures 4.16 and 4.28. The first consists of multiple tow fish in series, while the second consists of them in parallel. In the latter case each fish is connected to a secondary cable, which in turn is coupled to the primary tow cable, resulting in a series of junctions (*i.e.* j_1, j_2, j_3 , etc, as shown in Figure 4.28).



Two-Part Tow 1 – Path of Vehicles
Figure 4.13



Two-Part Tow 1 - Depth
Figure 4.14



Two-Part Tow 1 - Pitch Angle
Figure 4.15

Key to Graphs

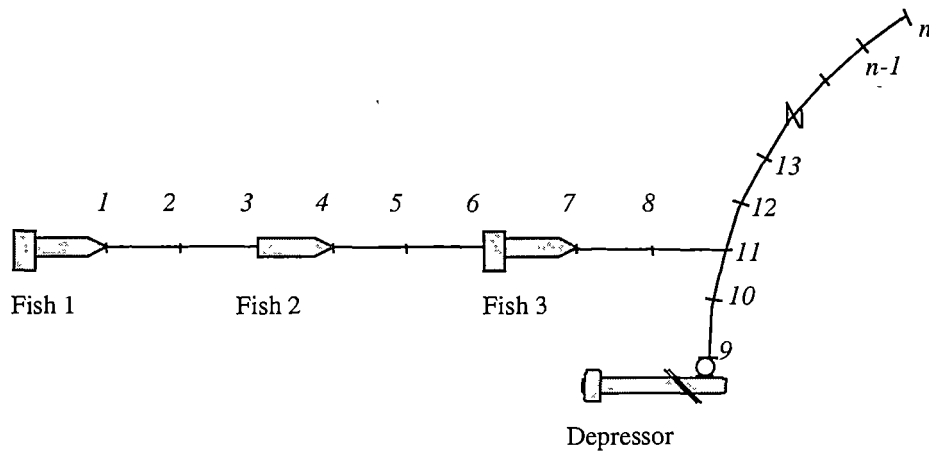
- surface ship
- fish
- depressor

- X-axis** – time (seconds)
- linear motion** – metres
- depth** – metres
- pitch angle** – degrees, (+) down

4.5 Multiple Tows in Series

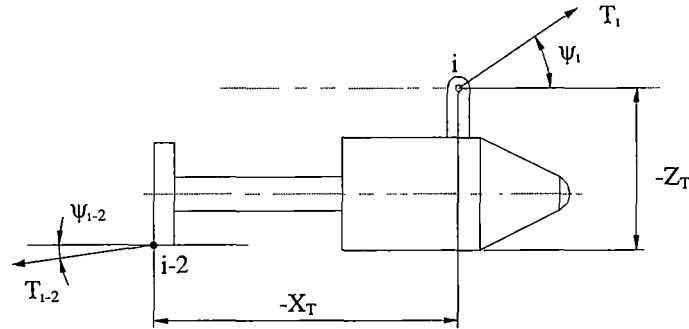
Considering Figure 4.16, it is seen that the fish in the towed system separate the secondary cable. Thus, each fish has two nodes, *i.e.* the tow cable node (usually forward) and the aft node to which the second cable is attached. Figure 4.17 shows the tow fish with the tow (forward) and aft cables at the respective nodes. Thus, when the forces and moments are calculated, it is essential to include the tension terms of the second cable, with due consideration to its location and transformation matrix. The node representing the fish and hence the node solved for the fish equations of motion, will be the forward tow point node for each fish considered.

The solution technique follows a similar routine to that explained in sub-section 4.3.5, however incorporating the additional tow fish equations and the secondary cable separations. The solution procedure explained below uses the lumped mass model shown in Figure 4.16.



Multiple Tow Fish in Series

Figure 4.16



Tow Fish with Two Cables at Two Separate Nodes

Figure 4.17

The solution commences by carrying out steps 3 to 12 in the solution procedure described in sub-section 4.3.5, from node 1, representing the first fish in the system, and continuing along the secondary cable until node 3, *i.e.* the aft node on the second fish, is reached. The equations for the second fish are then solved by solving the equations for the node representing it, *i.e.* node 4, including the tension of cable segment 2, previously calculated. The solution again continues through steps 3 to 12 along the cable until node 6, which is the aft node of fish three, is reached. Following a similar process to that for fish two, the solution again commences from node 7 and continues to the surface node "n". The latter part of the solution has to take into consideration the discontinuity of the junction and the depressor (if present), as explained for the two-part tow in sub-section 4.3.

Then, steps 9 and 10 are carried out in line with the surface excitation, and the tentative tensions are updated using the tension correction terms as described in sub-section 12. The tension terms are then checked for convergence as in step 13, with the

loop consisting of steps 3 to 13 repeated until convergence is achieved. The simulation is then incremented as explained in step 14.

This method of solution yields accurate results, but if the number of cables separated by the fish exceeds three, the time step required for convergence is extremely small, resulting in unacceptably slow simulation run times. The reason for this can be explained by considering nodes 4, 5, and 6. Since both ends of this cable will be subjected to errors during the iteration period, large time steps will introduce large errors, which will effect the convergence, resulting in instability. In order to allow for larger time steps and hence a faster solution time, the solution procedure was modified as explained below.

Referring again to Figure 4.16, the solution technique adapted is to individually solve the cables separated by the tow fish for each time step, and then to couple these cables via the respective tow fish. This procedure can be summarised as follows.

The solution technique divides the cable configuration into a number of cable sub-systems, with the divisions carried out at the tow fish separating the cables. In Figure 4.16 for example, this would consist of three cable sub-systems, *i.e.*,

- cable sub-system 1 : node 1 to node 3
- cable sub-system 2 : node 4 to node 6
- cable sub-system 3 : node 7 to node “n”

The solution commences by completing steps 2 to 13 in sub-section 4.3.5 for cable sub-system 3. This begins by first solving for fish three via the solution of the equations of motion for its representative node, *i.e.* node 7. The solution then continues along cable sub-system 3, until node “n” is reached, which enables the surface node motion to be entered via step 2. (Note: this cable sub-system may incorporate the junction and depressor, and thus will be required to be solved as described in sub-section 4.3.3). The loop-consisting of steps 3 to 13 is repeated until acceptable convergence is achieved for this cable sub-system, *i.e.* until cable sub-system 3 is solved subject to its boundary conditions.

Once this is achieved, the position of node 6 at the aft end of the third fish, is calculated by adding the angular displacement vector of fish three to the linear position of node 7, *i.e.* the tow point of fish three. The position of node 6 will be the driving function for cable sub-system 2, (*i.e.* nodes 4 to 6). The solution for this cable

sub-system is then effected by solving fish two via the solution of the equations of motion of its representative node, *i.e.* node 4, and progressing along the cable up to node 6, *i.e.* the end of cable sub-system 2. This process will consist of completing steps 3 to 13 in sub-section 4.3.5, until convergence is achieved, thus solving cable system 2 to its boundary conditions.

This is followed by obtaining node 3 on fish two in a similar manner to that explained for node 6, which will act as the driving function for cable sub-system 1. The latter can then be solved in a similar manner to cable sub-system 2. On completing these solutions, step 14 in sub-section 4.3.5 is carried out by incrementing the time and repeating the process until the simulation end time is reached.

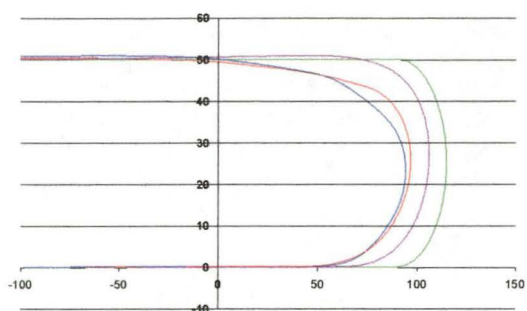
When a node representing a fish is solved during the solution of a cable sub-system, for example, when solving node 4 representing fish 2 during the solution of cable sub-system 2 (see Figure 4.17), the tension of the cable fitted to its aft end, *i.e.* cable segment 2, is unknown. This is due to the aft end cable segment tension not been calculated for the current time step, since segment 2 is solved during the solution of cable sub-system 1, which only commences after the completion of the solution of cable sub-system 2. In order to overcome this problem, the cable tension of segment 2, obtained in the previous time step is used for the solution of the equations of motion of node 4 representing fish 2.

Fish 1	41.2 kg	
Cable Sub-System 1	30 m	3 segments
Fish 2	30 kg	
Cable Sub-System 2	30 m	3 segments
Depressor	300 kg	
Primary Cable	55 m	5 segments

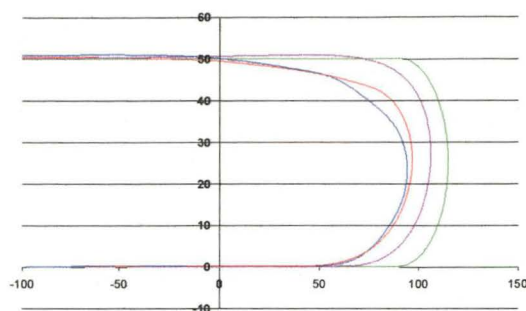
Series Multi-Tow Configuration Information

Table 4.2

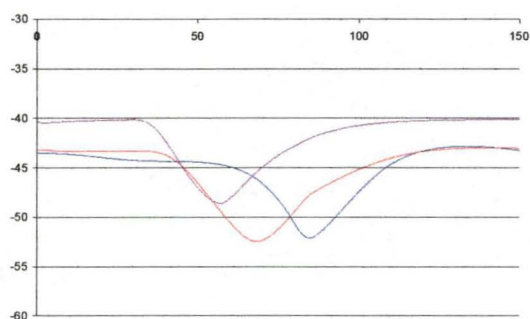
The error thus introduced will be acceptably small, if a relatively small time step is used in the solution procedure. This can be seen by comparing the results of the same tow configuration solved using the more accurate but slower method and the modified faster solution. A typical multi-tow configuration consisting of two towed fish and a depressor in series, (similar to Figure 1.1(g)), was solved using both solution techniques. The information on the tow is given in Table 4.2, while the surface excitation was the 180 degree manoeuvre at 3 metres per second described previously.



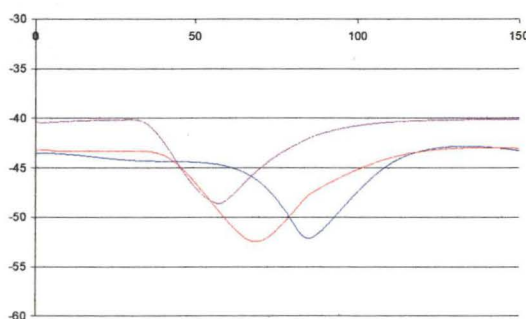
Series Multi-Tow – Path - Fast
Figure 4.18



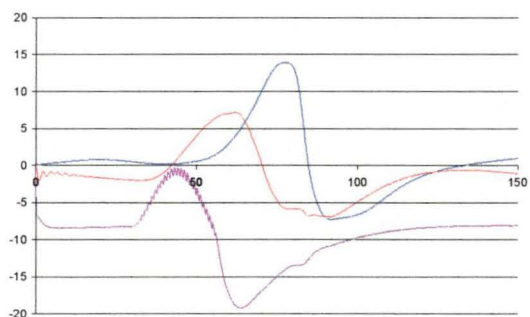
Series Multi-Tow - Path - Slow
Figure 4.19



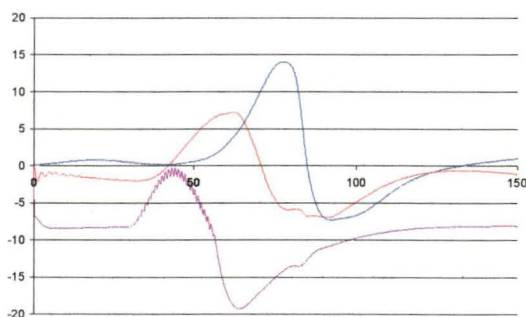
Series Multi-Tow – Depth - Fast
Figure 4.20



Series Multi-Tow – Depth - Slow
Figure 4.21



Series Multi-Tow - Pitch Angle - Fast
Figure 4.22



Series Multi-Tow - Pitch Angle - Slow
Figure 4.23

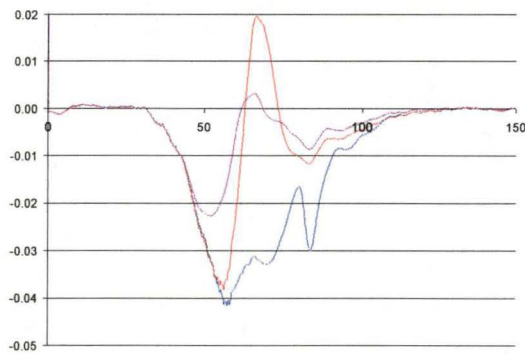
Key to Graphs

■ ship ■ fish 2
■ fish 1 ■ depressor
X-axis – time (seconds)

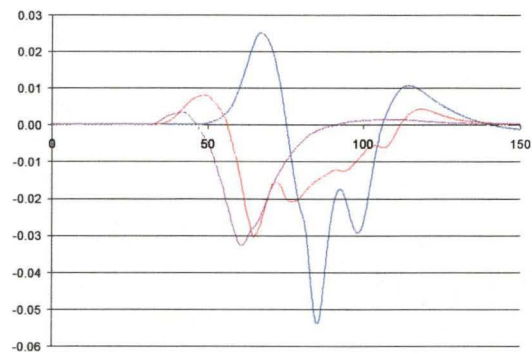
motion – metres
depth – metres
pitch angle – degrees, (+) down

The path of the vehicles, the depth of the tows, and the two fish pitch angles obtained using the fast and slow methods are given in Figures 4.18, 4.20, 4.22 and Figures 4.19, 4.21, 4.23 respectively. Figures 4.24 to 4.27 give the difference curves between

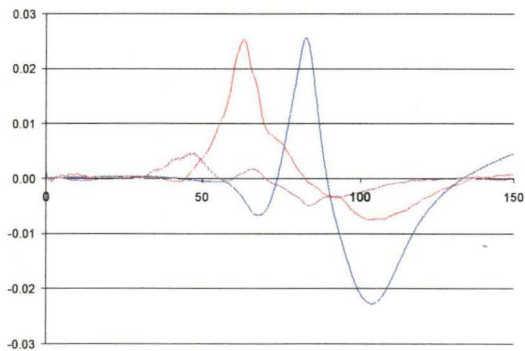
the results obtained from the two methods. It is clear from these figures that the errors introduced by separately solving each sub-system are small. However it allows the use of a time step more than 15 times larger than that for the more accurate method, resulting in it being more than 15 times faster. Thus, given the increase in speed and the marginal loss in accuracy, the selected method is acceptable for the simulation of multiple tows in series.



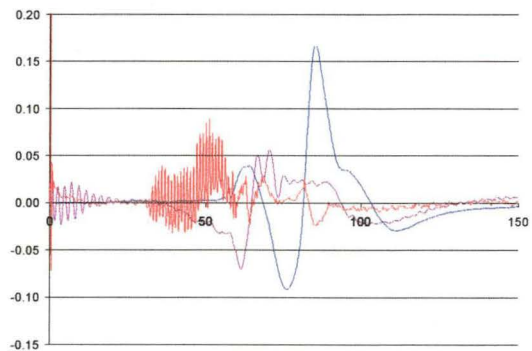
Difference Curve – X Direction
Figure 4.24



Difference Curve – Y Direction
Figure 4.25



Difference Curve – Depth
Figure 4.26

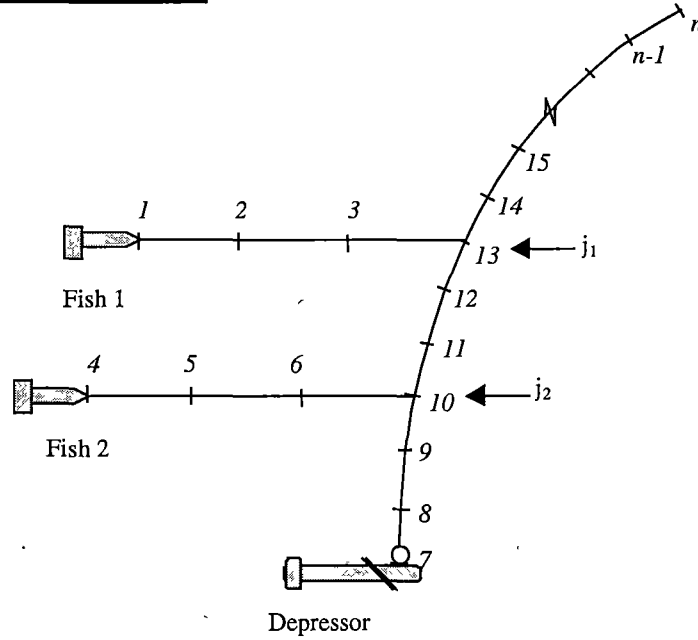


Difference Curve – Pitch Angle
Figure 4.27

Key to Graphs – same as for Figures 4.18 to 4.23.

The results also highlight the sensitivity of the results to the size of the time step. Although the method solving each sub-system separately uses a time step around 15 times larger than that for the more accurate method, there are no significant differences in the results. This is due to the iterative process removing any errors introduced by the larger time step. Therefore, the operator can select the largest time step that ensures numerical stability, as it will have very little effect on the accuracy. These aspects will be discussed later in Chapter 5.

4.6 Multiple Tows in Parallel



Multiple Tow Fish in Parallel

Figure 4.28

Figure 4.28 shows a multiple tow system, where two fish are towed in parallel, *i.e.* where each fish is attached to its own secondary cable, which in turn is connected to the primary tow cable. The required depth is maintained *via* a depressor fitted to the lower end of the primary cable. Although the example shown in Figure 4.28 has only two parallel tow fish, the computer model is capable of solving up to five parallel tow fish and can be easily modified to solve configurations having more parallel tow fish.

The modelling of the system is similar to that for a two-part tow, however, with due regard shown to the multiple junctions in the system. Each junction, *i.e.* nodes 10 and 13 in Figure 4.28, is modelled as described in sub-section 3.4.1, resulting in a set of equations similar to that given by equation (3.32).

In addition, the tow fish represented by nodes 1 and 4, will have only one cable segment attached to them, *i.e.* cable segments 1 and 4 respectively. Thus, the modelling will be as described in sub-section 3.5, resulting in equations similar to equations (3.102). The resulting set of equations can be presented in a matrix form as described in equation (4.32). However, the matrix $[E_i F_i G_i CD]$ will have a greater number of non-zero terms outside the tri-diagonal band, as well as a number of zero terms on the outer diagonal of the tri-diagonal band. For example, for the system shown in Figure 4.28 having two parallel tow fish, the matrix will be,

$$\begin{array}{cccccccccccccccc} C_1 & C_2 & C_3 & C_4 & C_5 & C_6 & C_7 & C_8 & C_9 & C_{10} & C_{11} & C_{12} & C_{13} & C_{14} & \cdots & C_{n-2} & C_{n-1} \\ R_1 & -F_1 & G_1 & & & & & & & & & & & & & & (\text{row } f_1) \\ R_2 & E_2 & -F_2 & G_2 & & & & & & & & & & & & & \\ R_3 & & E_3 & -F_3 & 0 & & & & & & & C_1 & C_2 & & & & (\text{row } f_{2-1}) \\ R_4 & & & 0 & -F_4 & G_4 & & & & & & & & & & & (\text{row } f_2) \\ R_5 & & & & E_5 & -F_5 & G_5 & & & & & & & & & & \\ R_6 & & & & & E_6 & -F_6 & 0 & & C_3 & C_4 & & & & & & (\text{row } D-1) \\ R_7 & & & & & & 0 & -F_7 & G_7 & & & & & & & & (\text{row } D) \\ R_8 & & & & & & & E_8 & -F_8 & G_8 & & & & & & & \\ R_9 & & & & & & & & E_9 & -F_9 & G_9 & & & & & & \\ R_{10} & & & & & & & & & D_3 & D_4 & & & & & & \\ R_{11} & & & & & & & & & & & G_{10} & & & & & (\text{row } j_2) \\ R_{12} & & & & & & & & & & & E_{11} & -F_{11} & G_{11} & & & \\ R_{13} & & & & & & & & & & & & E_{12} & -F_{12} & G_{12} & & \\ R_{14} & & & & & & & & & & & & & E_{13} & -F_{13} & G_{13} & (\text{row } j_1) \\ \vdots & & & & & & & & & & & & & & & & \\ R_{n-2} & & & & & & & & & & & & & & & E_{n-2} & -F_{n-2} & G_{n-2} \\ R_{n-1} & & & & & & & & & & & & & & & E_{n-1} & -F_{n-1} & G_{n-1} \end{array}$$

(4.47)

This matrix has to be converted to a true tri-diagonal matrix $[E_i F_i G_i]$, to be solved in the manner described by equations (4.37) to (4.40). The conversion process is adapted from that described for the conversion of matrix (4.33) to (4.35), since the terms lying outside the tri-diagonal band can be described with reference to the positions of the tow fish, junctions, and depressor. The process described below should be considered in conjunction with the conversion explained in sub-section 4.3.3.

The first phase, consists of eliminating all D_i terms. This commences at row “2” by eliminating term E_2 with the aid of row “1”. The elimination process is then continued from rows “2” to “ f_2-1 ” by successively eliminating all E_i terms with the aid of the row immediately above the row being manipulated. The resulting row “ f_2-1 ”, which is now devoid of term E_{f_2-1} , can be used to eliminate terms D_1 and D_2 .

Skipping row “f₂”, the elimination process of E₁ from rows “f₂+1” to “D-1” is carried out in a similar fashion to that explained above. As in the previous case, the resulting row “D-1”, can then be used to eliminate terms D₃ and D₄. In the example shown (*i.e.* equation (4.47)), this should result in all D_i terms being eliminated. At the end of this elimination process, in addition to the elimination of all the D_i terms, the E₁ terms from rows “2” to “D”, would have converted to zero.

The second phase of the elimination process is the elimination of the C_i terms. Using row “j₂-1”, the term C_4 in row “D-1” is eliminated. This is then followed by row “j₂-

2", which is used to eliminate the term C_3 also in row "D-1". This elimination process will introduce new terms along row "D-1", between columns " j_2-2 " and "D+1". These additional terms can be eliminated by continuing the process of elimination using row " j_2-3 ", followed by row " j_2-4 " and so on, until row "D" is reached. This will also ensure that the zero term G_{D-1} , will convert to a non-zero term.

A similar elimination process is then carried out for terms C_1 and C_2 , located on row " f_2-1 ", by commencing the elimination process with row " j_1-1 " to eliminate the term C_2 , followed by row " j_1-2 " to eliminate the term C_1 and so on, until row " f_2 " is reached. This process will ensure that any additional terms introduced on to row " f_2-1 " between columns " j_1-2 " to " f_2+1 " will be eliminated. In addition, the elimination process will also convert the term G_{f_2-1} to a non-zero term. The conversion of all the G_i terms that are zero to non-zero values is essential to ensure that the solution process for a true tri-diagonal matrix as explained from equations (4.37) to (4.40), has no divisions by zero.

The resulting matrix will be a true tri-diagonal matrix $[E_i F_i G_i]$, which will be as shown in equations (4.35) and (4.36) and solved using the Thomas algorithm as explained in sub-section 4.3.3 to yield the tension correction terms δT_i^{t+1} . The solution process for the multiple tow system will be as explained for the two-part tow, *i.e.* steps 1 to 14 in sub-section 4.3.5, with the only difference being the modification in converting the matrix to a true tri-diagonal matrix in step 11.

The conversion explained above would be similar for a tow configuration consisting of more parallel tows and hence more C_i and D_i terms, as their positions will be known as a function of the positions of the tow fish, junctions, and depressor. This allows the elimination process explained above to be applied.

Fish 1	26 kg	
Secondary Cable 1	20 m	4 segments
Fish 2	26 kg	
Secondary Cable 2	20 m	4 segments
Fish 3	26 kg	
Secondary Cable 3	20 m	4 segments
Depressor	85 kg	
Primary Cable	125 m	10 segments

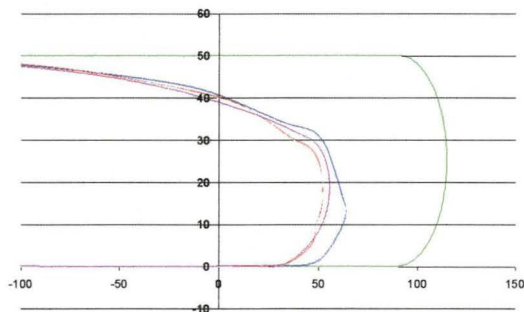
Parallel Multi-Tow Configuration Information

Table 4.3

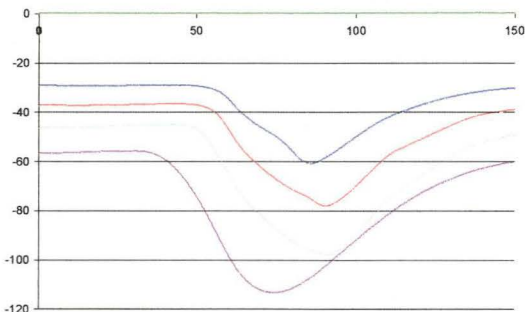
Figures 4.29 to 4.31 give the results of a multi-tow having three fish plus the depressor in parallel. Information on the tow is given in Table 4.3. The surface excitation again is the 180 degree manoeuvre at 3 metres per second.

From Figure 4.29, as expected the tow fish turn inside the turning circle of the surface vessel. The inevitable slowing down of the fish results in an increase in their depth and pitch angles, as shown in Figures 4.30 and 4.31. With a parallel multi-tow, it is important to consider the change in depth of the parallel tows as they may make contact with each other and get “entangled”. Although Figure 4.30 only shows the depth of the towed fish, it is prudent to look at the positions of the secondary cables in full, to prevent contact between them. The program is able to supply the positions of the cable nodes to enable this investigation.

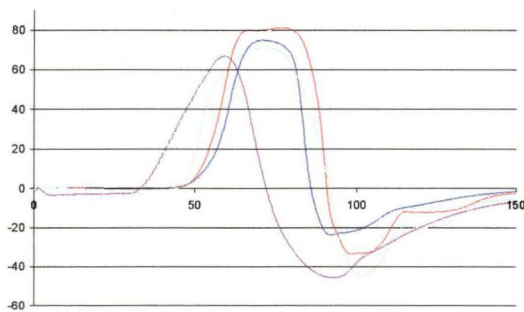
The computer flowcharts for the modelling techniques explained in Chapter 3 and the solution procedure described in this chapter are given in Appendix B.



Parallel Multi-Tow – Path
Figure 4.29



Parallel Multi-Tow – Depth
Figure 4.30



Parallel Multi-Tow - Pitch Angle
Figure 4.31

Key to Graphs

- ship
- fish 1
- fish 2
- fish 3
- depressor

- X-axis** – time (seconds)
- motion** – metres
- depth** – metres
- pitch angle** – degrees, (+) down

CHAPTER 5

ANALYSIS OF THE NUMERICAL METHOD

5.1 Introduction

In Chapter 2, the modelling of a continuous cable system was briefly described, and the equations of motion were derived as second order coupled non-linear partial differential equations, (see equations (2.9)). In order to solve these equations, they first have to be converted into second order coupled non-linear ordinary differential equations.

One method of achieving this is to model the cable structure using the lumped mass method as explained in Chapter 3. The resulting ordinary differential equations are then solved using a numerical integration scheme that gives the change in the cable configuration over time, *i.e.* a time domain simulation. In Chapter 4, the solution procedure employed in this project was detailed.

Since the equations are non-linear, an iterative process, such as the Newton-Raphson iteration process, is required at each time step. Thus, the solution obtained from the numerical integration scheme is checked for accuracy with the aid of a constraint relationship. This relationship will enable the results to be *improved* through the iteration process, until an acceptable level of accuracy is achieved. In addition to being accurate, the selected numerical technique must be stable, *i.e.* it should converge to a solution.

In engineering, the use of numerical techniques is widespread. Although, most engineers are conversant with the use of numerical techniques, and are aware that the procedure should be stable and accurate, many are unsure of the mechanics involved in satisfying these criteria, a point not lost on mathematicians. Therefore, this section looks briefly at the numerical techniques, and analyses the stability and accuracy of these methods, with an emphasis on the technique used in this project. It is not intended to carry out a detailed study, as that is left respectfully in the “domain” of the mathematician. Text such as Ames (1969), Gear (1971), and Wood (1990) provide a good mathematical analysis of such numerical methods, while Bathe (1982) gives

engineers a brief but concise description on the accuracy and stability requirements of popular numerical schemes in engineering.

The integration of ordinary differential equations can be classified as *implicit* or *explicit*. Consider the equation,

$$\frac{d\bar{u}}{dt} = f(\bar{u}, t) \quad (5.1)$$

where

\bar{u} : arbitrary vector varying with time “t”

\bar{f} : vector, which is a function of both “ \bar{u} ” and “t”.

If during the integration, “ \bar{f} ” is obtained only for known values of “ \bar{u} ”, the integration is said to be explicit. However, if “ \bar{f} ” must be obtained for values of “ \bar{u} ” that are calculated from “ \bar{f} ”, then the integration is said to be implicit.

The general form of an explicit time integration scheme is given by,

$$\ddot{\bar{R}}^t = f(\bar{R}^{t+1}, \bar{R}^t, \bar{R}^{t-1}, \bar{R}^{t-2}, \dots) \quad (5.2)$$

where “ \bar{R} ” is the displacement and “t” is the time.

From equation (5.2) it is seen that the displacement at “t+1” (*i.e.* \bar{R}^{t+1}), depends only upon the values *up to* time “t”. The most popular explicit integration scheme is the Central Difference (CD) method, (Walton and Polachek (1959) and Bathe (1982)).

Implicit schemes can be represented by,

$$\ddot{\bar{R}}^{t+1} = f(\bar{R}^{t+1}, \bar{R}^t, \bar{R}^{t-1}, \bar{R}^{t-2}, \dots) \quad (5.3)$$

In this case, the displacement at “t+1” (*i.e.* \bar{R}^{t+1}), depends upon the values *up to and inclusive* of those at time “t+1”. Therefore, these generally require an iteration process in the solution technique. A number of implicit schemes are used in engineering, including the Newmark, Houbolt, and Wilson- θ methods, (Bathe (1982) and Thomas (1993) give details of these methods in engineering applications).

The integration schemes for ordinary differential equations can be further divided into a number of groups, and the more popular ones are discussed here.

p-Step Algorithms

These numerical algorithms are given by,

$$\sum_{t=0}^p \{ (\alpha^t \Delta t^{-2} \underline{\underline{m}} + \gamma^t \Delta t^{-1} \underline{\underline{c}} + \beta^t \underline{\underline{k}}) \bar{\underline{R}}^{N+t} - \beta^t \bar{\underline{f}}^{N+t} \} = 0 \quad (5.4)$$

where

$\alpha^t, \beta^t, \gamma^t$: parameters of the multi-step integration algorithm
 $\underline{\underline{m}}, \underline{\underline{c}}, \underline{\underline{k}}$: system mass, damping, and stiffness matrices respectively
 $\bar{\underline{R}}^N$: displacement vector at time “N”
 $\bar{\underline{f}}$: external load vector

Thus, to obtain $\bar{\underline{R}}^p$ it is required to use the values corresponding to times 0 to p-1. For example, if the algorithm was a two-step algorithm, then $\bar{\underline{R}}^p$ will depend on times p-2 and p-1.

One-Step p-Stage Algorithms

These are of the form,

$$\bar{\underline{R}}^{t+1} = \underline{\underline{A}}_p \bar{\underline{R}}^t + \underline{\underline{L}}_p \bar{\underline{f}}^{t+1} \quad (5.5)$$

where

$$\bar{\underline{R}}^{t^T} = \left[\bar{\underline{R}}^t, \dot{\bar{\underline{R}}}^t, \ddot{\bar{\underline{R}}}^t, \dots, \bar{\underline{R}}^{t^{p-1}} \right]^T$$

$\bar{\underline{f}}$: external load vector

$\underline{\underline{A}}_p$: amplification matrix

$\underline{\underline{L}}_p$: p x p load operator

t : time

Note: $\underline{\underline{A}}_p$ and $\underline{\underline{L}}_p$ will be dealt with in detail later in sub-section 5.5.2 of this chapter.

To obtain \bar{R}^{t+1} , the values at time “t” are used, (*i.e.* one-step). However, “p-1” derivatives of R^t are used, (*i.e.* p-stage). For example, if the algorithm is a one-step two-stage algorithm, then \bar{R}^{t+1} will depend on R^t and \dot{R}^t .

In cable models the common algorithms used are single-step, multi-step, and multiple evaluation schemes. The first uses simple low-order formulae based on a truncated Taylor series. Only one function is evaluated at every step, thus resulting in low accuracy. However the accuracy can be improved if the derivatives can be explicitly calculated. The hinged rod cable method explained in Chapter 2 uses a single-step integration scheme.

The multi-step method uses a number of values obtained in previous iteration steps to recalculate their values. This allows their values to be *improved* through an iterative procedure until sufficient convergence is achieved. Increasing the number of previous values in the iteration process enables schemes involving higher order terms to be incorporated, thus increasing accuracy. Common methods consist of *predictor-corrector* schemes, where explicit formulae give a *prediction* of the required solution of an implicit *corrector*. The solution described in Chapter 4 follows this method.

The final group, multiple evaluation schemes, reduces the error by calculating the values at a number of intermediate positions within the given step. An example is the *Runge-Kutta* method, used by Ractliffe (1984) and Sanders (1982) to solve underwater cable / riser and towed systems, respectively.

The selection of the numerical solution procedure depends on the balance between accuracy / stability of the schemes and the computational effort required. In dynamic cable / body models, modes of motion occur within the system, and oscillate at a rate on the scale of milliseconds. The ratio of the fastest to the slowest normal mode of motion is referred to as the “stiffness ratio”. A system having a large ratio (usually above a ratio of 10000), is deemed to be stiff.

Although these high frequency modes do not greatly influence the motion of the system, they affect the stability of the numerical scheme used in the solution process. Therefore, the step size used in explicit integration solution schemes should be sufficiently small to follow these rapid variations. Implicit integration schemes are usually stable for all time steps. However, the time step is limited due to two conditions:

- the loss of accuracy due to the size of the time step; and
- instability due to the propagation of the errors introduced by the iteration scheme required for non-linear systems.

Usually numerical methods utilising higher order schemes are more accurate, but they require greater computational effort. However, these methods do not always increase in stability. In some cases, the increase can be marginal, while in others it may even reduce in comparison with a related lower-order scheme.

When selecting more accurate higher-order schemes for systems with very high frequency modes, the schemes must have sufficiently large stability regions to enable a practical step length to be used. A number of quasi-Newton iteration schemes can achieve this, although they require a high computational load. Therefore, the scheme selected should balance the accuracy, stability, and computational load.

The Houbolt method used in this project is a higher-order scheme with a sufficiently large stability region, (Hilber *et al.* (1977)). Although the computational time is greater than that of a lower order system (*e.g.* an Euler type integrator), it proved to be sufficiently competitive against models using such lower order schemes. Note: although a number of numerical methods were used during the computer modelling phase, the Houbolt scheme was ultimately selected for the project.

5.1.1 Derivation of the Houbolt Scheme

Since the numerical scheme used here is the Houbolt scheme, it is prudent at this juncture to discuss its derivation. The Houbolt method is a three step ($p = 3$) method. (Note: some texts refer to the Houbolt scheme as a four-step method. However, in this thesis the notation given by Wood (1990) will be used, *i.e.* $p = 0$ to 3).

Multi-step numerical algorithms are generally described by equation (5.4). If the **second order differential equation** is of the form,

$$\ddot{\mathbf{R}} = \mathbf{\bar{F}} \quad (5.6)$$

then equation (5.4) will reduce to,

$$\sum_{t=0}^p \{ \alpha^t \bar{R}^{N+t} - \Delta t^2 \beta^t \bar{F}^{N+t} \} = 0 \quad (5.7)$$

where \bar{R}^N is the displacement at time “N”. Since $p = 3$, equation (5.7) becomes,

$$\alpha^0 \bar{R}^N + \alpha^1 \bar{R}^{N+1} + \alpha^2 \bar{R}^{N+2} + \alpha^3 \bar{R}^{N+3} = \Delta t^2 \bar{F}^{N+3} \quad (5.8)$$

Note: $\beta^0 = \beta^1 = \beta^2 = 0$ and $\beta^3 = 1$, since the method is implicit and the number of functional evaluations are to be minimised.

The associated local truncation error ($L_{\Delta t}(\bar{R}^N \Delta t)$) is estimated by using the exact solution of equation (5.6) in the integration scheme given by equation (5.7). Thus,

$$L_{\Delta t}(\bar{R}^N \Delta t) = \sum_{t=0}^3 \{ \alpha^t \bar{R}^{N+t} - \Delta t^2 \beta^t \bar{F}^{N+t} \} \quad (5.9)$$

Expanding equation (5.9) in a Taylor series about \bar{R}^N yields,

$$L_{\Delta t}(\bar{R}^N \Delta t) = C^0 \bar{R}^N + \Delta t C^1 \dot{\bar{R}}^N + \Delta t^2 C^2 \ddot{\bar{R}}^N + \Delta t^3 C^3 \dddot{\bar{R}}^N \quad (5.10)$$

where C^t are constants obtained by the expansion of the terms in (5.9) and collating the coefficients of terms having the same power. Therefore, from equations (5.8) and (5.10) we obtain,

$$C^0 = \alpha^0 + \alpha^1 + \alpha^2 + \alpha^3 \quad (5.11a)$$

$$C^1 = \alpha^1 + 2\alpha^2 + 3\alpha^3 \quad (5.11b)$$

$$C^2 = 1/2 (\alpha^1 + 4\alpha^2 + 9\alpha^3) - 1 \quad (5.11c)$$

$$C^3 = 1/6 (\alpha^1 + 8\alpha^2 + 27\alpha^3) - 3 \quad (5.11d)$$

It is required that the error in the scheme is at least of the second order. Inspection of equation (5.9) indicates that the difference equation has an order of accuracy of q if,

$$C^0 = C^1 = C^2 = \dots = C^q = C^{q+1} = 0 \quad \text{and} \quad (5.12a)$$

$$C^{q+2} \neq 0 \quad (5.12b)$$

Thus, for accuracy of the second order,

$$C^0 = C^1 = C^2 = C^3 = 0 \quad (5.13)$$

which reduces equations (5.11) to,

$$\alpha^0 = -(\alpha^1 + \alpha^2 + \alpha^3) \quad (5.14a)$$

$$\alpha^1 = -(2\alpha^2 + 3\alpha^3) \quad (5.14b)$$

$$\alpha^1 = 2 - (4\alpha^2 + 9\alpha^3) \quad (5.14c)$$

$$\alpha^1 = 18 - (8\alpha^2 + 27\alpha^3) \quad (5.14d)$$

Solving the above simultaneous equations yields,

$$\alpha^0 = -1, \quad \alpha^1 = 4, \quad \alpha^2 = -5, \quad \text{and} \quad \alpha^3 = 2 \quad (5.15)$$

Now substituting into equation (5.8) and using equation (5.6) we have,

$$\ddot{\bar{R}}^{N+3} = \frac{1}{\Delta t^2} (2\bar{R}^{N+3} - 5\bar{R}^{N+2} + 4\bar{R}^{N+1} - \bar{R}^N) \quad (5.16)$$

which is the **acceleration** for the Houbolt scheme.

Let us now consider a **first order differential equation** of the form,

$$\dot{\bar{R}} = \bar{F} \quad (5.17)$$

In a similar process to the second order differential equation explained above, equation (5.17) can be expressed in the finite difference scheme as,

$$\alpha^0 \bar{R}^N + \alpha^1 \bar{R}^{N+1} + \alpha^2 \bar{R}^{N+2} + \alpha^3 \bar{R}^{N+3} = \Delta t \bar{F}^{N+3} \quad (5.18)$$

Again, the associated local truncation error ($L_{\Delta t}(\bar{R}^N \Delta t)$) is estimated as,

$$L_{\Delta t}(\bar{R}^N \Delta t) = \sum_{t=0}^3 \{ \alpha^t \bar{R}^{N+t} - \Delta t \beta^t \bar{F}^{N+t} \} \quad (5.19)$$

Now expanding equation (5.19) in a Taylor series and collating the coefficients of terms having the same power gives,

$$C^0 = \alpha^0 + \alpha^1 + \alpha^2 + \alpha^3 \quad (5.20a)$$

$$C^1 = \alpha^1 + 2\alpha^2 + 3\alpha^3 - 1 \quad (5.20b)$$

$$C^2 = 1/2 (\alpha^1 + 4\alpha^2 + 9\alpha^3) - 3 \quad (5.20c)$$

$$C^3 = 1/6 (\alpha^1 + 8\alpha^2 + 27\alpha^3) - 9/2 \quad (5.20d)$$

Inspection of equation (5.19) indicates that the difference equation has an order of accuracy of q if,

$$C^0 = C^1 = C^2 = \dots = C^q = 0 \quad \text{and} \quad (5.21a)$$

$$C^{q+1} \neq 0 \quad (5.21b)$$

Therefore, for accuracy of the second order,

$$C^0 = C^1 = C^2 = 0 \quad (5.22)$$

Thus, using equations (5.17a), (5.17b) and (5.17c) we have,

$$\alpha^0 = 3/2 - \alpha^3 \quad (5.23a)$$

$$\alpha^1 = 3\alpha^3 - 4 \quad (5.23b)$$

$$\alpha^2 = 5/2 - 3\alpha^3 \quad (5.23c)$$

These three relationships do not facilitate the complete solution of the coefficients, *i.e.* the relationships will depend on the value selected for α^3 . However, it is possible to obtain a solution if the accuracy is increased to the third order. This will result in,

$$C^3 = 0 \quad (5.24)$$

Thus, we obtain,

$$\alpha^0 = -2/6, \quad \alpha^1 = 3/2, \quad \alpha^2 = -6/2, \quad \text{and} \quad \alpha^3 = 11/6 \quad (5.25)$$

Now substituting into equation (5.18) and using equation (5.17) gives,

$$\dot{\bar{R}}^{N+3} = \frac{1}{6\Delta t} (11\bar{R}^{N+3} - 18\bar{R}^{N+2} + 9\bar{R}^{N+1} - 2\bar{R}^N) \quad (5.26)$$

which is the **velocity** for the Houbolt scheme.

5.2 Comparison between the Lumped Mass Model and the Continuous Cable Model

5.2.1 Continuous Cable Model

In Chapter 3, the cable was modelled by dividing it into a number of segments. The cable system will now be modelled and investigated as a continuous system, (see Schram and Reyle (1968), Patton (1972), and Brook (1990) for a detailed explanation of this modelling technique). The derivation of these equations was considered briefly in Chapter 2, and will be expanded in this sub-section.

Figure 2.1 shows the Cartesian coordinate system and the cable orientation, which yields the transformation matrices $[\Lambda]$ between the Cartesian coordinates (X, Y, Z) and the local coordinates (X', Y', Z') located along the cable. This was derived as equation (2.3) in Chapter 2 and is reproduced below.

$$[\Lambda] = \begin{bmatrix} \cos\phi \cos\psi & \sin\phi \cos\psi & \sin\psi \\ -\sin\phi & \cos\phi & 0 \\ -\cos\phi \sin\psi & -\sin\phi \sin\psi & \cos\psi \end{bmatrix} \quad (5.27)$$

Note: the inverse of the above transformation matrix is equal to the transpose of the matrix or,

$$[\Lambda]^{-1} = [\Lambda]^T \quad (5.28)$$

The spatial coordinates of the cable is defined as follows. The length along the cable is represented by “s”, the length of an *unstretched* segment of the cable is represented

by “ δs ”, and the *stretched* length by “ δs_1 ”. Then from Figure 2.1, considering the geometric relationships between the angles and the spatial derivatives gives a set of *constitutive relationships* as,

$$\frac{\partial x}{\partial s_1} = \text{Cos } \phi \text{ Cos } \psi \quad (5.29a)$$

$$\frac{\partial y}{\partial s_1} = \text{Sin } \phi \text{ Cos } \psi \quad (5.29b)$$

$$\frac{\partial z}{\partial s_1} = \text{Sin } \psi \quad (5.29c)$$

where x , y , and z are the displacements in the X , Y , and Z directions.

The relationship between the stretched length “ δs_1 ” and the unstretched length “ δs ” is given by the local strain of the element as,

$$\frac{\delta s_1}{\delta s} = 1 + \epsilon \quad (5.30)$$

where “ ϵ ” is the local strain in the cable element when stretched. Thus, the constitutive relationships given in equations (5.29) become,

$$\frac{\partial x}{\partial s} = (1 + \epsilon) \text{Cos } \phi \text{ Cos } \psi \quad (5.31a)$$

$$\frac{\partial y}{\partial s} = (1 + \epsilon) \text{Sin } \phi \text{ Cos } \psi \quad (5.31b)$$

$$\frac{\partial z}{\partial s} = (1 + \epsilon) \text{Sin } \psi \quad (5.31c)$$

Figure 2.2 shows the tensile force and the external forces on the cable segment. By resolving these forces into the Cartesian coordinate directions, X , Y , and Z , we obtain the equations of motion as,

$$\mu_c \frac{\partial^2 x}{\partial t^2} \delta s = (T + \delta T) \text{Cos } (\phi + \delta \phi) \text{Cos } (\psi + \delta \psi) - T \text{Cos } \phi \text{ Cos } \psi + F_{ox} \delta s \quad (5.32a)$$

$$\mu_c \frac{\partial^2 y}{\partial t^2} \delta s = (T + \delta T) \sin(\phi + \delta\phi) \cos(\psi + \delta\psi) - T \sin \phi \cos \psi + F_{oy} \delta s \quad (5.32b)$$

$$\mu_c \frac{\partial^2 z}{\partial t^2} \delta s = (T + \delta T) \sin(\psi + \delta\psi) - T \sin \psi + F_{oz} \delta s \quad (5.32c)$$

where

$F_{ox,y,z}$: external forces except the tension forces per unit stretched length of cable,
(i.e. hydrodynamic, mass, and buoyancy forces)

s : the arc length of any unstretched point along the cable

T : cable tension

μ_c : cable mass per unit length

ϕ : horizontal angle of the cable with the X axis

ψ : vertical angle of the cable with the X-Y plane

δ : represents the change in the parameter

If we expand the trigonometric terms and take limits for the changes in the parameters s , T , ψ , and ϕ , we get,

$$\delta s \rightarrow 0, \quad \delta T \rightarrow 0, \quad \delta \psi \rightarrow 0, \quad \text{and} \quad \delta \phi \rightarrow 0$$

Equation (5.32) then reduces to,

$$\frac{\partial}{\partial s} (T \cos \phi \cos \psi) + F_{ox} = \mu_c \frac{\partial^2 x}{\partial t^2} \quad (5.33a)$$

$$\frac{\partial}{\partial s} (T \sin \phi \cos \psi) + F_{oy} = \mu_c \frac{\partial^2 y}{\partial t^2} \quad (5.33b)$$

$$\frac{\partial}{\partial s} (T \sin \psi) + F_{oz} = \mu_c \frac{\partial^2 z}{\partial t^2} \quad (5.33c)$$

Thus, equations (5.31) and (5.33) describe the motion of the cable system.

Before the solution of these equations is attempted, manipulating the above-mentioned sets of equations reduces them to typical wave equations. Substituting the constitutive relationships of equations (5.31) into the appropriate equations in (5.33) gives,

$$\mu_c \cdot \frac{\partial^2 x}{\partial t^2} = \frac{\partial}{\partial s} \left(\frac{T}{1 + \epsilon} \cdot \frac{\partial x}{\partial s} \right) + F_{ox} \quad (5.34a)$$

$$\mu_c \cdot \frac{\partial^2 y}{\partial t^2} = \frac{\partial}{\partial s} \left(\frac{T}{1 + \epsilon} \cdot \frac{\partial y}{\partial s} \right) + F_{oy} \quad (5.34b)$$

$$\mu_c \cdot \frac{\partial^2 z}{\partial t^2} = \frac{\partial}{\partial s} \left(\frac{T}{1 + \epsilon} \cdot \frac{\partial z}{\partial s} \right) + F_{oz} \quad (5.34c)$$

These are the wave equations (Kreyszig (1993)) of the continuous cable system.

Equations (5.31) and (5.33) describe the motion of the continuous three-dimensional dynamic cable system. Therefore, these equations have to be solved to obtain the configuration of the cable system. The solution procedure for these equations is much simpler if they are first transformed into the local coordinate system (X' , Y' , Z') by multiplying by the transformation matrix $[\Lambda]$.

First consider equations (5.33), they can be transformed into the local coordinates and expressed in matrix form as,

$$[\Lambda] \cdot \begin{bmatrix} \frac{\partial}{\partial s} (T \cos \phi \cos \psi) \\ \frac{\partial}{\partial s} (T \sin \phi \cos \psi) \\ \frac{\partial}{\partial s} (T \sin \psi) \end{bmatrix} + [\Lambda] \cdot \begin{bmatrix} F_{ox} \\ F_{oy} \\ F_{oz} \end{bmatrix} = \mu_c [\Lambda] \cdot \begin{bmatrix} \frac{\partial V_x}{\partial t} \\ \frac{\partial V_y}{\partial t} \\ \frac{\partial V_z}{\partial t} \end{bmatrix} \quad (5.35)$$

where

$$\frac{\partial V_x}{\partial t} = \frac{\partial^2 x}{\partial t^2}, \quad \frac{\partial V_y}{\partial t} = \frac{\partial^2 y}{\partial t^2}, \quad \text{and} \quad \frac{\partial V_z}{\partial t} = \frac{\partial^2 z}{\partial t^2}$$

First considering the left hand side tension terms, the multiplication can be expanded and simplified to give,

$$[\Lambda] \cdot \begin{bmatrix} \frac{\partial}{\partial s}(T \cos \phi \cos \psi) \\ \frac{\partial}{\partial s}(T \sin \phi \cos \psi) \\ \frac{\partial}{\partial s}(T \sin \psi) \end{bmatrix} = \begin{bmatrix} \frac{\partial T}{\partial s} \\ T \cos \psi \frac{\partial \phi}{\partial s} \\ T \frac{\partial \psi}{\partial s} \end{bmatrix} \quad (5.36)$$

Now considering the global external forces on the cable (F_{ox} , F_{oy} , F_{oz}), the “local” external forces ($F_{ox'}$, $F_{oy'}$, $F_{oz'}$) are defined as,

$$[F_{ox'}, F_{oy'}, F_{oz'}]^T = [\Lambda] \cdot [F_{ox}, F_{oy}, F_{oz}]^T \quad (5.37)$$

Similarly, the global cable velocities (V_x , V_y , V_z), can be expressed as a function of the local velocities ($V_{x'}$, $V_{y'}$, $V_{z'}$) as,

$$[V_x, V_y, V_z]^T = [\Lambda]^T \cdot [V_{x'}, V_{y'}, V_{z'}]^T \quad (5.38)$$

To obtain expressions for the global acceleration in terms of the local acceleration, differentiating equation (5.38) with respect to time gives,

$$\left[\frac{\partial V_x}{\partial t}, \frac{\partial V_y}{\partial t}, \frac{\partial V_z}{\partial t} \right]^T = \frac{\partial [\Lambda]^T}{\partial t} [V_{x'}, V_{y'}, V_{z'}]^T + [\Lambda]^T \left[\frac{\partial V_{x'}}{\partial t}, \frac{\partial V_{y'}}{\partial t}, \frac{\partial V_{z'}}{\partial t} \right]^T \quad (5.39)$$

Multiplying equation (5.39) by the transformation matrix, expanding, and simplifying gives,

$$[\Lambda] \cdot \begin{bmatrix} \frac{\partial V_x}{\partial t} \\ \frac{\partial V_y}{\partial t} \\ \frac{\partial V_z}{\partial t} \end{bmatrix} = \begin{bmatrix} \frac{\partial V_{x'}}{\partial t} - V_{z'} \frac{\partial \psi}{\partial t} - V_{y'} \cos \psi \frac{\partial \phi}{\partial t} \\ \frac{\partial V_{y'}}{\partial t} + V_{x'} \cos \psi \frac{\partial \phi}{\partial t} - V_{z'} \sin \psi \frac{\partial \phi}{\partial t} \\ \frac{\partial V_{z'}}{\partial t} + V_{x'} \frac{\partial \psi}{\partial t} + V_{y'} \sin \psi \frac{\partial \phi}{\partial t} \end{bmatrix} \quad (5.40)$$

Now substituting equations (5.36), (5.37), and (5.40) into equation (5.35) and simplifying gives,

$$\frac{\partial T}{\partial s} - \mu_c \left(\frac{\partial V_{x'}}{\partial t} - V_{z'} \frac{\partial \psi}{\partial t} - V_{y'} \cos \psi \frac{\partial \phi}{\partial t} \right) + F_{ox'} = 0 \quad (5.41a)$$

$$T \cos \psi \frac{\partial \phi}{\partial s} - \mu_c \left(\frac{\partial V_{y'}}{\partial t} + V_{x'} \cos \psi \frac{\partial \phi}{\partial t} - V_{z'} \sin \psi \frac{\partial \phi}{\partial t} \right) + F_{oy'} = 0 \quad (5.41b)$$

$$T \frac{\partial \psi}{\partial s} - \mu_c \left(\frac{\partial V_{z'}}{\partial t} + V_{x'} \frac{\partial \psi}{\partial t} + V_{y'} \sin \psi \frac{\partial \phi}{\partial t} \right) + F_{oz'} = 0 \quad (5.41c)$$

The constitutive relationships given in equations (5.31) can also be expressed in terms of the local velocities. Differentiating equations (5.31) with respect to time gives,

$$\frac{\partial V_{x'}}{\partial s} = (1 + \epsilon) \left[-\cos \phi \sin \psi \frac{\partial \psi}{\partial t} - \sin \phi \cos \psi \frac{\partial \phi}{\partial t} \right] + \cos \phi \cos \psi \frac{\partial \epsilon}{\partial t} \quad (5.42a)$$

$$\frac{\partial V_{y'}}{\partial s} = (1 + \epsilon) \left[-\sin \phi \sin \psi \frac{\partial \psi}{\partial t} + \cos \phi \cos \psi \frac{\partial \phi}{\partial t} \right] + \sin \phi \cos \psi \frac{\partial \epsilon}{\partial t} \quad (5.42b)$$

$$\frac{\partial V_{z'}}{\partial s} = (1 + \epsilon) \cos \psi \frac{\partial \psi}{\partial t} + \sin \psi \frac{\partial \epsilon}{\partial t} \quad (5.42c)$$

By expressing the global velocities in terms of the local velocities, and simplifying gives,

$$\frac{\partial V_{x'}}{\partial s} - \frac{\partial \epsilon}{\partial t} - V_{z'} \frac{\partial \psi}{\partial s} - V_{y'} \cos \psi \frac{\partial \phi}{\partial s} = 0 \quad (5.43a)$$

$$\frac{\partial V_{y'}}{\partial s} - (1 + \epsilon) \frac{\partial \psi}{\partial t} + V_{x'} \frac{\partial \psi}{\partial s} + V_{y'} \sin \psi \frac{\partial \phi}{\partial s} = 0 \quad (5.43b)$$

$$\frac{\partial V_{z'}}{\partial s} - (1 + \epsilon) \cos \psi \frac{\partial \phi}{\partial t} + V_{x'} \cos \psi \frac{\partial \phi}{\partial s} - V_{z'} \sin \psi \frac{\partial \phi}{\partial s} = 0 \quad (5.43c)$$

In addition to the above equations, the relationship between the tension and the strain in the cable is defined as,

$$\frac{\partial T}{\partial t} = \frac{\partial T}{\partial \epsilon} \frac{\partial \epsilon}{\partial t} \quad (5.44)$$

Assuming a linear variation of tension, equation (5.44) simplifies to,

$$T = \frac{\partial T}{\partial \epsilon} \cdot \epsilon \quad (5.45)$$

Now using equation (5.45) in equations (5.41) and (5.43), the following set of equations describing the motion of the cable in the directions tangential and normal to the cable (*i.e.* local coordinates) is obtained.

$$\frac{\partial \bar{U}}{\partial t} + \underline{\underline{Au}} \frac{\partial \bar{U}}{\partial s} + \underline{\underline{Bu}} = 0 \quad (5.46)$$

where

\bar{U} : vector consisting of $[V_{x'}, V_{y'}, V_{z'}, \epsilon, \phi, \psi]^T$

$$\underline{\underline{Au}} = \begin{bmatrix} 0 & -\frac{V_{y'}}{1+\epsilon} & -\frac{V_{z'}}{1+\epsilon} & -\frac{1}{\mu_c} \frac{\partial T}{\partial \epsilon} & Au_1 & -\frac{V_{z'} V_{x'}}{1+\epsilon} \\ 0 & \frac{V_{x'} - V_{z'} \tan \psi}{1+\epsilon} & 0 & 0 & Au_2 & \\ 0 & \frac{V_{y'} \tan \psi}{1+\epsilon} & \frac{V_{x'}}{1+\epsilon} & 0 & Au_3 & \left[\frac{V_{x'}^2}{1+\epsilon} - \frac{T}{\mu_c} \right] \\ -1 & 0 & 0 & 0 & \frac{V_{y'} \cos \psi}{V_{z'}} & \\ 0 & -\frac{1}{(1+\epsilon) \cos \psi} & 0 & 0 & -\frac{(V_{x'} - V_{z'} \tan \psi)}{1+\epsilon} & 0 \\ 0 & 0 & -\frac{1}{1+\epsilon} & 0 & -\frac{V_{y'} \sin \psi}{1+\epsilon} & -\frac{V_{x'}}{1+\epsilon} \end{bmatrix}$$

$$\underline{\underline{Bu}} = \frac{1}{\mu_c} [-F_{ox'}, -F_{oy'}, -F_{oz'}, 0 \ 0 \ 0]^T$$

and where

$$Au_1 = \frac{-V_{z'} V_{y'} \sin \psi - V_{y'} \cos \psi (V_{x'} - V_{z'} \tan \psi)}{1+\epsilon}$$

$$Au_2 = -\frac{T \cos \psi}{\mu_c} + \frac{\cos \psi (V_{x'} - V_{z'} \tan \psi)^2}{1+\epsilon}$$

$$Au_3 = \frac{V_{x'} V_{y'} \sin \psi + V_{y'} \cos \psi (V_{x'} - V_{z'} \tan \psi)}{1+\epsilon}$$

5.2.2 Wave Speeds

Let us now look at the solution of the continuous cable model developed in the previous sub-section. For the six equations given in matrix form in equation (5.46), the determinant is written as,

$$\left| \underline{\underline{Au}} - \lambda_w \underline{\underline{I}} \right| = 0 \quad (5.47)$$

where $\underline{\underline{I}}$ is an unity matrix and λ_w represents the eigenvalues of the system.

The six characteristics of the equations can be derived using classical eigenvalue theory, (Patton (1972)), as,

$$\lambda_{w1,2} = \pm \sqrt{\frac{1}{\mu_c} \cdot \frac{dT}{d\varepsilon}} \quad (5.48a)$$

$$\lambda_{w3,4} = \pm \sqrt{\frac{1}{\mu_c} \cdot \frac{\varepsilon}{(1+\varepsilon)} \cdot \frac{dT}{d\varepsilon}} \quad (5.48b)$$

$$\lambda_{w5,6} = \pm \sqrt{\frac{1}{\mu_c} \cdot \frac{\varepsilon}{(1+\varepsilon)} \cdot \frac{dT}{d\varepsilon}} \quad (5.48c)$$

Since two of the roots are repeated, the equations are a mixed hyperbolic-parabolic system of partial differential equations. The characteristic values obtained in (5.48a) represent the speeds at which the *tensile disturbance* (tensile stress wave) travels along the line, with the positive travelling down the line and the negative up the line. The characteristic values obtained in (5.48b) and (5.48c) represent the speeds at which the *transverse disturbance* (transverse flexural wave) travels along the line, again with the positive travelling down the line and the negative up the line. Although the two speeds in equations (5.48b) and (5.48c) are equal in value, the first is in the X'-Y' plane while the second is in the X'-Z' plane.

5.2.3 Relationship between Continuous and Discrete Systems

Now let us look at the relationship between the equations for the continuous system and those developed for the discrete system, (*i.e.* the lumped mass model). The latter system was developed in Chapter 3, and the relevant equations will be referred to in this sub-section.

The equations describing the motion of the nodes in a discrete system are those derived in equations (3.14) in Chapter 3. For simplicity, the added mass terms will be neglected, thus these equations reduce to:

$$m_i \cdot \ddot{x}_i = F_{ix} \quad (5.49a)$$

$$m_i \cdot \ddot{y}_i = F_{iy} \quad (5.49b)$$

$$m_i \cdot \ddot{z}_i = F_{iz} \quad (5.49c)$$

since $m_{i11} = m_{i22} = m_{i33} = m_i$.

Now using equations (3.27), the external forces can be expanded to include the tension terms as,

$$m_i \cdot \ddot{x}_i = T_i \cos \phi_i \cos \psi_i - T_{i-1} \cos \phi_{i-1} \cos \psi_{i-1} + F_{iox} \quad (5.50a)$$

$$m_i \cdot \ddot{y}_i = T_i \sin \phi_i \cos \psi_i - T_{i-1} \sin \phi_{i-1} \cos \psi_{i-1} + F_{ioy} \quad (5.50b)$$

$$m_i \cdot \ddot{z}_i = T_i \sin \psi_i - T_{i-1} \sin \psi_{i-1} + F_{ioz} \quad (5.50c)$$

Considering Figure 3.1, for segment “i” it is noted that,

$$\cos \phi_i \cos \psi_i = \frac{x_{i+1} - x_i}{l_i (1 + \epsilon_i)} \quad (5.51a)$$

$$\sin \phi_i \cos \psi_i = \frac{y_{i+1} - y_i}{l_i (1 + \epsilon_i)} \quad (5.51b)$$

$$\sin \psi_i = \frac{z_{i+1} - z_i}{l_i (1 + \epsilon_i)} \quad (5.51c)$$

where l_i is the unstretched length and ϵ_i is the strain of segment “i”. A similar set can be written to describe the angles of segment “i-1”. Thus, equations (5.50) can be written as,

$$m_i \cdot \ddot{x}_i = T_i \frac{x_{i+1} - x_i}{l_i(1 + \epsilon_i)} - T_{i-1} \frac{x_i - x_{i-1}}{l_{i-1}(1 + \epsilon_{i-1})} + F_{iox} \quad (5.52a)$$

$$m_i \cdot \ddot{y}_i = T_i \frac{y_{i+1} - y_i}{l_i(1 + \epsilon_i)} - T_{i-1} \frac{y_i - y_{i-1}}{l_{i-1}(1 + \epsilon_{i-1})} + F_{ioy} \quad (5.52b)$$

$$m_i \cdot \ddot{z}_i = T_i \frac{z_{i+1} - z_i}{l_i(1 + \epsilon_i)} - T_{i-1} \frac{z_i - z_{i-1}}{l_{i-1}(1 + \epsilon_{i-1})} + F_{ioz} \quad (5.52c)$$

From here on for simplicity, we will only consider the equations in the X-direction. Now using a Taylor expansion for the coordinates in the X-direction, coordinates x_{i+1} and x_i are expanded about $x_{i+1/2}$ (*i.e.* the mean between the two coordinates) as,

$$\begin{aligned} x_{i+1} = x_{i+1/2} &+ \frac{(x_{i+1} - x_{i+1/2})}{1} \frac{\partial x}{\partial s} \Big|_{i+1/2} + \frac{(x_{i+1} - x_{i+1/2})^2}{2!} \frac{\partial^2 x}{\partial s^2} \Big|_{i+1/2} + \\ &\frac{(x_{i+1} - x_{i+1/2})^3}{3!} \frac{\partial^3 x}{\partial s^3} \Big|_{i+1/2} + \frac{(x_{i+1} - x_{i+1/2})^4}{4!} \frac{\partial^4 x}{\partial s^4} \Big|_{i+1/2} + \frac{(x_{i+1} - x_{i+1/2})^5}{5!} \frac{\partial^5 x}{\partial s^5} \Big|_{i+1/2} + \dots \end{aligned} \quad (5.53)$$

$$\begin{aligned} x_i = x_{i+1/2} &+ \frac{(x_i - x_{i+1/2})}{1} \frac{\partial x}{\partial s} \Big|_{i+1/2} + \frac{(x_i - x_{i+1/2})^2}{2!} \frac{\partial^2 x}{\partial s^2} \Big|_{i+1/2} + \\ &\frac{(x_i - x_{i+1/2})^3}{3!} \frac{\partial^3 x}{\partial s^3} \Big|_{i+1/2} + \frac{(x_i - x_{i+1/2})^4}{4!} \frac{\partial^4 x}{\partial s^4} \Big|_{i+1/2} + \frac{(x_i - x_{i+1/2})^5}{5!} \frac{\partial^5 x}{\partial s^5} \Big|_{i+1/2} + \dots \end{aligned} \quad (5.54)$$

where “s” define the spatial coordinates.

Now consider a lumped mass system where all segments are similar, thus having the same length, *i.e.* $l_i = l_{i-1} = 1$. Then by substituting $x_{i+1} - x_{i+1/2} = 1/2$ and $x_i - x_{i+1/2} = -1/2$ in equations (5.53) and (5.54), and subtracting one from the other we have,

$$x_{i+1} - x_i = l \frac{\partial x}{\partial s} \Big|_{i+1/2} + \frac{l^3}{3!2^2} \frac{\partial^3 x}{\partial s^3} \Big|_{i+1/2} + \frac{l^5}{5!2^4} \frac{\partial^5 x}{\partial s^5} \Big|_{i+1/2} + O(l^7) \quad (5.55)$$

where $O(l^7)$ is the asymptotic notation of the terms having an order of 7. Following a similar procedure for coordinates x_i and x_{i-1} about $x_{i-1/2}$ we have,

$$x_i - x_{i-1} = l \left. \frac{\partial x}{\partial s} \right|_{i-1/2} + \frac{l^3}{3!2^2} \left. \frac{\partial^3 x}{\partial s^3} \right|_{i-1/2} + \frac{l^5}{5!2^4} \left. \frac{\partial^5 x}{\partial s^5} \right|_{i-1/2} + O(l^7) \quad (5.56)$$

(Note: a similar set of equations can be written for the coordinates in the Y and Z directions).

Employing equations (5.55) and (5.56) in equation (5.52a), (*i.e.* the equation along the X-direction), and dividing by “1” we have,

$$\begin{aligned} \frac{m_i \ddot{x}_i}{1} = & \frac{T_i}{1(1 + \epsilon_i)} \left[\left. \frac{\partial x}{\partial s} \right|_{i+1/2} + \frac{l^2}{3!2^2} \left. \frac{\partial^3 x}{\partial s^3} \right|_{i+1/2} + \frac{l^4}{5!2^4} \left. \frac{\partial^5 x}{\partial s^5} \right|_{i+1/2} + O(l^7) \right] - \\ & \frac{T_{i-1}}{1(1 + \epsilon_{i-1})} \left[\left. \frac{\partial x}{\partial s} \right|_{i-1/2} + \frac{l^2}{3!2^2} \left. \frac{\partial^3 x}{\partial s^3} \right|_{i-1/2} + \frac{l^4}{5!2^4} \left. \frac{\partial^5 x}{\partial s^5} \right|_{i-1/2} + O(l^7) \right] + \frac{F_{iox}}{1} \end{aligned} \quad (5.57)$$

Separating into terms of a similar order in “1” gives,

$$\begin{aligned} \frac{m_i \ddot{x}_i}{1} = & \frac{1}{1} \left[\frac{T_i}{(1 + \epsilon_i)} \left. \frac{\partial x}{\partial s} \right|_{i+1/2} - \frac{T_{i-1}}{(1 + \epsilon_{i-1})} \left. \frac{\partial x}{\partial s} \right|_{i-1/2} \right] + \\ & \frac{1}{24} \left[\frac{T_i}{(1 + \epsilon_i)} \left. \frac{\partial^3 x}{\partial s^3} \right|_{i+1/2} - \frac{T_{i-1}}{(1 + \epsilon_{i-1})} \left. \frac{\partial^3 x}{\partial s^3} \right|_{i-1/2} \right] + \\ & \frac{l^3}{1920} \left[\frac{T_i}{(1 + \epsilon_i)} \left. \frac{\partial^5 x}{\partial s^5} \right|_{i+1/2} - \frac{T_{i-1}}{(1 + \epsilon_{i-1})} \left. \frac{\partial^5 x}{\partial s^5} \right|_{i-1/2} \right] + O(l^7) + \frac{F_{iox}}{1} \end{aligned} \quad (5.58)$$

For any variable (say R) of the cable segment, R_i represents its value at node “i”, while $R_{i-1/2}$ and $R_{i+1/2}$ represent its values along the cable segments just prior to and after node “i” respectively. Now using a Taylor expansion for $R_{i+1/2}$ and $R_{i-1/2}$ about R_i , and subtracting one from the other gives,

$$R_{i+1/2} - R_{i-1/2} = l \left. \frac{\partial R}{\partial s} \right|_i + \frac{l^3}{3!2^2} \left. \frac{\partial^3 R}{\partial s^3} \right|_i + \frac{l^5}{5!2^4} \left. \frac{\partial^5 R}{\partial s^5} \right|_i + O(l^7) \quad (5.59)$$

From the numbering system used for the lumped mass model (Figure 3.4), it is seen that coordinate $x_{i+1/2}$ lies in segment i and coordinate $x_{i-1/2}$ lies in element i-1. Thus, using equation (5.59) in equation (5.58) we have,

$$\begin{aligned}
\frac{m_1 \cdot \ddot{x}_1}{1} = & \frac{\partial}{\partial s} \left[\frac{T}{(1+\epsilon)} \frac{\partial x}{\partial s} \right] + \frac{l^2}{24} \frac{\partial^3}{\partial s^3} \left[\frac{T}{(1+\epsilon)} \frac{\partial x}{\partial s} \right] + \frac{l^4}{1920} \frac{\partial^5}{\partial s^5} \left[\frac{T}{(1+\epsilon)} \frac{\partial x}{\partial s} \right] + \dots + \\
& \frac{l^2}{24} \left\{ \frac{\partial}{\partial s} \left[\frac{T}{(1+\epsilon)} \frac{\partial^3 x}{\partial s^3} \right] + \frac{l^2}{24} \frac{\partial^3}{\partial s^3} \left[\frac{T}{(1+\epsilon)} \frac{\partial^3 x}{\partial s^3} \right] + \frac{l^4}{1920} \frac{\partial^5}{\partial s^5} \left[\frac{T}{(1+\epsilon)} \frac{\partial^3 x}{\partial s^3} \right] + \dots + \right\} + \\
& \frac{l^4}{1920} \left\{ \frac{\partial}{\partial s} \left[\frac{T}{(1+\epsilon)} \frac{\partial^5 x}{\partial s^5} \right] + \frac{l^2}{24} \frac{\partial^3}{\partial s^3} \left[\frac{T}{(1+\epsilon)} \frac{\partial^5 x}{\partial s^5} \right] + \frac{l^4}{1920} \frac{\partial^5}{\partial s^5} \left[\frac{T}{(1+\epsilon)} \frac{\partial^5 x}{\partial s^5} \right] + \dots + \right\} \\
& + \dots + \frac{F_{iox}}{1}
\end{aligned} \tag{5.60}$$

Taking limits as $l \rightarrow 0$ gives,

$$\frac{m}{1} \cdot \frac{\partial^2 x}{\partial t^2} = \frac{\partial}{\partial s} \left(\frac{T}{1+\epsilon} \cdot \frac{\partial x}{\partial s} \right) + \frac{F_{iox}}{1} \tag{5.61}$$

where $m_1 = m_{1-1} = m$, since all segments are similar. Now since,

$$\ddot{x} = \frac{\partial^2 x}{\partial t^2} = \text{acceleration in the X-direction}$$

$$\mu_c = \frac{m}{1} = \text{the unit mass per unstretched length of the cable}$$

$$F_{ox} = \frac{F_{iox}}{1} = \text{the external forces, except the tension forces per unstretched length of the cable}$$

equation (5.61) reduces to,

$$\mu_c \cdot \frac{\partial^2 x}{\partial t^2} = \frac{\partial}{\partial s} \left(\frac{T}{1+\epsilon} \cdot \frac{\partial x}{\partial s} \right) + F_{ox} \tag{5.62a}$$

$$\mu_c \cdot \frac{\partial^2 y}{\partial t^2} = \frac{\partial}{\partial s} \left(\frac{T}{1+\epsilon} \cdot \frac{\partial y}{\partial s} \right) + F_{oy} \tag{5.62b}$$

$$\mu_c \cdot \frac{\partial^2 z}{\partial t^2} = \frac{\partial}{\partial s} \left(\frac{T}{1+\epsilon} \cdot \frac{\partial z}{\partial s} \right) + F_{oz} \tag{5.62c}$$

where equations (5.62b) and (5.62c) are the component equations in the Y and Z directions, which are obtained from equations in (5.52b) and (5.52c) respectively.

Equations (5.62) are identical to those given by equations (5.34), *i.e.* the wave equations describing the motion of the continuous cable system. Therefore, we can conclude that the lumped mass system developed in Chapter 3 is a true representation of the continuous cable system.

5.2.4 Effects due to Discretisation

Now let us look at the effect on the continuous system as it passes over into the ordinary differential equations describing the lumped mass model. Again for simplicity only the equations in the X-direction are considered.

Referring back to sub-section 5.2.3, substituting equations (5.55) and (5.56) in equation (5.52a) gave equation (5.60). Neglecting terms of order greater than l^2 , reduces equation (5.60) to,

$$\frac{m_i \ddot{x}_i}{1} = \frac{\partial}{\partial s} \left[\frac{T}{(1 + \epsilon)} \frac{\partial x}{\partial s} \right] + \frac{l^2}{24} \frac{\partial^3}{\partial s^3} \left[\frac{T}{(1 + \epsilon)} \frac{\partial x}{\partial s} \right] + \frac{l^2}{24} \frac{\partial}{\partial s} \left[\frac{T}{(1 + \epsilon)} \frac{\partial^3 x}{\partial s^3} \right] + \frac{F_{iox}}{1} \quad (5.63)$$

In order to simplify the investigation, assume that the cable is “stiff” and the tension is constant, *i.e.*,

$$\epsilon \ll 1 \quad (5.64)$$

$$\frac{\partial T}{\partial s} \approx 0 \quad (5.65)$$

Using the above conditions in equation (5.63) gives,

$$\frac{m}{1} \frac{\partial^2 x}{\partial t^2} = T \frac{\partial^2 x}{\partial s^2} + \frac{T l^2}{12} \frac{\partial^4 x}{\partial s^4} + \frac{F_{iox}}{1} \quad (5.66)$$

where $m_i = m_{i-1} = m$, since all segments are similar and $\ddot{x} = \frac{\partial^2 x}{\partial t^2}$.

Neglecting the external force F_{ox} , (again for simplicity), gives,

$$\frac{m}{T l} \frac{\partial^2 x}{\partial t^2} = \frac{\partial^2 x}{\partial s^2} + \frac{l^2}{12} \frac{\partial^4 x}{\partial s^4} \quad (5.67)$$

Similar equations can be developed for the Y and Z directions by using equations (5.52b) and (5.52c) respectively.

Inspection of equation (5.67) shows that it is not an ideal wave equation, however it can still transmit waves along the cable. The solution to this equation is given in Huang (1992), and is of the following form,

$$x = x_0 e^{(\sqrt{-1} (\omega t - k_w s))} \quad (5.68)$$

given that,

$$\omega_w = k_w \sqrt{\frac{TI}{m}} \sqrt{1 - \frac{l^2}{12} k_w^2} \quad (5.69)$$

where

ω_w : wave frequency

k_w : wave number

Further, the wave speed (C_w) is defined as,

$$C_w = \frac{\omega_w}{k_w} = \sqrt{\frac{TI}{m}} \sqrt{1 - \frac{l^2}{12} k_w^2} \quad (5.70)$$

The dependence of the wave speed on the wave number results in the wave no longer being non-dispersive, as is the case with a continuous cable. Therefore, the effect of the wavelength has to be considered during the analysis. Note: the wavelength (l_w) is give by,

$$l_w = \frac{2\pi}{k_w} \quad (5.71)$$

For example, consider the case where $k_w \ll 1$. Then from equation (5.69), the wave frequency becomes,

$$\omega_w = k_w \sqrt{\frac{TI}{m}} \quad (5.72)$$

which gives the wave speed from equation (5.70) as,

$$C_w = \sqrt{\frac{TI}{m}} \quad (5.73)$$

Thus, the wave speed for this condition is independent of the wave number. Therefore, if the segment length is small or the wavelength is relatively large, then the discretisation has little effect.

Now consider the wave equation given by (5.70). The maximum frequency occurs when the wave number reaches,

$$k_w = \sqrt{\frac{3T}{ml}} \quad (5.74)$$

If excitation frequencies above this frequency are encountered, these wave fronts will be cut-off, (Huang (1992)). Thus, responses above this frequency will disperse as they travel along the cable model, *i.e.* the lumped mass models truncate the high frequency responses of the system. However, for most engineering applications this is acceptable, as the high frequency, low amplitude responses are of little interest.

The geometric discretisation can also result in parasitical motion of the lumped masses. The tangential stiffness (k_t) of a single lumped mass is linearly dependent on the relative tangential displacement, and is given by,

$$k_t = 2 E A_i l_i \quad (5.75)$$

where

- E : modulus of elasticity
- A_i : cross sectional area of the cable segment
- l_i : length of the cable segment

The normal stiffness (k_n) is non-linearly dependent on the normal displacement (δ_n) as,

$$k_n = \frac{E A_i \delta_n}{l_i^2} \quad (5.76)$$

If the damping is neglected, then the resonant frequencies of the parasitical motions are given by,

$$\omega = \sqrt{\frac{k}{M_{\text{total}}}} \quad (5.77)$$

where

ω : resonant frequencies

k : either k_t or k_n , depending on the resonant frequency

M_{total} : total mass of the lumped mass, *i.e.* its mass plus the added mass.

5.3 Stability and Accuracy

Given the long simulation time required for the solution of dynamic time domain cable system models, the mathematical representation and the solution technique must be sufficiently accurate and stable. The errors that can enter during the integration process are divided into two categories:

- truncation error – the difference between the exact solution of the partial differential equation and the exact solution of the difference equation; and
- numerical (round off) error - the difference between the exact solution of the difference equation and the numerical solution of the difference equation.

Generally the former is much larger than the latter. Investigations by O'Brian *et al.* (1950-51) show that the stability issues encountered in numerical schemes are due to truncation errors rather than due to numerical errors in the scheme.

Usually all implicit time integration schemes are unconditionally stable, while explicit schemes are only conditionally stable. Therefore, explicit schemes require a time step that is *less* than a defined critical value, while the implicit schemes have no limiting time step. However, when using implicit schemes for non-linear systems, large time steps will cause the numerical integration scheme to “blow out”, *i.e.* become unstable.

The reason for this is the truncation error introduced by the required iteration scheme, (*i.e.* the Newton-Raphson scheme in the case of the towed system model of this project).

Thus, the selection of the time step is dependent on the accuracy and stability of the numerical scheme. Therefore, the time step should be sufficiently small to ensure accuracy and stability are met, but large enough to prevent long simulation times.

Numerical stability depends not on the original set of equations, but on the numerical scheme used. Stability requires that the amplification of any errors entering the solution process should be limited. There are a number of methods for assessing the stability of a numerical scheme. These methods, which are discussed in the following sub-sections, include:

- von Neumann method;
- Routh-Hurwitz method; and
- matrix stability method.

During the analysis, four popular numerical integration schemes used in engineering will be discussed. This includes the Houbolt integration scheme used in this work. The four methods discussed are given below:

Central Difference Scheme

$$\dot{\bar{R}}^{t+1} = \frac{\bar{R}^{t+2} - \bar{R}^t}{2\Delta t} \quad (5.78a)$$

$$\ddot{\bar{R}}^{t+1} = \frac{\bar{R}^t - 2\bar{R}^{t+1} + \bar{R}^{t+2}}{\Delta t^2} \quad (5.78b)$$

Houbolt Scheme

$$\dot{\bar{R}}^{t+1} = \frac{11\bar{R}^{t+1} - 18\bar{R}^t + 9\bar{R}^{t-1} - 2\bar{R}^{t-2}}{6\Delta t} \quad (5.79a)$$

$$\ddot{\bar{R}}^{t+1} = \frac{2\bar{R}^{t+1} - 5\bar{R}^t + 4\bar{R}^{t-1} - \bar{R}^{t-2}}{\Delta t^2} \quad (5.79b)$$

Newmark- β Scheme

$$\dot{\bar{\mathbf{R}}}^{t+1} = \dot{\bar{\mathbf{R}}}^t - (1-\gamma)\ddot{\bar{\mathbf{R}}}^t \Delta t + \gamma\ddot{\bar{\mathbf{R}}}^{t+1} \Delta t \quad (5.80a)$$

$$\bar{\mathbf{R}}^{t+1} = \bar{\mathbf{R}}^t + \dot{\bar{\mathbf{R}}}^t \Delta t + (1-2\beta)\ddot{\bar{\mathbf{R}}}^t \frac{\Delta t^2}{2} + 2\beta\ddot{\bar{\mathbf{R}}}^{t+1} \frac{\Delta t^2}{2} \quad (5.80b)$$

Wilson- θ Scheme

$$\dot{\bar{\mathbf{R}}}^{t+\theta\Delta t} = \frac{3.(\bar{\mathbf{R}}^{t+\theta\Delta t} - \bar{\mathbf{R}}^t)}{\theta.\Delta t} - 2.\dot{\bar{\mathbf{R}}}^t - \frac{\theta.\Delta t}{2}.\ddot{\bar{\mathbf{R}}}^t \quad (5.81a)$$

$$\ddot{\bar{\mathbf{R}}}^{t+\theta\Delta t} = \frac{6.(\bar{\mathbf{R}}^{t+\theta\Delta t} - \bar{\mathbf{R}}^t)}{\theta^2.\Delta t^2} - 2.\ddot{\bar{\mathbf{R}}}^t - \frac{6}{\theta.\Delta t}.\dot{\bar{\mathbf{R}}}^t \quad (5.81b)$$

On inspecting the schemes, it is seen that the first is an explicit scheme, while the others are implicit schemes. Further, the implicit schemes are multi-step algorithms. It is also seen that the Central Difference and Houbolt schemes require special starting procedures, since information from the previous time steps to the simulation start time are required. The Newmark- β and Wilson- θ schemes, however, do not require such starting procedures.

Bathe (1982) states that the starting procedure used in the Houbolt scheme for linear systems influences the results. However Thomas (1993), by studying the results of the same simulation using a number of starting procedures, shows that the results for non-linear cable systems using the Houbolt scheme are independent of the starting procedure employed. The conclusion drawn is that the iterative process utilised in non-linear systems “removes” the sensitivity of the scheme to the starting procedure. This was demonstrated in sub-section 4.5 of Chapter 4, where the use of two different time steps yielded the same results for a series multi-tow system.

5.4 von Neumann (Fourier) and Routh-Hurwitz Methods

In this investigation the stability characteristics of the approximate integration scheme are investigated using the versatile matrix stability method. This is carried out in sub-section 5.5. However, a brief introduction to the other two methods are presented in this sub-section.

5.4.1 von Neumann (Fourier) Method

Von Neumann's (also known as the Fourier) stability method is the more traditional method of investigating the stability of numerical methods. Although it has limitations, it is successfully used to investigate many (especially explicit) numerical schemes. Examples of such investigations on underwater cable systems are given in Walton and Polachek (1959) and Huang (1994).

The method was developed by Professor J von Neumann, and consists of introducing a line of errors represented by a Fourier series at the mesh points of the computational network at $t = 0$. Then the propagation of the line of errors through the integration scheme is investigated. For the scheme to be stable, the error should **not** grow during the integration.

Although the method assumes linear systems, it is possible to investigate non-linear systems by applying the method successively to a sequence of overlapping small time regions.

Von Neumann's stability method is briefly described below, however for a more detailed study the reader is directed to O'Brien *et al.* (1950-51) and Ames (1969).

The Fourier series representation of the line of errors is introduced at $t = 0$ as,

$$\text{Error} = \sum_i A_i e^{i\beta_i R} \quad (5.82)$$

where

R : variable, *e.g.* displacement

β_i : real positive number

For stability, the sum of the above errors must reduce to the correct error value at each mesh point of the line.

Due to the system being linear, it is possible to use linear superposition to obtain the complete effect. Thus, it is only required to consider a single error term, *i.e.*,

$$e^{i\beta R} \quad (5.83)$$

Now one must seek a solution for the partial differential equation that reduces to equation (5.83) at $t = 0$. The solution will be of the form,

$$e^{\alpha R} e^{i\beta R} \quad (5.84)$$

The above is then substituted into the difference equation, and the condition for the error **not** to grow is ascertained. For this condition to be satisfied,

$$e^{\alpha R} \leq 1 \quad (5.85)$$

Therefore, the difference equation with the substituted error term is rearranged to give an expression for $e^{\alpha R}$. Then it is possible to find the conditions for the expression to be equal to or less than 1.

Shortcomings in this method are its inability to include boundary conditions and the requirement to linearise the equations prior to the investigation. However, as stated at the beginning of this sub-section, it has been used by a number of researchers to investigate algorithms employed in the solution of underwater cable systems.

5.4.2 Routh-Hurwitz Method

The Routh-Hurwitz method is a technique of identifying the stability region by applying the z transformation,

$$\lambda = \frac{(1 + z)}{(1 - z)} \quad (5.86)$$

which maps the circle $|\lambda| = 1$ into the imaginary axis $\text{Re } z = 0$ and the interior of the circle into the half plane $\text{Re } z < 0$. Then the Routh-Hurwitz condition states that the necessary and sufficient condition for stability is that the roots of the characteristic polynomial must have negative real parts. This method is explained in Hilber (1976) and Wood (1990), with the latter using it to determine the stability requirements of a number of numerical integration schemes.

5.5 Matrix Stability Method

This is an extremely versatile approach to analyse the stability of numerical schemes. It is derived by using the two basic approaches utilised in the investigation of the dynamics of structures:

- the direct integration of the equations of motion; and
- the modal analysis.

In the former, the equations are integrated using a numerical step-by-step procedure, the term *direct* implying that prior to this procedure the equations are not transformed in any manner. The solution procedure utilised in Chapter 4 is of this type.

The latter approach consists of changing the basis from the element coordinate basis to an eigenvector basis, associated with the natural frequencies (or eigenvalues) of the undamped problem. Thus, it generates an alternate set of equations that can be integrated more efficiently by a direct integration scheme than the unmodified equations of motion.

It reasons that if the modal form and the unmodified equations are integrated using the same scheme, the results should be the same. Therefore, it is possible to analyse the modal form of equations, to determine the accuracy and stability of the direct integration scheme.

5.5.1 Modal Superposition

Consider the general representation of the equations of motion of the cable,

$$\underline{\underline{m}}\ddot{\underline{\underline{R}}} + \underline{\underline{c}}\dot{\underline{\underline{R}}} + \underline{\underline{k}}\underline{\underline{R}} = \underline{\underline{F}} \quad (5.87)$$

where

- $\underline{\underline{m}}$: cable mass matrix
- $\underline{\underline{c}}$: cable damping matrix
- $\underline{\underline{k}}$: cable stiffness matrix
- $\underline{\underline{R}}$: time dependent displacement vector
- $\underline{\underline{F}}$: time dependent external load vector

The set of equations represented by equation (5.87) is assembled for a discrete system by superposition of the equations representing each individual node. If the number of nodes in the system is “n”, then the matrices in equation (5.87) will be square matrices of nth order, while the vectors will be column matrices of a similar order.

Now to convert equation (5.87) to the eigenvector basis. The transformation of the displacement from the element coordinate basis to the eigenvector basis is given by,

$$\bar{\underline{\underline{R}}} = \underline{\underline{\Lambda}}_m \bar{\underline{\underline{R}}}_m \quad (5.88)$$

where

$\bar{\underline{\underline{R}}}_m$: time dependent modal displacement vector

$\underline{\underline{\Lambda}}_m$: modal transformation matrix

The modal transformation matrix is obtained as follows. Since the eigenvalues are not affected by the damping in the system or the external forces, it is possible to neglect these terms in equation (5.87) during the conversion. Thus, equation (5.87) reduces to,

$$\underline{\underline{m}} \ddot{\underline{\underline{R}}} + \underline{\underline{k}} \underline{\underline{R}} = 0 \quad (5.89)$$

The solution for equation (5.89) will be of the form,

$$\bar{\underline{\underline{R}}} = \bar{\underline{\underline{\theta}}} \text{Sin } \omega_n (t - t_c) \quad (5.90)$$

where

$\bar{\underline{\underline{\theta}}}$: vector of the order n, (that will be shown later to be the eigenvectors), where
“n” is the number of nodes in the discrete system

t : time

t_c : time constant

ω_n : frequency of vibration, *i.e.* natural frequency of vector $\bar{\underline{\underline{\theta}}}$

Substituting equation (5.90) into equation (5.89) gives the generalised eigenproblem, which enables the calculation of $\bar{\underline{\underline{\theta}}}$ and ω_n. Thus,

$$\underline{\underline{k}} \bar{\theta} = \omega_n^2 \underline{\underline{m}} \bar{\theta} \quad (5.91)$$

Since the eigenvalue “ λ ” is defined as,

$$\lambda = \omega_n^2 \quad (5.92)$$

it is possible to write the above equation as,

$$\underline{\underline{k}} \bar{\theta} = \lambda \underline{\underline{m}} \bar{\theta} \quad (5.93)$$

The eigenproblem in equation (5.93) yields “ n ” eigensolutions,

$$(\lambda_1, \bar{\theta}_1), (\lambda_2, \bar{\theta}_2), (\lambda_3, \bar{\theta}_3), \dots, (\lambda_n, \bar{\theta}_n) \quad (5.94)$$

where the eigenvectors are $\underline{\underline{m}}$ -orthonormalised, *i.e.* must have the following relationship,

$$\bar{\theta}_i^T \underline{\underline{m}} \bar{\theta}_j = \delta_{ij} \quad \begin{cases} = 1; & i = j \\ = 0; & i \neq j \end{cases} \quad (5.95)$$

and where δ_{ij} is the Kronecker delta, (note: the above is equal to a unity matrix, $\underline{\underline{I}}$).

The vector $\bar{\theta}_i$ is called the i^{th} -mode shape vector and λ_i is the corresponding eigenvalue. Thus, equation (5.89) is satisfied by any of the “ n ” displacement solutions, *i.e.*,

$$\bar{R} = \bar{\theta}_i \sin \omega_m (t - t_c), \quad \text{where } i = 1, 2, 3, \dots, n \quad (5.96)$$

Now defining matrices $\underline{\underline{\Theta}}$ and $\underline{\underline{\lambda}}$ as,

$$\underline{\underline{\Theta}} = [\bar{\theta}_1 \quad \bar{\theta}_2 \quad \bar{\theta}_3 \quad \dots \quad \bar{\theta}_n] = \text{matrix that stores the eigenvectors along its columns}$$

$$\underline{\underline{\lambda}} = \begin{bmatrix} \lambda_1 & & & & \\ & \lambda_2 & & & \\ & & \lambda_3 & & \\ & & & \dots & \\ & & & & \lambda_n \end{bmatrix} = \text{matrix that stores the eigenvalues along its diagonal}$$

it is possible to write the “n” solutions to equation (5.93) as,

$$\underline{\underline{k}} \underline{\underline{\Theta}} = \underline{\underline{m}} \underline{\underline{\Theta}} \lambda \quad (5.97)$$

Since the eigenvectors are $\underline{\underline{m}}$ -orthonormal, we have,

$$\underline{\underline{\Theta}}^T \underline{\underline{m}} \underline{\underline{\Theta}} = \underline{\underline{I}} \quad (5.98a)$$

$$\underline{\underline{\Theta}}^T \underline{\underline{k}} \underline{\underline{\Theta}} = \underline{\underline{\lambda}} \quad (5.98b)$$

Thus, it is seen that $\underline{\underline{\Theta}}$ is suitable to be used as the modal transformation matrix $\underline{\underline{\Lambda}}_m$, so equation (5.88) becomes,

$$\underline{\underline{R}} = \underline{\underline{\Theta}} \underline{\underline{R}}_m \quad (5.99)$$

Therefore, the set of equations represented by equation (5.87) is transformed into the eigenvector basis as,

$$\ddot{\underline{\underline{R}}}_m + \underline{\underline{\Theta}}^T \underline{\underline{c}} \underline{\underline{\Theta}} \dot{\underline{\underline{R}}}_m + \underline{\underline{\lambda}} \underline{\underline{R}}_m = \underline{\underline{\Theta}}^T \underline{\underline{F}} \quad (5.100)$$

where the damping and external force terms have been included to complete the equation. From the above transformation, it is noted that the mass and stiffness matrices in equation (5.100) are decoupled. In order to easily analyse the equation, it would be advantageous to also have the damping matrix decoupled. In general, the damping matrix cannot be constructed in a similar manner to the mass and stiffness matrices. The approach is to approximate the overall energy dissipation during the system response.

The analysis is made easier if the damping is assumed to be proportionate, *i.e.*,

$$\theta_i^T \underline{\underline{c}} \theta_j = 2 \omega_m \zeta_i \delta_{ij} \quad (5.101)$$

where “ δ_{ij} ” is the Kronecker delta and “ ζ ” is the modal damping ratio. Therefore, it is assumed that the eigenvectors θ_i , (where $i = 1, 2, 3, \dots, n$), are also $\underline{\underline{c}}$ -orthonormal. Thus, the “n” constituent equations in equation (5.100) will be of the same form. The damping matrix is generally obtained using a linear combination of the mass and stiffness matrices. For example, Rayleigh damping can be assumed to be of the form,

$$\underline{\underline{c}} = \alpha \underline{\underline{m}} + \beta \underline{\underline{k}} \quad (5.102)$$

where α and β are constants determined from two given damping ratios corresponding to two unequal natural frequencies. When the system has more than two natural frequencies, then the two average damping ratio values are used in equation (5.102). A more advanced method of obtaining the damping matrix for systems with more than two natural frequencies, using Caughey series is described in Bathe (1982).

5.5.2 Stability Analysis

As stated previously, integration of the modal form and of the unmodified equations, using the same scheme should give the same result. Therefore, by analysing the modal form of the equations it is possible to determine the accuracy and stability of the direct integration scheme. This method requires only the variables Δt , ω_n , and ζ_i , (where $i = 1, 2, 3, \dots, n$), to be considered in the analysis, and not the complete stiffness and mass matrices. In addition, since all “n” equations in (5.100) are of a similar form, only one general expression needs to be studied. This is written as,

$$\ddot{\bar{\mathbf{R}}}_m + 2\zeta\omega_n\dot{\bar{\mathbf{R}}}_m + \omega_n^2\bar{\mathbf{R}}_m = \bar{\mathbf{f}} \quad (5.103)$$

where

$\bar{\mathbf{R}}_m$: time dependent modal displacement vector

$\bar{\mathbf{f}}$: external load vector

ζ : modal damping ratio

ω_n : natural frequency of the mode

In light of the solution characteristic of the direct integration method, it is required to estimate the integration error in the solution of equation (5.103) as a function of $\Delta t/t_{n,\min}$, ζ , and $\bar{\mathbf{f}}$, where $t_{n,\min}$ is the minimum natural period of the cable mesh.

Note: It is the time ratio $\Delta t/t_{n,\min}$, (*i.e.* the ratio of the time step to the minimum natural period of the cable mesh), and not the absolute time step that governs the criteria for stability and accuracy, (Hearn and Thomas (1991)). This can be explained by considering a fixed time step, Δt . An increase in the time ratio $\Delta t/t_{n,\min}$ means that natural period $t_{n,\min}$ is decreasing, *i.e.* the natural frequency is increasing. Thus,

the use of a larger time ratio results in the higher modes being inaccurately integrated. This concept will be discussed further after the conditions for stability and accuracy are obtained.

One method of estimating the integration error of the solution technique employed for equation (5.103) is the use of the amplification matrix (also referred to as the approximation operator) and load operator introduced in equation (5.5). These will depend on the integration scheme used in the solution, and give the relationship between the quantities at the required time step as a function of the quantities of the previous time steps and the external forces respectively. The relationship is generally defined as,

$$\hat{\mathbf{R}}^{t+1} = \underline{\underline{\mathbf{A}_p}} \hat{\mathbf{R}}^t + \underline{\underline{\mathbf{L}_p}} \bar{\mathbf{f}}^{t+1} \quad (5.104)$$

where

$\hat{\mathbf{R}}$: vector storing the solution quantities, (*e.g.* displacements, velocities, *etc.*)

$\underline{\underline{\mathbf{A}_p}}$: amplification matrix

$\underline{\underline{\mathbf{L}_p}}$: load operator

Since the load operator does not influence the numerical stability of the scheme, the analysis is carried out with no external load. Thus, equation (5.104) reduces to,

$$\hat{\mathbf{R}}^{t+1} = \underline{\underline{\mathbf{A}_p}} \hat{\mathbf{R}}^t \quad (5.105)$$

Inspection of equation (5.105) reveals that it is possible to recursively calculate the solution at any given time as,

$$\hat{\mathbf{R}}^{t+m} = \underline{\underline{\mathbf{A}_p}}^m \hat{\mathbf{R}}^t \quad (5.106)$$

where superscript “m” represents the number of time intervals, *i.e.*,

$$t^{t+m} = t^t + (m \cdot \Delta t) \quad (5.107)$$

For stability and accuracy, the amplification matrix in equation (5.106) must remain bounded. Therefore, in order to investigate the stability and accuracy of an integration method, it is required to derive the amplification matrix for that scheme.

The derivation of the amplification matrix for the Houbolt scheme is given later in this sub-section, while the derivations for the other three methods discussed in this sub-section are given in Bathe (1982).

Once the amplification matrix for the integration scheme is obtained, the spectral decomposition of the matrix is used to analyse the stability. Thus,

$$\underline{\underline{A}}_p = \underline{\underline{P}} \underline{\underline{J}} \underline{\underline{P}}^{-1} \quad (5.108)$$

where

$\underline{\underline{P}}$: matrix of eigenvectors of $\underline{\underline{A}}_p$

$\underline{\underline{J}}$: Jordan form of $\underline{\underline{A}}_p$, with eigenvalues (λ_{p_i}) of $\underline{\underline{A}}_p$ along its leading diagonal.

Now considering $\underline{\underline{A}}_p^2$, we obtain,

$$\underline{\underline{A}}_p^2 = \underline{\underline{P}} \underline{\underline{J}} \underline{\underline{P}}^{-1} \underline{\underline{P}} \underline{\underline{J}} \underline{\underline{P}}^{-1} \quad (5.109)$$

Since $\underline{\underline{P}}^{-1} \underline{\underline{P}} = \underline{\underline{I}}$, we get,

$$\underline{\underline{A}}_p^2 = \underline{\underline{P}} \underline{\underline{J}}^2 \underline{\underline{P}}^{-1} \quad (5.110)$$

Similarly, by continuing in this manner we obtain for “m” time steps,

$$\underline{\underline{A}}_p^m = \underline{\underline{P}} \underline{\underline{J}}^m \underline{\underline{P}}^{-1} \quad (5.111)$$

i.e. a recursive relationship is obtained for the amplification matrix. Expanding equation (5.111) we obtain,

$$\underline{\underline{A}}_p^m = \begin{bmatrix} p_{11} & p_{12} & \dots & p_{1n} \\ p_{21} & p_{22} & \dots & p_{2n} \\ \dots & \dots & \dots & \dots \\ p_{n1} & p_{n2} & \dots & p_{nn} \end{bmatrix} \begin{bmatrix} \lambda_{p1}^m & 0 & \dots & 0 \\ 0 & \lambda_{p2}^m & \dots & 0 \\ \dots & \dots & \dots & \dots \\ 0 & 0 & 0 & \lambda_{p3}^m \end{bmatrix} \begin{bmatrix} p_{11} & p_{12} & \dots & p_{1n} \\ p_{21} & p_{22} & \dots & p_{2n} \\ \dots & \dots & \dots & \dots \\ p_{n1} & p_{n2} & \dots & p_{nn} \end{bmatrix}^{-1} \quad (5.112)$$

where

p_{ab} : eigenvector terms of $\underline{\underline{Ap}}$
 λ_{pi} : where $i = 1, 2, 3, \dots, n$
 eigenvalues of $\underline{\underline{Ap}}$

On inspecting equation (5.112), it is possible to deduce the requirements for $\underline{\underline{Ap}}$ to remain bounded as “m” increases, *i.e.*,

requirement for $\underline{\underline{Ap}} \rightarrow 0$ as $m \rightarrow \infty$

This occurs if the *maximum absolute value of the eigenvalues* (λ_{pi}) is equal to or less than one. Thus,

$$\max |\lambda_{pi}| \leq 1, \quad \text{where } i = 1, 2, 3, \dots, n \quad (5.113)$$

The maximum absolute value of the eigenvalues is defined as the *spectral radius* $p(\underline{\underline{Ap}})$, *i.e.*,

$$p(\underline{\underline{Ap}}) = \max |\lambda_{pi}| \quad \text{where } i = 1, 2, 3, \dots, n \quad (5.114)$$

Thus,

$$p(\underline{\underline{Ap}}) \leq 1 \quad (5.115)$$

Therefore, the stability criterion for the integration method employed is:

The spectral radius of the amplification matrix should be equal to or less than one.

It should also be noted, that smaller the spectral radius, more rapid is the convergence of the integration scheme.

5.5.3 Stability of the Houbolt Integration Scheme

The preceding explanation addresses the general stability requirements for a numerical integration scheme. Now let us investigate the scheme used in this project, *i.e.* the Houbolt scheme given by equations (5.79) and reproduced below.

$$\dot{\bar{R}}^{t+1} = \frac{11\bar{R}^{t+1} - 18\bar{R}^t + 9\bar{R}^{t-1} - 2\bar{R}^{t-2}}{6\Delta t} \quad (5.79a)$$

$$\ddot{\bar{R}}^{t+1} = \frac{2\bar{R}^{t+1} - 5\bar{R}^t + 4\bar{R}^{t-1} - \bar{R}^{t-2}}{\Delta t^2} \quad (5.79b)$$

The equation of motion to be investigated was reduced to a modal form in equation (5.103), which is reproduced below with due regard to the time intervals, *i.e.* at time “ $t+1$ ”.

$$\ddot{\bar{R}}_m^{t+1} + 2\zeta\omega_n \dot{\bar{R}}_m^{t+1} + \omega_n^2 \bar{R}_m^{t+1} = \bar{f}^{t+1} \quad (5.116)$$

Substituting equations (5.79a) and (5.79b) into equation (5.116) gives the recursive relationship inclusive of the amplification matrix as,

$$\begin{bmatrix} \bar{R}_m^{t+1} \\ \dot{\bar{R}}_m^t \\ \ddot{\bar{R}}_m^{t-1} \end{bmatrix} = \underline{\underline{A_p}} \begin{bmatrix} \bar{R}_m^t \\ \dot{\bar{R}}_m^{t-1} \\ \ddot{\bar{R}}_m^{t-2} \end{bmatrix} + \underline{\underline{L_p}} \bar{f}^{t+1} \quad (5.117)$$

with

$$\underline{\underline{A_p}} = \begin{bmatrix} \frac{5\alpha_p}{\omega_n^2 \Delta t^2} + 6\beta_p & -\frac{4\alpha_p}{\omega_n^2 \Delta t^2} - 3\beta_p & \frac{\alpha_p}{\omega_n^2 \Delta t^2} + \frac{2\beta_p}{3} \\ 1 & 0 & 0 \\ 0 & 1 & 0 \end{bmatrix}$$

$$\underline{\underline{L_p}} = \begin{bmatrix} \alpha_p \\ \omega_n^2 \\ 0 \\ 0 \end{bmatrix}$$

and where

$$\alpha_p = \left(\frac{2}{\omega_n^2 \Delta t^2} + \frac{11\zeta}{3\omega_n \Delta t} + 1 \right)^{-1}$$

$$\beta_p = \frac{\zeta \alpha_p}{\omega_n \Delta t}$$

The stability condition for the Houbolt scheme is measured by obtaining the spectral radius of the amplification matrix $\underline{\underline{A_p}}$ obtained above. Thus, it is required to calculate the eigenvalues of $\underline{\underline{A_p}}$, which are obtained from,

$$\det(\underline{\underline{A_p}} - \lambda \underline{\underline{I}}) = \lambda^3 + 2A_1 \lambda^2 + A_2 \lambda + A_3 = 0 \quad (5.118)$$

where

A_1 : $\frac{1}{2}$ trace $\underline{\underline{A_p}}$

A_2 : sum of principle minors of $\underline{\underline{A_p}}$

A_3 : determinant of $\underline{\underline{A_p}}$

A plot of the spectral radius versus the time ratio $\Delta t/t_{n,mn}$ for the Houbolt scheme (assuming no damping) is given in Figure 5.1. It is seen from this figure that the spectral radius is less than “1” for all values of $\Delta t/t_{n,mn}$. Therefore, the Houbolt scheme is deduced to be unconditionally stable. Note: although the inclusion of damping will change the shape of the curve, it does not significantly change the stability characteristics at low damping ratios.

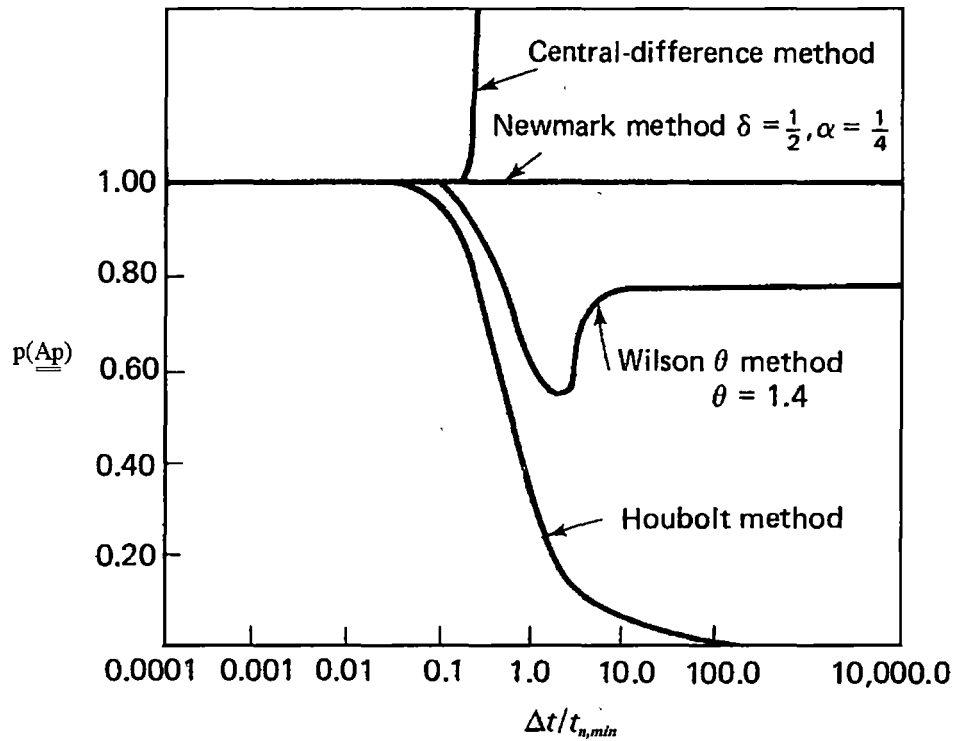
Similar curves are also produced in Figure 5.1 for the other three numerical integration schemes considered in this sub-section, *i.e.* the Central Differential, Wilson- θ , and Newmark- β schemes respectively. From these curves the conditions for stability for the respective schemes are obtainable. Details of the stability analysis of these methods are given in Bathe (1982) and Wood (1990).

Inspection of these curves shows that as $\Delta t/t_{n,mn}$ increases, the spectral radius of the Houbolt scheme is the smallest. Therefore, it has the fastest rate of convergence of the four schemes considered.

The explicit Central Difference scheme is conditionally stable, *i.e.* the time step has to be less than a critical value. It can be shown by following a similar procedure to that described for the Houbolt scheme in equations (5.117) and (5.118), that the condition for stability of the Central Difference scheme is,

$$\Delta t \leq \frac{t_{n,min}}{\pi} \quad (5.119)$$

For the Wilson- θ , and Newmark- β schemes, the stability is controlled by selecting appropriate values for the relevant parameters, (see equations (5.80) and (5.81)).



(Bathe (1982))

Spectral Radius of Numerical Integration Schemes with Zero Damping
Figure 5.1

5.5.4 Non-linear Systems

The forgoing stability analysis was based on the system being linear. However, from Chapters 3 and 4 we know that the mathematical model for the towed cable system is non-linear. This means that the coefficients of the equations of motion change with time.

Since the Houbolt scheme was shown in sub-section 5.5.3 to be unconditionally stable, it can be successfully used to solve the non-linear underwater tow model. As in linear systems, the Houbolt scheme being implicit, considers the equilibrium of the system at the “next” time step, *i.e.* at time = $t+1$. However, since the system is non-

linear, an iterative process is required to solve the equations for each time step. The iterative process used in the solution and explained in Chapter 4 is the Newton-Raphson iteration scheme. This form of iteration is called a **predictor-corrector** method, as the values predicted from the system equations are repeatedly corrected until convergence is achieved.

Two criteria that affect such iteration schemes are:

- the selection of a correct *convergence tolerance*, which is the difference between the exact solution of the difference equation and the accepted solution; and
- the *truncation error*, which is due to the neglecting of higher order terms from the Taylor series expansion.

Either one will introduce errors into the iteration process, which may grow during the integration resulting in:

- inaccuracies entering the results; and / or
- stability problems.

Consider the solution technique outlined in Chapter 4. The correction terms for the iteration process are obtained by the Taylor expansion of equation (4.13), thus yielding equation (4.15) reproduced below.

$$ER_i^{t+1} = \tilde{ER}_i^{t+1} + \frac{\partial \tilde{ER}_i^{t+1}}{\partial T_{i-1}^{t+1}} \cdot \delta T_{i-1}^{t+1} + \frac{\partial \tilde{ER}_i^{t+1}}{\partial T_i^{t+1}} \cdot \delta T_i^{t+1} + \frac{\partial \tilde{ER}_i^{t+1}}{\partial T_{i+1}^{t+1}} \cdot \delta T_{i+1}^{t+1} + \text{higher order terms} = 0 \quad (5.120)$$

It is assumed that the tentative values of the tow configuration are sufficiently close to the solution, thus enabling the higher order terms to be neglected. This is acceptable if the time step is sufficiently small, as the solution of the previous time step (*i.e.* time t) is used as the tentative values for the current time step (*i.e.* time $t+1$). However, if the time step is large, then the higher order terms cannot be neglected, as the error thus introduced may cause the iteration process to “blow up”. A similar situation

occurs if the forcing function is large, as the changes introduced at each time step are significant.

It is possible to increase the accuracy by including some higher order terms into the process. For example, the second order terms can be calculated by differentiating equation (4.11) with respect to the tensions of the relevant cable segments to the required order, (although the actual differentiation is not carried out here, it is a straightforward partial differential process). However, the additional computational effort this introduces does not offer a significant advantage over the use of a smaller time step with a solution scheme excluding the higher order terms.

In general, the stability of implicit numerical schemes utilised for non-linear systems can be maintained by using a sufficiently small time step. The limiting condition for the time step has been investigated by a number of researchers based on experience and the testing of practical schemes (*e.g.* Bathe (1982), Wood (1990), and Thomas (1993)), and is predicted as,

$$\Delta t \leq \frac{t_{n,min}}{10} \quad (5.121)$$

This also meets the accuracy requirement discussed in the next sub-section.

Note: In Belytschko & Schoeberle (1975) and Hughes (1977) numerical schemes for non-linear systems in structures are analysed for stability using an energy stability criteria, *i.e.* the boundedness of the energy in the discrete system relative to its initial energy is postulated to imply stability. This consists of first developing an inequality for the energy of the discrete system at a particular time step as a function of the previous time step. Then the condition under which the energy at the time step is bounded relative to the energy of the previous time step is developed. However, this method was not adopted in this study, as the method described above gives acceptable results.

5.6 Accuracy

From the previous sub-section it was deduced that the time step for conditionally stable integration schemes (such as the Central Difference System), is governed by the stability requirements, (*e.g.* equation (5.119)). However, for unconditionally stable

schemes such the Houbolt scheme, the time step must be selected to yield the required accuracy.

As stated for the stability criteria, it is possible to analyse the direct integration of the equations of motion by studying the modal form of these equations. Thus, the accuracy of the integration scheme is obtained by analysing the accuracy of equation (5.103) as a function of $\Delta t / t_{n,min}$, ζ , and \bar{f} .

The accuracy of the numerical schemes is measured by using two criteria, *i.e.* the **period elongation** and the **amplitude decay** of the solution, shown in Figure 5.2. These give the deviation of the numerical solution against the exact solution, and Figure 5.3 shows these parameters for the three implicit integration methods. It is seen from the latter curves, that the accuracy is acceptable at low ratios of $\Delta t / t_{n,min}$, *i.e.* when,

$$\frac{\Delta t}{t_{n,min}} \leq 0.1 \quad (5.122)$$

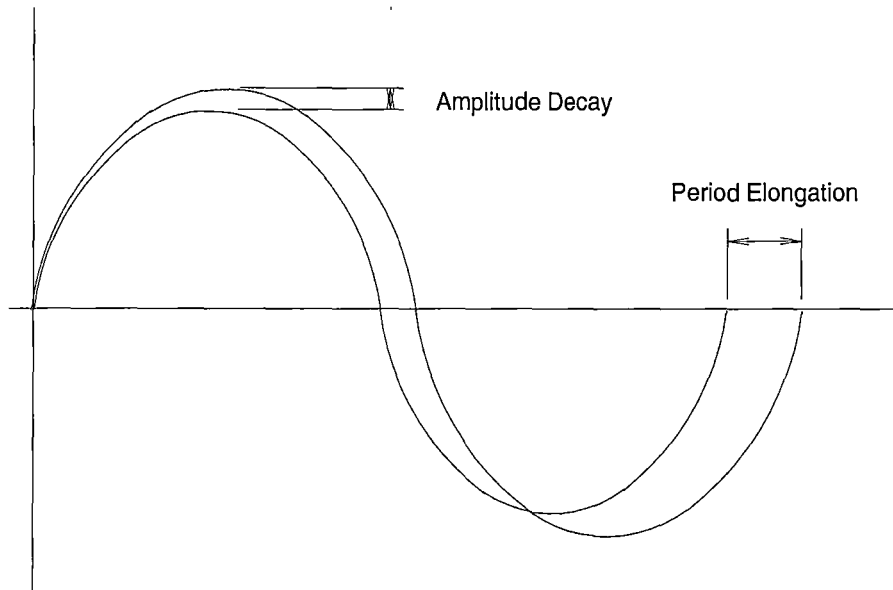
Wood (1990) investigated these parameters for the Newmak- β and Wilson- θ schemes. In this thesis, we will apply a similar investigation to the Houbolt scheme. Inspection of the Houbolt scheme given by equations (5.79), reveals that it is generally a multi-step scheme, and specifically a three step scheme. Therefore, the analysis will concentrate on multi-step algorithms.

As stated in sub-section 5.5.2, the integration of the unmodified equations and their modal form, using the same scheme should give the same result. Therefore, by analysing the modal form of the equations, it is possible to determine the accuracy of the direct integration scheme. The conversion of the equations of motion to the modal form was explained in sub-sections 5.5.1 and 5.5.2, resulting in equation (5.103), reproduced below,

$$\ddot{\bar{R}}_m + 2\zeta\omega_n \dot{\bar{R}}_m + \omega_n^2 \bar{R}_m = \bar{f} \quad (5.123)$$

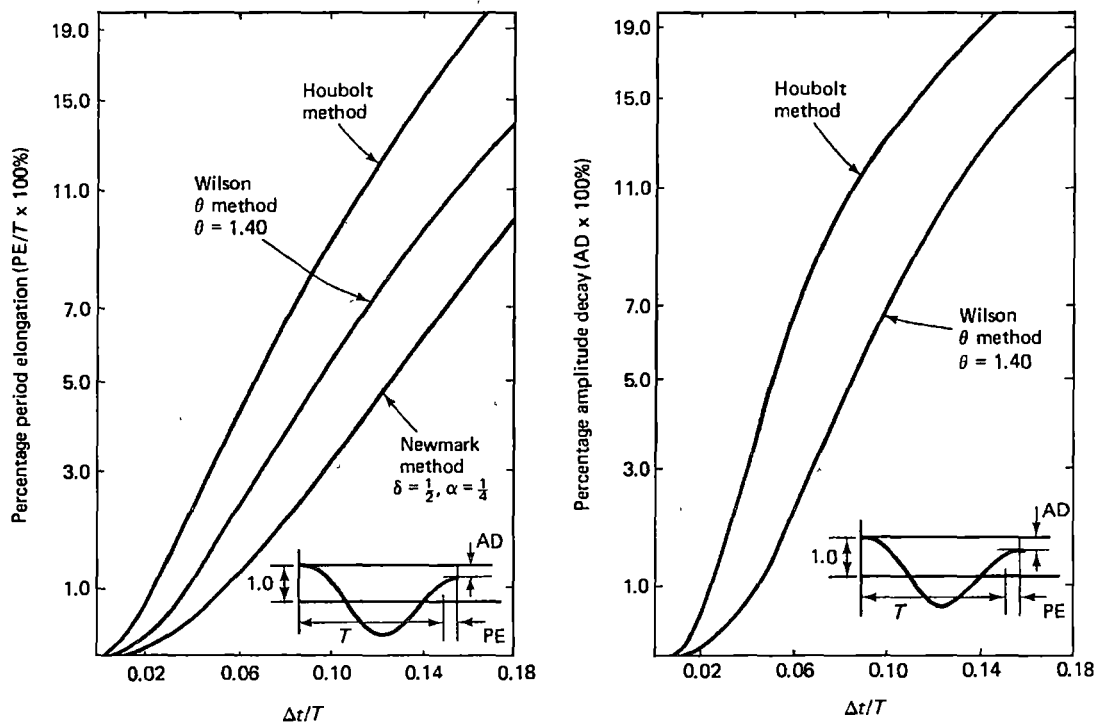
where all terms are as given in equation (5.103).

In order to solve the above equation, it is replaced by a p-step algorithm. Thus, using equation (5.4) we get,



Amplitude Decay and Period Elongation

Figure 5.2



(Bathe (1982))

Amplitude Decay and Period Elongation of Numerical Integration Schemes

Figure 5.3

$$\sum_{t=0}^p \{(\alpha^t \Delta t^{-2} + 2\gamma^t \zeta \omega_n \Delta t^{-1} + \beta^t \omega_n^2) \bar{R}_m^{N+t} - \beta^t \bar{f}^{N+t}\} = 0 \quad (5.124)$$

where

$\alpha^t, \beta^t, \gamma^t$: parameters of the multi-step integration algorithm
 \bar{R}_m^{N+t} : modal displacement at time “N+t”
 \bar{f}^{N+t} : external load vector at time “N+t”

The local truncation error ($L_{\Delta}(\bar{R}^N \Delta t)$) is obtained by using the exact solution of equation (5.123) in the integration scheme given by equation (5.124).

Thus,

$$L_{\Delta}(\bar{R}_m^N \Delta t) = \sum_{t=0}^p \{(\alpha^t \Delta t^{-2} + 2\gamma^t \zeta \omega_n \Delta t^{-1} + \beta^t \omega_n^2) \bar{R}_m^{N+t} - \beta^t \bar{f}^{N+t}\} = O(\Delta t^a) \quad (5.125)$$

where superscript “a” is the power of the “ Δt ” term and $O(\Delta t^a)$ is the asymptotic notation of the error having an order of “a”. The error is of the order of the lowest “ Δt ” term in equation (5.125).

5.6.1 Accuracy Analysis of the Houbolt Scheme

The converted modal form of the equations of motion of the system is given in equation (5.123). Inspection of equation (5.125) reveals that the external force terms, \bar{f}^{N+t} , combine in the same manner as the stiffness term, $\omega_n^2 \bar{R}_m^{N+t}$. Thus, to simplify the analysis, the external force vector will be omitted. Hence, equation (5.123) can be written as,

$$\ddot{\bar{R}}_m + 2\zeta \omega_n \dot{\bar{R}}_m + \omega_n^2 \bar{R}_m = 0 \quad (5.126)$$

where all terms are as given in equation (5.103).

The Houbolt scheme is given by equations (5.79). Therefore, by substituting equations (5.79a) and (5.79b) into equation (5.126), and dropping the subscript “m” for clarity, we obtain,

$$\begin{aligned} & \frac{1}{\Delta t^2} (2.\bar{R}^{t+1} - 5.\bar{R}^t + 4.\bar{R}^{t-1} - \bar{R}^{t-2}) + \\ & \frac{\zeta \omega_n}{3.\Delta t} (11.\bar{R}^{t+1} - 18.\bar{R}^t + 9.\bar{R}^{t-1} - 2.\bar{R}^{t-2}) + \omega_n^2 \bar{R}^{t+1} = 0 \end{aligned} \quad (5.127)$$

Inspection of the Houbolt scheme given by equations (5.79), reveals that it is a three-step ($p = 3$) integration scheme. Therefore, representing equation (5.126) in the general form for a p -step algorithm, *i.e.* as in equation (5.124), gives,

$$\sum_{t=0}^3 (\alpha^t \Delta t^{-2} + 2\gamma^t \zeta \omega_n \Delta t^{-1} + \beta^t \omega_n^2) R^{N+t} = 0 \quad (5.128)$$

Comparing equations (5.127) and (5.128) gives the parameters α^t , β^t , and γ^t as,

$$\alpha^0 = -1 \quad \alpha^1 = 4 \quad \alpha^2 = -5 \quad \alpha^3 = 2 \quad (5.129a)$$

$$\gamma^0 = -1/3 \quad \gamma^1 = 3/2 \quad \gamma^2 = -3 \quad \gamma^3 = 11/6 \quad (5.129b)$$

$$\beta^0 = 0 \quad \beta^1 = 0 \quad \beta^2 = 0 \quad \beta^3 = 1 \quad (5.129c)$$

As stated previously, the truncation error is obtained by using the exact solution in the numerical algorithm, (see equation (5.125)). The exact solution to equation (5.126) is given by,

$$e^{\Gamma t} = e^{(-\zeta \omega_n \pm i \omega_n \sqrt{1-\zeta^2})t} = e^{\omega_n (-\cos v \pm i \sin v)t} \quad (5.130)$$

where

$$\zeta = \cos v$$

$$\Gamma = \omega_n (-\cos v \pm i \sin v)$$

The characteristic polynomial of the p -step algorithm of equation (5.130) is given by,

$$\sum_{t=0}^3 (\alpha^t \Delta t^{-2} + 2\gamma^t \zeta \omega_n \Delta t^{-1} + \beta^t \omega_n^2) r^t = 0 \quad (5.131)$$

This has an approximate principle root equal to,

$$e^{\tilde{\Gamma}\Delta t} = e^{(\Gamma + \delta)\Delta t} \quad (5.132)$$

where “ δ ” is the error and

$$\tilde{\Gamma} = \Gamma + \delta \quad (5.133)$$

This means that the approximate solution is multiplied at each time step by $e^{(\Gamma + \delta)\Delta t}$ instead of $e^{\Gamma\Delta t}$. Substituting equation (5.132) in equation (5.131) and expanding the exponential term as a series gives,

$$\sum_{t=0}^p (\alpha^t \Delta t^{-2} + 2\gamma^t \zeta \omega_n \Delta t^{-1} + \beta^t \omega_n^2) \times \left(1 + t \Delta t \tilde{\Gamma} + t^2 \frac{\Delta t^2}{2!} \tilde{\Gamma}^2 + t^3 \frac{\Delta t^3}{3!} \tilde{\Gamma}^3 + \dots \right) = 0 \quad (5.134)$$

Collating the terms having a similar order of Δt yields,

$$\begin{aligned} \Delta t^{-2} \sum_{t=0}^p \alpha^t + \Delta t^{-1} \left(\tilde{\Gamma} \sum_{t=0}^p t \alpha^t + 2\zeta \omega_n \sum_{t=0}^p \gamma^t \right) \\ + \tilde{\Gamma}^2 \sum_{t=0}^p t^2 \alpha^t / 2! + 2\zeta \omega_n \tilde{\Gamma} \sum_{t=0}^p t \gamma^t + \omega_n^2 \sum_{t=0}^p \beta^t \\ + \tilde{\Gamma} \Delta t \left(\tilde{\Gamma}^2 \sum_{t=0}^p t^3 \alpha^t / 3! + 2\zeta \omega_n \tilde{\Gamma} \sum_{t=0}^p t^2 \gamma^t / 2! + \omega_n^2 \sum_{t=0}^p t \beta^t \right) + \dots = 0 \end{aligned} \quad (5.135)$$

Now using the parameters α^t , β^t , and γ^t obtained for the Houbolt scheme in equations (5.129), the following conditions are obtained,

$$\sum_{t=0}^p \alpha^t = \sum_{t=0}^p t \alpha^t = \sum_{t=0}^p \gamma^t = 0 \quad (5.136)$$

$$\sum_{t=0}^p t^2 \alpha^t / 2! = \sum_{t=0}^p t \gamma^t = \sum_{t=0}^p \beta^t = 1 \quad (5.137)$$

and

$$\sum_{t=0}^p t \beta_t = \sum_{t=0}^p t^2 \gamma_t / 2! = \sum_{t=0}^p t^3 \alpha_t / 3! = 3 \quad (5.138)$$

Substituting equations (5.136), (5.137), and (5.138) into equation (5.135) reduces it to,

$$\left(\tilde{\Gamma}^2 + 2\zeta\omega_n\tilde{\Gamma} + \omega_n^2\right) + 3\Delta t\left(\tilde{\Gamma}^3 + 2\zeta\omega_n\tilde{\Gamma}^2 + \omega_n^2\tilde{\Gamma}\right) + O\left(\Delta t^2\right) = 0 \quad (5.139)$$

where $O(\Delta t^2)$ is the asymptotic notation of the error having an order of “2”.

Substituting equation (5.133) into equation (5.139) gives,

$$\begin{aligned} &\left\{\left(\Gamma^2 + 2\zeta\omega_n\Gamma + \omega_n^2\right) + 2\delta\left(\Gamma + \zeta\omega_n\right)\right\} + \\ &3\Delta t\left\{\left[\Gamma\left(\Gamma^2 + 2\zeta\omega_n\Gamma + \omega_n^2\right) + 3\Gamma^2\delta + 4\zeta\omega_n\Gamma\delta + \omega_n^2\delta\right] + O\left(\Delta t^2\right)\right\} = 0 \end{aligned} \quad (5.140)$$

where all terms of δ^2 and above are included in $O(\Delta t^2)$.

Since equation (5.130) is an exact solution to equation (5.126), the latter gives,

$$\Gamma^2 + 2\zeta\omega_n\Gamma + \omega_n^2 = 0 \quad (5.141)$$

Using equation (5.141) in equation (5.140) and simplifying gives,

$$\left\{2\delta\left(\Gamma + \zeta\omega_n\right)\right\} + 3\Delta t\left\{2\Gamma^2\delta + 2\zeta\omega_n\Gamma\delta\right\} + O\left(\Delta t^2\right) = 0 \quad (5.142)$$

Referring to equation (5.130), where $\Gamma = \omega_n(-\cos v \pm i \sin v)$ and $\zeta = \cos v$, we have,

$$\Gamma = \omega_n(-\zeta \pm i \sin v) \quad or, \quad (5.143a)$$

$$\Gamma + \zeta\omega_n = \pm i\omega_n \sin v \quad (5.143b)$$

Without the loss of generality, considering the plus sign and substituting equation (5.143b) into equation (5.142) gives,

$$i2\delta\omega_n \sin v + 3\Delta t\left\{2\Gamma^2\delta + 2\zeta\omega_n\Gamma\delta\right\} + O\left(\Delta t^2\right) = 0 \quad (5.144)$$

Having obtained an expression for the error, it is now required to separate the error term into its components, *i.e.* the amplitude decay and period elongation. Thus, we define,

$$\delta = -\delta_a + i\delta_p \quad (5.145)$$

where

δ : error

δ_a : amplitude error, which increases the damping by a small quantity δ_a

δ_p : phase error, which increases the frequency of oscillation by a small quantity $\delta_p/2\pi$. This can also be expressed as a period increase, *i.e.*,

$$\frac{2\pi}{(\omega_n \sin v + \delta_p)} - \frac{2\pi}{\omega_n \sin v} = -\frac{2\pi\delta_p}{(\omega_n^2 \sin^2 v)} \quad (5.146)$$

or as a fractional period increase of

$$-\frac{\delta_p}{(\omega_n \sin v)} \quad (5.147)$$

Now substituting equation (5.145) into equation (5.144) gives,

$$i2(-\delta_a + i\delta_p)\omega_n \sin v + 6\Delta t(-\delta_a + i\delta_p)\{\Gamma^2 + \zeta\omega_n \Gamma\} + O(\Delta t^2) = 0 \quad (5.148)$$

From equation (5.130) we have,

$$\Gamma = \omega_n (-\cos v \pm i \sin v) \quad (5.149)$$

Using *de Moivre's* theorem, equation (5.149) becomes,

$$(-\cos v + i \sin v)^a = (-1)^a (\cos v - i \sin v)^a = (-1)^a (\cos av - i \sin av) \quad (5.150)$$

Considering the plus sign in equation (5.149) we have,

$$\Gamma^a = \omega_n^a (-1)^a (\cos av - i \sin av) \quad (5.151)$$

Substituting equation (5.151) into equation (5.148) gives,

$$\begin{aligned}
& -2\delta_p \omega_n \sin v - i 2\delta_a \omega_n \sin v \\
& + 6\omega_n^2 \Delta t \{ \delta_a \cos^2 v - \delta_a \cos 2v + \delta_p \sin 2v - \delta_p \cos v \sin v \} \\
& + i 6\omega_n^2 \Delta t \{ \delta_p \cos 2v - \delta_p \cos^2 v + \delta_a \sin 2v - \delta_a \cos v \sin v \} + O(\Delta t^2) = 0
\end{aligned} \tag{5.152}$$

Separating out the real and imaginary parts gives,

$$\begin{aligned}
2\delta_p \omega_n \sin v = \\
+ 6\omega_n^2 \Delta t \{ \delta_a \cos^2 v - \delta_a \cos 2v + \delta_p \sin 2v - \delta_p \cos v \sin v \} + O(\Delta t^2)
\end{aligned} \tag{5.153}$$

$$\begin{aligned}
2\delta_a \omega_n \sin v = \\
+ 6\omega_n^2 \Delta t \{ \delta_p \cos 2v - \delta_p \cos^2 v + \delta_a \sin 2v - \delta_a \cos v \sin v \} + O(\Delta t^2)
\end{aligned} \tag{5.154}$$

Inspection of equations (5.153) and (5.154) shows that the error terms δ_a and δ_p are of the order Δt^2 . Therefore, it is stated that the *amplitude and phase errors are $O(\Delta t^2)$* . The actual expressions for the respective error terms can be obtained by solving the above equations. However, this will not be attempted in this work, as equations (5.153) and (5.154) are adequate to meet our requirements.

It is interesting to note that if the three terms in equation (5.138) were not equal to each other, then the phase error (δ_p) would be $O(\Delta t^2)$, while the amplitude error (δ_a) would remain $O(\Delta t)$.

Wood (1990) showed that stability issues occur if a higher order accuracy is pursued. Therefore, as shown in Figure 5.3, errors in the order of $O(\Delta t^2)$ are acceptable providing the time step is relatively small. Thus, a time step conforming to,

$$\frac{\Delta t}{t_{n,mn}} \leq 0.1 \tag{5.155}$$

is sufficient to give the accuracy required.

This can be explained by considering a mode within the system having a natural period “ $t_{n,a}$ ”, where “a” represents the mode in question. For accuracy of the solution,

$$\frac{\Delta t}{t_{n,a}} \leq 0.1 \quad (5.156)$$

If this is not the case, the mode will be integrated inaccurately, resulting in errors being introduced into the solution. The selection of the time ratio in accordance to (5.156) results in an accurate integration of the modes that conforms to,

$$t_{n,i} \leq t_{n,a} \quad (5.157)$$

where “i” represents the modes. However, higher modes, *i.e.* any mode where the period is greater than “ $t_{n,a}$ ”, will introduce errors during the integration. Therefore, to ensure accuracy in all modes, “ $t_{n,a}$ ” should represent the highest mode, hence, the condition defined by equation (5.155).

The requirement for accuracy can also be seen by inspecting the spectral radius shown in Figure 5.1. When the ratio $\Delta t/t_{n,mm} \leq 0.1$, the spectral radius is equal to one. Therefore, the solution has no amplification. However, as the time ratio increases, the spectral radius falls below one, resulting in a damping effect on the solution, *i.e.* introducing amplitude damping.

5.7 Natural Frequencies of the Model

As seen from equations (5.121) and (5.155), the conditions to maintain stability and accuracy of numerical schemes with non-linear systems are the same. Therefore, to ensure stability and accuracy of the numerical integration of non-linear systems, (such as the underwater tow model), the time step should be smaller than one tenth of the smallest natural period of the cable mesh.

In order to conform to the above, it is required to calculate the natural frequencies of the cable mesh system, which in turn will yield the respective natural periods.

In conventional structural dynamic analysis, the displacements are considered to be small, thus the system mass and stiffness matrices can be considered to be constant. This yields constant natural frequencies for the system. However, cable systems undergo considerable displacement, resulting in time dependent mass and stiffness matrices, and hence time dependent natural frequencies. Ideally, therefore, the time

step should be adjusted during the simulation time to ensure adequate accuracy and stability.

However, as the time step limit is only a guide, and not a critical value as in an explicit numerical integration scheme, it is sufficient to obtain an approximate value for the natural frequencies. It is then possible to use a time step that is sufficiently lower than the smallest natural period (corresponding to the highest natural frequency), in order to achieve the required accuracy and stability.

To calculate the natural frequencies and hence the natural periods, we first need to convert the tow model into an eigenproblem. Since the damping and external forces will have no effect on the natural frequencies, the general equation of motion, *i.e.* equation (5.87), is reduced to represent free vibration without damping, *i.e.*,

$$\underline{\underline{m}}\ddot{\underline{\underline{R}}} + \underline{\underline{k}}\underline{\underline{R}} = 0 \quad (5.158)$$

where $\underline{\underline{m}}$ and $\underline{\underline{k}}$ are the mass and stiffness matrices respectively. The solution for equation (5.158) will be of the form,

$$\underline{\underline{R}} = \underline{\underline{\theta}} \sin \omega_n (t - t_c) \quad (5.159)$$

where

- $\underline{\underline{\theta}}$: vector of the order n , (that was shown in sub-section 5.5.1 to be the eigenvectors), where “ n ” is the number of nodes in the discrete system
- t : time
- t_c : time constant
- ω_n : frequency of vibration, *i.e.* natural frequency of the vector $\underline{\underline{\theta}}$

Substituting equation (5.159) into equation (5.158) gives the generalised eigenproblem, which enables the calculation of $\underline{\underline{\theta}}$ and ω_n . Thus,

$$\underline{\underline{k}}\underline{\underline{\theta}} = \omega_n^2 \underline{\underline{m}}\underline{\underline{\theta}} \quad (5.160)$$

Since the eigenvalue “ λ ” is defined as,

$$\lambda = \omega_n^2 \quad (5.161)$$

it is possible to write the above equation as,

$$\underline{\underline{k}} \bar{\underline{\theta}} = \lambda \underline{\underline{m}} \bar{\underline{\theta}} \quad (5.162)$$

Thus, we obtain the eigenvalues (λ) from the characteristic polynomial of equation (5.162) as,

$$\det(\underline{\underline{k}} - \lambda \underline{\underline{m}}) = 0 \quad (5.163)$$

Solving equation (5.163) yields the natural frequencies of the system.

Therefore, let us first reduce the equations of motion to the form given by equation (5.158). The equations of motion for the nodes representing the tow system are given by equations (3.14) in Chapter 3 as,

$$m_{i11} \cdot \ddot{x}_i + m_{i12} \cdot \ddot{y}_i + m_{i13} \cdot \ddot{z}_i = F_{ix} \quad (5.164a)$$

$$m_{i21} \cdot \ddot{x}_i + m_{i22} \cdot \ddot{y}_i + m_{i23} \cdot \ddot{z}_i = F_{iy} \quad (5.164b)$$

$$m_{i31} \cdot \ddot{x}_i + m_{i32} \cdot \ddot{y}_i + m_{i33} \cdot \ddot{z}_i = F_{iz} \quad (5.164c)$$

where the terms m_{iab} are given in equations (3.7). Now using equations (3.27) in the above equations, the external forces can be expanded to include the tension terms as,

$$\begin{aligned} m_{i11} \cdot \ddot{x}_i + m_{i12} \cdot \ddot{y}_i + m_{i13} \cdot \ddot{z}_i \\ = T_i \cos \phi_i \cos \psi_i - T_{i-1} \cos \phi_{i-1} \cos \psi_{i-1} + F_{iox} \end{aligned} \quad (5.165a)$$

$$\begin{aligned} m_{i21} \cdot \ddot{x}_i + m_{i22} \cdot \ddot{y}_i + m_{i23} \cdot \ddot{z}_i \\ = T_i \sin \phi_i \cos \psi_i - T_{i-1} \sin \phi_{i-1} \cos \psi_{i-1} + F_{ioy} \end{aligned} \quad (5.165b)$$

$$\begin{aligned} m_{i31} \cdot \ddot{x}_i + m_{i32} \cdot \ddot{y}_i + m_{i33} \cdot \ddot{z}_i \\ = T_i \sin \psi_i - T_{i-1} \sin \psi_{i-1} - F_{ioz} \end{aligned} \quad (5.165c)$$

Using the relationships for the cable segment angles defined in equations (5.51), in equations (5.165) gives,

$$m_{i11} \cdot \ddot{x}_i + m_{i12} \cdot \ddot{y}_i + m_{i13} \cdot \ddot{z}_i = T_i \frac{x_{i+1} - x_i}{l_i (1 + \epsilon_i)} - T_{i-1} \frac{x_i - x_{i-1}}{l_{i-1} (1 + \epsilon_{i-1})} + F_{iox} \quad (5.166a)$$

$$m_{i21} \cdot \ddot{x}_i + m_{i22} \cdot \ddot{y}_i + m_{i23} \cdot \ddot{z}_i = T_i \frac{y_{i+1} - y_i}{l_i (1 + \epsilon_i)} - T_{i-1} \frac{y_i - y_{i-1}}{l_{i-1} (1 + \epsilon_{i-1})} + F_{ioy} \quad (5.166b)$$

$$m_{i31} \cdot \ddot{x}_i + m_{i32} \cdot \ddot{y}_i + m_{i33} \cdot \ddot{z}_i = T_i \frac{z_{i+1} - z_i}{l_i (1 + \epsilon_i)} - T_{i-1} \frac{z_i - z_{i-1}}{l_{i-1} (1 + \epsilon_{i-1})} + F_{ioz} \quad (5.166c)$$

Expanding the tension terms and separating the coordinates yields,

$$\begin{aligned} m_{i11} \cdot \ddot{x}_i + m_{i12} \cdot \ddot{y}_i + m_{i13} \cdot \ddot{z}_i = & \frac{T_i}{l_i (1 + \epsilon_i)} x_{i+1} - \left(\frac{T_i}{l_i (1 + \epsilon_i)} + \frac{T_{i-1}}{l_{i-1} (1 + \epsilon_{i-1})} \right) x_i \\ & + \frac{T_{i-1}}{l_{i-1} (1 + \epsilon_{i-1})} x_{i-1} + F_{iox} \end{aligned} \quad (5.167a)$$

$$\begin{aligned} m_{i21} \cdot \ddot{x}_i + m_{i22} \cdot \ddot{y}_i + m_{i23} \cdot \ddot{z}_i = & \frac{T_i}{l_i (1 + \epsilon_i)} y_{i+1} - \left(\frac{T_i}{l_i (1 + \epsilon_i)} + \frac{T_{i-1}}{l_{i-1} (1 + \epsilon_{i-1})} \right) y_i \\ & + \frac{T_{i-1}}{l_{i-1} (1 + \epsilon_{i-1})} y_{i-1} + F_{ioy} \end{aligned} \quad (5.167b)$$

$$\begin{aligned} m_{i31} \cdot \ddot{x}_i + m_{i32} \cdot \ddot{y}_i + m_{i33} \cdot \ddot{z}_i = & \frac{T_i}{l_i (1 + \epsilon_i)} z_{i+1} - \left(\frac{T_i}{l_i (1 + \epsilon_i)} + \frac{T_{i-1}}{l_{i-1} (1 + \epsilon_{i-1})} \right) z_i \\ & + \frac{T_{i-1}}{l_{i-1} (1 + \epsilon_{i-1})} z_{i-1} + F_{ioz} \end{aligned} \quad (5.167c)$$

Representing equations (5.167) in matrix form gives,

$$\begin{bmatrix} m_{i11} & m_{i12} & m_{i13} \\ m_{i21} & m_{i22} & m_{i23} \\ m_{i31} & m_{i32} & m_{i33} \end{bmatrix} \cdot \begin{bmatrix} \ddot{x}_i \\ \ddot{y}_i \\ \ddot{z}_i \end{bmatrix} =
\begin{bmatrix} T_{ia} & 0 & 0 & T_{ib} & 0 & 0 & T_{ic} & 0 & 0 \\ 0 & T_{ia} & 0 & 0 & T_{ib} & 0 & 0 & T_{ic} & 0 \\ 0 & 0 & T_{ia} & 0 & 0 & T_{ib} & 0 & 0 & T_{ic} \end{bmatrix} \cdot \begin{bmatrix} x_{i+1} \\ y_{i+1} \\ z_{i+1} \\ x_i \\ y_i \\ z_i \\ x_{i-1} \\ y_{i-1} \\ z_{i-1} \end{bmatrix} + \begin{bmatrix} F_{iox} \\ F_{ioy} \\ F_{ioz} \end{bmatrix} \quad (5.168)$$

where

$$T_{ia} = \frac{T_i}{l_i(1 + \epsilon_i)}$$

$$T_{ib} = -\left(\frac{T_i}{l_i(1 + \epsilon_i)} + \frac{T_{i-1}}{l_{i-1}(1 + \epsilon_{i-1})} \right)$$

$$T_{ic} = \frac{T_{i-1}}{l_{i-1}(1 + \epsilon_{i-1})}$$

Equations (5.167) represent the equations of motion for node i. Similar equations can be produced for each node of the tow system. These equations are then assembled to produce a set of equations for the complete system as,

$$\underline{\underline{m}} \ddot{\underline{\underline{R}}} + \underline{\underline{k}} \underline{\underline{R}} = \underline{\underline{F}}_o \quad (5.169)$$

where the term $\underline{\underline{F}}_o$ includes all external forces and the damping forces introduced by the interaction between the cable / fish and the surrounding water. Therefore, this term can be neglected when calculating the natural frequencies, resulting in equation (5.169) being similar to equation (5.158). The eigenvalues can therefore, be calculated using the characteristic polynomial as defined in equation (5.163) as,

$$\det(\underline{\underline{k}} - \lambda \underline{\underline{m}}) = 0 \quad (5.170)$$

The actual calculation of the eigenvalues (and hence the natural frequencies) is tedious, especially if a large number of elements / nodes are present in the model. This gives large mass and stiffness matrices, which requires an iterative process to calculate the eigenvalues.

Bathe (1982) gives a comprehensive description of the various methods available for the calculation of eigenvalues of systems having large mass and stiffness matrices. Thomas (1993) carries out such a calculation for a mooring cable model in two-dimensions.

5.8 Estimation of the Time Step

In practice, a simpler and quicker method to estimate an appropriate time step for the dynamic simulation of the tow model is desirable. This can be achieved by using the wave speed obtained from the continuous cable model developed in sub-section 5.2.2.

Consider the propagation of a wave. The period due to the wave is given by,

$$t_p = \frac{l_w}{C_w} \quad (5.171)$$

where

t_p : period of the cycle
 l_w : wavelength
 C_w : wave speed

In sub-section 5.2.2, the wave propagation speeds along a continuous cable were given by equations (5.48) reproduced below,

$$\lambda_{w1,2} = \pm \sqrt{\frac{1}{\mu_c} \cdot \frac{dT}{d\epsilon}} \quad (5.48a)$$

$$\lambda_{w3,4} = \pm \sqrt{\frac{1}{\mu_c} \cdot \frac{\epsilon}{(1 + \epsilon)} \cdot \frac{dT}{d\epsilon}} \quad (5.48b)$$

$$\lambda_{w5,6} = \pm \sqrt{\frac{1}{\mu_c} \cdot \frac{\epsilon}{(1 + \epsilon)} \cdot \frac{dT}{d\epsilon}} \quad (5.48c)$$

From the above it is seen that equations (5.48b) and (5.48c) are the same. In addition, although each equation represents two speeds, the magnitudes of the two speeds are the same, with the difference being limited to their directions. Therefore, equation (5.48a) represents the speed at which the *tensile disturbance* (tensile stress wave) travels along the line, while equations (5.48b) and (5.48c) represent the speed at which the *transverse disturbance* (transverse flexural wave) travels along the line. In short, there are two wave speeds, *i.e.*, the longitudinal wave speed (λ_{wL}) and the transverse wave speed (λ_{wT}), given by,

$$\lambda_{wL} = \sqrt{\frac{1}{\mu_c} \cdot \frac{dT}{d\epsilon}} \quad (5.172)$$

$$\lambda_{wT} = \sqrt{\frac{1}{\mu_c} \cdot \frac{\epsilon}{(1 + \epsilon)} \cdot \frac{dT}{d\epsilon}} \quad (5.173)$$

First consider the longitudinal wave speed given by equation (5.172). Rearranging equation (5.45) as,

$$\frac{\partial T}{\partial \epsilon} = \frac{T}{\epsilon} \quad (5.174)$$

and substituting into equation (5.172) gives,

$$\lambda_{wL} = \sqrt{\frac{1}{\mu_c} \cdot \frac{T}{\epsilon}} \quad (5.175)$$

Now from Hook's law of elasticity we have,

$$\frac{T}{\epsilon} = E \cdot A \quad (5.176)$$

where E is the modulus of elasticity of the cable material and A is the cross sectional area of the cable. Substituting equation (5.176) into (5.175) gives,

$$\lambda_{wL} = \sqrt{\frac{E \cdot A}{\mu_c}} \quad (5.177)$$

The relationship between the mass per unit length of the cable (μ_c) and the density of the cable material (ρ_c) is given by,

$$\frac{\mu_c}{A} = \rho_c \quad (5.178)$$

Substituting equation (5.178) into equation (5.177) gives the longitudinal wave speed as,

$$\lambda_{wL} = \sqrt{\frac{E}{\rho_c}} \quad (5.179)$$

Now let us look at the transverse wave speed given by equation (5.173). Again substituting equation (5.174) into equation (5.173) gives,

$$\lambda_{wT} = \sqrt{\frac{1}{\mu_c} \cdot \frac{T}{(1 + \epsilon)}} \quad (5.180)$$

Since the strain in the cable is relatively small, *i.e.* $\epsilon \ll 1$, equation (5.180) reduces to,

$$\lambda_{wT} = \sqrt{\frac{T}{\mu_c}} \quad (5.181)$$

The relationship between the tension and the stress in the cable is given by,

$$T = \sigma \cdot A \quad (5.182)$$

where σ is the stress in cable when stretched and A is the cross sectional area of the cable. Substituting equation (5.182) into (5.181) gives,

$$\lambda_{wT} = \sqrt{\frac{\sigma \cdot A}{\mu_c}} \quad (5.183)$$

Converting the mass per unit length into the density of the cable material by using equation (5.178) in equation (5.183) gives the transverse wave speed as,

$$\lambda_{wT} = \sqrt{\frac{\sigma}{\rho_c}} \quad (5.184)$$

Thus, the longitudinal and transverse wave speeds are given by equations (5.179) and (5.184) respectively.

Referring to equation (5.171), it is noted that the lowest period is obtained if the largest wave speed (represented by C_w) is used. From equations (5.179) and (5.184) it is seen that the longitudinal wave speed (λ_{wL}) is greater than the transverse wave speed (λ_{wT}). Therefore, it is the longitudinal wave speed that should be used in equation (5.171). Thus, the period is given by,

$$t_p = \frac{l_w}{\lambda_{wL}} = l_w \sqrt{\frac{\rho_c}{E}} \quad (5.185)$$

In sub-sections 5.5 and 5.6 we identified that the time step for the numerical integration scheme should be less than one tenth of the smallest natural period of the cable mesh to ensue stability and accuracy, (equations (5.121), and (5.155)). However, Bathe (1982) and Ractliffe (1984) suggests that the time step can be less than a *cut-off time period*, which considers only the lower frequencies that tend to dominate the response. The time period value obtained in equation (5.185) suits this criterion, and can be used to estimate a suitable time step. Thus, the requirement for stability and accuracy is that the time step is less than one tenth of the cut-off period, *i.e.*,

$$\Delta t \leq \frac{t_p}{10} \quad (5.186)$$

Substituting from equation (5.185) into equation (5.186) gives,

$$\Delta t \leq \frac{l_w}{10} \sqrt{\frac{\rho_c}{E}} \quad (5.187)$$

Since we are considering an element mesh, the wavelength (l_w) can be replaced by the length of the smallest element (l_m) in the lumped mass model. Thus, equation (5.187) becomes,

$$\Delta t \leq \frac{l_m}{10} \sqrt{\frac{\rho_c}{E}} \quad (5.188)$$

Since the higher frequencies contribute little to the solution, very little is gained in the way of accuracy by using very small time steps (Thomas (1993)). Thus, it is possible to use larger time steps than that specified in equation (5.188), provided that stability and convergence difficulties are not encountered in the iteration process required for the non-linear system. However, equation (5.188) can be used as a guide when selecting an appropriate time step for the time domain simulation of cable systems.

CHAPTER 6

EXPERIMENTAL METHODS AND VALIDATION

6.1 Introduction

In the previous chapters, the development of the two-part tow and multi-tow computer models was detailed. In order to supplement the data from the computer model and to validate the model, a series of experiments were carried out. These included:

- scaled model tests in the circulating water channel at the Australian Maritime College; and
- full scale trials using DSTO towed side scan sonar gear, deployed from RAN vessels.

This chapter explains the experimental procedure and evaluates the results obtained. A summary of the results from the scaled model tests and the full scale trials is provided in Appendix A. A selection of the validation runs, *i.e.* the comparison of the scaled model results against equivalent computer simulations, is also presented.

The drag and lift coefficients for the scaled models used in the circulating water channel were obtained experimentally using a horizontal planar-motion-mechanism (HPMM) having a 6 DOF load cell. These experiments and the processing of these coefficients to enable their input into the computer model are also described in this chapter.

6.2 Scaled Model Trials

The scaled model trials carried out in the circulating water channel at the Australian Maritime College contributed to the study of the two-part tow in two ways, *i.e.*:

- the validation of the computer model; and
- the response due to varying the tow configuration parameters.

The latter parameters included cable lengths, location of the junction along the primary cable, type of depressor, use of a drogue, and the change in excitation amplitude and frequency.

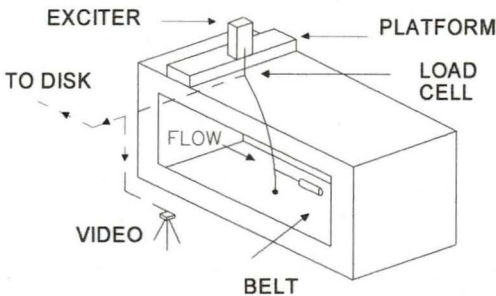
The circulating water channel is shown in Figures 6.1 and 6.2. It consists of a varying cross sectional water channel, with flow correction screens at its entrance. Four hydraulically driven pumps circulate fresh water through the channel. The upper surface is open to the atmosphere, while the lower surface consists of a moving belt. This configuration allows for a uniform flow profile across the investigation region within the channel.



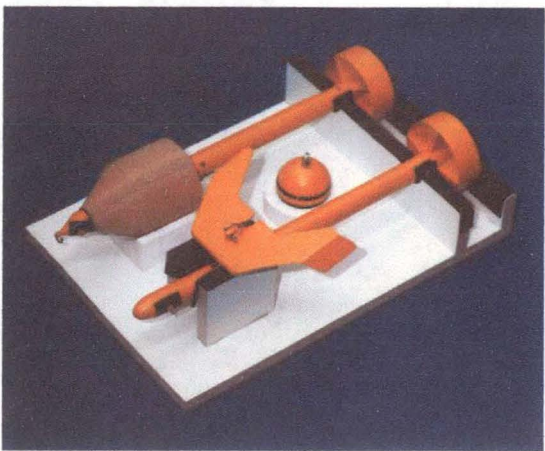
Circulating Water Channel
Figure 6.1



Top View of Channel
Figure 6.2



Experimental Procedure
Figure 6.3



Scaled Models
Figure 6.4

A seamless glass window (Figure 6.1) allows for an unrestricted view of the channel's working section. A motorised platform (Figure 6.2) located on rails at the upper surface, enables the lowering of experimental apparatus into the fluid flow.

Figure 6.3 shows the experimental set-up for the scaled model test in the circulating water channel. The configuration was excited by an "elliptical exciter" located on the motorised platform at the upper water surface. The motion of the towed fish was recorded on video and digitised using reference points on the towed body. By locating the video camera at different positions, it was possible to record the surge, sway, heave, pitch, and yaw motions. The tension values at the surface tow point were also recorded via a load cell.

The scaled models used in the circulating water channel are shown in Figure 6.4. They consisted of a neutrally buoyant tow fish and two depressors, *i.e.* a fish with a depressor wing (giving negative lift) and a ball type depressor that acted as a clump weight. The scaling factor for the models were determined by the size of the circulating water channel, in order to reduce the end effects and maintain the full configuration within the working section of the channel. Therefore, the scale factor selected was one thirds ($1/3$) the full scale configuration.

In order to compare the results between the computer model and the scaled model tests, it was required to calculate the various inertia and hydrodynamic coefficients of the fish and depressor. These included the mass, added mass, and the hydrodynamic force and moment coefficients. These were obtained using a mixture of experimental techniques and theoretical approximations. The calculation of the hydrodynamic force and moment coefficients is described in sub-section 6.5.

6.2.1 Scaled Model Trial Configurations

The scaled model experiments carried out in the circulating water channel consisted of the following tow configurations:

- single part tow;
- two-part tow with the secondary cable attached to the depressor;
- two-part tow with the secondary cable attached to a point along the primary cable; and

- two-part tow with a drogue fitted to the aft end of the towed fish.

The lengths of the following tow cables were also varied to give different cable configurations, (see Figure 1.2 for a description of these lengths):

- secondary cable;
- cable between the junction and the depressor, (effectively changing the primary cable length); and
- cable between the towed fish and the drogue, (when fitted).

In addition, two types of depressors were used, *i.e.* a depressor fish equipped with a negative lift wing and a ball type depressor that acted as a clump weight, (see Figure 6.4). The water velocity was maintained at 1 metre per second for all runs.

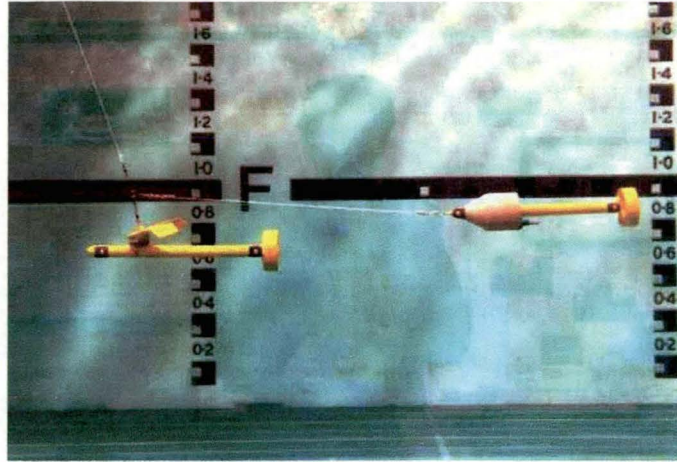
The experimental runs were again divided into two groups, depending on the direction of excitation. These were:

- vertical excitation, where the excitation motion was surge (X), heave (Z), or a combination of the two; and
- horizontal excitation, where the excitation motion was sway (Y).

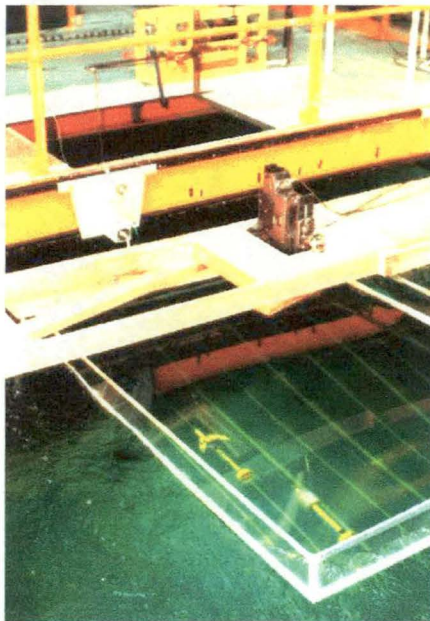
Each configuration was tested for varying excitation amplitudes and frequencies. Table A1 in Appendix A gives the data for the individual runs. Note: the excitation frequency is given as the excitation period, *i.e.* the reciprocal of the frequency.

Figure 6.5 shows the two-part tow utilising a depressor fish, set up to investigate the vertical motions, (*i.e.* surge, heave, and pitch). Figure 6.6 is the same configuration set up for horizontal motions, (*i.e.* surge, sway, and yaw). A Perspex bottomed platform was “moored” on the water surface above the tow configuration to enable clear photography of the latter.

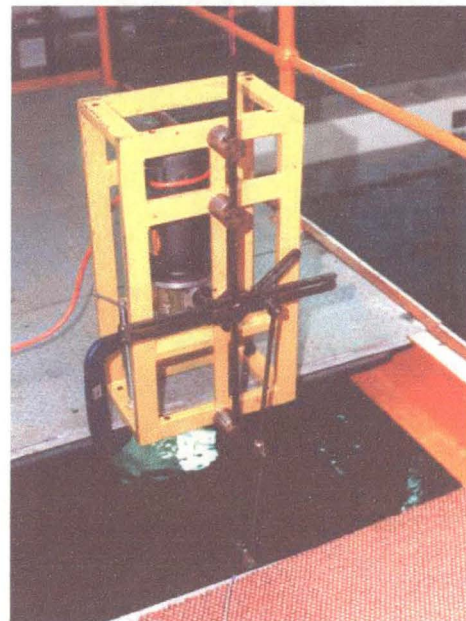
The configuration was excited by an elliptical exciter (Figure 6.7), located at the water surface and capable of providing excitation in all three linear directions. The exciter was set up to ensure that the cable model remained submerged throughout each run.



Recording of Vertical Motion
Figure 6.5



Recording of Horizontal Motion
Figure 6.6



Surface Excitation Mechanism
Figure 6.7

6.3 Scaled Model Test Results

The motions of the towed fish and depressor were obtained on video and digitised using reference points on the towed bodies. The recording of these motions depended on the excitation direction. In the vertical excitation runs, the vertical linear motions (surge and heave) and the vertical angular motion (pitch), of the depressor and towed

fish were recorded. For the ball type depressor, only the linear motions were recorded, as the pitch of a “clump” weight is of little relevance.

In the horizontal excitation runs, the horizontal linear motions (surge and sway) and the horizontal angular motion (yaw), of the towed fish were recorded. The horizontal motions of the depressor were not recorded due to the inability to video tape its motion from above, as the towed fish obstructed the view of the depressor, (see Figure 6.6).

Table A2 in Appendix A summarises the results from these runs. It gives the maximum amplitudes of the relevant linear and angular displacements of the depressor and towed fish.

In order to simplify the analysis of the results, the displacement amplitudes of similar configurations and excitations were plotted against the excitation periods. Due to the number of graphs involved, all of them are not reproduced in this text, however, a selection is given at appropriate locations in this chapter. Note: It is possible to reproduce these graphs by simply plotting the data given in Table A2, using a basic spreadsheet or plotting software.

A number of conventional (single part) tow configurations were also tested under horizontal excitation. These allowed for direct comparison between the equivalent single part and two-part tow configurations. However, with vertical excitation, no single part tow configurations were tested, as the necessary comparison was carried out by considering the relative motions between the depressor and towed fish.

6.3.1 Response of the Two-Part Tow due to Vertical Excitation

Let us first investigate the general behaviour of the two-part tow undergoing vertical excitation, *i.e.* excitation in the X and Z directions. Figures 6.8 to 6.16 give the response of similar two-part tow configurations under varying excitation amplitudes and frequencies. Figures 6.8 to 6.12 represent two-part tow configurations utilising the depressor fish, where the first three figures deal with an increasing Z-direction excitation amplitude, while the latter three deals with a decreasing X-direction excitation amplitude. Similarly, Figures 6.13 to 6.16 represent equivalent two-part tow configurations using a ball type depressor. Again the first two figures deal with an increasing Z-direction excitation amplitude, while the latter three deal with a decreasing X-direction excitation amplitude.

On inspecting Figures 6.8 to 6.16, it is clear that the response of the towed fish is substantially better than that of the depressor, especially at the higher excitation frequencies. This is due to the inherent decoupling effect of the two-part tow configuration.

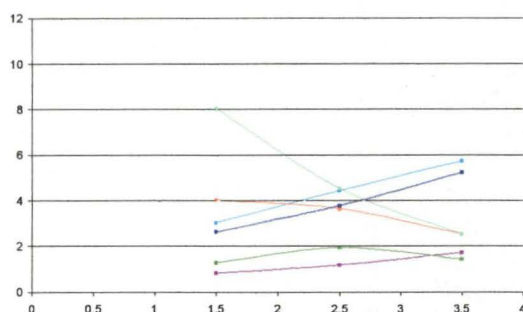
Response to Varying Excitation Frequency

In the configuration utilising the depressor fish (Figures 6.8 to 6.12), as the excitation frequency increases, the surge of the depressor fish tends to reduce, while its heave and pitch amplitudes increase. The latter motion increases substantially as the excitation frequency increases.

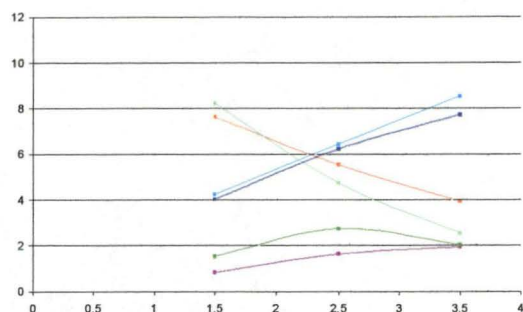
In the case of the ball type depressor (Figures 6.13 to 6.16), its motions (surge and heave), are relatively “flat”, *i.e.* they show little change as the excitation frequency changes. This is due to the effect of gravity forces dominating the hydrodynamic forces. This is also the reason for the surge of the depressor ball to be much lower than its heave. The latter motion does increase marginally as the excitation frequency increases, which is probably due to the inertia effect of the depressor ball. The surge amplitude of the depressor tends to mirror the excitation amplitude in that direction, and does drop slightly as the excitation frequency increases.

In both depressor type configurations, at high frequency excitations all motions of the towed fish tend to reduce due to the decoupling effect of the two-part tow. It tends to reduce the transmission of the heave motion from the depressor to the towed fish effectively. However, in surge motion the reduction is less significant, and in the case of the ball type depressor, the surge of the towed fish tends to be slightly higher than that of the depressor, (Figures 6.13 to 6.16).

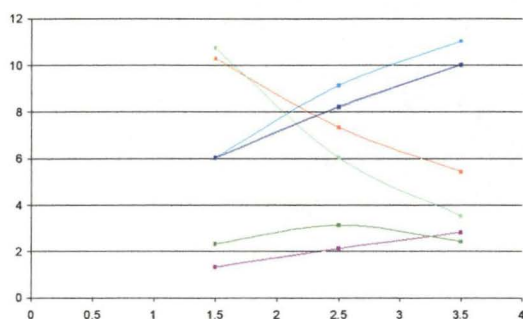
In the case of the fish type depressor (Figures 6.8 to 6.12), a marked improvement is noted in the towed fish pitch amplitude at the higher excitation frequencies, over that of the depressor. However, at the lower frequencies they tend to be closer. When considering the pitch amplitude of the towed fish in isolation, the response degrades slightly as the frequency increases, and then improves at the higher frequency end. This change is not overly significant, and as shown later is dependent on the length of the secondary cable and the location of the junction.



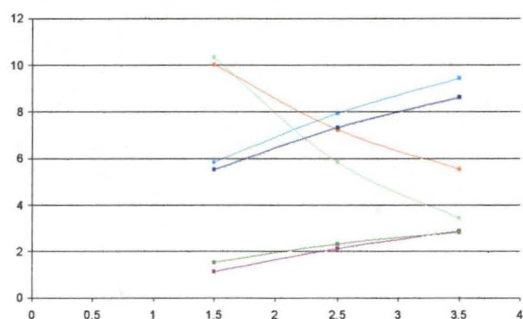
**Depressor and Towed Fish Response
for Configurations C11 to C13
Figure 6.8**



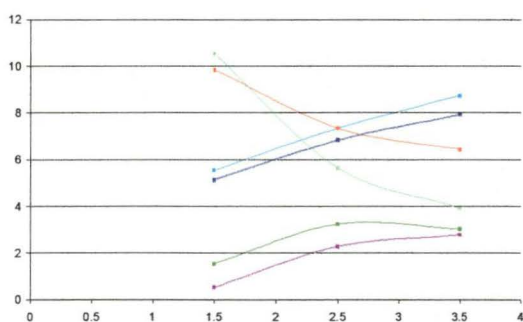
**Depressor and Towed Fish Response
for Configurations C21 to C23
Figure 6.9**



**Depressor and Towed Fish Response
for Configurations C31 to C33
Figure 6.10**



**Depressor and Towed Fish Response
for Configurations B31 to B33
Figure 6.11**



**Depressor and Towed Fish Response
for Configurations A31 to A33
Figure 6.12**

Key to Graphs

- depressor surge (cm)
 - depressor heave (cm)
 - depressor pitch (degrees)
 - fish surge (cm)
 - fish heave (cm)
 - fish pitch (degrees)
- X-axis** period (seconds)

Note:

- Figures 6.8 to 6.10 give an **increasing change** in the **Z excitation amplitude** for a tow configuration with a fish type depressor
- Figures 6.10 to 6.12 give a **decreasing change** in the **X excitation amplitude** for a tow configuration with a fish type depressor

Response to Varying Excitation Amplitudes

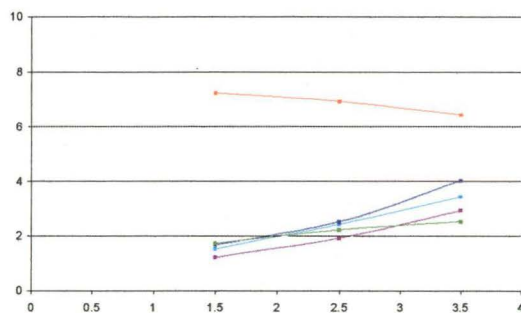
Let us first look at the response due to an increase in the X-direction excitation amplitude. Such an increase for the tow configuration with a depressor fish (Figures 6.12, 6.11 and 6.10), results in an expected and noticeable increase in the surge motions of the depressor and the towed fish. This increase tends to be greater at the lower frequencies of excitation, while the overall increase is fairly similar for the two bodies, (possibly slightly greater for the depressor).

There is a very small reduction in the heave amplitude of the depressor and the towed fish. The pitch amplitudes of the two bodies undergo a slight reduction at low frequencies, but increase in the higher frequency range. These changes are slightly larger for the towed fish, which indicates that the increase in surge excitation does marginally influence the other motions of the towed fish.

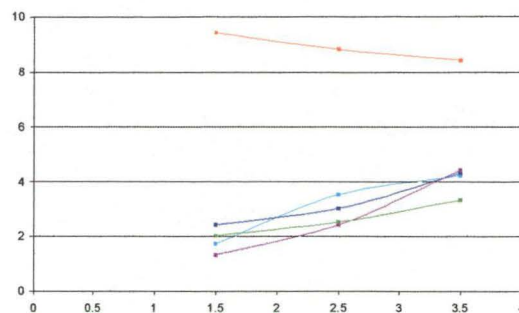
In the configuration with the ball type depressor (Figures 6.16, 6.15 to 6.14), the surge of the depressor tends to be low and relatively similar to the X-direction excitation amplitude. As the latter increases, the surge amplitude of the depressor and towed fish tends to increase, especially at the lower frequencies. The surge of the towed fish is also seen to be slightly higher than that of the depressor.

The heave, on the other hand, is much lower for the towed fish, due to the decoupling effect of the two-part tow. The depressor heave decreases slightly as the X-direction excitation increases, especially at the lower frequency end. The effect due to the increase in the X-direction excitation amplitude on the heave and pitch amplitudes of the towed fish is not easily identifiable, as these amplitudes fluctuate and tend to undergo very little change at the higher frequencies.

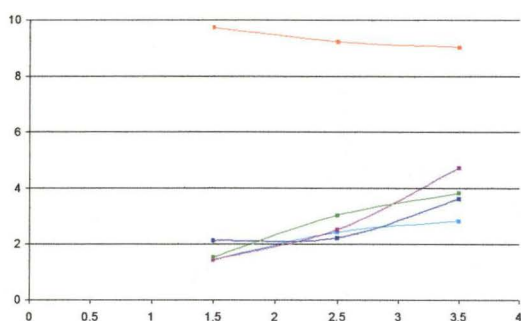
Now let us look at the response due to an increase in the Z-direction excitation amplitude. As this increases, the depressor and towed fish in the tow configuration with a depressor fish (Figures 6.8 to 6.10), both undergo increases in the surge amplitude, especially at the lower frequencies. The heave amplitude of the depressor increases significantly, especially at the higher frequencies. However, for the towed fish its increase is marginal, with very little difference at the higher frequencies. The pitch amplitude increases for both the depressor and towed fish, although the increase is much smaller for the latter and is not dependent on the frequency. However, for the depressor, the increase is much higher at the higher excitation frequencies.



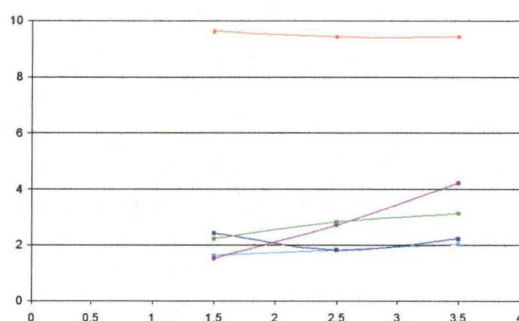
**Depressor and Towed Fish Response
for Configurations I21 to I23
Figure 6.13**



**Depressor and Towed Fish Response
for Configurations I31 to I33
Figure 6.14**



**Depressor and Towed Fish Response
for Configurations H31 to H33
Figure 6.15**



**Depressor and Towed Fish Response
for Configurations G31 to G33
Figure 6.16**

Key to Graphs

■	depressor surge (cm)	■	fish surge (cm)
■	depressor heave (cm)	■	fish heave (cm)
■	depressor pitch (degrees)	■	fish pitch (degrees)
X-axis period (seconds)			

Note:

- Figures 6.13 to 6.14 give an **increasing change** in the **Z excitation amplitude** for a tow configuration with a ball type depressor
- Figures 6.14 to 6.16 give a **decreasing change** in the **X excitation amplitude** for a tow configuration with a ball type depressor

For the tow configuration with a ball type depressor (Figures 6.13 and 6.14), when the Z-direction excitation amplitude is increased, a slight increase occurs in the surge amplitude of the depressor, while its heave amplitude increases significantly across the frequency range. The towed fish on the other hand has a slight increase in surge across the frequency range, (very similar to that of the depressor), while the heave and

pitch increases slightly at the lower frequencies and remains virtually constant at the higher frequencies.

Thus, for the tow configurations using either type of depressor, an increase in the X-direction excitation amplitude results in the surge amplitude of both the depressor and the towed fish increasing. The increase in the tow fish heave is kept to a minimum due to the decoupling effect, although its pitch can marginally increase. An increase in the Z-direction excitation amplitude results in the depressor following suit in both tow configurations. However, for the towed fish the surge motion increases, thus keeping the changes in the heave and pitch amplitudes small, *i.e.* the decoupling effect improves the latter two motions.

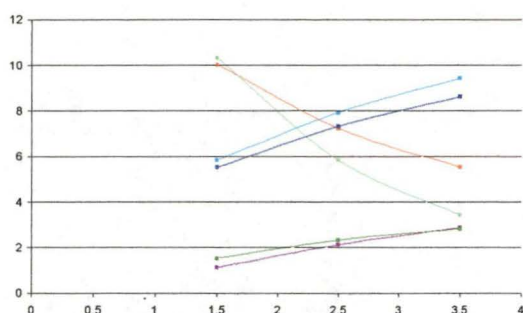
Response to Varying the Location of the Junction along the Primary Cable

Figures 6.17 and 6.18 represent the motion of two-part tow configurations utilising a depressor fish, with the former having the junction along the primary cable, while the latter has the secondary cable directly fitted to the depressor. Figures 6.19 and 6.20 deals with a similar pair, but utilising a ball type depressor.

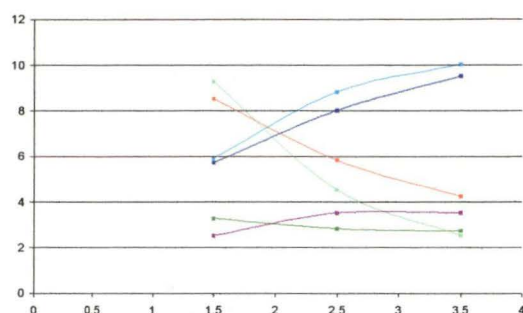
First consider the tow configuration with the depressor fish, (Figures 6.17 and 6.18). At higher excitation frequencies, the surge amplitudes of the depressor and towed fish undergo very little change due to the variation of the junction along the primary cable. At lower frequencies, the surge increases as the junction moves closer to the depressor. The depressor tends to have a slightly larger surge displacement than the towed fish and this gap tends to increase as the junction is moved away from the depressor.

The heave and pitch amplitudes of the depressor fish increase when the junction is moved higher along the primary cable. However, the same displacement amplitudes for the towed fish reduce as the junction moves away (*i.e.* above) from the depressor.

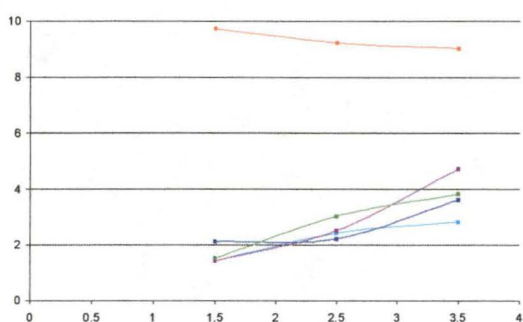
Figures 6.19 and 6.20 compare the response of varying the location of the junction on a two-part tow configuration utilising a ball type depressor. At low excitation frequencies, the location of the junction has little effect on the surge amplitudes of the depressor and towed fish. However, at higher frequencies, they are slightly lower when the secondary cable is secured directly to the depressor, although these changes are so small that they may not be significant.



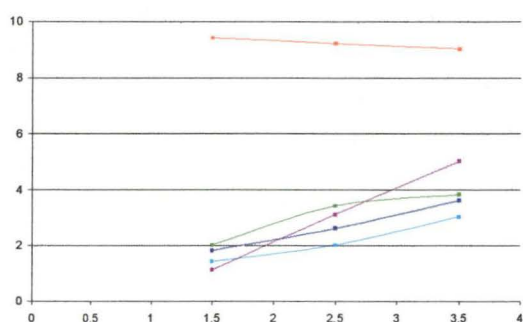
**Depressor and Towed Fish Response
for Configurations B31 to B33
Figure 6.17**



**Depressor and Towed Fish Response
for Configurations E31 to E33
Figure 6.18**



**Depressor and Towed Fish Response
for Configurations H31 to H33
Figure 6.19**



**Depressor and Towed Fish Response
for Configurations K31 to K33
Figure 6.20**

Key to Graphs

■	depressor surge (cm)	■	fish surge (cm)
■	depressor heave (cm)	■	fish heave (cm)
■	depressor pitch (degrees)	■	fish pitch (degrees)
X-axis period (seconds)			

The heave motion of the depressor displays very little change with varying location of the junction along the primary cable. However, the heave and pitch amplitudes of the towed fish are less when the junction is moved away (*i.e.* above) the depressor at low to medium frequencies of excitation, although a slight reversal occurs at high excitation frequencies.

Thus, considering the two depressors, from Figures 6.17 and 6.18 (*i.e.* for the depressor fish), it is evident that the depressor response improves when the secondary cable is directly fitted to it. This may be due to the tension of the secondary cable

acting to damp the motion of the depressor. With the ball type depressor, very little change occurs in the depressor motion, again as its weight dominates the motion.

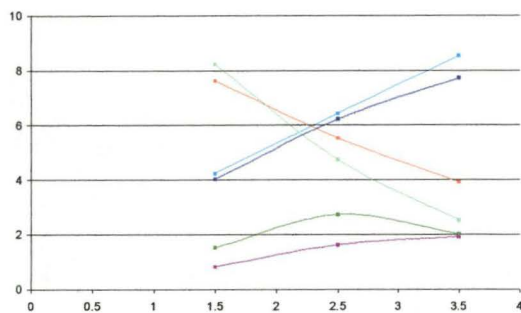
For the towed fish in the configuration utilising the depressor fish, the motion is better when the junction is located a distance above the depressor, although this improvement is extremely small in surge. With a ball type depressor, again the towed fish shows better response with the junction located above the depressor, except at high excitation frequencies. These findings are in line with those obtained from the computer simulation given in sub-section 4.4 of Chapter 4. Note: if the junction is too close to the surface, the surface excitation will adversely effect the junction and hence the towed fish, thus negating the decoupling effect of the two-part tow.

Response to Varying the Length of the Secondary Cable

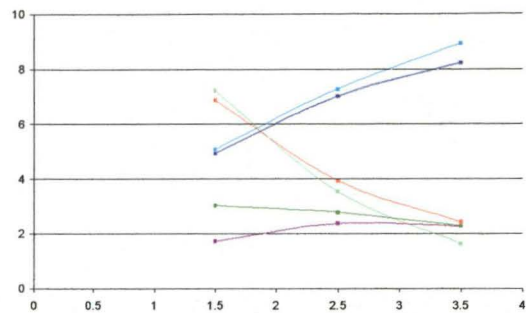
Let us now look at the effect of varying the length of the secondary cable has on the motions of the bodies. Figures 6.21 to 6.26 give three pairs of tow configurations, with the length of the secondary cable reduced from 0.8 metres to 0.5 metres in the second of each pair. Figures 6.21 to 6.24 are two-part tow configurations utilising a depressor fish, with the last two having the secondary cable attached directly to the depressor fish. Figures 6.25 and 6.26 use a ball type depressor.

For the situation with the junction above the depressor (Figures 6.21 and 6.22), it is seen that a reduction in the secondary cable length results in a slight increase in the depressor surge, (especially at the higher frequencies of excitation), while its heave and pitch amplitudes tend to reduce. From Figures 6.23 and 6.24 (*i.e.* with the secondary cable attached directly to the depressor fish), the change in the depressor surge amplitude reduces significantly, while the heave and pitch amplitudes increase marginally, especially at the higher frequencies. This is due to the coupling effect of the depressor fish and the towed fish being inversely proportional to the length of the secondary cable.

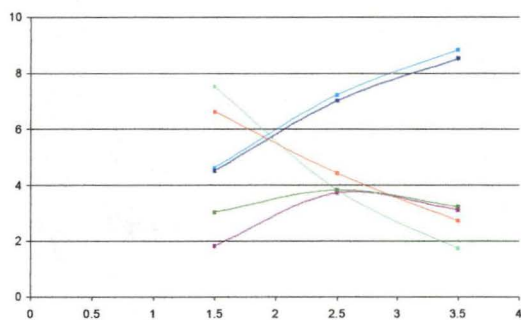
Considering the towed fish, all three amplitudes increase as the secondary cable is shortened, especially at high frequencies. The increase in the surge amplitude is relatively small, however the increase in heave and pitch amplitudes is significant. When the secondary cable is short, the pitch tends to increase slightly with the excitation frequency. By comparing Figures 6.23 and 6.24 it is seen that the dependence of the towed fish amplitudes on the secondary cable length reduces, when the secondary cable is fitted closer to the depressor.



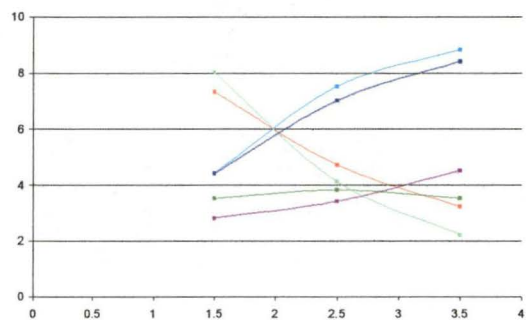
**Depressor and Towed Fish Response
for Configurations C21 to C23
Figure 6.21**



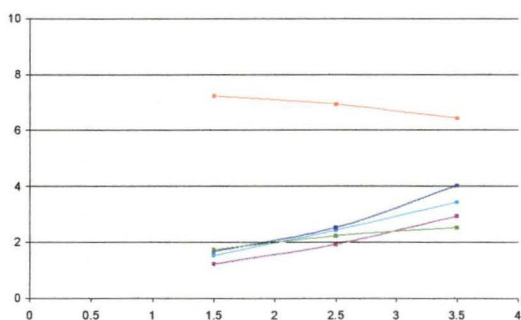
**Depressor and Towed Fish Response
for Configurations X21 to X23
Figure 6.22**



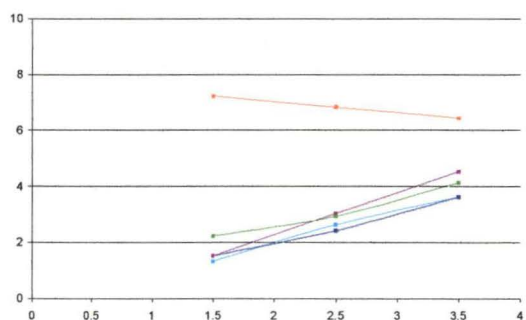
**Depressor and Towed Fish Response
for Configurations F21 to F23
Figure 6.23**



**Depressor and Towed Fish Response
for Configurations T21 to T23
Figure 6.24**



**Depressor and Towed Fish Response
for Configurations I21 to I23
Figure 6.25**



**Depressor and Towed Fish Response
for Configurations AH21 to AH23
Figure 6.26**

Key to Graphs

- | | |
|-----------------------------|------------------------|
| ■ depressor surge (cm) | ■ fish surge (cm) |
| ■ depressor heave (cm) | ■ fish heave (cm) |
| ■ depressor pitch (degrees) | ■ fish pitch (degrees) |
| X-axis period (seconds) | |

Figures 6.25 and 6.26 deals with the same scenario, but utilising a ball type depressor. Very little effect occurs to the motions of the depressor due to shortening the length of the secondary cable, except for a small increase in surge and a small decrease in heave at the lower frequencies. The lack of any significant difference is again due to the weight dominating its motion. Very little effect on these results is noticed by varying the location of the junction along the primary cable length. For the towed fish, a very small increase is noted in the surge amplitude as the length of the secondary cable is reduced. However, the heave and pitch increase significantly, especially at the lower frequencies of excitation.

In summary, for both types of depressors, the towed fish amplitudes tend to increase as the secondary cable is shortened. This is due to the increased coupling effect of the shorter cable. Although this has very little effect on the ball type depressor, the performance of the fish type depressor improves in a tow-part tow configuration having the junction above the depressor. The reason may be attributed to the effect of the secondary cable tension acting on the depressor fish.

Response to the use of Fish Type and Ball Type Depressors

Figures 6.17 to 6.20 can again be used to compare the response of the towed bodies, due to the utilisation of the fish type and ball type depressors in the two-part tow configuration. It is seen that the depressor surge amplitude is much lower for the ball type. Although the depressor surge amplitude drops in both types as the frequency of excitation increases, the drop is much lower in the ball type, since its motion is far less dependent on the excitation frequency. This is due to the dominant weight effect on its motion.

The heave amplitudes of both types of depressors increase with the excitation frequency. However, this increase is prominent and greater with the fish type depressor, whereas for the ball type depressor the heave amplitude, like the surge amplitude, tends to be “flatter”. At low frequencies of excitation, the heave is a lot lower for the fish type depressor. However, as the frequency increases they tend to equalise, and may even swap over at very high frequencies.

For the towed fish, the surge with a ball type depressor is lower, since the ball itself has very low surge amplitude. In both cases, the surge amplitude will fall as the frequency increases, however the surge is “flatter” with the ball type depressor. On the other hand, the heave and pitch amplitudes of the towed fish are “flatter” with the

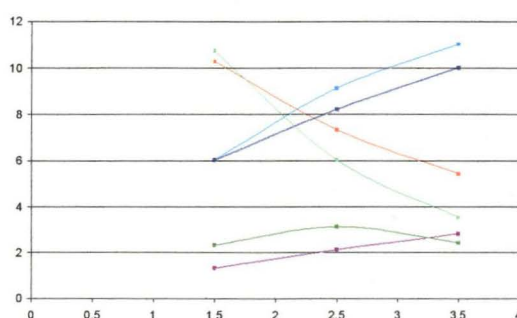
fish type depressor. In the latter configuration, these motions are significantly less when the junction is moved away (*i.e.* above) the depressor. In both cases, the heave and pitch amplitudes of the towed fish drop as the frequency increases. With the ball type depressor, these amplitudes are seen to be more dependent on the frequency, especially when the secondary cable is directly attached to the depressor.

At lower frequencies, the depressor fish gives better performance, while the ball type depressor seems to be better at the other end of the frequency spectrum. The latter also is better in damping out large X-direction excitation.

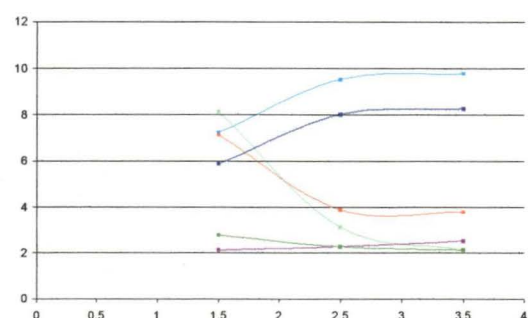
Response to the use of a Drogue

The last test in the vertical direction was to identify the effect of a drogue fitted to the aft end of the towed fish. Figures 6.27 to 6.30 describe the motion of a two-part tow utilising a depressor fish and a drogue. The first is without a drogue, while the next three have a drogue fitted to the towed fish via a cable of length 0.3, 0.4, and 0.6 metres respectively. The effect of the drogue is not seen to be of great significance, especially at higher frequencies of excitation. However, at the lower frequencies a slight improvement is noted in the towed fish heave and pitch amplitudes. At higher frequencies, the drogue can adversely effect these motions marginally.

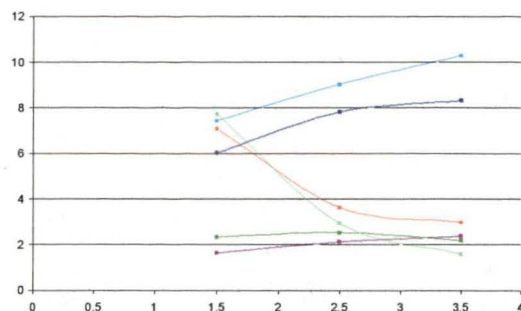
Figures 6.31 to 6.33 describe the motion for a similar tow configuration, however utilising a ball type depressor. The first is without a drogue, while the next two have a drogue fitted to the towed fish via a cable of length 0.3 and 0.6 metres respectively. In this case there is a slight improvement in the surge amplitude of the towed fish at higher frequencies of excitation. However, the heave and pitch amplitudes tend to deteriorate slightly.



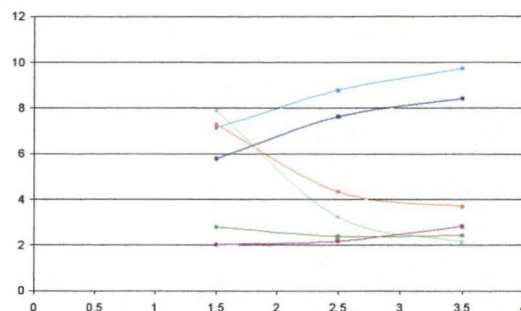
**Depressor and Towed Fish Response
for Configurations C31 to C33
Figure 6.27**



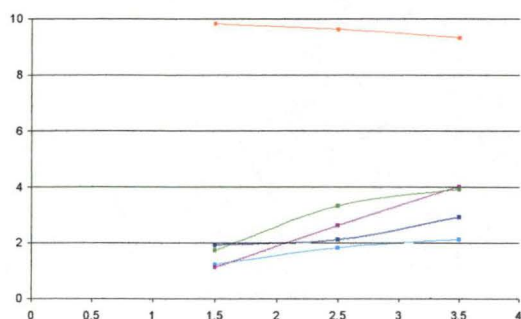
**Depressor and Towed Fish Response
for Configurations AA62 to AA64
Figure 6.28**



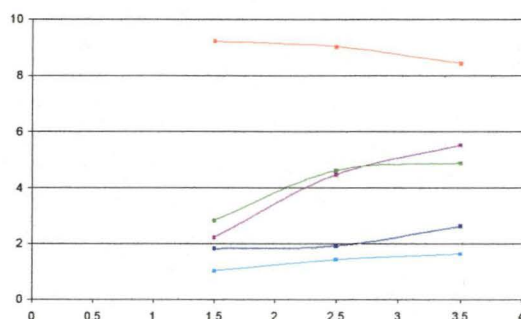
**Depressor and Towed Fish Response
for Configurations AA42 to AA44
Figure 6.29**



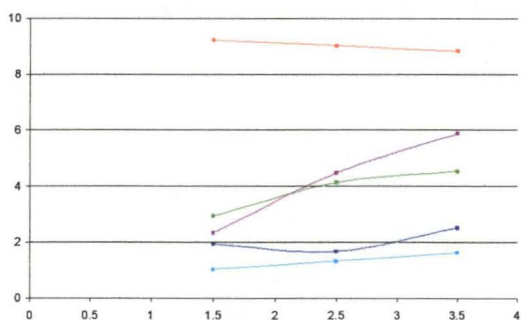
**Depressor and Towed Fish Response
for Configurations AB42 to AB44
Figure 6.30**



**Depressor and Towed Fish Response
for Configurations J31 to J33
Figure 6.31**



**Depressor and Towed Fish Response
for Configurations AC22 to AC24
Figure 6.32**



**Depressor and Towed Fish Response
for Configurations AD22 to AD24
Figure 6.33**

Key to Graphs

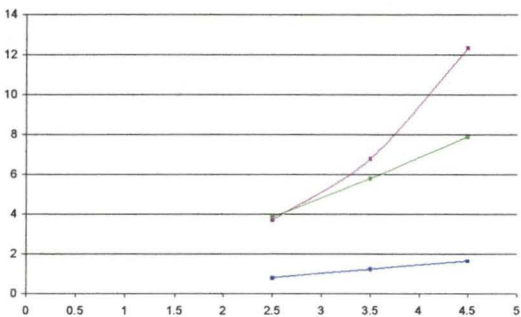
- depressor surge (cm)
- depressor heave (cm)
- depressor pitch (degrees)
- fish surge (cm)
- fish heave (cm)
- fish pitch (degrees)
- X-axis** period (seconds)

Thus, the use of a drogue seems to adversely effect the motion with a ball type depressor, and provides little improvement with a fish type depressor at lower excitation frequencies. Therefore, it may not warrant its use to improve the vertical response of a two-part tow configuration.

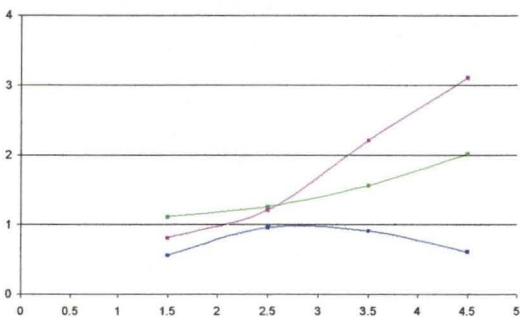
6.3.2 Response of the Two-Part Tow due to Horizontal Excitation

Let us now investigate the behaviour of the two-part tow undergoing horizontal excitation, *i.e.* excitation in the Y-direction. Only the motion of the towed fish was recorded, as the latter obstructed the view of the depressor, (see Figure 6.6). Therefore, a number of equivalent single part tows were carried out to quantify the improvement due to the two-part tow configuration.

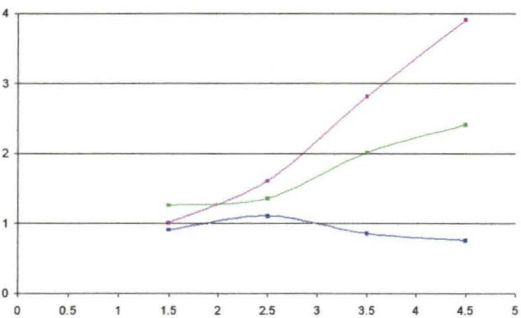
Figures 6.34, 6.36, and 6.37 give the response of a single part tow and two equivalent two-part tows respectively. The first of the two-part tows utilises a depressor fish, while the second utilises a ball type depressor.



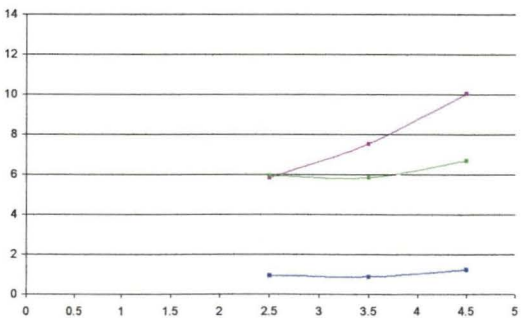
Towed Fish Response for Configurations YY21 to YY23
Figure 6.34



Towed Fish Response for Configurations YA11 to YA14
Figure 6.35



Towed Fish Response for Configurations YA21 to YA24
Figure 6.36



Towed Fish Response for Configurations WA21 to WA23
Figure 6.37

Key to Graphs

- fish surge (cm)
- fish yaw (degrees)
- fish sway (cm)
- X-axis period (seconds)

On inspecting these figures, it is seen that the response of the towed fish is substantially better with the two-part tow, especially using the depressor fish. No significant change is noted for the surge motion, except for a slight improvement at the low frequency end. For the two-part tow configuration with a depressor fish, the improvement in the sway and yaw amplitudes are significant.

For the ball type depressor, the improvements are mainly in the lower excitation frequency region, while in some cases, the single part tow may prove better at higher frequencies. Overall the inherent decoupling effect of the two-part tow configuration greatly improves the response of the towed vehicle under the influence of horizontal excitation.

Response to Varying Excitation Frequency

Let us now look at the effect of varying the frequency of the Y-direction excitation amplitude. Figures 6.35 to 6.37 give the response of the two-part tow configuration as a function of the Y-direction excitation frequency, with the first two dealing with a depressor fish and the latter utilising a ball type depressor.

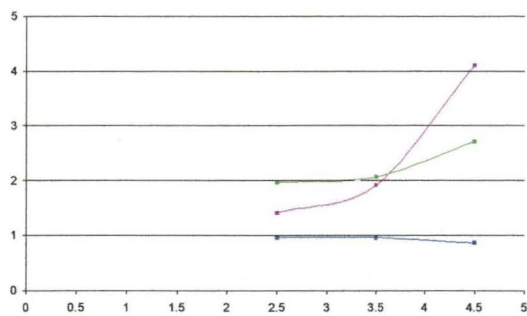
On inspecting Figures 6.35 and 6.36 for the tow utilising a depressor fish, it is seen that an increase in excitation frequency reduces the sway and yaw amplitudes of the towed fish, although the rate of reduction reduces as the frequency increases. The surge on the other hand remains reasonably “flat”, increasing a little as the frequency increases and then dropping off.

In Figure 6.37 for the tow utilising a ball type depressor, an increase in the excitation frequency reduces the sway amplitude of the towed fish. In this case, the rate of reduction dramatically increases at higher frequencies, *i.e.* opposite to that of the fish type depressor. The yaw amplitude tends to be “flat” over the low to medium frequency range, with only a marginal drop as the frequency increases. However, at high frequencies, it follows the heave motion and drops off significantly.

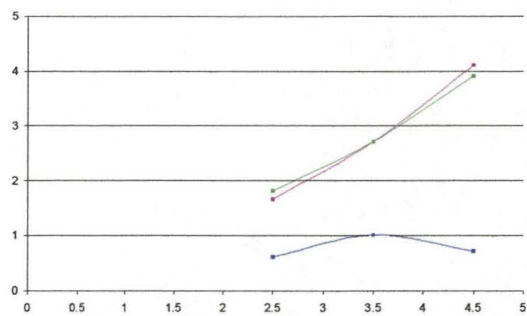
Response to Varying Y-Direction Excitation Amplitude

The response due to an increase in the Y-direction excitation amplitude for the tow configuration with a depressor fish is given in Figures 6.35 and 6.36. As expected all three displacement amplitudes, (*i.e.* surge, sway, and yaw), increase as the Y-direction excitation increases.

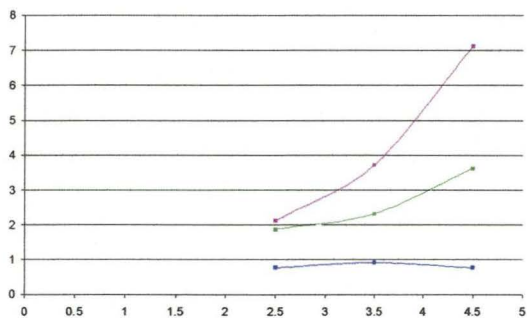
Response to Varying the Location of the Junction along the Primary Cable



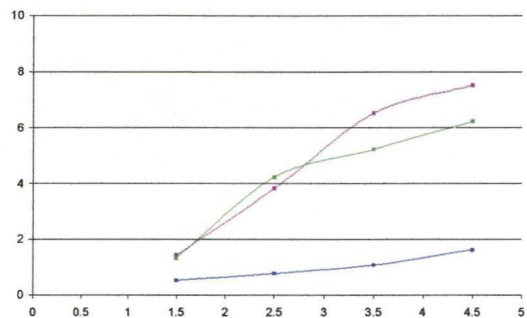
Towed Fish Response for Configurations YD21 to YD23
Figure 6.38



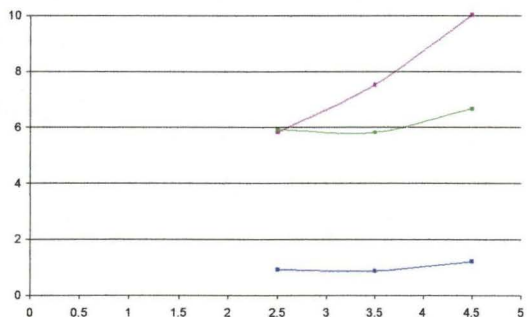
Towed Fish Response for Configurations YG21 to YG23
Figure 6.39



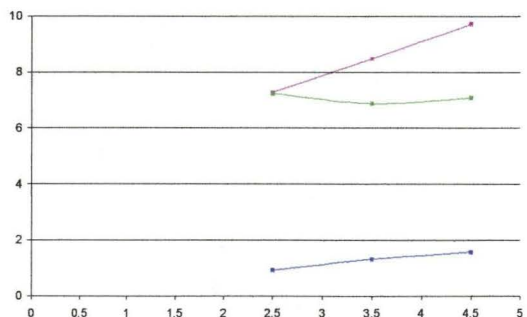
Towed Fish Response for Configurations YC21 to YC23
Figure 6.40



Towed Fish Response for Configurations WC21 to WC24
Figure 6.41



Towed Fish Response for Configurations WA21 to WA23
Figure 6.42



Towed Fish Response for Configurations WB21 to WB24
Figure 6.43

Key to Graphs

- fish surge (cm)
- fish yaw (degrees)
- fish sway (cm)
- X-axis period (seconds)

Figures 6.38 to 6.40 represent the motion of two-part tow configurations utilising a depressor fish, with the distance from the depressor to the junction being 0.5, 0.25, and 0.0 meters respectively. Figures 6.41 and 6.43 deal with a similar set, but utilising a ball type depressor.

For the configuration having the depressor fish (Figures 6.38 to 6.40), the “flat” surge curve of the towed fish tends to remain unchanged with the relocation of the junction, except for a possible slight deterioration at the high frequency end. The sway tends to increase as the junction moves closer to the depressor, especially when the secondary cable is fitted directly to the depressor, and at low frequencies. The yaw amplitude also shows an increase as the junction moves closer to the depressor.

Now considering Figures 6.41 and 6.43 for the configuration with a ball type depressor, again the surge tends to remain “flat” with very little change. The sway and yaw amplitudes however, tend to increase significantly across the frequency range.

Thus, the movement of the junction closer to the depressor in both tow configurations tends to adversely effect the sway and yaw motions of the towed fish. Again as in the vertical excitation situation, care must be taken to prevent the junction being too close to the surface, as it will negate the decoupling effect of the two-part tow.

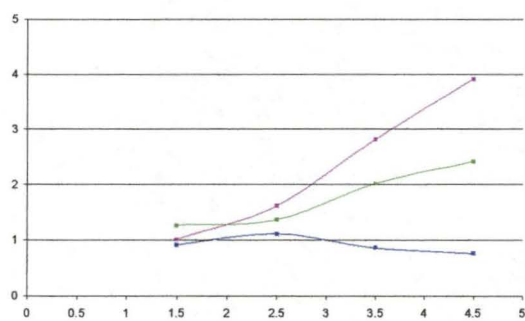
Response to Varying the Length of the Secondary Cable

Let us now look at the effect on the motion of the bodies, due to the varying length of the secondary cable. Figures 6.44 to 6.47 represent the effect of reducing the length of the secondary cable from 0.8 metres to 0.5 metres, with the first two utilising a depressor fish, and the latter two utilising a ball type depressor.

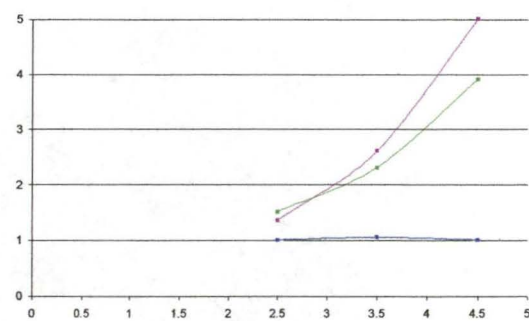
Considering first the configuration with the depressor fish, it is seen that the towed fish surge amplitude increases slightly at low frequencies, but possibly reverses at the higher frequencies. The sway on the other hand tends to increase significantly at low frequencies, but tends to remain unchanged or even possibly swap over at the higher frequencies. The yaw amplitude tends to increase slightly across the frequency range.

Now considering the configuration with the ball type depressor (Figures 6.46 and 6.47), as the secondary cable shortens the tow fish surge remains approximately constant, possibly with a slight increase at the lower frequency range. The sway and

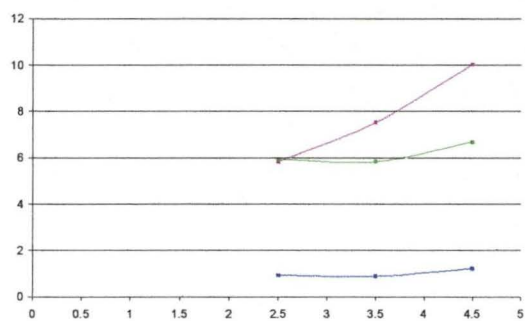
yaw amplitudes tend to increase significantly at the lower frequencies but equalise at the higher frequencies.



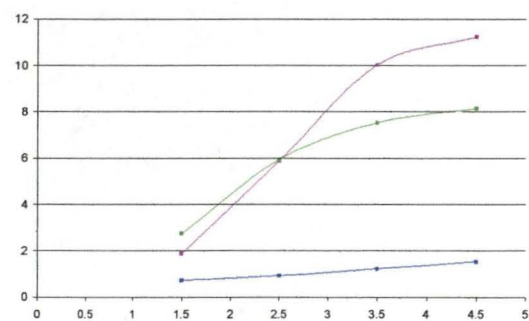
Towed Fish Response for Configurations YA21 to YA24
Figure 6.44



Towed Fish Response for Configurations YB21 to YB23
Figure 6.45



Towed Fish Response for Configurations WA21 to WA23
Figure 6.46



Towed Fish Response for Configurations WD21 to WD24
Figure 6.47

Key to Graphs

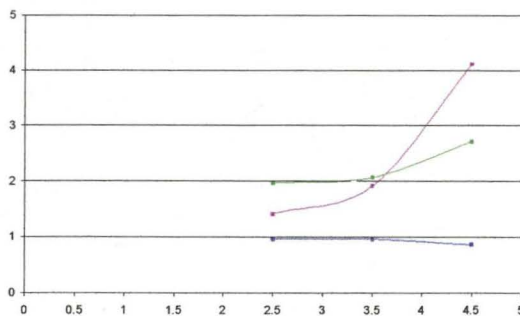
- | | |
|-------------------|-------------------------|
| ■ fish surge (cm) | ■ fish yaw (degrees) |
| ■ fish sway (cm) | X-axis period (seconds) |

Thus, in both configurations as expected the shorter cable adversely effects the sway and yaw motions, especially at the lower frequencies. The improvements in the higher frequencies are relatively insignificant.

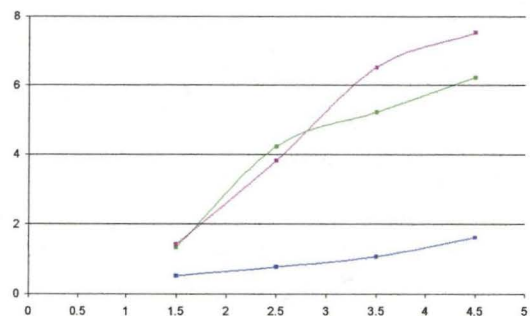
Response to the use of Fish Type and Ball Type Depressors

Figures 6.48 and 6.49 compare the motion of the towed bodies, due to the utilisation of the fish type and ball type depressors respectively. The surge amplitude varies little between the two configurations, although the depressor fish configuration does

seem to have a slight advantage at the lower frequency end. However, when considering the sway and yaw amplitudes, the improvement in the response when using a depressor fish is highly significant, although the difference reduces at the higher frequencies.



Towed Fish Response for Configurations YD21 to YD23
Figure 6.48



Towed Fish Response for Configurations WC21 to WC24
Figure 6.49

Key to Graphs

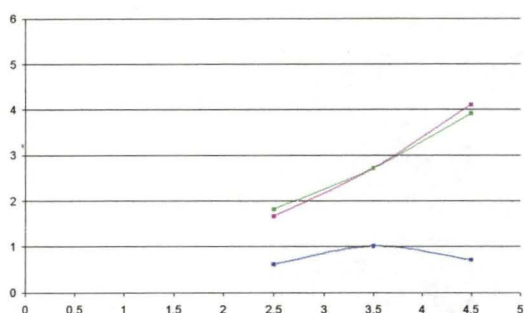
- fish surge (cm)
- fish sway (cm)
- fish yaw (degrees)
- X-axis period (seconds)

The reason for the higher towed fish response amplitude with the ball type depressor, is the larger lateral motion imparted to the depressor. The momentum of the ball tends to swing the depressor from side to side, with very little damping due to the low hydrodynamic forces present on the ball. This in turn causes the towed fish to accelerate in the lateral direction. The depressor fish on the other hand creates larger hydrodynamic forces that tend to damp out the lateral motions.

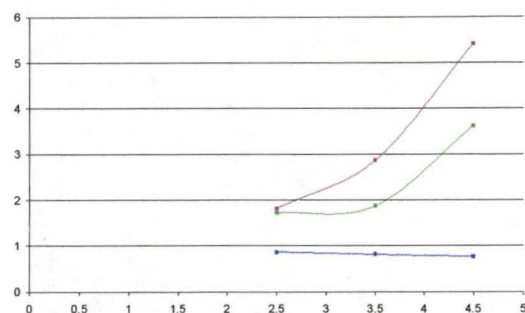
Therefore, it can be concluded that although the difference in the vertical movements are not significant, (see sub-section 6.3.1), the fish type depressor has a clear advantage when it comes to the horizontal excitation.

Response to the use of a Drogue

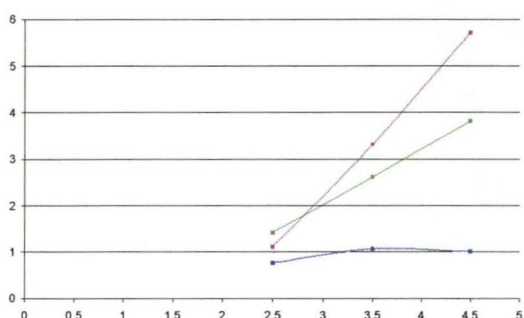
Finally let us look at the effect on the horizontal displacements due to the fitting of a drogue to the aft end of the towed fish. Figures 6.50 to 6.52 describe the motion of two-part tow configurations fitted with a drogue and utilising a depressor fish, while Figures 6.53 and 6.55 utilise a ball type depressor. Each set consists of a two-part tow without a drogue, followed by two configurations, each having a drogue fitted using a 0.3 and 0.5 metre cable respectively.



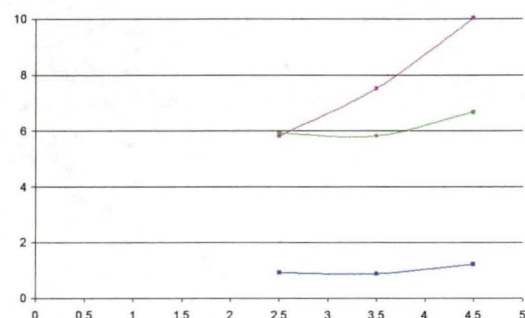
**Towed Fish Response for
Configurations YG21 to YG23
Figure 6.50**



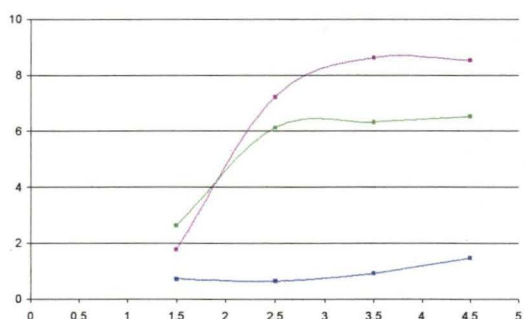
**Towed Fish Response for
Configurations YE21 to YE23
Figure 6.51**



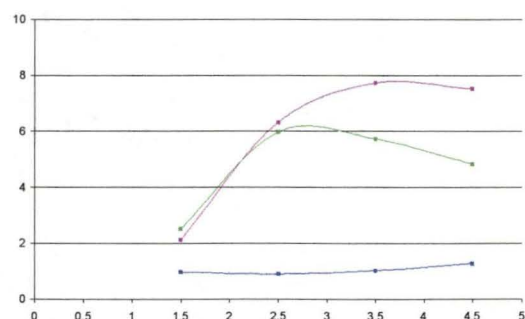
**Towed Fish Response for
Configurations YF21 to YF23
Figure 6.52**



**Towed Fish Response for
Configurations WA21 to WA23
Figure 6.53**



**Towed Fish Response for
Configurations WE21 to WE24
Figure 6.54**



**Towed Fish Response for
Configurations WF21 to WF24
Figure 6.55**

Key to Graphs

■ fish surge (cm)
■ fish sway (cm)

■ fish yaw (degrees)
X-axis period (seconds)

For the configuration utilising the depressor fish, very little change is noticed in the surge amplitude. The sway tends to increase at lower frequencies, but remains closer at the higher frequency end, while the yaw amplitude marginally reduces. However, none of the changes are significant. With the ball type depressor, the surge again remains approximately constant. The sway and yaw amplitudes tend to reduce slightly at the lower frequency range and remain relatively unchanged at the other end of the frequency spectrum.

As with the vertical excitation, the drogue has very little effect on the response of the towed fish.

6.3.3 Conclusion from the Scaled Model Trial Results

From the above analysis of the vertical and horizontal motions, it is clear that the two-part tow offers a much more stable platform, due to the inherent decoupling effect of the configuration. In general, as the excitation frequency increases, the response of the towed fish improves, although the same is not true for the depressor. Although there is little difference in the vertical motions of the towed fish due to the fish and ball type depressors, a significant improvement is gained by utilising the former in the horizontal direction. However, the ball type depressor is more suitable to dampen out surge excitation.

The two-part tow is able to absorb heave excitation, with a slight increase in the tow fish surge amplitude. An increase in surge excitation is however transmitted to the towed fish, although its effect on the angular motion is restricted. In the case of lateral (sway) excitation, a slight increase occurs in the sway and yaw amplitudes of the towed fish, although the rate of increase is reduced via the two-part tow configuration.

It was also noted that locating the junction a distance above the depressor improves the response, although it should not be too close to the surface. Directly connecting the secondary cable to the depressor does improve the response of the depressor, but adversely affects the motion of the towed fish. Although increasing the length of the secondary cable improves the response of the towed fish, beyond a given length there would be little, if any, improvement.

The use of a drogue seems to only marginally improve the low frequency response of the two-part tow, and in some cases adversely affects the response at higher

frequencies, albeit in a relatively small way. The marginal improvement and the possible deterioration of the response may not warrant the use of such devices, especially given the difficulties in deploying and recovering a two-part tow with a drogue from a “cluttered” after deck of a small surface vessel, typical of those used for inshore and coastal operations.

6.4 Full Scale Trials

As stated in Chapter 1, the project was initiated due to adverse results from towed sonar operations of the Royal Australian Navy (RAN), due to the effect of surface vessel motion. The tow in question was a conventional tow arrangement as shown in Figure 1.3, towing a Klein side scan sonar vehicle.



Full Scale Trial Single Part Tow
Figure 6.56



Full Scale Trial Two-Part Tow
Figure 6.57



Aft Deck of Deploying Vessel
Figure 6.58



Deploying of Two-Part Tow
Figure 6.59

In order to investigate the behaviour of the towed fish, the Defence Science and Technology Organisation (DSTO), carried-out a number full-scale trials using the conventional tow arrangement in 1993. The objective was to document the behaviour of the tow fish under usual tow conditions, and investigate the effects of varying parameters of the tow configuration. These included the change of the tow point location and the inclusion of a depressor wing. The results from these trials showed that there was a significant exceedence of the motion limits stipulated for efficient sonar operations. This was verified in the trials conducted jointly by the author and DSTO, as shown later in this sub-section.

In 1994 and 1995, AMC and DSTO conducted further trials with both the conventional and two-part tow configurations in Jervis Bay and Port Phillip Bay. In both cases, DSTO side scan sonar vehicles were deployed from Royal Australian Navy vessels using the relevant onboard gear. The objectives were to compare the two configurations under varying conditions and to investigate the behaviour of the two-part tow by varying the tow configuration parameters. Figures 6.56 and 6.57 show the single and two-part tow arrangements used in the trials. Figures 6.58 and 6.59 show the surface vessel and the deploying of the two-part tow.

Discussions with the sonar operators established the limiting parameters given in Table 6.1. Note: although the operational roll and heave rate limits were higher than those given in the table, they were set to be compatible to the other rate limits.

Motion	Rate Limits
Surge	1 m/s
Sway	1 m/s
Heave	1 m/s
Roll	6.28 deg/s
Pitch	6.28 deg/s
Yaw	1.05 deg/s

Full Scale Trail – Limiting Parameters
Table 6.1

The trial in Jervis Bay in 1994 detailed in Table A3 in Appendix A, consisted of 50 single part tow and 22 two-part tow runs. The trial in Port Phillip Bay in 1995 detailed in Table A4, consisted of 25 single part tow and 30 two-part tow runs. In this text, the above two trials will be referred to as ***Trial 1*** and ***Trial 2*** respectively.

From Tables A3 and A4 it is seen that the various tow configurations investigated included:

- change in cable length;
- direction of tow to swell, (i.e. into, against, and across); and
- the use of a depressor wing.

For the two-part tow, the secondary cable length was maintained at 10 metres throughout all runs in both trials.

The information on the motion of the sonar vehicle was obtained via a motion and environment measuring system located in the vehicle. This unit known as TOWfish Data Acquisition System (*TOWDAS*) was supplied by DSTO. It contains three gyros and three accelerometers arranged in the X, Y and Z axis, two inclinometers, depth sensor, internal and external temperature sensors, and leak detectors. The gyros and accelerometers measure rates of change in the six degrees of freedom and the inclinometers measure static pitch and roll. Data was acquired at a rate of 50 samples per second on each of the gyros and accelerometers and 2 samples per second on each of the other sensors. These were transmitted to an interface controller located on the towing vessel, which displayed the system status on a series of indicators and transmitted the data to a computer for data display and storage. The surface tow point cable tension was also recorded via a load cell.

6.4.1 Full Scale Trial Results

The recorded files were processed using dedicated computer programs to convert them into text files and to analyse the data. In order to remove any high frequency noise, the data was filtered through a 0.1 to 25 Hz window. The linear motions, *i.e.* surge, sway, and heave, which were recorded as accelerations, were then integrated to give the respective rates, *i.e.* in metres per second (m/s). The processed data was then compared against the stipulated rate limits using a computer program, which provided the following:

- average deviation and standard deviation of the absolute rates of the six motions;

- percentages for each of the six rates exceeding the above stipulated limits;
- percentage that at least one of the six rates exceeded the relevant stipulated limits; and
- probability density of the six rates.

Tables A5 and A6 in Appendix A summarise the results form Trials 1 and 2 respectively. The average values for all of the runs in each Trial are reproduced in Tables 6.2 and 6.3.

Single Part Tow

Rates	Roll	Pitch	Yaw	Surge	Sway	Heave	Any
Av Deviation	5.85	1.35	1.58	0.17	0.08	0.07	
Av St Dev	0.08	0.14	0.11	0.28	0.24	0.22	
Av % Excess	32.46	1.48	54.43	0.59	0.00	0.00	65.38

Two-Part Tow

Rates	Roll	Pitch	Yaw	Surge	Sway	Heave	Any
Av Deviation	1.84	0.76	0.51	0.09	0.04	0.06	
Av St Dev	0.07	0.10	0.08	0.24	0.26	0.26	
Av % Excess	1.06	0.05	10.04	0.00	0.00	0.00	10.78

Trail 1 – Summary of Results

Table 6.2

Single Part Tow

Rates	Roll	Pitch	Yaw	Surge	Sway	Heave	Any
Av Deviation	7.62	1.17	1.86	0.06	0.09	0.11	
Av St Dev	0.04	0.05	0.04	0.17	0.16	0.14	
Av % Excess	42.45	0.09	59.97	0.00	0.03	0.25	72.27

Two-Part Tow

Rates	Roll	Pitch	Yaw	Surge	Sway	Heave	Any
Av Deviation	3.27	1.07	0.85	0.11	0.09	0.04	
Av St Dev	0.06	0.07	0.04	0.21	0.17	0.16	
Av % Excess	12.86	0.16	30.58	0.02	0.00	0.00	36.80

Trail 2 – Summary of Results

Table 6.3

In both cases it is seen that the two-part tow reduces the wave induced motion of the towed fish in comparison to the equivalent single part tow. In Trial 1 (Table 6.2), it is seen that the percentage exceeding the rate limit of at least one motion is reduced from 65.38 to 10.78, *i.e.* a reduction of 83.51%. In Trail 2 (Table 6.3), this reduces from 72.27 to 36.80 *i.e.* a reduction of 49.08%.

The results also allow for comparison of the tow fish behaviour under varying conditions. Tables A7 to A11 in Appendix A show the comparison between compatible runs in Trial 2, (Note: a similar comparison was carried out on the results of Trial 1, however, it is not reproduced in this text). In these comparisons, only the percentage exceeding at least one rate limit, yaw rate limit, and pitch rate limit were considered. In addition, average deviation, standard deviation, and the percentage significance of any change in comparison to the first run in each group were also obtained, (a group being the number of runs being compared). The latter is the probability against the sample averages of the same distribution taking the same values indicated. The (+/-) sign give the direction of change of the average deviation in comparison to the run. A ± 99 change gives the most significant variation. The runs selected for comparison are usually compatible in all aspects except for the parameter being analysed.

Direction to Swell

Table A7 looks at the effect on the tow fish motion due to the direction of tow to the swell. The table consists of four sections, where the single part and two-part tows were each investigated to compare their behaviour with the change in direction, *i.e.* with the swell (0) versus across the swell (90), and with the swell (0) versus into the swell (180).

In the single part tow, a drop was noted in the percentage exceeding the rate limit of at least one motion, as the direction of motion changed from being with the direction of the swell to across, and then into the swell. There was also a drop in the yaw rates with a corresponding increase in the pitch rate, when the above changes in directions occurred. However, the changes in the rates are insufficient to make a significant difference, which is reinforced by the percentage significance of the changes in each group.

Considering the two-part tow, it was noted that the percentage exceeding the rate limit of at least one motion increased when the direction of motion moved from being with

the swell, with the highest change occurring when travelling across the swell. This trend also held true for the yaw and pitch rates. However the changes were again of low significance.

Change in Cable Length

Table A8 shows the effect due to the change in the primary cable length. In the two-part tow the change in length was limited to the primary cable, as the secondary cable was kept constant at 10 metres. Again the analysis looks at the single and two-part tows separately. In each group, the shorter cable is the first run, and the comparison is carried out against it.

In the single part tow, the increase in cable length resulted in a drop in the percentage exceeding the rate limits of at least one motion. Considering the yaw and pitch rates separately, a decrease was noted in the yaw rate, but an increase occurred in the pitch rate, although the increase is relatively small. The latter however seems to be significant, judging by the percentage significance of the changes in each group.

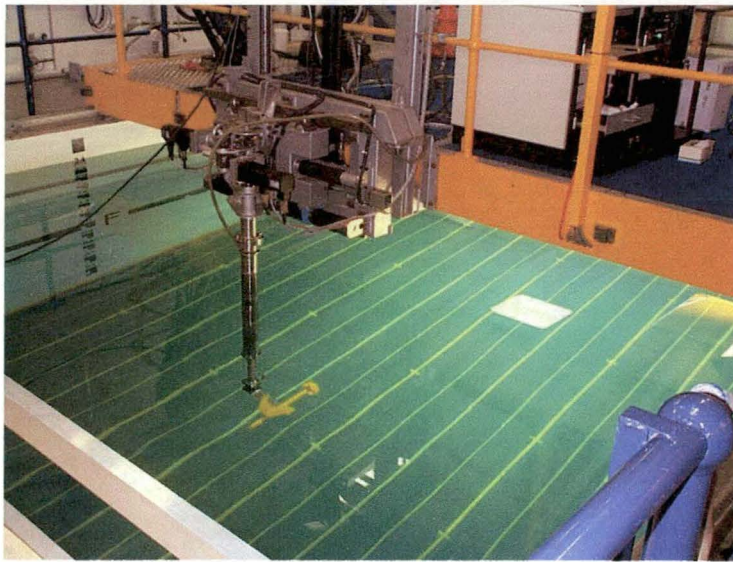
For the two-part tow, the increase in cable length seemed to have very little improvement in the given rates, except for the pitch rate. In the latter the drop is substantial, which seems to be significant given the high percentage significance of the changes in most groups. This may be of importance since it may not be required to have long primary cables when utilising a two-part tow arrangement to decouple the motion of the surface vessel and the towed fish. Obviously, this will assist with the deploying of the tow gear and equipment, especially from small surface vessels such as coastal trawlers. The same however, cannot be said for a single part tow.

Single versus Two-Part Tow

Table A11 compares the two-part tow runs with compatible single part tow runs carried out during the trial. It is clearly evident from these results that the two-part is far less susceptible to external excitation than its equivalent single part tow. Using a compatible two-part tow in preference to a single part tow, results in approximately a 60% reduction in the percentage exceeding the rate limit of at least one motion.

6.5 Scaled Model Hydrodynamic Coefficients

As stated earlier, the scaled model tests were used to validate the computer program. Therefore, it was required to obtain the force and moment hydrodynamic coefficients for the tow fish and depressors. These coefficients were obtained by using the horizontal planar-motion-mechanism (HPMM) fitted with a six degree of freedom load cell and located at the circulating water channel as shown in Figure 6.60. Although ideally the load cell should be placed within the model at its centroid, the relatively small size of the models did not permit this. Therefore, they were attached to the load cell via a specially built low drag connecting bracket.



Use of HPMM to Obtain the Hydrodynamic Coefficients

Figure 6.60

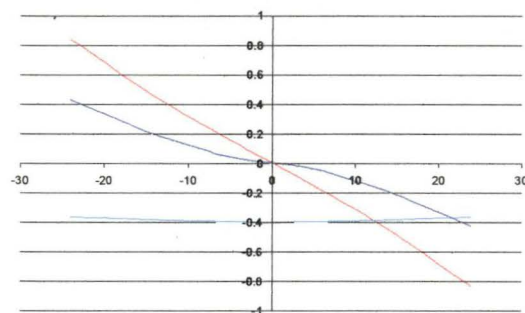
The recorded values from the HPMM were then manipulated to give the forces and moments acting at the tow point of the model. This was essential since the computer model requires these forces and moments at the tow point of each body, (see subsection 3.5 of Chapter 3). The procedure of obtaining the above can be summarised as follows:

- correct the data by removing any zeroing errors;
- subtract the forces and moments generated by the connecting bracket;
- subtract the cross coupling terms due to the offset location of the model with respect to the load cell; and

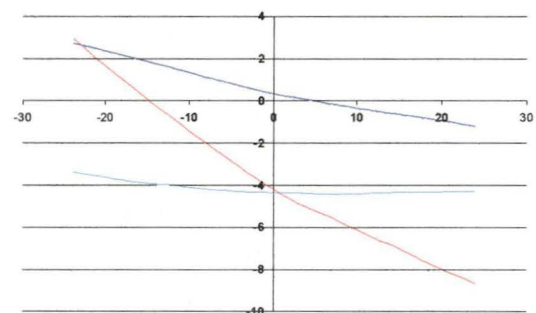
- translate the forces and moments to the tow point of the model.

The forces and moments for the models were obtained for angles of incidence from 0 degrees to 25 degrees. (The angle of incidence being the angle the model's centreline makes with the flow direction). In order to prevent flow interference between the horizontal planar-motion-mechanism and the tow fish, the latter was only rotated in front of the mechanism. The opposite rotation was obtained by swapping over the model in relation to the mechanism.

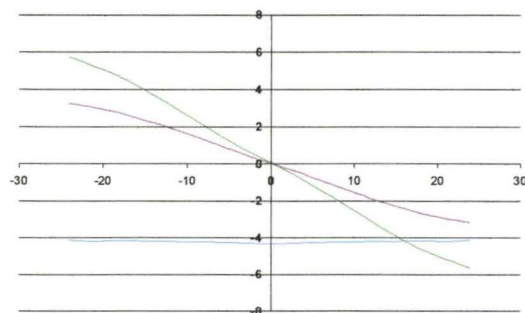
The forces and moments obtained were converted to coefficients by the respective force and moment equations described in sub-section 2.5 of Chapter 2. The coefficients thus obtained for the tow fish and depressor fish were plotted against the angle of incidence as shown in Figures 6.61 to 6.63.



Coefficients for Tow Fish
Figure 6.61



Vertical Coefficients for Depressor
Figure 6.62



Horizontal Coefficients for Depressor
Figure 6.63

Key to Graphs

- surge coefficient
 - heave coefficient
 - sway coefficient
 - pitch coefficient
 - yaw coefficient
- X-axis** angle of incidence (degrees)

Note: For the tow fish, the horizontal and vertical coefficients are similar.

Since the tow fish is symmetrical about the X-Z and X-Y planes, the coefficients shown in Figure 6.61 were used in both the vertical and horizontal directions.

The computer model requires the force and moment coefficient curves to be fed in via a third order polynomial equation, as a function of the tangent of the angle of incidence, (see sub-section 3.5 in Chapter 3). Thus, utilising a curve fitting technique, the curves are represented in the following format.

$$\text{Coefficient} = a + b \tan \varphi + c \tan^2 \varphi + d \tan^3 \varphi \quad (6.1)$$

where

a, b, c, d : constants defining the equation

φ : angle of incidence of the vehicle to the flow direction

The horizontal planar-motion-mechanism is also capable of calculating the hydrodynamic acceleration coefficients of the bodies. However, as the models were relatively simple, the hydrodynamic inertia coefficients were obtained by theoretical approximation. The methods for such approximations are given in number of fluid mechanics publications such as Humphreys and Watkinson (1978), Gerhart and Gross (1985), and Clauss *et al.* (1992). Similarly, all coefficients for the ball type depressor were obtained using theoretical approximations.

6.6 Validation of the Computer Program

In order to confirm that the computer model accurately simulates the behaviour of towed systems, a number of the scaled model runs were used to validate the two-part computer model. The results from the computer model proved to emulate those obtained from the equivalent scaled model tests, thus successfully validating the computer program.

Three examples of these validation runs are reproduced in this sub-section. These consist of two runs under vertical (X-Z plane) excitation, utilising a ball and fish type depressor respectively, and the other under horizontal (Y-Z plane) excitation utilising a depressor fish. The results consist of the relevant linear and angular displacements of the towed fish and depressor, as well as the surface tow point tension. The dimensions and specifications for the runs, together with the equivalent scaled model run identification labels, are given in Table 6.4. All three simulations were carried out using a time step of 0.001 seconds and a tension error limit of 1 N.

Figures 6.64 to 6.71 compare the results from the computer model for the two-part tow with a ball type depressor under vertical excitation, against its equivalent test run, *i.e.* run I31. The excitation frequency and amplitudes are as in Table 6.4.

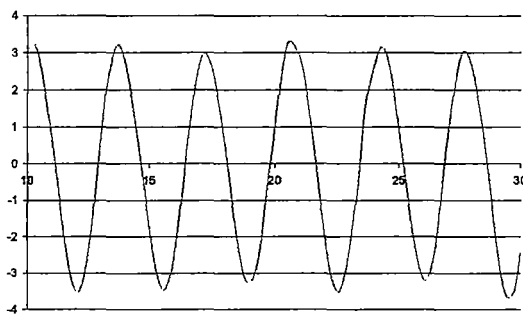
	I31	C31	YA22	No. of Segments
Primary Cable	1.5 m	1.5 m	1.5 m	8 (6 + 2)
Secondary Cable	0.8 m	0.8 m	0.8 m	5
Depressor to Junction Cable	0.25 m	0.25 m	0.25 m	2
Depressor Type	Ball	Fish	Fish	
Excitation Frequency	0.2857 Hz	0.2857 Hz	0.2857 Hz	(Note: period = 3.5 seconds)
X Amplitude	0.035 m	0.035 m	0.035 m	
Y Amplitude	0.0 m	0.0 m	0.0 m	
Z Amplitude	0.1 m	0.1 m	0.1 m	

Cable Diameter	2.2 mm
Cable Mass per Unit Length	3.013 g
Cable Tangential Drag Coefficient	0.2
Cable Normal Drag Coefficient	1.2
Cable Tangential Inertia Coefficient	0.1
Cable Normal Inertia Coefficient	1.0

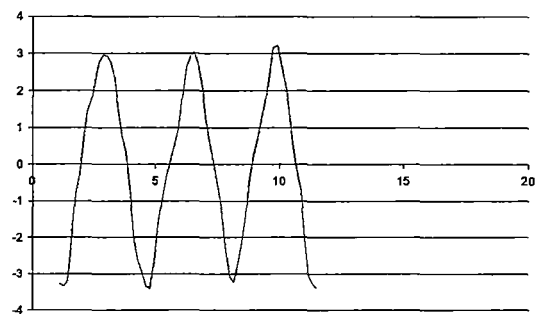
Tow Configuration Information for Validation Runs

Table 6.4

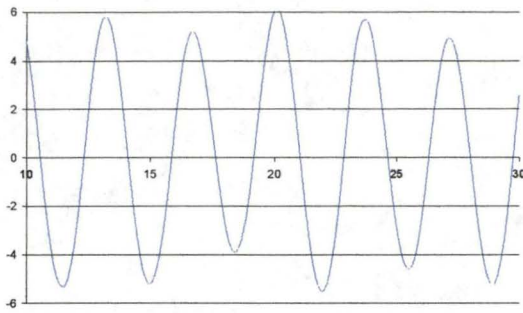
The X-axis in all graphs is the period in seconds. The pitch angles are the deviation about the mean angle of incidence of the models. The surge and heave are also manipulated to give the displacement from the steady state condition. In the experimental results, when more than one displacement is produced on a graph, the phase between them should be disregarded, as they are selected arbitrarily. Further, the experimental results have been averaged and “smoothened” to remove any effects due to turbulence and measuring errors.



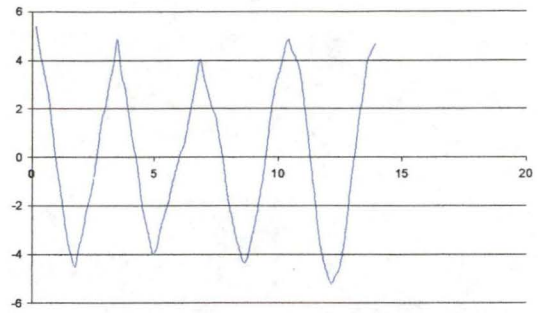
Pitch Angle of Tow Fish for I31 –
Computer - Degrees
Figure 6.64



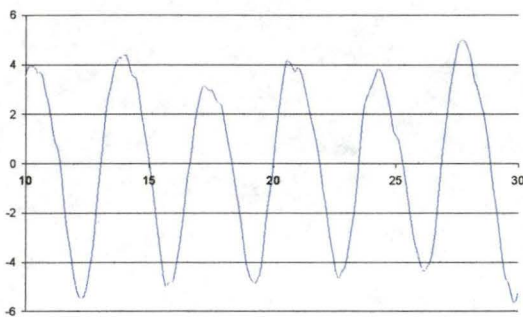
Pitch Angle of Tow Fish for I31 –
Experiment - Degrees
Figure 6.65



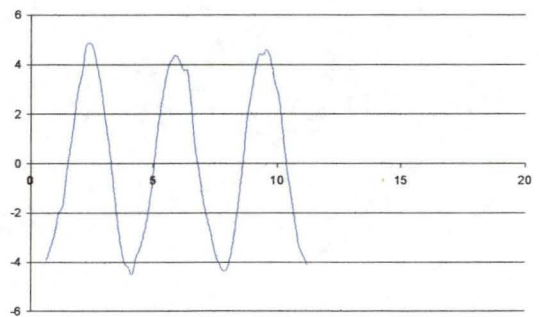
**Heave of Tow Fish for I31 – Computer
– Centimetres
Figure 6.66**



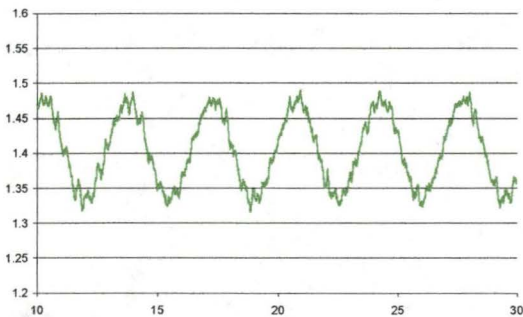
**Heave of Tow Fish for I31 –
Experiment - Centimetres
Figure 6.67**



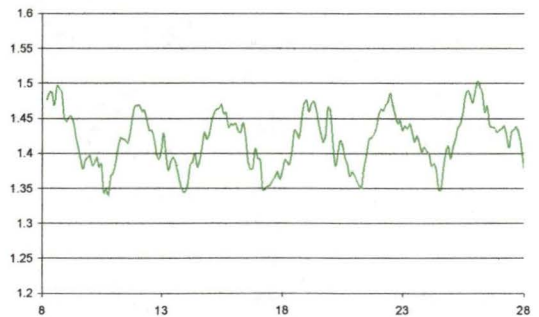
**Surge of Tow Fish for I31 – Computer
– Centimetres
Figure 6.68**



**Surge of Tow Fish for I31 –
Experiment - Centimetres
Figure 6.69**



**Tension at Surface for I31 – Computer
– Kilograms
Figure 6.70**



**Tension at Surface for I31 –
Experimental - Kilograms
Figure 6.71**

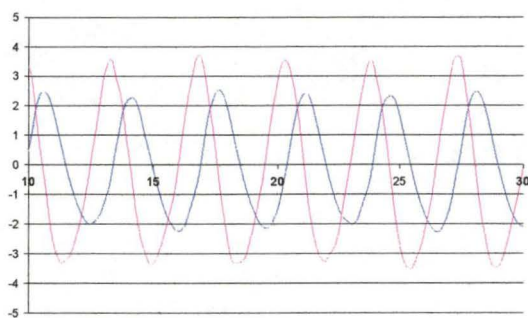
Key to Graphs

■ fish displacement
■ depressor displacement

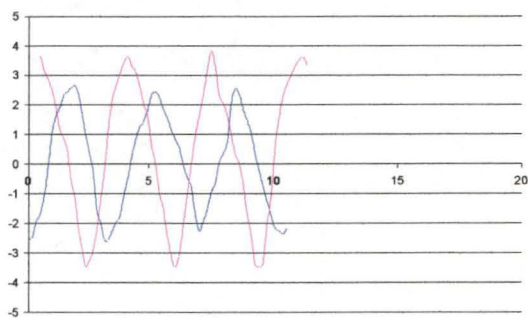
■ surface node tension
X-axis period (seconds)

The tension values from the computer program were filtered to remove the high frequency response. This is done by the use of a low pass filter or by a moving point average, the latter used here as it is readily available in most spreadsheet packages.

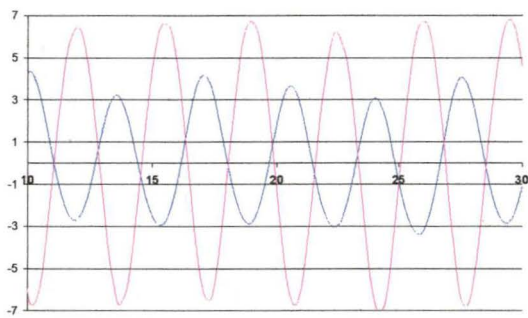
Figures 6.72 to 6.79 compares the results from the computer model for the two-part tow utilising a depressor fish under vertical excitation, against its equivalent test run, *i.e.* run C31. The excitation frequency and amplitudes are as in Table 6.4. Note: the previous run (I31) and this one (C31) allows for a comparison of the two-part tow utilising different depressor types, as they are otherwise similar.



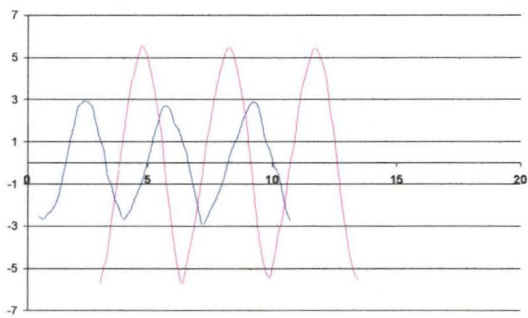
**Pitch Angle of Tow Fish and Depressor
for C31 – Computer - Degrees
Figure 6.72**



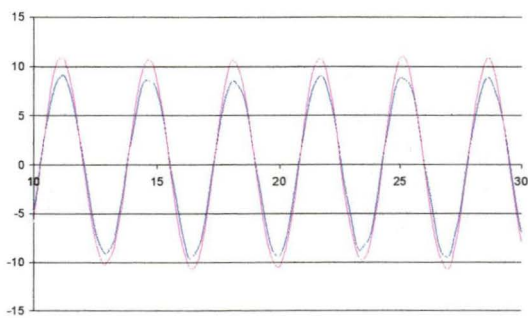
**Pitch Angle of Tow Fish and Depressor
for C31 – Experiment - Degrees
Figure 6.73**



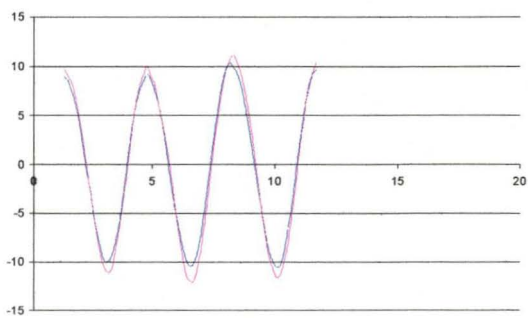
**Heave of Tow Fish and Depressor for
C31 – Computer - Centimetres
Figure 6.74**



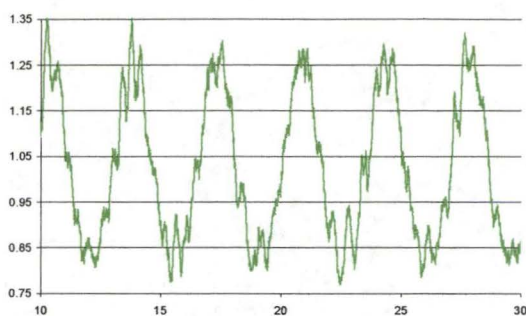
**Heave of Tow Fish and Depressor for
C31 – Experiment - Centimetres
Figure 6.75**



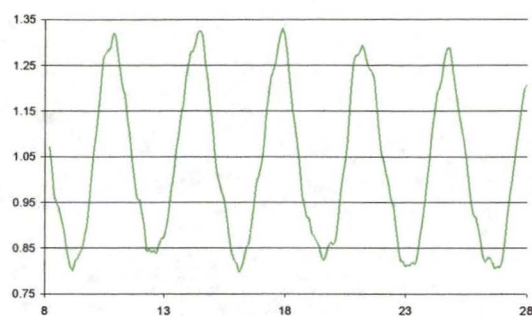
**Surge of Tow Fish for C31 – Computer
- Centimetres
Figure 6.76**



**Surge of Tow Fish for C31 –
Experimental – Centimetres
Figure 6.77**



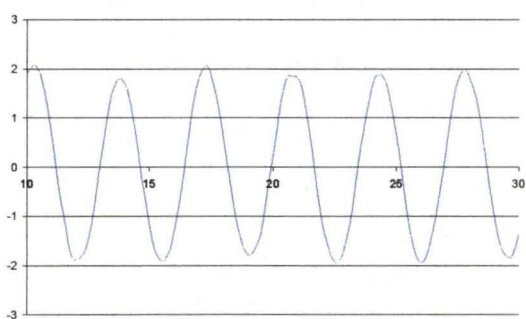
**Tension at Surface for C31 –
Computer - Kilograms
Figure 6.78**



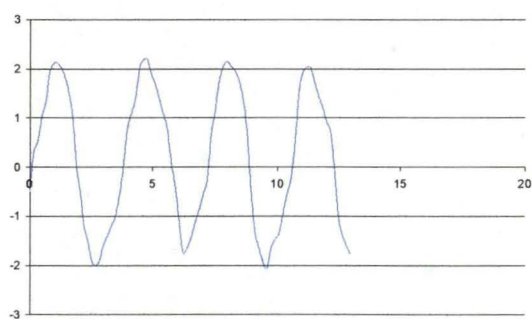
**Tension at Surface for C31 –
Experimental - Kilograms
Figure 6.79**

Key to Graphs – same as for Figures 6.64 to 6.71.

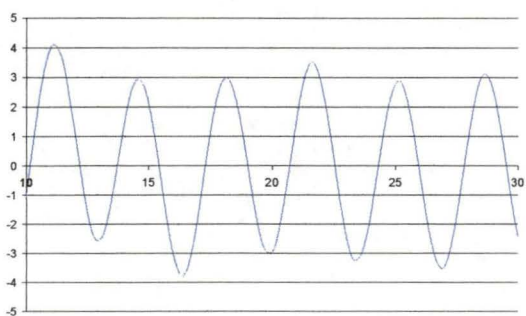
Finally Figures 6.80 to 6.83 show the yaw and sway results for the same tow configuration with a depressor fish under horizontal excitation, *i.e.* test run YA22. Again the configuration and excitation details are given in Table 6.4.



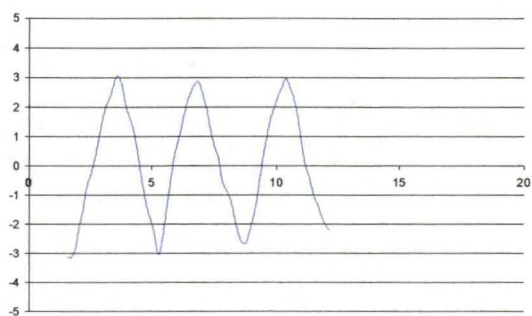
**Yaw Angle of Tow Fish for YA22 –
Computer - Degrees
Figure 6.80**



**Yaw Angle of Tow Fish for YA22 –
Experiment - Degrees
Figure 6.81**



**Sway of Tow Fish for YA22 –
Computer – Centimetres
Figure 6.82**



**Sway of Tow Fish for YA22 –
Experiment - Centimetres
Figure 6.83**

Key to Graphs – same as for Figures 6.64 to 6.71.

Table 6.5 gives the averages and standard deviations of the differences between the computer and experimental results, as a percentage of the amplitude of the relevant motions for the three examples considered.

I31 – Fish	Pitch	Heave	Surge
Average	-0.65	8.73	-0.21
Standard Deviations	13.72	19.45	14.61
C31 – Fish	Pitch	Heave	Surge
Average	-2.75	8.6	0.52
Standard Deviations	14.5	18.65	8.74
C31 – Depressor	Pitch	Heave	Surge
Average	-9.03	-0.76	2.79
Standard Deviations	11.57	17.72	10.63
YA22 – Fish	Yaw	Sway	
Average	-6.66	-5.68	
Standard Deviations	10.99	15.49	

Statistical Analysis of the Computer and Experimental Results

Table 6.5

As seen from the Figures 6.64 to 6.83 and Table 6.5, there is good correlation between the results from the computer program and the equivalent scaled model tests. This should be considered in light of the small dimensions of the configuration, the approximations in the derivation of some coefficients, and the inevitable errors in the experimental procedures and analysis.

Thus, it can be concluded that the computer program is a good representation of the actual two-part tow. Therefore, it can be used with a high degree of confidence to simulate the behaviour of such configurations.

CHAPTER 7

CONCLUSION

7.1 Summary

The main objective of this project was to investigate the use of a two-part underwater tow to minimise the transmission of wave induced motions from the surface tow vessel to the towed underwater body. This was carried out in three stages, *i.e.* the computer simulation of the two-part tow, scaled model tests of the tow configuration, and full scale trials. During the simulation stage, the computer model was expanded to deal with series and parallel multi-tow systems.

The description of the various conventional, two-part and multi-tow configurations was followed by an extensive review of the literature in modelling of cable / towing systems as well as the techniques utilised to solve these models. The literature review of the cable modelling looked at early analytical techniques right up to state of the art finite difference / element methods. These ranged from early one dimensional static models through to quasi static models, culminating in three-dimensional dynamic models.

The commonly employed three-dimensional dynamic cable modelling techniques were analysed to select an appropriate method for this project. Each modelling technique was explained in detail and analysed to deduce its attributes and limitations. The method of characteristics and the finite difference method both use complex solution procedures, so the inclusion of the junction and multiple towed bodies would require substantial modification and add to the complexity of the solution procedure. In addition, the behaviour of the models under slack cable conditions is debatable. For these reasons these two modelling techniques were rejected.

The incorporation of the junction in the hinged rod model was also found to be tedious and could further complicate the representation of parallel multi-tow configurations. In addition, as the model does not support longitudinal wave propagation, it cannot represent the dynamic effect due to rapid cable top motion. Therefore, this method too was rejected.

The finite element method can represent two-part and multi-tow configurations. However, it offers no advantages over the lumped-mass method and uses a more complex set of equations, with the solution process being slower due to the use of matrix algebra. In the lumped-mass system, due to the redistribution of forces from the segments to the adjacent nodes, the representation of the junction in the towed cable system is simplified. This provides an elegant method of modelling series and parallel multi-tow systems. In addition, the lumping of the forces at the nodes facilitates the integration of the towed fish model with that of the cable. Therefore, the latter method was selected to represent the two-part and multi-tow cable systems.

One area within fluid dynamics that is continuously being investigated is the prediction of the cable drag and inertia forces. A description of such prediction methods and the equations generally used to predict these forces were also presented. These equations include coefficients, which are usually predicted by experimental data, although some researchers have put forward analytical techniques. The effects of surface roughness, inclination to the flow direction, oscillations of the flow/cable, and vortex shedding, on these coefficients were also discussed. Examples of the experimental data used for the prediction of these coefficients were presented and the selection of the appropriate coefficients was explained.

Also discussed were the methods available to model underwater vehicles. Again the methods available to predict the relevant hydrodynamic coefficients were discussed, with a combination of experimental and theoretical approximations selected to predict the coefficients of the underwater bodies of the towed system.

The three-dimensional dynamic modelling of the tow configuration was described in detail. The cable was divided into a number of lumped masses separated by elastic segments. This allowed the junction to be represented as a node, with more than two cable segments attached to it. By modelling the cable as a continuous system and comparing it with the lumped-mass model, it was shown that the latter was a true representation of the continuous system. The effects due to this discretisation were also discussed.

The cable was modelled with three degrees of freedom about the global axis system, while the towed fish was modelled with six degrees of freedom about its local axis system. This required that the latter be manipulated to ensure integration with the cable model, thus providing adequate coupling of forces and motions. To enable this,

the modelling of the towed fish was carried out about its tow point, requiring the translation of all forces, moments and inertia effects.

The versatility of the dynamic modelling technique enabled the model to have more than one junction, thus allowing for the modelling of parallel multi-tow systems. The program was also modified to facilitate series multi-tow systems, by incorporating an aft tow point to the tow fish.

The solution for the dynamic model commences from a quasi-static model, that also allows for preliminary low level investigations. The dynamic model uses the values from the quasi-static model as initial tentative values and employs a time stepping technique, solving the dynamic equations subject to the boundary conditions. The driving function for the model is the path of motion of the upper end of the cable, *i.e.* the surface tow vessel. The non-linear differential equations describing the motion of the system are solved using the Houbolt scheme, *i.e.* an implicit multi-step numerical integration scheme. Since the equations are non-linear, the solution requires an iteration process. This is achieved using a Newton-Raphson iteration process based on the constraint equation for the constitutive stress-strain relationship of each cable segment. This results in a *predictor-corrector* solution scheme.

The solution procedure results in a set of equations expressed by a tri-diagonal matrix, which can be solved using the well known Thomas algorithm. However, the discontinuity of the junction will result in zero terms in the tri-diagonal band and non-zero terms outside the band. In order to facilitate a fast solution, the matrix is converted into its true tri-diagonal form by manipulation. This solution procedure enables a rapid solution to the parallel multi-tow configuration, *i.e.* a system having a number of junctions.

In the case of a series multi-tow system, the configuration is divided into separate cable systems at each tow fish, which are solved separately. They are then interfaced through the geometry of the appropriate tow fish. The error introduced by solving the cable systems separately as opposed to solving them as one system is shown to be insignificant, although the increase in solution speed is substantial. Examples of program outputs were also presented for the various tow configurations.

One of the problems encountered during such numerical solution techniques is numerical instability. Although a number of researchers have done work in structural dynamics to explain these phenomenon, very little work has been carried out with

underwater cable systems. Therefore, this work has explained the operation of explicit and implicit integration schemes, identified reasons for numerical instability, and attempted to identify the requirements for stability and accuracy.

Although a number of numerical schemes were used during the development stages, the Houbolt scheme was finally selected for the modelling. Therefore, the investigation is centred around this scheme. It was derived from first principles and the “mechanics” of the integration scheme was explained. Methods available to investigate the stability and accuracy requirements were discussed, including the requirements for non-linear systems. An appropriate method was selected and used on the Houbolt scheme to derive an acceptable time step to meet these conditions. This time step is dependent on the natural frequencies of the cable system, and since the calculation of these frequencies is tedious, a simpler method based on the wave speeds of the continuous cable system was derived. It was also seen that the iteration process required due to the non-linear equations of motion, removed any errors that were introduced by the starting procedure or by the use of larger time steps.

The investigation was supplemented by scaled model and full scale trial data, while the former was also used to validate the computer program. Both experiments clearly showed that the two-part tow offered a much more stable platform, due to the inherent decoupling effect of the configuration. The two-part tow is able to absorb heave excitation, with a slight increase in the tow fish surge amplitude. An increase in surge excitation is however transmitted to the towed fish, although its effect on the angular motions are restricted. In the case of lateral (sway) excitation, a slight increase occurs in the sway and yaw amplitudes of the towed fish, although the rate of increase is reduced via the two-part tow configuration.

Increasing the length of the secondary cable improves the response of the towed fish, although beyond a given length there will be little, if any, improvement. The same can be said with regard to the length of the primary cable.

Although there is little difference in the tow fish response under vertical excitation due to the utilisation of a fish or ball type depressor, a significant improvement is gained by utilising the former under horizontal excitation. The location of the junction a distance above the depressor also improves the response. Directly connecting the secondary cable to the depressor does improve the response of the depressor, but adversely effects the motion of the towed fish. The marginal

improvement due to the use of a drogue does not warrant the use of such devices, especially given the difficulties in deployment and recovery.

Inspection of the results from the computer model compared to those from the scaled model tests showed good agreement, thus successfully validating the computer program. The validation required the calculation of the hydrodynamic coefficients for the scaled models, which were obtained using a horizontal planar-motion-mechanism.

7.2 Conclusions and Recommendations

The use of the two-part tow is a cheap but effective method of reducing the transmission of wave induced surface vessel motion along the tow cable to the towed underwater body. In order to optimise the tow configuration, its parameters have to be adjusted to suit the towing conditions and the underwater bodies. Although this is possible by trialing a number of full scale configurations, it is financially and time-wise more efficient to carry out computer simulations of the various configurations to decide upon an acceptable arrangement.

The computer model developed during this project is ideally suited for this task. Since the quasi-static model can be run separately, it provides the user with an adequate tool to carry out initial investigations, especially since it requires only basic input information. It can be used to identify the approximate parameters to achieve the required depth and trail.

Once this is achieved, the dynamic model can be initiated to investigate the behaviour of the system. The tow cable and underwater vehicle parameters can then be modified during these dynamic runs to obtain the required response. These parameters include: primary and secondary cable lengths, location of junction along primary cable, mass, buoyancy and hydrodynamic coefficients of the cable and towed bodies, and the tow speed and direction. The simulation also allows the operator to plan surface vessel manoeuvres during towing operations, to prevent contact between towed bodies, cables, and underwater objects.

The model is able to simulate conventional, two-part, multi-tow systems. With the two-part tow, the model is able to vary the location of the junction along the primary cable length, which to the best of the author's knowledge, is a feature not found on other towing models. The multi-tow configurations allow for two variations, *i.e.*

series and parallel multiple towed systems. In such tows, simulation is of importance due to the difficulties in deploying the tows and the possible contact between the number of towed bodies and cables. In addition, the number of parameters that can be changed is also greater, thus offering a larger number of combinations.

The experimental data obtained during this project will assist operators in deciding on the parameters that will improve the response of the tow configurations. These will assist in the selection of the preliminary configuration.

In general, based on the experimental work and results from the computer simulations, the following conditions were found to improve the response of a two-part tow configuration.

The junction is best located along the primary cable length as opposed to being at the depressor, as the latter configuration increases the coupling between the two cables. Although longer primary and secondary cables do improve the decoupling of the motions, it is not required to have excessively long cables as the improvements are not significant for very long cable lengths. The use of a depressor fish, with adequate hydrodynamic damping is preferable to a clump weight, as the latter imparts larger motions to the cables. This is especially true with horizontal motions, *i.e.* sway and yaw motions. However, the clump weight does prove to be better in reducing surge motion. Under certain conditions the latter can be beneficial, as the two-part tow inherently tends to reduce heave, sway and associated angular motions at the expense of surge motion.

The dynamic simulation requires a sufficiently small time step to ensure accuracy and stability. Due to the non-linear equations of motion, the time step cannot be easily predicted using existing theories, although these effects were investigated in detail. However, a guide to predict an approximate time step, based on the wave speeds of the cable system, is presented. In practice, the operator should attempt to use the largest possible time step, as the iteration process removes any errors introduced.

Due to the nature of the model, unrealistic input data, especially with regard to the cable and tow body hydrodynamic coefficients, can lead to numerical instability. Therefore, operators should ensure that the input values are realistic and possess the required physical damping. Continuous instability during simulation runs may warrant the inspection and correction of these coefficients. These coefficients can be obtained using experimental data and/or theoretical approximations. The information

provided in this thesis on the prediction of these coefficients should assist operators with this task.

7.3 Future Work

Future work can be divided into a number of areas. These include the following:

- DSTO is currently developing a modified Klein sonar platform that incorporates adjustable control surfaces. This allows the operator to control the trajectory of the tow fish from the surface. The towed fish model in the computer program can be modified to incorporate movable control surfaces, thus allowing the operator to simulate the motion. A further step from this would be the incorporation of an adaptive control system, allowing the control surfaces to be automatically adjusted to maintain the required altitude and attitude.
- The versatility of the program enables it to be modified to represent a number of different tow configurations. These could include a variety of multi-tow configurations not already incorporated within the program. Thus, the program can be modified to meet the requirements of specific operations in the offshore, military, and maritime industries.
- A variety of full scale tows, covering conventional, two-part, and multi-tow configurations, would be beneficial to further validate and refine the model.
- The model can be improved to include a number of operational effects, including the upper end of the tow cable being above the water surface, sheared flow (*i.e.* the current velocity changing with water depth), the effect of waves on the velocity of the surrounding water relative to the cable, and the effect of vortex induced motions and forces.
- As the finite element method is also able to model the cable junction, it may be beneficial to develop an equivalent simulation model using this technique and compare the results of the two programs. This will no doubt add to the hotly debated topic, as to the merits or otherwise of each method, aggressively promoted by each school.

- As stated earlier, very little work has been done in investigating the stability and accuracy criteria with underwater cable systems. This thesis attempts to identify some of these criteria, however, a lot more work is required to thoroughly understand the mechanisms involved with the numerical stability of the iteration process and the implicit integration scheme used to solve the non-linear set of equations. The depth of the area is such that it would require a study purely dedicated to the stability and accuracy requirements.
- Considering the practical operations, one major drawback of the two-part tow is the difficulties faced with the deployment and recovery of the configuration from small coastal vessels. The requirement to deploy two fish one after the other is hindered by the available after deck space and the weight of the units. The deployment of a single launch unit, that separates into two parts after deployment, would be greatly appreciated by the operators. The recovery process too would be simplified if the reverse could be facilitated. Such a design could be developed and incorporated into the existing computer model to predict deploying and recovery operations.

As a final comment, it can be concluded that the objectives of this project were achieved, *i.e.* the successful simulation of the two-part underwater tow and the investigation to improve its behaviour under the influence of wave induced surface excitation. In addition, the project was successfully expanded to include series and parallel multi-tow configurations.

Although a number of investigations have been carried out dealing with aspects of underwater towing operations, the strength of this investigation lies in that it combines these aspects into one study, *i.e.* mathematical modelling, computer simulation, prediction of the hydrodynamic coefficients, scaled model experiments, full scale trials, and the analysis of the numerical technique.

BIBLIOGRAPHY

1. Abkowitz, M.A., "Stability and Motion Control of Ocean Vehicle", The MIT Press, Massachusetts, 1969.
2. Ablow, C.M. and Schechter, S., "Numerical Simulation of Undersea Cable Dynamics", Ocean Engineering, Vol 10, No 6, 1983, pp. 443-457.
3. Achenbach, E., "Influence of Surface Roughness on the Cross-flow Around a Circular Cylinder", Journal of Fluid Mechanics, Vol 46, Part 2, 1971, pp. 321-335.
4. Allen, D.W., "Vortex-Induced Vibration of Deepwater Risers", OTC 5530, Offshore Technology Conference, Houston, Texas, May 1998, pp. 209-215.
5. Ames, W.F., Numerical Methods for Partial Differential Equations", Academic Press Inc., Boston, 1969.
6. Asplin, R.G. and Christensson, C.G., "A New Generation Side Scan Sonar", IEEE, CH2585-8/88/0000-0329, 1988, pp. 329-334.
7. Bathe, K.J., "Finite Element Procedures in Engineering Analysis", Prentice-Hall Inc, New Jersey, 1982.
8. Bathe, K.J. and Wilson, E.L., "Stability and Accuracy Analysis of Direct Integration Methods", Earthquake Engineering and Structural Dynamics, John Wiley & Sons, Vol 1, 1973, pp. 283-291.
9. Belytschko, T., Chiapetta, R.L. and Bartel, H.D., "Efficient Large Scale Non-Linear Transient Analysis by Finite Elements", Int. Journal for Numerical Methods in Engineering, John Wiley & Sons, Vol 10, 1976, pp. 579-596.
10. Belytschko, T., Holmes, N. and Mullen, R., "Explicit Integration – Stability, Solution Properties, Cost", ASME Applied Mechanics Symposia Series, Finite Element Analysis of Transient Nonlinear Structural Behaviour, Vol AMD14, Houston, Texas, November – December 1975, pp. 1-21.
11. Belytschko, T. and Schoeberie, D.F., "On the Unconditional Stability of an Implicit Algorithm for Nonlinear Structural Dynamics", Journal of Applied Mechanics, 97, Houston, Texas, December 1975, pp. 865-869.
12. Bergan, P.G. and Mollestad, E., "An Automatic Time-Stepping Algorithm for Dynamic Problems", Computer Methods in Applied Mechanics and Engineering, Vol 49, 1985, pp. 299-318.
13. Bergdahl, L.M. and Rask, I., "Dynamic vs Quasi-Static Design of Catenary Mooring Systems", OTC 5530, 19th Offshore Technology Conference, Houston, Texas, April 1987, pp. 397-404.

14. Bernitsas, M.M., "A Three Dimensional Non-linear Large Deflection Model for Dynamic Behaviour of Risers, Pipelines, and Cables", *Journal of Ship Research*, Vol 26, No. 1 March 1982, pp. 59-64.
15. Berteaux, H.O., "Buoy Engineering", Wiley, New York, 1976.
16. Bettles, R.W. and Chapman, D.A., "The Experimental Verification of a Towed Body and Cable Dynamic Response Theory", *Ocean Engineering*, Vol 12, No 5, 1985, pp. 453-469.
17. Brook, A.K., "The Design of Catenary Mooring Systems for Offshore Vessels", *Offshore Gothenborg*, 1985, pp. 303-322.
18. Brook, A.K., "A Theoretical Investigation of the Static and Dynamic Behaviour of Ship Mooring Lines", PhD Thesis, University of Newcastle upon Tyne, UK, March 1990.
19. Brook, A.K., "The Static and Dynamic Analysis of Moored Vessels in Irregular Seas", 6th Int. Conference on Behaviour of Offshore Structures (BOSS '92), Vol 1, London, July 1992, pp. 251-264.
20. Brooks, I.H., "A Pragmatic Approach to Vortex Induced Vibration of a Drilling Riser", OTC 5522, 19th Offshore Technology Conference, Houston, Texas, April 1987, pp. 327-332.
21. Bourget, P.L. and Marichal, D., "Study of the Vortex Shedding Influence on the Drag Coefficient and the Shape of Immersed Flexible Cylinders", Int. Conference CADMO, 1986, pp. 427-436.
22. Bourget, P.L. and Marichal, D., "Remarks about Variations in the Drag Coefficient of a Circular Cylinder Moving Through Water", *Ocean Engineering*, Vol 17, No 6, 1990, pp. 569-585.
23. Burgess, J.J., "Bending Stiffness in a Simulation of Undersea Cable Development", 2nd Int. Offshore and Polar Engineering Conference, San Francisco, June 1992, pp. 308-315.
24. Burgess, J.J., "Equation of Motion of a Submerged Cable with Bending Stiffness", 12th Int. Conference on Offshore Mechanics and Arctic Engineering, ASME, Calgary, 1992, pp. 283-289.
25. Cannon, T.C. and Genin, J., "Three Dimensional Dynamic Behaviour of a Flexible Towed Cable", *Aeronautical Quarterly*, August 1972, pp. 201-210.
26. Casarella, J. and Parsons, M., "A Survey of Investigation and Motion of Cable Systems Under Hydrodynamic Loading", *MTS Journal*, Vol 4, No 4, July-August 1970, pp. 27-44.
27. Chakrabarti, S.K. and Cotter, D.C., "Hydrodynamic Coefficients of Mooring Tower", OTC 4496, 15th Offshore Technology Conference, Houston, Texas, May 1983, pp. 449-458.

28. Chakrabarti, S.K., "Nonlinear Methods in Offshore Engineering", Developments in Marine Technology 5, Elsevier, New York, 1990.
29. Chapman, D.A., "Towed Cable Behaviour During Ship Turning Manoeuvres", Ocean Engineering, Vol 11, No 4, 1984, pp. 327-361.
30. Chapman, D.A., "Theory for Three Dimensional Dynamic Simulation of a Towed Cable-Body System", PhD Thesis, University of Bath, UK, 1987.
31. Chauduri, J., McNamara, J.F and O'Brian, P.J., "Nonlinear Dynamic Analysis of Hybrid Riser System for Deepwater Applications", OTC 5466, 19th Offshore Technology Conference, Houston, Texas, April 1987, pp. 405-416.
32. Chen, Y. and Lin, F., "General Drag Force Linearisation for Nonlinear Analysis of Marine Risers", Ocean Engineering, Vol 16, No 3, 1989, pp. 265-280.
33. Chiou, R.B. and Leonard, J.W., "Analysis of Multi-Leg Mooring by Spatial Integration", 1st European Offshore Mechanics Symposium, Trondheim, August 1990, pp. 474-481.
34. Choo, Y. and Casarella, J., "Hydrodynamic Resistance of Towed Cables", Journal of Hydraulics, October 1971, Vol 5, No 4, pp. 126-131.
35. Choo, Y. and Casarella, J., "A Survey of Analytical Methods for Dynamic Simulation of Cable-Body Systems", Journal of Hydraulics, Vol 4, No 4, October 1973, pp. 137-144.
36. Clauss, G., Lehmann, E., and Ostergaard, C, (translated by Shields, M.J.), "Offshore Structures Volume 1, Conceptual Design and Hydromechanics", Springer-Verlag, London, 1992.
37. Connaire, A.D. and McNamara, J.F., "Aspects of Non-linear Three-Dimensional Mooring Line Dynamics", 16th Int. Conference on Offshore Mechanics and Arctic Engineering, ASME, Vol 1-A, Yokohama, April 1997, pp. 211-219.
38. Cordelle, F., "Simulation of the Dynamic Behaviour of Mooring Buoys in Waves", 2nd Int. Symposium on Ocean Engineering and Ship Handling, SSPA, Gottenburg, 1983, pp. 267-280.
39. Dreyer, T.P. and Murray, D.M., "On the Modelling of Two-Dimensional Segmented Representations of Cable Shape", Ocean Engineering, Vol 11, No 6, 1984, pp. 609-625.
40. Delmer, T.N., Stephens, T.C., and Coe, J.N., "Numerical Simulation of Towed Cables", Ocean Engineering, Vol 10, No 2, 1983, pp. 119-132.
41. Dercksen, A., Huijsmans, R.H.M., and Wichers, J.E.W., "An Improved Method for Calculating the Contribution of Hydrodynamic Chain Damping on Low Frequency Vessel Motion", OTC 6967, 24th Offshore Technology Conference, Houston, Texas, May 1992, pp. 209-217.

42. de Wit, G., "Choice of Umbilical Cable for Submersibles – Footprint Optimisation", OTC 4278, 14th Offshore Technology Conference, Houston, Texas, May 1982, pp. 561-570.
43. Douglas, J.F., Gasiorek, J.M., and Swaffield, J.A., "Fluid Mechanics", Second Edition, Longman Scientific and Technical, Essex, 1985.
44. Eames, M.C., "Steady-State Theory of Towing Cables", Quartely Transaction, Royal Institute of Naval Architects, Vol 110, No. 2, London, April, 1967, pp. 185-206.
45. Fage, A and Warsap, J.H. "The Effects of Turbulence and Surface Roughness on the Drag of a Circular Cylinder", ARC R & M 1283, 1930.
46. Ferriss, D.H., "Approximate Determination of the Configuration of an Underwater Cable Subjected to Steady Hydrodynamic Loading", Division of Information Technology and Computing, National Physics Laboratory, 1980.
47. Fidler, J., "Methods of Predicting Submersible Hydrodynamic Characteristics", Report NEAR-TR-139, Neilson Engineering and Research Inc., Naval Coastal Systems Centre, July 1978, pp. 238-278.
48. Gear, C.W., "Numerical Initial Value Problems in Ordinary Differential Equations", Prentice-Hall Inc, New Jersey, 1971.
49. Greenhow, M. and Ahn, S.I., "Added Mass and Damping of Horizontal Circular Cylinder Sections", Ocean Engineering, Vol 15, No 5, 1988, pp. 495-504.
50. Gerhart, P.M. and Gross, R.H., "Fundamentals of Fluid Mechanics", Addison-Wesley Publishing Company, Massachusetts, 1985.
51. Gertler, M. and Hagen, G.R., "Standard Equations of Motion for Submarine Simulation", Naval Ship Research and Development Centre, SR 009 01 01, June 1967.
52. Griffin, O.M., "Vortex Induced Vibration of Marine Cable Structures", NRL Memorandum Report 560, Naval Research Laboratory, June 1985.
53. Grosenbaugh, M.A., Yoerger, D.R., and Triantafyllou, M.S., "A Full Scale Experimental Study of the Effect of Shear Current on the Vortex Induced Vibration and Quasi-Static Configuration of a Long Tow Cable", 8th Int. Conference on Offshore Mechanics and Arctic Engineering, ASME, The Hague, March 1989.
54. Grosenbaugh, M.A., "The Effect of Unsteady Motion on the Drag Forces and Flow-Induced Vibrations of a Long Vertical Tow Cable", 1st European Offshore Mechanics Symposium, Trondheim, August 1990, pp. 464-473.

55. Hansen, H. T., Skomedal, N.G., and Vada, T., "Computation of Vortex Induced Fluid Loading and Response Interaction of Marine Risers", 8th Int. Conference on Offshore Mechanics and Arctic Engineering, ASME, The Hague, March 1989.
56. Haritos, N. and He, D.T., "A Total Lagrangian Formulation of a Cable Finite Element", Civil and Agriculture Engineering, Report RR/STRUCT/02/1989, University of Melbourne, 1989.
57. Haritos, N. and He, D.T., "A Finite Element Formulation for Cables Suitable for Dynamic Modeling", Mathematics and Computers in Simulation 32, North Holland, 1990, pp. 179-184.
58. Haritos, N. and He, D.T., "Modelling the Response of Cable Elements in an Ocean Environment", Finite Element in Analysis and Design 19, Elsevier Science Publications, 1992, pp. 19-32.
59. Haritos, N. and He, D.T., "Modelling the Response of Single-Point Mooring-Systems in a Wave Environment", Maritime Technology Conference, Sydney.
60. Hartnup, G.C., Airey, R.G., Patel, S., and Lyons, G.J., "Large Scale Tests for Vortex Shedding Effects on Mooring Risers", OTC 4593, 15th Offshore Technology Conference, Houston, Texas, May 1983, pp. 113-118.
61. Healey, A.J., Papoulias, F.A., and Lienard, D., "Multivariable Sliding Mode Control for Autonomous Diving and Steering of Unmanned Underwater Vehicles", pp. 293-314.
62. Hearn, G.E. and Thomas, D.O., "The Influence of Practical Time Integration Schemes on Dynamic Mooring Line Analysis", OTC 6604, 23rd Offshore Technology Conference, Houston, Texas, May 1991, pp. 397-409.
63. Henderson, J.F. and Wright, R.C., "The Use of Active Controls on Underwater Towed Bodies", 2nd Int. Conference on Computer Modelling in Ocean Engineering, Barcelona, October 1991.
64. Henderson, J.F. and Wright, R.C., "Underwater Terrain Following Using Active Controls on a Towed Vehicle", Underwater Technology, Autumn 1993, pp. 14-21.
65. Herstein, I.N., and Winter, D.J., "Matrix Theory and Linear Algebra", Macmillian Publishing Company, New York, 1988.
66. Hilber, H.M., "Analysis and Design of Numerical Integration Methods in Structural Dynamics", PhD Thesis, University of California, USA, 1976.
67. Hilber, H.M., Hughes, T.J.R., and Taylor, R.L., "Improved Numerical Dissipation for Time Integration Algorithms in Structural Dynamics", Earthquake Engineering and Structural Dynamics, John Wiley & Sons, 1977, Vol 5, pp. 283-292.

68. Hopkin, D., "The Dynamics and Control of an Underwater Towed Vehicle", Masters Thesis, University of British Columbia, Vancouver, B.C., 1989.
69. Hopkin, D., Davies, M., and Gartshore, I., "Trajectory and Altitude Control of an Underwater Towed Vehicle", Int. Conference on Modelling and Control of Marine Craft, Exeter, April 1990, pp. 227-251.
70. Horton, K.J., Ferrer, C.M., Watson, K.P., and Charvoz, D.C., "Measurements of the Hydrodynamic Characteristics of Stranded Cables", OTC 5521, 19th Offshore Technology Conference, Houston, Texas, April 1987, pp. 317-325.
71. Hover, F.S., Grosenbaugh, M.A., and Htriantafyllou, M.S., "Modelling the Dynamics of a Deeply-Towed Underwater Vehicle System", 1st European Offshore Mechanics Symposium, Trondheim, August 1990, pp. 457-463.
72. Huang, S., "Analysis and Control of Marine Cable Systems", PhD Thesis, Strathclyde University, UK, Mach 1992.
73. Huang, S., "Dynamic Analysis of Three Dimensional Marine Cables", Ocean Engineering, Vol 21, No 6, 1994, pp. 587-605.
74. Huang, S. and Vassalos, D., "A Semi-Analytical treatment of Three Dimensional Statics of Marine Cables", Ocean Engineering, Vol 20, No 4, 1993, pp. 409-420.
75. Huang, S. and Vassalos, D., "Analysis of Taut-Slack Marine Cable Dynamics", Int. Conference on Offshore Mechanics and Arctic Engineering, ASME, 1995, pp. 401-406.
76. Huang, T.S. and Leonard, J.W., "Dynamic Response of Viscoelastic Cable Elements", Ocean Engineering, Vol 17, No 12, 1990, pp. 23-34.
77. Huang, T.S. and Leonard, J.W., "Lateral Stability of a Submarine Flexible Hoseline", Ocean Engineering, 1990, Vol 17, No 12, pp. 35-52.
78. Hughes, T.J.R., "A Note on the Stability of Newmark's Algorithm in Nonlinear Structural Dynamics", Int. Journal for Numerical Methods in Engineering, Vol 11, No 2, 1977, pp. 383-386.
79. Humphreys, D.E. and Watkinson, K.W., "Prediction of Acceleration Hydrodynamic Coefficients for Underwater Vehicles from Geometric Parameters", Technical Report TR 327-78, Naval Coastal Systems Centre, February 1978.
80. Humphreys, D.E., "Development of the Equations of Motion and Transfer Functions for Underwater Vehicles", Naval Coastal Systems Laboratory, Technical Report TR NCSL 287-76, July 1976.
81. Humphreys, D.E., "Dynamics and Hydrodynamics of Ocean Vehicles", IEEE, CH1685-7/81/0000-0088, 1981, pp. 88-91.

82. Huse, E., "Influence of Mooring Line Damping upon Rig Motions", OTC 5204, 18th Offshore Technology Conference, Houston, Texas, May 1986, pp. 433-438.
83. Imlay, F.H., "The Complete Expression for 'Added Mass' of a Rigid Body Moving in an Ideal Fluid", Research and Development Report 1528 Hydrodynamics Laboratory, David Taylor Model Basin, July 1961.
84. Ishii, K. Okamoto, T., and Tachibana, N., "Development of a Flexible Marine Riser System", OTC 5164, 18th Offshore Technology Conference, Houston, Texas, May 1986, pp. 121-129.
85. Ivers, D.W. and Mudie, J.D., "Towing a Long Cable at Slow Speeds: A Three Dimensional Dynamic Model", MTS Journal, Vol 7, No. 3, May-June 1973, pp. 23-31.
86. Jacobsen, V., Bruschi, P., Simantiras, P., and Vitali, L., "Vibration Suppression Devices for Long Slender Tubulars", OTC 8156, Offshore Technology Conference, Houston, Texas, May 1996, pp. 71-80.
87. Jefferys, E.R. and Patel, M.H., "On the Dynamics of Taut Mooring Systems", Engineering Structures, Vol 4, January 1982, pp. 37-43.
88. Johansson, P.I., "A Finite Element Model for Dynamic Analysis of Mooring Cables", PhD Thesis, Massachusetts Institute of Technology, USA, 1976.
89. Johansson, P.I., "Non-Linear Dynamic Response of a Mooring Line", Det Norske Veritas, Publication No. 106, March 1977.
90. Kamman, J.W. and Huston, R.L., "Modelling of Submerged Cable Dynamics", Technical Report No: N00014-76C-0139, Office of Naval Research, 1983.
91. Kamman, J.W. and Huston, R.L., "Modelling of Submerged Cable Dynamics", Journal of Computers and Structures, Vol 20, No 1-3, 1985, pp. 623-629.
92. Kamman, J.W., Nguyen, T.C., and Crane, J.W., "Modelling Towed Cable System Dynamics", Oceans '89, Vol 5, 1989.
93. Kamman, J.W. and Nguyen, T.C., "Modelling Towed Cable System Dynamics", Technical Memorandum, NCSC TM 492-88, May 1990.
94. Kato, M., Abe, T., Tamiya, M., and Kumakiri, T., "Drag Forces on Oscillating Cylinders in a Uniform Flow", OTC 4591, 15th Offshore Technology Conference, Houston, Texas, May 1983, pp. 95-102.
95. Kato, N., "Vibration Analysis of Underwater Towed System" Journal of the Society of Naval Architecture of Japan, Vol 162, November 1987, pp. 345-355.
96. Kazerooni, H. and Sheridan, T.B., "General Purpose Digital Simulation of Underwater Vehicles", IEEE, CH1685-7/81/0000-0123, 1981, pp. 123-126.
97. Keulegan, G.H. and Carpenter, L.H., "Forces on Cylinders and Plates in an Oscillating Fluid" Journal of Research of the National Bureau of Standards, Vol 60, No. 5, May 1958, pp. 423-440.

98. Kim, Y.H., Vandiver, J.K., and Holler, R., "Vortex-Induced Vibration and Drag Coefficient of Long Cable Subjected to Sheared Flows", 4th Int. Conference on Offshore Mechanics and Arctic Engineering, ASME, Vol II, Dallas, Feb 1985, pp. 584-592.
99. Kinoshita, T., and Takaiwa, K. "The Effect of Current upon Hydrodynamic Forces Acting on Mooring Chain" Journal of Kansai Society of Naval Architecture, No. 203, December 1986.
100. Kokkinowrachos, K. and Giese, K., "Static and Dynamic Analysis for the Design of Flexible Risers in Floating Offshore Production Systems", 3rd Int. Symposium on Practical Design of Ship and Mobile Units, PRADS '87, Trondheim, June 1987, pp. 211-223.
101. Kokkinowrachos, K., Giese, K. and Markoulidis, P., "Comparative Evaluation of Numerical Methods for Non-Linear Flexible Riser Problems", Workshop on Ocean Engineering, Wageningen, November 1987, pp.233-249.
102. Koterayama, W., "Motions of Moored Floating Body and Dynamics of Mooring Lines in Regular Waves", from the Transaction of the West-Japan Society of Naval Architects, No53, 1977, pp. 99-126.
103. Koterayama, W., Kyozuka, Y., Nakamura, M., Ohkusu, M., and Kashiwagi, M., "The Motion of a Depth Controllable Towed Vehicle", 7th Int. Conference on Offshore Mechanics and Arctic Engineering, ASME, Houston, 1988, pp. 423-430.
104. Koterayama, W., Nakamura, M., and Hu, C., "Slow Drift Damping Force due to Viscous Force acting on Mooring Lines and Floating Structure", 7th Int. Conference on Behaviour of Offshore Structures (BOSS '94), Vol 2, Massachusetts, July 1994, pp. 97-112.
105. Kreyszig, E., "Advanced Engineering Mathematics", John Wiley and Sons, Inc, New York, 1993.
106. Kuhtz, S., Bearman, P.W., and Graham, J.M.R., "Experiments on Fixed and Compliant Cylinders in Oscillatory Flow at Low β Numbers", 8th Int. Conference on Behaviour of Offshore Structures (BOSS '97), Vol 2, Delft, July 1997, pp. 79-93.
107. Kuwan, C.T. and Bruen, F.J., "Mooring Line Dynamics: Comparison of Time Domain, Frequency Domain, and Quasi-Static Analyses", OTC 6657, 23rd Offshore Technology Conference, Houston, Texas, May 1991, pp. 95-108.
108. Kwapisz, L., "On a Method of Increasing Accuracy of Numerical Determination of a Line Shape in the Flow", HYDRONAV '97, 12th Int. Conference on Hydrodynamics in Ship Design, Wroclaw, 1997, pp. 303-313.

109. Labbe, J.R., Nikkel, K.G., and Wang, E., "Sensitivity of Marine Riser Response to the Choice of Hydrodynamic Coefficients", OTC 4592, 15th Offshore Technology Conference, Houston, Texas, May 1983, pp. 103-112.
110. Larsen, C.M., Leira, B.J., Olufsen, A., and Sodahl, N., "Design Methods for Flexible Risers", 6th Int. Conference on Behaviour of Offshore Structures (BOSS '92), Vol 2, London, July 1992, pp. 1253-1269.
111. Lax, P.D., and Richtmyer, R.D., "Survey of the Stability of Linear Finite Difference Equations", Communication on Pure and Applied Mathematics, Vol 9, 1956, pp. 267-293.
112. Lindahl, J. and Sjoberg, A., "Dynamic Analysis of Mooring Cables", 2nd Int. Symposium on Ocean Engineering and Ship Handling, Swedish Maritime Research Centre SSPA, Gothenburg, 1983, pp. 281-319.
113. Leira, B.J. and Olufsen, A., "Short-Crested Sea and Riser Estimation", OTC 5467, 19th Offshore Technology Conference, Houston, Texas, April 1987, pp. 417-425.
114. Leonard, J.W., "Curved Finite Element Approximation to Nonlinear Cables", OTC 1533, 4th Offshore Technology Conference, Houston, Texas, May 1972, pp. 225-236.
115. Leonard, J.W., "Non-linear Dynamics of Curved Cable Elements", American Society of Civil Engineers, Journal of the Engineering Mechanics Division, EM3, 99, 1973, pp. 293-309.
116. Leonard, J.W. and Nath, J.H., "Comparison of Finite Element and Lumped Parameter Methods for Oceanic Cables", Engineering Structures, Vol 2, July 1981, pp. 153-167.
117. Leonard, J.W. and Recker, W.W., "Non-linear Dynamics of Cable with Low Initial Tension", American Society of Civil Engineers, Journal of the Engineering Mechanics Division, Vol 98, No. EM2, April 1972, pp. 293-309.
118. Leonard, J.W. and Tuah, H., "Non-linear Deterministic and Stochastic Response of Cable Systems with Large Bodies under Hydrodynamic Loads", Engineering Structures, Vol 8, April 1986, pp. 153-167.
119. Marichal, D. and Jacquot, C., "Study of the Dynamical Behaviour of Immersed Cables", Computer Modelling in Ocean Engineering, Rotterdam, 1988, pp. 631-638.
120. McNamara, J.F. and Hibbitt, H.D., "Numerical Analysis of Flexible Pipes and Risers in Offshore Applications", Offshore Mechanics and Arctic Engineering Speciality Symposium on "Offshore and Arctic Frontiers", 9th Annual ETEC Conference, New Orleans, February 1986, pp. 343-351.

121. McNamara, J.F. and O'Brien, P.J., "Response of Flexible Pipelines to Ocean Wave Loading", 4th Irish Durability and Fracture Conference, Queen's University, Belfast, September 1986, pp. 306-316.
122. McNamara, J.F., O'Brien, P.J., and Gilroy, S.G., "Non-linear Analysis of Flexible Risers Using Hybrid Finite Elements", 5th Int. Symposium on Offshore Mechanics and Arctic Engineering, ASME, Tokyo, April 1986, pp. 371-377.
123. Milinazzo, F., Wilkie, M., and Latchman, S.A., "An Efficient Algorithm for Simulating the Dynamics of Towed Cable Systems", *Ocean Engineering*, Vol 14, No 6, 1987, pp. 513-526.
124. Miller, B.L., "The Hydrodynamic Drag Coefficient of Roughened Circular Cylinders" Transaction, Royal Institute of Naval Architects, London, 1976, pp. 55-70.
125. Miller, R.T., "Dynamics of Towed Underwater Vehicle", Report 219, US Navy Defense Laboratory, Panama City, November 1963.
126. Morison, J.R., O'Brien, M.P., Johnson, J.W., and Schaaf, S.A., "The Forces Exerted by Surface Waves on Piles", *Petroleum Transaction, AIME*, Vol 189, 1950, pp. 149-154.
127. Nakajima, T., Seizo, M. and Masataka, F., "On The Dynamic Analysis of Multi-Component Mooring Lines", OTC 4309, 14th Offshore Technology Conference, Houston, Vol 3, 1982, pp. 105-120.
128. Nakamura, Y., Koterayama, W., and Kyozyuka, W., "Slow Drift Oscillation of Semi-Submersibles and Dynamic Tension of Mooring Lines", 1st Pacific/Asia Offshore Mechanics Symposium, Seoul, June 1990, pp.191-196.
129. Newmark, N.M., "A Method of Computation for Structural Dynamics", *Journal of Engineering Mechanics Division, ASCE*, July 1959, Vol 85, EM3, pp. 67-94.
130. Ormberg, H., Fylling, I.J., and Morch, M., "Dynamic Response in Anchor Lines: Numerical Simulation Compared with Field Measurements", OTC 4497, 15th Offshore Technology Conference, Houston, Texas, May 1983, pp. 459-468.
131. O'Brien, G.G., Hyman, M.A., and Kaplan, S., "A Study of the Numerical Solution of Partial Differential Equations", *Journal of Mathematics and Physics*, Vol 29-30, 1950-51, pp. 223-251.
132. O'Brien, T., "General Solution of Suspended Cable Problems", *Journal of the Structural Division, American Society of Civil Engineers*, Vol 93, No. ST1, February 1967, pp. 2391-2404.
133. Packwood, A.R., "Performance of Segmented Swept and Unswept Cable Fairing at Low Reynolds Numbers", *Ocean Engineering*, Vol 17, No 4, 1990, pp. 393-407.

134. Palo, P.A., Meggitt, D.J., and Nordell, W.J., "Dynamic Cable Analysis Models", OTC 4500, 15th Offshore Technology Conference, Houston, Texas, May 1983, pp. 487-494.
135. Papoulias, F.A., "Stability and Bifurcations of Towed Underwater Vehicles in the Dive Plane", Journal of Ship Research, Vol 36, No 3, September 1992, pp. 255-267.
136. Park, H., "A Tension Measurement Method of a Towing Cable or a Buoy Cable", Ocean Engineering, Vol 20, No 2, 1993, pp. 163-170.
137. Park, K.C. and Underwood, P.G., "A Variable-Step Central Difference Method for Structural Dynamic Analysis – Part 1. Theoretical Aspects", Computer Methods in Applied Mechanics and Engineering, 22, 1980, pp. 241-258.
138. Patel, M.H., "Dynamics of Offshore Structures", Butterworth, London, 1989.
139. Patton, K.T., "The Response of Cable-Moored Axisymmetric Buoys to Ocean Wave Excitation", PhD Thesis, University of Rhode Island, USA, 1972.
140. Paul, B. and Soler, A.I., "Cable Dynamics and Optimum Towing Strategies for Submersibles", MTS Journal, Vol 6, No. 2, March-April 1972, pp. 34-42.
141. Pedersen, P.T. and Junqi, Y., "Mathematical Model for Space Curved Marine Pipelines and Risers", 3rd Int. Symposium on Practical Design of Ship and Mobile Units, PRADS '87, Trondheim, June 1987, pp. 224-235.
142. Peuker, M., Kokkinowrachos, K., and Giese, K., "Development of Flexible Risers for Floating Offshore Production", OTC 5469, 19th Offshore Technology Conference, Houston, Texas, April 1987, pp. 439-450.
143. Peyrot, A.H., "Marine Cable Structures", Journal of the Structural Division, American Society of Civil Engineers, Vol 106, No. ST12, December 1980, pp. 2391-2404.
144. Peyrot, A.H. and Goulois, A.M., "Analysis of Cable Structures", Journal of Computers and Structures, Vol 10, No. 5, 1979, pp. 805-813.
145. Pode, L., "Tables for Computing the Equilibrium Configuration of a Flexible Cable in a Uniform Stream", Report 687, NSD 830-100, The David Taylor Model Basin, March 1951.
146. Polderdijk, S.H., "Response of Anchor Lines to Excitation at the Top", 4th Int. Conference on Behaviour of Offshore Structures (BOSS '85), Delft, July 1985, pp. 347-358.
147. Press, W.H., Flannery, B.P., Teukolsky, S.A., and Vetterling, W.T., "Numerical Recipes, The Art of Scientific Computing", Cambridge University Press, Cambridge, 1986.
148. Preston, J.M., "Stability of Towfish as Sonar Platforms and Benefits of the Two-Part Tow", Defence Research Establishment Pacific, December 1989.

149. Ractliffe, A.T., "Development of a Comprehensive Simulation Model of a Single Point Mooring System", Transaction, Royal Institute of Naval Architects, London, 1980, pp. 33-44.
150. Ractliffe, A.T., "Dynamic Response of Flexible Catenary Risers", Int. Symposium on Floating Production Systems, Royal Institute of Naval Architects, London, March, 1984.
151. Randhawa, P., "Dynamic Simulation of an Underwater Catenary ", BEng Thesis, Australian Maritime College, November 1995.
152. Ranmuthugala, S.D., "The Dynamics of a Two-Part Underwater Tow", Workshop on Ship Hydrodynamics, AMECRC, Launceston, December 1992.
153. Ranmuthugala, S.D. and Gottschalk, S.A., "Dynamic Simulation of a Two-Part Underwater Tow", Offshore Australia Conference, Melbourne, November 1993, Vol 2, Section I-1.
154. Ranmuthugala, S.D. and Gottschalk, S.A., "Investigation into the Dynamic Behaviour of a Two-Part Underwater Tow", Int. Conference on Hydrodynamics (ICH'D'94), Wuxi, October 1994, pp. 663-670.
155. Ranmuthugala, S.D., "Experimental Validation of the Dynamic Behaviour of a Two-Part Underwater Tow", 6 Asian Conference on Fluid Dynamics, Singapore, May 1995, Vol 2, pp. 1078-1081.
156. Ranmuthugala, S.D. and Anderson, B.A., "Investigation into The Dynamics of Two-Part and Multiple Tow Configurations", 16th Int. Conf. on OMAE, Yokohama, Japan, Nov 1997, Vol 1, pp. 31-38.
157. Ranmuthugala, S.D., "Dynamics of Two-Part and Multiple Tows", AME98, Sydney, June 1998.
158. Ranmuthugala, S.D., "Modelling and Related Numerical Stability Requirements of Underwater Towed Bodies", Shallow Survey 99, Int. Conference on High Resolution Survey in Shallow Waters, Sydney, October 1999.
159. Ranmuthugala, S.D., "Modelling And Related Numerical Stability Criteria Of Underwater Two-Part And Multiple Towed Systems" Final Report, Task D2, Australian Maritime Engineering CRC, Launceston, June 2000.
160. Reid, R.O., "Dynamics of Deep-Sea Mooring Lines", Final Report, Project 204, Ref. 68-11F, A & M College of Texas, Texas, July 1968.
161. Rogers, A.C., "Assessment of Vortex Suppression Devices for Production Risers and Towed Deep Ocean Pipe Strings", OTC 4594, 15th Offshore Technology Conference, Houston, Texas, May 1983, pp. 119-126.
162. Russell, G.T. and Bellec, P., "The Investigation of Submersible Manoeuvrability by Simulation", IEEE, CH1685-7/81/0000-0137, 1981, pp. 0137-0141.

163. Sanders, J.V., "A Three Dimensional Dynamic Analysis of a Towed System", *Ocean Engineering*, Vol 9, No 5, 1982, pp. 483-499.
164. Sarpkaya, T., "Vortex Induced Oscillations", *Journal of Applied Mechanics*, ASME, Vol 46, No. 1, March 1975, pp. 241-258.
165. Sarpkaya, T., "Forces on Cylinders and Spheres in a Sinusoidally Oscillating Fluid", *Journal of Applied Mechanics*, ASME, Vol 42, No. 1, March 1975, pp. 32-37.
166. Sarpkaya, T., "The Hydrodynamics Resistance Roughened Cylinders in Harmonic Flow", *Transaction, Royal Institute of Naval Architects*, London, 1977, pp. 41-55.
167. Sarpkaya, T., "Hydroelastic Response of Cylinder in Harmonic Flow", *Transaction, Royal Institute of Naval Architects*, London, 1979, pp. 103-110.
168. Sarpkaya, T., "Hydrodynamic Lift and Drag on Rough Circular Cylinders", OTC 6518, 23rd Offshore Technology Conference, Houston, Texas, May 1991, pp. 191-197.
169. Schram, J.W. and Reyle, S.P., "A Three-Dimensional Dynamic Analyses of a Towed System", *Journal of Hydronautics*, October 1968, Vol 2, No 4, pp. 213-220.
170. Shafiee-far, M., Massie, W.W., and Vugts, J.H., "The Validity of Morison Equation Extensions", OTC 8064, Offshore Technology Conference, Houston, Texas, May 1996, pp. 331-340.
171. Srivastava, S.K. and Ganapathy, C., "Experimental Investigation on Loop Manoeuvre of Underwater Towed Array System", *Ocean Engineering*, Vol 25, No 1, 1998, pp. 85-102.
172. Skop, R.A. and O'Hara, G.J., "A Method for the Analysis of Internally Redundant Structural Cable Arrays", *MTS Journal*, Vol 6, No. 1, January-February 1972, pp. 6-18.
173. Slaouti, A. and Bao, X.L., "On the Use of the Morison Equation in the Vortex Shedding Range of Keulegan-Carpenter Numbers from 6 to 22", 8th Int. Conference on Behaviour of Offshore Structures (BOSS '97), Vol 2, Delft, July 1997, pp. 47-63.
174. Somasundaran, T.P., Vendhan, C.P., and Idichandy V.G., "Hydrodynamic Loading on a Compliant Cylinder", 16th Int. Conference on Offshore Mechanics and Arctic Engineering, ASME, Vol 1-A, Yokohama, April 1997, pp. 65-72.
175. Soylemez, M., "A General Method for Calculating Hydrodynamic Forces", *Ocean Engineering*, Vol 23, No 5, 1996, pp. 423-445.

176. Summey, D.C. and Smith, N.S., "The Development and Application of Underwater Vehicle Design Techniques", IEEE, CH1685-7/81/0000-1160, 1981, pp. 1160-1164.
177. Sun, Y., Leonard, J.W., and Chiou, R.B., "Simulation of Unsteady Oceanic Cable Deployment by Direct Integration with Suppression", Ocean Engineering, Vol 21, No 3, 1994, pp. 243-256.
178. Sun, Y. and Leonard, J.W., "Dynamics of Ocean Cables with Local Low Tension Regions", Ocean Engineering, Vol 25, No 6, 1998, pp. 443-463.
179. Suhara, T., Koterayama, F., Hiyama, H., and Koga, Y., "Behaviour and Tension of Oscillating Chain in Water (III)", Naval Architecture and Ocean Engineering, Vol 22, Dec 1984, pp. 137-145.
180. Suhara, T., Koterayama, F., Hiyama, H., and Koga, Y., "Approximate Analysis of Oscillation of Mooring Line", 3rd Int. Symposium on Practical Design of Ship and Mobile Units, PRADS '87, Trondheim, June 1987, pp. 247-256.
181. Syck, J.M., "Dynamics of Undersea Cables", NUSC Technical Report 6313, Naval Underwater System Centre, Connecticut, May 1981.
182. Teng, B. and Li, Y. "The Wave Current Force Spectrum on Inclined Cylinders", Ocean Engineering, Vol 18, No 6, 1991, pp. 535-553.
183. Thomas, D.O., "A Numerical Investigation of the Time Integration Schemes Applied to the Dynamic Solution of Mooring Lines", PhD Thesis, University of Newcastle upon Tyne, UK, March 1993.
184. Tsinipizoglou, S., "Three Dimensional Dynamic Analysis of Composite Mooring Lines", 3rd Int. Congress on Marine Technology, Vol 1, Int. Maritime Association of East Mediterranean, Athens, May-June 1984, pp. 321.
185. Triantafyllou, M.S., "Preliminary Design of Mooring Systems", Journal of Ship Research, Vol 26, No. 1, March 1982, pp. 25-35.
186. Triantafyllou, M.S. and Blier, A., "The Dynamics of Inclined Taut and Slack Marine Cables", OTC 4498, 15th Offshore Technology Conference, Houston, Texas, May 1983, pp. 469-476.
187. Triantafyllou, M.S., "Linear Dynamics of Cable and Chains", The Shock and Vibration Digest, Volume 16, No. 3, Vibration Institute, Illinois, December 1984.
188. Triantafyllou, M.S., Blier, A., and Shin, H., "Static and Fatigue Analysis of Multi-leg Mooring System", MIT Sea Grant Program, Report MITSG 86-21, Massachusetts Institute of Technology, Cambridge, August 1986.
189. Triantafyllou, M.S., "Cable Mechanics for Moored Floating Systems", 7th Int. Conference on Behaviour of Offshore Structures (BOSS '94), Vol 2, Massachusetts, July 1994, pp. 57-78.

190. Triantafyllou, M.S., Yue, D.K.P., and Tein, D.Y.S., "Damping of Moored Floating Structures", OTC 7489, 26th Offshore Technology Conference, Houston, Texas, May 1994, pp. 215-224.
191. Tuah, H. and Leonard, J.W., "Dynamic Response of Viscoelastic Cable Element", Ocean Engineering, Vol 17, No 1/2, 1990, pp. 23-34.
192. Tuah, H. and Leonard, J.W., "Strumming of Nonlinear Cable Elements using Modal Superposition", Engineering Structures, Vol 14, No. 5, pp. 282-290.
193. Underwood, P.G. and Park, K.C., "A Variable-Step Central Difference Method for Structural Dynamic Analysis – Part 2. Implementation and Performance Evaluation", Computer Methods in Applied Mechanics and Engineering, 23, 1980, pp. 259-279.
194. van den Boom, H.J.J., "Dynamic Behaviour of Mooring Lines", 4th Int. Conference on Behaviour of Offshore Structures (BOSS '85), Delft, July 1985, pp. 359-368.
195. van den Boom, H.J.J., Dekker, J.N., and van Elsacker, A.W., "Dynamic Aspects of Offshore Riser and Mooring Concepts", OTC 5531, 19th Offshore Technology Conference, Houston, Texas, April 1987, pp. 405-416.
196. van den Boom, H.J.J. and van Walree, F., "Hydrodynamic Aspects of Offshore Risers", OTC 6438, 22nd Offshore Technology Conference, Houston, Texas, May 1990, pp. 153-164.
197. van Oortmerssen, G., van der Vegt, J.J.W., and van Walree, F., "Forces on Cylinders in Oscillatory Flow: a Comparison of the Results of Numerical and Physical Models".
198. Vandiver, J. K., "Drag Coefficients of Long Flexible Cylinders", OTC 4490, 15th Offshore Technology Conference, Houston, Texas, May 1983, pp. 405-414.
199. Vandiver, J. K., "The Prediction of Lockin Vibration of Flexible Cylinders in a Sheared Flow", OTC 5006, 17th Offshore Technology Conference, Houston, Texas, May 1985, pp. 405-412.
200. Vandiver, J. K. and Chung, T.Y., "Hydrodynamic Damping on Flexible Cylinders in Sheared Flow", OTC 5524, 19th Offshore Technology Conference, Houston, Texas, April 1987, pp. 343-353.
201. Vandiver, J.K., "Research Challenges in the Vortex-Induced Vibration Prediction of Marine Risers", OTC 8698, Offshore Technology Conference, Houston, Texas, May 1998, pp. 155-163.
202. Vinje, T., "Statistical Distribution of Hydrodynamic Forces on Objects in Current and Waves", Norwegian Maritime Research, No. 2/1980.
203. Walshaw, A.C. and Jobson, D.A., "Mechanics of Fluid", Third Edition, Longman Group Ltd, Essex, 1979.

204. Walton, T.S. and Polachek, H., "Calculation of Transient Motion of Submerged Cables", *Mathematics of Computation*, Vol XIV, 1959, pp. 27-46.
205. Webster, R.L., , "Nonlinear Static and Dynamic Response of Underwater Cable Structures using the Finite Element Method", OTC 2232, 7th Offshore Technology Conference, Houston, Texas, 1975, pp. 753-764.
206. Whitney, A.K. and Nikkel, K.G., " Effects of Shear Flow on Vortex Shedding Induced Vibration of Marine Risers", OTC 4595, 15th Offshore Technology Conference, Houston, Texas, May 1983, pp. 127-136.
207. Wilson, B.W., "Characteristics of Anchor Cables in Uniform Ocean Currents", Technical Report, No. 204-1, A & M College of Texas, Texas, April 1960.
208. Wilson, J.F., "Dynamics of Offshore Structures", John Wiley & Sons, New York, 1984.
209. Winget, J.M. and Huston, R.L., "Cable Dynamics – A Finite Segment Approach", *Journal of Computers and Structures*, Vol 6, 1979, pp. 457-480.
210. Wingham, P.J., "Methods for Reducing Ship Induced Attitude Variations of Passive Towed Bodies", *Advances in Underwater Technology*, pp. 89-97.
211. Wingham, P.J. and Henderson, J.F., "Wind Tunnel Tests on the A.R.E. Towfish 1", UTH Tech Memo 51/88(C), University of Bath, September 1988.
212. Wood, W.L., "Practical Time-Stepping Schemes", Clarendon Press, Oxford, 1990.
213. Yilmaz, O. and Incecik, A., "Extreme Motion Response Analysis of Moored Semi-Submersibles", *Ocean Engineering*, Vol 23, No 6, 1996, pp. 497-517.
214. Yoshida, K. and Suzuki, H., "Criteria for Stress Evaluation of Underwater Line Structures", 3rd Int. Symposium on Practical Design of Ship and Mobile Units, PRADS '87, Trondheim, June 1987, pp. 237-246.
215. Yoshida, K., Suzuki, H., and Oka, N., "A Lift Force Model and Response Analysis of Underwater Line Structures Subjected to Waves" OTC 5218, 18th Offshore Technology Conference, Houston, Texas, May 1986, pp. 547-555.
216. Zare, K. and Datta, T.K., "Dynamic Response of Lazy-S Risers in Random Sea", OTC 6440, 22nd Offshore Technology Conference, Houston, Texas, May 1990, pp. 177-184.
217. Zienkiewicz, O.C., "A New Look at the Newmark, Houbolt and Other Time Stepping Formulas. A weighted Residual Approach", *Earthquake Engineering and Structural Dynamics*, Vol 5, 1977, pp. 413-418.

APPENDIX A

EXPERIENTIAL RESULTS

Code	Primary	Second	J to Dep	Dep	F to Drg	X	Y	Z	T
A11	1.5	0.8	0.25	Fish		0	0	0.05	3.5
A12	1.5	0.8	0.25	Fish		0	0	0.05	2.5
A13	1.5	0.8	0.25	Fish		0	0	0.05	1.5
A21	1.5	0.8	0.25	Fish		0	0	0.075	3.5
A22	1.5	0.8	0.25	Fish		0	0	0.075	2.5
A23	1.5	0.8	0.25	Fish		0	0	0.075	1.5
A31	1.5	0.8	0.25	Fish		0	0	0.1	3.5
A32	1.5	0.8	0.25	Fish		0	0	0.1	2.5
A33	1.5	0.8	0.25	Fish		0	0	0.1	1.5
B11	1.5	0.8	0.25	Fish		0.02	0	0.05	3.5
B12	1.5	0.8	0.25	Fish		0.02	0	0.05	2.5
B13	1.5	0.8	0.25	Fish		0.02	0	0.05	1.5
B21	1.5	0.8	0.25	Fish		0.02	0	0.075	3.5
B22	1.5	0.8	0.25	Fish		0.02	0	0.075	2.5
B23	1.5	0.8	0.25	Fish		0.02	0	0.075	1.5
B31	1.5	0.8	0.25	Fish		0.02	0	0.1	3.5
B32	1.5	0.8	0.25	Fish		0.02	0	0.1	2.5
B33	1.5	0.8	0.25	Fish		0.02	0	0.1	1.5
C11	1.5	0.8	0.25	Fish		0.035	0	0.05	3.5
C12	1.5	0.8	0.25	Fish		0.035	0	0.05	2.5
C13	1.5	0.8	0.25	Fish		0.035	0	0.05	1.5
C21	1.5	0.8	0.25	Fish		0.035	0	0.075	3.5
C22	1.5	0.8	0.25	Fish		0.035	0	0.075	2.5
C23	1.5	0.8	0.25	Fish		0.035	0	0.075	1.5
C31	1.5	0.8	0.25	Fish		0.035	0	0.1	3.5
C32	1.5	0.8	0.25	Fish		0.035	0	0.1	2.5
C33	1.5	0.8	0.25	Fish		0.035	0	0.1	1.5
D21	1.5	0.8	0	Fish		0	0	0.075	3.5
D22	1.5	0.8	0	Fish		0	0	0.075	2.5
D23	1.5	0.8	0	Fish		0	0	0.075	1.5
D31	1.5	0.8	0	Fish		0	0	0.1	3.5
D32	1.5	0.8	0	Fish		0	0	0.1	2.5
D33	1.5	0.8	0	Fish		0	0	0.1	1.5
E21	1.5	0.8	0	Fish		0.02	0	0.075	3.5
E22	1.5	0.8	0	Fish		0.02	0	0.075	2.5
E23	1.5	0.8	0	Fish		0.02	0	0.075	1.5
E31	1.5	0.8	0	Fish		0.02	0	0.1	3.5
E32	1.5	0.8	0	Fish		0.02	0	0.1	2.5
E33	1.5	0.8	0	Fish		0.02	0	0.1	1.5
F21	1.5	0.8	0	Fish		0.035	0	0.075	3.5
F22	1.5	0.8	0	Fish		0.035	0	0.075	2.5
F23	1.5	0.8	0	Fish		0.035	0	0.075	1.5
F31	1.5	0.8	0	Fish		0.035	0	0.1	3.5
F32	1.5	0.8	0	Fish		0.035	0	0.1	2.5
F33	1.5	0.8	0	Fish		0.035	0	0.1	1.5

Scaled Model Tests AMC – Information

Table A1

PTO

Continued from previous page

Code	Primary	Second	J to Dep	Dep	F to Drg	X	Y	Z	T
G21	1.5	0.8	0.25	Ball		0	0	0.075	3.5
G22	1.5	0.8	0.25	Ball		0	0	0.075	2.5
G23	1.5	0.8	0.25	Ball		0	0	0.075	1.5
G31	1.5	0.8	0.25	Ball		0	0	0.1	3.5
G32	1.5	0.8	0.25	Ball		0	0	0.1	2.5
G33	1.5	0.8	0.25	Ball		0	0	0.1	1.5
H21	1.5	0.8	0.25	Ball		0.02	0	0.075	3.5
H22	1.5	0.8	0.25	Ball		0.02	0	0.075	2.5
H23	1.5	0.8	0.25	Ball		0.02	0	0.075	1.5
H31	1.5	0.8	0.25	Ball		0.02	0	0.1	3.5
H32	1.5	0.8	0.25	Ball		0.02	0	0.1	2.5
H33	1.5	0.8	0.25	Ball		0.02	0	0.1	1.5
I21	1.5	0.8	0.25	Ball		0.035	0	0.075	3.5
I22	1.5	0.8	0.25	Ball		0.035	0	0.075	2.5
I23	1.5	0.8	0.25	Ball		0.035	0	0.075	1.5
I31	1.5	0.8	0.25	Ball		0.035	0	0.1	3.5
I32	1.5	0.8	0.25	Ball		0.035	0	0.1	2.5
I33	1.5	0.8	0.25	Ball		0.035	0	0.1	1.5
J21	1.5	0.8	0	Ball		0	0	0.075	3.5
J22	1.5	0.8	0	Ball		0	0	0.075	2.5
J23	1.5	0.8	0	Ball		0	0	0.075	1.5
J31	1.5	0.8	0	Ball		0	0	0.1	3.5
J32	1.5	0.8	0	Ball		0	0	0.1	2.5
J33	1.5	0.8	0	Ball		0	0	0.1	1.5
K21	1.5	0.8	0	Ball		0.02	0	0.075	3.5
K22	1.5	0.8	0	Ball		0.02	0	0.075	2.5
K23	1.5	0.8	0	Ball		0.02	0	0.075	1.5
K31	1.5	0.8	0	Ball		0.02	0	0.1	3.5
K32	1.5	0.8	0	Ball		0.02	0	0.1	2.5
K33	1.5	0.8	0	Ball		0.02	0	0.1	1.5
L21	1.5	0.8	0	Ball		0.035	0	0.075	3.5
L22	1.5	0.8	0	Ball		0.035	0	0.075	2.5
L23	1.5	0.8	0	Ball		0.035	0	0.075	1.5
L31	1.5	0.8	0	Ball		0.035	0	0.1	3.5
L32	1.5	0.8	0	Ball		0.035	0	0.1	2.5
L33	1.5	0.8	0	Ball		0.035	0	0.1	1.5
S21	1.5	0.5	0	Fish		0	0	0.075	3.5
S22	1.5	0.5	0	Fish		0	0	0.075	2.5
S23	1.5	0.5	0	Fish		0	0	0.075	1.5
S31	1.5	0.5	0	Fish		0	0	0.1	3.5
S32	1.5	0.5	0	Fish		0	0	0.1	2.5
S33	1.5	0.5	0	Fish		0	0	0.1	1.5
T21	1.5	0.5	0	Fish		0.035	0	0.075	3.5
T22	1.5	0.5	0	Fish		0.035	0	0.075	2.5
T23	1.5	0.5	0	Fish		0.035	0	0.075	1.5
T31	1.5	0.5	0	Fish		0.035	0	0.1	3.5
T32	1.5	0.5	0	Fish		0.035	0	0.1	2.5
T33	1.5	0.5	0	Fish		0.035	0	0.1	1.5

Scaled Model Tests AMC – Information (continued)

Table A1

PTO

Continued from previous page

Code	Primary	Second	J to Dep	Dep	F to Drg	X	Y	Z	T
V21	1.5	0.5	0.25	Fish		0	0	0.075	3.5
V22	1.5	0.5	0.25	Fish		0	0	0.075	2.5
V23	1.5	0.5	0.25	Fish		0	0	0.075	1.5
V31	1.5	0.5	0.25	Fish		0	0	0.1	3.5
V32	1.5	0.5	0.25	Fish		0	0	0.1	2.5
V33	1.5	0.5	0.25	Fish		0	0	0.1	1.5
X21	1.5	0.5	0.25	Fish		0.035	0	0.075	3.5
X22	1.5	0.5	0.25	Fish		0.035	0	0.075	2.5
X23	1.5	0.5	0.25	Fish		0.035	0	0.075	1.5
X31	1.5	0.5	0.25	Fish		0.035	0	0.1	3.5
X32	1.5	0.5	0.25	Fish		0.035	0	0.1	2.5
X33	1.5	0.5	0.25	Fish		0.035	0	0.1	1.5
AA12	1.5	0.8	0.25	Fish	0.4	0	0	0.075	3.5
AA13	1.5	0.8	0.25	Fish	0.4	0	0	0.075	2.5
AA14	1.5	0.8	0.25	Fish	0.4	0	0	0.075	1.5
AA22	1.5	0.8	0.25	Fish	0.4	0	0	0.1	3.5
AA23	1.5	0.8	0.25	Fish	0.4	0	0	0.1	2.5
AA24	1.5	0.8	0.25	Fish	0.4	0	0	0.1	1.5
AA32	1.5	0.8	0.25	Fish	0.4	0.035	0	0.075	3.5
AA33	1.5	0.8	0.25	Fish	0.4	0.035	0	0.075	2.5
AA34	1.5	0.8	0.25	Fish	0.4	0.035	0	0.075	1.5
AA42	1.5	0.8	0.25	Fish	0.4	0.035	0	0.1	3.5
AA43	1.5	0.8	0.25	Fish	0.4	0.035	0	0.1	2.5
AA44	1.5	0.8	0.25	Fish	0.4	0.035	0	0.1	1.5
AA52	1.5	0.8	0.25	Fish	0.3	0	0	0.1	3.5
AA53	1.5	0.8	0.25	Fish	0.3	0	0	0.1	2.5
AA54	1.5	0.8	0.25	Fish	0.3	0	0	0.1	1.5
AA62	1.5	0.8	0.25	Fish	0.3	0.035	0	0.1	3.5
AA63	1.5	0.8	0.25	Fish	0.3	0.035	0	0.1	2.5
AA64	1.5	0.8	0.25	Fish	0.3	0.035	0	0.1	1.5
AB22	1.5	0.8	0.25	Fish	0.6	0	0	0.1	3.5
AB23	1.5	0.8	0.25	Fish	0.6	0	0	0.1	2.5
AB24	1.5	0.8	0.25	Fish	0.6	0	0	0.1	1.5
AB42	1.5	0.8	0.25	Fish	0.6	0.035	0	0.1	3.5
AB43	1.5	0.8	0.25	Fish	0.6	0.035	0	0.1	2.5
AB44	1.5	0.8	0.25	Fish	0.6	0.035	0	0.1	1.5
AB52	1.5	0.8	0.25	Fish	0.6	0	0	0.075	3.5
AB53	1.5	0.8	0.25	Fish	0.6	0	0	0.075	2.5
AB54	1.5	0.8	0.25	Fish	0.6	0	0	0.075	1.5
AB62	1.5	0.8	0.25	Fish	0.6	0.035	0	0.1	3.5
AB63	1.5	0.8	0.25	Fish	0.6	0.035	0	0.1	2.5
AB64	1.5	0.8	0.25	Fish	0.6	0.035	0	0.1	1.5
AC22	1.5	0.8	0	Ball	0.3	0	0	0.1	3.5
AC23	1.5	0.8	0	Ball	0.3	0	0	0.1	2.5
AC24	1.5	0.8	0	Ball	0.3	0	0	0.1	1.5
AC42	1.5	0.8	0	Ball	0.3	0.035	0	0.1	3.5
AC43	1.5	0.8	0	Ball	0.3	0.035	0	0.1	2.5
AC44	1.5	0.8	0	Ball	0.3	0.035	0	0.1	1.5

Scaled Model Tests AMC – Information (continued)

Table A1

PTO

Continued from previous page

Code	Primary	Second	J to Dep	Dep	F to Drg	X	Y	Z	T
AD22	1.5	0.8	0	Ball	0.6	0	0	0.1	3.5
AD23	1.5	0.8	0	Ball	0.6	0	0	0.1	2.5
AD24	1.5	0.8	0	Ball	0.6	0	0	0.1	1.5
AD42	1.5	0.8	0	Ball	0.6	0.035	0	0.1	3.5
AD43	1.5	0.8	0	Ball	0.6	0.035	0	0.1	2.5
AD44	1.5	0.8	0	Ball	0.6	0.035	0	0.1	1.5
AG21	1.5	0.5	0.25	Ball		0	0	0.075	3.5
AG22	1.5	0.5	0.25	Ball		0	0	0.075	2.5
AG23	1.5	0.5	0.25	Ball		0	0	0.075	1.5
AG31	1.5	0.5	0.25	Ball		0	0	0.1	3.5
AG32	1.5	0.5	0.25	Ball		0	0	0.1	2.5
AG33	1.5	0.5	0.25	Ball		0	0	0.1	1.5
AH21	1.5	0.5	0.25	Ball		0.035	0	0.075	3.5
AH22	1.5	0.5	0.25	Ball		0.035	0	0.075	2.5
AH23	1.5	0.5	0.25	Ball		0.035	0	0.075	1.5
AH31	1.5	0.5	0.25	Ball		0.035	0	0.1	3.5
AH32	1.5	0.5	0.25	Ball		0.035	0	0.1	2.5
AH33	1.5	0.5	0.25	Ball		0.035	0	0.1	1.5
AJ21	1.5	0.5	0	Ball		0	0	0.075	3.5
AJ22	1.5	0.5	0	Ball		0	0	0.075	2.5
AJ23	1.5	0.5	0	Ball		0	0	0.075	1.5
AJ31	1.5	0.5	0	Ball		0	0	0.1	3.5
AJ32	1.5	0.5	0	Ball		0	0	0.1	2.5
AJ33	1.5	0.5	0	Ball		0	0	0.1	1.5
AK21	1.5	0.5	0	Ball		0.035	0	0.075	3.5
AK22	1.5	0.5	0	Ball		0.035	0	0.075	2.5
AK23	1.5	0.5	0	Ball		0.035	0	0.075	1.5
AK31	1.5	0.5	0	Ball		0.035	0	0.1	3.5
AK32	1.5	0.5	0	Ball		0.035	0	0.1	2.5
AK33	1.5	0.5	0	Ball		0.035	0	0.1	1.5
YA11	1.5	0.8	0.25	Fish		0	0.1	0	4.5
YA12	1.5	0.8	0.25	Fish		0	0.1	0	3.5
YA13	1.5	0.8	0.25	Fish		0	0.1	0	2.5
YA14	1.5	0.8	0.25	Fish		0	0.1	0	1.5
YA21	1.5	0.8	0.25	Fish		0	0.15	0	4.5
YA22	1.5	0.8	0.25	Fish		0	0.15	0	3.5
YA23	1.5	0.8	0.25	Fish		0	0.15	0	2.5
YA24	1.5	0.8	0.25	Fish		0	0.15	0	1.5
YB11	1.5	0.5	0.25	Fish		0	0.1	0	4.5
YB12	1.5	0.5	0.25	Fish		0	0.1	0	3.5
YB13	1.5	0.5	0.25	Fish		0	0.1	0	2.5
YB21	1.5	0.5	0.25	Fish		0	0.15	0	4.5
YB22	1.5	0.5	0.25	Fish		0	0.15	0	3.5
YB23	1.5	0.5	0.25	Fish		0	0.15	0	2.5
YC21	1.5	0.8	0	Fish		0	0.15	0	4.5
YC22	1.5	0.8	0	Fish		0	0.15	0	3.5
YC23	1.5	0.8	0	Fish		0	0.15	0	2.5

Scaled Model Tests AMC – Information (continued)

Table A1

PTO

Continued from previous page

Code	Primary	Second	J to Dep	Dep	F to Drg	X	Y	Z	T
YD21	1.5	0.8	0.5	Fish		0	0.15	0	4.5
YD22	1.5	0.8	0.5	Fish		0	0.15	0	3.5
YD23	1.5	0.8	0.5	Fish		0	0.15	0	2.5
YE21	1.5	0.8	0.25	Fish	0.3	0	0.15	0	4.5
YE22	1.5	0.8	0.25	Fish	0.3	0	0.15	0	3.5
YE23	1.5	0.8	0.25	Fish	0.3	0	0.15	0	2.5
YF21	1.5	0.8	0.25	Fish	0.5	0	0.15	0	4.5
YF22	1.5	0.8	0.25	Fish	0.5	0	0.15	0	3.5
YF23	1.5	0.8	0.25	Fish	0.5	0	0.15	0	2.5
YG21	1.5	0.8	0.25	Fish		0	0.15	0	4.5
YG22	1.5	0.8	0.25	Fish		0	0.15	0	3.5
YG23	1.5	0.8	0.25	Fish		0	0.15	0	2.5
YY11	1.5					0	0.1	0	4.5
YY12	1.5					0	0.1	0	3.5
YY13	1.5					0	0.1	0	2.5
YY21	1.5					0	0.15	0	4.5
YY22	1.5					0	0.15	0	3.5
YY23	1.5					0	0.15	0	2.5
WA21	1.5	0.8	0.25	Ball		0	0.15	0	4.5
WA22	1.5	0.8	0.25	Ball		0	0.15	0	3.5
WA23	1.5	0.8	0.25	Ball		0	0.15	0	2.5
WB21	1.5	0.8	0	Ball		0	0.15	0	4.5
WB22	1.5	0.8	0	Ball		0	0.15	0	3.5
WB23	1.5	0.8	0	Ball		0	0.15	0	2.5
WC21	1.5	0.8	0.5	Ball		0	0.15	0	4.5
WC22	1.5	0.8	0.5	Ball		0	0.15	0	3.5
WC23	1.5	0.8	0.5	Ball		0	0.15	0	2.5
WC24	1.5	0.8	0.5	Ball		0	0.15	0	1.5
WD21	1.5	0.5	0.25	Ball		0	0.15	0	4.5
WD22	1.5	0.5	0.25	Ball		0	0.15	0	3.5
WD23	1.5	0.5	0.25	Ball		0	0.15	0	2.5
WD24	1.5	0.5	0.25	Ball		0	0.15	0	1.5
WE21	1.5	0.8	0.25	Ball	0.3	0	0.15	0	4.5
WE22	1.5	0.8	0.25	Ball	0.3	0	0.15	0	3.5
WE23	1.5	0.8	0.25	Ball	0.3	0	0.15	0	2.5
WE24	1.5	0.8	0.25	Ball	0.3	0	0.15	0	1.5
WF21	1.5	0.8	0.25	Ball	0.5	0	0.15	0	4.5
WF22	1.5	0.8	0.25	Ball	0.5	0	0.15	0	3.5
WF23	1.5	0.8	0.25	Ball	0.5	0	0.15	0	2.5
WF24	1.5	0.8	0.25	Ball	0.5	0	0.15	0	1.5

Scaled Model Tests AMC – Information
Table A1

Code	Period	Dep	Max amplitude		Fish	Max amplitude	
		Surge cm	Heave cm	Pitch deg	Surge cm	Heave cm	Pitch deg
A11	3.5	3.6	2.8	2.5	3.4	1.6	1.5
A12	2.5	3.2	3.6	3	2.95	1.1	2
A13	1.5	2.5	3.5	4.5	2.6	0.6	1.2
A21	3.5	6.5	4.4	2.9	5.5	2.8	2.5
A22	2.5	5.8	5.3	4.2	5	2	2.1
A23	1.5	4.3	7.1	7.8	4	0.35	1.5
A31	3.5	8.7	6.4	3.9	7.9	2.75	3
A32	2.5	7.3	7.3	5.6	6.8	2.25	3.2
A33	1.5	5.5	9.8	10.5	5.1	0.5	1.5
B11	3.5	4.5	2.6	2.5	4.4	1.55	1.5
B12	2.5	3.9	3.4	4.3	3.6	1.3	1
B13	1.5	3.6	3.3	8.5	2.4	0.7	1.5
B21	3.5	7.1	4.1	2.5	6.6	1.8	3.2
B22	2.5	6	5.4	4.1	5.4	1.4	2.3
B23	1.5	4.3	7.1	7.5	3.8	0.7	1.7
B31	3.5	9.4	5.5	3.4	8.6	2.85	2.8
B32	2.5	7.9	7.2	5.8	7.3	2.1	2.3
B33	1.5	5.8	10	10.3	5.5	1.1	1.5
C11	3.5	5.7	2.5	2.5	5.2	1.7	1.4
C12	2.5	4.4	3.6	4.5	3.75	1.15	1.9
C13	1.5	3	4	8	2.6	0.8	1.25
C21	3.5	8.5	3.9	2.5	7.7	1.9	2
C22	2.5	6.4	5.5	4.7	6.2	1.6	2.7
C23	1.5	4.2	7.6	8.2	4	0.8	1.5
C31	3.5	11	5.4	3.5	10	2.8	2.4
C32	2.5	9.1	7.3	6	8.2	2.1	3.1
C33	1.5	6	10.25	10.7	6	1.3	2.3
D21	3.5	6.2	4.2	3.4	6	3.2	3.25
D22	2.5	5.85	4.4	4.1	5.4	3.3	3.75
D23	1.5	4.1	6.3	7.1	4.1	1.9	2.7
D31	3.5	9.1	5.3	3.25	8.1	4.7	4.3
D32	2.5	7.5	6.5	5	7.3	3.7	3.3
D33	1.5	7.9	6	8	5.6	2	3.2
E21	3.5	7.7	2.9	2	7.2	4.1	2.8
E22	2.5	6.3	4.4	3.5	6.3	2.7	2.5
E23	1.5	4.4	6.5	6.9	4.3	1.5	2.2
E31	3.5	10	4.2	2.5	9.5	3.5	2.7
E32	2.5	8.8	5.8	4.5	8	3.5	2.8
E33	1.5	5.9	8.5	9.25	5.7	2.5	3.25
F21	3.5	8.8	2.7	1.7	8.5	3.1	3.2
F22	2.5	7.2	4.4	3.8	7	3.7	3.8
F23	1.5	4.6	6.6	7.5	4.5	1.8	3
F31	3.5	11.2	3.9	2.6	10	3	2.8
F32	2.5	9.3	5.7	4.7	8.8	3.7	3.6
F33	1.5	6.2	8.8	9.3	6.1	2.2	3.2
G21	3.5	1.4	7.2		2	2.7	3.2
G22	2.5	1.2	7.2		1.6	2	2.4
G23	1.5	1.2	7.25		1.4	1	1.7
G31	3.5	2	9.4		2.2	4.2	3.1
G32	2.5	1.8	9.4		1.8	2.7	2.8
G33	1.5	1.6	9.6		2.4	1.5	2.2

Scaled Model Tests AMC – Results

Table A2

PTO

Continued from previous page

Code	Period	Dep	Max amplitude		Fish	Max amplitude	
		Surge cm	Heave cm	Pitch deg	Surge cm	Heave cm	Pitch deg
H21	3.5	2.8	6.4		2.9	2.9	2.8
H22	2.5	2.4	6.4		2.5	2.4	2.6
H23	1.5	1.3	7.2		1.8	1.2	1.4
H31	3.5	2.8	9		3.6	4.7	3.8
H32	2.5	2.4	9.2		2.2	2.5	3
H33	1.5	1.4	9.7		2.1	1.4	1.5
I21	3.5	3.4	6.4		4	2.9	2.5
I22	2.5	2.4	6.9		2.5	1.9	2.2
I23	1.5	1.5	7.2		1.65	1.2	1.7
I31	3.5	4.2	8.4		4.3	4.4	3.3
I32	2.5	3.5	8.8		3	2.4	2.5
I33	1.5	1.7	9.4		2.4	1.3	2
J21	3.5	2	6.9		2.5	4	3.2
J22	2.5	1.6	7		1.8	1.8	2.2
J23	1.5	1.2	7.4		1.6	1	1.1
J31	3.5	2.1	9.3		2.9	4	3.9
J32	2.5	1.8	9.6		2.1	2.6	3.3
J33	1.5	1.2	9.8		1.9	1.1	1.7
K21	3.5	2.5	6.6		3	4	3.1
K22	2.5	1.7	6.8		1.8	2.3	2.8
K23	1.5	1	7		1.5	1	1.2
K31	3.5	3	9		3.6	5	3.8
K32	2.5	2	9.2		2.6	3.1	3.4
K33	1.5	1.4	9.4		1.8	1.1	2
L21	3.5	3.8	6		4.2	3.4	3.2
L22	2.5	2	6.8		2.6	2.1	2.3
L23	1.5	1.2	7		1.4	1	1.4
L31	3.5	4.2	8		4.8	4.5	4.1
L32	2.5	2.5	9		2.8	3	3
L33	1.5	1.2	9.8		1.7	1	1.6
S21	3.5	7	3.7	2.4	6.5	3.9	3.1
S22	2.5	6.5	4.25	3.55	6.2	3.4	3.7
S23	1.5	4.5	6.5	7.1	4.5	2.6	3.1
S31	3.5	9.4	5.1	3.2	9	4.8	3.5
S32	2.5	8.9	5.6	4.3	8.3	4.5	4.6
S33	1.5	5.9	8.9	9.75	5.9	2.9	4.6
T21	3.5	8.8	3.2	2.2	8.4	4.5	3.5
T22	2.5	7.5	4.7	4.1	7	3.4	3.8
T23	1.5	4.4	7.3	8	4.4	2.8	3.5
T31	3.5	11	4.3	2.35	10	3.6	3.2
T32	2.5	9.2	6.15	5	8.6	4.4	4.1
T33	1.5	5.85	9.05	9.9	5.6	3.1	4.5
V21	3.5	6.6	3.6	2.6	5.7	2.8	2.7
V22	2.5	6.35	4	3.4	5.7	2.2	2.3
V23	1.5	4.75	6.2	6.8	4.4	1.7	2.2
V31	3.5	9.1	4.85	3.6	8.2	3.6	2.7
V32	2.5	8.4	5.8	4.35	7.6	3	2.8
V33	1.5	6.7	8.6	9.45	5.9	2.2	2.8

Scaled Model Tests AMC – Results (continued)

Table A2

PTO

Continued from previous page

Code	Period	Dep	Max amplitude		Fish	Max amplitude	
		Surge cm	Heave cm	Pitch deg	Surge cm	Heave cm	Pitch deg
X21	3.5	8.9	2.4	1.6	8.2	2.25	2.25
X22	2.5	7.25	3.9	3.5	7	2.35	2.75
X23	1.5	5.05	6.85	7.2	4.9	1.7	3
X31	3.5	8.2	3.65	2.1	9.8	2.7	2.7
X32	2.5	9.3	5.35	4.15	8.8	2.5	3.1
X33	1.5	6.15	8.75	9.9	5.9	1.9	3.3
AA12	3.5	6.2	3.6	2.4	5.4	2.5	1.5
AA13	2.5	5.7	3.7	3.1	5	1.8	2.1
AA14	1.5	5.4	4.4	5.4	5	1.75	1.5
AA22	3.5	8.4	4.6	2.55	7.4	2.85	2.2
AA23	2.5	7.8	4.75	3.35	6.6	2.4	2.35
AA24	1.5	7.3	7.35	7.8	5.4	1.65	2.2
AA32	3.5	7.8	1.6	2.1	7	1.6	1.3
AA33	2.5	7.5	2.6	2.95	6	1.3	2.1
AA34	1.5	5.6	4.4	6.8	4.2	1	1.8
AA42	3.5	10.25	2.95	1.55	8.3	2.35	2.15
AA43	2.5	9	3.6	2.9	7.8	2.1	2.5
AA44	1.5	7.4	7.05	7.7	6	1.6	2.3
AA52	3.5	8	5.4	2.7	7.2	3.25	2.3
AA53	2.5	7.45	5.5	3.9	6.4	2.9	2.75
AA54	1.5	7.2	7.3	8.4	5.3	1.85	2.55
AA62	3.5	9.75	3.75	2.1	8.25	2.5	2.1
AA63	2.5	9.5	3.85	3.1	8	2.25	2.25
AA64	1.5	7.2	7.1	8.1	5.85	2.1	2.75
AB22	3.5	7.7	5.1	3.35	6.95	3.2	2.7
AB23	2.5	7.3	5.2	3.8	6.3	2.75	3.05
AB24	1.5	7	7	7.3	5.45	2.05	2.9
AB42	3.5	9.7	3.65	2.1	8.4	2.8	2.4
AB43	2.5	8.75	4.3	3.2	7.6	2.15	2.35
AB44	1.5	7.1	7.25	7.85	5.75	2	2.75
AB52	3.5	8	4.85	3	6.9	3.25	2.45
AB53	2.5	8.15	4.75	3.6	6.45	2.75	2.25
AB54	1.5	7.35	7.2	7.7	5.4	1.9	2.7
AB62	3.5	9.8	3.35	2	8.4	2.55	2.15
AB63	2.5	9.5	4.15	3.05	7.75	1.8	2.45
AB64	1.5	7.1	7.7	8	5.7	1.8	2.4
AC22	3.5	1.6	8.4		2.6	5.5	4.85
AC23	2.5	1.4	9		1.9	4.45	4.6
AC24	1.5	1	9.2		1.8	2.2	2.8
AC42	3.5	3	8.2		4.25	5.4	4.35
AC43	2.5	2.2	8.6		2.7	3.85	3.65
AC44	1.5	1.3	9.2		1.75	2.1	2.9
AD22	3.5	1.6	8.8		2.5	5.85	4.5
AD23	2.5	1.3	9		1.65	4.45	4.1
AD24	1.5	1	9.2		1.9	2.3	2.9
AD42	3.5	3	8		3.75	5.3	4.25
AD43	2.5	2.4	6.8		2.8	4	4.1
AD44	1.5	1.6	7.2		1.8	2.25	3

Scaled Model Tests AMC – Results (continued)

Table A2

PTO

Continued from previous page

Code	Period	Dep	Max amplitude		Fish	Max amplitude	
		Surge cm	Heave cm	Pitch deg	Surge cm	Heave cm	Pitch deg
AG21	3.5	1.65	6.8		2.1	5.2	4.2
AG22	2.5	1.4	7		1.75	3.1	3.4
AG23	1.5	1	7.2		1.7	1.35	2
AG31	3.5	2.2	9.2		2.8	6.2	4.9
AG32	2.5	1.8	9.4		2.2	3.6	4
AG33	1.5	1.3	9.8		2.6	2	3.1
AH21	3.5	3.6	6.4		3.6	4.5	4.1
AH22	2.5	2.6	6.8		2.4	3	2.9
AH23	1.5	1.3	7.2		1.5	1.5	2.2
AH31	3.5	4.2	8.2		5	5.9	5.1
AH32	2.5	2.6	8.6		2.75	3.9	4.2
AH33	1.5	1.4	9.4		2.4	2	2.8
AJ21	3.5	1.8	7		2.2	5.6	4.9
AJ22	2.5	1.3	7.2		1.6	3.6	4.4
AJ23	1.5	0.8	7.6		1.3	1.1	2.1
AJ31	3.5	2.2	8.8		2.8	6.8	5.6
AJ32	2.5	1.6	9.2		2	4.3	4.9
AJ33	1.5	1.2	9.6		1.9	1.65	2.5
AK21	3.5	4.2	6		4.5	4.9	4.5
AK22	2.5	2.4	6.8		2.7	3.3	3.9
AK23	1.5	1.1	7.2		1.2	1.4	2.2
AK31	3.5	4.6	8.6		4.8	6.4	5.5
AK32	2.5	3.3	9.2		3.3	4.2	4.5
AK33	1.5	1.5	9.6		1.5	1.4	2.6
Code	Period	Dep	Max amplitude		Fish	Max amplitude	
		Surge cm	Sway cm	Yaw deg	Surge cm	Sway cm	Yaw deg
YA11	4.5				0.6	3.1	2
YA12	3.5				0.9	2.2	1.55
YA13	2.5				0.95	1.2	1.25
YA14	1.5				0.55	0.8	1.1
YA21	4.5				0.75	3.9	2.4
YA22	3.5				0.85	2.8	2
YA23	2.5				1.1	1.6	1.35
YA24	1.5				0.9	1	1.25
YB11	4.5				1	4.75	3.25
YB12	3.5				0.7	1.9	1.95
YB13	2.5				0.75	1.3	2
YB21	4.5				1	5	3.9
YB22	3.5				1.05	2.6	2.3
YB23	2.5				1	1.35	1.5
YC21	4.5				0.75	7.1	3.6
YC22	3.5				0.9	3.7	2.3
YC23	2.5				0.75	2.1	1.85
YD21	4.5				0.85	4.1	2.7
YD22	3.5				0.95	1.9	2.05
YD23	2.5				0.95	1.4	1.95

Scaled Model Tests AMC – Results (continued)

Table A2 PTO

Continued from previous page

Code		Dep	Max amplitude		Fish	Max amplitude	
		Surge cm	Sway cm	Yaw deg	Surge cm	Sway cm	Yaw deg
YE21		4.5			0.75	5.4	3.6
YE22		3.5			0.8	2.85	1.85
YE23		2.5			0.85	1.8	1.7
YF21		4.5			1	5.7	3.8
YF22		3.5			1.05	3.3	2.6
YF23		2.5			0.75	1.1	1.4
YG21		4.5			0.7	4.1	3.9
YG22		3.5			1	2.7	2.7
YG23		2.5			0.6	1.65	1.8
YY11		4.5			1.6	9.3	5.65
YY12		3.5			0.95	5	4.2
YY13		2.5			0.9	2.7	2.7
YY21		4.5			1.6	12.3	7.85
YY22		3.5			1.2	6.75	5.75
YY23		2.5			0.75	3.65	3.8
WA21		4.5			1.2	10	6.65
WA22		3.5			0.85	7.5	5.8
WA23		2.5			0.9	5.8	5.9
WB21		4.5			1.55	9.7	7.05
WB22		3.5			1.3	8.45	6.85
WB23		2.5			0.9	7.25	7.2
WC21		4.5			1.6	7.5	6.2
WC22		3.5			1.05	6.5	5.2
WC23		2.5			0.75	3.8	4.2
WC24		1.5			0.5	1.4	1.3
WD21		4.5			1.5	11.2	8.1
WD22		3.5			1.2	10	7.5
WD23		2.5			0.9	5.85	5.9
WD24		1.5			0.7	1.85	2.7
WE21		4.5			1.45	8.5	6.5
WE22		3.5			0.9	8.6	6.3
WE23		2.5			0.62	7.2	6.1
WE24		1.5			0.7	1.75	2.6
WF21		4.5			1.25	7.5	4.8
WF22		3.5			1	7.7	5.7
WF23		2.5			0.88	6.3	5.95
WF24		1.5			0.95	2.1	2.5

Scaled Model Tests AMC – Results
Table A2

File	Type	Primary Cable	Second Cable	Dir to Swell	Wing	Tow Point
ST1-1	Single	10	-	with	no	forward
ST2-1	Single	10	-	into	no	forward
ST3-1	Single	10	-	across	no	forward
ST4-1	Single	10	-	with	no	forward
ST5-1	Single	10	-	across	no	forward
ST6-1	Single	10	-	into	no	forward
ST7-1	Single	20	-	into	no	forward
ST8-1	Single	20	-	with	no	forward
ST9-1	Single	20	-	across	no	forward
ST10-1	Single	20	-	with	no	forward
ST11-1	Single	20	-	into	no	forward
ST12-1	Single	20	-	across	no	forward
ST13-1	Single	20	-	across	no	forward
ST14-1	Single	20	-	with	no	forward
ST15-1	Single	20	-	into	no	forward
ST16-1	Single	20	-	with	yes	forward
ST17-1	Single	20	-	into	yes	forward
ST18-1	Single	20	-	across	yes	forward
ST19-1	Single	20	-	into	yes	forward
ST20-1	Single	60	-	into	yes	forward
ST21-1	Single	60	-	with	yes	forward
ST22-1	Single	60	-	-	yes	forward
ST23-1	Single	60	-	with	yes	forward
ST24-1	Single	60	-	into	no	forward
ST25-1	Single	60	-	with	no	forward
ST26-1	Single	60	-	into	no	forward
ST27-1	Single	60	-	with	no	forward
ST28-1	Single	60	-	into	no	forward
ST29-1	Single	60	-	with	no	forward
ST30-1	Single	60	-	into	yes	forward
ST31-1	Single	60	-	with	yes	forward
ST32-1	Single	60	-	into	yes	forward
ST33-1	Single	60	-	with	yes	forward
ST34-1	Single	20	-	with	yes	forward
ST35-1	Single	20	-	into	yes	forward
ST36-1	Single	20	-	across	yes	forward
ST37-1	Single	20	-	across	yes	forward
ST38-1	Single	20	-	with	yes	forward
ST39-1	Single	20	-	into	yes	forward
ST40-1	Single	20	-	with	yes	forward
ST41-1	Single	20	-	into	yes	forward
ST42-1	Single	20	-	across	yes	forward
ST43-1	Single	20	-	across	yes	forward
ST44-1	Single	20	-	with	yes	forward
ST45-1	Single	20	-	into	yes	forward
ST46-1	Single	20	-	with	no	forward
ST47-1	Single	20	-	into	no	forward
ST48-1	Single	20	-	across	no	forward
ST49-1	Single	20	-	across	no	forward
ST50-1	Single	20	-	with	no	forward

Trial 1 – Tow Information

Table A3

PTO

Continued from previous page

Trial 1 – Jervis Bay

Tow-PartTow

1994

File	Type	Primary Cable	Second Cable	Dir to Swell	Wing	Tow Point
TT1-1	Two Part	10	10	across	no	forward
TT2-1	Two Part	10	10	into	no	forward
TT3-1	Two Part	10	10	with	no	forward
TT4-1	Two Part	20	10	into	no	forward
TT5-1	Two Part	20	10	across	no	forward
TT6-1	Two Part	20	10	with	no	forward
TT7-1	Two Part	20	10	into	no	forward
TT8-1	Two Part	20	10	135 deg	no	forward
TT9-1	Two Part	20	10	across	no	forward
TT10-1	Two Part	20	10	into	no	forward
TT11-1	Two Part	20	10	across	no	forward
TT12-1	Two Part	20	10	with	no	forward
TT13-1	Two Part	20	10	into	yes	forward
TT14-1	Two Part	20	10	across	yes	forward
TT15-1	Two Part	20	10	into	no	aft
TT16-1	Two Part	20	10	with	no	aft
TT17-1	-	-	-	-	-	
TT18-1	-	-	-	-	-	
TT19-1	-	-	-	-	-	
TT20-1	-	-	-	-	-	
TT21-1	Two Part	50	10	into	no	forward
TT22-1	Two Part	50	10	with	no	forward

Trial 1 – Tow Information (continued)

Table A3

Trial 2 – Port Phillip Bay**Single Tow****1995**

File	Type	Primary Cable	Second Cable	Dir to Swell	Wing	Tow Point	Speed
ST1-2	Single	20	-	with	no	forward	5.5
ST2-2	Single	20	-	across	no	forward	5.7
ST3-2	Single	20	-	into	no	forward	5.6
ST4-2	Single	20	-	with	no	forward	5.6
ST5-2	Single	20	-	across	no	forward	5.7
ST6-2	Single	20	-	into	no	forward	5.6
ST7-2	Single	20	-	with	no	forward	8.5
ST8-2	Single	20	-	across	no	forward	8.6
ST9-2	Single	20	-	into	no	forward	8.5
ST10-2	Single	15	-	with	yes	forward	5.5
ST11-2	Single	15	-	across	yes	forward	5.5
ST12-2	Single	15	-	into	yes	forward	?
ST13-2	Single	15	-	?	yes	forward	8.4
ST14-2	Single	35	-	across	yes	forward	5.6
ST15-2	Single	35	-	with	yes	forward	6.2
ST16-2	Single	35	-	into	yes	forward	4.6
ST17-2	Single	35	-	across	yes	forward	7.5
ST18-2	Single	35	-	with	yes	forward	8
ST19-2	Single	35	-	into	yes	forward	7.9
ST20-2	Single	40.5	-	across	no	forward	5.7
ST21-2	Single	40.5	-	with	no	forward	5.6
ST22-2	Single	40.5	-	into	no	forward	5.4
ST23-2	Single	40.5	-	across	no	forward	7.8
ST24-2	Single	40.5	-	with	no	forward	8.3
ST25-2	Single	40.5	-	into	no	forward	7.5

Trial 2 – Port Phillip Bay**Two-Part Tow****1995**

File	Type	Primary Cable	Second Cable	Dir to Swell	Wing	Tow Point	Speed
TT1-2	Two Part	20	10	across	no	forward	4.7
TT2-2	Two Part	20	10	with	no	forward	5.7
TT3-2	Two Part	20	10	across	no	forward	5.7
TT4-2	Two Part	20	10	into	no	forward	5.9
TT5-2	Two Part	20	10	across	no	forward	6.2
TT6-2	Two Part	20	10	with	no	forward	6.7
TT7-2	Two Part	20	10	into	no	forward	7.5
TT8-2	Two Part	20	10	with	no	forward	7.9
TT9-2	Two Part	20	10	across	no	forward	7.9
TT10-2	Two Part	-	-	-	-	-	-
TT11-2	Two Part	15	10	with	yes	forward	4.9
TT12-2	Two Part	15	10	across	yes	forward	5.2
TT13-2	Two Part	15	10	into	yes	forward	5
TT14-2	Two Part	15	10	across	yes	forward	5.4
TT15-2	Two Part	15	10	with	yes	aft	5.3
TT16-2	Two Part	15	10	into	yes	aft	5.1
TT17-2	Two Part	15	10	with	yes		8.1
TT18-2	Two Part	15	10	across	yes		8

Trial 2 – Tow Information (continued)**Table A4****PTO**

Continued from previous page

TT19-2	Two Part	15	10	across	yes		8
TT20-2	Two Part	15	10	into	yes		7.7
TT21-2	Two Part	-	-	-	-	-	-
TT22-2	Two Part	15	10	with	yes	forward	8
TT23-2	Two Part	15	10	across	yes	forward	8
TT24-2	Two Part	15	10	into	yes	forward	8.4
TT25-2	Two Part	40	10	into	no	forward	5.6
TT26-2	Two Part	40	10	across	no	forward	5.8
TT27-2	Two Part	40	10	with	no	forward	6.3
TT28-2	Two Part	40	10	across	no	forward	8
TT29-2	Two Part	40	10	into	no	forward	8
TT30-2	Two Part	40	10	with	no	forward	7.8

Trial 2 – Tow Information (continued)

Table A4

Trial 1 – Jervis Bay**1994**

Filtering: 0.1 - 25 Hz

Surge Rate Limit: 1 m/s

Roll Rate Limit: 6.28 deg/s

Sway Rate Limit: 1 m/s

Pitch Rate Limit: 6.28 deg/s

Heave Rate Limit: 1 m/s

Yaw Rate Limit: 1.05 deg/s

Single Tow

File	Rates	Roll	Pitch	Yaw	Surge	Sway	Heave	Any
ST1-1	Av Deviation	10.14	1.36	2.17	0.22	0.07	0.05	
	St Dev	0.056	0.114	0.044	0.36	0.183	0.151	
	% Excess	63.93	0.01	71.68	0	0	0	87.53
ST2-1	Av Deviation	12.31	1.65	2.49	0.11	0.07	0.1	
	St Dev	0.054	0.135	0.045	0.176	0.194	0.192	
	% Excess	70.3	0.32	75.92	0	0	0	91.11
ST3-1	Av Deviation	12.34	1.41	2.7	0.09	0.09	0.07	
	St Dev	0.08	0.072	0.061	0.177	0.243	0.182	
	% Excess	70.39	0.08	77.22	0	0	0	91.93
ST4-1	Av Deviation	12.76	2.22	2.86	0.34	0.08	0.06	
	St Dev	0.077	0.119	0.16	0.283	0.24	0.212	
	% Excess	68.73	2.79	75.64	1.81	0	0	91.54
ST5-1	Av Deviation	13.19	2.34	3.82	0.15	0.14	0.09	
	St Dev	0.086	0.141	0.145	0.207	0.199	0.148	
	% Excess	70.15	4.04	81.98	0	0	0	93.88
ST6-1	Av Deviation	12.74	2.49	3.4	0.18	0.14	0.11	
	St Dev	0.041	0.057	0.093	0.168	0.144	0.136	
	% Excess	69.49	4.73	80.58	0	0	0	93.38
ST7-1	Av Deviation	6.74	1.02	1.7	0.1	0.06	0.05	
	St Dev	0.068	0.071	0.091	0.206	0.207	0.181	
	% Excess	45.15	0	62.36	0	0	0	76.61
ST8-1	Av Deviation	6.86	1.01	1.81	0.09	0.06	0.05	
	St Dev	0.066	0.047	0.097	0.261	0.181	0.231	
	% Excess	46.35	0	65.5	0	0	0	79.08
ST9-1	Av Deviation	7.18	1.05	2.09	0.07	0.06	0.06	
	St Dev	0.034	0.062	0.054	0.195	0.201	0.244	
	% Excess	48.91	0	70.4	0	0	0	83.46
ST10-1	Av Deviation	7.29	1.03	1.76	0.14	0.06	0.03	
	St Dev	0.055	0.1	0.061	0.442	0.236	0.318	
	% Excess	49.66	0.01	64.27	0	0	0	81.23
ST11-1	Av Deviation	7.93	1.24	2.19	0.09	0.06	0.05	
	St Dev	0.054	0.056	0.05	0.241	0.141	0.175	
	% Excess	52.95	0.01	72.04	0	0	0	85.69
ST12-1	Av Deviation	7.31	1.13	1.97	0.06	0.06	0.05	
	St Dev	0.046	0.059	0.059	0.157	0.153	0.272	
	% Excess	49.47	0.05	67.8	0	0	0	82.71
ST13-1	Av Deviation	5.03	1.06	1.64	0.06	0.07	0.05	
	St Dev	0.053	0.094	0.101	0.233	0.206	0.171	
	% Excess	31.85	0.01	60.27	0	0	0	71.43
ST14-1	Av Deviation	4.6	0.88	1.1	0.09	0.09	0.03	
	St Dev	0.047	0.121	0.141	0.605	0.498	0.175	
	% Excess	27.62	0	44.52	0	0	0	58.57
ST15-1	Av Deviation	4.76	0.97	1.22	0.11	0.05	0.05	
	St Dev	0.041	0.083	0.106	0.292	0.144	0.287	
	% Excess	29.23	0	48.59	0	0	0	61.5
ST16-1	Av Deviation	2.2	0.72	0.66	0.08	0.03	0.03	
	St Dev	0.082	0.107	0.075	0.517	0.252	0.114	
	% Excess	2.9	0	20.03	0	0	0	22

Trial 1 – Tow Results (continued)**Table A5****PTO**

Continued from previous page

File	Rates	Roll	Pitch	Yaw	Surge	Sway	Heave	Any
ST17-1	Av Deviation	3.87	1.09	1.12	0.18	0.06	0.06	
	St Dev	0.128	0.08	0.101	0.237	0.204	0.155	
	% Excess	19.86	0	44.71	0	0	0	53.98
ST18-1	Av Deviation	2.69	0.95	0.98	0.09	0.06	0.06	
	St Dev	0.086	0.066	0.095	0.168	0.292	0.187	
	% Excess	6.95	0	39.03	0	0	0	42.67
ST19-1	Av Deviation	5.48	1.15	1.32	0.22	0.12	0.09	
	St Dev	0.064	0.213	0.162	0.255	0.307	0.258	
	% Excess	35.67	0.14	51.29	0.24	0	0	68.55
ST20-1	Av Deviation	3.19	2.31	1.33	0.26	0.07	0.11	
	St Dev	0.042	0.252	0.245	0.196	0.183	0.2	
	% Excess	11.54	4.65	52.25	0.51	0	0	58.63
ST21-1	Av Deviation	4.04	1.1	0.98	0.28	0.12	0.08	
	St Dev	0.063	0.117	0.154	0.224	0.286	0.157	
	% Excess	21.28	0.17	37.33	0.04	0	0	49.67
ST22-1 - Not Complete								
ST23-1	Av Deviation	2.56	1.2	0.96	0.27	0.11	0.08	
	St Dev	0.34	0.276	0.363	0.34	0.276	0.289	
	% Excess	7.06	0.59	32.35	0.98	0	0	35.16
ST24-1	Av Deviation	3.07	3.35	1.22	0.32	0.06	0.16	
	St Dev	0.115	0.276	0.124	0.272	0.186	0.215	
	% Excess	10.63	14.64	47.51	2.23	0	0	57.39
ST25-1	Av Deviation	13.18	1.57	2.39	0.42	0.11	0.14	
	St Dev	0.153	0.333	0.088	0.619	0.417	0.484	
	% Excess	73.24	0.9	75	8.35	0	0	93.14
ST26-1	Av Deviation	3.41	4.16	1.42	0.41	0.06	0.18	
	St Dev	0.165	0.276	0.21	0.278	0.259	0.225	
	% Excess	14.19	21.19	52.29	5.66	0	0	65.9
ST27-1	Av Deviation	8.74	1.67	1.71	0.42	0.12	0.13	
	St Dev	0.182	0.21	0.12	0.348	0.299	0.287	
	% Excess	53.75	0.65	62.92	4.21	0	0	80.46
ST28-1	Av Deviation	4.35	2.24	1.53	0.27	0.07	0.14	
	St Dev	0.215	0.32	0.195	0.264	0.257	0.221	
	% Excess	23.35	4.76	55.62	0.84	0	0	65.12
ST29-1	Av Deviation	5.67	0.89	1.41	0.23	0.14	0.09	
	St Dev	0.074	0.211	0.121	0.443	0.404	0.378	
	% Excess	36.79	0.03	53.16	0.31	0	0	67.57
ST30-1	Av Deviation	2.62	2.28	0.84	0.31	0.06	0.12	
	St Dev	0.111	0.256	0.165	0.23	0.173	0.185	
	% Excess	7.07	4.97	31.13	2.08	0	0	39.63
ST31-1	Av Deviation	3.54	0.91	1.14	0.29	0.14	0.09	
	St Dev	0.083	0.157	0.12	0.314	0.278	0.347	
	% Excess	16.18	0.01	45.79	0.33	0	0	53.14
ST32-1	Av Deviation	4.28	2.53	1.49	0.31	0.12	0.12	
	St Dev	0.077	0.41	0.199	0.241	0.198	0.267	
	% Excess	24.03	7.46	56.63	1.06	0	0	67.89
ST33-1	Av Deviation	4.51	0.96	1.34	0.29	0.25	0.1	
	St Dev	0.068	0.241	0.197	0.307	0.346	0.274	
	% Excess	26.17	0.09	50.43	0.36	0	0	61.6
ST34-1	Av Deviation	4.05	0.91	1.18	0.06	0.04	0.04	
	St Dev	0.03	0.055	0.038	0.171	0.227	0.2	
	% Excess	21.31	0	47.36	0	0	0	57.81
ST35-1	Av Deviation	3.79	0.93	1.11	0.08	0.03	0.05	
	St Dev	0.047	0.043	0.049	0.145	0.246	0.15	
	% Excess	18.58	0	44.56	0	0	0	54.12
ST36-1	Av Deviation	4.19	1.17	1.37	0.16	0.07	0.07	
	St Dev	0.034	0.114	0.093	0.42	0.374	0.201	
	% Excess	23.17	0.01	53.39	0	0	0	63.74

Trial 1 – Tow Results (continued)

Table A5

PTO

Continued from previous page

File	Rates	Roll	Pitch	Yaw	Surge	Sway	Heave	Any
ST37-1	Av Deviation	3.67	0.82	1.27	0.15	0.1	0.06	
	St Dev	0.051	0.352	0.238	0.485	0.335	0.286	
	% Excess	17.14	0	49.28	0	0	0	56.9
ST38-1	Av Deviation	3.3	0.64	0.88	0.05	0.04	0.04	
	St Dev	0.037	0.049	0.055	0.277	0.21	0.149	
	% Excess	12.81	0	34.23	0	0	0	41.72
ST39-1	Av Deviation	2.49	0.68	0.61	0.09	0.04	0.05	
	St Dev	0.043	0.085	0.079	0.147	0.19	0.163	
	% Excess	4.55	0	17.06	0	0	0	20.33
ST40-1	Av Deviation	2.39	0.78	1.25	0.07	0.04	0.04	
	St Dev	0.079	0.059	0.052	0.374	0.233	0.221	
	% Excess	4.28	0	50.21	0	0	0	51.45
ST41-1	Av Deviation	1.52	0.72	0.93	0.1	0.04	0.04	
	St Dev	0.059	0.091	0.106	0.222	0.169	0.133	
	% Excess	0.24	0	36.07	0	0	0	36.15
ST42-1	Av Deviation	2.23	0.95	1.32	0.13	0.07	0.05	
	St Dev	0.072	0.101	0.075	0.293	0.236	0.202	
	% Excess	3.86	0	52.04	0	0	0	53.13
ST43-1	Av Deviation	2.23	1.24	1.16	0.13	0.07	0.07	
	St Dev	0.071	0.105	0.099	0.21	0.324	0.207	
	% Excess	2.6	0	46.68	0	0	0	47.68
ST44-1	Av Deviation	4.52	1.04	1.25	0.06	0.04	0.05	
	St Dev	0.06	0.034	0.037	0.221	0.167	0.155	
	% Excess	26.82	0	50.09	0	0	0	62.15
ST45-1	Av Deviation	2.77	1.04	0.97	0.11	0.03	0.05	
	St Dev	0.054	0.046	0.058	0.166	0.187	0.157	
	% Excess	7.65	0	38.64	0	0	0	42.42
ST46-1	Av Deviation	9.86	0.87	1.69	0.06	0.04	0.02	
	St Dev	0.109	0.048	0.078	0.202	0.157	0.185	
	% Excess	60.44	0	61.98	0	0	0	82.68
ST47-1	Av Deviation	6.63	0.95	1.38	0.07	0.04	0.03	
	St Dev	0.122	0.097	0.083	0.233	0.118	0.115	
	% Excess	44.98	0	54.28	0	0	0	71.51
ST48-1	Av Deviation	9.84	1.23	2.03	0.14	0.1	0.06	
	St Dev	0.12	0.139	0.074	0.634	0.412	0.302	
	% Excess	60.47	0.04	67.7	0	0	0	85.24
ST49-1	Av Deviation	7.85	1.34	2.43	0.07	0.08	0.07	
	St Dev	0.044	0.088	0.104	0.23	0.208	0.329	
	% Excess	51.82	0.05	72.41	0	0	0	85.19
ST50-1	Av Deviation	6.68	1.02	1.86	0.04	0.06	0.03	
	St Dev	0.051	0.058	0.059	0.234	0.116	0.208	
	% Excess	45.22	0	65.09	0	0	0	79.1
Averages	Av Deviation	5.85	1.35	1.58	0.17	0.08	0.07	
	Av St Dev	0.08	0.14	0.11	0.28	0.24	0.22	
	Av % Excess	32.46	1.48	54.43	0.59	0.00	0.00	65.38

Tow-Part Tow

File	Rates	Roll	Pitch	Yaw	Surge	Sway	Heave	Any
TT1-1	Av Deviation	1.62	0.78	0.54	0.09	0.03	0.05	
	St Dev	0.096	0.16	0.106	0.252	0.147	0.163	
	% Excess	0.41	0	11.65	0	0	0	11.98
TT2-1	Av Deviation	1.37	1.62	0.44	0.16	0.02	0.08	
	St Dev	0.135	0.196	0.137	0.171	0.24	0.202	
	% Excess	0.35	0.85	6.13	0	0	0	7.04
TT3-1	Av Deviation	1.4	0.68	0.42	0.09	0.02	0.05	
	St Dev	0.154	0.201	0.159	0.23	0.172	0.244	
	% Excess	0.14	0	4.91	0	0	0	5.04

Trial 1 – Tow Results (continued)

Table A5

PTO

Continued from previous page

File	Rates	Roll	Pitch	Yaw	Surge	Sway	Heave	Any
TT4-1	Av Deviation	2.22	0.84	0.56	0.1	0.03	0.06	
	St Dev	0.049	0.088	0.053	0.187	0.263	0.201	
	% Excess	2.78	0	12.76	0	0	0	14.67
TT5-1	Av Deviation	2.11	0.73	0.57	0.08	0.04	0.06	
	St Dev	0.085	0.112	0.068	0.262	0.201	0.372	
	% Excess	1.9	0	13.94	0	0	0	15.32
TT6-1	Av Deviation	2.2	0.67	0.56	0.07	0.04	0.03	
	St Dev	0.054	0.054	0.053	0.25	0.227	0.19	
	% Excess	2.47	0	13.44	0	0	0	15.15
TT7-1	Av Deviation	1.89	0.77	0.51	0.08	0.03	0.04	
	St Dev	0.07	0.09	0.082	0.188	0.27	0.201	
	% Excess	0.97	0	9.59	0	0	0	10.13
TT8-1	Av Deviation	1.82	0.062	0.51	0.07	0.06	0.06	
	St Dev	0.044	0.07	0.071	0.34	0.292	0.261	
	% Excess	0.82	0	9.63	0	0	0	10.13
TT9-1	Av Deviation	2.02	0.84	0.61	0.08	0.06	0.09	
	St Dev	0.048	0.099	0.085	0.182	0.275	0.28	
	% Excess	1.48	0	16.96	0	0	0	17.88
TT10-1	Av Deviation	1.97	0.75	0.55	0.08	0.03	0.04	
	St Dev	0.069	0.1	0.077	0.213	0.255	0.235	
	% Excess	1.26	0	12.92	0	0	0	13.79
TT11-1	Av Deviation	1.82	0.62	0.51	0.07	0.06	0.07	
	St Dev	0.048	0.098	0.09	0.181	0.353	0.323	
	% Excess	0.69	0	9.94	0	0	0	10.47
TT12-1	Av Deviation	1.86	0.6	0.5	0.06	0.03	0.03	
	St Dev	0.092	0.085	0.082	0.28	0.254	0.228	
	% Excess	1	0	8.92	0	0	0	9.68
TT13-1	Av Deviation	1.86	0.75	0.48	0.07	0.03	0.03	
	St Dev	0.068	0.078	0.096	0.175	0.196	0.207	
	% Excess	0.88	0	8.39	0	0	0	8.91
TT14-1	Av Deviation	1.77	0.61	0.48	0.07	0.05	0.05	
	St Dev	0.102	0.091	0.113	0.242	0.358	0.303	
	% Excess	0.63	0	8.5	0	0	0	8.95
TT15-1	Av Deviation	1.97	1.24	0.53	0.15	0.07	0.13	
	St Dev	0.056	0.152	0.052	0.169	0.342	0.266	
	% Excess	1.61	0	11.39	0	0	0	12.27
TT16-1	Av Deviation	1.77	0.59	0.45	0.07	0.03	0.03	
	St Dev	0.07	0.062	0.058	0.375	0.271	0.336	
	% Excess	0.5	0	6.6	0	0	0	6.91
TT17-1 to 21-1 Not Complete								
TT21-1	Av Deviation	1.9	0.86	0.52	0.11	0.08	0.09	
	St Dev	0.043	0.119	0.069	0.342	0.347	0.277	
	% Excess	0.89	0	10.87	0	0	0	11.42
TT22-1	Av Deviation	1.59	0.67	0.41	0.08	0.05	0.04	
	St Dev	0.046	0.03	0.057	0.306	0.301	0.41	
	% Excess	0.21	0	4.15	0	0	0	4.27
Averages	Av Deviation	1.84	0.76	0.51	0.09	0.04	0.06	
	Av St Dev	0.07	0.10	0.08	0.24	0.26	0.26	
	Av % Excess	1.06	0.05	10.04	0.00	0.00	0.00	10.78

Trial 1 – Tow Results

Table A5

Trial 2 – Port Phillip Bay**1995**

Filtering: 0.1 - 25 Hz

Surge Rate Limit: 1 m/s

Roll Rate Limit: 6.28 deg/s

Sway Rate Limit: 1 m/s

Pitch Rate Limit: 6.28 deg/s

Heave Rate Limit: 1 m/s

Yaw Rate Limit: 1.05 deg/s

Single Tow

File	Rates	Roll	Pitch	Yaw	Surge	Sway	Heave	Any
ST1-2	Av Deviation	16.11	0.93	3.25	0.03	0.05	0.05	
	St Dev	0.021	0.025	0.023	0.232	0.102	0.103	
	% Excess	83.54	0	83.62	0	0	0	97.5
ST2-2	Av Deviation	14.18	1.08	3.01	0.04	0.05	0.06	
	St Dev	0.051	0.056	0.048	0.112	0.127	0.186	
	% Excess	78.43	0.01	80.75	0	0	0	94.68
ST3-2	Av Deviation	13.16	1.02	2.79	0.03	0.05	0.06	
	St Dev	0.04	0.055	0.035	0.073	0.185	0.097	
	% Excess	75.94	0	80	0	0	0	93.53
ST4-2	Av Deviation	15.59	0.95	3.21	0.03	0.05	0.04	
	St Dev	0.035	0.034	0.037	0.31	0.161	0.155	
	% Excess	82.78	0	83.51	0	0	0	97.01
ST5-2	Av Deviation	14.03	1.02	3.03	0.04	0.05	0.05	
	St Dev	0.053	0.036	0.047	0.098	0.125	0.139	
	% Excess	78.71	0	81.69	0	0	0	94.85
ST6-2	Av Deviation	12.83	0.95	2.76	0.03	0.04	0.06	
	St Dev	0.04	0.045	0.033	0.128	0.141	0.186	
	% Excess	74.86	0	80.04	0	0	0	93
ST7-2	Av Deviation	4.81	0.91	0.85	0.03	0.09	0.05	
	St Dev	0.043	0.04	0.04	0.167	0.186	0.128	
	% Excess	29.83	0	32.01	0	0	0	50.04
ST8-2	Av Deviation	4.96	0.91	0.89	0.04	0.1	0.04	
	St Dev	0.06	0.095	0.058	0.295	0.165	0.118	
	% Excess	31.2	0.01	34.24	0	0	0	52.29
ST9-2	Av Deviation	4.43	0.85	0.82	0.03	0.08	0.04	
	St Dev	0.027	0.023	0.028	0.212	0.229	0.144	
	% Excess	25.97	0	30.28	0	0	0	46.23
ST10-2	Av Deviation	3.1	1.08	1.37	0.05	0.04	0.05	
	St Dev	0.021	0.033	0.031	0.283	0.161	0.104	
	% Excess	10.36	0	54.06	0	0	0	58.89
ST11-2	Av Deviation	3.17	1.12	1.48	0.05	0.04	0.06	
	St Dev	0.025	0.026	0.033	0.145	0.213	0.118	
	% Excess	11.44	0	57.09	0	0	0	62.06
ST12-2	Av Deviation	3.22	1.12	1.53	0.04	0.04	0.07	
	St Dev	0.023	0.025	0.041	0.148	0.158	0.122	
	% Excess	11.7	0	58.6	0	0	0	63.4
ST13-2	Av Deviation	6.36	1.84	1.77	0.16	0.22	0.37	
	St Dev	0.029	0.036	0.027	0.168	0.178	0.169	
	% Excess	43.13	0.57	63.55	0	0.04	3.19	79.86
ST14-2	Av Deviation	3.17	1.42	1.56	0.15	0.06	0.24	
	St Dev	0.032	0.095	0.061	0.168	0.133	0.233	
	% Excess	11.49	0.03	58.53	0	0	0.29	63.32
ST15-2	Av Deviation	3.37	1.22	1.45	0.08	0.06	0.19	
	St Dev	0.037	0.034	0.033	0.138	0.235	0.148	
	% Excess	14.05	0	55.62	0	0	0.01	61.62
ST16-2	Av Deviation	2.79	1.57	1.27	0.12	0.06	0.27	
	St Dev	0.037	0.067	0.055	0.143	0.167	0.144	
	% Excess	7.35	0.13	50.86	0	0	0.48	54.66
ST17-2	Av Deviation	4.93	1.75	1.78	0.12	0.25	0.31	
	St Dev	0.029	0.031	0.041	0.167	0.157	0.105	
	% Excess	30.67	0.52	63.94	0	0.32	0.89	75.21

Trial 2 – Tow Results**Table A6****PTO**

Continued from previous page

File	Rates	Roll	Pitch	Yaw	Surge	Sway	Heave	Any
ST18-2	Av Deviation	4.88	1.77	1.71	0.09	0.23	0.31	
	St Dev	0.032	0.025	0.031	0.189	0.168	0.201	
	% Excess	30.47	0.45	62.72	0	0.01	1.27	74.6
ST19-2	Av Deviation	4.68	1.7	1.63	0.09	0.24	0.26	
	St Dev	0.027	0.028	0.038	0.159	0.154	0.117	
	% Excess	28.52	0.36	60.83	0	0.26	0.18	71.75
ST20-2	Av Deviation	11.94	1.25	2.55	0.07	0.05	0.04	
	St Dev	0.065	0.097	0.044	0.184	0.152	0.176	
	% Excess	71.24	0.01	76.25	0	0	0	91.01
ST21-2	Av Deviation	15.59	0.97	3.07	0.03	0.06	0.03	
	St Dev	0.028	0.032	0.015	0.182	0.111	0.13	
	% Excess	82.47	0.01	82.39	0	0	0	97.11
ST22-2	Av Deviation	8.91	1.29	2.06	0.04	0.04	0.04	
	St Dev	0.049	0.068	0.046	0.079	0.131	0.098	
	% Excess	60.44	0.04	71.27	0	0	0	85.4
ST23-2	Av Deviation	4.64	0.83	0.85	0.04	0.09	0.05	
	St Dev	0.055	0.059	0.042	0.144	0.176	0.082	
	% Excess	27.81	0	32.24	0	0	0	48.46
ST24-2	Av Deviation	4.49	0.75	0.85	0.03	0.09	0.05	
	St Dev	0.02	0.027	0.038	0.139	0.137	0.111	
	% Excess	26.51	0	32.19	0	0	0	47.73
ST25-2	Av Deviation	5.1	0.9	0.86	0.04	0.09	0.05	
	St Dev	0.038	0.074	0.066	0.21	0.215	0.13	
	% Excess	32.43	0	33.03	0	0	0	52.62
Averages	Av Deviation	7.62	1.17	1.86	0.06	0.09	0.11	
	Av St Dev	0.04	0.05	0.04	0.17	0.16	0.14	
	Av % Excess	42.45	0.09	59.97	0.00	0.03	0.25	72.27

Tow-Part Tow

File	Rates	Roll	Pitch	Yaw	Surge	Sway	Heave	Any
TT1-2	Av Deviation	2.57	0.62	0.63	0.05	0.03	0.02	
	St Dev	0.106	0.098	0.06	0.147	0.14	0.154	
	% Excess	5.59	0	18.13	0	0	0	20.64
TT2-2	Av Deviation	2.44	0.6	0.61	0.05	0.03	0.02	
	St Dev	0.042	0.045	0.022	0.195	0.108	0.167	
	% Excess	3.94	0	16.86	0	0	0	17.99
TT3-2	Av Deviation	2.43	0.57	0.61	0.06	0.03	0.02	
	St Dev	0.042	0.027	0.024	0.174	0.111	0.103	
	% Excess	3.71	0	16.51	0	0	0	17.57
TT4-2	Av Deviation	2.26	0.89	0.66	0.06	0.04	0.02	
	St Dev	0.057	0.043	0.031	0.175	0.17	0.14	
	% Excess	2.82	0	20.71	0	0	0	22.61
TT5-2	Av Deviation	2.25	0.9	0.68	0.07	0.05	0.02	
	St Dev	0.046	0.043	0.042	0.149	0.129	0.146	
	% Excess	2.59	0	21.18	0	0	0	22.75
TT6-2	Av Deviation	2.31	0.91	0.69	0.07	0.04	0.02	
	St Dev	0.04	0.034	0.036	0.235	0.128	0.168	
	% Excess	2.85	0	22.39	0	0	0	24.09
TT7-2	Av Deviation	2.79	1.2	0.82	0.06	0.05	0.03	
	St Dev	0.033	0.029	0.028	0.208	0.168	0.12	
	% Excess	7.28	0.05	30.55	0	0	0	33.95
TT8-2	Av Deviation	2.88	1.25	0.86	0.07	0.06	0.03	
	St Dev	0.047	0.04	0.033	0.216	0.102	0.15	
	% Excess	8	0.06	32.68	0	0	0	36.33
TT9-2	Av Deviation	2.91	1.28	0.84	0.08	0.06	0.03	
	St Dev	0.03	0.057	0.021	0.293	0.199	0.151	
	% Excess	8.59	0.04	31.79	0	0	0	35.63
TT10-2 - Incomplete Run								

Trial 2 – Tow Results (continued)

Table A6

PTO

Continued from previous page

File	Rates	Roll	Pitch	Yaw	Surge	Sway	Heave	Any
TT11-2	Av Deviation	2.92	0.86	0.74	0.1	0.04	0.03	30.57
	St Dev	0.05	0.057	0.028	0.23	0.202	0.148	
	% Excess	8.64	0	25.31	0	0	0	
TT12-2	Av Deviation	2.92	0.86	0.72	0.09	0.04	0.03	29.5
	St Dev	0.047	0.045	0.03	0.176	0.197	0.175	
	% Excess	8.77	0	24.25	0	0	0	
TT13-2	Av Deviation	2.7	0.75	0.67	0.08	0.03	0.02	25.06
	St Dev	0.08	0.09	0.051	0.26	0.191	0.126	
	% Excess	6.71	0	20.96	0	0	0	
TT14-2	Av Deviation	2.89	0.87	0.75	0.14	0.04	0.03	31.45
	St Dev	0.069	0.072	0.048	0.446	0.206	0.129	
	% Excess	8.62	0	26.05	0	0	0	
TT15-2	Av Deviation	2.97	0.83	0.75	0.08	0.05	0.03	31.27
	St Dev	0.086	0.068	0.042	0.192	0.117	0.202	
	% Excess	9.31	0	25.84	0	0	0	
TT16-2	Av Deviation	2.74	0.76	0.69	0.09	0.04	0.02	26.63
	St Dev	0.066	0.056	0.039	0.222	0.196	0.139	
	% Excess	7.42	0	22.15	0	0	0	
TT17-2	Av Deviation	4.94	1.75	1.2	0.17	0.22	0.09	63.74
	St Dev	0.063	0.118	0.06	0.285	0.247	0.233	
	% Excess	31.08	0.44	48.31	0	0	0	
TT18-2	Av Deviation	4.95	1.92	1.23	0.2	0.26	0.1	63.94
	St Dev	0.063	0.099	0.038	0.176	0.187	0.175	
	% Excess	30.9	0.55	49.02	0	0	0	
TT19-2	Av Deviation	5.04	1.9	1.34	0.3	0.26	0.11	67.41
	St Dev	0.076	0.137	0.054	0.235	0.183	0.211	
	% Excess	31.63	0.74	53	0.57	0	0	
TT20-2	Av Deviation	4.66	1.85	1.19	0.25	0.29	0.11	61.53
	St Dev	0.104	0.221	0.094	0.158	0.168	0.27	
	% Excess	27.86	0.39	47.61	0	0	0	
TT21-2- Incomplete run								
TT22-2	Av Deviation	4.98	1.86	1.25	0.23	0.22	0.1	64.64
	St Dev	0.054	0.091	0.05	0.159	0.207	0.159	
	% Excess	31.56	0.71	49.46	0	0	0	
TT23-2	Av Deviation	5.05	1.82	1.28	0.23	0.22	0.1	66.15
	St Dev	0.068	0.129	0.06	0.175	0.226	0.193	
	% Excess	31.83	0.91	51.2	0	0.06	0	
TT24-2	Av Deviation	4.81	1.77	1.29	0.21	0.2	0.09	65.38
	St Dev	0.057	0.106	0.046	0.174	0.252	0.167	
	% Excess	29.8	0.64	51.71	0	0	0	
TT25-2	Av Deviation	2.25	0.52	0.56	0.03	0.03	0.02	14.42
	St Dev	0.05	0.036	0.048	0.169	0.117	0.122	
	% Excess	2.42	0	13.71	0	0	0	
TT26-2	Av Deviation	2.43	0.57	0.62	0.05	0.03	0.02	18.98
	St Dev	0.037	0.044	0.023	0.206	0.142	0.148	
	% Excess	4.05	0	17.7	0	0	0	
TT27-2	Av Deviation	2.55	0.59	0.64	0.03	0.03	0.02	21.36
	St Dev	0.063	0.03	0.043	0.253	0.148	0.11	
	% Excess	5.14	0	19.68	0	0	0	
TT28-2	Av Deviation	3.32	0.78	0.87	0.04	0.05	0.02	39.24
	St Dev	0.038	0.031	0.031	0.183	0.126	0.158	
	% Excess	13.13	0	33.59	0	0	0	
TT29-2	Av Deviation	3.18	0.77	0.82	0.04	0.05	0.02	36.06
	St Dev	0.05	0.044	0.034	0.122	0.16	0.114	
	% Excess	11.69	0	30.71	0	0	0	
TT30-2	Av Deviation	3.38	0.83	0.9	0.02	0.05	0.03	41.39
	St Dev	0.043	0.044	0.03	0.202	0.157	0.185	
	% Excess	14.19	0	35.18	0	0	0	
Averages	Av Deviation	3.27	1.07	0.85	0.11	0.09	0.04	36.80
	Av St Dev	0.06	0.07	0.04	0.21	0.17	0.16	
	Av % Excess	12.86	0.16	30.58	0.02	0.00	0.00	

Trial 2 – Tow Results (continued)

Table A6

Single Tow

% Excess				Av Dev (Std Dev) %Sign					
Run	Yaw	Pitch	Any	Yaw	Pitch	Wing	Dirn	Len	Vel
ST1	83.62	0	97.5	3.25(0.07)	0.93(0.02)	NW	0	20	5.5
ST2	80.75	0.01	94.68	3.01(0.14)-84	1.08(0.06)+97	NW	90	20	5.7
ST4	83.51	0	97.01	3.21(0.12)	0.95(0.03)	NW	0	20	5.6
ST5	81.69	0	94.85	3.03(0.14)-64	1.02(0.04)+82	NW	90	20	5.7
ST7	32.01	0	50.04	0.85(0.03)	0.91(0.04)	NW	0	20	8.5
ST8	34.24	0.01	52.29	0.89(0.05)+47	0.91(0.09)+ 2	NW	90	20	8.6
ST10	54.06	0	58.89	1.37(0.04)	1.08(0.04)	W	0	15	5.5
ST11	57.09	0	62.06	1.48(0.05)+90	1.12(0.03)+58	W	90	15	5.5
ST15	55.62	0	61.62	1.45(0.05)	1.22(0.04)	W	0	35	6.2
ST14	58.53	0.03	63.32	1.56(0.10)+67	1.42(0.13)+82	W	90	35	5.6
ST18	62.72	0.45	74.6	1.71(0.05)	1.77(0.04)	W	0	35	8
ST17	63.94	0.52	75.21	1.78(0.07)+54	1.75(0.05)-21	W	90	35	7.5
ST21	82.39	0.01	97.11	3.07(0.05)	0.97(0.03)	NW	0	40.5	5.6
ST20	76.25	0.01	91.01	2.55(0.11)-99	1.25(0.12)+97	NW	90	40.5	5.7
ST24	32.19	0	47.73	0.85(0.03)	0.75(0.02)	NW	0	40.5	8.3
ST23	32.24	0	48.46	0.85(0.04)+ 2	0.83(0.05)+85	NW	90	40.5	7.8
Averages first line			73.06	1.97	1.07				
Averages other lines			72.73	1.89	1.17				

ST1	83.62	0	97.5	3.25(0.07)	0.93(0.02)	NW	0	20	5.5
ST3	80	0	93.53	2.79(0.10)-99	1.02(0.06)+84	NW	180	20	5.6
ST4	83.51	0	97.01	3.21(0.12)	0.95(0.03)	NW	0	20	5.6
ST6	80.04	0	93	2.76(0.09)-99	0.95(0.04)+ 2	NW	180	20	5.6
ST7	32.01	0	50.04	0.85(0.03)	0.91(0.04)	NW	0	20	8.5
ST9	30.28	0	46.23	0.82(0.02)-52	0.85(0.02)-83	NW	180	20	8.5
ST10	54.06	0	58.89	1.37(0.04)	1.08(0.04)	W	0	15	5.5
ST12	58.6	0	63.4	1.53(0.06)+96	1.12(0.03)+59	W	180	15	?
ST15	55.62	0	61.62	1.45(0.05)	1.22(0.04)	W	0	35	6.2
ST16	50.86	0.13	54.66	1.27(0.07)-96	1.57(0.11)+99	W	180	35	4.6
ST18	62.72	0.45	74.6	1.71(0.05)	1.77(0.04)	W	0	35	8
ST19	60.83	0.36	71.75	1.63(0.06)-64	1.70(0.05)-70	W	180	35	7.9
ST21	82.39	0.01	97.11	3.07(0.05)	0.97(0.03)	NW	0	40.5	5.6
ST22	71.27	0.04	85.4	2.06(0.09)-99	1.29(0.09)+99	NW	180	40.5	5.4
ST24	32.19	0	47.73	0.85(0.03)	0.75(0.02)	NW	0	40.5	8.3
ST25	33.03	0	52.62	0.86(0.06)+11	0.90(0.07)+96	NW	180	40.5	7.5
Averages first line			73.06	1.97	1.07				
Averages other lines			70.07	1.72	1.18				

Trial 2 – Results – Direction to Swell

Table A7

PTO

Continued from previous page

Two-Part Tow

% Excess				Av Dev (Std Dev) %Sign					
Run	Yaw	Pitch	Any	Yaw	Pitch	Wing	Dirn	Len	Vel
TT2	16.86	0	17.99	0.61(0.01)	0.60(0.03)	NW	0	20	5.7
TT3	16.51	0	17.57	0.61(0.01)+2	0.57(0.02)-63	NW	90	20	5.7
TT6	22.39	0	24.09	0.69(0.02)	0.91(0.03)	NW	0	20	6.7
TT5	21.18	0	22.75	0.68(0.03)-19	0.90(0.04)-14	NW	90	20	6.2
TT8	32.68	0.06	36.33	0.86(0.03)	1.25(0.05)	NW	0	20	7.9
TT9	31.79	0.04	35.63	0.84(0.02)-43	1.28(0.07)+25	NW	90	20	7.9
TT11	25.31	0	30.57	0.74(0.02)	0.86(0.05)	W	0	15	4.9
TT12	24.25	0	29.5	0.72(0.02)-49	0.86(0.04)+2	W	90	15	5.2
TT15	25.84	0	31.27	0.75(0.03)	0.83(0.06)	W	0	15	5.3
TT14	26.05	0	31.45	0.75(0.04)+2	0.87(0.06)+33	W	90	15	5.4
TT17	48.31	0.44	63.74	1.20(0.07)	1.75(0.21)	W	0	15	8.1
TT18	49.02	0.55	63.94	1.23(0.05)+26	1.92(0.19)+43	W	90	15	8
TT19	53	0.74	67.41	1.34(0.07)+81	1.90(0.26)+32	W	90	15	8
TT22	49.46	0.71	64.64	1.25(0.06)	1.86(0.17)	W	0	15	8
TT23	51.2	0.91	66.15	1.28(0.08)+23	1.82(0.23)-10	W	90	15	8
TT27	19.68	0	21.36	0.64(0.03)	0.59(0.02)	NW	0	40	6.3
TT26	17.7	0	18.98	0.62(0.01)-47	0.57(0.03)-47	NW	90	40	5.8
TT30	35.18	0	41.39	0.90(0.03)	0.83(0.04)	NW	0	40	7.8
TT28	33.59	0	39.24	0.87(0.03)-54	0.78(0.02)-74	NW	90	40	8
Averages first line			36.82	0.85	1.05				
Averages other lines			39.26	0.89	1.15				

TT2	16.86	0	17.99	0.61(0.01)	0.60(0.03)	NW	0	20	5.7
TT4	20.71	0	22.61	0.66(0.02)+95	0.89(0.04)+99	NW	180	20	5.9
TT8	32.68	0.06	36.33	0.86(0.03)	1.25(0.05)	NW	0	20	7.9
TT7	30.55	0.05	33.95	0.82(0.02)-71	1.20(0.03)-56	NW	180	20	7.5
TT11	25.31	0	30.57	0.74(0.02)	0.86(0.05)	W	0	15	4.9
TT13	20.96	0	25.06	0.67(0.03)-91	0.75(0.07)-79	W	180	15	5
TT15	25.84	0	31.27	0.75(0.03)	0.83(0.06)	W	0	15	5.3
TT16	22.15	0	26.63	0.69(0.03)-83	0.76(0.04)-65	W	180	15	5.1
TT22	49.46	0.71	64.64	1.25(0.06)	1.86(0.17)	W	0	15	8
TT20	47.61	0.39	61.53	1.19(0.11)-33	1.85(0.41)-2	W	180	15	7.7
TT24	51.71	0.64	65.38	1.29(0.06)+33	1.77(0.19)-26	W	180	15	8.4
TT27	19.68	0	21.36	0.64(0.03)	0.59(0.02)	NW	0	40	6.3
TT25	13.71	0	14.42	0.56(0.03)-96	0.52(0.02)-99	NW	180	40	5.6
TT30	35.18	0	41.39	0.90(0.03)	0.83(0.04)	NW	0	40	7.8
TT29	30.71	0	36.06	0.82(0.03)-95	0.77(0.03)-76	NW	180	40	8
Averages first line			34.79	0.82	0.97				
Averages other lines			35.7	0.84	1.06				

Trial 2 – Results – Direction to Swell (continued)
Table A7

Single Tow

% Excess				Av Dev (Std Dev) %Sign					
Run	Yaw	Pitch	Any	Yaw	Pitch	Wing	Dirn	Len	Vel
ST1	83.62	0	97.5	3.25(0.07)	0.93(0.02)	NW	0	20	5.5
ST21	82.39	0.01	97.11	3.07(0.05)-95	0.97(0.03)+67	NW	0	40.5	5.6
ST4	83.51	0	97.01	3.21(0.12)	0.95(0.03)	NW	0	20	5.6
ST21	82.39	0.01	97.11	3.07(0.05)-71	0.97(0.03)+31	NW	0	40.5	5.6
ST7	32.01	0	50.04	0.85(0.03)	0.91(0.04)	NW	0	20	8.5
ST24	32.19	0	47.73	0.85(0.03)+2	0.75(0.02)-99	NW	0	40.5	8.3
ST2	80.75	0.01	94.68	3.01(0.14)	1.08(0.06)	NW	90	20	5.7
ST20	76.25	0.01	91.01	2.55(0.11)-98	1.25(0.12)+77	NW	90	40	5.7
ST5	81.69	0	94.85	3.03(0.14)	1.02(0.04)	NW	90	20	5.7
ST20	76.25	0.01	91.01	2.55(0.11)-99	1.25(0.12)+92	NW	90	40	5.7
ST8	34.24	0.01	52.29	0.89(0.05)	0.91(0.09)	NW	90	20	8.6
ST23	32.24	0	48.46	0.85(0.04)-46	0.83(0.05)-55	NW	90	40.5	7.8
ST3	80	0	93.53	2.79(0.10)	1.02(0.06)	NW	180	20	5.6
ST22	71.27	0.04	85.4	2.06(0.09)-99	1.29(0.09)+99	NW	180	40.5	5.4
ST6	80.04	0	93	2.76(0.09)	0.95(0.04)	NW	180	20	5.6
ST22	71.27	0.04	85.4	2.06(0.09)-99	1.29(0.09)+99	NW	180	40.5	5.4
ST9	30.28	0	46.23	0.82(0.02)	0.85(0.02)	NW	180	20	8.5
ST25	33.03	0	52.62	0.86(0.06)+48	0.90(0.07)+51	NW	180	40.5	7.5
ST10	54.06	0	58.89	1.37(0.04)	1.08(0.04)	W	0	15	5.5
ST15	55.62	0	61.62	1.45(0.05)+77	1.22(0.04)+98	W	0	35	6.2
ST11	57.09	0	62.06	1.48(0.05)	1.12(0.03)	W	90	15	5.5
ST14	58.53	0.03	63.32	1.56(0.10)+53	1.42(0.13)+96	W	90	35	5.6
Averages first line			76.37	2.13	0.98				
Averages other lines			74.62	1.9	1.1				
ST12	58.6	0	63.4	1.53(0.06)	1.12(0.03)	W	180	15	?
ST16	50.86	0.13	54.66	1.27(0.07)-99	1.57(0.11)+99	W	180	35	4.6
ST19	60.83	0.36	71.75	1.63(0.06)+74	1.70(0.05)+99	W	180	35	7.9
Averages first line			63.4	1.53	1.12				
Averages other lines			63.2	1.45	1.64				

Two-Part Tow

% Excess				Av Dev (Std Dev) %Sign					
Run	Yaw	Pitch	Any	Yaw	Pitch	Wing	Dirn	Len	Vel
TT1	18.13	0	20.64	0.63(0.04)	0.62(0.06)	NW	90	20	4.7
TT26	17.7	0	18.98	0.62(0.01)-17	0.57(0.03)-53	NW	90	40	5.8
TT9	31.79	0.04	35.63	0.84(0.02)	1.28(0.07)	NW	90	20	7.9
TT28	33.59	0	39.24	0.87(0.03)+61	0.78(0.02)-99	NW	90	40	8
TT3	16.51	0	17.57	0.61(0.01)	0.57(0.02)	NW	90	20	5.7
TT26	17.7	0	18.98	0.62(0.01)+34	0.57(0.03)+2	NW	90	40	5.8
TT5	21.18	0	22.75	0.68(0.03)	0.90(0.04)	NW	90	20	6.2
TT26	17.7	0	18.98	0.62(0.01)-93	0.57(0.03)-99	NW	90	40	5.8

Trial 2 – Results – Cable Length

Table A8

PTO

Continued from previous page

% Excess				Av Dev (Stnd Dev) %Sign					
Run	Yaw	Pitch	Any	Yaw	Pitch	Wing	Dirn	Len	Vel
TT2	16.86	0	17.99	0.61(0.01)	0.60(0.03)	NW	0	20	5.7
TT27	19.68	0	21.36	0.64(0.03)+64	0.59(0.02)-23	NW	0	40	6.3
TT6	22.39	0	24.09	0.69(0.02)	0.91(0.03)	NW	0	20	6.7
TT27	19.68	0	21.36	0.64(0.03)-80	0.59(0.02)-99	NW	0	40	6.3
TT8	32.68	0.06	36.33	0.86(0.03)	1.25(0.05)	NW	0	20	7.9
TT30	35.18	0	41.39	0.90(0.03)+66	0.83(0.04)-99	NW	0	40	7.8
TT4	20.71	0	22.61	0.66(0.02)	0.89(0.04)	NW	180	20	5.9
TT25	13.71	0	14.42	0.56(0.03)-99	0.52(0.02)-99	NW	180	40	5.6
TT7	30.55	0.05	33.95	0.82(0.02)	1.20(0.03)	NW	180	20	7.5
TT29	30.71	0	36.06	0.82(0.03)+2	0.77(0.03)-99	NW	180	40	8
Averages first line			25.73	0.71	0.91				
Averages other lines			25.64	0.7	0.64				

Trial 2 – Results – Cable Length (continued)
Table A8

Single Tow

% Excess				Av Dev (Stnd Dev) %Sign					
Run	Yaw	Pitch	Any	Yaw	Pitch	Wing	Dirn	Len	Vel
ST1	83.62	0	97.5	3.25(0.07)	0.93(0.02)	NW	0	20	5.5
ST7	32.01	0	50.04	0.85(0.03)-99	0.91(0.04)-32	NW	0	20	8.5
ST4	83.51	0	97.01	3.21(0.12)	0.95(0.03)	NW	0	20	5.6
ST7	32.01	0	50.04	0.85(0.03)-99	0.91(0.04)-56	NW	0	20	8.5
ST21	82.39	0.01	97.11	3.07(0.05)	0.97(0.03)	NW	0	40.5	5.6
ST24	32.19	0	47.73	0.85(0.03)-99	0.75(0.02)-99	NW	0	40.5	8.3
ST2	80.75	0.01	94.68	3.01(0.14)	1.08(0.06)	NW	90	20	5.7
ST8	34.24	0.01	52.29	0.89(0.05)-99	0.91(0.09)-88	NW	90	20	8.6
ST5	81.69	0	94.85	3.03(0.14)	1.02(0.04)	NW	90	20	5.7
ST8	34.24	0.01	52.29	0.89(0.05)-99	0.91(0.09)-75	NW	90	20	8.6
ST20	76.25	0.01	91.01	2.55(0.11)	1.25(0.12)	NW	90	40	5.7
ST23	32.24	0	48.46	0.85(0.04)-99	0.83(0.05)-99	NW	90	40.5	7.8
ST3	80	0	93.53	2.79(0.10)	1.02(0.06)	NW	180	20	5.6
ST9	30.28	0	46.23	0.82(0.02)-99	0.85(0.02)-99	NW	180	20	8.5
ST6	80.04	0	93	2.76(0.09)	0.95(0.04)	NW	180	20	5.6
ST9	30.28	0	46.23	0.82(0.02)-99	0.85(0.02)-96	NW	180	20	8.5
ST22	71.27	0.04	85.4	2.06(0.09)	1.29(0.09)	NW	180	40.5	5.4
ST25	33.03	0	52.62	0.86(0.06)-99	0.90(0.07)-99	NW	180	40.5	7.5
ST15	55.62	0	61.62	1.45(0.05)	1.22(0.04)	W	0	35	6.2
ST18	62.72	0.45	74.6	1.71(0.05)+99	1.77(0.04)+99	W	0	35	8
ST14	58.53	0.03	63.32	1.56(0.10)	1.42(0.13)	W	90	35	5.6
ST17	63.94	0.52	75.21	1.78(0.07)+92	1.75(0.05)+97	W	90	35	7.5
ST16	50.86	0.13	54.66	1.27(0.07)	1.57(0.11)	W	180	35	4.6
ST19	60.83	0.36	71.75	1.63(0.06)+99	1.70(0.05)+73	W	180	35	7.9
Averages first line			85.31	2.5	1.14				
Averages other lines			55.62	1.07	1.09				

Two-Part Tow

% Excess				Av Dev (Stnd Dev) %Sign					
Run	Yaw	Pitch	Any	Yaw	Pitch	Wing	Dirn	Len	Vel
TT1	18.13	0	20.64	0.63(0.04)	0.62(0.06)	NW	90	20	4.7
TT3	16.51	0	17.57	0.61(0.01)-35	0.57(0.02)-55	NW	90	20	5.7
TT5	21.18	0	22.75	0.68(0.03)+69	0.90(0.04)+99	NW	90	20	6.2
TT9	31.79	0.04	35.63	0.84(0.02)+99	1.28(0.07)+99	NW	90	20	7.9
Averages first line			20.64	0.63	0.62				
Averages other lines			25.32	0.71	0.92				
TT1	18.13	0	20.64	0.63(0.04)	0.62(0.06)	NW	90	20	4.7
TT3	16.51	0	17.57	0.61(0.01)-35	0.57(0.02)-55	NW	90	20	5.7
TT5	21.18	0	22.75	0.68(0.03)+69	0.90(0.04)+99	NW	90	20	6.2
TT9	31.79	0.04	35.63	0.84(0.02)+99	1.28(0.07)+99	NW	90	20	7.9
TT26	17.7	0	18.98	0.62(0.01)	0.57(0.03)	NW	90	40	5.8
TT28	33.59	0	39.24	0.87(0.03)+99	0.78(0.02)+99	NW	90	40	8

Trial 2 – Results – Tow Speed

Table A9

PTO

Continued from previous page

% Excess				Av Dev (Std Dev) %Sign					
Run	Yaw	Pitch	Any	Yaw	Pitch	Wing	Dirn	Len	Vel
TT2	16.86	0	17.99	0.61(0.01)	0.60(0.03)	NW	0	20	5.7
TT6	22.39	0	24.09	0.69(0.02)+99	0.91(0.03)+99	NW	0	20	6.7
TT8	32.68	0.06	36.33	0.86(0.03)+99	1.25(0.05)+99	NW	0	20	7.9
TT27	19.68	0	21.36	0.64(0.03)	0.59(0.02)	NW	0	40	6.3
TT30	35.18	0	41.39	0.90(0.03)+99	0.83(0.04)+99	NW	0	40	7.8
TT4	20.71	0	22.61	0.66(0.02)	0.89(0.04)	NW	180	20	5.9
TT7	30.55	0.05	33.95	0.82(0.02)+99	1.20(0.03)+99	NW	180	20	7.5
TT25	13.71	0	14.42	0.56(0.03)	0.52(0.02)	NW	180	40	5.6
TT29	30.71	0	36.06	0.82(0.03)+99	0.77(0.03)+99	NW	180	40	8
TT11	25.31	0	30.57	0.74(0.02)	0.86(0.05)	W	0	15	4.9
TT17	48.31	0.44	63.74	1.20(0.07)+99	1.75(0.21)+99	W	0	15	8.1
TT15	25.84	0	31.27	0.75(0.03)	0.83(0.06)	W	0	15	5.3
TT17	48.31	0.44	63.74	1.20(0.07)+99	1.75(0.21)+99	W	0	15	8.1
TT11	25.31	0	30.57	0.74(0.02)	0.86(0.05)	W	0	15	4.9
TT22	49.46	0.71	64.64	1.25(0.06)+99	1.86(0.17)+99	W	0	15	8
TT15	25.84	0	31.27	0.75(0.03)	0.83(0.06)	W	0	15	5.3
TT22	49.46	0.71	64.64	1.25(0.06)+99	1.86(0.17)+99	W	0	15	8
TT12	24.25	0	29.5	0.72(0.02)	0.86(0.04)	W	90	15	5.2
TT18	49.02	0.55	63.94	1.23(0.05)+99	1.92(0.19)+99	W	90	15	8
TT19	53	0.74	67.41	1.34(0.07)+99	1.90(0.26)+99	W	90	15	8
TT23	51.2	0.91	66.15	1.28(0.08)+99	1.82(0.23)+99	W	90	15	8
TT14	26.05	0	31.45	0.75(0.04)	0.87(0.06)	W	90	15	5.4
TT18	49.02	0.55	63.94	1.23(0.05)+99	1.92(0.19)+99	W	90	15	8
TT19	53	0.74	67.41	1.34(0.07)+99	1.90(0.26)+99	W	90	15	8
TT23	51.2	0.91	66.15	1.28(0.08)+99	1.82(0.23)+99	W	90	15	8
TT13	20.96	0	25.06	0.67(0.03)	0.75(0.07)	W	180	15	5
TT20	47.61	0.39	61.53	1.19(0.11)+99	1.85(0.41)+99	W	180	15	7.7
TT24	51.71	0.64	65.38	1.29(0.06)+99	1.77(0.19)+99	W	180	15	8.4
TT16	22.15	0	26.63	0.69(0.03)	0.76(0.04)	W	180	15	5.1
TT20	47.61	0.39	61.53	1.19(0.11)+99	1.85(0.41)+99	W	180	15	7.7
TT24	51.71	0.64	65.38	1.29(0.06)+99	1.77(0.19)+99	W	180	15	8.4
TT20	47.61	0.39	61.53	1.19(0.11)	1.85(0.41)	W	180	15	7.7
TT24	51.71	0.64	65.38	1.29(0.06)+54	1.77(0.19)-12	W	180	15	8.4
Averages first line			27.59	0.71	0.82				
Averages other lines			52.42	1.08	1.5				
TT18	49.02	0.55	63.94	1.23(0.05)	1.92(0.19)	W	90	15	8
TT19	53	0.74	67.41	1.34(0.07)+78	1.90(0.26)-4	W	90	15	8
TT23	51.2	0.91	66.15	1.28(0.08)+39	1.82(0.23)-25	W	90	15	8
Averages first line			63.94	1.23	1.92				
Averages other lines			66.78	1.31	1.86				

Trial 2 – Results – Tow Speed (continued)

Table A9

PTO

Continued from previous page

% Excess				Av Dev (Stnd Dev) %Sign					
Run	Yaw	Pitch	Any	Yaw	Pitch	Wing	Dirn	Len	Vel
TT19	53	0.74	67.41	1.34(0.07)	1.90(0.26)	W	90	15	8
TT23	51.2	0.91	66.15	1.28(0.08)-40	1.82(0.23)-16	W	90	15	8
Averages first line			67.41	1.34	1.9				
Averages other lines			66.15	1.28	1.82				
TT13	20.96	0	25.06	0.67(0.03)	0.75(0.07)	W	180	15	5
TT16	22.15	0	26.63	0.69(0.03)+32	0.76(0.04)+9	W	180	15	5.1
Averages first line			25.06	0.67	0.75				
Averages other lines			26.63	0.69	0.76				

Trial 2 – Results – Tow Speed (continued)
Table A9

Single Tow

% Excess			Av Dev (Std Dev) %Sign						
Run	Yaw	Pitch	Any	Yaw	Pitch	Wing	Dirn	Len	Vel
ST11	57.09	0	62.06	1.48(0.05)	1.12(0.03)	W	90	15	5.5
ST2	80.75	0.01	94.68	3.01(0.14)+99	1.08(0.06)-42	NW	90	20	5.7
ST14	58.53	0.03	63.32	1.56(0.10)	1.42(0.13)	W	90	35	5.6
ST20	76.25	0.01	91.01	2.55(0.11)+99	1.25(0.12)-62	NW	90	40	5.7
ST19	60.83	0.36	71.75	1.63(0.06)	1.70(0.05)	W	180	35	7.9
ST25	33.03	0	52.62	0.86(0.06)-99	0.90(0.07)-99	NW	180	40.5	7.5
ST12	58.6	0	63.4	1.53(0.06)	1.12(0.03)	W	180	15	?
ST3	80	0	93.53	2.79(0.10)+99	1.02(0.06)-88	NW	180	20	5.6
ST13	63.55	0.57	79.86	1.77(0.05)	1.84(0.07)	W	?	15	8.4
ST9	30.28	0	46.23	0.82(0.02)-99	0.85(0.02)-99	NW	180	20	8.5
ST15	55.62	0	61.62	1.45(0.05)	1.22(0.04)	W	0	35	6.2
ST21	82.39	0.01	97.11	3.07(0.05)+99	0.97(0.03)-99	NW	0	40.5	5.6
ST16	50.86	0.13	54.66	1.27(0.07)	1.57(0.11)	W	180	35	4.6
ST22	71.27	0.04	85.4	2.06(0.09)+99	1.29(0.09)-95	NW	180	40.5	5.4
ST17	63.94	0.52	75.21	1.78(0.07)	1.75(0.05)	W	90	35	7.5
ST23	32.24	0	48.46	0.85(0.04)-99	0.83(0.05)-99	NW	90	40.5	7.8
ST18	62.72	0.45	74.6	1.71(0.05)	1.77(0.04)	W	0	35	8
ST24	32.19	0	47.73	0.85(0.03)-99	0.75(0.02)-99	NW	0	40.5	8.3
Averages first line			67.39	1.58	1.5				
Averages other lines			72.97	1.87	0.99				

Two-Part Tow

% Excess			Av Dev (Std Dev) %Sign						
Run	Yaw	Pitch	Any	Yaw	Pitch	Wing	Dirn	Len	Vel
TT12	24.25	0	29.5	0.72(0.02)	0.86(0.04)	W	90	15	5.2
TT1	18.13	0	20.64	0.63(0.04)-95	0.62(0.06)-99	NW	90	20	4.7
TT11	25.31	0	30.57	0.74(0.02)	0.86(0.05)	W	0	15	4.9
TT2	16.86	0	17.99	0.61(0.01)-99	0.60(0.03)-99	NW	0	20	5.7
TT15	25.84	0	31.27	0.75(0.03)	0.83(0.06)	W	0	15	5.3
TT2	16.86	0	17.99	0.61(0.01)-99	0.60(0.03)-99	NW	0	20	5.7
TT14	26.05	0	31.45	0.75(0.04)	0.87(0.06)	W	90	15	5.4
TT3	16.51	0	17.57	0.61(0.01)-99	0.57(0.02)-99	NW	90	20	5.7
TT20	47.61	0.39	61.53	1.19(0.11)	1.85(0.41)	W	180	15	7.7
TT7	30.55	0.05	33.95	0.82(0.02)-99	1.20(0.03)-87	NW	180	20	7.5
TT16	22.15	0	26.63	0.69(0.03)	0.76(0.04)	W	180	15	5.1
TT4	20.71	0	22.61	0.66(0.02)-59	0.89(0.04)+97	NW	180	20	5.9
TT13	20.96	0	25.06	0.67(0.03)	0.75(0.07)	W	180	15	5
TT4	20.71	0	22.61	0.66(0.02)-18	0.89(0.04)+92	NW	180	20	5.9
TT22	49.46	0.71	64.64	1.25(0.06)	1.86(0.17)	W	0	15	8
TT8	32.68	0.06	36.33	0.86(0.03)-99	1.25(0.05)-99	NW	0	20	7.9

Trial 2 – Results – Depressor Wing (continued)

Table A10

PTO

Continued from previous page

% Excess			Av Dev (Stnd Dev) %Sign			Wing	Dirn	Len	Vel
Run	Yaw	Pitch	Any	Yaw	Pitch				
TT17	48.31	0.44	63.74	1.20(0.07)	1.75(0.21)	W	0	15	8.1
TT6	22.39	0	24.09	0.69(0.02)-99	0.91(0.03)-99	NW	0	20	6.7
TT23	51.2	0.91	66.15	1.28(0.08)	1.82(0.23)	W	90	15	8
TT9	31.79	0.04	35.63	0.84(0.02)-99	1.28(0.07)-97	NW	90	20	7.9
TT24	51.71	0.64	65.38	1.29(0.06)	1.77(0.19)	W	180	15	8.4
TT7	30.55	0.05	33.95	0.82(0.02)-99	1.20(0.03)-99	NW	180	20	7.5
TT18	49.02	0.55	63.94	1.23(0.05)	1.92(0.19)	W	90	15	8
TT9	31.79	0.04	35.63	0.84(0.02)-99	1.28(0.07)-99	NW	90	20	7.9
TT19	53	0.74	67.41	1.34(0.07)	1.90(0.26)	W	90	15	8
TT9	31.79	0.04	35.63	0.84(0.02)-99	1.28(0.07)-97	NW	90	20	7.9
Averages first line			48.25	1.01	1.37				
Averages other lines			27.28	0.73	0.97				

Trial 2 – Results – Depressor Wing (continued)
Table A10

% Excess			Av Dev (Stnd Dev) %Sign						
Run	Yaw	Pitch	Any	Yaw	Pitch	Wing	Dirn	Len	Vel
ST1	83.62	0	97.5	3.25(0.07)	0.93(0.02)	NW	0	20	5.5
TT2	16.86	0	17.99	0.61(0.01)-99	0.60(0.03)-99	NW	0	20	5.7
ST4	83.51	0	97.01	3.21(0.12)	0.95(0.03)	NW	0	20	5.6
TT2	16.86	0	17.99	0.61(0.01)-99	0.60(0.03)-99	NW	0	20	5.7
ST7	32.01	0	50.04	0.85(0.03)	0.91(0.04)	NW	0	20	8.5
TT8	32.68	0.06	36.33	0.86(0.03)+16	1.25(0.05)+99	NW	0	20	7.9
ST2	80.75	0.01	94.68	3.01(0.14)	1.08(0.06)	NW	90	20	5.7
TT3	16.51	0	17.57	0.61(0.01)-99	0.57(0.02)-99	NW	90	20	5.7
ST2	80.75	0.01	94.68	3.01(0.14)	1.08(0.06)	NW	90	20	5.7
TT5	21.18	0	22.75	0.68(0.03)-99	0.90(0.04)-98	NW	90	20	6.2
ST5	81.69	0	94.85	3.03(0.14)	1.02(0.04)	NW	90	20	5.7
TT3	16.51	0	17.57	0.61(0.01)-99	0.57(0.02)-99	NW	90	20	5.7
TT5	21.18	0	22.75	0.68(0.03)-99	0.90(0.04)-97	NW	90	20	6.2
TT1	18.13	0	20.64	0.63(0.04)-99	0.62(0.06)-99	NW	90	20	4.7
ST8	34.24	0.01	52.29	0.89(0.05)	0.91(0.09)	NW	90	20	8.6
TT9	31.79	0.04	35.63	0.84(0.02)-61	1.28(0.07)+99	NW	90	20	7.9
ST3	80	0	93.53	2.79(0.10)	1.02(0.06)	NW	180	20	5.6
TT4	20.71	0	22.61	0.66(0.02)-99	0.89(0.04)-94	NW	180	20	5.9
ST6	80.04	0	93	2.76(0.09)	0.95(0.04)	NW	180	20	5.6
TT4	20.71	0	22.61	0.66(0.02)-99	0.89(0.04)-68	NW	180	20	5.9
ST9	30.28	0	46.23	0.82(0.02)	0.85(0.02)	NW	180	20	8.5
TT7	30.55	0.05	33.95	0.82(0.02)+2	1.20(0.03)+99	NW	180	20	7.5
ST10	54.06	0	58.89	1.37(0.04)	1.08(0.04)	W	0	15	5.5
TT11	25.31	0	30.57	0.74(0.02)-99	0.86(0.05)-99	W	0	15	4.9
TT15	25.84	0	31.27	0.75(0.03)-99	0.83(0.06)-99	W	0	15	5.3
ST21	82.39	0.01	97.11	3.07(0.05)	0.97(0.03)	NW	0	40.5	5.6
TT27	19.68	0	21.36	0.64(0.03)-99	0.59(0.02)-99	NW	0	40	6.3
ST24	32.19	0	47.73	0.85(0.03)	0.75(0.02)	NW	0	40.5	8.3
TT30	35.18	0	41.39	0.90(0.03)+75	0.83(0.04)+94	NW	0	40	7.8
ST11	57.09	0	62.06	1.48(0.05)	1.12(0.03)	W	90	15	5.5
TT12	24.25	0	29.5	0.72(0.02)-99	0.86(0.04)-99	W	90	15	5.2
TT14	26.05	0	31.45	0.75(0.04)-99	0.87(0.06)-99	W	90	15	5.4
ST20	76.25	0.01	91.01	2.55(0.11)	1.25(0.12)	NW	90	40	5.7
TT26	17.7	0	18.98	0.62(0.01)-99	0.57(0.03)-99	NW	90	40	5.8
ST23	32.24	0	48.46	0.85(0.04)	0.83(0.05)	NW	90	40.5	7.8
TT28	33.59	0	39.24	0.87(0.03)+31	0.78(0.02)-61	NW	90	40	8
ST22	71.27	0.04	85.4	2.06(0.09)	1.29(0.09)	NW	180	40.5	5.4
TT25	13.71	0	14.42	0.56(0.03)-99	0.52(0.02)-99	NW	180	40	5.6
ST25	33.03	0	52.62	0.86(0.06)	0.90(0.07)	NW	180	40.5	7.5
TT29	30.71	0	36.06	0.82(0.03)-46	0.77(0.03)-91	NW	180	40	8
Averages first line			75.39	2.04	0.99				
Averages other lines			26.48	0.71	0.81				

Trial 2 – Results – Single vs Two-Part Tow

Table A11

PTO

Continued from previous page

% Excess			Av Dev (Std Dev) %Sign						
Run	Yaw	Pitch	Any	Yaw	Pitch	Wing	Dirn	Len	Vel
ST12	58.6	0	63.4	1.53(0.06)	1.12(0.03)	W	180	15	?
TT13	20.96	0	25.06	0.67(0.03)-99	0.75(0.07)-99	W	180	15	5
TT16	22.15	0	26.63	0.69(0.03)-99	0.76(0.04)-99	W	180	15	5.1
Averages first line			63.4	1.53	1.12				
Averages other lines			25.84	0.68	0.76				
ST12	58.6	0	63.4	1.53(0.06)	1.12(0.03)	W	180	15	?
TT20	47.61	0.39	61.53	1.19(0.11)-99	1.85(0.41)+92	W	180	15	7.7
TT24	51.71	0.64	65.38	1.29(0.06)-99	1.77(0.19)+99	W	180	15	8.4
Averages first line			63.4	1.53	1.12				
Averages other lines			63.45	1.24	1.81				
ST15	55.62	0	61.62	1.45(0.05)	1.22(0.04)	W	0	35	6.2
TT27	19.68	0	21.36	0.64(0.03)-99	0.59(0.02)-99	NW	0	40	6.3
ST18	62.72	0.45	74.6	1.71(0.05)	1.77(0.04)	W	0	35	8
TT30	35.18	0	41.39	0.90(0.03)-99	0.83(0.04)-99	NW	0	40	7.8
ST14	58.53	0.03	63.32	1.56(0.10)	1.42(0.13)	W	90	35	5.6
TT26	17.7	0	18.98	0.62(0.01)-99	0.57(0.03)-99	NW	90	40	5.8
ST17	63.94	0.52	75.21	1.78(0.07)	1.75(0.05)	W	90	35	7.5
TT28	33.59	0	39.24	0.87(0.03)-99	0.78(0.02)-99	NW	90	40	8
ST16	50.86	0.13	54.66	1.27(0.07)	1.57(0.11)	W	180	35	4.6
TT25	13.71	0	14.42	0.56(0.03)-99	0.52(0.02)-99	NW	180	40	5.6
ST19	60.83	0.36	71.75	1.63(0.06)	1.70(0.05)	W	180	35	7.9
TT29	30.71	0	36.06	0.82(0.03)-99	0.77(0.03)-99	NW	180	40	8
Averages first line			66.86	1.57	1.57				
Averages other lines			28.58	0.73	0.68				

Trial 2 – Results – Single vs Two-Part Tow (continued)
Table A11

APPENDIX B

COMPUTER PROGRAM FLOWCHARTS

The flowcharts detailing the computer programs developed to predict the behavior of two-part and multi-tow configurations are presented below. These include the quasi-static and dynamic model for the conventional, two-part and series multi-tows. The parallel multi-tow is similar to these flowcharts with minor modification. The major difference is the matrix solution subroutine and it is given at the end of this Appendix.

List of Program Flowcharts

Overall Computer Program Flowchart for the Two-Part Tow	335
Quasi-Static Main Program	336
Subroutine Initial Data	338
Subroutine Node Weight	339
Subroutine Depressor Weight	340
Subroutine Top Weight	341
Subroutine Bottom Weight	341
Subroutine Junction Weight	341
Subroutine Segment Weight	342
Subroutine Fish Weight	342
Subroutine Fish Lift Drag	342
Subroutine Cable Drag	343
Subroutine Node Drag	343
Subroutine Cable Angle	344
Subroutine Junction Angle	345
Subroutine Depressor Angle	346
Subroutine Angle Adjust	347
Subroutine Adjust Error	347
Subroutine Correct Angle	348
Subroutine Calculate Tension	349
Subroutine Tail Tension	349
Subroutine Make XY	349
Subroutine Coordinate	350
Subroutine Coordinate Calculate	351
Dynamic Main Program	352
Subroutine Initial Data	356
Subroutine Cable Area	357
Subroutine Cable Transformation Matrix	358

Subroutine Fish Transformation Matrix	358
Subroutine Fish Mass Matrix	358
Subroutine Node Weights	359
Subroutine Fish Mass Matrix 3 DOF Local	360
Subroutine Top Equation Coefficients	360
Subroutine Surface Conditions	361
Subroutine Top Conditions	362
Subroutine Fish Force Moment	363
Subroutine Cable Added Mass	365
Subroutine Inertia Coefficient	366
Subroutine Cable Drag	367
Subroutine Cable Velocity	368
Subroutine Node Acceleration	368
Subroutine Node Coordinate	369
Subroutine Node Velocity	369
Subroutine Equation Coefficient	370
Subroutine Node Drag	373
Subroutine Fish Angular Velocity Angle	374
Subroutine Fish Angular Acceleration	374
Subroutine Segment Angle Horizontal	375
Subroutine Segment Angle Vertical	375
Subroutine Correct Tension	376
Subroutine Tail Tension	378
Subroutine Convert Matrix	379
Subroutine Eliminate C	382
Subroutine Increment Values	383
Subroutine Free Array	384
Multi Tow in Parallel	385
Subroutine Convert Matrix – Multi Tow	385

Nomenclature for Flowcharts

The majority of the symbols used in the program flowcharts are those defined in the Nomenclature at the beginning of the thesis. However, some symbols are specific to the program flowcharts and are defined below or within each flowchart.

Variables

A_e	equivalent area of any additional mass at the node
A_{ab}	where $a = 1, 2, 3$ and $b = 1, 2, 3$ mass matrix terms of the <i>manipulated</i> equation of motion of fish “f”
A_{fab}	where $a = 1$ to 6 and $b = 1$ to 6 mass matrix terms of the equation of motion of fish “f”
A_{fl_f}, B_{fl_f}	variables A_{fl}, B_{fl} as defined in the Nomenclature
Astore	storage variable for variable A
$A_{\omega x, y, z}$	surface excitation amplitude in the X, Y and Z directions
B21, B23	variables B_{21}, B_{23} as defined in the Nomenclature
$B_{f_{gu, v, w}}$	buoyancy force on fish along local axes
C_{ati}	tangential added mass coefficient of cable segment “i”

C_{ani}	normal added mass coefficient of cable segment “i”
$C_{D,Lf}$	drag and lift force coefficients of fish for static model
C_{ni}	cable drag coefficient in the normal direction
C_{ti}	cable drag coefficient in the tangential direction
cabbeg	node at start of cable system
cabend	node at end of cable system
check	absolute error of the horizontal angle (ψ) between two iterations
checkstore	storage variable for the absolute error of the horizontal angle (ψ) between two iterations
CTR	incremental step counter
$CTRM_{iab}$	<i>where $a = 1,2,3$ and $b = 1,2,3$</i> transformation matrix of cable segment “i”
C_{abfc}	<i>where $a = X',Y',Z'$, $b = pitch$, and $c = 1,2,3,4$</i> Coefficients of third order polynomial representing force coefficients of fish, (note: force “a” due to angle “b” of order “c”)
C_{abfc}	<i>where $a = roll, pitch, yaw$, $b = pitch$, and $c = 1,2,3,4$</i> Coefficients of third order polynomial representing moment coefficients of fish, (note: moment “a” due to angle “b” of order “c”)
de	equivalent diameter of any additional mass at the node
$DEN\phi$	denominator of the tangent of the horizontal angle
$DEN\psi$	denominator of the tangent of the vertical angle
$D_{fu,v,w}$	drag force on fish along local axes
EM_i	modulus of elasticity of cable element “i”
$F_{din,t}$	drag forces on cable segment “i” in the normal and tangential directions
$F2_{dN,D}$	components of the drag forces on second (tail) cable segment of tow fish in the Y and X directions
$FfDrag_f$	drag forces on fish “f”
$FfLift_f$	lift forces on fish “f”
FH_f, FV_f	total force on the fish in the horizontal and vertical directions
FILE	true (1) or false (0) operator to identify surface node position input
FIRST	true (1) or false (0) operator to identify initial operations
$Ff_{u,v,wf}$	total force on the fish in the local directions
$FTRM_{fab}$	<i>where $a = 1,2,3$ and $b = 1,2,3$</i> transformation matrix of fish “f”
fishnode	cable node representing the fish
f_r	surface excitation frequency in hertz
k	iteration counter
l_{ext}	stretched length of cable segment
$Mf_{u,v,wf}$	moment on fish about local axes at tow point
$Mf_{gu,v,w}$	force on fish due to gravity along local axes
m_{iab}	<i>where $a = 1,2,3$ and $b = 1,2,3$</i> mass matrix terms of cable segment i
m_{iabL}	<i>where $a = 1,2,3$ and $b = 1,2,3$</i> storage variable for mass matrix terms
mf_f	mass of fish “f”
Ndt	total number of time steps
$NUM\phi$	numerator of the tangent of the horizontal angle
$NUM\psi$	numerator of the tangent of the vertical angle
noofcables	number of cable systems in the tow configurations
nooffish	number of fish in the tow configurations

pd_f, rd_f, yd_f	damping of fish in pitch, roll and yaw
SCL	iteration scale factor to force convergence
T_t	tension of second (tail) cable of tow fish
$T_{tx,z}$	tension of second (tail) cable of tow fish in the X and Z directions
Terror	absolute error of tension terms between iterations
Terrormax	maximum value of Terror
TP_{ANG}	pitch angle of fish with flow direction
TP_{YAW}	yaw angle of fish with flow direction
tinct	time incremental counter
time	simulation time
V	horizontal velocity of the cable relative to the surrounding fluid
V_{ei}	volume of any additional mass at node “i”
V_{eqnt}	equivalent velocity
V_{f_f}	volume of towed fish “f”
$V_{n,t}$	velocity of cable relative to the surrounding fluid in the normal and tangential directions
$V_{x,y,z,t}$	tow velocity in the X, Y and Z directions
W1	weight due to second (tail) cable on tow fish
W_{f_f}	net weight in water of towed fish “f”
x_{Gf}, y_{Gf}, z_{Gf}	components of the distance from the tow point (1) to the centre of gravity (G) of tow fish “f”, measured from the tow point and positive in the directions of the local axes system.
x_{tf}, y_{tf}, z_{tf}	components of the distance from the tow point (1) to the tail (second) tow point (t) of tow fish “f”, measured from the tow point and positive in the directions of the local axes system.
x_{0f}, y_{0f}, z_{0f}	components of the distance from the tow point (1) to the centroid (0) of tow fish “f”, measured from the tow point and positive in the directions of the local axes system.
Y_{drf}, Y_{dyf}	damping in Y direction due to roll and sway
Z_{dpf}	damping in Z direction due to pitch

Greek Symbols

ψ_{error}	error in horizontal angle (ψ)
ψ_{error1}	2π minus the absolute value of ψ_{error}
ψ_{store}	storage variable for horizontal angle (ψ)
ψ_{error1}	second storage variable for horizontal angle
v	surface excitation amplitude control variable
ω_r	surface excitation frequency in radians per second

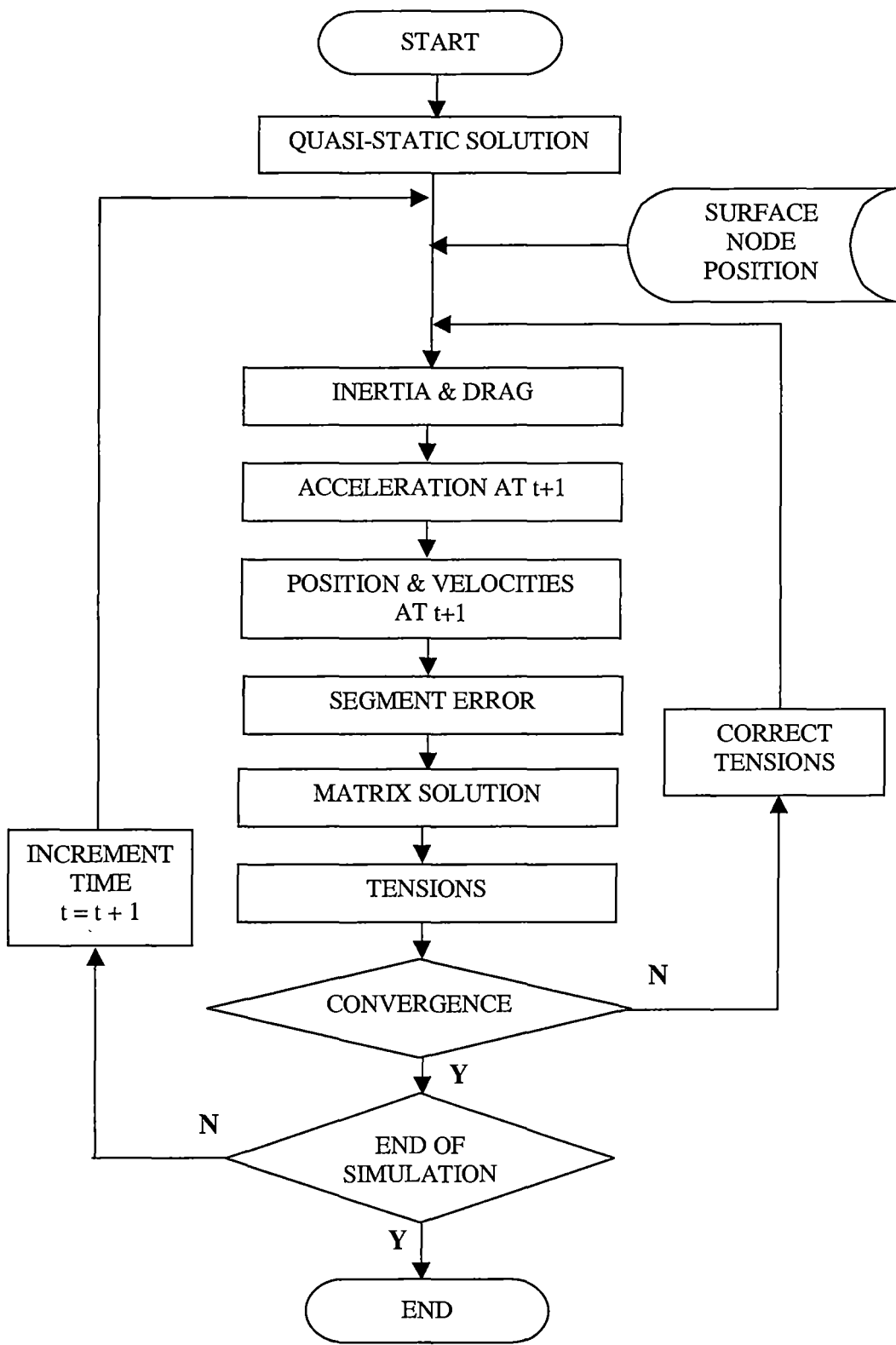
Subscripts

an	adjacent node
c	cable system
t	second (tail) cable of fish, (not used as time in flowcharts)

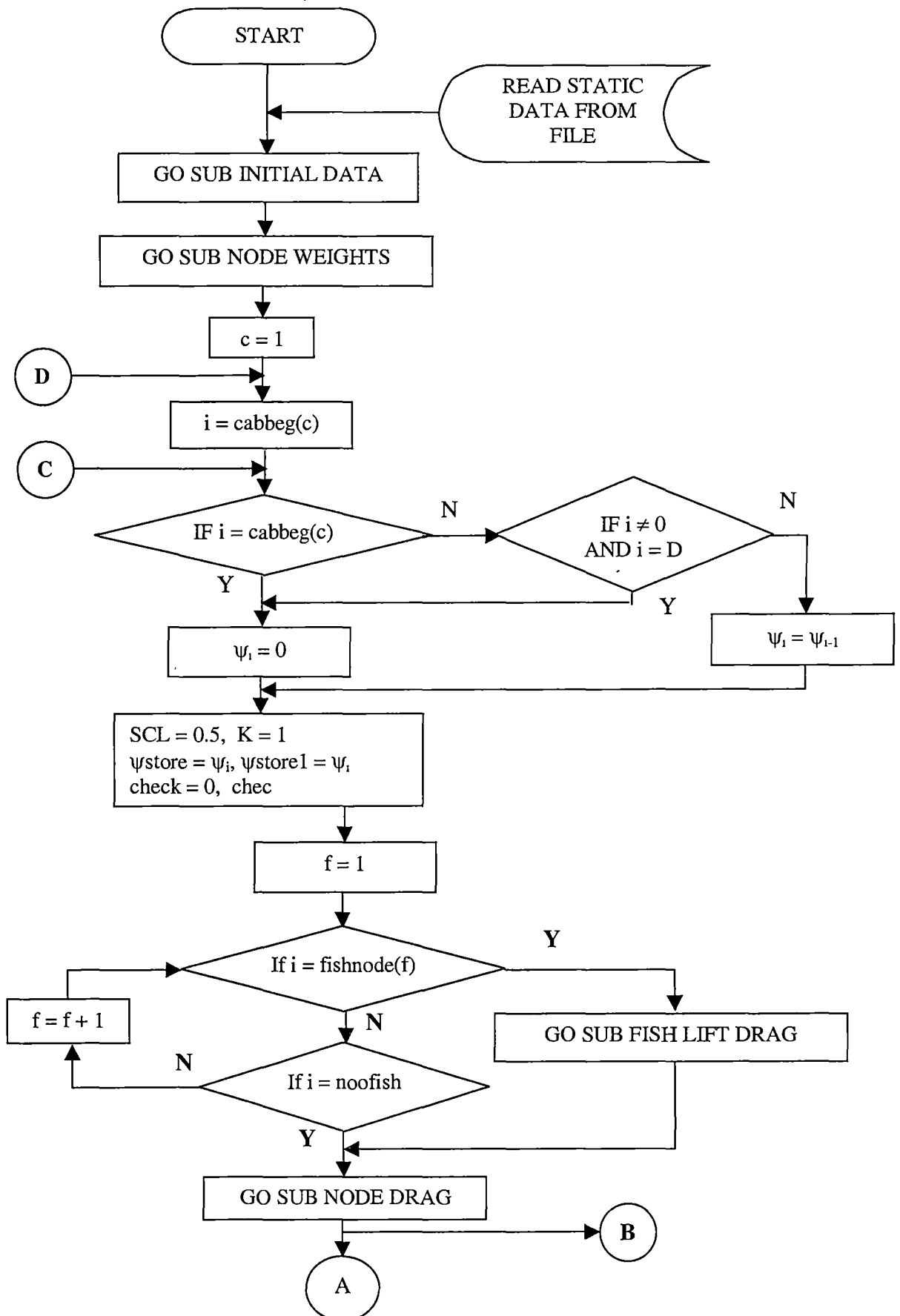
Superscripts

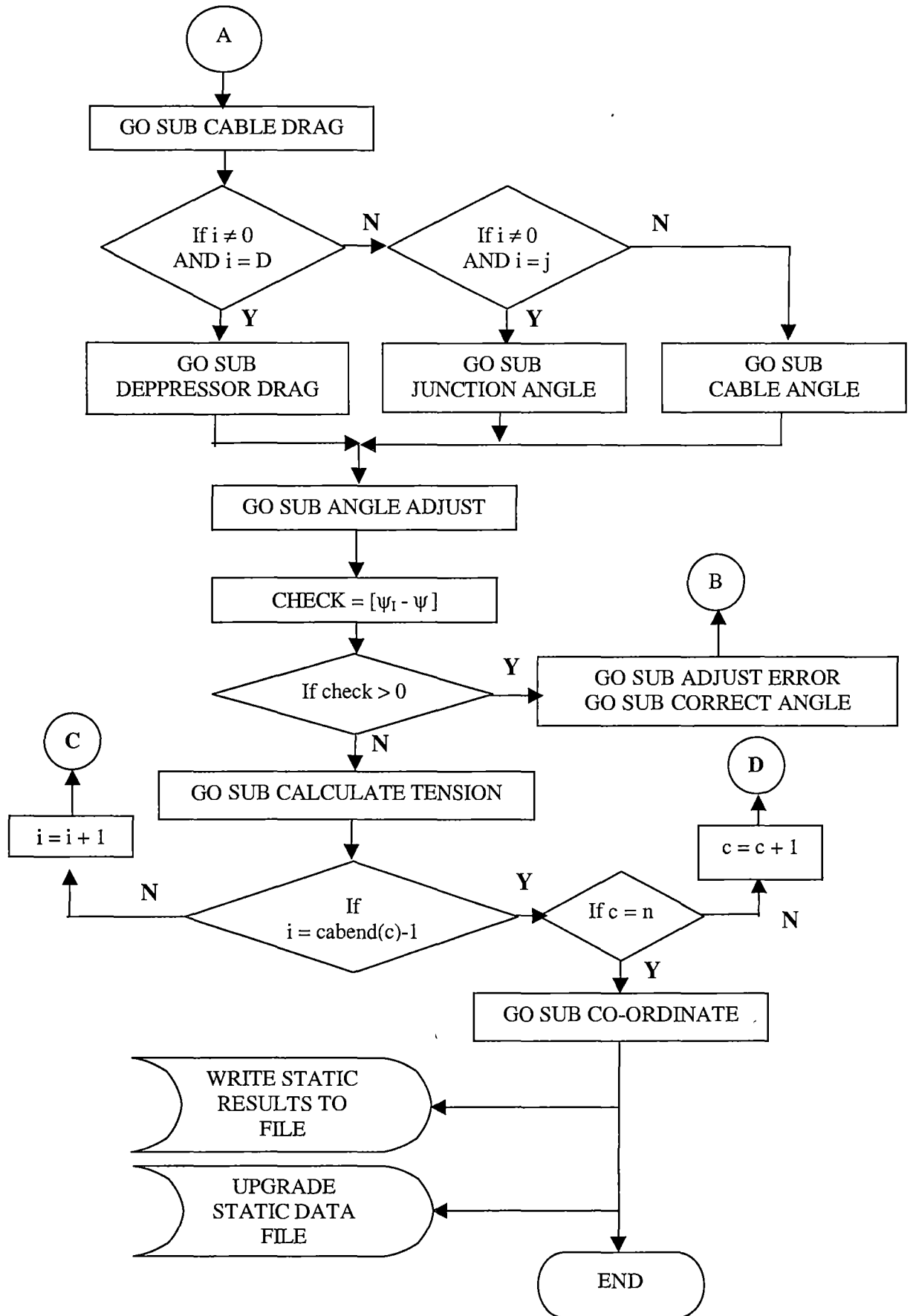
m	convergence correction superscript
t	time

Overall Computer Program Flowchart for the Two-Part Tow

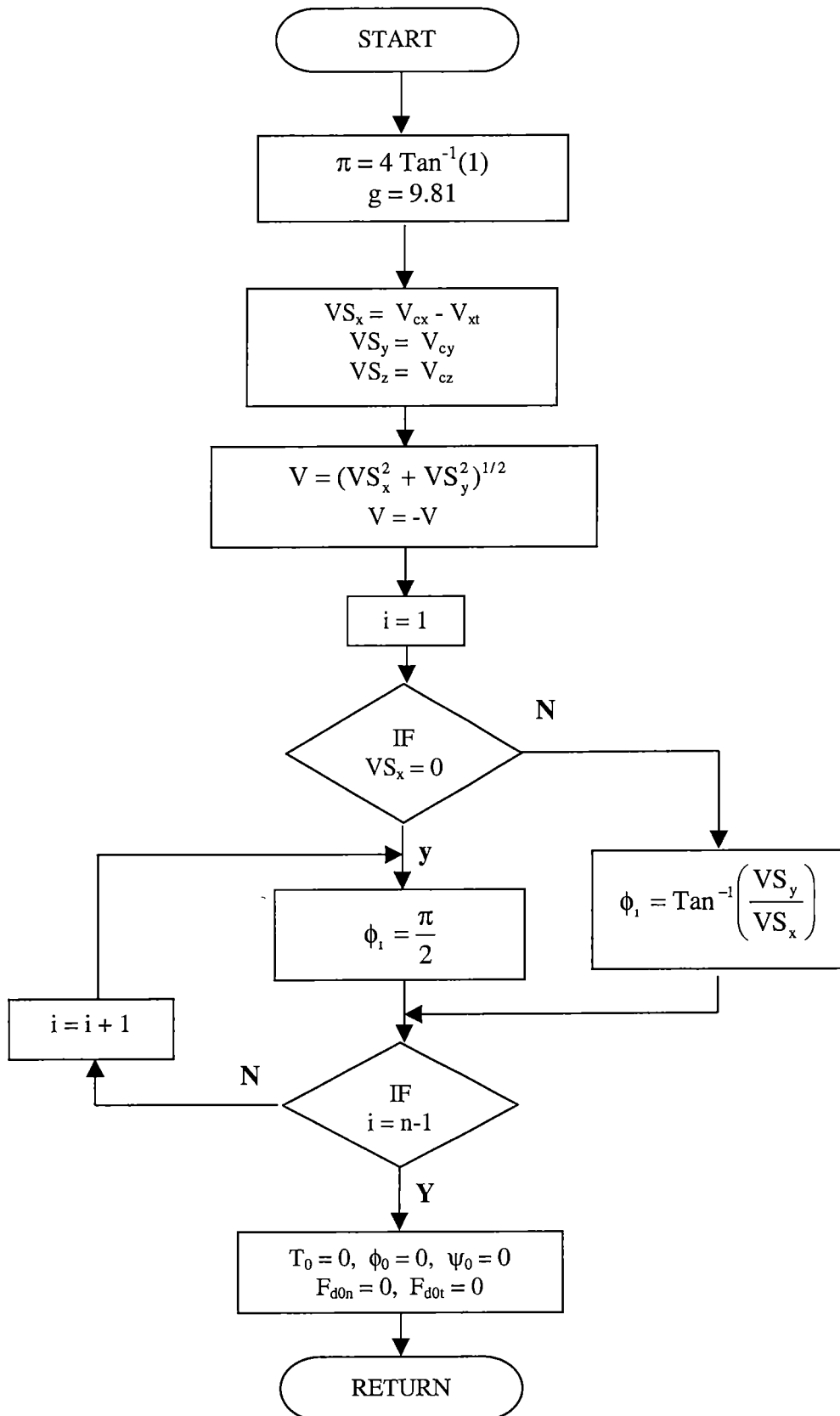


Quasi-Static Main Program

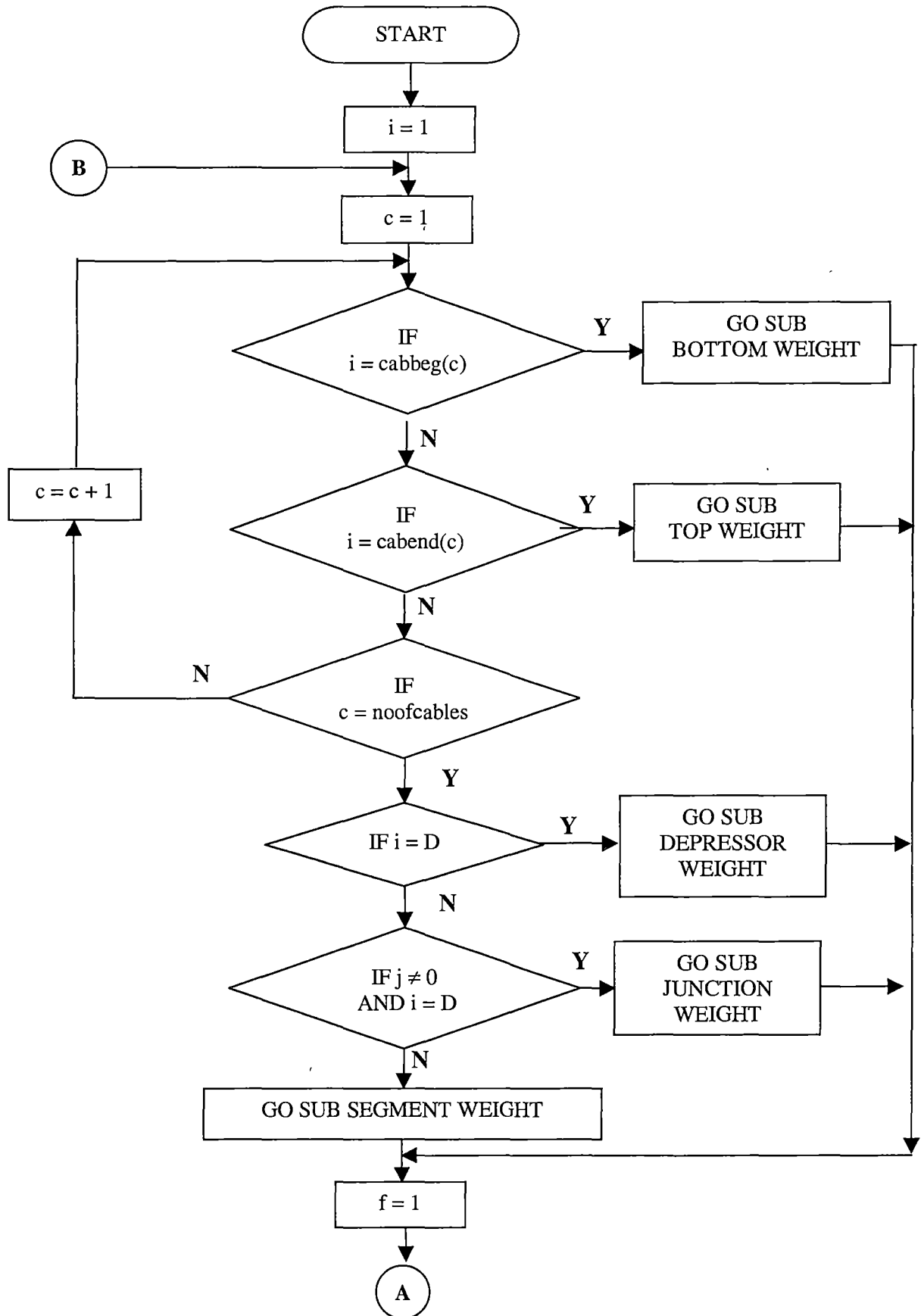


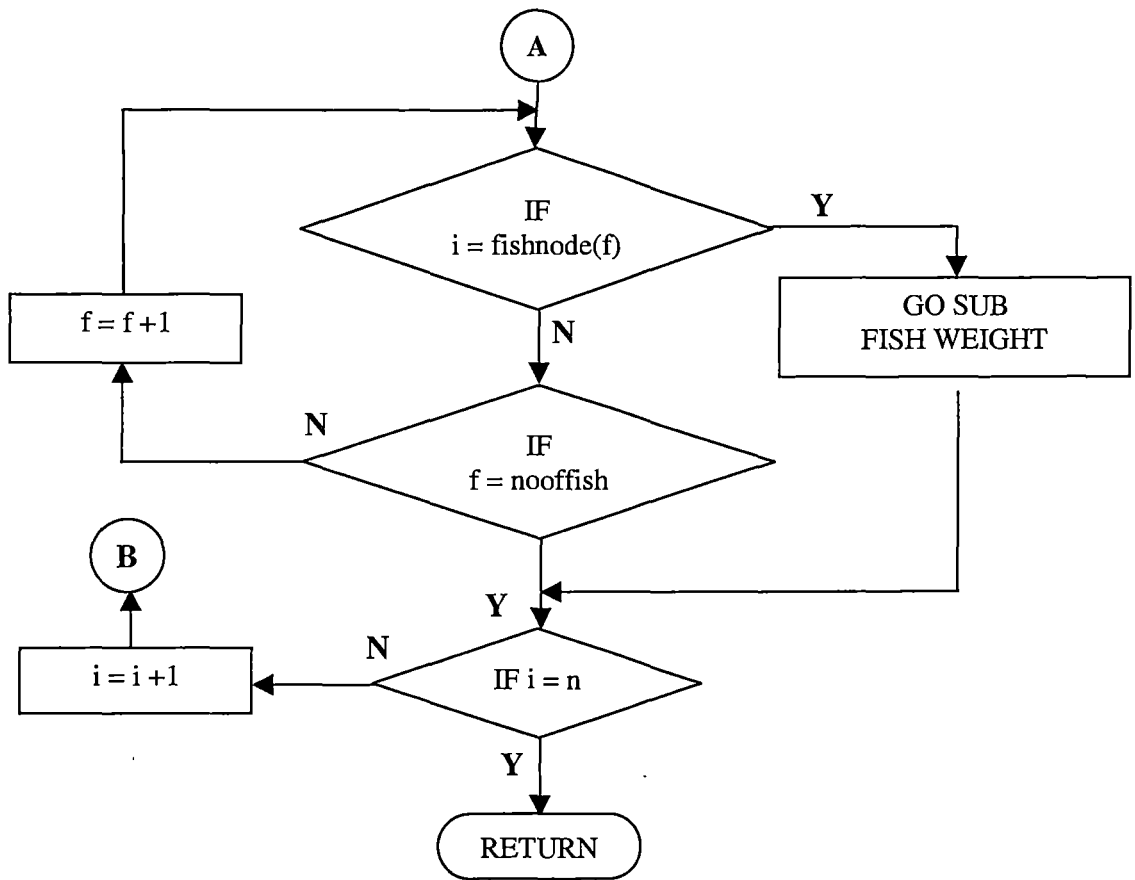


Subroutine Initial Data

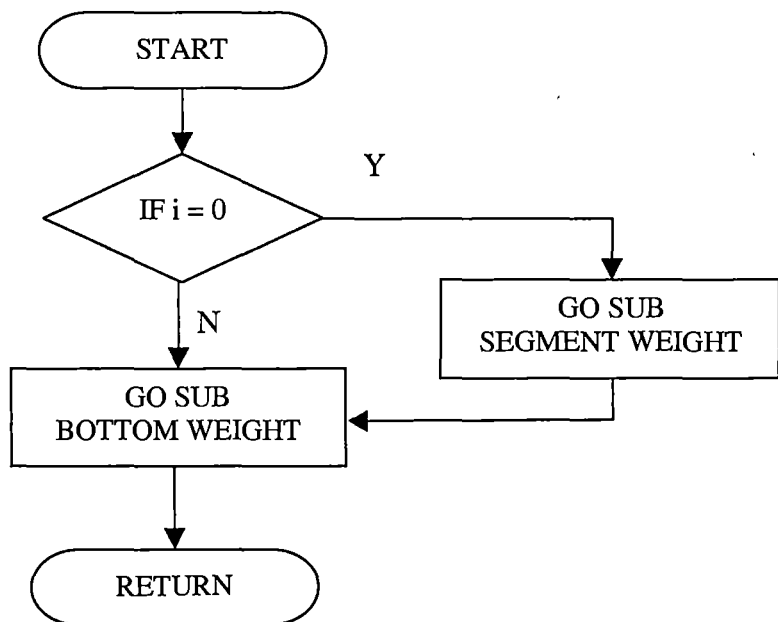


Subroutine Node Weight

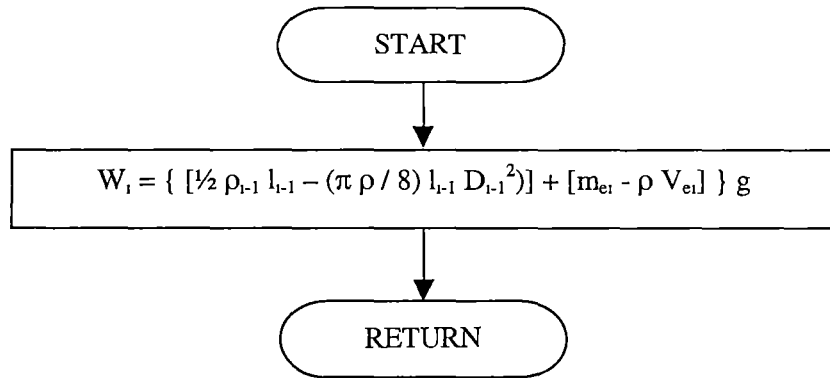




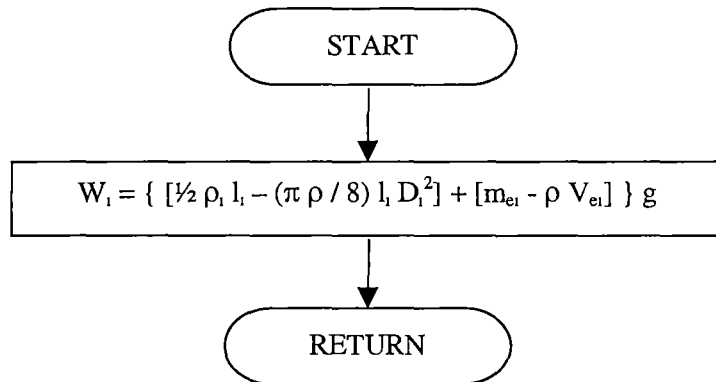
Subroutine Depressor Weight



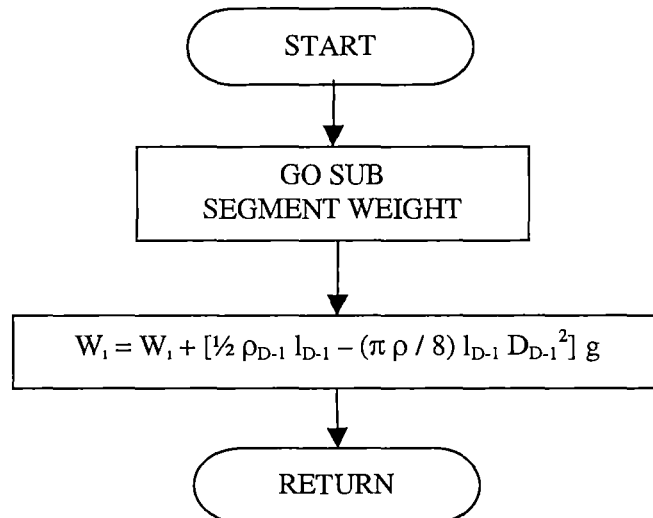
Subroutine Top Weight



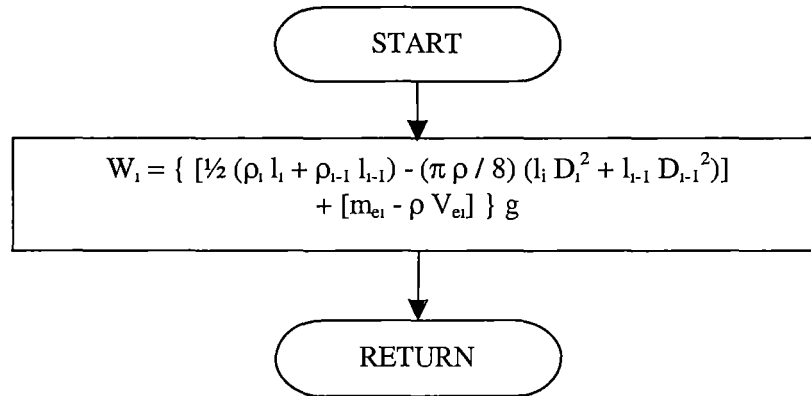
Subroutine Bottom Weight



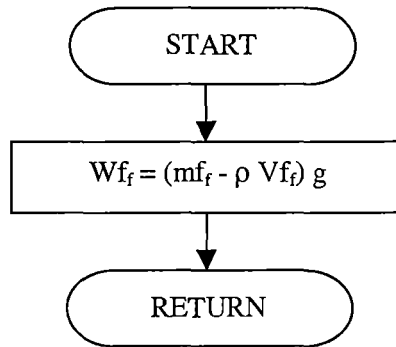
Subroutine Junction Weight



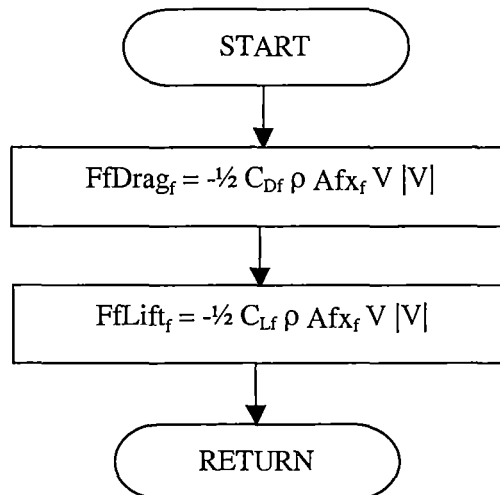
Subroutine Segment Weight



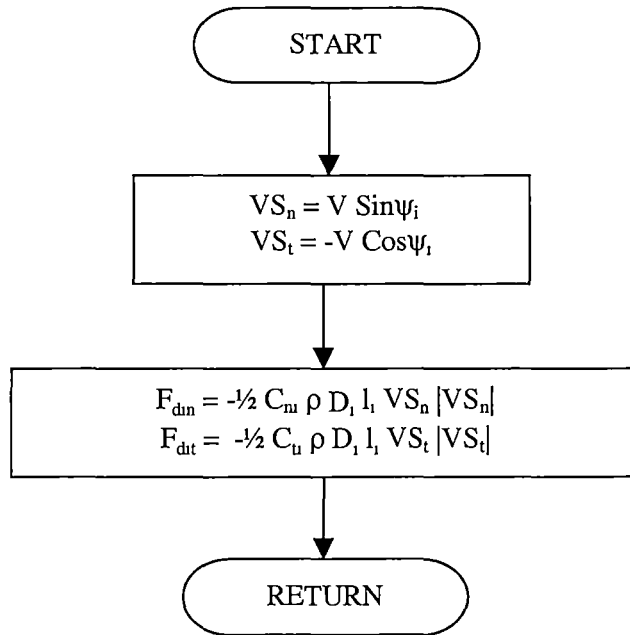
Subroutine Fish Weight



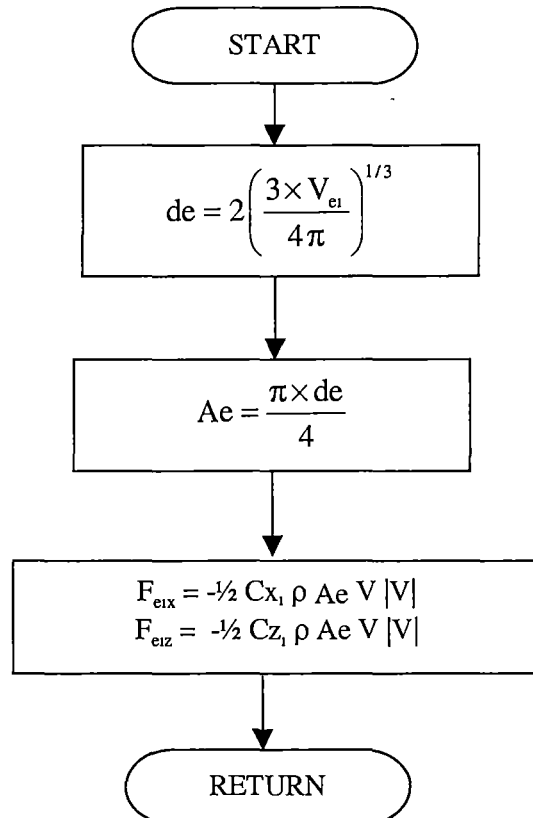
Subroutine Fish Lift Drag



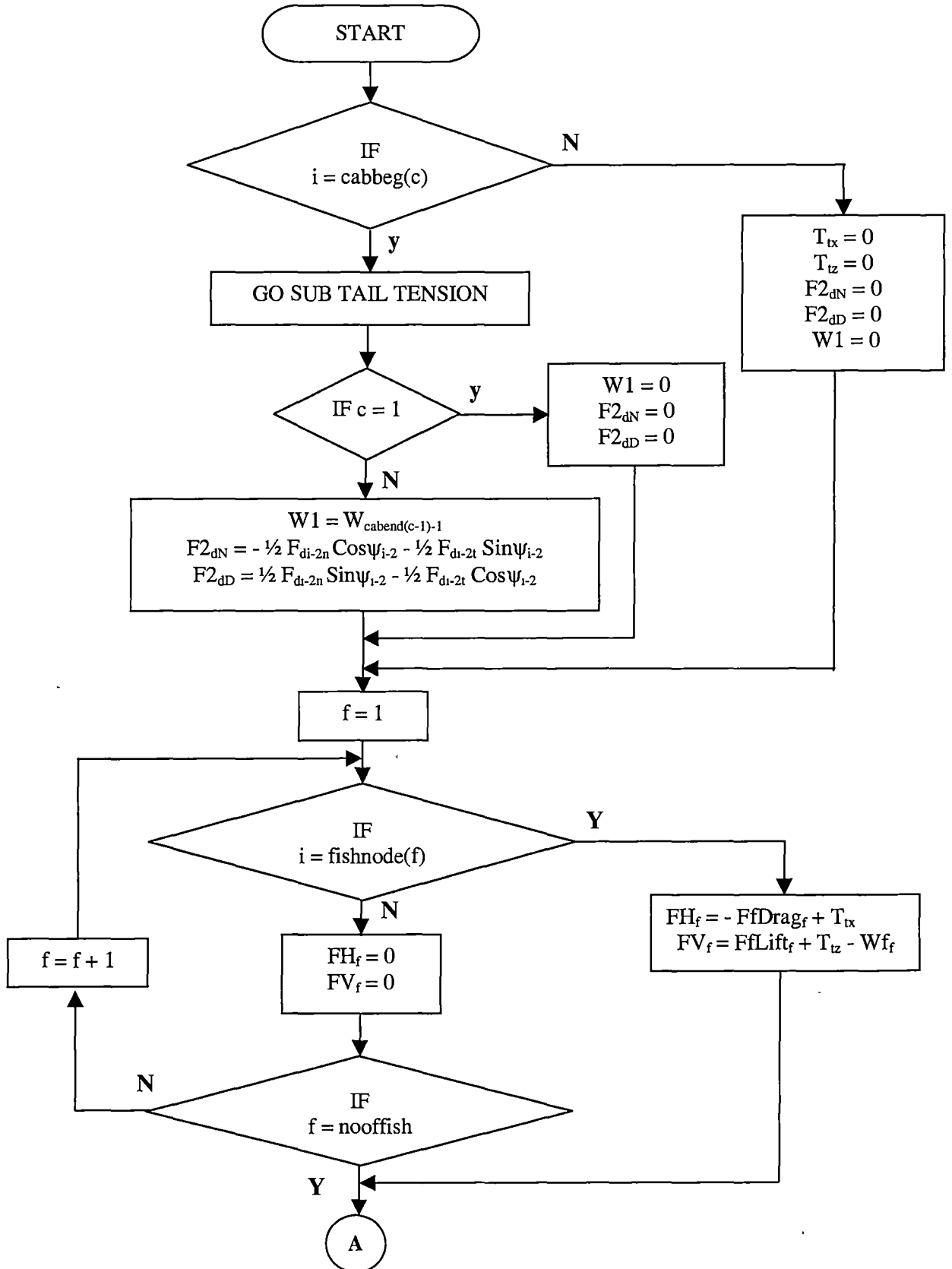
Subroutine Cable Drag

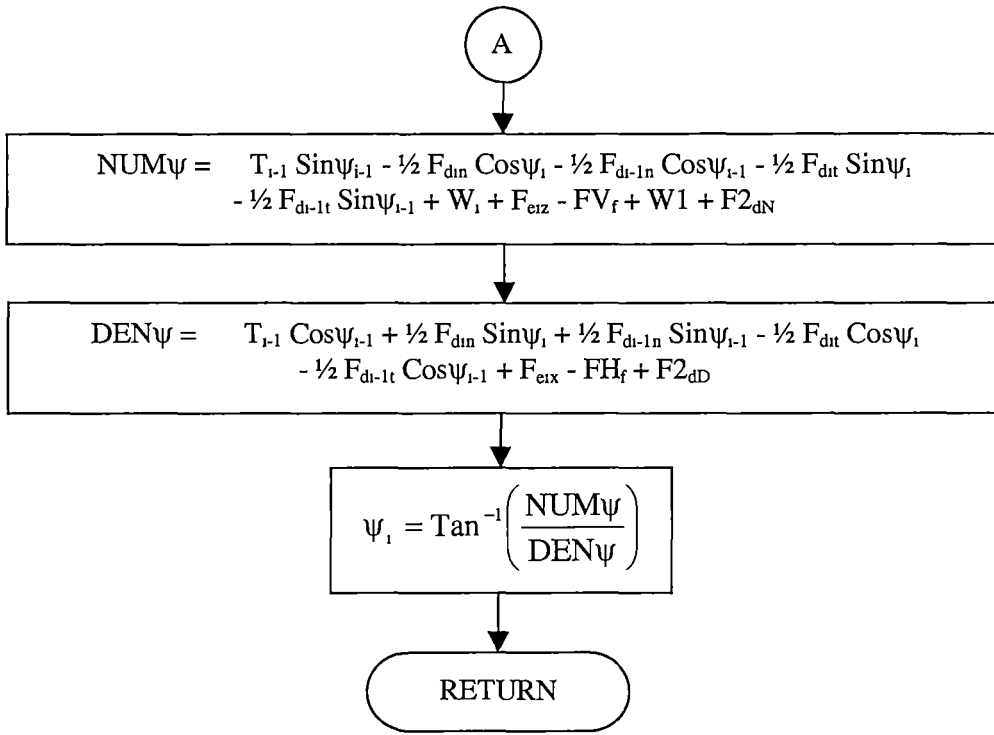


Subroutine Node Drag

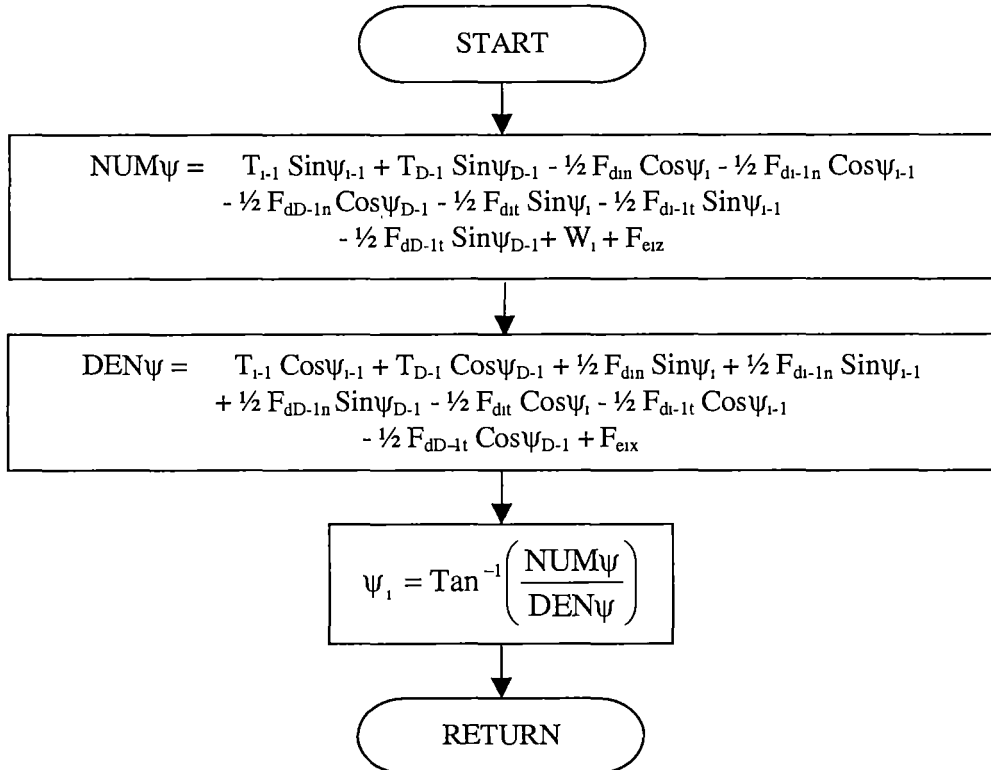


Subroutine Cable Angle

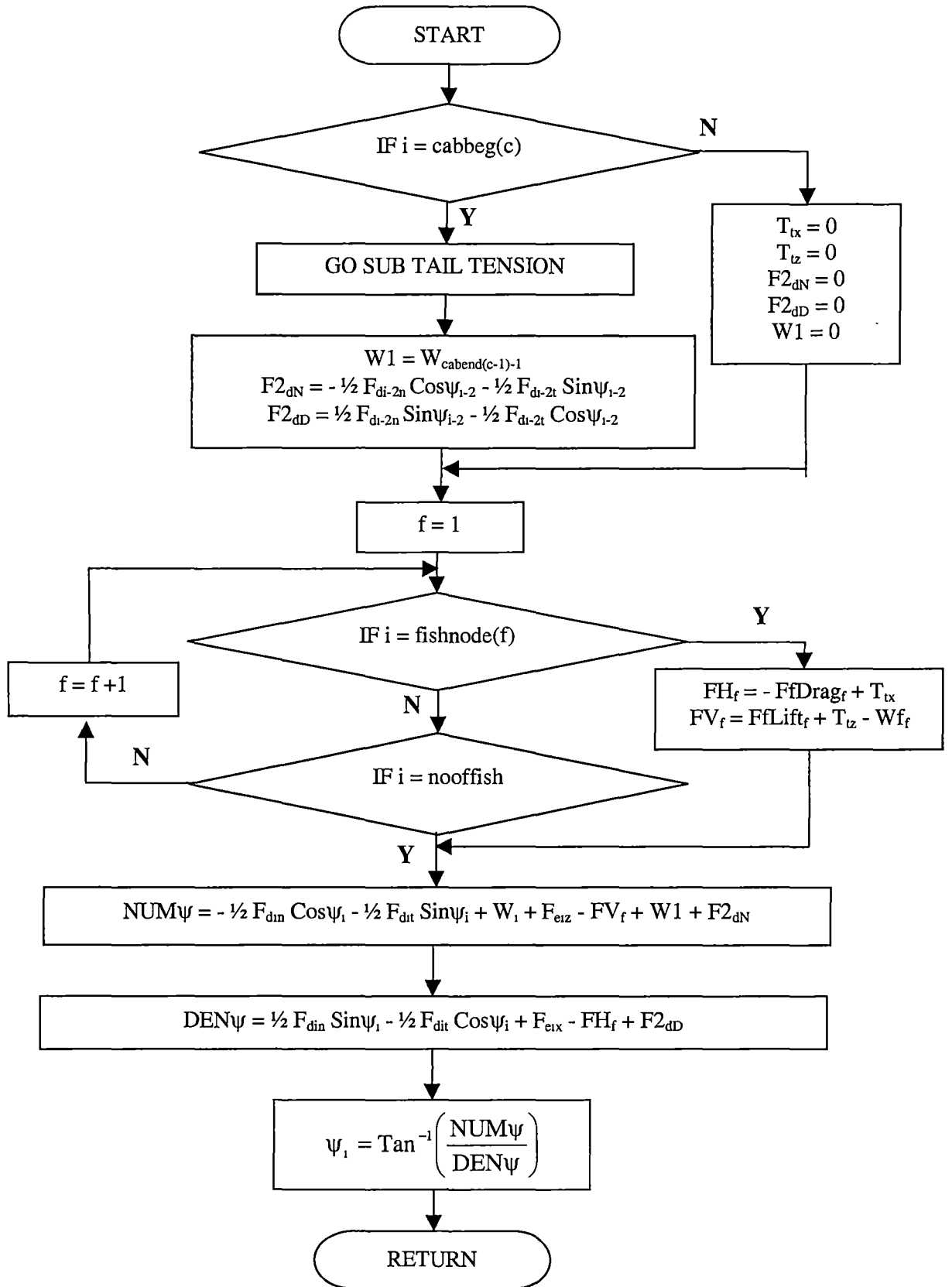




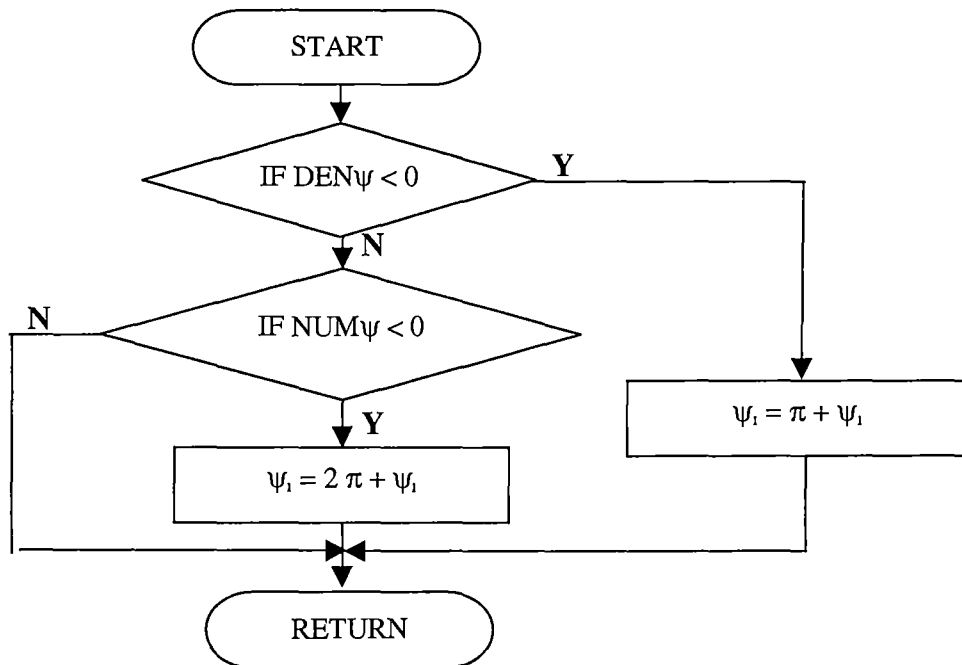
Subroutine Junction Angle



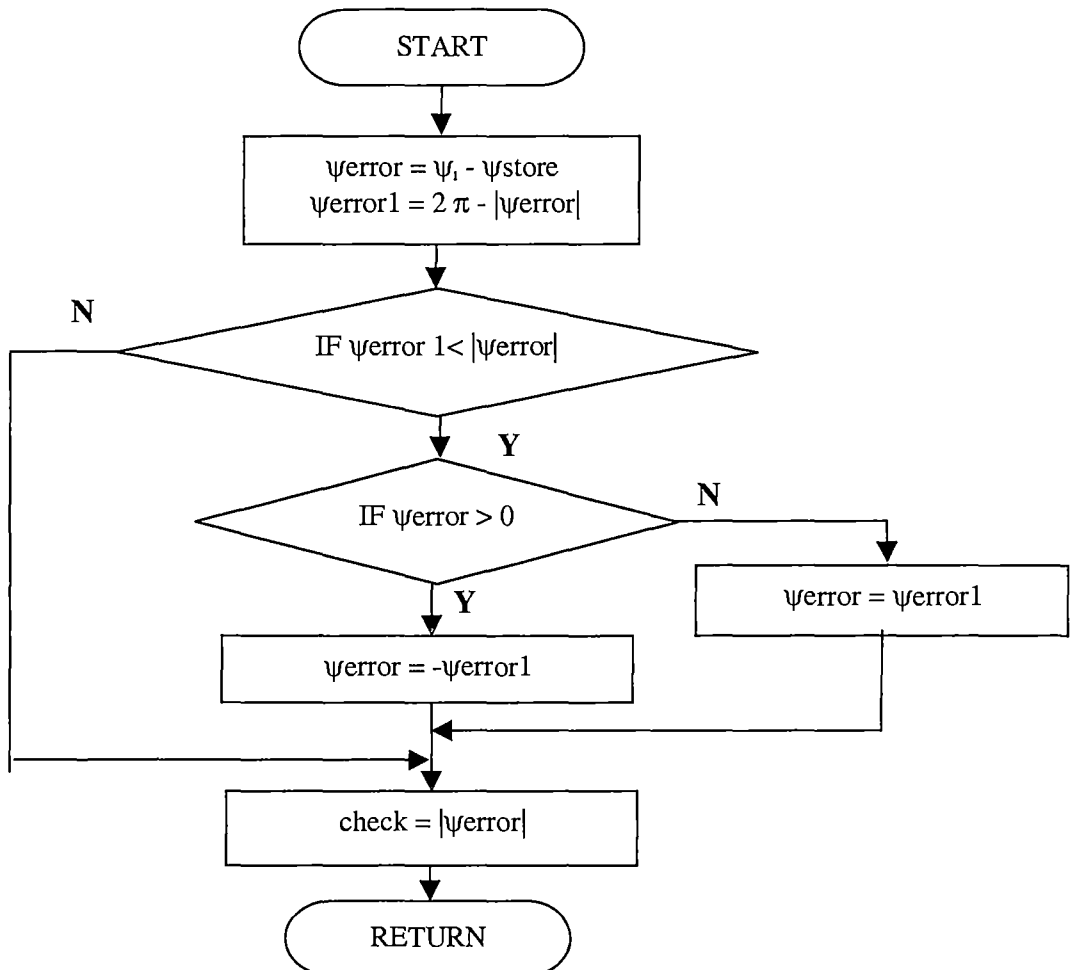
Subroutine Depressor Angle



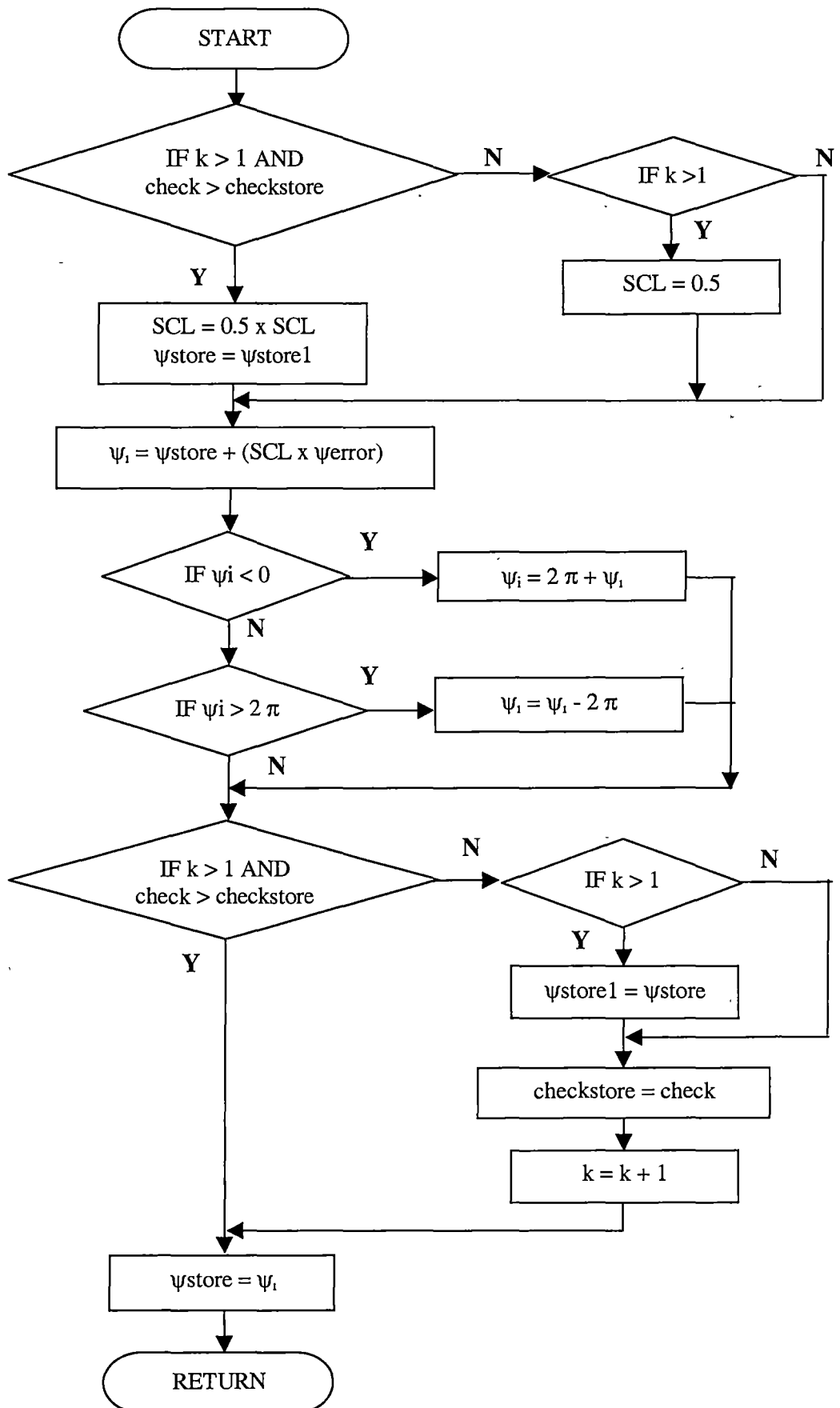
Subroutine Angle Adjust



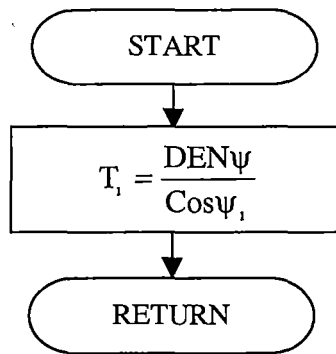
Subroutine Adjust Error



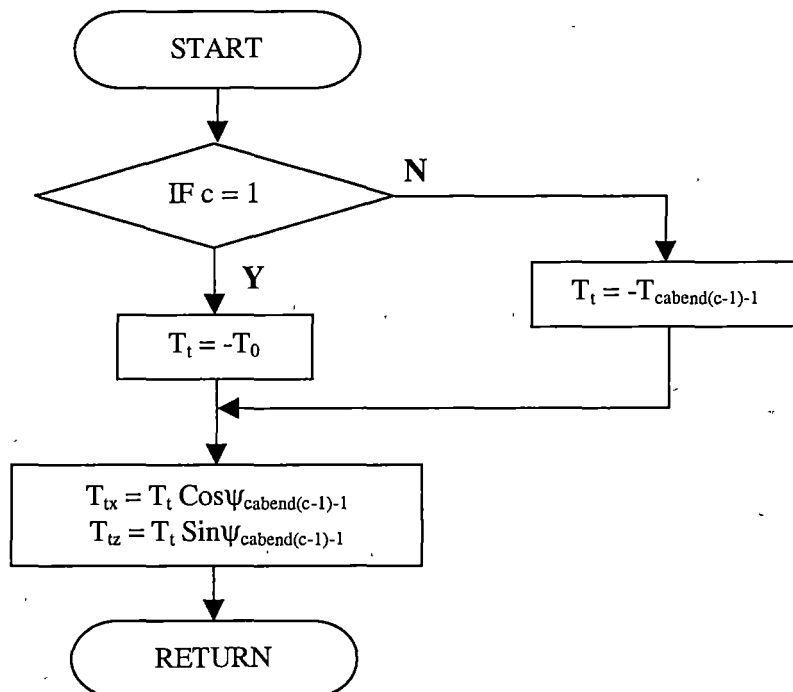
Subroutine Correct Angle



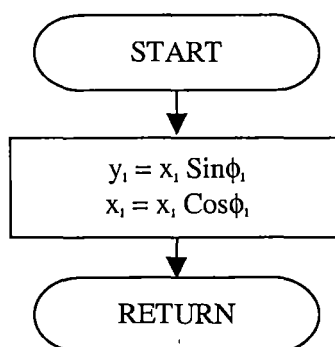
Subroutine Calculate Tension



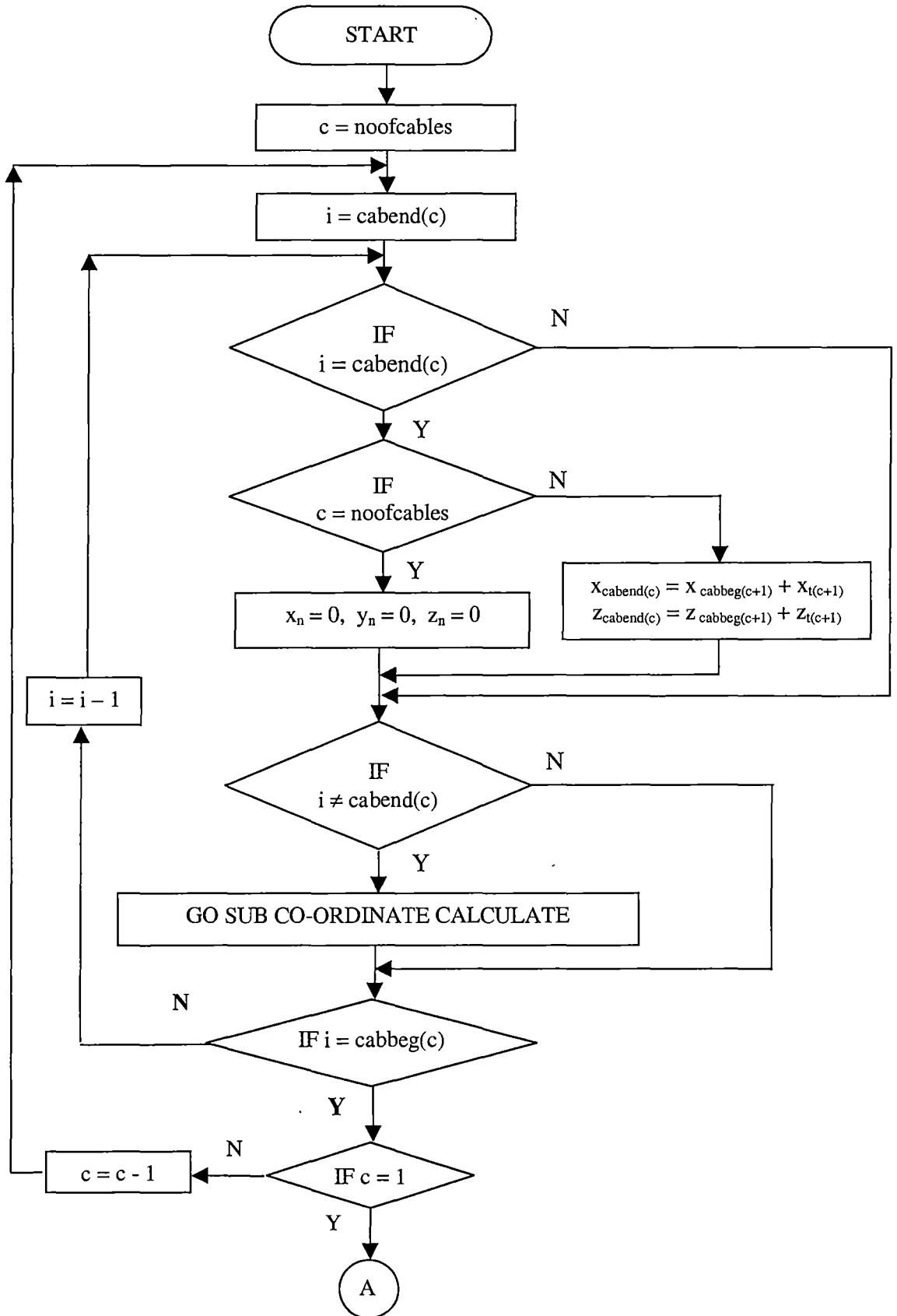
Subroutine Tail Tension

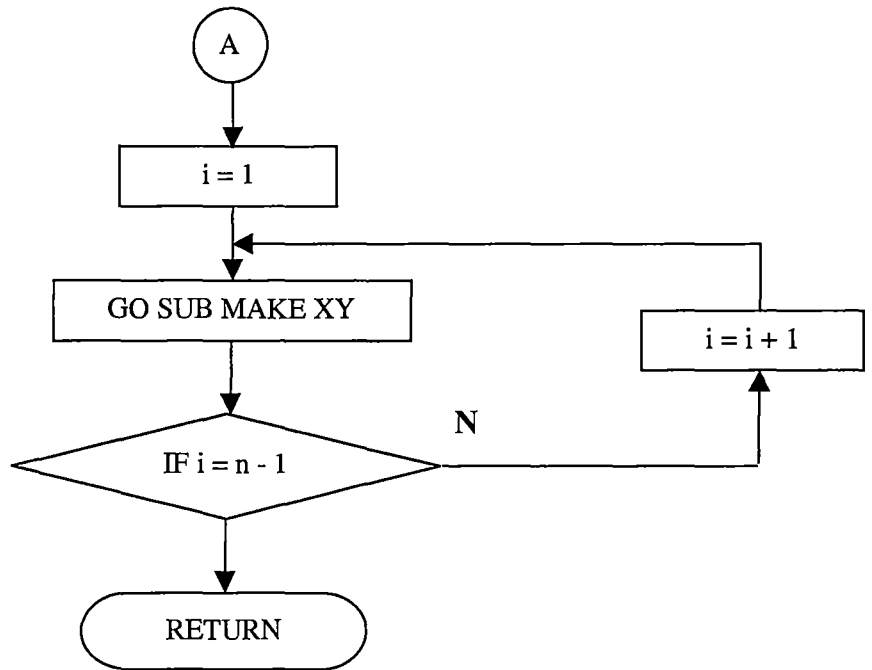


Subroutine Make XY

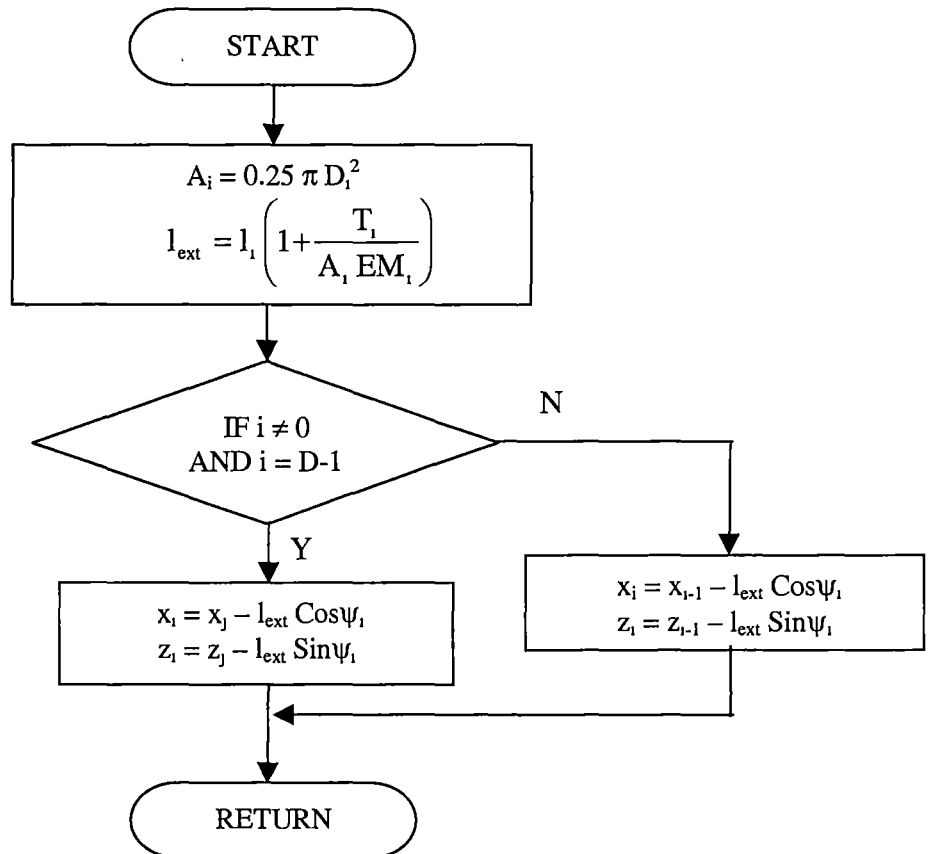


Subroutine Coordinate

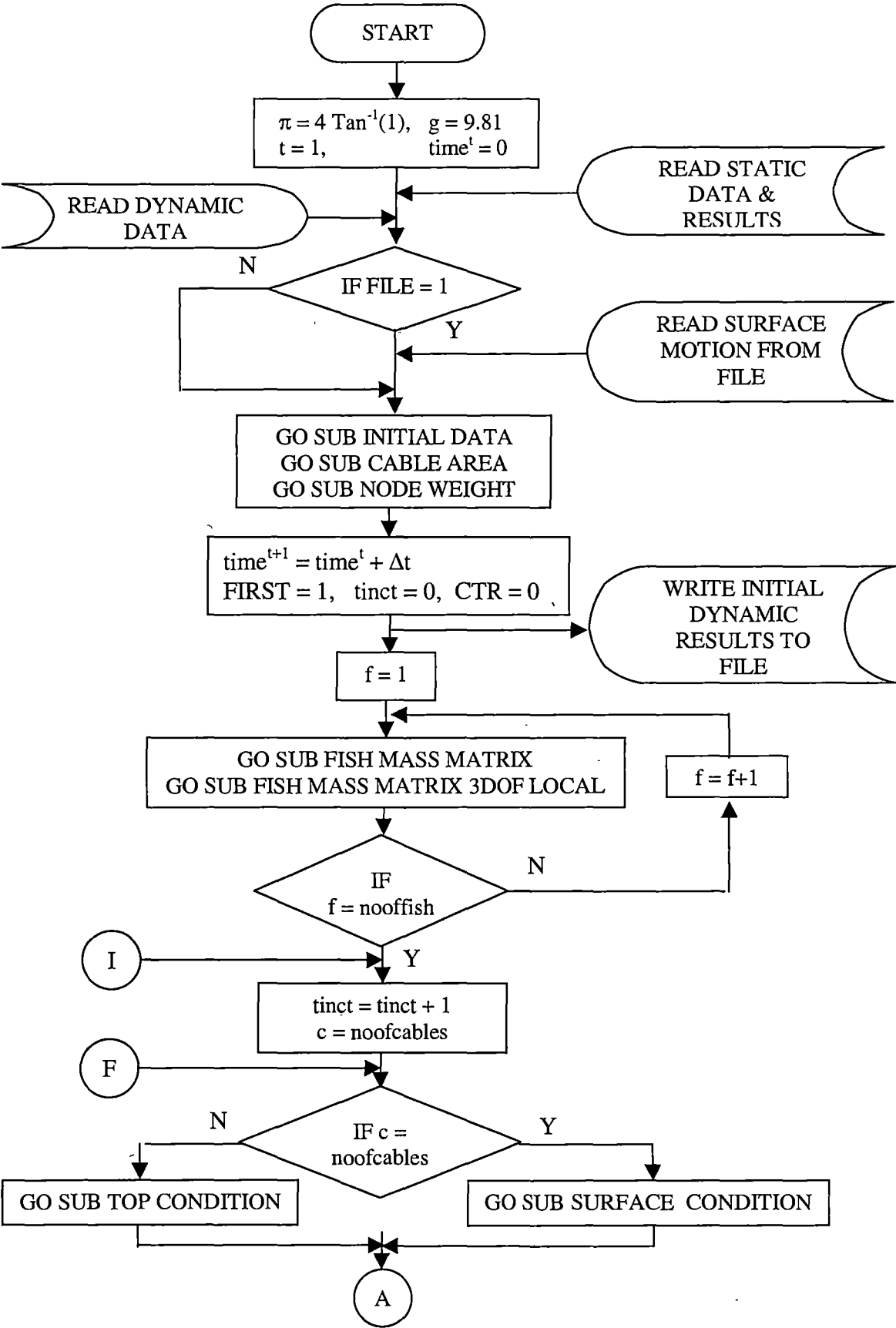


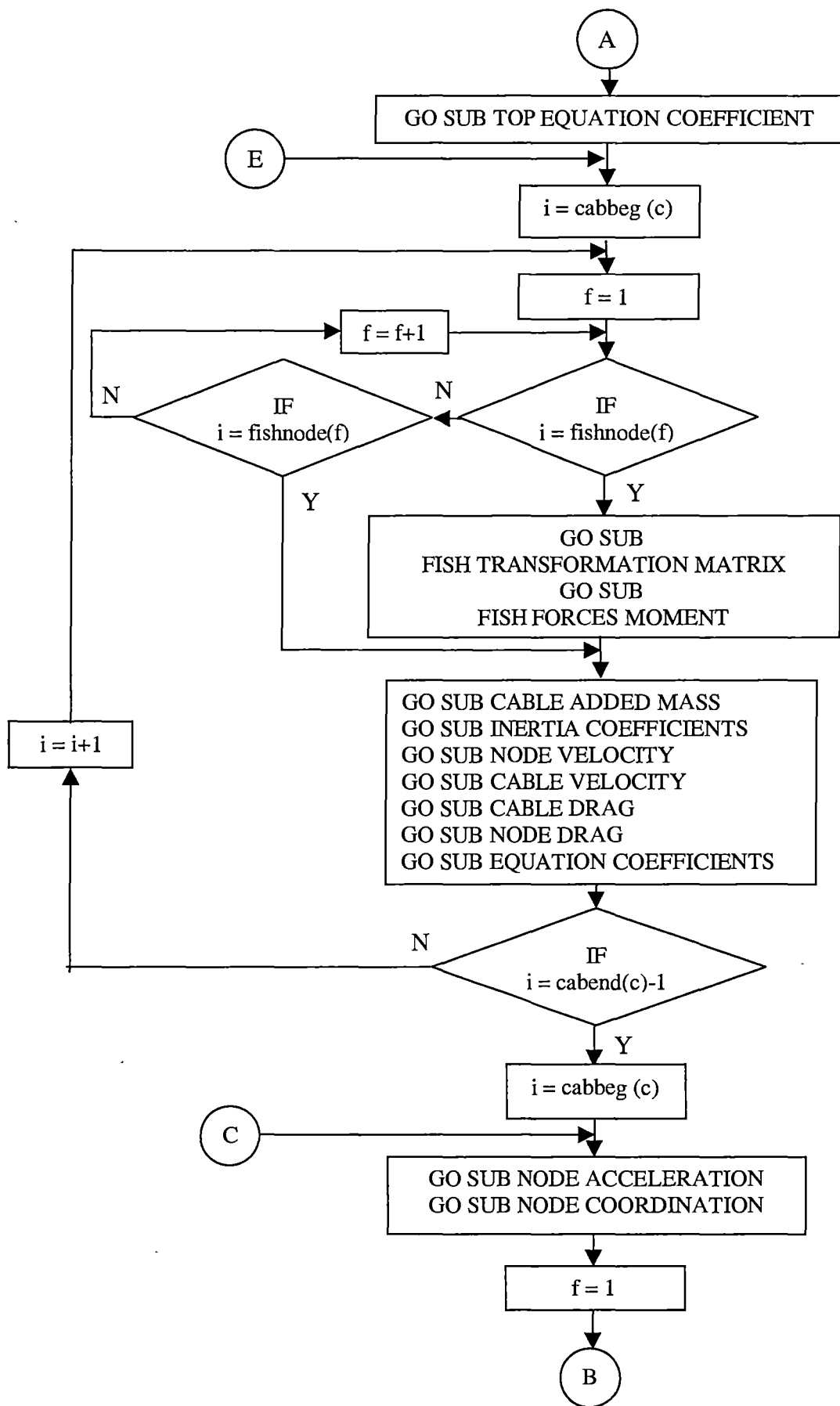


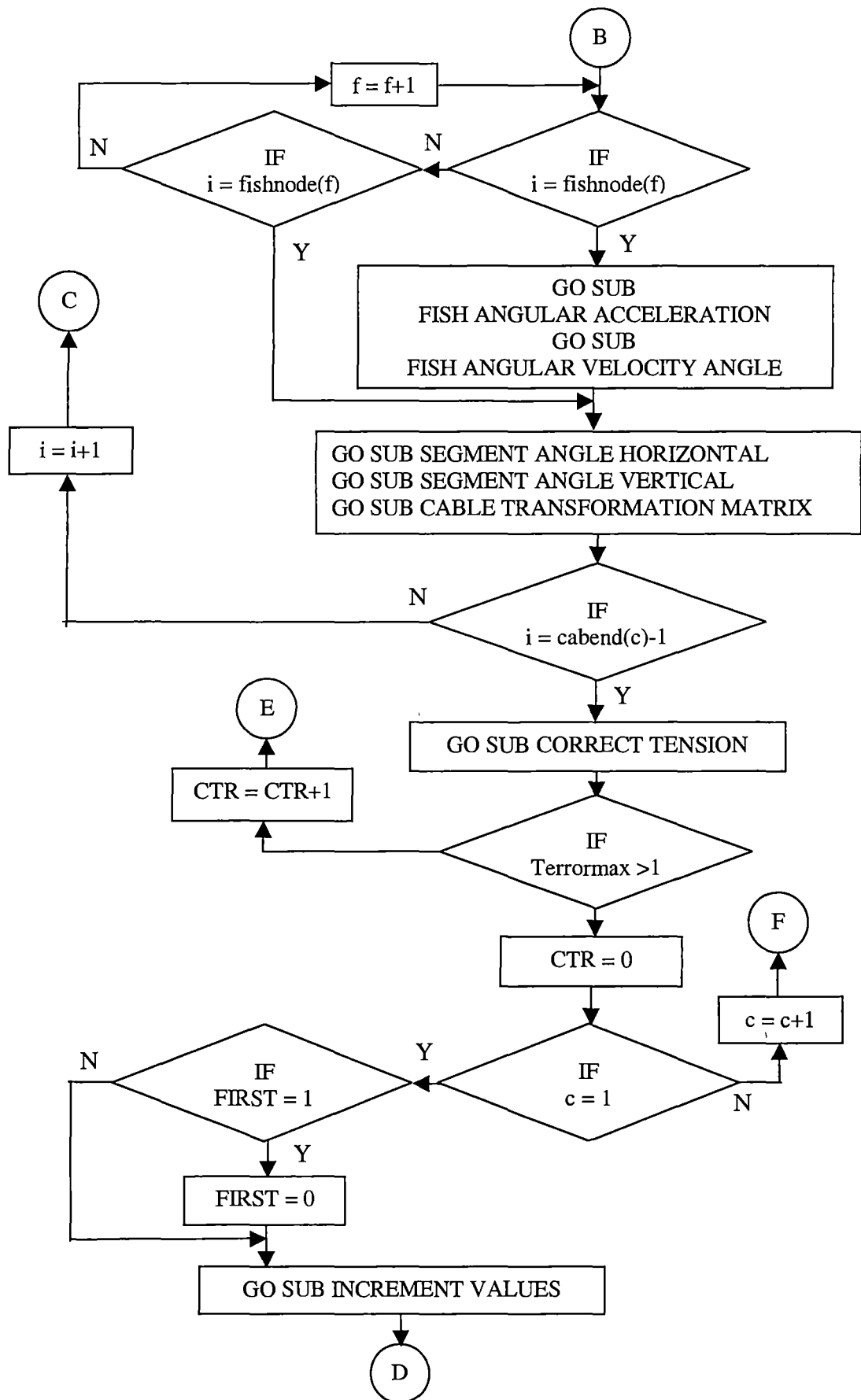
Subroutine Coordinate Calculate

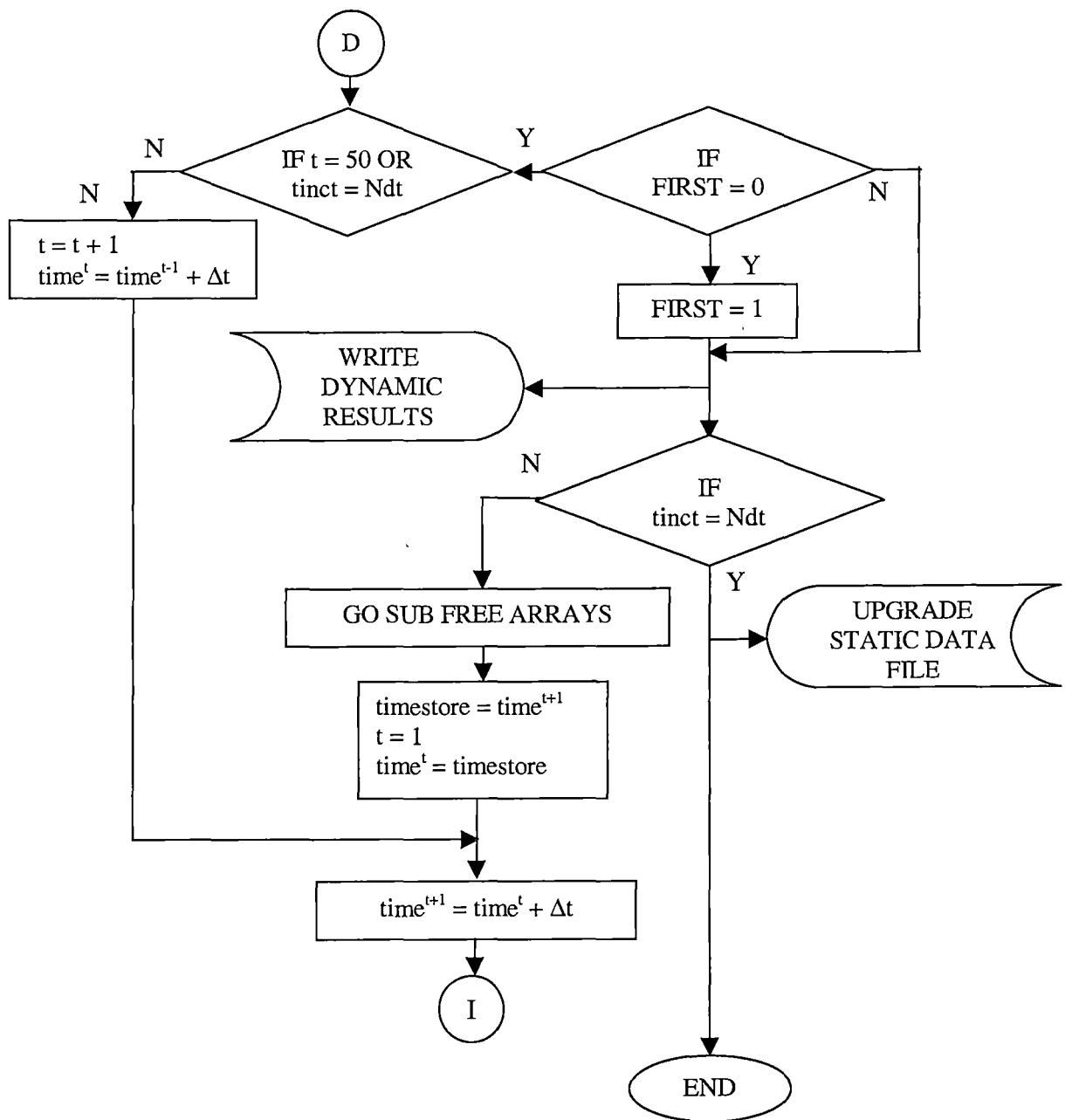


Dynamic Main Program

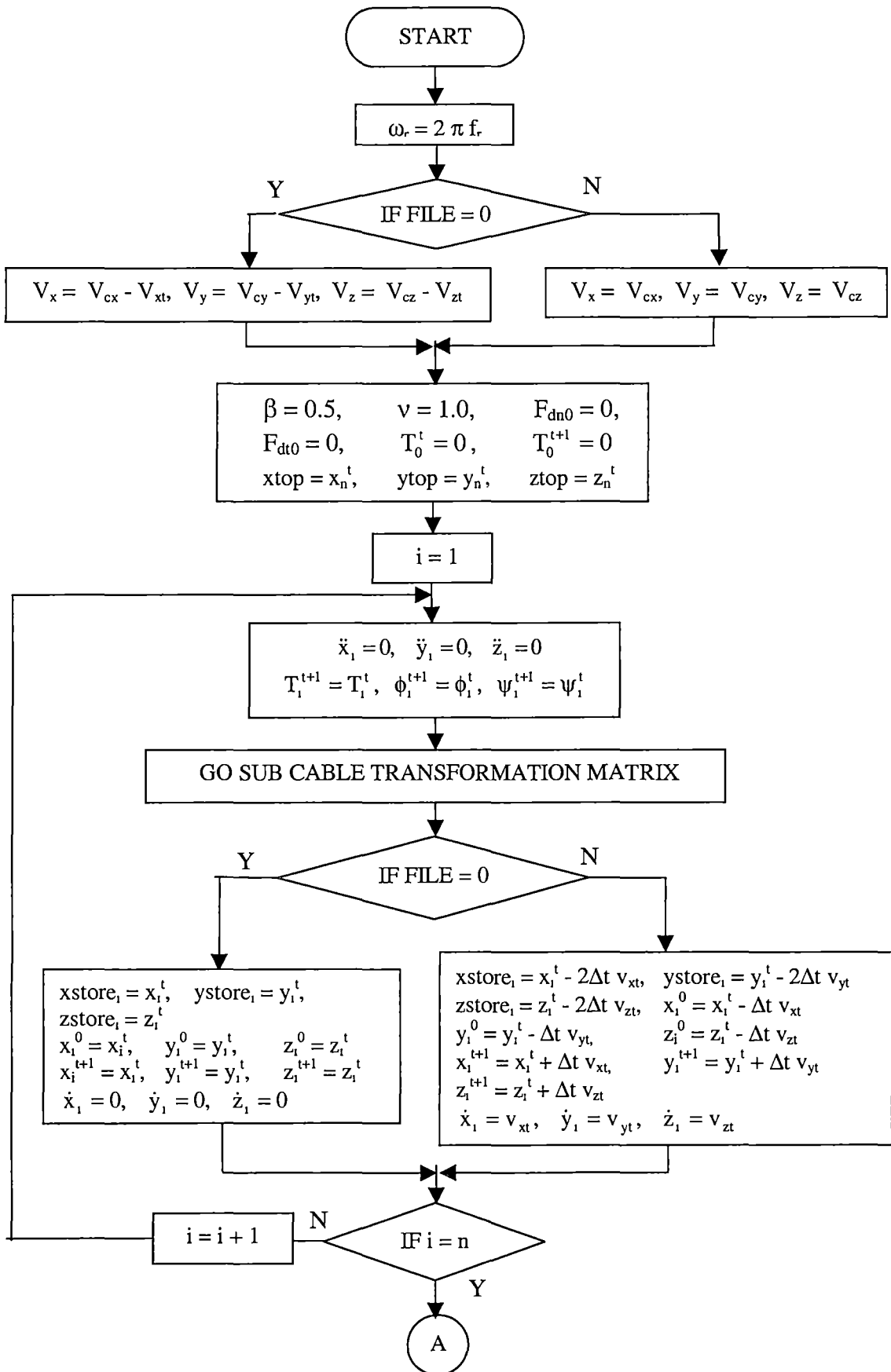


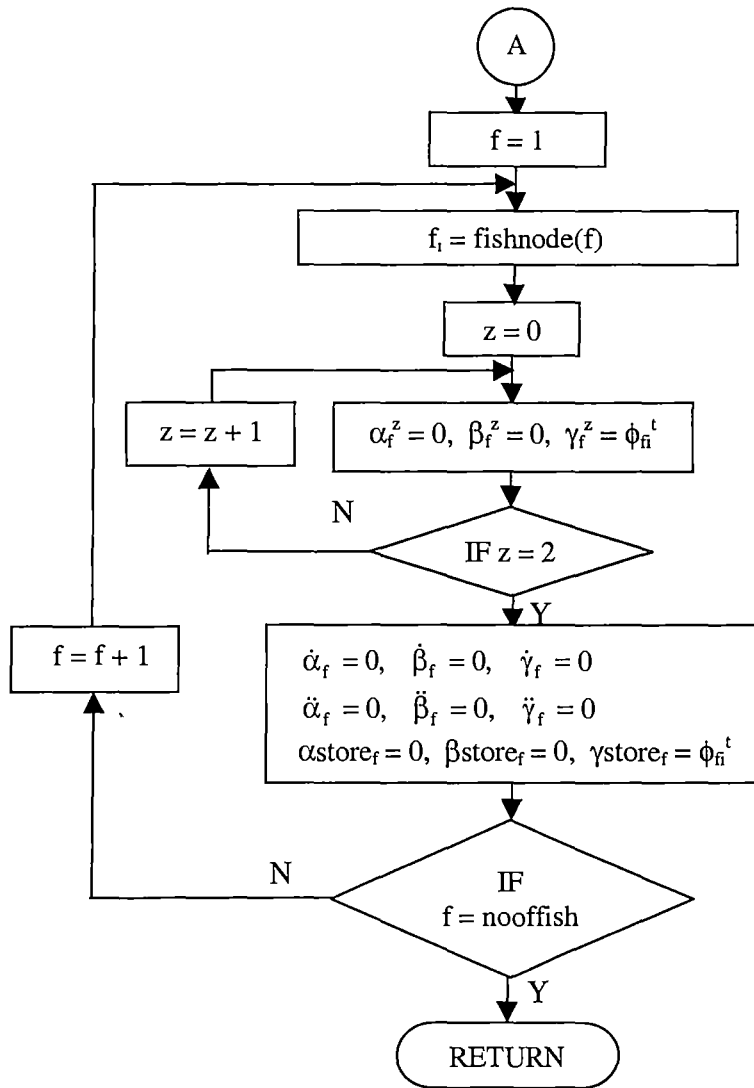




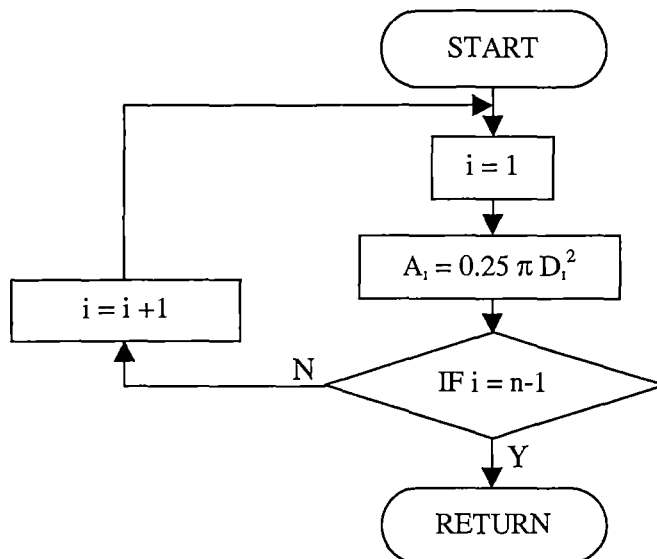


Subroutine Initial Data

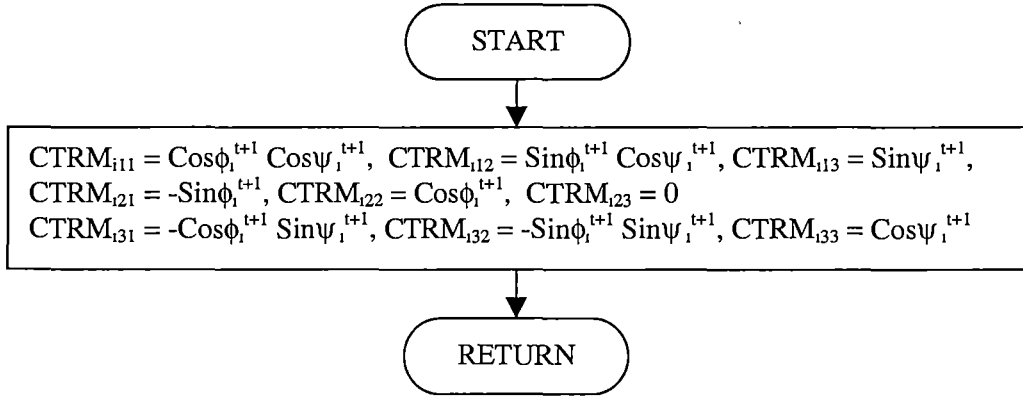




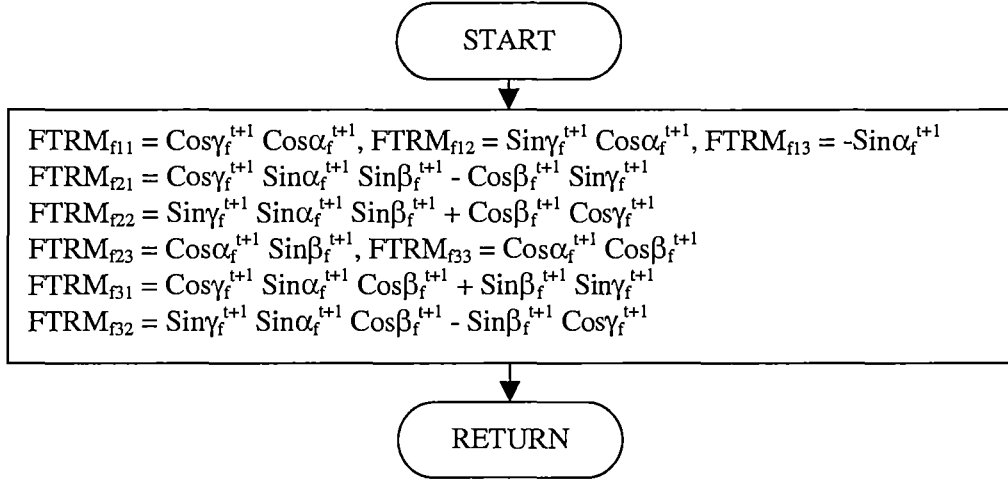
Subroutine Cable Area



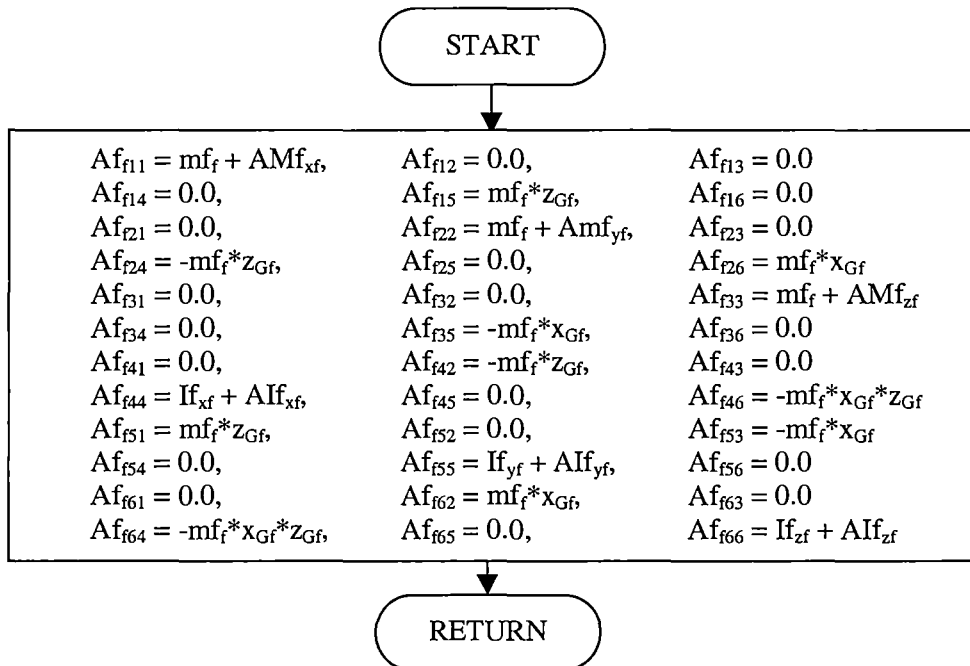
Subroutine Cable Transformation Matrix



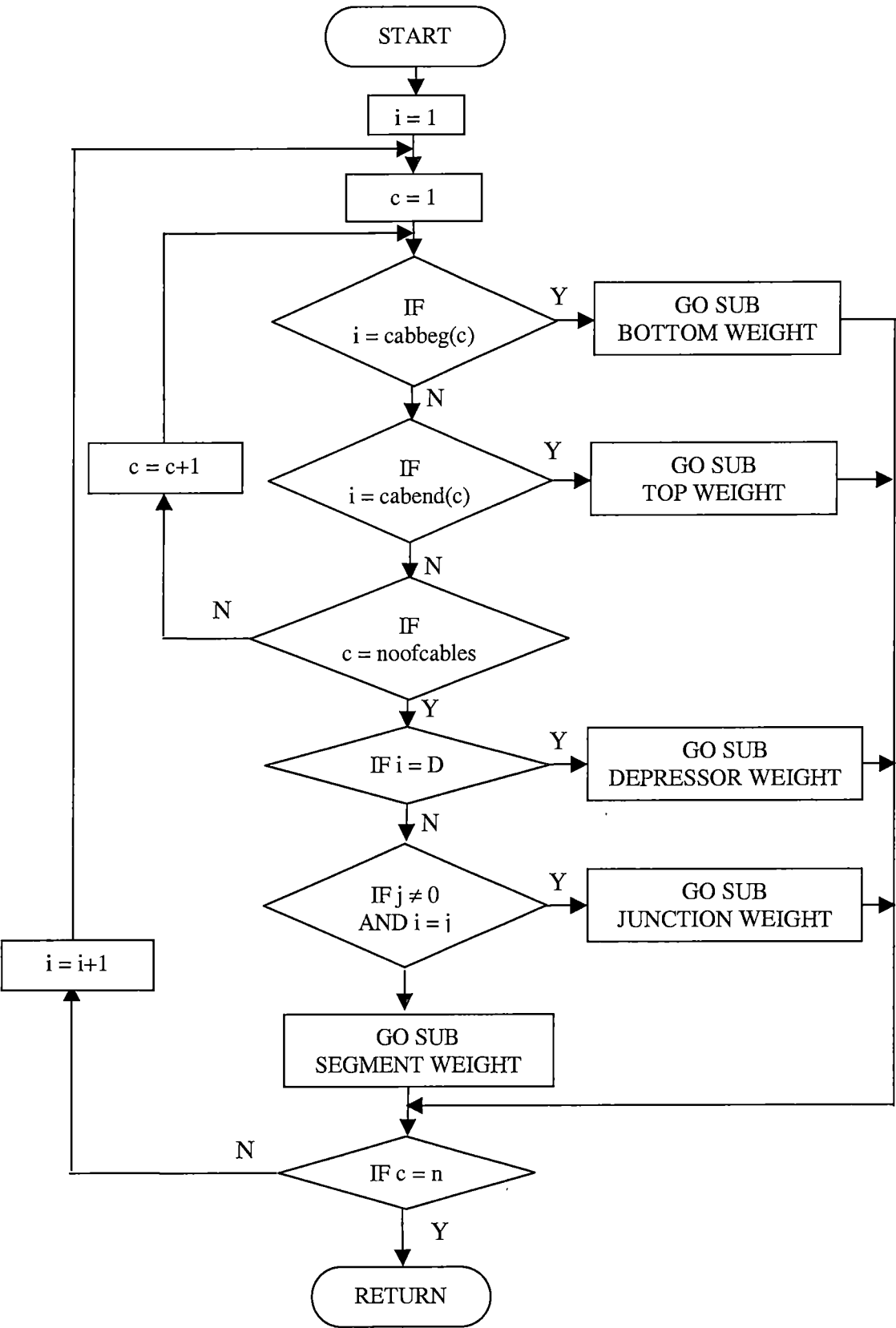
Subroutine Fish Transformation Matrix



Subroutine Fish Mass Matrix

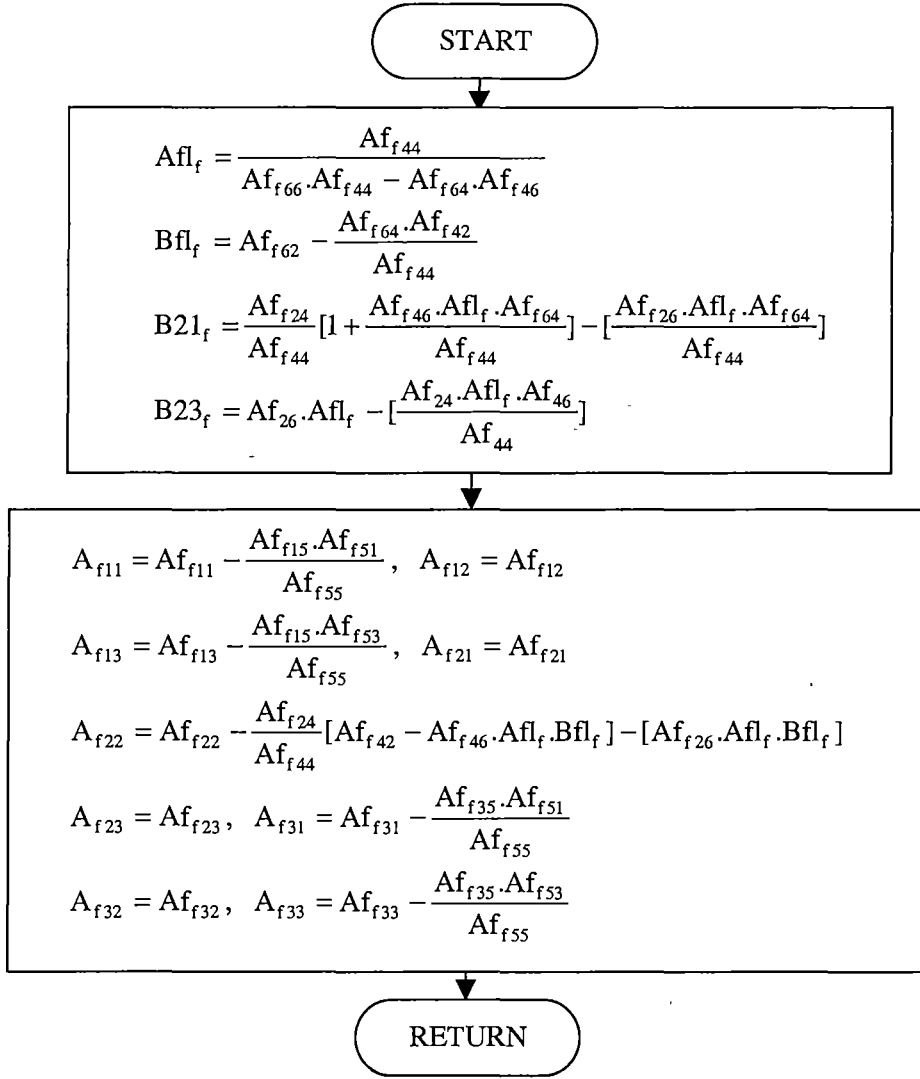


Subroutine Node Weights

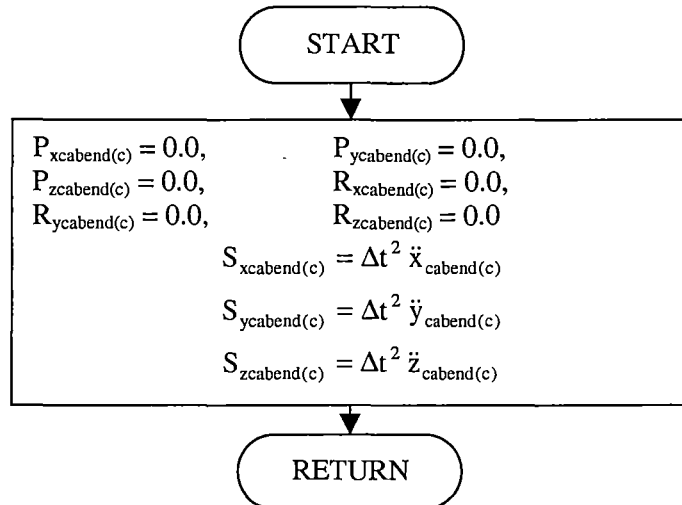


The subroutines called up in this subroutine are the same as for the equivalent Static program.

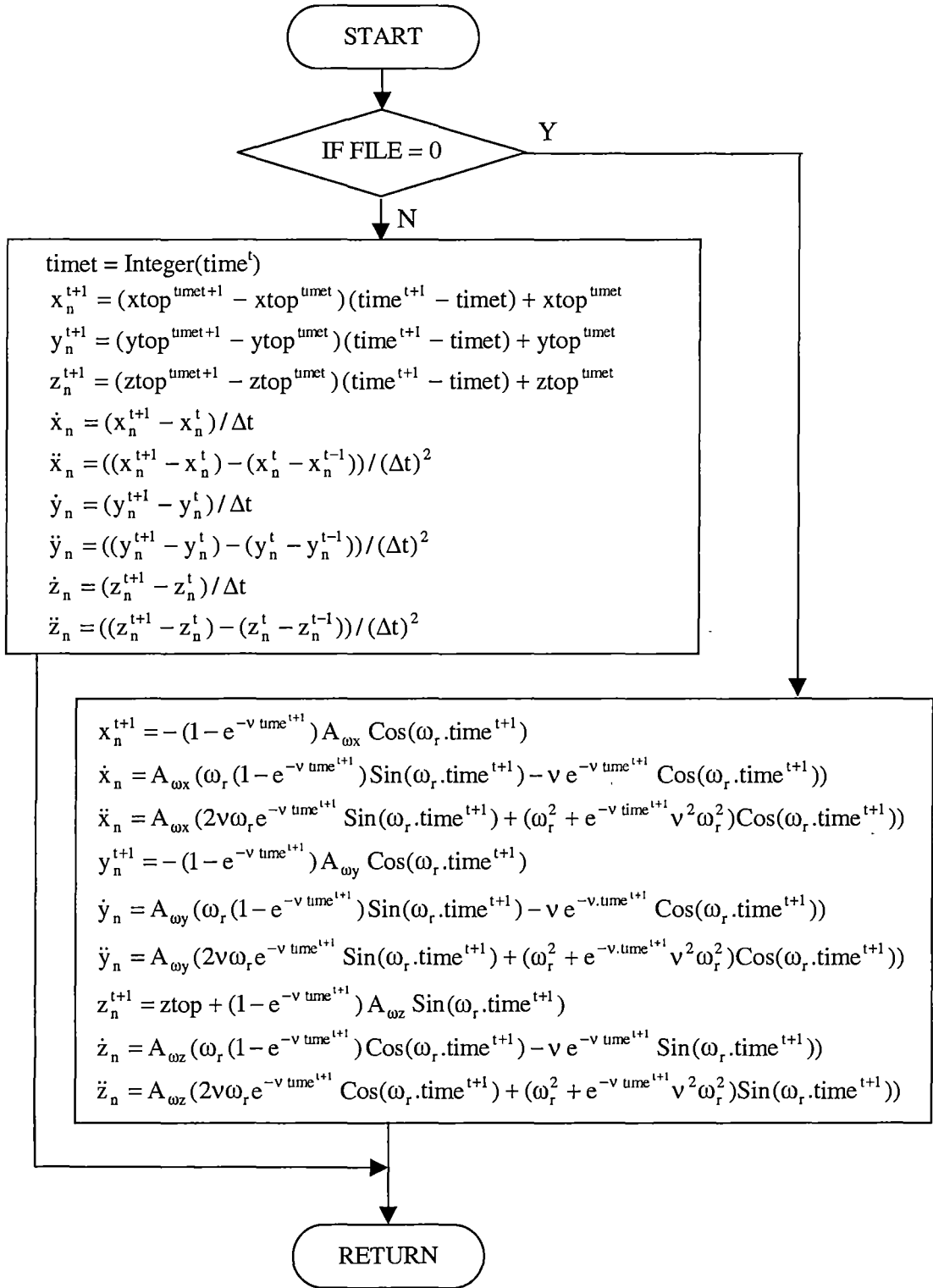
Subroutine Fish Mass Matrix 3 DOF Local



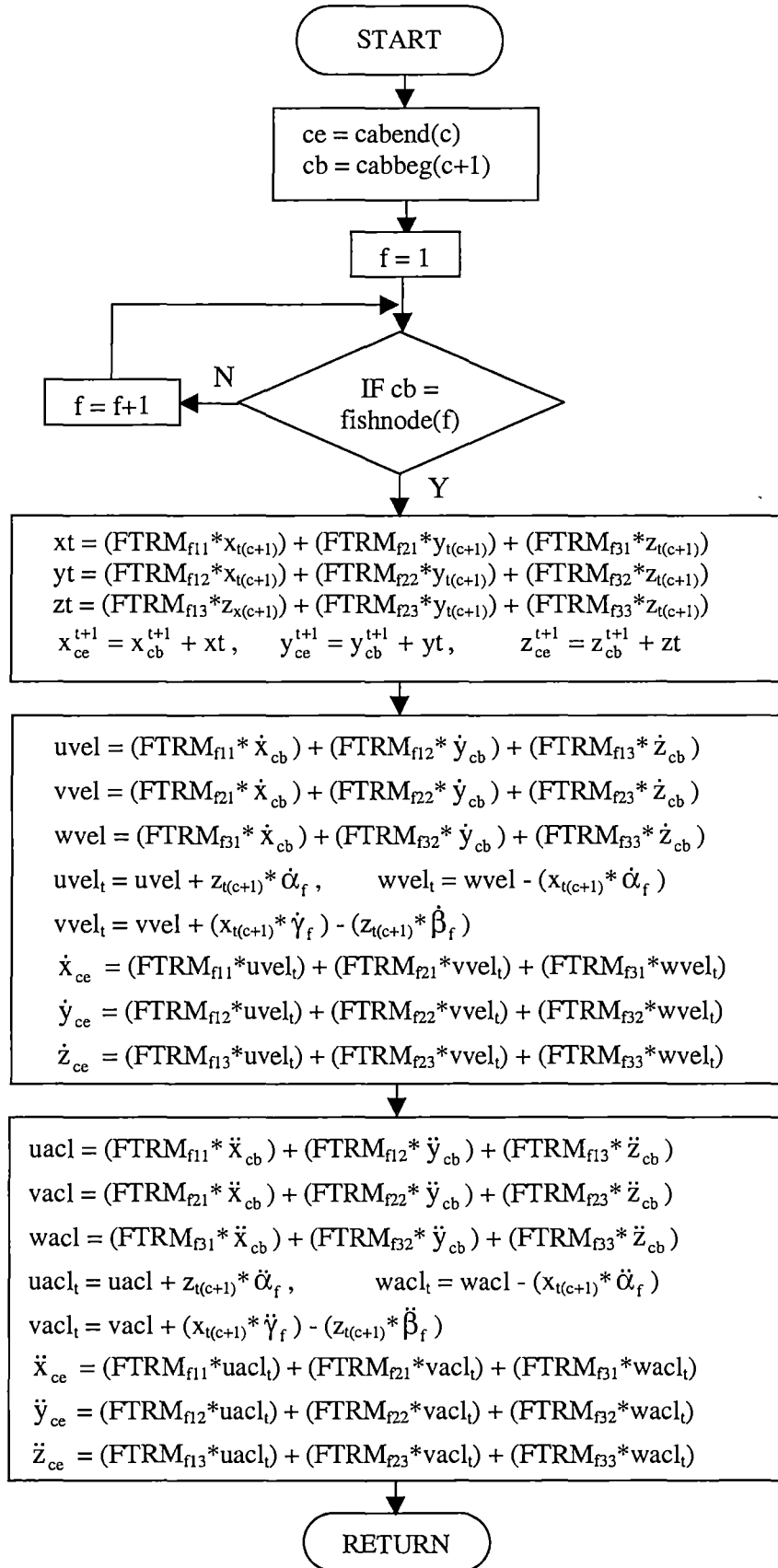
Subroutine Top Equation Coefficients



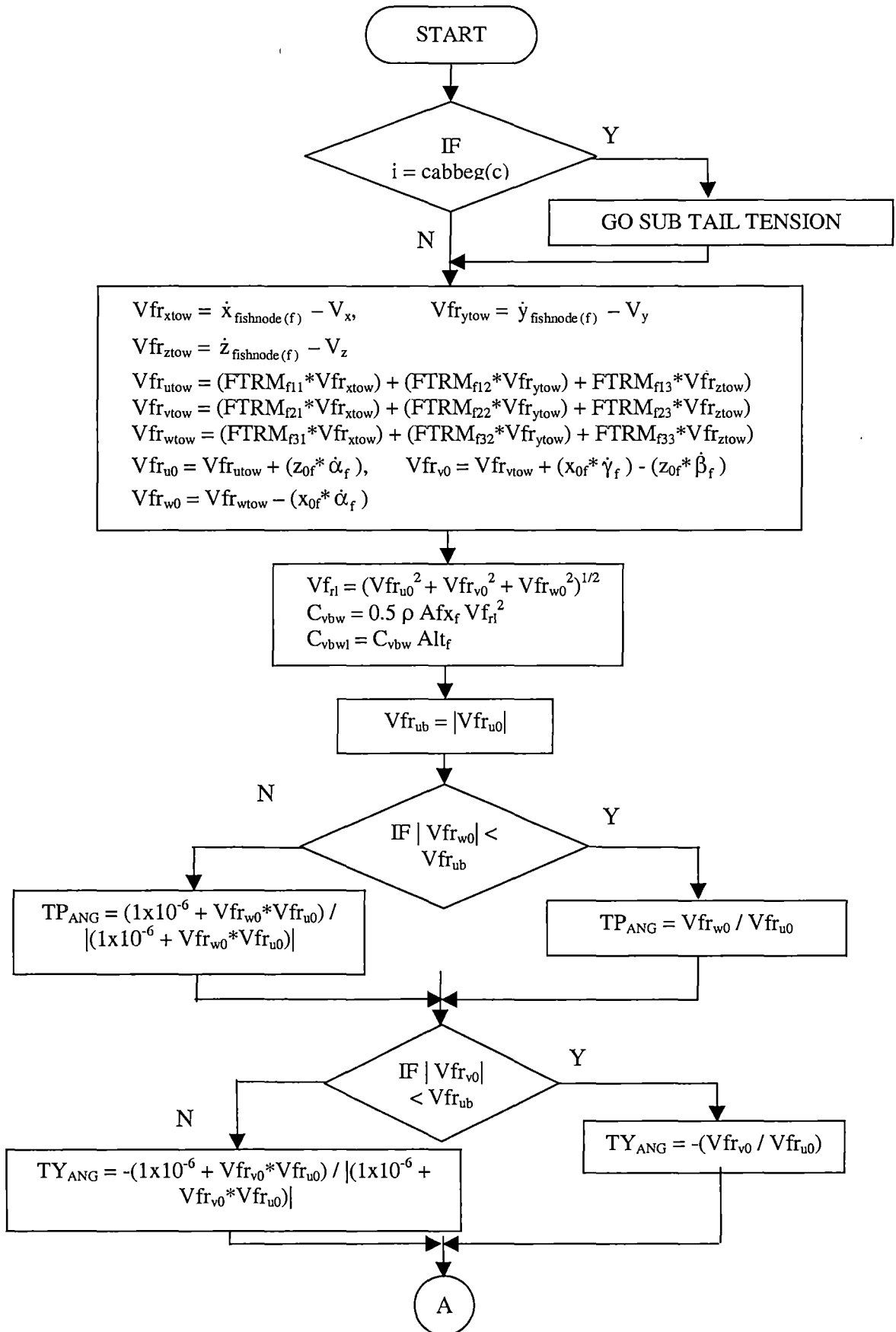
Subroutine Surface Conditions

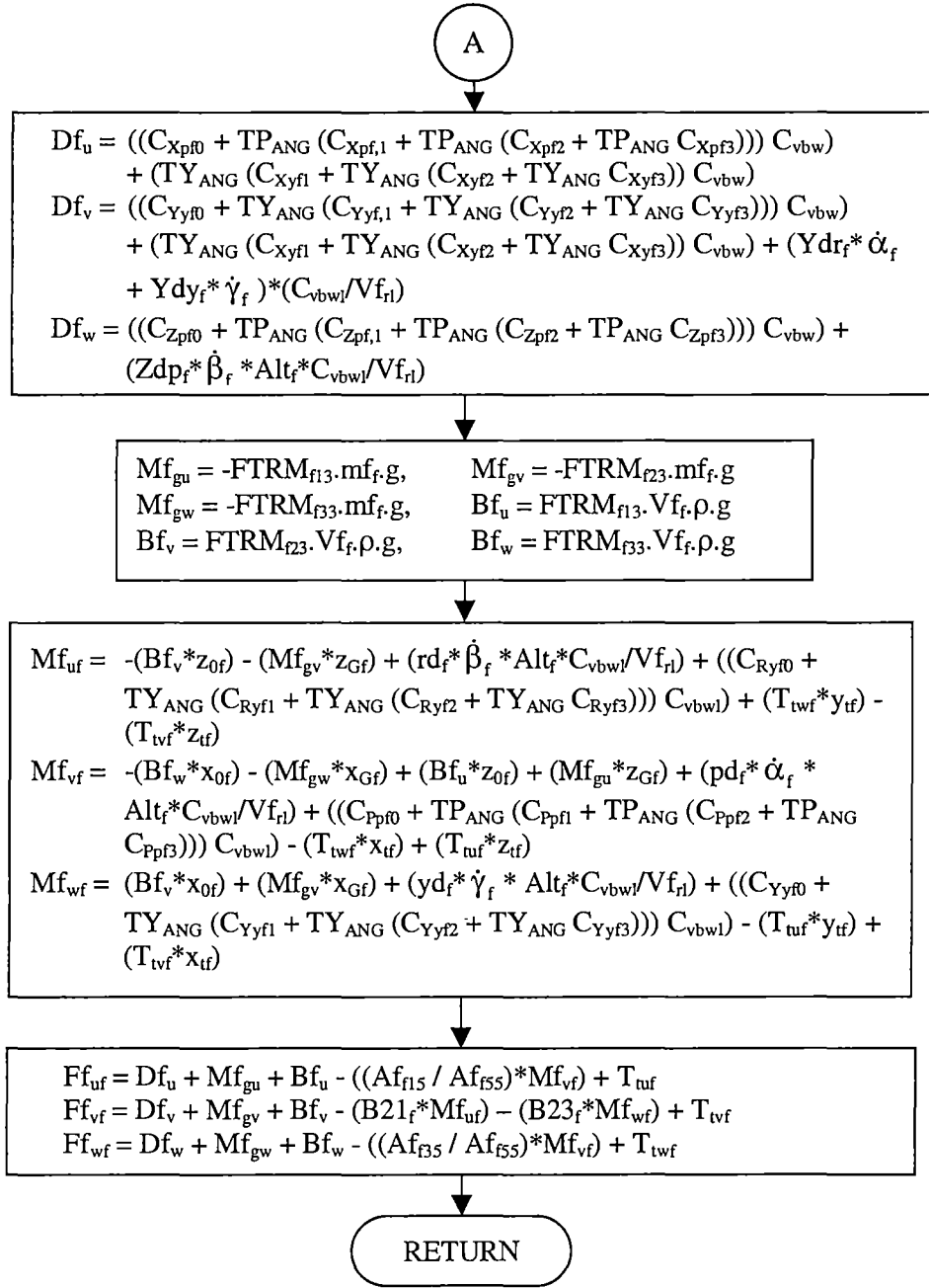


Subroutine Top Conditions

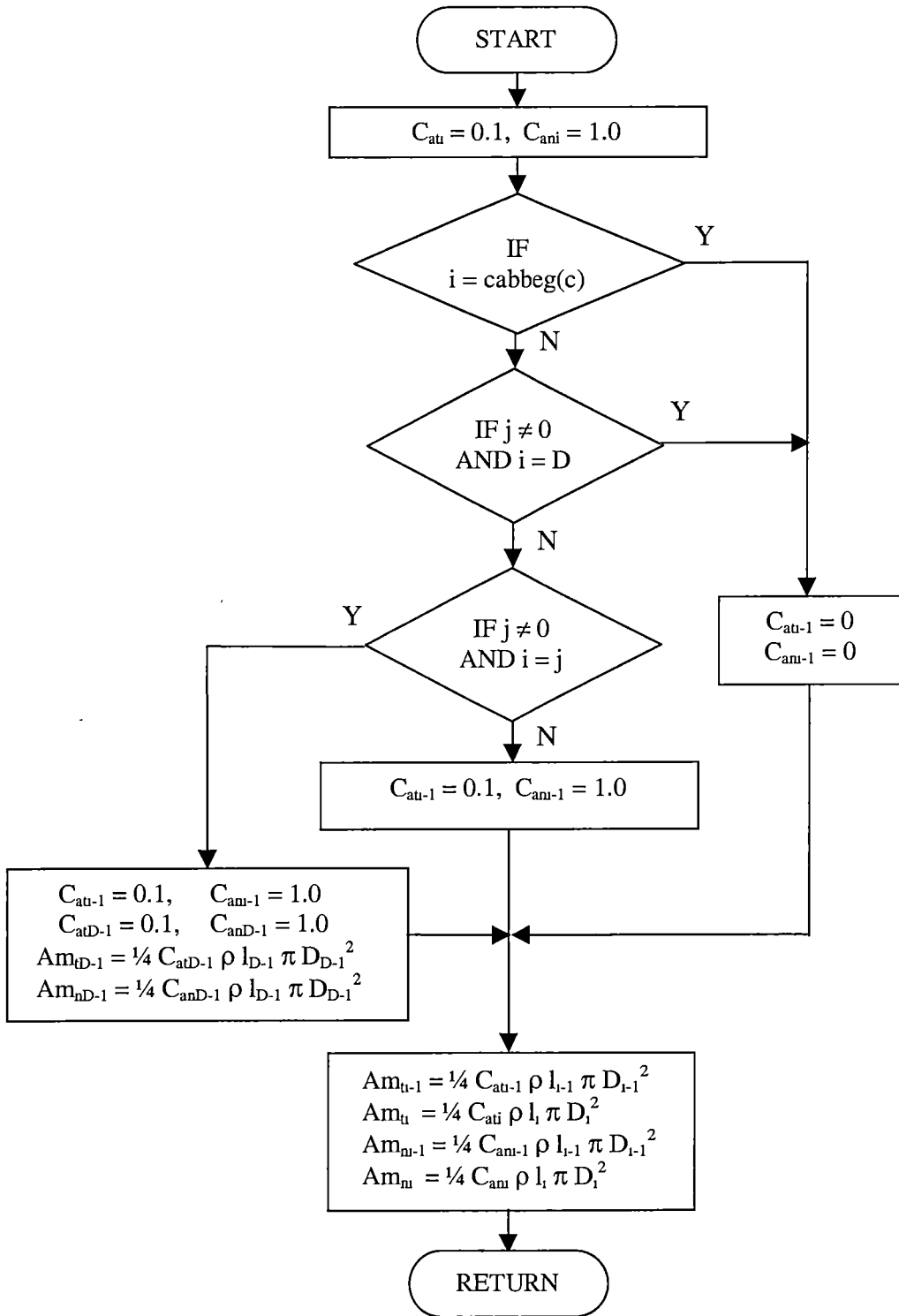


Subroutine Fish Force Moment

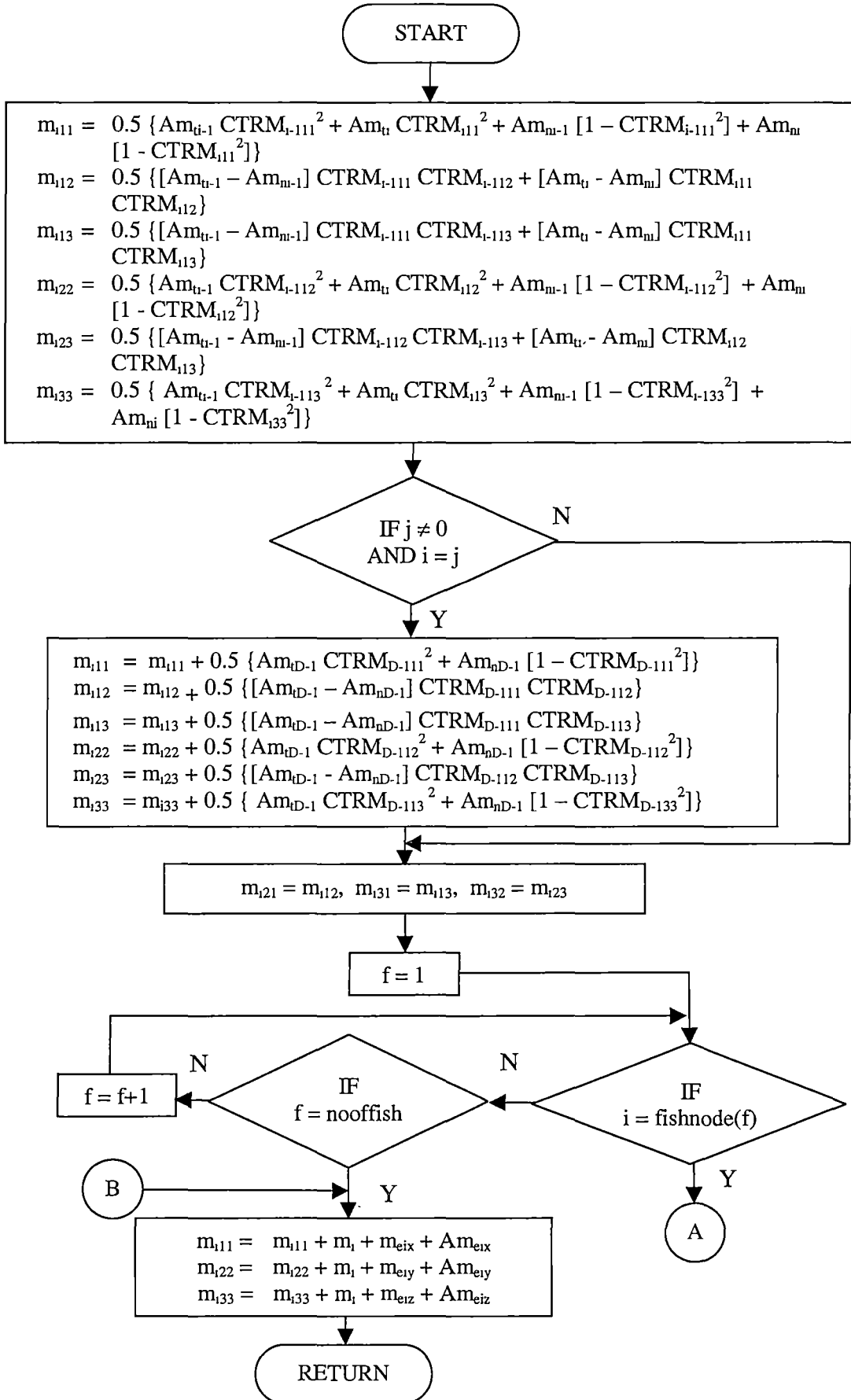


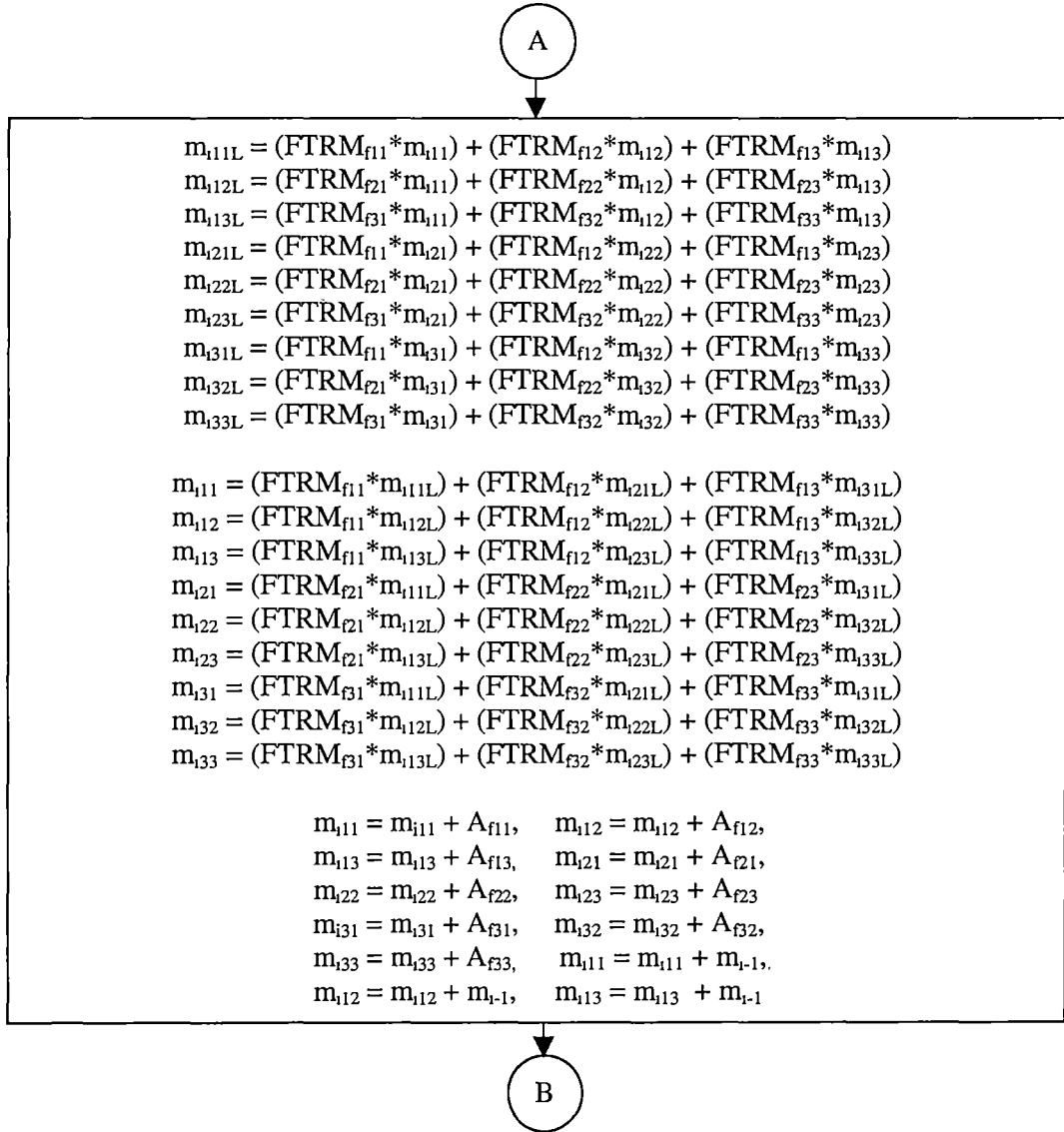


Subroutine Cable Added Mass

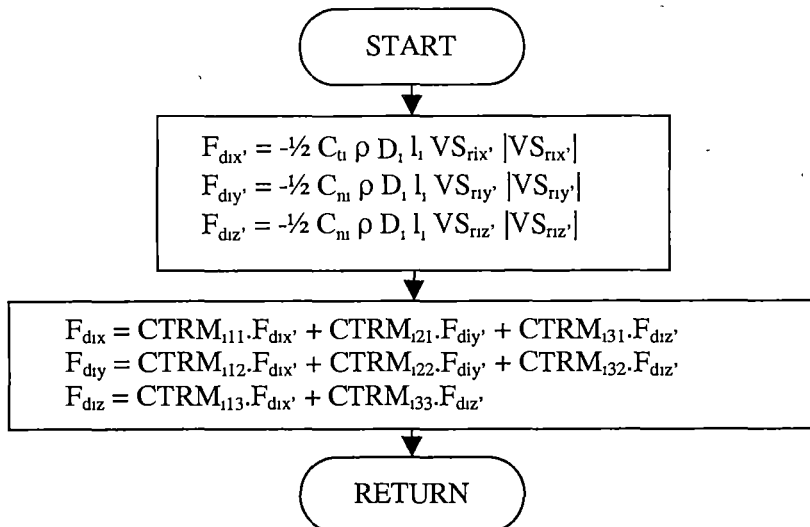


Subroutine Inertia Coefficient

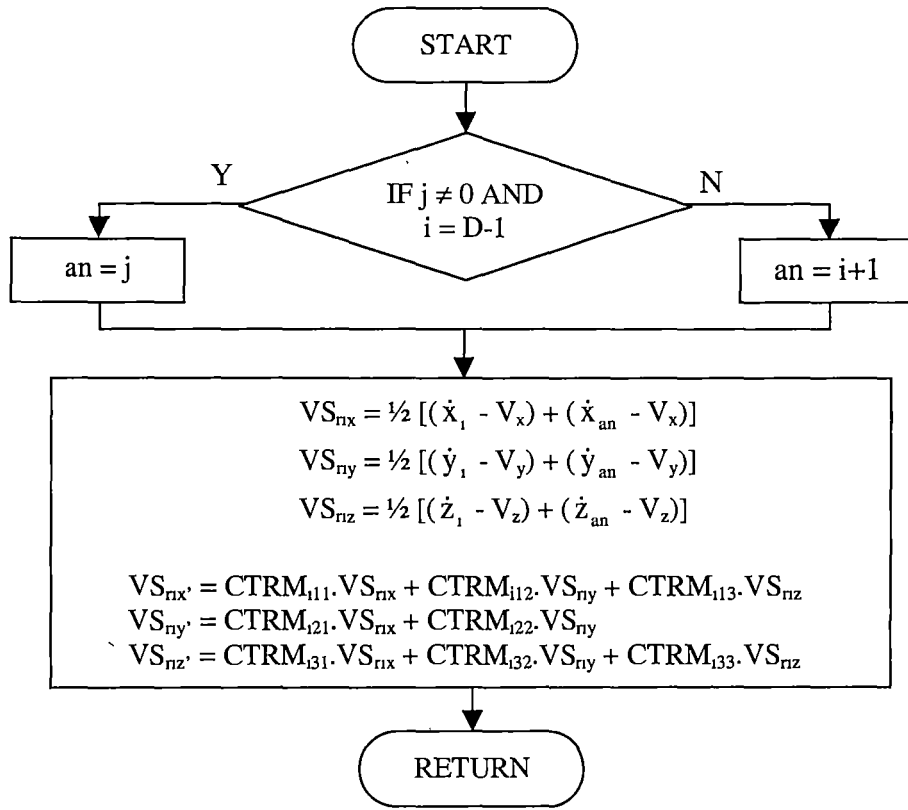




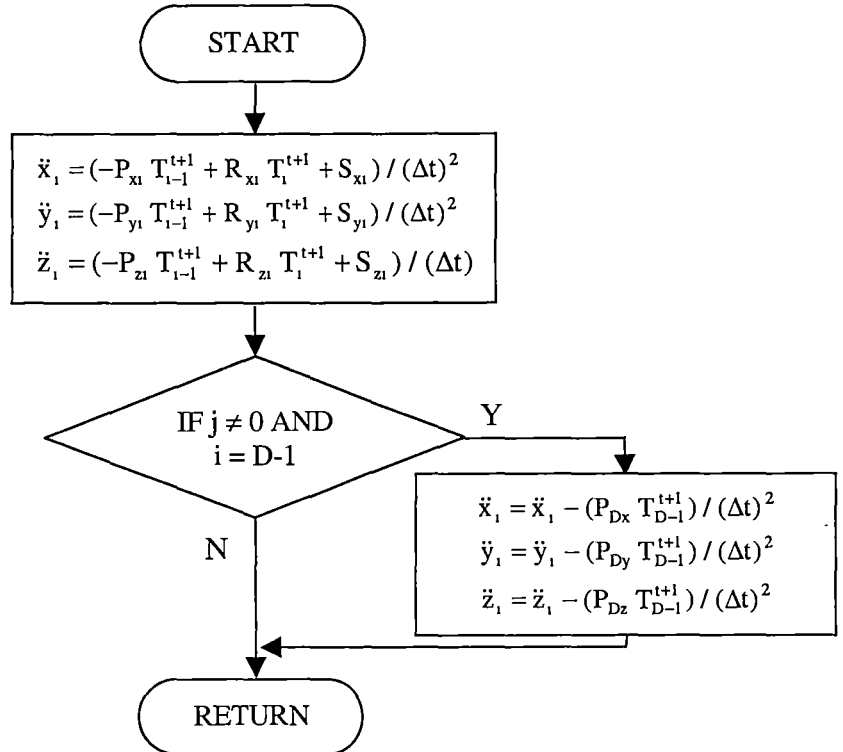
Subroutine Cable Drag



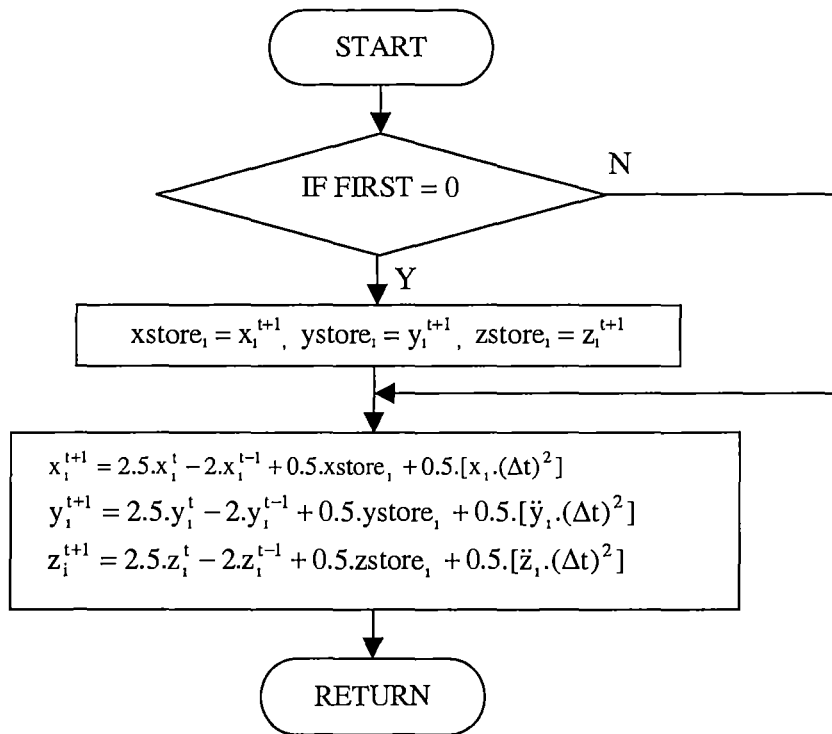
Subroutine Cable Velocity



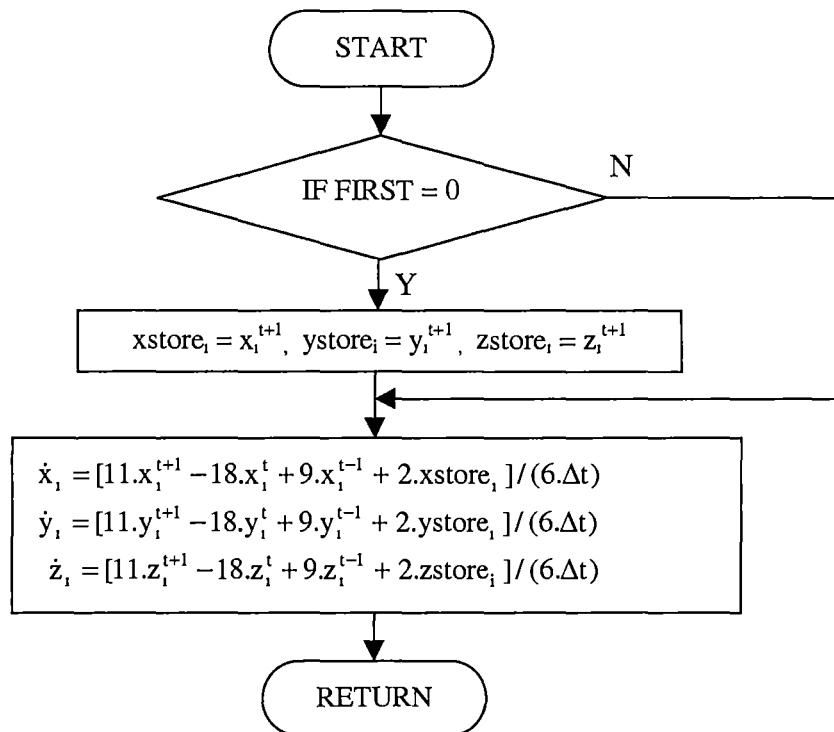
Subroutine Node Acceleration



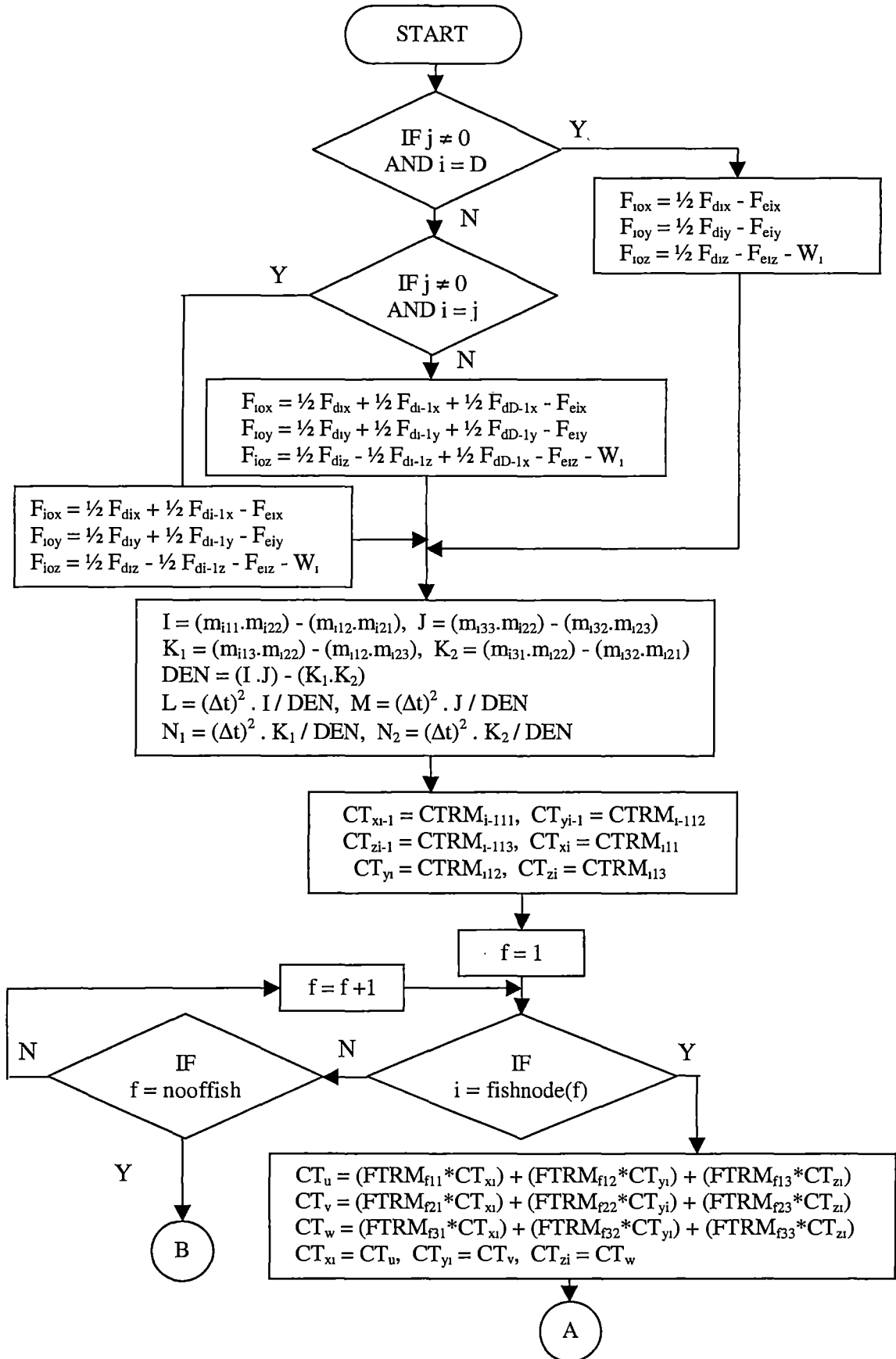
Subroutine Node Coordinate

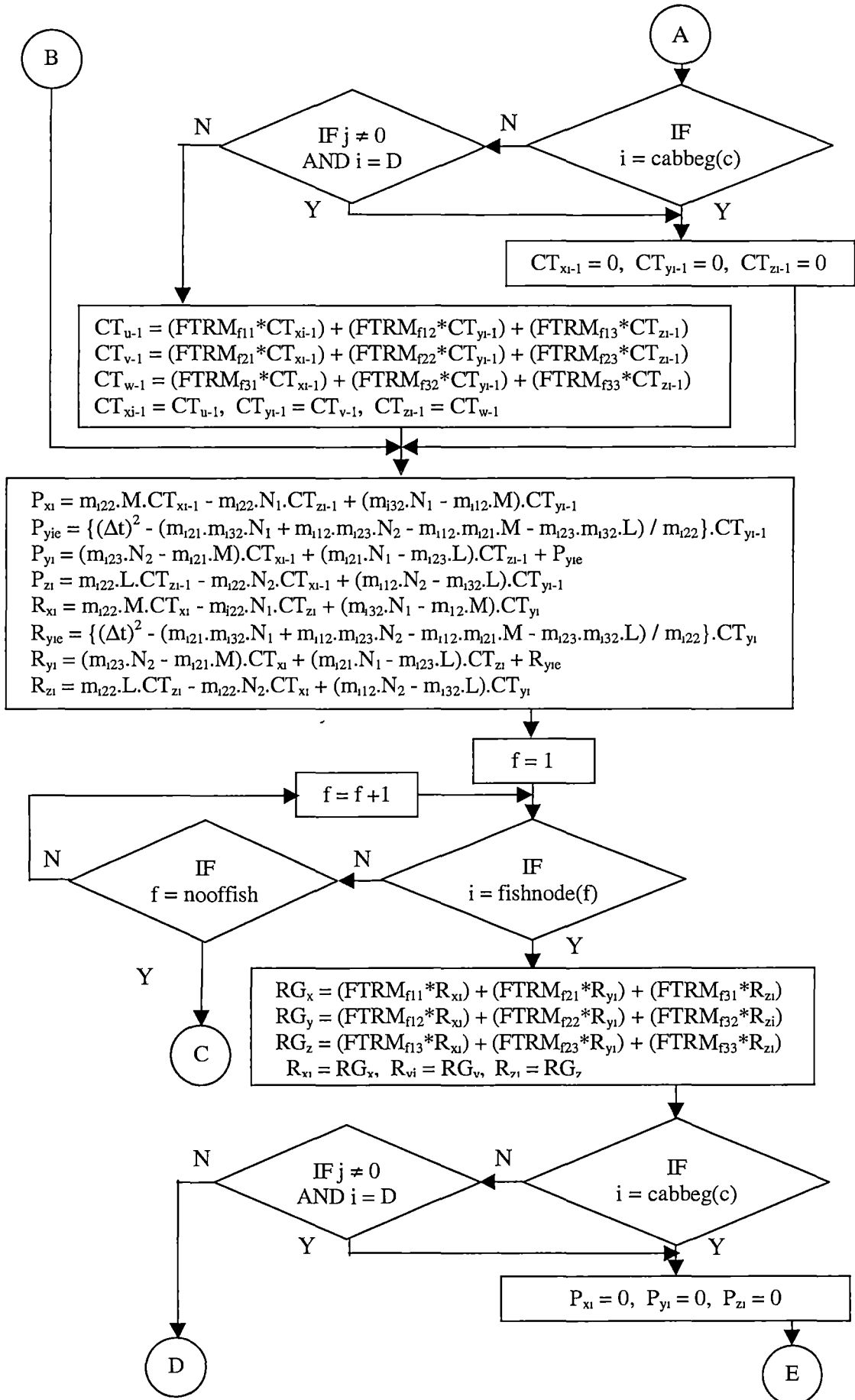


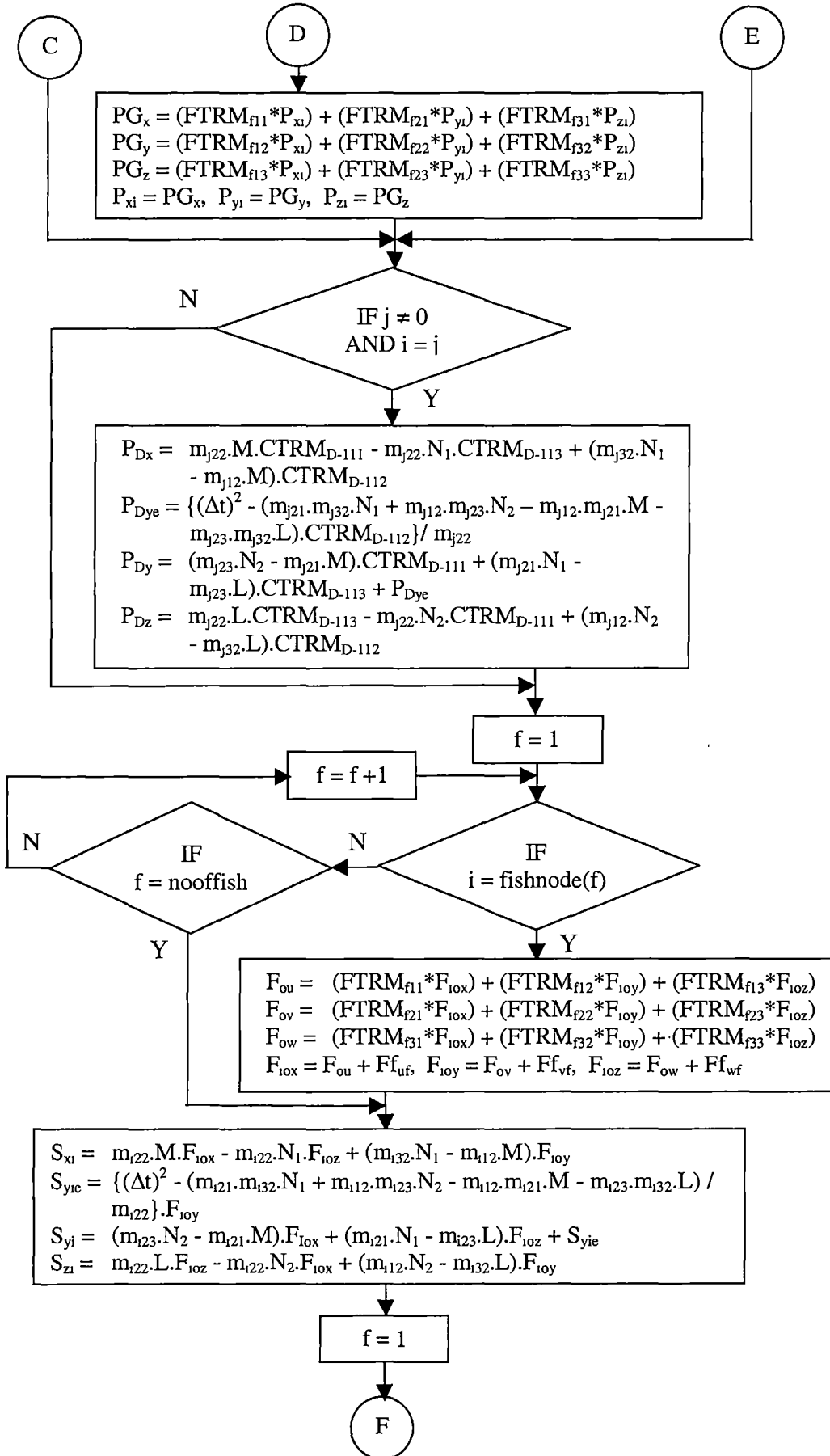
Subroutine Node Velocity

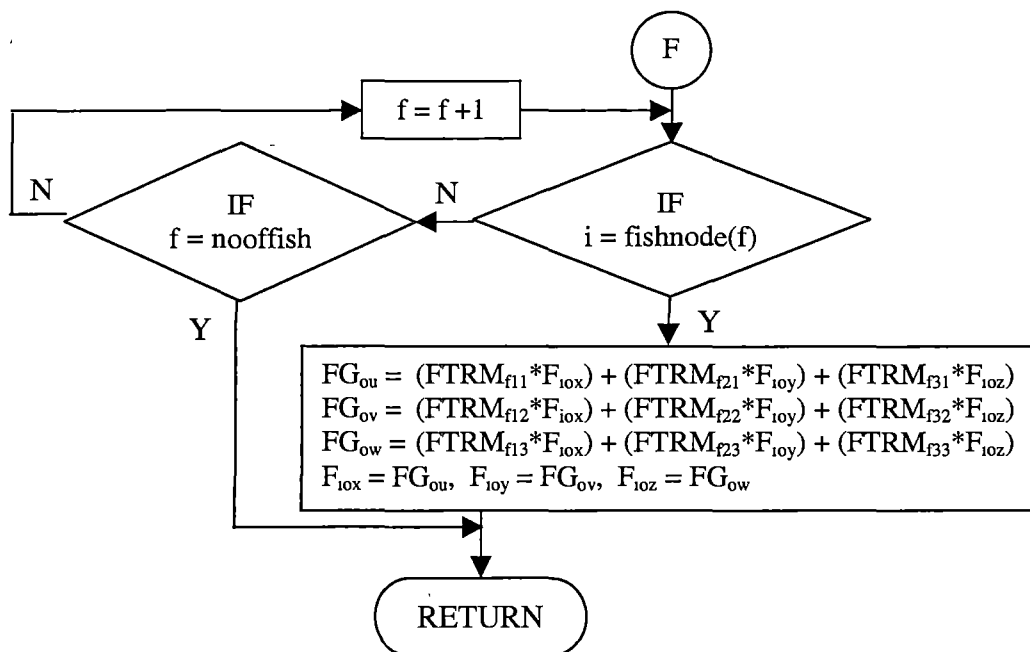


Subroutine Equation Coefficient

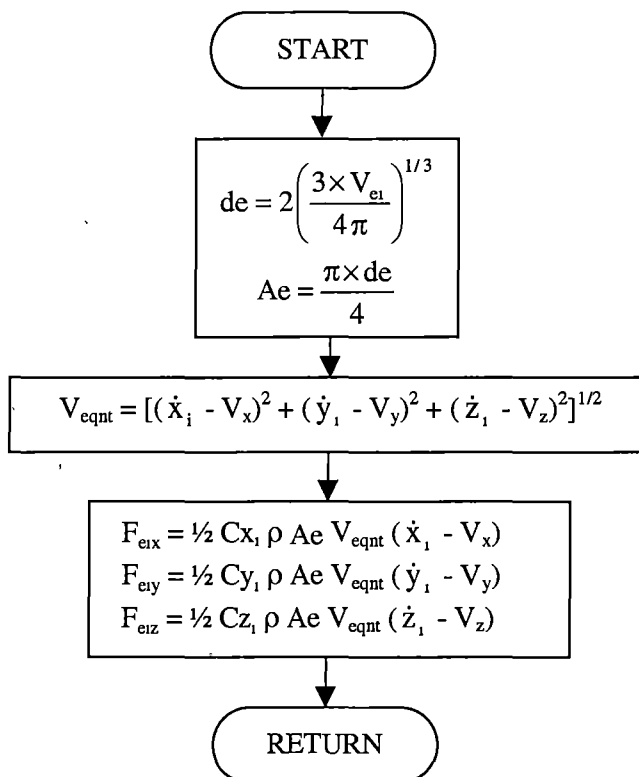




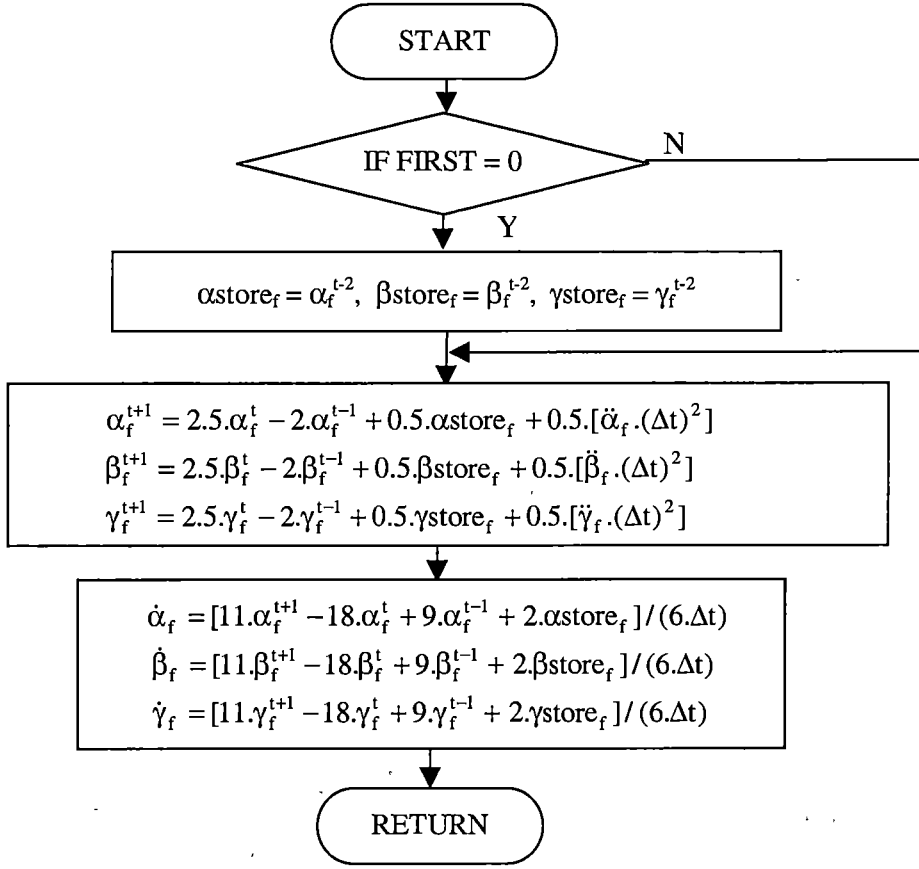




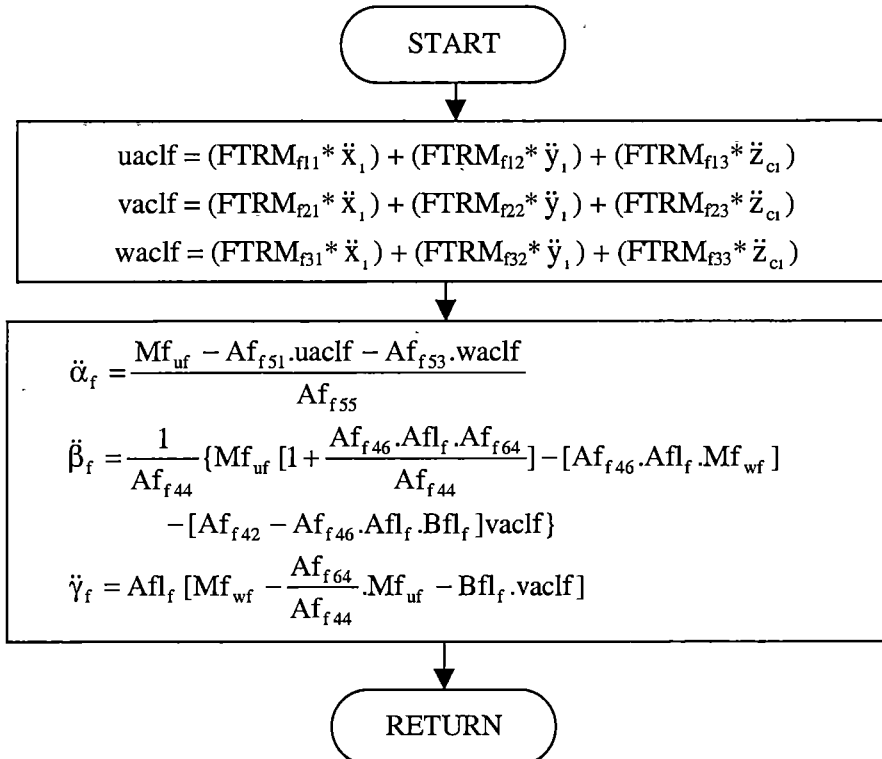
Subroutine Node Drag



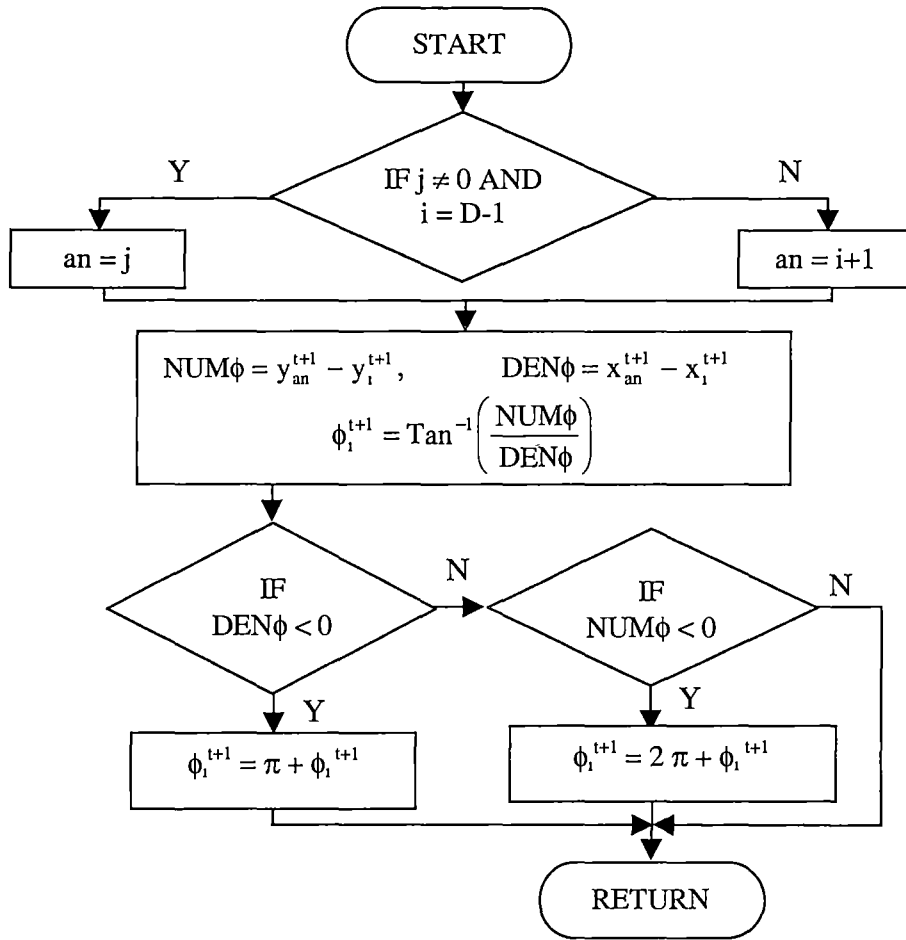
Subroutine Fish Angular Velocity Angle



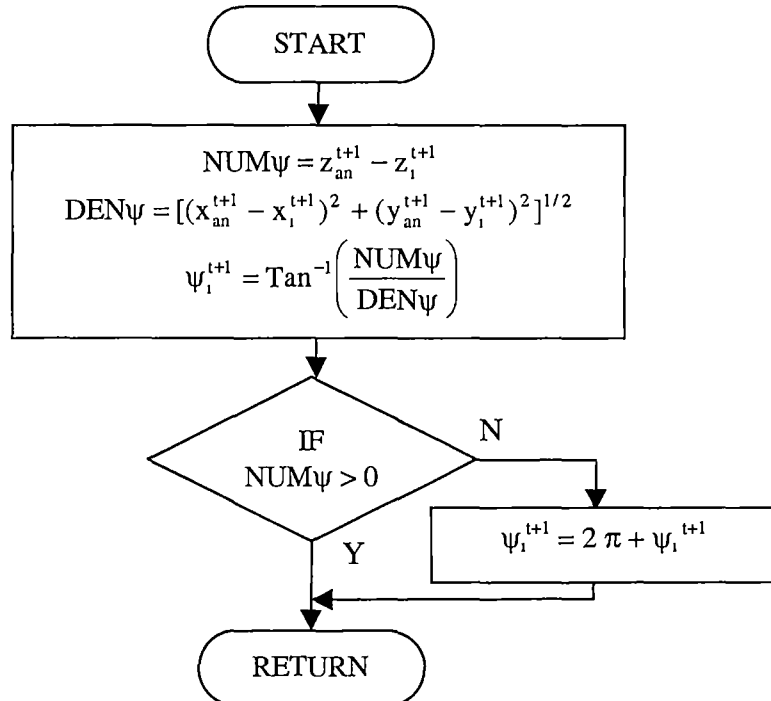
Subroutine Fish Angular Acceleration



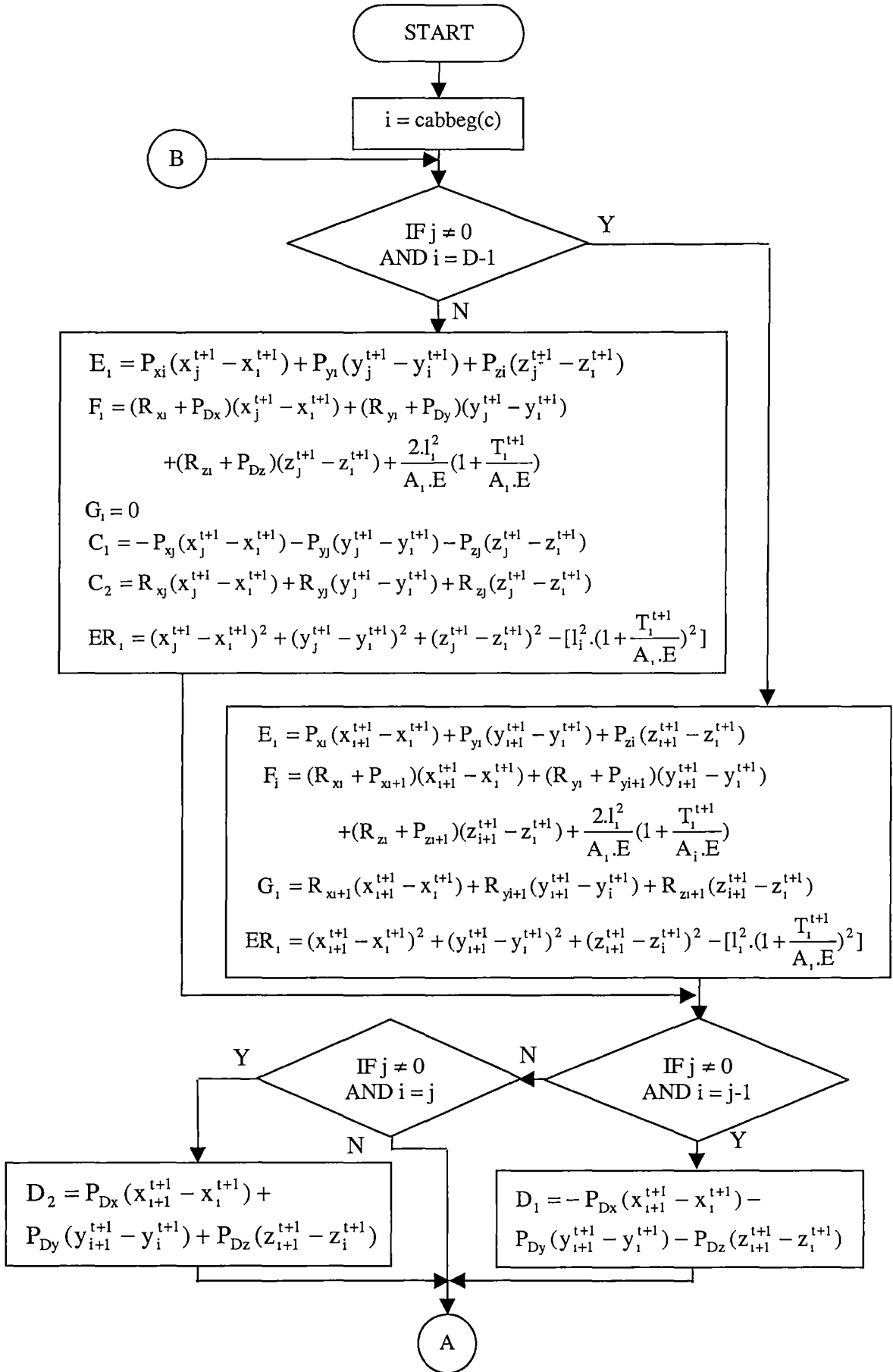
Subroutine Segment Angle Horizontal

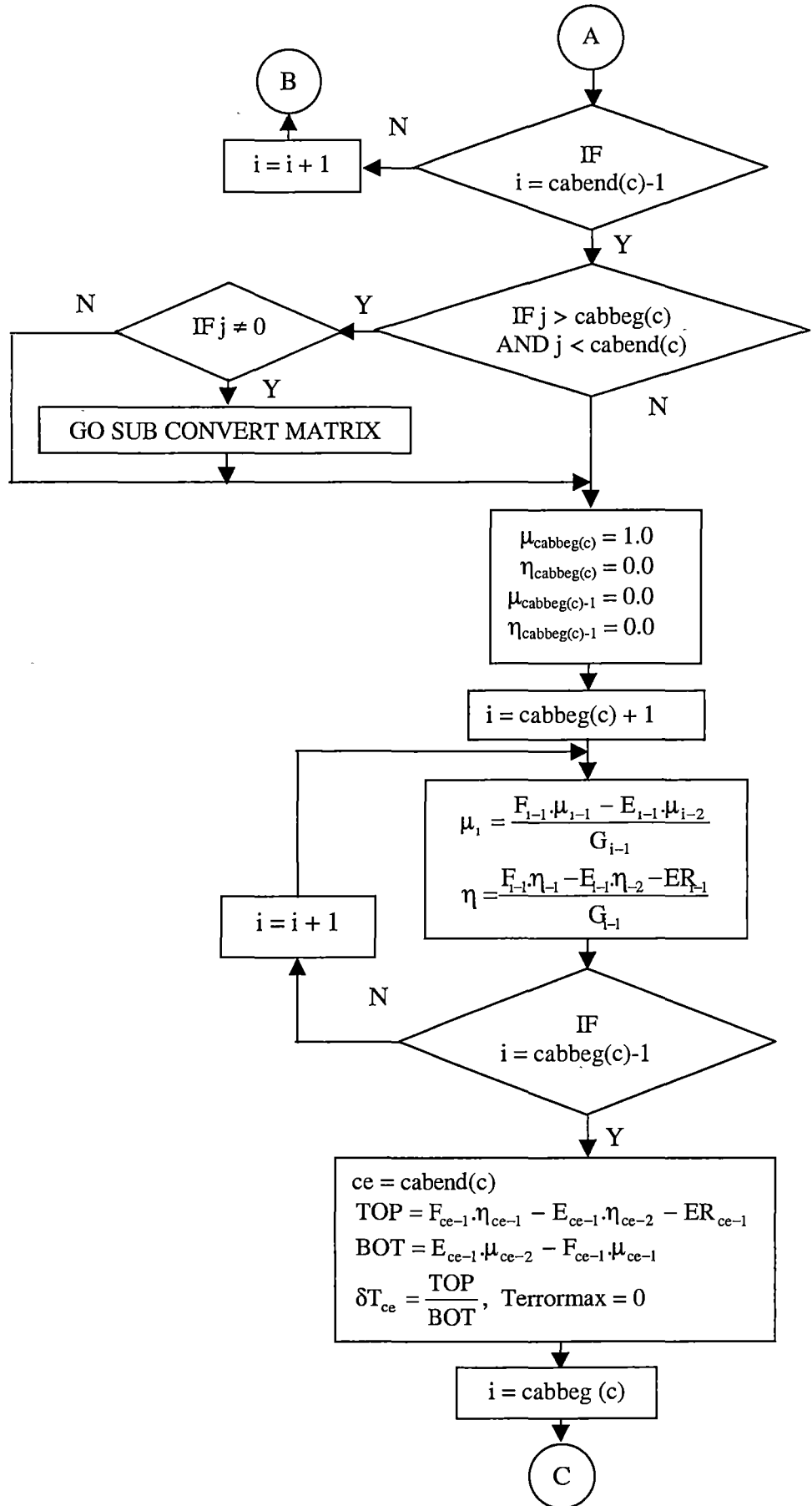


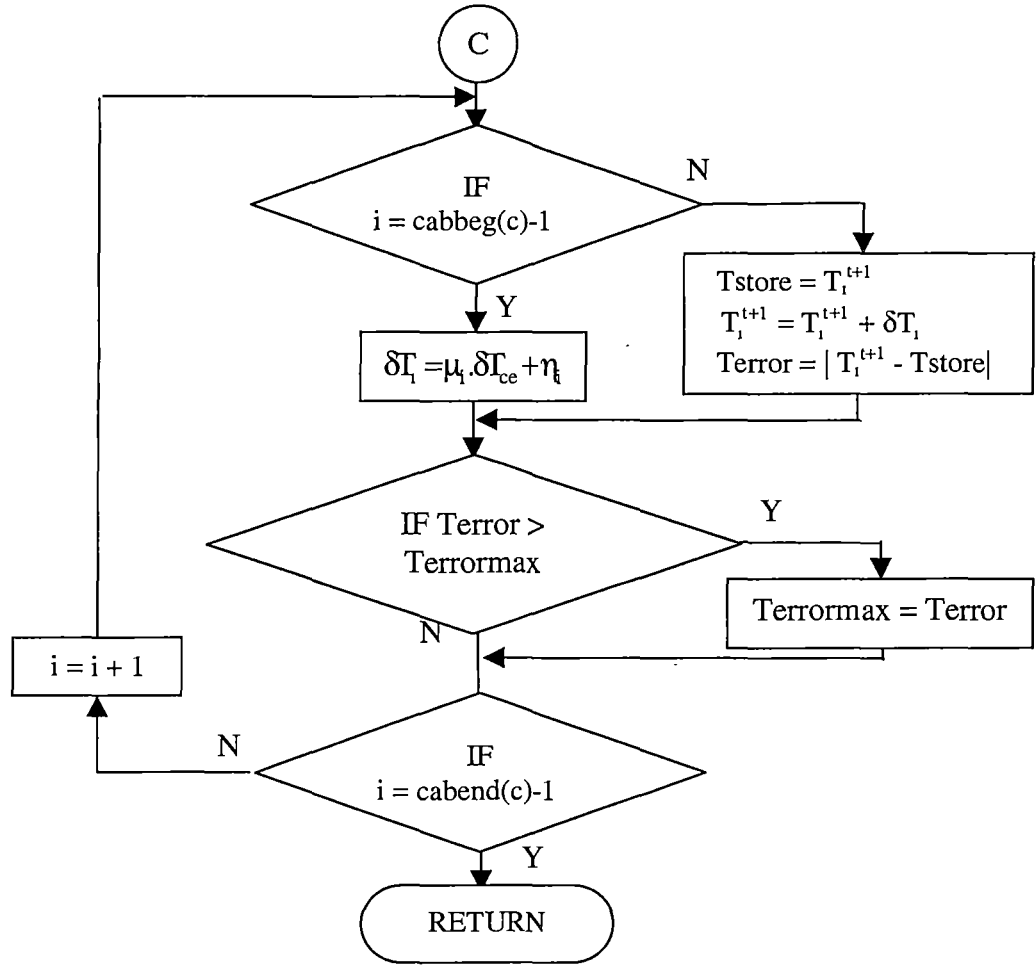
Subroutine Segment Angle Vertical



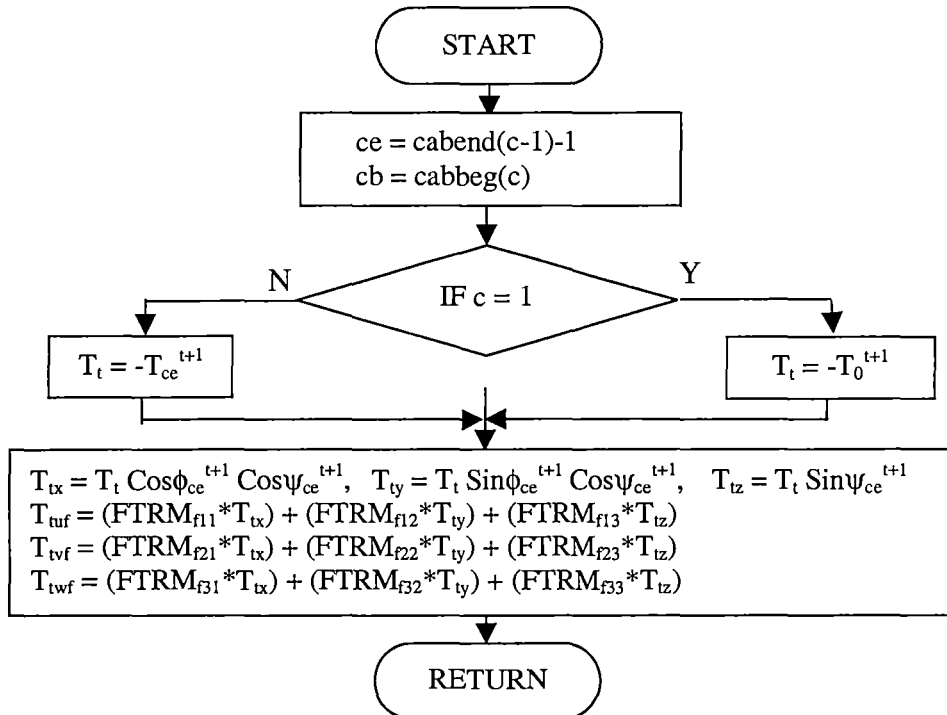
Subroutine Correct Tension



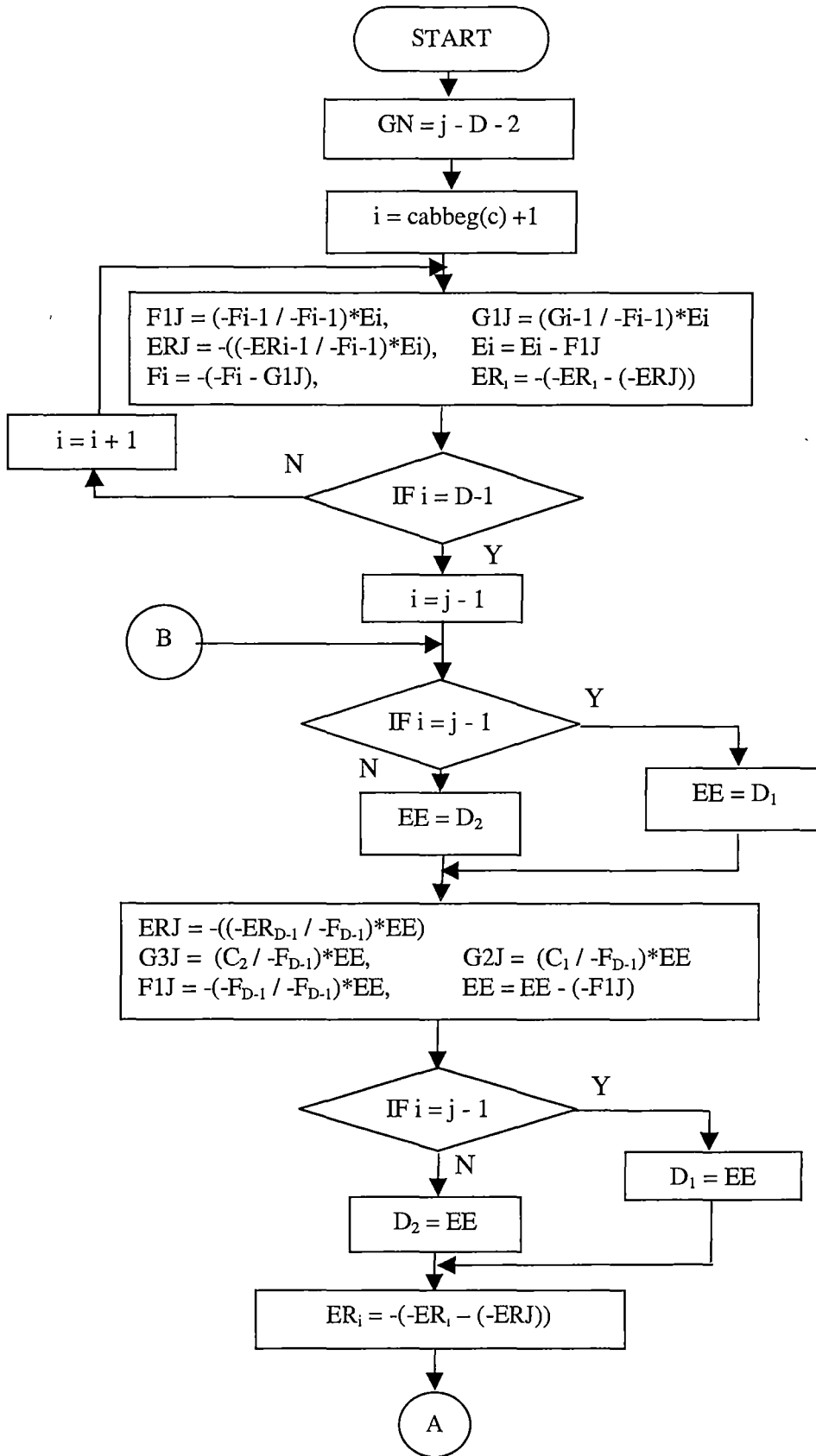


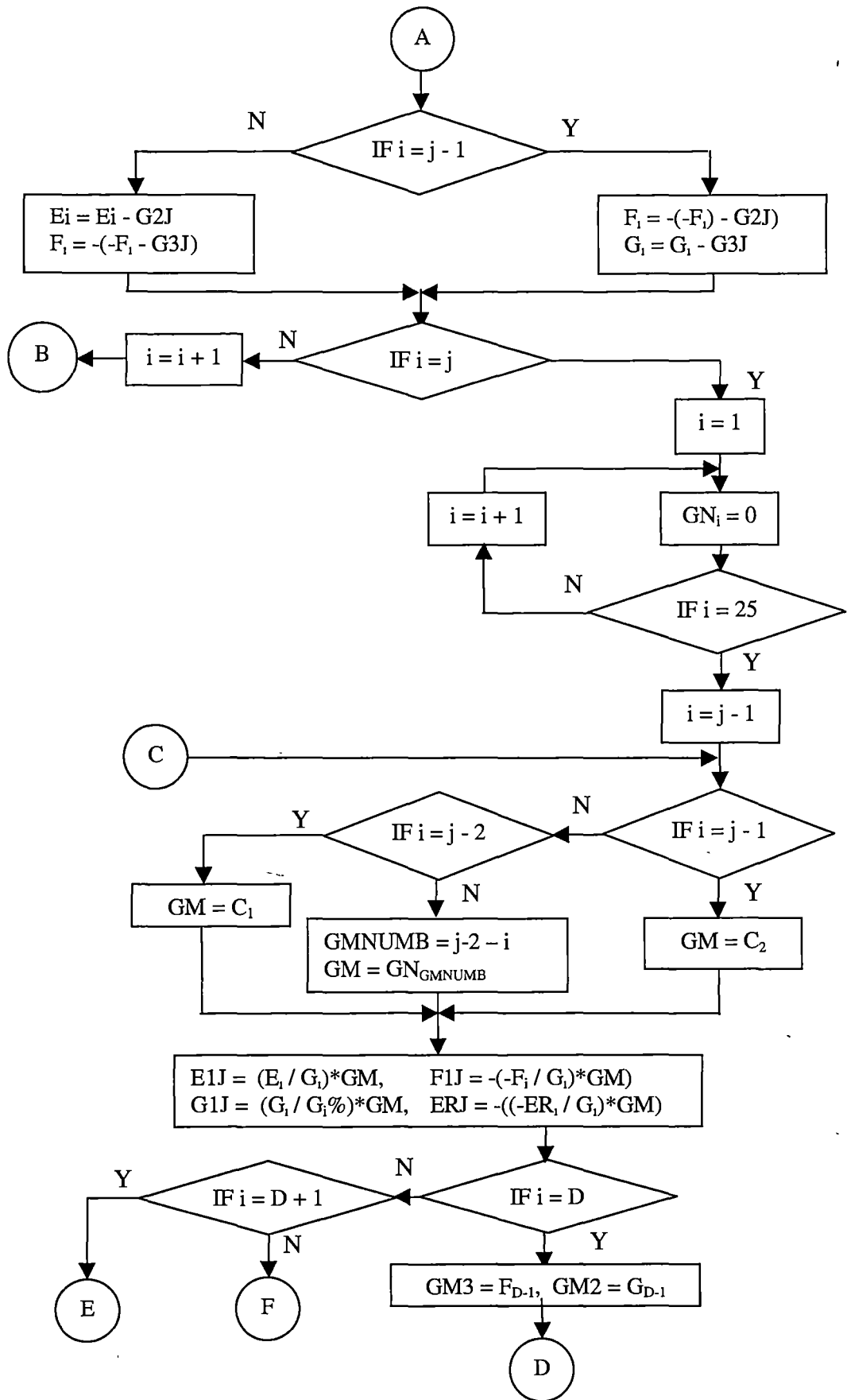


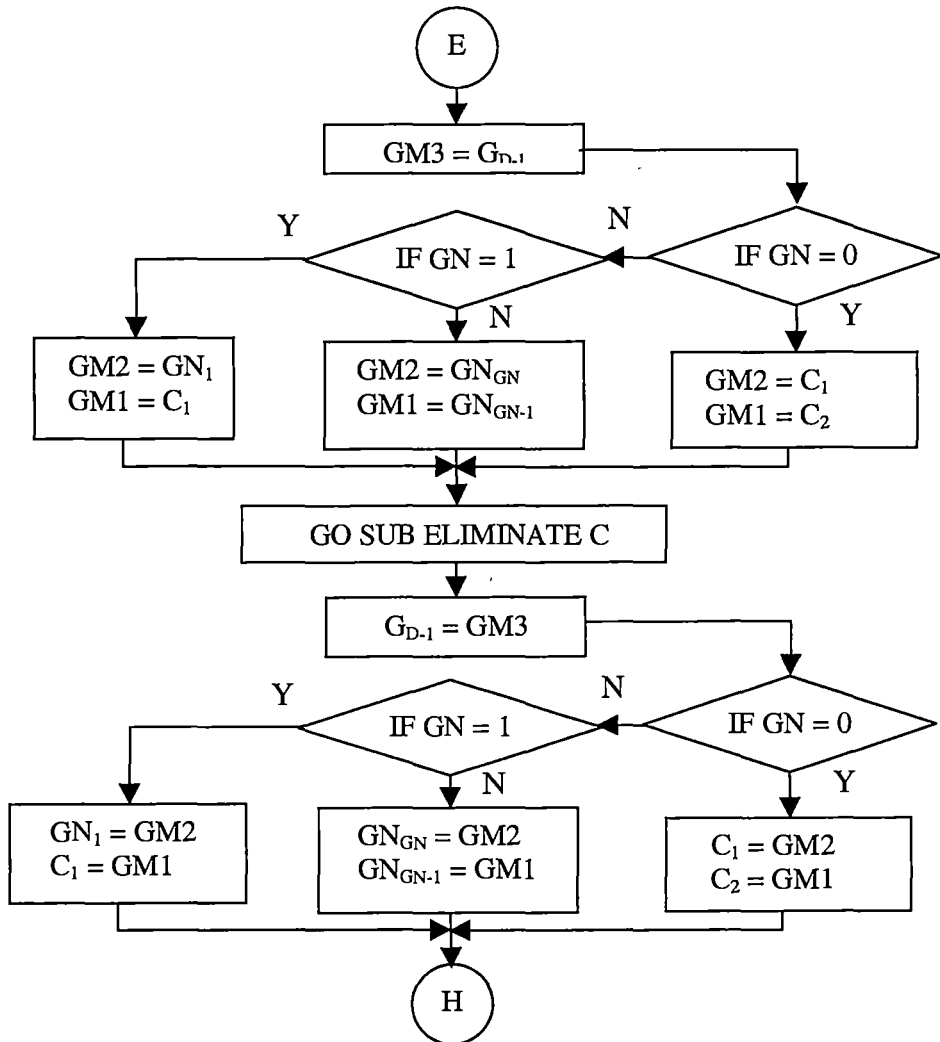
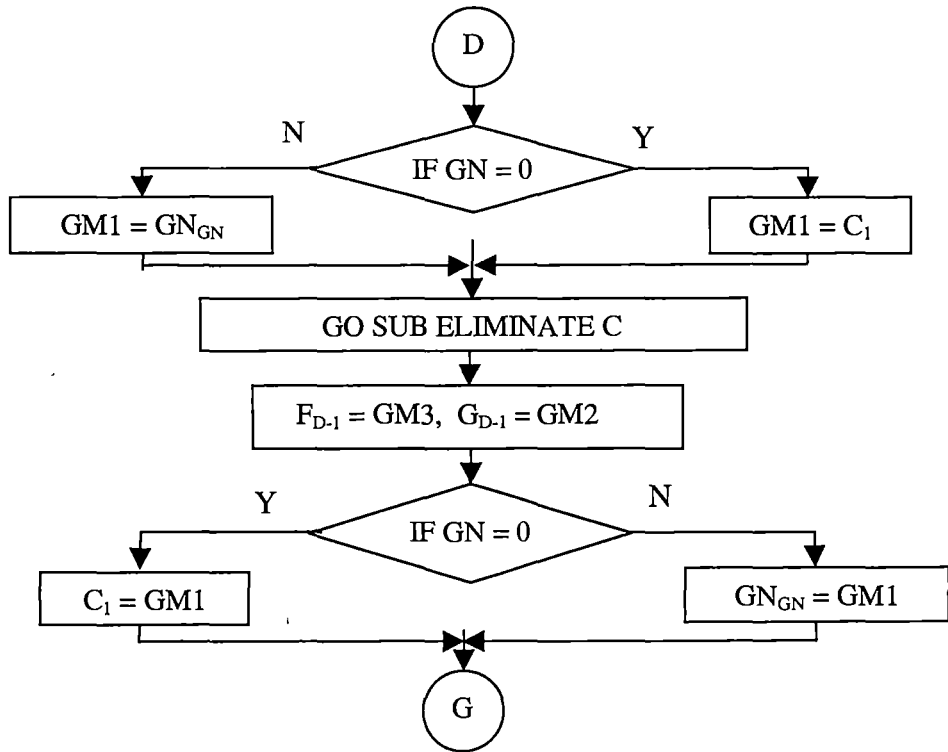
Subroutine Tail Tension

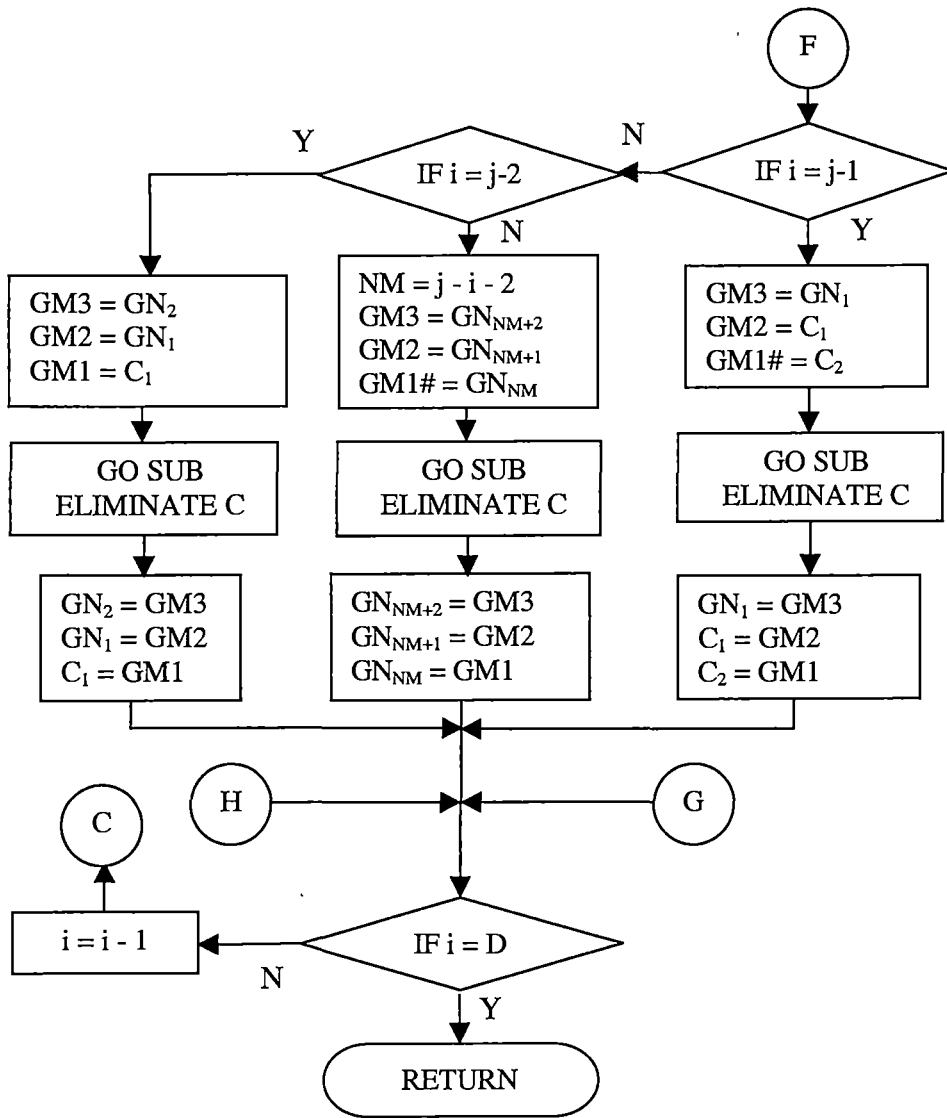


Subroutine Convert Matrix

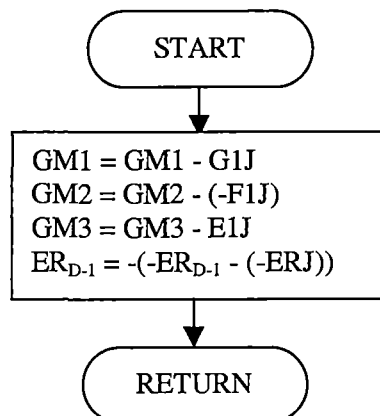




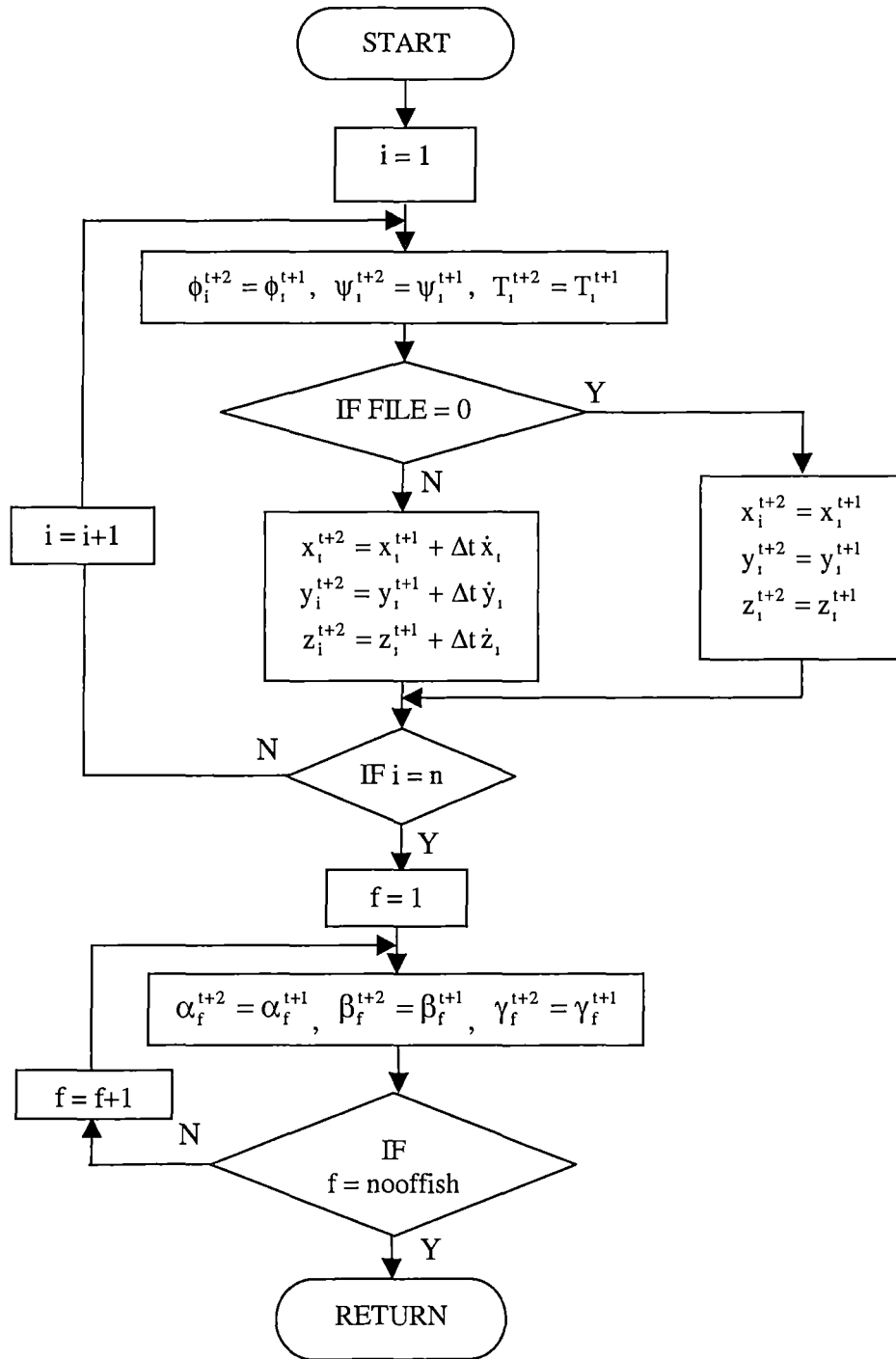




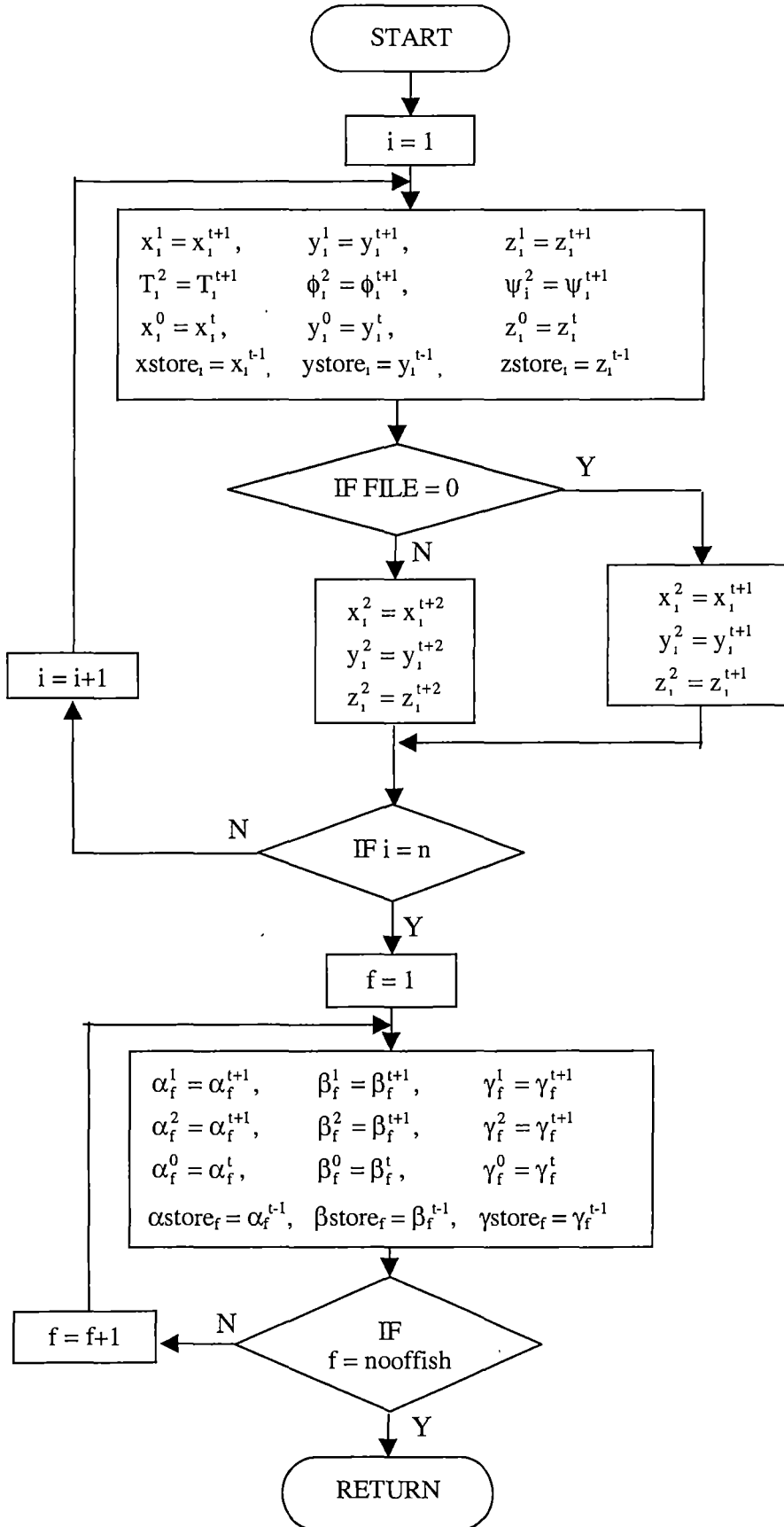
Subroutine Eliminate C



Subroutine Increment Values



Subroutine Free Array



Multi Tow in Parallel

For the multi-tow in parallel, the program is slightly different to that explained above. However, as the differences are small, only the matrix conversion subroutine is given here. The input data should include the number of junctions and the node positions of these junctions. In *Subroutine Eliminate C*, simply replace the subscript “D-I” with “*lastnode(a)*”. The additional variables are:

a variable representing each parallel tow
 firstnode(a) first node of the parallel tow “a”
 juntno(a) node number of the junction in parallel tow “a”
 lastnode(a) last node of the parallel tow “a”
 nooftows number of cable systems in the tow configuration

Subroutine Convert Matrix – Multi Tow

